

MMET 02

## Conference Proceedings

2002 International Conference on

# MATHEMATICAL METHODS IN ELECTROMAGNETIC THEORY

DISTRIBUTION STATEMENT A  
Approved for Public Release  
Distribution Unlimited

Kiev, Ukraine  
September 10-13, 2002

# CONFERENCE PROCEEDINGS

*2002 International Conference on*

# MATHEMATICAL METHODS IN ELECTROMAGNETIC THEORY

# MMET\*02

Volume 2

**DISTRIBUTION STATEMENT A**

Approved for Public Release  
Distribution Unlimited

*Kiev, Ukraine*

*September 10-13, 2002*

20030110 025



*Organized and sponsored by*

IEEE AP/MTT/AES/ED/GRS/NPS/EMB Societies East Ukraine Joint Chapter

*in cooperation with*

Scientific Council of NAS on Radio Physics and Microwave Electronics  
Institute of Radio-Physics and Electronics of NAS  
National Technical University of Ukraine – Kiev Polytechnic Institute  
Ukrainian National URSI Committee

*technically co-sponsored by*

IEEE AP, MTT and ED Societies  
URSI

*We wish to thank the following for their contribution to the success  
of this conference:*

IEEE ED, MTT and AP Societies  
European Office of Aerospace Research and Development  
European Research Office, USARDSG-UK  
TICRA

2002 International Conference on Mathematical Methods in Electromagnetic Theory

IEEE Catalog Number: 02EX554  
ISBN: 0-7803-7391-X

Library of Congress: 2002100182

This material is based upon work supported by the European Office of Aerospace Research and development, Air Force Office of Scientific Research, Air Force Research Laboratory, under Contract No. F61775-02-WF065.

Copyright and Reprint Permission: Abstracting is permitted with credit to the source. Libraries are permitted to photocopy beyond the limit of U.S. copyright law for private use of patrons those articles in this volume that carry a code in the bottom of the first page, provided the per-copy fee indicated in the code is paid through Copyright Clearance Center, 222 Rosewood Drive, Danvers, MA 01923. For other copying, reprint or republication permission, write to IEEE Copyrights Manager, IEEE Service Center, 445, Hoes Lane, P.O. Box 1331, Piscataway, NJ 08855-1331. All rights reserved. Copyright © 2002 by the IEEE, Inc.

REPORT DOCUMENTATION PAGE			Form Approved OMB No. 0704-0188	
Public reporting burden for this collection of information is estimated to average 1 hour per response, including the time for reviewing instructions, searching existing data sources, gathering and maintaining the data needed, and completing and reviewing the collection of information. Send comments regarding this burden estimate or any other aspect of this collection of information, including suggestions for reducing this burden to Washington Headquarters Services, Directorate for Information Operations and Reports, 1215 Jefferson Davis Highway, Suite 1204, Arlington, VA 22202-4302, and to the Office of Management and Budget, Paperwork Reduction Project (0704-0188), Washington, DC 20503.				
1. AGENCY USE ONLY (Leave blank)		2. REPORT DATE		3. REPORT TYPE AND DATES COVERED
		2002		Conference Proceedings, 10-13 September 2002
4. TITLE AND SUBTITLE			5. FUNDING NUMBERS	
2002 International Conference on Mathematical Methods in Electromagnetic Theory (MMET 02), Volume 2			N62558-02-M-6003	
6. AUTHOR(S)				
7. PERFORMING ORGANIZATION NAME(S) AND ADDRESS(ES)			IEEE catalog no. 02EX554	
National Academy of Sciences, Ukraine			ISBN 0-7803-7391-X	
9. SPONSORING/MONITORING AGENCY NAME(S) AND ADDRESS(ES)			10. SPONSORING/MONITORING AGENCY REPORT NUMBER	
USARDSG-UK, Fiscal Office, Edison House, 223 Old Marylebone Road, London NW1 5 <sup>th</sup> , UK			R&D 9294-EE-02	
11. SUPPLEMENTARY NOTES				
Conference Proceedings of the 2002 International Conference on Mathematical Methods in Electromagnetic Theory, Volumes 1 (pages 1-340) and 2 (pages 341-696) based on work supported by the European Office of Aerospace Research and development, Air Force Office of Scientific Research, Air Force Research Laboratory, under contract no. F61775-02-WF065, IEEE Catalog Number 02EX554, ISBN 0-7803-7391-X, 696 pages total..				
12a. DISTRIBUTION/AVAILABILITY STATEMENT			12b. DISTRIBUTION CODE	
Approved for Public Release.			A	
ABSTRACT (Maximum 200 words)				
Table of Contents- Volume 2. See attached with presentation titles of the sessions listed below:				
WIENER-HOPF AND FUNCTION-THEORETIC METHODS GRATINGS AND FREQUENCY-SELECTIVE SURFACES ANTENNA ANALYSIS AND SYNTHESIS NUMERICAL TECHNIQUES SCATTERING AND RADAR CROSS SECTION WAVEGUIDE CIRCUITS COMPOSITE MEDIA AND METAMATERIALS ANALYTICAL REGULARIZATION PROPAGATION AND SIGNAL PROCESSING BEAMS AND PLASMAS EIGENVALUE PROBLEMS				
14. SUBJECT TERMS			15. NUMBER OF PAGES	
US Army Research, Ukraine, Wiener-Hopf, Function-Theoretic methods, Waveguide, Electromagnetic waves, Gratings, Diffraction, Scattering, Antenna Analysis, Electromagnetic field, Reflector antenna, Numerical techniques, Wavelet, Antenna, Apertures, Radar, Dielectric, Waveguide circuits, Electrodynamic properties, Bandpass filter, Mode-matching method, Eigenwaves, Composite media, Metamaterials, Analytical regularization, Magnetoactive plasma, Chiral layer, Backscattering, Propagation, Signal processing, Beams, Plasma				
			16. PRICE CODE	
17. SECURITY CLASSIFICATION OF REPORT	18. SECURITY CLASSIFICATION OF THIS PAGE	19. SECURITY CLASSIFICATION OF ABSTRACT	20. LIMITATION OF ABSTRACT	
Unclassified	Unclassified	Unclassified	Unlimited	

**WIENER-HOPF AND FUNCTION-THEORETIC METHODS:** Phase radiation characteristics of an open-ended circular waveguide; Frechet differentiability of a field operator for scattering from an open screen; Reflection of surface waves and their coupling with wave beams at anisotropically perturbed impedance plane; Axial symmetric wave diffraction by a circular waveguide cavity; On the method of solution of the wave equation with periodic coefficients; Fractional cylindrical functions implementation for electromagnetic waves scattering analysis; Integro-differential potentials for the analysis of a fractal cover properties; Integro-differential charges and currents distribution on the fractal medium topology.

**GRATINGS AND FREQUENCY-SELECTIVE SURFACES:** Mathematical simulation of impedance diffraction gratings; Analysis of frequency selective structure with fractal elements; Electromagnetic wave diffraction by double-layer periodic grating of curvilinear metal strips; FEM and its generalization for the diffraction by polygonal profile gratings; Electromagnetic characteristic of doubly-periodic magnetodielectric layer bounded by two uniform media; Scattering of electromagnetic waves by homogeneous dielectric gratings with perfectly conducting strip; Simulation of the finite photonic crystal-based adaptive antenna; A combination of up- and down-going plane waves used to describe the field inside grooves of a deep grating; Scattering and absorption of light by nano-thickness negative-dielectric strip gratings; Reconstruction of periodic boundary between dielectric media; Reflective properties of grid structures with dielectric coating; Comparative study of integration schemes used on differential theory of gratings; Eigenwaves in the layered medium of bi-periodic strip arrays; Mathematical models of electromagnetic wave scattering by two-element strip grating with perpendicularly magnetized gyrotropic medium; Dispersive and diffraction analysis of integrated periodic waveguide structure.

**ANTENNA ANALYSIS AND SYNTHESIS:** Calculation of electromagnetic field in near field zone of reflector antenna with edge radar absorbing coating; Analysis of reflector pattern in different frequency ranges in the backward hemisphere; To the problem of analysis of dielectric rod antennas; Statistical analysis of internal parameters of radiating systems with reactance elements; An algorithm of the sidelobe level optimization for the dual shaped symmetric reflector antenna; Fitness function calculation technique in the yagi-uda antennas evolutionary design; Evaluation of uncertainty budget for antenna calibrations; Antenna arrays synthesis according to the sector pattern by multiparametric method of regularization.

**NUMERICAL TECHNIQUES:** A study for the fast solution of electromagnetic scattering problems: a wavelet based approach; Symbolic computation techniques for aperture antennas; The 2,5-D electromagnetic analysis in time domain mode; Calculation of leakage through apertures on coaxial cable braided screens; Efficient CFIE-mom analysis of 3-D PEC scatterers in layered media; The partial region method in 2-D electromagnetic and acoustic problems; Dielectric parameters recognition by using a waveguide cavity and a rigorous processing algorithm; Drop shaped monopole antenna and its interaction with the user's head; Building Trefftz finite elements for electromagnetic problems.

**SCATTERING AND RADAR CROSS SECTION:** Calculation of near-zone electromagnetic fields scattered by complex shape airborne objects and estimation of their angular coordinates by onboard antenna systems; Mathematical methods in some diffraction problems for domains with defects; Application of the method of auxiliary sources for the analysis of plane wave scattering by impedance spheres; Volume singular integral equations method for solving of diffraction problem of electromagnetic waves on dielectric body in a box; Radar cross section of a perfectly conducting, flat, polygonal plate over a dielectric, lossy half-space: a closed form, physical optics expression; Electromagnetic modeling of the jet aircraft intake with the interior impeller; Finite element analysis of scattering from 2D-objects of arbitrary composition; Radioabsorbing material optimal using in the reduction of aircraft radar cross-section; Minimization of the field diffracted from a convex impedance body to the shadow region.

**WAVEGUIDE CIRCUITS:** Influence of defects on electrodynamic properties of a semi-infinite periodic sequence of the metal-dielectric scatterers; Waveguide filters on the lumped elements; Wave scattering by a cylindrical obstacle in a generalized waveguide; Capacitive iris bandpass filter with spurious harmonic modes suppression; Data preprocessing for generalized mode-matching method; Mode-matching approach for the calculation of a waveguide tee distorted by semi-plates in the branching region; The effects of resonance energy absorption in lossy waveguide-dielectric resonators; Diffraction on the eigenwaves on an inclined medium interface in the waveguides with metallic walls.

**COMPOSITE MEDIA AND METAMATERIALS:** The second or the third harmonic generation on a nonlinear film in a Bragg resonator; Analytical investigation of periodic media with negative parameters; Investigation of composite materials with controllable electrodynamic properties; Simplified analysis of split ring resonator used in backward meta-material; The analytical method of investigation of Faraday chiral media; Scattering of a wave beam by inhomogeneous anisotropic chiral layer; Modeling of electromagnetic field from mobile phone distributed in the human head phantom; The mechanisms of gravitophotophoresis for aerosol aggregates in the free-molecular regime.

**ANALYTICAL REGULARIZATION:** The plane H-polarized wave diffraction by a metal grating with a magnetoactive plasma; Wave diffraction by axially symmetrical system of finite soft cylinders; Diffraction by a screened chiral layer with a grating; Resonant coupling of cavity-backed slots; Radiation characteristics of a 2D parabolic reflector antenna excited by the H-polarized complex source; Electromagnetic waves scattering on an unclosed cone with an isotropic one inside; Electromagnetic backscattering from a triangular dielectric cylinder; Simulation of a discrete Luneburg lens fed by a conformal printed antenna.

**PROPAGATION AND SIGNAL PROCESSING:** The filter for horn antenna multifrequency data processing; On unique estimation of azimuth-elevation-carriers by volume arrays; Comparing techniques for proving unsatisfiability; Modified method of geometric electromagnetics for the analysis of radio field in marine tropospheric waveguides; Nonlinear stage of propagation of wave disturbances in the topside ionosphere; The technique for calculating of HF-signals characteristics taking into consideration ionosphere; waveguide propagation; Electrodynamical model of the receiving antenna in terms of a waveguide representation of the HF field; Evaluation of the atmospheric aerosol particle size in the reflective layer produced by strong solar flares; On possibility of Schumann resonance observations within industrial areas. **BEAMS AND PLASMAS:** Bistability of nonlinear surface polaritons in conducting antiferromagnets; Propagation of intra-subband plasmons in a weakly disordered array of quantum wires; Calculation of impedance of a sharp plasma boundary with a mixed-type electron scattering in anomalous skin-effect conditions; Radiophysical characteristics of a radiator from the gas discharge plasma; Radiation by self-oscillating relativistic charged particle moving along periodic structure; Interaction of a non-relativistic electron beam with a semiconductor cylinder in an external magnetic field; An analytical method for construction of single particle electron trajectories in free electron lasers; Collisionless damping of surface plasma oscillations and possibilities of its revers at the interaction with charged particle flows; Peculiarities of nonlinear stabilization of the plasma-beam instability in semiconductor GaAs.

**EIGENVALUE PROBLEMS:** Eigenoscillations near cascade of thin disks between the pair of parallel planes; Influence of an elliptical non-uniformity of dielectric sphere on spectral characteristics of resonance oscillations; On perturbation of the spectrum of planar dielectric waveguide by refraction index profile; Numerical investigation of eigenoscillations near a honeycomb in a circular channel; Existence theorems for eigenoscillations in 3-D rectangular waveguides; Some aspects of the slow waves in the circular waveguide with azimuthally magnetized ferrite rod; Dispersion characteristics of a waveguide with periodic impedance of walls; The problem of orthogonality of eigenwaves in a waveguide partially filled with a lossy dielectric; Rotor stator acoustic interaction, death and birth of resonance frequency; Characteristics of spatially-developed square multimode resonators.

**MMET\*02 Chairman**

Prof. E. I. Veliev, IRE NASU, Kharkov, Ukraine

**MMET\*02 Organizing Committee**

Prof. V. I. Naidenko, NTUU-KPI, Kiev  
*Local Organization Chairman*

Mr. H. A. Borsch, NTUU-KPI, Kiev  
*Local organization and technical support*

Dr. V. G. Drygailo, NTUU-KPI, Kiev  
*Director of the Science Library*

Dr. E. V. Guseva, NTUU-KPI, Kiev  
*Local organization and technical support*

Dr. Y. M. Kuleshov, IRE NASU, Kharkov  
*IEEE East Ukraine Joint Chapter Chairman*

Prof. L. N. Litvinenko, IRA NASU, Kharkov  
*Ukrainian National URSI Committee Vice-Chairman*

Mr. A. A. Nosich, KNU, Kharkov  
*System administrator and technical support*

Prof. V.I. Pravda, NTU-KPI, Kiev  
*Dean of Dept. Radio Engineering*

Dr. A. Shishkova, KNU, Kharkov  
*Secretary and web designer*

Mrs. S. Spivakova, KNPU, Kharkov  
*Proceedings editor and designer*

Mr. A. D. Ustimenko, IRE NAS, Kharkov  
*Local Organization Manager*

Prof. V. M. Yakovenko, IRE NASU, Kharkov  
*Ukrainian National URSI Committee Vice-Chairman*

Prof. F. J. Yanovsky, National Aviation University, Kiev  
*Local Organization Coordinator*

Prof. M. Z. Zgurovsky, NTUU-KPI, Kiev  
*Rector*

**Preceding Pages Blank**

**MMET\*02 CHAIRMAN**

Prof. E. I. Veliev, IRE NASU, Kharkov, Ukraine

**MMET\*02 Technical Program Committee****Co-Chairmen:**

Prof. A. I. Nosich, IRE NASU, Kharkov, Ukraine

Dr. W. Ross Stone, IEEE AP-S & URSI, San Diego, USA

**Members:**

Prof. T. Benson, University of Nottingham, UK  
Prof. O. Breinbjerg, TU of Denmark, Lyngby, Denmark  
Prof. N. Engheta, University of Pennsylvania, Philadelphia, USA  
Prof. Y. V. Gandel, Kharkov National University, Ukraine  
Prof. F. Gardiol, Ecole Polytechnique, Lausanne, Switzerland  
Prof. M. Hashimoto, Osaka Electro-Communication University, Japan  
Prof. A. Jacob, Technical University of Braunschweig, Germany  
Prof. A. A. Kirilenko, IRE NASU, Kharkov, Ukraine  
Prof. K. Kobayashi, Chuo University, Tokyo, Japan  
Prof. M. Marciniak, Institute of Telecommunications, Warsaw, Poland  
Prof. Z. T. Nazarchuk, PMI NASU, Lviv, Ukraine  
Prof. M. Ney, ENSTB, Brest, France  
Prof. Y. Okuno, Kumamoto University, Japan  
Prof. A. Samokhin, Moscow TU of Radio Electronics, Russia  
Prof. H. Shigesawa, Doshisha University, Kyoto, Japan  
Prof. S. V. Sukhinin, IH SB RAS, Novosibirsk, Russia  
Prof. I. Sukhoivanov, Kharkov NU of Radio Electronics, Ukraine  
Prof. D. I. Vavriv, IRA NASU, Kharkov, Ukraine  
Dr. S. N. Vorobyov, IRA NASU, Kharkov, Ukraine  
Prof. T. Yamasaki, Nihon University, Tokyo, Japan  
Prof. F. J. Yanovsky, National Aviation University, Kiev, Ukraine  
Dr. N. P. Yashina, IRE NASU, Kharkov, Ukraine  
Prof. L. P. Yatsuk, Kharkov National University, Ukraine



## CHAIRMEN'S WELCOME

*Dear Colleagues –*

We are happy to open MMET\*02 in Kiev, over-a-thousand years old capital of the eleven years old independent Ukraine. The venue of the conference, this time, is the largest technical university of Ukraine, NTUU-KPI, or *Kyivska Politekhnika*.

As with the previous MMET conferences held in 1990-2000, we have tried to follow our several basic traditions. One of them is the idea that a cross-fertilization of mathematicians and microwave engineers is a natural necessity that should be promoted by all means. There are many other meetings covering *only* applied mathematics or computing and *only* microwaves or physics. MMET is a unique combination of the both. Therefore the technical program is a mixture of fundamental mathematical studies into boundary-value problems of wave scattering and studies into applications and implementations of various analysis methods. Another eternal idea is that interaction with the Western science has always been and still is very important for Ukrainians, Russians, Belarussians, Georgians, and other Eastern Europeans. Therefore we intended to attract as many as possible keynote speakers from the West Europe, America and Japan, from one hand, and good contributed papers from the East Europe, from the other hand. At the same time we still believe that having two working languages and massive poster sessions, as done sometimes, is a wrong way of international conference organization in our conditions. Instead, MMET gives one a chance to train in writing and presenting a paper in the major international science language, which is English. Still another traditional idea is to help young scientists from low-income regions come and participate, even if they travel from very far away. Humiliation of a 50-Euro a month salary of a scientist should be neutralized, at least once in two years, by an opportunity to join the holiday of MMET.

This year the Technical Program Committee had invited 28 papers and accepted 148 contributed ones, out of 161 submitted. We enjoyed working with all the members of Local Organizing Committee and Technical Program Committee. We are extremely thankful to the staff and executives of the Department of Radio Engineering and the Scientific Library of NTUU-KPI. All of us should kindly thank the editing group that prepared the conference proceedings and supported the Website of MMET\*02. The generosity of the conference sponsors is greatly appreciated.

We thank everybody of participants who have come to Kiev this September despite many other professional commitments. We hope to see you at the future conferences in Ukraine.

Eldar I. Veliev and Alexander I. Nosich

It looks like MMET\*02 has quite a nice program. Congratulations! Best wishes with the conference.

W. Ross Stone

# MMET\*02 PAPERS GEOGRAPHY

	ENTITY	PAPERS
1	UKRAINE	83
2	RUSSIA	33
3	TURKEY	8
4	JAPAN	6
5	FRANCE	4
6	BELARUS	3
7	DENMARK	3
8	GERMANY	3
9	GREECE	3
10	ITALY	3
11	USA	3
12	BULGARIA	2
13	GEORGIA	2
14	SWITZERLAND+TURKEY	2
15	UKRAINE+FRANCE	2
16	UKRAINE+JAPAN	2
17	AUSTRIA	1
18	BELGIUM	1
19	CROATIA	1
20	CZECH REPUBLIC	1
21	IRAN	1
22	JORDAN	1
23	MEXICO	1
24	The NETHERLANDS	1
25	POLAND	1
26	SWEDEN	1
27	UK	1
28	UKRAINE+DENMARK	1
29	UKRAINE+TURKEY	1
30	UKRAINE+UK	1
<b>TOTAL</b>		<b>176</b>

# TABLE OF CONTENTS

## *Volume I*

### PLENARY SESSIONS

01	<b>A. Andrenko</b> , Study and microwave applications of artificial periodic substrate PBG planar circuits.....	21
02	<b>A. Baghai-Wadji</b> , Measures for accelerating EM computations.....	27
03	<b>Yu. Smirnov, S. Ivleeva</b> , Propagation of electromagnetic waves in open cylindrical waveguides with nonlinear media.....	33
04	<b>F. Molinet</b> , Hybrid numerical-asymptotic method for the calculation of the coupling between elements of a conformal microstrip patch array.....	38
05	<b>T. Magath, K. Schuenemann</b> , Application of evolution strategies in optimal design problems involving diffraction gratings.....	42
06	<b>A. Freni, P. De Vito, A. Mori</b> , A BMIA/AIM formulation for the analysis of large stacked patch antennas.....	48
07	<b>A. Hoorfar</b> , Evolutionary computational techniques in electromagnetics....	54
08	<b>G. Vandenbosch, M. Vrancken, and B. Van Thielen</b> The use of hierarchy in modeling tools for planar structures.....	61
09	<b>V. L. Derbov, V. V. Serov, I. L. Plastun, S. V. Shilov</b> , Time-dependent self-action of periodically modulated laser beams in resonant media.....	67
10	<b>G. Fikioris</b> , On the solvability and application of numerical methods to Hallen's equation.....	73
11	<b>P. O. Savenko, B. M. Podlevskii, M. D. Tkach, M. I. Andriychuk</b> , Some classes of nonlinear synthesis problems for radiation systems: theory and methods of solution.....	79
12	<b>V. Daniele</b> , The Wiener-Hopf factorization method for the diffraction by wedges having arbitrary aperture angle .....	87
13	<b>H. Shigesawa, M. Tsuji</b> , Basic properties of leaky modes in printed- circuit transmission lines.....	93
14	<b>A. Kirilenko</b> , Large-scale discretization and generalized mode-matching as a basis for fast electromagnetic solvers.....	99
15	<b>H. Baudrand, W. Sidina, B. Damienne</b> The concept of waves: theory and applications in electronic problems.....	100

16	<b>G. Kyriacou</b> , Analytical study of microwave structures printed on anisotropic substrates based on the Wiener-Hopf technique.....	105
17	<b>E. Hasanov</b> , Complex and real rays in three dimensional Minkowski space	112
18	<b>F. Zolla, D. Felbacq</b> , Artificial anisotropy.....	118
19	<b>A. Krokhin, J. Arriaga, P. Halevi</b> , Homogenization of photonic crystals.....	124
20	<b>V.G. Daniele, R. E. Zich</b> , Approximated factorizations for kernels involved in the scattering due by a wedge at skew incidence.....	130
21	<b>M. Ney, S. Le Maguer</b> , The transmission-line matrix (TLM) method: an efficient tool for problem segmentation (diakoptics).....	136
22	<b>T. Jablonskii</b> , Spectral properties of the operator describing EM wave propagation in anisotropic dielectric guiding structures with arbitrary transversal inhomogeneity.....	141
23	<b>A. Nosich</b> , Infinite-sheet branching of the habitat of the natural-frequencies of open resonators as a result of admission of infinite boundaries.....	150
24	<b>S. Koshikawa, K. Kobayashi</b> , Wiener-Hopf analysis of the RCS of two canonical, parallel-plate waveguide cavities with material loading.....	152
25	<b>S. V. Sukhinin, D. A. Kondratenko</b> , Wave transmission trough inhomogeneous chain of transparent obstacles.....	157
26	<b>G. Schneider, A. Jacob</b> , Adapted grids for the wavelet-based simulation of complex planar circuits.....	163
27	<b>A. Samokhin</b> , Volume singular integral equation method in electromagnetic theory.....	169
28	<b>N. Engheta</b> , Electromagnetics of complex media and metamaterials.....	175

## TIME-DOMAIN METHODS

01	<b>K. P. Gaikovich</b> , Evolution equation for near-field thermal radio emission...	183
02	<b>M. S. Antyufeyeva, O. A. Tretyakov</b> , Time-domain electromagnetic fields in a resonator with dispersive medium.....	186
03	<b>A. N. Dumin, V. A. Katrich</b> , Energy transformation of a transient wave on radiating aperture.....	189
04	<b>V. A. Doroshenko</b> , Excitation of a slotted bicone by an impulse magnetic dipole.....	192
05	<b>S. Martynyuk, F. Dubrovka, P. Edenhofer</b> A novel dual-polarized Ku-band antenna subarray.....	195

06	A. Nerukh, T. Benson, Integral equations in time domain for electromagnetic fields of waveguide structures.....	198
07	I. S. Maksymov, G. I. Churyumov, Photonic Green's functions calculation by using FDTD method.....	201
08	N. N. Ruzhytska, A. G. Nerukh, D. A. Nerukh. Calculation of complexity of a pulse transformation in time-varying medium.....	204
09	N. Sakhnenko, A. Nerukh, Investigation of electromagnetic field in a plate-parallel waveguide with time varying medium.....	207
10	V. A. Ruchenkov, K. N. Klimov, B. V. Sestroretsky, M. A. Drize, Y. P. Bolshakov, Direct study of fields and radiation patterns of antennas with the account of closely located objects.....	210
11	A. Y. Butrym, O. A. Tretyakov, Electromagnetic signals in a waveguide filled with an inhomogeneous time-variant medium.....	213
12	A. I. Vyazmitinova, Accurate "absorbing" conditions for nonsinusoidal problems of diffraction for compact objects.....	216
13	O. Puzanov, Modeling of videopulse scattering by plane layered dielectric structures in the presence of errors.....	219
14	I. Araz, O. Cerezci, Z. Demir, Terminated two-wire transmission line suspended in air illuminated by electromagnetic field and measurement of differential mode current.....	222

## COMPUTATIONAL OPTOELECTRONICS

01	A. M. Gomilko, A. A. Gourjii, V. B. Katok, V. G. Levandovskyy, Y. D. Shchepkina, Single-mode fiber with a reduced non-zero dispersion in wide range of wavelength.....	227
02	E. Kartchevski, G. Hanson, Mathematical analysis of the guided modes of an integrated optical guide.....	230
03	I. Vorgul, A. Vukovic, P. Sewell, T. Benson, Full vectorial analysis of optical fibre facet.....	233
04	I. A. Sukhoivanov, V. V. Lysak, A. Shulika, Mathematical modelling of un-symmetrical optical mirrors for femtosecond impulse generation.....	236
05	E. A. Romanova, S. B. Gaal, Modelling of radiation field excited on sharp waveguide discontinuities by numerical and semi-analytical methods.....	239
06	M. I. Ayzatsky, K. Y. Kramarenko, Coupled oscillations in the theory of layered dielectric.....	242



- 07 **V. Katok, M. Kotenko, O. Ometsinska**, Stratification method for analysis of the radial inhomogeneous dielectric waveguide: a new approach towards realization.....245

## PRINTED ANTENNAS AND CIRCUITS

- 01 **A. M. Lerer, G. P. Sinyavsky, D. E. Zelenchuk**, Diffraction of electromagnetic wave by an array of complex shape microstrip reflectors.....251
- 02 **V. Schejbal, Z. Raida, Z. Novacek**, Comparison of CAD formulas, moment method and experiments for rectangular microstrip antennas..... 254
- 03 **S. Arslanagic, P. Meincke, E. Jorgensen, O. Breinbjerg**, A line integral representation of the physical optics far field from plane PEC scatterers illuminated by electric or magnetic Hertzian dipoles.....257
- 04 **L. M. Karpukov, S. N. Romanenko, R. D. Pulov**, Closed-form Green's function and its using for analysis of microstrip antennas..... 260
- 05 **J. V. Rassokhina, A. N. Rudiakova, V. G. Krizhanovski**, Accurate analysis of PBG structures for high efficiency power amplifier design..... 263
- 06 **A. O. Kasyanov, V. A. Obukhovets, V. I. Zagorovsky**, Numerical simulation of the microstrip phased array..... 266
- 07 **A. N. Rudiakova, Ju. V. Rassokhina, V. G. Krizhanovski**, The photonic bandgap microstrip class-E amplifier..... 267
- 08 **V. Naidenko, E. Guseva**, Diffraction of a plane H-polarised electromagnetic wave by two sequentially included stratified periodic dielectric structures..... 270

## GEORADAR AND REMOTE SENSING

- 01 **Yu. A. Averyanova, A. A. Averyanov, F. J. Yanovsky**, Wind flight conditions model.....275
- 02 **I. Prokopenko, K. Prokopenko**, Nonparametric algorithm for a detection of random process disorder in the signals of radar remote sensing.....278
- 03 **F. J. Yanovsky**, Doppler-polarimetric retrieval of rain rate and turbulence intensity in precipitation.....281
- 04 **Y. S. Khraisat**, Relationship between an interval of correlation of echo-signal envelope and turbulence intensity in radar reflecting volume of cloud or precipitation..... 287

- 05 A. Vertiy, S. Gavrilov, Methods of improving of the subsurface objects images reconstructed by the tomography process.....290
- 06 F. Dikmen, A. Alkumru, O. Yildirim, An ART algorithm for imaging of buried cylindrical bodies illuminated by gaussian beams.....293
- 07 A. V. Muzychenko, A. Z. Sazonov, O. I. Sukharevsky, Estimation of geometrical parameters of perfectly conducting cylindrical object buried in dielectric half-space by its scattering characteristics.....296
- 08 M. V. Andreev, O. O. Drobakhin, D. Yu. Saltykov, Application of wavelet analysis for detection of cylindrical objects in dielectric layer using characteristic of reflection.....299
- 09 A. A. Palto, Parameters optimization for synthesizing aperture method at practical use of continuous radiation underground radar.....302

## WIRE AND WAVEGUIDE ANTENNAS

- 01 M. B. Protsenko, Curved-wire antennas solution technique.....307
- 02 L. M. Karpukov, V. M. Onufrienko, S. N. Romanenko, The properties of the fractal wire antenna.....310
- 03 N. P. Yeliseyeva, N.N. Gorobets, Radiation resistance of an electric dipole having different orientations when changing the position of a plane screen.....313
- 04 B. A. Arand, M. Hakkak, Analysis of vertical wire antenna above imperfect ground using discrete complex image method.....316
- 05 S. G. Vashtalov, Radiation from a planar waveguide with symmetrical flange.....319
- 06 M. B. Manuilov, Rigorous theory of rectangular waveguide arrays with finite flush mounted dielectric cover.....322
- 07 V. M. Morozov, V. I. Magro, M. Guarab, Solution of three-dimensional electromagnetic problems .....325
- 08 V. A. Katrich, V. I. Kiyko, L. P. Yatsuk, M. N. Nesterenko, Basis functions in the analysis of electrically long slots in rectangular waveguide with the induced magnetomotive forces method.....328
- 09 A. V. Gribovsky, A waveguide-based antenna array excited by a surface wave.....331

## *Volume II*

### WIENER-HOPF AND FUNCTION-THEORETIC METHODS

- 01 A.V. Shishkova, S. N. Pivnenko, O. S. Kim, N. N. Gorobets, Phase radiation characteristics of an open-ended circular waveguide.....361
- 02 Z. T. Nazarchuk, Y. P. Kulynych, Frechet differentiability of a field operator for scattering from an open screen..... 364
- 03 V. F. Borulko, Reflection of surface waves and their coupling with wave beams at anisotropically perturbed impedance plane.....367
- 04 D. B. Kuryliak, K. Kobayashi, S. Koshikawa, Z. T. Nazarchuk, Axial symmetric wave diffraction by a circular waveguide cavity..... 370
- 05 E. A. Gevorkyan, On the method of solution of the wave equation with periodic coefficients..... 373
- 06 D. V. Golovin, D. O. Batrakov, Fractional cylindrical functions implementation for electromagnetic waves scattering analysis..... 376
- 07 V. M. Lewykin, V. M. Onufriyenko, Integro-differential potentials for the analysis of a fractal cover properties..... 379
- 08 V. M. Onufriyenko, Integro-differential charges and currents distribution on the fractal medium topology..... 382

### GRATINGS AND FREQUENCY-SELECTIVE SURFACES

- 01 G. A. Kalinchenko, A. M. Lerer, A. A. Yachmenov, Mathematical simulation of impedance diffraction gratings.....387
- 02 A. O. Kasyanov, V. A. Obukhovets, Analysis of frequency selective structures with fractal elements..... 390
- 03 P. L. Mladyonov, Electromagnetic wave diffraction by double-layer periodic grating of curvilinear metal strips..... 395
- 04 G. Elschner, A. Rathsfeld, G. Schmidt, FEM and its generalization for the diffraction by polygonal profile gratings..... 398
- 05 N. V. Sidorchuk, V. V. Yachin, S. L. Prosvirnin, Electromagnetic characteristics of doubly-periodic magnetodielectric layer bounded by two uniform media..... 401
- 06 T. Yamasaki, T. Hinata, T. Hosono, Scattering of electromagnetic waves by homogeneous dielectric gratings with perfectly conducting strip.....404

07	<b>A. Bijamov, R. Zaridze, K. Tavzarashvili, V. Tabatadze,</b> Simulation of the finite photonic crystal –based adaptive antenna.....	407
08	<b>Y. Okuno, D. Q. Zhou, K. Yoshimoto, A. Matsushima, and T. Matsuda,</b> A combination of up- and down-going plane waves used to describe the field inside grooves of a deep grating.....	410
09	<b>T. L. Zinenko, A. I. Nosich,</b> Scattering and absorption of light by nano-thickness negative-dielectric strip gratings.....	413
10	<b>J. Chandezon, A. Poyedinchuk, N. Yashina,</b> Reconstruction of periodic boundary between dielectric media.....	416
11	<b>M. U. Sitsko, V. I. Demidchik,</b> Reflective properties of grid structures with dielectric coating.....	420
12	<b>K. Watanabe,</b> Comparative study of integration schemes used on differential theory of gratings.....	423
13	<b>S. L. Prosvirnin, D. O. Tyrnov,</b> Eigenwaves in the layered medium of biperiodic strip arrays.....	426
14	<b>Y. V. Gandel, V. V. Khoroshun,</b> Mathematical models of electromagnetic wave scattering by two-element strip grating with perpendicularly magnetized gyrotropic medium.....	429
15	<b>T. Bugrova,</b> Dispersive and diffraction analysis of integrated periodic waveguide structure.....	432

## ANTENNA ANALYSIS AND SYNTHESIS

01	<b>S. V. Nechitaylo, A. Z. Sazonov, O. I. Sukharevsky,</b> Calculation of electromagnetic field in near field zone of reflector antenna with edge radar absorbing coating.....	437
02	<b>G. V. Yermakov,</b> Analysis of reflector pattern in different frequency ranges in the backward hemisphere.....	440
03	<b>S. V. Buharov,</b> To the problem of analysis of dielectric rod antennas.....	443
04	<b>V. V. Ovsyanikov,</b> Statistical analysis of internal parameters of radiating systems with reactance elements.....	446
05	<b>M. V. Romanenko,</b> An algorithm of the sidelobe level optimization for the dual shaped symmetric reflector antenna.....	449
06	<b>S. N. Sorokin, V. V. Savelyev, E. V. Ivanchenko, M. P. Oleynik,</b> Fitness function calculation technique in the yagi–uda antennas evolutionary design.....	452

- 07 **B. Turetken, E. San, M. Yazici, I. Araz, A. I. Yurekli, M. Hekim**, Evaluation of uncertainty budget for antenna calibrations..... 455
- 08 **O. N. Nosenko, N. N. Gorobets**, Antenna arrays synthesis according to the sector pattern by multiparametric method of regularization..... 458

## NUMERICAL TECHNIQUES

- 01 **M. B. Kurt, N. Ari, O. Cerezci**, A study for the fast solution of electromagnetic scattering problems: a wavelet based approach..... 463
- 02 **N. Ari, A. Tesneli, S. S. Seker, O. Cerezci**, Symbolic computation techniques for aperture antennas..... 466
- 03 **T. V. Kamichev, K. N. Klimov, B. V. Sestroretsky, S. A. Ivanov**, The 2.5-D electromagnetic analysis in time domain mode..... 469
- 04 **B. Colak, O. Cerezci, Z. Demir, M. Yazici, B. Turetken, I. Araz**, Calculation of leakage through apertures on coaxial cable braided screens..... 473
- 05 **O. S. Kim, E. Jorgensen, P. Meincke, O. Breinbjerg**, Efficient CFIE-mom analysis of 3-D PEC scatterers in layered media..... 476
- 06 **T. Trifonov**, The partial region method in 2-D electromagnetic and acoustic problems..... 479
- 07 **A. Y. Poyedinchuk, A. A. Kirilenko, N. P. Yashina**, Dielectric parameters recognition by using a waveguide cavity and a rigorous processing algorithm..... 482
- 08 **G. Ghvedashvili, R. Zaridze, K. Tavzarashvili, G. Saparishvili, A. Bijamov**, Drop shaped monopole antenna and its interaction with the user's head..... 485
- 09 **Y. O. Shlepnev**, Building Trefftz finite elements for electromagnetic problems..... 488

## SCATTERING AND RADAR CROSS SECTION

- 01 **N. V. Barkhudaryan, A. Z. Sazonov, O. I. Sukharevsky**, Calculation of near-zone electromagnetic fields scattered by complex shape airborne objects and estimation of their angular coordinates by onboard antenna systems..... 493
- 02 **A. A. Gousenkova**, Mathematical methods in some diffraction problems for domains with defects..... 496



- 03 **M. Karamehmedovic, O. Breinbjerg**, Application of the method of auxiliary sources for the analysis of plane wave scattering by impedance spheres.... 499
- 04 **Yu. G. Smirnov, A. A. Tsupak**, Volume singular integral equations method for solving of diffraction problem of electromagnetic waves on dielectric body in a box..... 502
- 05 **H. T. Anastassiou**, Radar cross section of a perfectly conducting, flat, polygonal plate over a dielectric, lossy half-space: a closed form, physical optics expression..... 505
- 06 **V. N. Kisel, A. I. Fedorenko**, Electromagnetic modeling of the jet aircraft intake with the interior impeller..... 508
- 07 **A. M. Lebedev**, Finite element analysis of scattering from 2D-objects of arbitrary composition..... 511
- 08 **V. A. Vasilets, S. A. Gorelyshev, K. I. Tkachuk**, Radioabsorbing material optimal using in the reduction of aircraft radar cross-section..... 514
- 09 **A. A. Zvyagintsev, A. I. Ivanov**, Minimization of the field diffracted from a convex impedance body to the shadow region..... 517

## WAVEGUIDE CIRCUITS

- 01 **V. V. Khardikov, V. B. Kazanskiy**, Influence of defects on electrodynamic properties of a semi-infinite periodic sequence of the metal-dielectric scatterers..... 523
- 02 **A. R. Sorkin**, Waveguide filters on the lumped elements..... 526
- 03 **V. P. Chumachenko, I. V. Petrusenko**, Wave scattering by a cylindrical obstacle in a generalized waveguide..... 529
- 04 **A. Kirilenko, L. Mospan, V. Tkachenko**, Capacitive iris bandpass filter with spurious harmonic modes suppression..... 532
- 05 **A. A. Kirilenko, D. Yu. Kulik**, Data preprocessing for generalized mode-matching method..... 535
- 06 **S. F. Kulishenko, A. A. Kirilenko, S. L. Senkevich**, Mode-matching approach for the calculation of a waveguide tee distorted by semi-plates in the branching region..... 540
- 07 **L. B. Minakova, L. A. Rud**, The effects of resonance energy absorption in lossy waveguide-dielectric resonators..... 543
- 08 **I. N. Pleshchinskii, N. B. Pleshchinskii**, Diffraction on the eigenwaves on an inclined medium interface in the waveguides with metallic walls..... 546

## COMPOSITE MEDIA AND METAMATERIALS

- 01 V. F. Borulko, The second or the third harmonic generation on a nonlinear film in a Bragg resonator.....551
- 02 K. Vytovtov, Analytical investigation of periodic media with negative parameters..... 554
- 03 R. V. Kornev, V. I. Demidchik, Investigation of composite materials with controllable electrodynamic properties..... 557
- 04 S. Hrabar, J. Bartolic, Simplified analysis of split ring resonator used in backward meta-material..... 560
- 05 K. A. Vytovtov, The analytical method of investigation of Faraday chiral media..... 563
- 06 A. V. Malyuskin, D. N. Goryushko, A. A. Shmat'ko, S. N. Shulga, Scattering of a wave beam by inhomogeneous anisotropic chiral layer.....566
- 07 V. Goblyk, Y. Yakovenko, Modeling of electromagnetic field from mobile phone distributed in the human head phantom..... 569
- 08 A.A. Cheremisin, Yu .V. Vassilyev, The mechanisms of gravitophotophoresis for aerosol aggregates in the free-molecular regime..... 570

## ANALYTICAL REGULARIZATION

- 01 A. V. Brovenko, P. N. Melezhik, A. Ye. Poyedinchuk, The plane H-polarized wave diffraction by a metal grating with a magnetoactive plasma..... 573
- 02 E. Ozkan, F. Dikmen, Yu. Tuchkin, S. Tarapov, Wave diffraction by axially symmetrical system of finite soft cylinders..... 576
- 03 S. B. Panin, A. Ye. Poyedinchuk, Diffraction by a screened chiral layer with a grating..... 579
- 04 A.V. Sulima, Resonant coupling of cavity-backed slots..... 582
- 05 T. Oguzer, A. Nosich, A. Altintas, Radiation characteristics of a 2D parabolic reflector antenna excited by the H-polarized complex source..... 586
- 06 E. K. Semenova, V. A. Doroshenko, Electromagnetic waves scattering on an unclosed cone with an isotropic one inside.....589
- 07 L. N. Il'yashenko, Electromagnetic backscattering from a triangular dielectric cylinder.....592
- 08 S. Rondineau, A. I. Nosich, M. Himdi, J.-P. Daniel, Simulation of a discrete Luneburg lens fed by a conformal printed antenna.....594

## PROPAGATION AND SIGNAL PROCESSING

- 01 Y.V. Kondratyev, O O. Drobakhin, The filter for horn antenna multifrequency data processing..... 599
- 02 I. Urazghildiiev, C. C. Logothetis, A. Rydberg, K. Wallin, On unique estimation of azimuth-elevation-carriers by volume arrays..... 602
- 03 O. Tveretina, H. Zantema, Comparing techniques for proving unsatisfiability..... 605
- 04 A. Bychkov, A. Bychkov, Modified method of geometric electromagnetics for the analysis of radio field in marine tropospheric waveguides..... 608
- 05 V. B. Ivanov, M. V. Tolstikov, Nonlinear stage of propagation of wave disturbances in the topside ionosphere..... 611
- 06 A. V. Oinats, V. I. Kurkin, S. N. Ponomarchuk, The technique for calculating of HF-signals characteristics taking into consideration ionosphere waveguide propagation..... 614
- 07 V. V. Khakhinov, Electrodynamics model of the receiving antenna in terms of a waveguide representation of the HF field..... 617
- 08 Y. Goncharenko, F. Kivva, Evaluation of the atmospheric aerosol particle size in the reflective layer produced by strong solar flares..... 620
- 09 A. V. Shvets, V. K. Ivanov, A. V. Varavin, On possibility of Schumann resonance observations within industrial areas..... 623

## BEAMS AND PLASMAS

- 01 N. N. Beletskii, S. A. Borysenko, Bistability of nonlinear surface polaritons in conducting antiferromagnets..... 629
- 02 Y. V. Bludov, Propagation of intra-subband plasmons in a weakly disordered array of quantum wires..... 632
- 03 V. I. Miroshnichenko, V. M. Ostroushko, Calculation of impedance of a sharp plasma boundary with a mixed-type electron scattering in anomalous skin-effect conditions..... 635
- 04 V. V. Ovsyanikov, A. N. Gordienko, Radiophysical characteristics of a radiator from the gas discharge plasma..... 638
- 05 A. N. Opanasenko, Radiation by self-oscillating relativistic charged particle moving along periodic structure..... 641

- 06 **A. F. Rusanov, V. M. Yakovenko**, Interaction of a non-relativistic electron beam with a semiconductor cylinder in an external magnetic field..... 644
- 07 **K. V. Ilyenko, V. A. Goryashko, T. Yu. Yatsenko, B. P. Yefimov**, An analytical method for construction of single particle electron trajectories in free electron lasers..... 647
- 08 **I. V. Yakovenko, V. M. Yakovenko**, Collisionless damping of surface plasma oscillations and possibilities of its revers at the interaction with charged particle flows..... 650
- 09 **Yu. O. Averkov, V. M. Yakovenko**, Peculiarities of nonlinear stabilization of the plasma-beam instability in semiconductor GaAs..... 653

## EIGENVALUE PROBLEMS

- 01 **I. S. Chikichev**, Eigenoscillations near cascade of thin disks between the pair of parallel planes..... 659
- 02 **Yu. F. Filipov, Yu. V. Prokopenko**, Influence of an elliptical non-uniformity of dielectric sphere on spectral characteristics of resonance oscillations..... 662
- 03 **V. V. Linnik, N. B. Pleshchinskii**, On perturbation of the spectrum of planar dielectric waveguide by refraction index profile..... 665
- 04 **A. I. Makarov**, Numerical investigation of eigenoscillations near a honeycomb in a circular channel..... 668
- 05 **I. B. Yumov**, Existence theorems for eigenoscillations in 3-D rectangular waveguides..... 671
- 06 **G. Georgiev, M. Georgieva-Grosse**, Some aspects of the slow waves in the circular waveguide with azimuthally magnetized ferrite rod..... 674
- 07 **V. Bondarev, L. Logacheva**, Dispersion characteristics of a waveguide with periodic impedance of walls..... 677
- 08 **L. P. Yatsuk, A. A. Komyachko, Yu. V. Zhironkin**, The problem of orthogonality of eigenwaves in a waveguide partially filled with a lossy dielectric..... 680
- 09 **E. R. Bartuli**, Rotor stator acoustic interaction, death and birth of resonance frequency..... 683
- 10 **V. I. Naidenko, H. A. Borsch**, Characteristics of spatially-developed square multimode resonators..... 686

**WIENER-HOPF  
AND  
FUNCTION-  
THEORETIC  
METHODS**



## PHASE RADIATION CHARACTERISTICS OF AN OPEN-ENDED CIRCULAR WAVEGUIDE

A.V. Shishkova<sup>1</sup>, S.N. Pivnenko<sup>2</sup>, O.S. Kim<sup>2</sup>, N.N. Gorobets<sup>1</sup>

<sup>1</sup> Kharkov National University, 4 Svobody sq., Kharkov, 61077, Ukraine

Phone: +380-572-434525, fax: +380-572-471816, e-mail: shann@online.kharkiv.com

<sup>2</sup> Technical University of Denmark, Oersteds Plads, 348, 2800 Kgs. Lyngby, Denmark

Phone: +45-4525-3860, fax: +45-4593-1634, e-mail: sp@oersted.dtu.dk

### ABSTRACT

Analytic expressions for phase radiation characteristics of a semi-infinite open-ended circular waveguide regardless of its aperture size and operating frequency have been obtained making use of the rigorous Weinstein's theory. The analysis of phase radiation patterns has been carried out for the dominant mode (TE<sub>11</sub>) as well as for the high order modes TM<sub>01</sub> and TE<sub>01</sub>, both for a single and multimode propagation. The measurement of radiation characteristics of an open-ended circular waveguide has been carried out at the DTU-ESA Spherical Near-Field Antenna Test Facility. It is shown that the theoretical results are in a good agreement with the experimental ones.

### ANALYTIC EXPRESSION FOR PHASE RADIATION PATTERN

For the first time, a rigorous solution of the electromagnetic diffraction problem for an open-ended circular waveguide (OE-CWG) by the Wiener-Hopf method was proposed by L. A. Weinstein [1]. He obtained analytic expressions and carried out a thorough analysis of amplitude radiation patterns for the case of single mode diffraction at an OE-CWG. When an open-ended waveguide is used as a feed in an antenna system, both the amplitude and phase radiation characteristics are needed thus allowing the polarization characteristics of the feed to be calculated. In this paper, the analytic expressions for the phase radiation characteristics of a semi-infinite OE-CWG are obtained regardless of its aperture size and operating frequency. According to the Weinstein's theory the explicit expression for the amplitude radiation pattern contains finite products proportional to the number of high order modes propagating in the waveguide of the given size. The phase radiation pattern, in general, contains an infinite sum, such as:

$$K = \lim_{M \rightarrow \infty} \frac{2w_0}{\pi} \left[ \ln \frac{2M\pi}{v_1 + \sqrt{v_1^2 - x^2}} - \frac{\pi}{w_0} \sum_{n=N_E+1}^M \arcsin \frac{w_0}{\sqrt{v_n^2 - v_0^2}} \right], \quad (1)$$

where  $v_n$  is a  $n$ -th root of the Bessel function of the first kind,  $v = \sqrt{k^2 - w^2}$  is a transverse wavenumber, and  $w$  is a longitudinal wavenumber.

In order to obtain an analytic expression for the phase radiation pattern, a method of summation of rational series using poly-gamma functions [2] has been employed. According to this method, there is an explicit expression for the following infinite series:

$$\sum_{n=\tilde{N}}^{\infty} \left( \frac{1}{n} - \frac{1}{n+1/4} \right) = \left( \Psi \left( \tilde{N} + \frac{1}{4} \right) - \Psi(\tilde{N}) \right), \quad (2)$$

where  $\Psi$  is the di-gamma function [2]. Employing asymptotic expressions for the roots of the Bessel function and expanding arccosine function in a series for a small value of argument, the infinite series in (1) can be reduced to the summation (2). The similar technique has been employed to obtain analytic expressions for the phase radiation pattern of an OE-CWG for both the symmetric and the non-symmetric excitation modes.

Investigation of the phase behavior on a whole radiation sphere has shown that the phase radiation patterns are not uniform for the symmetric excitation modes  $TM_{01}$  and  $TE_{01}$  as well as for the dominant mode  $TE_{11}$ . At the same time, it is well known that calculation of the phase radiation characteristics for a circular aperture under the Kirchhoff approximation without taking into account phenomena associated with mode transformation at the aperture and neglecting currents flowing on an exterior surface gives a fictitious phase center located in the center of the aperture [3]. Therefore, accounting for mode diffraction at the open end of a waveguide leads to the conclusion that a radiator in the form of OE-CWG has no phase center regardless of the excitation mode. However, when an OECWG is used as a feed in reflector or lens antennas, the phase error over the aperture associated with the non-uniform phase radiation pattern is quite small. Thus for the dominant mode excitation ( $TE_{11}$ ), the deviation of the phase pattern within the main lobe at  $-3$  dB does not exceed 2 degrees as compared to the direction of the main radiation maximum (See Fig. 1a). This remains valid for the whole operating frequency range of the single mode waveguide:  $1.84 < ka < 3.83$ , where  $k$  is a longitudinal wavenumber in the free space and  $a$  is the radius of the waveguide. For the

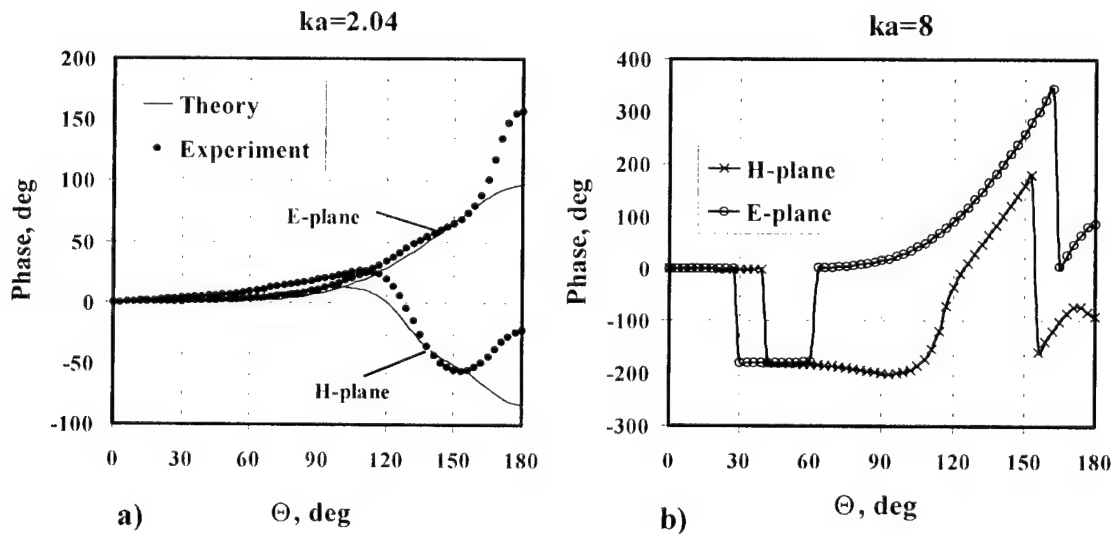


Fig.1. Phase radiation pattern of the single mode (a) and the multimode waveguide (b).

case of  $TE_{01}$  excitation ( $4.75 < ka < 6.5$ ), the deviation within the main lobe does not exceed 4 degrees, and for the  $TM_{01}$  case ( $3.0 < ka < 5.0$ ), it does not exceed 5 degrees. The maximum deviation of the phase radiation pattern within the main lobe is observed near cut-off frequencies: for  $TE_{01}$  mode with  $ka = 4.0$  it runs up to  $-21$  degrees and for  $TM_{01}$  mode with  $ka = 2.5$  it consists of 15 degrees. In the whole forward hemisphere the deviation of the phase radiation pattern can reach 30 degrees. The phase radiation pattern of an oversized waveguide can be considered almost uniform both within the main lobe and within first sidelobes (Fig. 1b).

### NEAR-FIELD PHASE RADIATION CHARACTERISTICS

The spherical wave expansion technique is used to analyze the general *near-field* radiation characteristics of an OE-CWG excited by the dominant mode  $TE_{11}$  as well as by the higher-order modes  $TE_{01}$  and  $TM_{01}$ . First, the coefficients of the spherical-wave expansion are obtained by matching the expansion with the far-fields. Then, the coefficients are used to calculate the near field.

An experimental verification of the calculated amplitude and phase radiation patterns has been made. The measurement of radiation characteristics of an open-ended circular waveguide has been carried out at the DTU-ESA Spherical Near-Field Antenna Test Facility. The measurement was performed at several frequencies for the dominant mode  $TE_{11}$  and for the  $TM_{01}$  mode as well. Two orthogonal complex components of the radiated field were accurately measured on a full sphere around the open-ended waveguide by a dual polarized probe. The measurement data were then transformed both to the far-field and to the near-field [4]. The theoretical amplitude and phase radiation characteristics of the waveguide were compared to the results obtained from the measurements (see Fig. 1a). It is seen that the theoretical results are in a good agreement with the experimental ones. Some differences yet observed can be explained by the difference between the simulated *semi-infinite* waveguide and the measured *finite* waveguide.

### CONCLUSION

The investigation of the phase radiation characteristics of an open-ended circular waveguide has shown that it has no phase center regardless of the excitation mode. Maximum deviation of the phase pattern from a constant is observed for the single mode propagation. In the multimode operation the phase radiation pattern is nearly uniform within the main lobe. In the near-field the phase radiation pattern is not uniform both for the single and multimode waveguides. As the distance to the aperture decreases, the deviation of the phase radiation pattern becomes more pronounced.

### REFERENCES

- [1] L.A. Weinstein. *The theory of diffraction and the factorization method*, The Boleyn Press, Boulder, Colorado, 1969.
- [2] M. Abramovits and I. A. Stegun. *Handbook of mathematical functions*, Appl. Mathem. series-55, 1964, pp. 84-90.
- [3] Yu.V. Shubarin. *Microwave antennas*, Izdat. Kharkov. Universiteta, 1960. (in Russian)
- [4] J.E. Hansen. *Spherical near-field antenna measurements*, London, Peter Peregrinus, 1988.

## FRECHET DIFFERENTIABILITY OF A FIELD OPERATOR FOR SCATTERING FROM AN OPEN SCREEN

Zinoviy T. Nazarchuk and Yaroslav P. Kulynych\*

Karpenko Physico-Mechanical Institute  
of National Academy of Sciences of Ukraine, Lviv, Ukraine  
E-mail: nazarch@ipm.lviv.ua; \*kulynych@ipm.lviv.ua

### ABSTRACT

The inverse problem, which we consider is to determine the shape of two-dimensional open screen from the knowledge of the field on a curve for the electromagnetic plane waves scattering.

Prof. R. Kress in his papers has proposed to reconstruct the scatterer's - shape from the knowledge of the far field pattern [1-2]. We extend this approach to the inverse problem of determining the shape of a two-dimensional open scatterer from the knowledge of the scattered field on a curve. In particular, we investigate the Frechet differentiability of a field operator for scattering from an open screen with the boundary as prerequisite for the theoretical foundation of the gradient methods or Newton type methods for the approximate solution of this nonlinear and improperly posed problem.

The aim of this paper is to provide a proof for Frechet differentiability with respect to the boundary of an operator, which maps the boundary of an open screen onto the scattered field and to obtain expression of this derivatives.

### STATEMENT OF THE PROBLEM

We consider the scattering of time-harmonic electromagnetic plane waves by a thin infinitely long cylindrical screen with a cross which is section described by an arc  $l \in R^2$  class  $C^3[a, b]$ , i.e.  $l = \{(x, f(x)) : x \in [a, b]\}$  where  $f(x)$  is an injective and three continuously differentiable function. The inverse problem consists in determination the shape of the screen from the knowledge of the field on curve  $S$ . Mathematically this problem can be interpreted as the solution with respect to  $l$  of a system operator equation

$$\begin{cases} \int_l j(s') H_0^{(1)}(kr) ds' = g(z), & z \in S, \\ \int_l j(s') H_0^{(1)}(kr) ds' = u(z), & z \in l. \end{cases} \quad (1)$$

Here,  $z = \{x, y\}$  - any point of  $R^2$ ,  $s'$  - arc abscissa of a point  $z' = \{x', y'\}$  of the contour  $l$ ,  $H_0^{(1)}(x)$  - Hankel function of zero order and of the first kind,  $g(z)$  - the given function on curve  $S$  and  $\bar{u}(s)$  - a value of the incident field at the points of curve  $l$ .

Let  $F$  the operator that maps a description  $f(x)$  of some admissible scatterer onto the corresponding scattered field  $g(z)$ ,  $z \in S$ . In terms of this operator the inverse problem consists in solution of the nonlinear and ill-posed equation for the function  $f$ ,

$$Ff = g \quad (2)$$

where  $g(z)$  is a (measured) scattered field.

In order to use Newton's method for the approximate solution of (2) it is necessary to establish the differentiability of operator  $F$  with respect to  $l$ .

## TECHNIQUE OF SOLUTION

To obtain characterizations of the derivatives we use a method, which is based on the classical theory of boundary integral operators [3]. From (1) we obtain

$$F = SK^{-1}R\bar{u}.$$

Here

$$K : C^{(0,\alpha)}(l) \Rightarrow C^{(1,\alpha)}(l), \quad K(\varphi; l) \equiv \int_l \varphi(s') \Phi(z, z') ds', \quad z \in l;$$

$$S : C^{(0,\alpha)}(l) \Rightarrow C^2(G), \quad S(\varphi; l) \equiv \int_l \varphi(s') \Phi(z, z') ds', \quad z \in G;$$

$$R : C^2(R^2) \Rightarrow C^2(l), \quad R(u; l) \equiv u|_l,$$

with  $\Phi(z, z') = \frac{H_0^{(1)}(kr)}{\sqrt{|s' - z_1||s' - z_{-1}|}}$ , where  $z_1$  and  $z_{-1}$  are extremities of the arc  $l$ ,  $G$  is any

domain of  $R^2$  for which  $\bar{G} \cap l = \emptyset$ .

The first step of the proof of a differentiability of the operator  $F$  consists in establishing that the mapping  $f \Rightarrow K$  is Frechet differentiable from  $C^3[a, b]$  into the space of bounded linear operators  $L(C^{0,\alpha}[a, b], C^{1,\alpha}[a, b])$  and that the derivative is given by  $h \Rightarrow K(\cdot; f, h)$ , where  $K(\cdot; f, h)$  denotes the integral operator

$$K'(\varphi; f, h)(x) = \int_a^b \frac{\varphi(\tau)}{\sqrt{(\tau - a)(\tau - b)}} [k_1(h; x, \tau) + k_2(h; x, \tau)] d\tau$$

with

$$k_1(h; x, \tau) = -kH_1^{(1)}(kr_f)J_f(\tau) \frac{f(x) - f(\tau)}{r_f} [h(x) - h(\tau)],$$

$$k_2(h; x, \tau) = H_0^{(1)}(kr_f) \frac{f'(\tau)}{J_f(\tau)} h'(\tau)$$

In the second step of the proof it is shown that mapping  $f \Rightarrow S$  is Frechet differentiable from  $C^3[a, b]$  into the space of bounded linear operators  $L(C^{0,\alpha}[a, b], C^2[G])$  and that the derivative is given by  $h \Rightarrow S'(\cdot; f, h)$ , where  $S(\cdot; f, h)$  denotes the integral operator

$$S'(\varphi; f, h)(x) = \int_a^b \frac{\varphi(\tau)}{\sqrt{(\tau - a)(\tau - b)}} [s_1(h; x, \tau) + s_2(h; x, \tau)] d\tau,$$

with

$$s_1(h; x, \tau) = -kH_1^{(1)}(kr)J_f(\tau) \frac{y-f(\tau)}{r} h(\tau), \quad s_2(h; x, \tau) = H_1^{(0)}(kr) \frac{f'(\tau)}{J_f(\tau)} h'(\tau).$$

It is easily to convinced, that  $f \Rightarrow R(\cdot; f)$  is Frechet differentiable one with the derivative  $R'(u; f, h) = u'_y(x, f(x))h(x)$ .

In the third step using the chain rule we finally obtain the Frechet differentiability of  $F$ . The derivative is given by

$$F'(f)h = S'(\phi_1; f, h) + S(K^{-1}(K'(\phi_1; f, h); f); f) + S(\phi_2; f)$$

where  $\phi_1 = K^{-1}(R(\bar{u}; f); f)$ ,  $\phi_2 = K^{-1}(R'(\bar{u}; f, h); f)$  For the actual numerical computation of the Frechet derivative of the operator  $F$  at first we determine  $\phi_1(x)$  by solving the integral equation

$$\int_a^b \frac{\phi_1(\tau)}{\sqrt{(\tau-a)(\tau-b)}} H_0^{(1)}(kr_f) J_f(\tau) d\tau = R(\bar{u}, f).$$

Further, we have to solve the integral equation

$$\int_a^b \frac{\phi_2(\tau)}{\sqrt{(\tau-a)(\tau-b)}} H_0^{(1)}(kr_f) J_f(\tau) d\tau = K'(\phi_1; f, h) + R'(u; f, h)$$

and at last we compute a sum

$$F'(f)h = S'(\phi_1; f, h) + S(\phi_2; f).$$

Hence, for numerical computation of the Frechet derivative it is necessary to solve two singular integral equations of the same type. The numerical methods for solving of such equations are known [4].

## REFERENCES

- [1]. Kress R. Freechet differentiability of the far field operator for scattering from a crack //J. Inv. Ill-Posed Problems. –1995. –№ 3. – P.305-313
- [2]. Kress, R. Inverse scattering form an open arc // Math. Meth. in the Appl. Sci.– 1995.– 18, № 2.–P.267–293.
- [3]. Potthast R. Freechet differentiability of boundary integral operators in inverse acoustic scattering // Inverse Problem. –1994. –10, № 4. – P.431-477.
- [4]. Panasyuk V.V., Savruk M.P. and Nazarchuk Z.T. Method of singular integral equations in two-dimensional diffraction problems.–Naukova Dumka Publ. House, Kiev, 1984 (in Russian).

# REFLECTION OF SURFACE WAVES AND THEIR COUPLING WITH WAVE BEAMS AT ANISOTROPICALLY PERTURBED IMPEDANCE PLANE

V. F. Borulko

Dept. of Radiophysics, Dnipropetrovsk National University, 13 Naukova St.,  
Dnipropetrovsk 49050 Ukraine  
Tel: 38 056 7254592, E-mail: borulko@hotmail.com

## ABSTRACT

Effects of coupling of waves at plane with spatially oscillating surface impedance (anisotropic and/or gyrotropic) are theoretically considered. A combination of the two processes is investigated. The first process is reflection of surface waves propagating along impedance surface. The second process is input-output coupling of falling paraxial wave electromagnetic beams (both TM and TE type) with both surface TM waves. This electromagnetics problem is important for consideration of devices combining functions of nonreciprocal antenna and microwave generator.

## INTRODUCTION

In open periodic waveguiding structures Bragg scattering can be observed in different forms [1]. Type of the wave transformation depends on from a value of perturbation period. If a perturbation wavenumber is twice as large as longitudinal wavenumber of surface wave, then coupling of two surface waves with opposite propagation directions occurs, that is reflection of surface waves is observed. If wavenumber of perturbation is equal to difference of longitudinal wavenumbers of surface and volume waves then a coupling of these waves secures, that is why we can obtain output of radiation from structure. Anisotropy of parameters causes coupling of waves with different polarization. If incident wave can excite surface wave reflected wave would be very differed from mirror one even if surface perturbation amplitude were small [2]. Open structures become more interesting when parameter perturbation is not periodic [3].

## METHOD OF ANALYSIS

In the paper physical effects of coupling of paraxial wave electromagnetic TM and TE beams falling on surface with spatially oscillating surface anisotropic impedance and two TM surface waves are theoretically considered. Moreover we suppose Bragg coupling (reflection) of surface waves. Asymptotic method [3] based on ideas of KBM method [4] is used. Perturbations are expressed as sum of sinusoidal components with small amplitudes smoothly varying along longitudinal coordinate. Amplitudes of incident TM and TE wave beams are smoothly varied across beam. The same small parameter  $\beta$  is used for all small values and as smoothness parameter [4]. For case  $\partial/\partial x \equiv 0$  all components of electromagnetic field are expressed in terms of  $x$  component of fields  $H_x$  and  $E_x$ . The potential functions  $H(y,z) \equiv H_x$  and  $E(y,z) \equiv E_x$  are determined by the solution of the following boundary-value problem:

$$\frac{\partial^2 H}{\partial z^2} + \frac{\partial^2 H}{\partial y^2} + k^2 H = 0, \quad \frac{\partial^2 E}{\partial z^2} + \frac{\partial^2 E}{\partial y^2} + k^2 E = 0, \quad (1)$$

$$\left( \frac{\partial H}{\partial y} + w_H H + w_{HE} \frac{\partial E}{\partial y} \right) \Big|_{y=0} = 0, \quad \left( E + w_E \frac{\partial E}{\partial y} - Z_{xx} H \right) \Big|_{y=0} = 0, \quad (2)$$

Impedance parameters  $w_H$ ,  $w_{HE}$  and  $w_E$  as functions of  $z$  are expressed through components of surface impedance tensor  $\mathbf{Z}$  in a form of sums of spatial harmonics

$$\begin{aligned} w_H &= i\omega \varepsilon Z_{xx} = w_{H,0} + \beta \sum_j w_{H,j}(\beta z) \exp(i\chi_j z) + \beta^2 \sum_{j,l} w_{H,j,l}(\beta z) \exp(i\chi_j z + i\chi_l z) \\ w_E &= iZ_{xz} / (\omega \mu) = w_{E,0} + \beta \sum_j w_{E,j}(\beta z) \exp(i\chi_j z), \\ w_{HE} &= \varepsilon Z_{zx} / \mu = \beta \sum_j w_{HE,j}(\beta z) \exp(i\chi_j z), \quad Z_{xx} = -\beta \sum_j w_{EH,j}(\beta z) \exp(i\chi_j z), \end{aligned}$$

where  $\chi_j$  is wavenumber of the  $j$ th spatial harmonics of the perturbation;  $w_{H,j}$ ,  $w_{E,j}$ ,  $w_{HE,j}$  and  $w_{EH,j}$  are amplitudes of these harmonics,  $w_{H,j,l}$  are amplitudes of the second order perturbation. Alongside with coordinate  $z$  we introduce a "smooth" variable  $\zeta = \beta z$  [4]. The Bragg coupling of surface waves and TM and TE beams occurs, when the wavenumber mismatches  $\eta_{V,s} = k_z + \chi_{pv(s)} - h_s$  ( $s = 1, 2$ ) become small. Here  $k_z$  is longitudinal wavenumber of the beams,  $h_s$  is longitudinal wavenumber of the surface wave, and  $pv(s)$  is integer-value function that coincide with the number of a spatial harmonic of the perturbation ensuring Bragg coupling. The Bragg reflection of a surface wave is observed if wavenumber mismatches  $\eta_{S,s,l} = -2h_s - \chi_l - \chi_{ps(s,l)}$  are close to zero. The solution of the boundary-value problem (1), (2) are searched as an asymptotic series on orders of small parameter  $\beta$  [3, 4].

$$\begin{aligned} H &= \sum_{s=1}^2 a_s \exp(-ih_s z - w y) + \beta a_H (\zeta + \beta y k_z / k_y) \exp(-ik_z z + ik_y y) + \Gamma_H \beta a_H (\zeta - \beta y k_z / k_y) \times \\ &\times \exp(-ik_z z + k_y y) + \beta u_1(a_1, a_2, k_z z, h_z, \chi z, \zeta, y) + \beta^2 u_2(a_1, a_2, k_z z, h_z, \chi z, \zeta, y) + \dots, \\ E &= \beta a_E (\zeta + \beta y k_z / k_y) \exp(-ik_z z + k_y y) + \Gamma_E \beta a_E (\zeta - \beta y k_z / k_y) \exp(-ik_z z - k_y y) + \\ &+ \beta v_1(a_1, a_2, k_z z, h_z, \chi z, \zeta, y) + \beta^2 v_2(a_1, a_2, k_z z, h_z, \chi z, \zeta, y) + \dots, \end{aligned} \quad (3)$$

where  $\Gamma_E$  and  $\Gamma_H$  are the reflection coefficients of plane waves from an undisturbed plane,  $k_y = \sqrt{k^2 - k_z^2}$ ,  $a_H$  and  $a_E$  are distributions of amplitudes of wave beams,  $u_n$  and  $v_n$  ( $n = 1, 2, \dots$ ) are  $2\pi$ -periodic versus  $k_z z$ ,  $h_s z$  and  $\chi_j z$  functions. First derivatives of complex amplitudes  $a_s$  are expressed in form of asymptotic expansions too [3, 4].

In a second approximation on small parameter value  $da_s/dz$  can be obtained as

$$\frac{da_s}{dz} = \beta^2 \left[ a_s A_{s,2} + \exp(-i\eta_{V,s} z) (a_H G_{s,2,V,H} + a_E G_{s,2,V,E}) + a_{3-s} \sum_l \exp(-i\eta_{S,s,l} z) G_{s,2,S,l} \right] \quad (4)$$

$$\text{where } A_{s,2} = -i w_{H,0} \left\{ \sum_j \left[ \frac{w_{HE,j} w_{EH,-j} i k_{-j}}{i k_{-j} w_{E,0} - 1} - \frac{w_{H,j} w_{H,-j}}{i k_{-j} - w_{H,0}} \right] - w_{H,0,0} \right\} / h_s,$$



$$G_{s,2,V,H} = 4w_{H,-pv(s)} k_y w_{H,0} / [(2h_s + \eta_{V,s})(ik_y - w_{H,0})], \quad G_{s,2,V,E} = 4w_{HE,-pv(s)} k_y w_{H,0} / \\ / [(2h_s + \eta_{V,s})(ik_y w_{E,0} - 1)], \quad G_{s,2,S,l} = -i2 w_{H,0} [w_{H,ps(s,l)} w_{H,l} / (ik_{3-s,l} - w_{H,0}) - \\ - ik_{3-s,l} w_{HE,ps(s,l)} w_{EH,l} / (ik_y w_{E,0} - 1)] / (2h_s + \eta_{S,s,l}),$$

Deciding the equation (4) we find variation of amplitude of the surface waves along longitudinal coordinate  $z$ . Then we can define the field, radiated from the surface.

## THE PHYSICAL EFFECTS

Total physical effect observed in the considered structure is result of combination of five phenomena – “unperturbed” specular reflections of volume TE and TM waves (they are characterized by parameters  $\Gamma_E$  and  $\Gamma_H$ ), transformation of these waves into two surface TM waves propagating in opposite directions along impedance surface (characterized by parameters  $G_{s,2,V,E}$  and  $G_{s,2,V,H}$ ), leaking and heat dissipation of energy of surface waves (characterized by parameters  $A_{s,2}$ ), mutual transformation (reflection) of surface waves (parameters  $G_{s,2,S,l}$ ). If rigorous exponentiality of perturbations and incident wave is disturbed physical pattern changes fundamentally – structure can be exited by a surface wave going from “a minus of infinity” or energy of falling volume waves can be transformed into energy to a surface wave going to “a plus of infinity”. Structures considered in the paper have high frequency and angular selectivity. They can be used as nonreciprocal reflector, transmitting or receiving antenna. Gyrotropy of impedance causes that antenna patterns for reception and transmission are essentially different. Combination of impedance gyrotropy and corrugation tilt allows using these structures as circulators concerning surface waves and TE wave beams.

## CONCLUSIONS

Asymptotic method based on method of Krylov, Bogoliubov and Mitropolsky have allowed us to consider phenomena of Bragg reflection and volume-surface coupling of surface waves and TM and TE waves in open anisotropic quasiperiodic waveguiding structure. Found solution is valid for small and not small values of mismatch; so we have no need to splice resonant and not resonant asymptotics. Obtained results will be useful for analysis of wave scattering by structures with small surface nonperiodically oscillating gyrotropic perturbations of parameters and for designing resonators, leaky-wave antennas or nonreciprocal devices with untraditional properties.

## REFERENCES

- [1] C. Elachi, "Waves in active and passive periodic structures: A review," *Proc. IEEE*, vol. 64, pp.1666-1698, Dec. 1976.
- [2] S. Tibuleac, R. Magnusson, T. A. Maldonado, P. P. Young, and T. R. Holzheimer, "Dielectric Frequency-Selective Structures Incorporating Waveguide Gratings," *IEEE Trans. On Microwave Theory and Techniques*, Vol. 48, No. 4, pp. 553-561, Apr. 2000.
- [3] V. F. Borulko, V. E. Ivanilov "Coupling of wave beam with surface wave at oscillated perturbation of surface impedance" in *Proc. of XXVIII Moscow International Conference "Antenna theory and techniques"*. - Moscow (Russia). - 1998. - P. 180-183.
- [4] N. N. Bogoliubov, Yu. A. Mitropolsky, *Asymptotic Methods in the Theory of Nonlinear Oscillations*. New York 1961.

## AXIAL SYMMETRIC WAVE DIFFRACTION BY A CIRCULAR WAVEGUIDE CAVITY

D. B. Kuryliak<sup>1)</sup>, K. Kobayashi<sup>2)</sup>, S. Koshikawa<sup>3)</sup>, and Z.T. Nazarchuk<sup>1)</sup>

<sup>1)</sup> Karpenko Physico-Mechanical Institute, National Academy of Sciences of Ukraine

5 Naukova St., 79601, Lviv, Ukraine

Tel: +380-322-637-038, Fax: +380-322-649-427, E-mail: kuryliak@ipm.lviv.ua;

nazarch@ipm.lviv.ua

<sup>2)</sup> Department of Electrical, Electronic, and Communication Engineering, Chuo University

1-13-27 Kasuga, Bunkyo-ku, Tokyo 112-8551, Japan

Tel: +81-3-3817-1869, Fax: +81-3-3817-1847, E-mail: kazuya@kazuya.elect.chuo-u.ac.jp

<sup>3)</sup> Laboratory, Antenna Giken Co., Ltd., 4-72 Miyagayato, Omiya 330-0011, Japan

Tel: +81-48-684-0712, Fax: +81-48-684-9960, E-mail: koshikawa@antenna-giken.co.jp

### INTRODUCTION

In this paper, we shall consider a three-dimensional (3-D) cavity formed by a finite circular waveguide with a planar termination at the open end, and analyze the axial symmetric diffraction problem by means of the Wiener-Hopf technique. The method of solution is similar to that we have developed for the analysis of parallel-plate waveguide cavities [1], but is more complicated because of the cylindrical geometry. The time factor is assumed to be  $e^{-i\omega t}$  and suppressed throughout this paper.

### WIENER-HOPF ANALYSIS OF THE PROBLEM

We consider a 3-D cavity formed by a finite circular waveguide with a planar termination, as shown in Fig. 1, where the cavity surface is perfectly conducting and of zero thickness. The cavity is assumed to be excited by a hypothetical generator with voltage of unit amplitude across an infinitesimally small gap at  $z=d(<L)$ . Thus the applied electric field becomes a uniform ring source given by  $e_z^i(\rho=b=0, z)=\delta(z-d)$ , where  $\delta(\cdot)$  is the Dirac delta function. Let the total field  $\phi^i(\rho, z)$  be

$$\phi^i(\rho, z) = \begin{cases} \phi^i(\rho, z) + \phi(\rho, z) & \text{for } 0 < \rho < b, \\ \phi(\rho, z) & \text{for } \rho > b, \end{cases} \quad (1)$$

where  $\phi^i(\rho, z)$  is the field excited in an infinitely long circular waveguide due to the ring source, and  $\phi(\rho, z)$  is the unknown scattered field satisfying the scalar Helmholtz equation. In the following analysis, we shall assume that the medium is slightly lossy. Applying the method established in our previous papers [1, 2], we derive the transformed wave equations as in

$$\hat{T}\Phi(\rho, \alpha) = 0 \text{ in } \rho > b \text{ for } |\tau| < k_2, \quad (2a)$$

$$\hat{T}\Psi_-(\rho, \alpha) = \alpha f(\rho) \text{ in } 0 < \rho < b \text{ for } \tau < k_2, \quad (2b)$$

$$\hat{T}[\Phi_1(\rho, \alpha) + e^{i\alpha L}\Psi_+(\rho, \alpha)] = -\alpha e^{-i\alpha L}g(\rho) \text{ in } 0 < \rho < b \text{ for } \tau > -k_2, \quad (2c)$$

where  $\hat{T} = d^2/d\rho^2 + \rho^{-1}d/d\rho - \gamma^2$ , and  $\gamma = (\alpha^2 - k^2)^{1/2}$  with  $\text{Re}\gamma > 0$ . In (2b,c),  $f(\rho)$  and  $g(\rho)$  are unknown inhomogeneous terms. The terms on the left-hand sides of (2a-c) are the Fourier transforms of the functions appearing in (1), and are defined by

$$\Phi(\rho, \alpha) = (2\pi)^{-1/2} \int_{-\infty}^{+\infty} \phi(\rho, z) e^{i\alpha z} dz \quad (3)$$

with  $\alpha = \text{Re}\alpha + i\text{Im}\alpha (\equiv \sigma + i\tau)$  and

$$\Phi(\rho, \alpha) = \Psi(\rho, \alpha) + \Phi_1(\rho, \alpha) - \Phi^i(\rho, \alpha), \quad (4)$$

$$\Psi(\rho, \alpha) = e^{-i\alpha L} \Psi_-(\rho, \alpha) + e^{+i\alpha L} \Psi_+(\rho, \alpha), \quad (5)$$

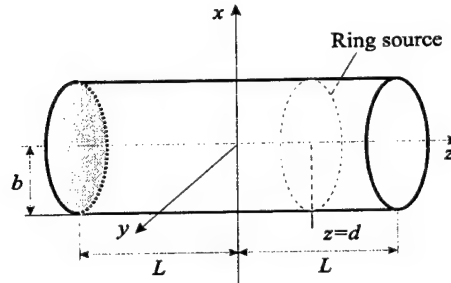


Fig. 1. Geometry of the problem.

where  $\Psi_-(\rho, \alpha) = \Phi_-(\rho, \alpha) + Q_-(\rho, \alpha)$ ,  $\Psi_+(\rho, \alpha) = \Phi_+(\rho, \alpha) + Q_+(\rho, \alpha)$ ,  $(6)$

$$\Phi_{\pm}(\rho, \alpha) = \pm \frac{1}{\sqrt{2\pi}} \int_{\pm L}^{\pm \infty} \phi(\rho, z) e^{i\alpha(z \mp L)} dz, \quad \Phi_1(\rho, \alpha) = \frac{1}{\sqrt{2\pi}} \int_{-L}^{+L} \phi'(\rho, z) e^{i\alpha z} dz. \quad (7)$$

Here  $\Phi^i(\rho, \alpha)$  and  $Q_{\pm}(\rho, \alpha)$  are known functions. In (4)-(7), the subscripts ' $\pm$ ' imply that the functions are regular in the half-planes  $\tau \gtrless \mp k_2$ , whereas the subscript '1' implies an entire function. In addition, the function  $\Phi(\rho, \alpha)$  defined by (3) is regular for  $|\tau| < k_2$ .

Solving (2a-c) for the unknown functions on the left-hand sides with the aid of the radiation condition and the boundary condition on the termination, we may derive a scattered field representation in the Fourier transform domain. Taking into account the boundary conditions at  $\rho = b$ , we derive the desired Wiener-Hopf equation. Applying the factorization and decomposition procedure, we finally obtain the exact solution with the result that

$$E_-(b, \alpha) + M_-(\alpha) \left[ J_E^{(1)}(\alpha) + \sum_{n=1}^{\infty} \frac{M_+(i\gamma_n) E_-(b, -i\gamma_n)}{i\gamma_n(\alpha - i\gamma_n)} \right] = M_-(\alpha) R_-(\alpha), \quad (8)$$

$$E_+(b, \alpha) - M_+(\alpha) \left[ J_E^{(2)}(\alpha) + \sum_{n=1}^{\infty} \frac{e^{-4\gamma_n L} M_+(i\gamma_n) E_+(b, i\gamma_n)}{i\gamma_n(\alpha + i\gamma_n)} \right] = M_+(\alpha) R_+(\alpha) \quad (9)$$

with

$$J_E^{(1,2)}(\alpha) = \frac{1}{2} \int_{\pm k}^{\pm i\infty \pm k} \frac{e^{\pm 2i\gamma L} M_{\pm}(\gamma) E_{\pm}(b, \gamma)}{\gamma^2 K_0(\gamma b) [K_0(\gamma b) - i\pi I_0(\gamma b)] \gamma - \alpha} d\gamma, \quad (10)$$

where  $R_{\pm}(\alpha)$  and  $M_{\pm}(\alpha)$  are known functions, and  $E_{\pm}(b, \alpha)$  are unknown functions denoting the Fourier transform of the  $z$ -component of the electric field at  $\rho = b$ . In (10),  $I_0(\cdot)$  and  $K_0(\cdot)$  are the modified Bessel functions of the first and second kinds, respectively. Equations (8) and (9) provide the exact solution of the Wiener-Hopf equation, but are formal since they contain the branch-cut integrals  $J_E^{(1,2)}(\alpha)$  with unknown integrands as well as infinite series with the unknown coefficients  $E_{\pm}(b, \pm i\gamma_n)$  for  $n=1, 2, 3, \dots$ . Applying the approximation procedure developed in [1, 2], we can derive an approximate solution convenient for numerical computation, but the details are omitted here.

## NUMERICAL RESULTS AND DISCUSSION

We shall now present numerical examples of the far field pattern for various physical parameters to discuss the scattering characteristics of the cavity. We have computed electric field components  $|e_z^*| = |e_z(\rho, z)R|$  and  $|e_\rho^*| = |e_\rho(\rho, z)R|$  as  $R \rightarrow \infty$ , where  $(R, \theta)$  is the cylindrical coordinates defined by  $z = R \cos \theta$ ,  $\rho = R \sin \theta$  for  $0 < \theta < \pi$ .

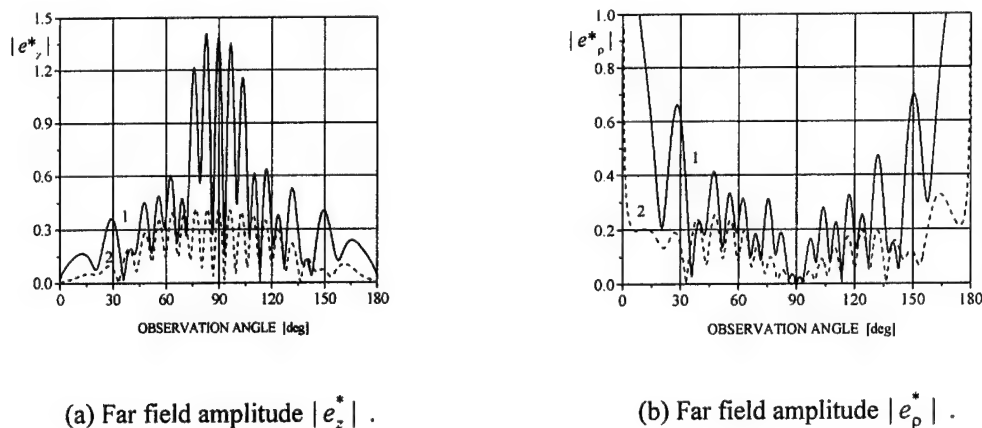


Fig. 2. Radiation pattern of electric field components  $e_z^*$  and  $e_\rho^*$  for  $d/L = 0$ .  
Line 1:  $2b = 10\lambda$ ,  $L/b = 1$ . Line 2:  $2b = 2\lambda$ ,  $L/b = 5$ .

Figure 2 shows the far field amplitude of  $e_z^*$  and  $e_\rho^*$  as a function of observation angle. It is seen from the figure that the radiated field oscillates rapidly with an increase of the cavity dimension. This sharp oscillation for larger cavities is due to the effect of the multiple diffraction between the aperture and the back corner. Next we evaluate the power of TM waves radiated from the cavity through the elementary surface  $dS = \sin \theta d\theta d\varphi$ . The radiated power  $P$  is found to be

$$P(\theta) \sim 0.5(\epsilon/\mu)^{1/2} |e_z(\rho, z)/\sin \theta|^2 R^2.$$

We investigate the power radiated from the cavities as a function of the observation angle and cavity parameters. We also show that, with an increase of the cross section of the cavity, dominant peaks of oscillations of the radiated power are formed in the region  $75^\circ < \theta < 105^\circ$ . The focusing effect of the radiated power in the direction  $\theta = 90^\circ$  is found for short cavities.

## ACKNOWLEDGMENTS

This work was supported in part by Chuo University as one of the 2000 Research Projects for Promotion of Advanced Research at Graduate School and by the Institute of Science and Engineering, Chuo University.

## REFERENCES

- [1] Kobayashi, K. and S. Koshikawa, "Wiener-Hopf analysis of the radar cross section of parallel-plate waveguide cavities," *Tech. Rep.*, no. KK96-3-8, Chuo Univ., Tokyo, March 1996.
- [2] Kuryliak, D. B., S. Koshikawa, K. Kobayashi, and Z. T. Nazarchuk, "Wiener-Hopf analysis of the axial symmetric wave diffraction problem for a circular waveguide cavity (*invited paper*)," *Proc. 2000 International Workshop on Direct and Inverse Wave Scattering* (September 25-29, 2000, Gebze, Turkey), pp. 2.67-2.81.

## ON THE METHOD OF SOLUTION OF THE WAVE EQUATION WITH PERIODIC COEFFICIENTS

E.A.Gevorkyan

Moscow State University of Economics, Statistics and Informatics

Contact address: Nezhinskaya str., 7, 119501, Moscow, Russia

Tel: (095)4427133, (095)4427066. Fax: (095)4427066.

E – mail: VBlagodatsikh@rector.mesi.ru

### ABSTRACT

The analytic method of solution of nonuniform wave equation of the problem of radiation of the magnetic moment, moving uniformly in the waveguide of arbitrary cross section with time – space periodic dielectric filling is given. The fields and the analytic expression for the Cerenkov energy losses of the magnetic moment in the region of strong (resonance) interaction between the radiation wave and the modulation wave are found.

Suppose that the source with magnetic moment  $\vec{m}(0,0,m_z)$  moves uniformly along the axis (oz – axis) of an ideal waveguide of arbitrary cross-section with nonmagnetic filling, whose permittivity is modulated in space and time according the periodic law

$$\varepsilon = \varepsilon_0 [1 + m \cos(k_0 z - ut)] \quad (1)$$

where  $m$  is the modulation index,  $k_0$  and  $u$  are the wave number and the phase velocity of the modulation wave,  $\varepsilon_0$  is the permittivity of the waveguide filling in the absence of modulation.

It can be shown that the longitudinal component of the magnetic vector  $H_z(x,y,z,t)$  as a potential of the transverse – electric (TE) field ( $E_z = 0, H_z \neq 0$ ) satisfies the following nonuniform partial differential equation

$$\Delta_{\perp} H_z + \frac{\partial^2 H_z}{\partial z^2} - \frac{1}{c^2} \frac{\partial}{\partial t} \left( \varepsilon \frac{\partial H_z}{\partial t} \right) = 4\pi \Delta_{\perp} m_z \quad , \quad (2)$$

where  $\Delta_{\perp} = \partial^2 / \partial x^2 + \partial^2 / \partial y^2$ ,  $c$  is the velocity of the light in vacuum.

In (2) let us pass to the variables

$$\xi = z - ut, \eta = \frac{z}{u} - \frac{u}{c^2} \int_0^{\xi} \frac{d\xi}{1 - \beta^2 \frac{\varepsilon}{\varepsilon_0}} \quad , \quad (3)$$

where  $b = 1 - \beta^2$ ,  $\beta = u / c \sqrt{\varepsilon_0}$ . After any algebraic transformations we receive

$$\Delta_{\perp} H_z + \frac{\partial}{\partial \xi} \left[ \left( 1 - \beta^2 \frac{\varepsilon}{\varepsilon_0} \right) \frac{\partial H_z}{\partial \xi} \right] - \frac{\varepsilon}{c^2 \left( 1 - \beta^2 \frac{\varepsilon}{\varepsilon_0} \right)} \frac{\partial^2 H_z}{\partial \eta^2} = -4\pi\varphi, \quad (4)$$

where

$$\varphi = -\Delta_{\perp} m_z, m_z = m_0 \frac{\delta(x-x_0)\delta(y-y_0)}{2\pi|u-v|} \int_{-\infty}^{\infty} e^{i\gamma(\eta-\eta_0)} d\gamma, \quad (5)$$

$$\eta_0 = \frac{v\xi}{u(v-u)} - \frac{1}{u} \int_0^{\xi} \frac{d\xi}{1 - \beta^2 \frac{\varepsilon}{\varepsilon_0}}, \quad (6)$$

$(x_0, y_0)$  is the point of intersection of trajectory of the magnetic moment with the cross section of the waveguide,  $m_0$  is the magnetic moment of the point source.

The equation (4) we can solve, suppose, that

$$H_z = \sum_{n=0}^{\infty} \psi_n(x, y) \int_{-\infty}^{\infty} e^{i\gamma\eta} H_n(\xi) d\gamma, \quad (7)$$

where  $\psi_n(x, y)$  are the eigenfunctions of the second boundary value problem for the transverse section of the waveguide, and expanding the right part of equation (4) on eigenfunctions  $\psi_n(x, y)$ . Thus from (4) we receive the ordinary differential equation of second order

$$\frac{d}{d\xi} \left[ \left( 1 - \beta^2 \frac{\varepsilon}{\varepsilon_0} \right) \frac{dH_n(\xi)}{d\xi} \right] + \frac{\chi_n^2}{1 - \beta^2 \frac{\varepsilon}{\varepsilon_0}} H_n(\xi) = -4\pi f_n(\xi), \quad (8)$$

where

$$f_n(\xi) = -\frac{m_0 \chi_n^2}{2\pi|u-v|} e^{i\gamma\eta_0} \psi_n(x_0, y_0), \quad (9)$$

$$\chi_n^2 = \frac{\gamma^2}{c^2} \varepsilon - \lambda_n^2 \left( 1 - \beta^2 \frac{\varepsilon}{\varepsilon_0} \right). \quad (10)$$

The equation (8) in the variable

$$S = \frac{k_0 b}{2\varepsilon_0} \int_0^\xi \frac{d\xi}{1 - \beta^2 \frac{\varepsilon}{\varepsilon_0}} \quad (11)$$

has a form

$$\frac{d^2 H_n(s)}{ds^2} + \frac{4\varepsilon_0^2 \chi_n^2}{k_0^2 b^2} H_n(s) = -4\pi \left( 1 - \beta^2 \frac{\varepsilon}{\varepsilon_0} \right) f_n(s), \quad (12)$$

where

$$f_n(s) = \frac{m_0 \lambda_n^2}{2\pi |u - v|} e^{-i \frac{2\gamma}{uk_0} \left( \frac{v}{v-u} - \frac{1}{b} \right) s} \psi_n(x_0, y_0). \quad (13)$$

The equation (12), as a Mathiew – Hill differential equation, we can solve, used the method, developed in our early articles [1–2]. Assuming a small modulation index  $m$ , after any transformations we receive the expression for  $H_z$  in variables  $z$  and  $t$  to the first approximation with respect to  $m$ . It gives the possibility to investigate the character of radiation in the region of strong interaction between the radiation wave and the modulation wave and find the Cerenkov energy losses of the magnetic moment in this case in the form

$$\left( \frac{dW}{dt} \right)_n = \frac{\pi m_0^2 \operatorname{sgn} \left( 1 - \frac{uv}{c^2} \varepsilon_0 \right) \left( 1 - \frac{v^2}{c^2} \varepsilon_0 \right) (1 - \beta^2)}{\varepsilon_0 (u - v) \left( 1 - \frac{uv}{c^2} \varepsilon_0 \right)} \psi_n^2(x_0, y_0). \quad (14)$$

Note that the result for the case of stationary but nonuniform filling of the waveguide we can receive from (4) passing there to the limit when  $u \rightarrow 0$ .

## REFERENCES

- [1] K.A.Barsukov, E.A.Gevorkyan. On the theory of propagation of electromagnetic waves in a waveguide filled with a nonstationary and nonhomogeneous dielectric material // Radiotekhnika i Elektronika.1983.- V. 28.-P. 237 – 241.
- [2] E.A. Gevorkyan. Transverse – magnetic electromagnetic waves in a waveguide with space – time multiperiodically modulated filling// Proceedings of International Conference on Mathematical Methods in Electromagnetic Theory. Kharkov, Ukraine, September 12 – 15.-2000.-P. 150 – 152.

## FRACTIONAL CYLINDRICAL FUNCTIONS IMPLEMENTATION FOR ELECTROMAGNETIC WAVES SCATTERING ANALYSIS

D.V. Golovin, D.O. Batrakov.

Kharkov National University, Ukraine  
Dmitry.O.Batrakov@univer.kharkov.ua

### ABSTRACT

An extension of a boundary integral method without using Green's function for solving electromagnetic boundary-value problems in layered media is presented. The generalization of the previous applications of that method to the case under consideration is achieved by using fractional cylindrical functions as the testing functions, which account for spatial inhomogeneity of the ambient medium. To illustrate advantages of such approach, numerical analyses are presented for 2D scattering problem involving penetrable cylinder of elliptical cross-section shape.

### INTRODUCTION

Employment of fractional cylindrical functions for analysis of electromagnetic wave scattering in the presence of bodies with coordinate surfaces was offered in [1,2]. But in our opinion, such functions can be used to solve many others problems of modern electromagnetic theory. Therefore, the attempt of expanding implementation area of such functions was undertaken. Two-dimensional scattering problem for homogeneous cylinders of arbitrary cross-section shape embedded in a plane layer is considered.

### PROBLEM STATEMENT AND BASIC EQUATIONS

Let suppose that as it shown in Fig.1 a permeable cylinder of arbitrary cross section  $S_p$  is situated in one layer of the three-layer structure. Introduce a coordinate system XYZ and suppose, that the impress sources  $f$  of monochromatic ( $\sim \exp(-i\omega t)$ ) wave and layers boundaries belongs to surrounding domain  $S_c$ . Cylinder formative is parallel to axis OX. The medium inside inclusion is described by material parameter  $\varepsilon_p(\vec{r})$  and

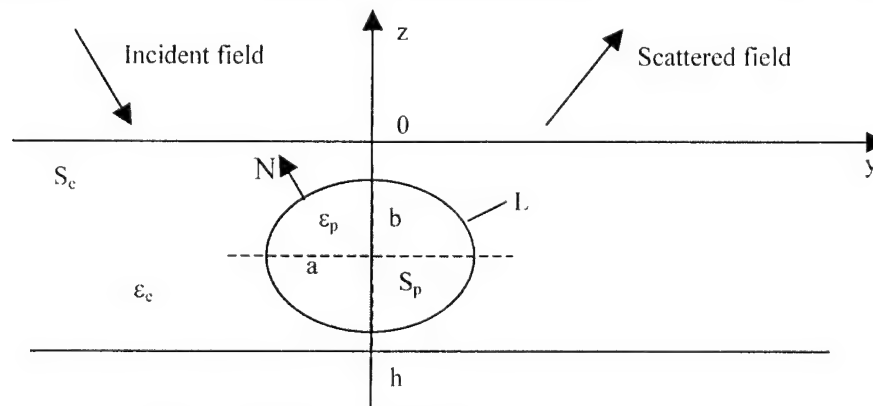


Fig. 1. Geometry of the problem.



wave number  $k_p(\vec{r})$ , and outside of inclusion -  $\varepsilon_e(\vec{r})$  and  $k(\vec{r})$  correspondingly.

Fields amplitudes outside and inside of inclusion satisfies to such equations:

$$\left[ \varepsilon(\vec{r}) \nabla_{\perp} \cdot \frac{1}{\varepsilon(\vec{r})} \nabla_{\perp} + k^2(\vec{r}) \right] \begin{Bmatrix} u_e(\vec{r}) \\ u_p(\vec{r}) \end{Bmatrix} = \begin{cases} \varepsilon(\vec{r}) \cdot f(\vec{r}), & (\vec{r} \in S_e) \\ 0, & (\vec{r} \in S_p) \end{cases} \quad (1)$$

(where  $\vec{r} = (0, x, y)$ ,  $\nabla_{\perp} = \left(0, \frac{\partial}{\partial y}, \frac{\partial}{\partial z}\right)$ ,  $f(\vec{r})$  - source density), and to boundary conditions:

$$u_e = u_p; \quad \frac{1}{\varepsilon} \frac{\partial u_e}{\partial N} = \frac{1}{\varepsilon_p} \frac{\partial u_p}{\partial N}; \quad (\vec{r} \in L). \quad (2)$$

They also satisfy continuity conditions for functions  $u_e$ ,  $1/\varepsilon$ ,  $\partial u_e / \partial N$ ,  $u_p$ ,  $1/\varepsilon$ ,  $\partial u_p / \partial N$  on structural boundaries in  $S_e, S_p$  and  $u_e$ , and satisfies radiation condition when  $r \rightarrow +\infty$ .  $\vec{N}$  - normal to  $L$  - contour of the scatterer, directed to  $S_e$ . In the case of excitation by vertically polarized wave ( $\vec{H} = \{H_x, 0, 0\}$ ,  $\vec{E} = \{0, E_y, E_z\}$ ), it is suitable to choose an x-components of magnetic field vectors as a functions  $u_e, u_p$ . As a result of manipulations described in [3], one can obtain following formulae for the scattered field:

$$u_{sc} = \int_L \frac{1}{\varepsilon(\vec{r}'_L)} \left[ G(\vec{r}, \vec{r}'_L) \frac{\partial u_e(\vec{r}'_L)}{\partial N'} - u_e(\vec{r}'_L) \frac{\partial G(\vec{r}, \vec{r}'_L)}{\partial N'} \right] dL'; \quad (\vec{r} \in S_e), \quad (4)$$

where  $G(\vec{r}, \vec{r}')$  - Green's function of a regular problem. We'll represent an unknown functions  $u_e$  and  $\partial u_e / \partial N$  as an expansions in terms of functions  $\xi_{\sigma}$  and  $\partial \xi_{\sigma} / \partial N$ :

$$u_e(\vec{r}) = \sum_{\sigma} \alpha_{\sigma} \xi_{\sigma}(\vec{r}); \quad \partial u_e(\vec{r}) / \partial N = \sum_{\sigma} \beta_{\sigma} \partial \xi_{\sigma}(\vec{r}) / \partial N. \quad (6)$$

Unlike previous papers, we'll choose the function  $\xi_{\sigma}(\vec{r})$  in a following way:

$$\xi_{\sigma}(\vec{r}) = \begin{cases} f_m(r) \cos(m\varphi) & \sigma = (m, e), m = 0, 1, 2, \dots \\ f_m(r) \sin(m\varphi) & \sigma = (m, o), m = 1, 2, \dots \end{cases}; \quad \varphi = \arg(\vec{r}), \quad (8)$$

where  $f_m(r) = J_{m+1}(r) / J_m(r)$ ,  $J_m(r)$  - Bessel functions of order  $m$ . We'll compute the wave functions using the fractional cylindrical ones, as it was shown in [3].

A possibility of fractional cylindrical functions application to the considered problem justified by presence of cylindrical inclusion with sufficiently smooth contour of cross-section. Unlike the results obtained in [2], the discussed problem is complicated by presence of dielectric layer and cylinder with sufficiently arbitrary cross-section.

## DESCRIPTION OF NUMERICAL ALGORITHM AND ANALYSIS OF OBTAINED RESULTS

In this section some numerical results based both on the analytical techniques developed in previous papers and a new algorithm for evaluating scattering diagrams by means of fractional cylindrical functions are presented. The goal of numerical experiments was to determine effectiveness of the proposed approach. Computations performed for dielectric elliptic cylinders, immersed in homogeneous dielectric layer. They show that for cylinders with transversal dimensions less than wavelength application of fractional

cylindrical functions does not give noticeable advantage. This fact can be easily explained, if one take into account, that the basic advantages of fractional functions related to their smooth behavior attached to large index and argument values [2]. Also it's necessary to mention, that the most effective this procedure became in a case of circular cylinder.

In Fig. 2 scattering diagrams, calculated by means of Bessel and fractional cylindrical functions are shown. Dielectric permeabilities of cylinder, layer, upper and lower half-spaces are equal to  $\varepsilon_p = 1.2$ ,  $\varepsilon_s = 3.0$ ,  $\varepsilon_e = 1.0$ ,  $\varepsilon_c = 2.0$  accordingly. Cylinder's radius is  $2.0 \cdot \lambda$ , layer's thickness -  $h = 6 \cdot \lambda$ , an inclusion embedding depth -  $Z_p = 3 \cdot \lambda$ . Incident wave length -  $\lambda = 1.5$  m. One can see, that when Bessel functions are used, scattering diagrams became steady only when  $M \geq 30$  ( $M$  maximum order of the scattering matrix). On the other hand, for fractional cylindrical functions analogous results can be obtained when  $M=20$ , and additional increasing of number of terms in decomposition does not leads to any changes.

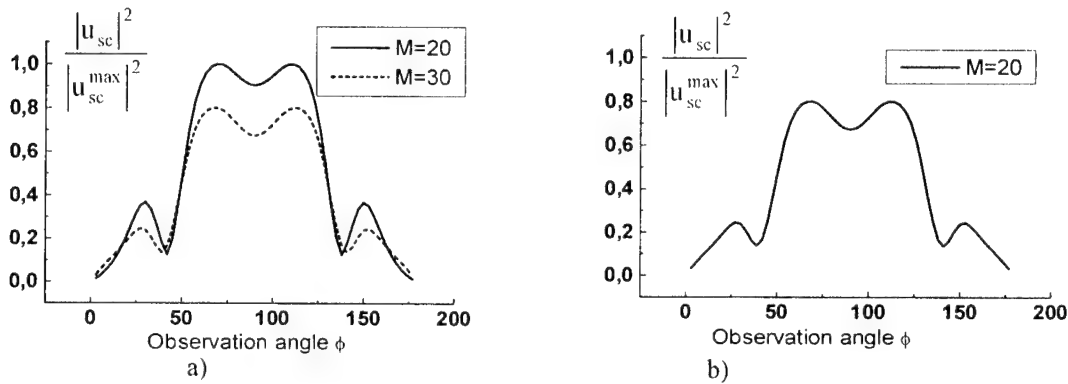


Fig.2. Scattered field diagram obtained for Bessel functions (a) and for fractional cylindrical functions (b).

## CONCLUSION

Obtained results show, that the fractional cylindrical functions within the framework of the null field method forms a successive base for solving a variety of scattering problems. Such problems in particular are essential elements in microwave and optical device design, nondestructive testing, remote sensing and thin film physics. The same technique can be applied to another diffraction problems (for example 3D problems) with only minor modifications.

## REFERENCES

- [1] Vorontsov A.A., Djachenko M.I., Mirovitskaya S.D. // Radiotekhnika i Elektronika (in Russian) 1985. V.30. № 8. P. 1483.
- [2] Vorontsov A.A., Mirovitskaya S.D // Radiotekhnika i Elektronika (in Russian) 1986. V.31. № 12. P. 2330.
- [3] Golovin D.V., Batrakov D.O. // Vestnik KNU. Radiophysika i Elektronika, 2002, № 514, P.83

## INTEGRO-DIFFERENTIAL POTENTIALS FOR THE ANALYSIS OF A FRACTAL COVER PROPERTIES

Vladimir M. Onufriyenko and Vladimir M. Lewykin \*

Zaporizhzhya National Technical University,  
Zhukovsky Str. 64, 69063, Zaporizhzhya, Ukraine  
E-mail: onufr@zstu.edu.ua

\*Zaporizhzhya National Technical University,  
Zhukovsky Str. 64, 69063, Zaporizhzhya, Ukraine  
E-mail: lewykin@yahoo.com

### ABSTRACT

We have considered stationary electric and magnetic fields of fractal objects with the help of differintegration methods. The equations of fractal electrostatic and magnetostatic potential at integro-differential form are proved and introduced. The offered ideas can be useful for modification numeric fields modelling techniques to solve electromagnetic problems for real objects with material structure irregularities consideration.

### INTRODUCTION

There are a number of modern numeric electromagnetic fields modelling techniques. Finite-Difference Time-Domain (FDTD), Method of Moments (MoM), and Finite Element Method (FEM) are the most popular and useful methods. The general essence of these methods consists in division of the approached ideal model of real physical object into elementary components the fields for which can be found on the basis of the classic Maxwell's theory. But the classic electromagnetic theory in which the object's geometry definition is based on concepts of point, line and plane (ideal objects) become impenetrable when the explanation of the field distribution of roughness fractal surfaces is needed. The examples of differintegration methods application for such complex electromagnetic problems were originally shown at [1].

### MAIN PART

Based on idea, that the fractal sets are adequate geometrical model for irregular contours and surfaces. Let us consider prefractal covering compact set, which is our proposed model of a contour with a current, as a limit of monotonously growing sequence of covering compact sets with the corresponding sequence of rising contours  $l \subset l_1 \subset \dots \subset l_i \subset \dots \subset l_n$ . The current near by  $l_n$  contour can be found as:

$$I(x) = \frac{1}{A(l, n)} \int_a^x dl_{n-1} \int_a^{l_{n-1}} dl_{n-2} \dots \int_a^{l_1} \rho(x') dx'.$$

The obtained repeated integral may be summarize by Riemann's-Liouville's definition of fractional integral

$$({}_a D_x^\alpha \rho)(x) = \frac{1}{\Gamma(\alpha)} \int_a^x \frac{\rho(x')}{(x - x')^{1-\alpha}} dx'. \quad (1)$$

As a result of usage fractal contour (surface) covering by compact sets, we have reduced a problem to construction a smoothing Hausdorf's measure on a physically prefractal layer with differintegration of an uniform electric charge density on a fractal point set projection to a smooth-faced segment [2].

Using of  $\alpha$ -order differintegral definition of fractal electric charge density  $\rho^\alpha(\mathbf{r}')$  located at  $\mathbf{r}'$  Eq. (1) enables to formulate the equations of classical electrostatics in terms of  $\alpha$ -characteristics. In analogy with the fractal electrostatic case, we may define fractal electric current density  $\mathbf{j}^\alpha(\mathbf{r})$  for magnetostatic field analysis. So the laws of electrostatics and magnetostatics for fractal objects can be summarized in two pairs of time-independent, uncoupled vector differintegral equations, namely the equations of fractal electrostatics

$$\nabla \cdot \mathbf{E}^\alpha(\mathbf{r}) = \frac{\rho^\alpha(\mathbf{r})}{\varepsilon_0}, \quad (2)$$

$$\nabla \times \mathbf{E}^\alpha(\mathbf{r}) = 0,$$

and the equations of fractal magnetostatics

$$\nabla \times \mathbf{H}^\alpha(\mathbf{r}) = \mu_0 \mathbf{j}^\alpha(\mathbf{r}), \quad (3)$$

$$\nabla \times \mathbf{H}^\alpha(\mathbf{r}) = 0.$$

The electrostatic field  $\mathbf{E}^\alpha(\mathbf{r})$  is irrotational and it may be expressed in terms of the gradient of a scalar field. If we denote this scalar field by  $-\phi^\alpha(\mathbf{r})$ , we get  $\mathbf{E}^\alpha(\mathbf{r}) = -\nabla \phi^\alpha(\mathbf{r})$ . Taking the divergence of this and using Eq. (2), we obtain Poisson's equation

$$\nabla^2 \phi^\alpha(\mathbf{r}) = -\nabla \cdot \mathbf{E}^\alpha(\mathbf{r}) = -\frac{\rho^\alpha(\mathbf{r})}{\varepsilon_0}. \quad (4)$$

The solution of Eq. (4)

$$\phi^\alpha(\mathbf{r}) = \frac{1}{4\pi\varepsilon_0} \int_V \frac{\rho^\alpha(\mathbf{r}')}{|\mathbf{r} - \mathbf{r}'|} dv' + c, \quad (5)$$

where the integration is taken over all source points  $\mathbf{r}'$  at which the charge density  $\rho^\alpha(\mathbf{r}')$  is non-zero and  $c$  is an arbitrary quantity which has a vanishing gradient. The scalar function  $\phi^\alpha(\mathbf{r})$  in Eq. (5) above is called the fractal electrostatic scalar potential. Consider the equations of magnetostatics Eq. (3) we got fractal magnetostatic vector potential with definition from  $\mathbf{B}^\alpha(\mathbf{r}) = \nabla \times \mathbf{A}^\alpha(\mathbf{r})$  as

$$\mathbf{A}^\alpha(\mathbf{r}) = \frac{\mu_0}{4\pi} \int_V \frac{\mathbf{j}^\alpha(\mathbf{r}')}{|\mathbf{r} - \mathbf{r}'|} dv' + \mathbf{a}(\mathbf{r}), \quad (6)$$

where  $\mathbf{a}(\mathbf{r})$  is an arbitrary vector field whose curl vanishes.

## CALCULUS EXAMPLES

As an example of using obtained expressions (Eq. 4-6) at FEM methods applications let us consider following problem

$$\nabla^2 \phi = -1 \text{ inside } B, \quad D^\alpha \phi|_A = C, \quad \phi|_B = 0, \quad (7)$$

where  $A$  border is a circle defined as  $\{x \cdot \cos(t); y \cdot \sin(t); 0 \leq t \leq 2\pi\}$  and  $B$  circle is infinity approximation defined as  $\{x \cdot 5 \cos(t); y \cdot 5 \sin(t); 0 \leq t \leq 2\pi\}$ .

Fractal boundary condition  $D^\alpha \phi|_A = C$  translates into  $\phi^{(\alpha)}|_A = C/(x-b)^{1-\alpha}$ ,  $1 \leq \alpha \leq 2$ .

The problem (7) was solved for  $b = -5$ ,  $C = 1$  parameters by finite element method with the help of FreeFEM+ software. The obtained potential surface for  $\alpha = 1.7$  is shown in Fig. 1. We demonstrate the  $XOZ$ -plane cut of potential distribution for  $\alpha$ -parameter varied from 1 up to 2 in Fig. 2.

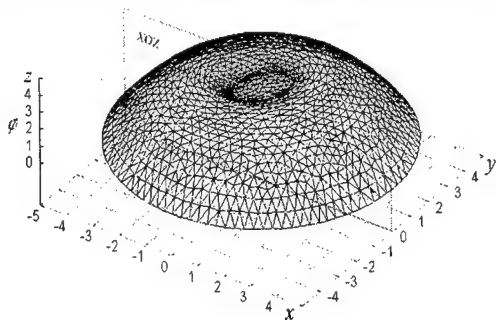


Fig. 1. 3D potential distribution for  $\alpha = 1.7$

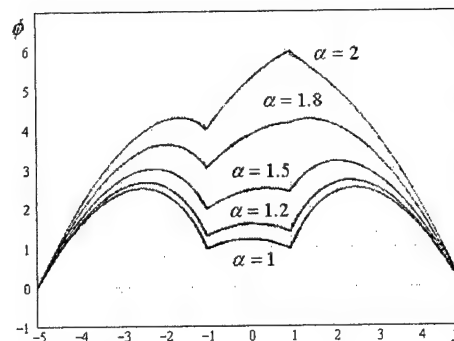


Fig. 2. Potential distribution for various  $\alpha$ -parameter

The problem (7) with  $\alpha = 1$  and  $\alpha = 2$  parameters of fractal boundary condition is equivalent of Dirichlet.

More interesting that at  $\alpha = 1.5$  calculation result is equal to solving of mixed problem with Dirichlet and Neumann boundary conditions like  $(\partial\phi/\partial\mathbf{n})|_A + \phi|_A = x$ .

## CONCLUSIONS

The application of fractional calculus enables to formulate the electromagnetic potential equations in terms of  $\alpha$ -characteristics. Formally proposed equations agree with the classical, at imposing on  $\alpha$ -characteristics additional boundary conditions.

Numeric decision of typical problem of potential theory has shown that definition of boundary conditions in the integro-differential form generalizes classical boundary conditions and is adequate for fractal surfaces with various levels of roughness. The offered ideas assumes to remove difficulties in investigations of singular distributions and can be useful for modification numeric fields modeling techniques to solve electromagnetic problems for real objects with structure irregularities consideration.

## REFERENCES

- [1] N. Engheta, On the Role of Fractional Calculus in Electromagnetic Theory// IEEE Antennas & Propagation Magazine, 1997, Vol.39, No. 4, pp.35-46.
- [2] V. Onufrienko, Telecommunications and Radio Engineering, 1999, Vol. 53, No. 4-5, pp.136-139.

## INTEGRO-DIFFERENTIAL CHARGES AND CURRENTS DISTRIBUTION ON THE FRACTAL MEDIUM TOPOLOGY

Vladymir M. Onufriyenko

Zaporizhzhya National Technical University,  
Zhukovsky Str. 64, Zaporizhzhya, 69063, Ukraine  
E-mail: onufr@zstu.edu.ua

### ABSTRACT

We will consider the geometric and physical aspects that permit introduction of the so-called  $\alpha$ -characteristics for studying the behavior of electromagnetic field components in the vicinity of a set of points with fractal properties. To estimate the  $\alpha$ -characteristics, possible algorithms are formulated, namely a geometric one involving evaluation of the Hausdorff measure and an analytical algorithm permitting the Hausdorff measure to be evaluated through application of fractional derivatives and integrals.

### INTRODUCTION

A great majority of real physical systems are of fractal nature in the respective range of scale sizes, characterized by the values of one or more respective fractal dimensions. Studies of a number of physical phenomena (such as small-angle scattering of X-rays, anomalies in the power-law dependences upon frequency of the electrical resistance or electrical energy dissipation [1], energy radiation and interaction of electromagnetic waves with impedance surfaces [2, 3], etc) have revealed the close relation of their performance to fractal properties of the boundaries and media involved. The possibility of the fractional calculus application to electrostatics was demonstrated in paper [4].

### FORMULATION

The well known technique of approximating to non-coordinate boundaries through covering the surface with simple compacts (like rectangles, circles, or ellipses) [5] permits application of numerical algorithms for solving boundary-value problems of electrodynamics.

Let us extend the technique of covering the boundaries and domains of existence of the electromagnetic field to the case of a smooth contour possessing fractally distributed geometric points over its certain section (physically, a highly jagged (rough) portion of the contour). To that end, we will consider a model of the contour section showing the properties of local uniformity and local self-similarity. Let fractal portion of the contour be approximated to with a segmented line with the links  $\Delta x_{i(k)}$  of constant length and the ends lying on the contour ( $k$ -number of covering generation). To represent the fractal contour approximately with points of the segmented line, let us cover it with a segmented line with links of a smaller length,  $\Delta x_{i(k+1)} < \Delta x_{i(k)}$ . Apart from higher order small values, the number  $N_{\Delta x_{i(k+1)}, \Delta x_{i(k)}}$  of the vertices of the segmented line with the link

length  $\Delta x_{i(k+1)}$  lying within one link of the segmented line with the link length  $\Delta x_{i(k)}$  will be equal to  $N_{\Delta x_{i(k+1)}\Delta x_{i(k)}} = f(\Delta x_{i(k)}/\Delta x_{i(k+1)})$ . For a covering line with  $\Delta x_{i(k+2)} < \Delta x_{i(k+1)}$ , we obtain similarly  $N_{\Delta x_{i(k+2)}\Delta x_{i(k+1)}} = f(\Delta x_{i(k+1)}/\Delta x_{i(k+2)})$ . On the other hand,  $N_{\Delta x_{i(k+1)}\Delta x_{i(k)}} \times N_{\Delta x_{i(k+2)}\Delta x_{i(k+1)}} = N_{\Delta x_{i(k+2)}\Delta x_{i(k)}}$ . Introducing the notation  $u = \Delta x_{i(k)}/\Delta x_{i(k+1)}$  and  $v = \Delta x_{i(k)}/\Delta x_{i(k+2)}$  we arrive at a functional equation  $f(x)f(y/x) = f(y)$  whose smooth solution is unique in the form of a power law,  $f(x) = x^\alpha$ . In this connection we are able to use the generalized measure of the manifold magnitude involving choice of a trial power function  $h(r) = \gamma(\alpha) \times r^\alpha$ , and covering of the multitude of points under study with elements  $B_i$  of length  $r_i$ , with formation of the Hausdorff  $\alpha$ -measure  $H^\alpha(E) = \lim_{\varepsilon \rightarrow 0} H_\varepsilon^\alpha(E) = \inf \{ \gamma(\alpha) \sum_i r_i^\alpha : E \subset \bigcup B_i, r_i < \varepsilon \}$ . That can serve as a measure of the extent and curvature of the continuous limiting line.

## RESULTS

The charge (current) density  $j_{\Delta x_{i(k+m)}}$  of  $(k+m)$  generation is determined as

$$j_{\Delta x_{i(k+m)}} = j_{\Delta x_{i(k)}} N_{\Delta x_{i(k+m)}\Delta x_{i(k)}}; j_{\Delta x_{i(k+m)}} \frac{\Delta x_{i(k+m)}}{(\Delta x_{i(k+m)})^{1-\alpha}} = j_{\Delta x_{i(k)}} \frac{\Delta x_{i(k)}}{(\Delta x_{i(k)})^{1-\alpha}}.$$

The charge (current) in fractal set is determined now by the Riemann - Liouville fractional integral  $J(x) = ({}_a I_x^\alpha j)(x)$ .

Differintegral  $D^\alpha j$  determines some the differintegral forms of a degree  $\alpha$  on  $\Omega$  with value in  $\bar{J}$  (imaging  $\Omega$  in  $L^\alpha(\Omega \subset \bar{E}, \bar{F})$ ):  $\bar{\omega}^\alpha(x) \cdot (\bar{X}) = (D^\alpha j)(x) \cdot \bar{X}$ .

Theorem. If  $\varphi_1, \varphi_2, \dots, \varphi_p$  - scalar differentiated functions on  $\Omega$ , the fractional differintegral forms  $d^\alpha \varphi_1 \wedge d^\alpha \varphi_2 \wedge \dots \wedge d^\alpha \varphi_p$  concerning some coordinate system in  $E$  can be represented as

$$d^\alpha \varphi_1 \wedge d^\alpha \varphi_2 \wedge \dots \wedge d^\alpha \varphi_p = \sum_{1 \leq i_1 < \dots < i_p \leq N} \frac{D^\alpha(\varphi_1, \dots, \varphi_p)}{D^\alpha(x_{i_1}, \dots, x_{i_p})} dx_{i_1} \wedge dx_{i_2} \wedge \dots \wedge dx_{i_p}.$$

If  $j^\alpha(x)$  - function in a coordinate neighbourhood  $(U, x)$  on  $E$ , the  $\alpha$  - forms  $\omega^\alpha$  in this neighbourhood is noted as  $j^\alpha(x) dx_1 \wedge \dots \wedge dx_m$ .

If the support of  $j^\alpha(x)$  belongs to  $U$ , on definition:  $\int_E j^\alpha = \int_{x(U)} j^\alpha(x) dx_1 \wedge \dots \wedge dx_m$ .

The  $\alpha$  - volume forms  $d^\alpha V = d^\alpha x_1 \wedge \dots \wedge d^\alpha x_m$  on a  $m$ -dimensional Riemannian manifold  $E$  induces a borel measure, which coincides with the Hausdorff-measure  $H^\alpha(U) = \int_U d^\alpha V$  for any open set  $U \subset E$ . Hence, for any integrable  $\alpha$  - forms  $j^\alpha$  on

E equality  $\int_E j^\alpha = \int_E \langle j^\alpha, \tau_E \rangle dH^\alpha$ , where  $\tau_E$  - vector, defining tangential plane is valid.

We have installed the formula of connection between integrals of the second type (from the  $\alpha$  - forms) and integrals of the first type (in respect of Hausdorff-measure).

The further development of the theory is carried out on the basis of interpretation of Dirac delta-function, which is determined as the  $\alpha$  - forms.

Electromagnetic field in fractal medium follows Maxwell (Abel) equations in the terms of  $\alpha$  - forms and  $\alpha$ -characteristics:

$$d^\alpha \vec{E}^{(\alpha)} = -\frac{\partial}{\partial t} \vec{B}^{(\alpha)} - \vec{j}_m^{(\alpha)}, \quad d^\alpha \vec{H}^{(\alpha)} = \frac{\partial}{\partial t} \vec{D}^{(\alpha)} + \vec{j}_e^{(\alpha)}, \quad d^\alpha \vec{D}^{(\alpha)} = \rho_e^{(\alpha)}, \quad d^\alpha \vec{B}^{(\alpha)} = \rho_m^{(\alpha)}.$$

We obtain fractional Green's function for the Helmholtz equation in the terms of the  $\alpha$  - characteristics with the relevant fractal boundary conditions [6-8].

## CONCLUSION

Generalizing the schemes outlined to include  $\alpha$ -differintegral forms Dirac delta-function will promote construction and further analysis of such mathematical models that would permit an adequate description of actual electromagnetic processes at fractal boundaries or in fractal media themselves (e.g., in the problems concerning «artificial» dielectrics, complex media and metamaterials, or power emission by «thick» contours and surfaces, etc).

## REFERENCES

- [1] L. Pietronero and E. Tosotti (Eds.). Fractals in physics: Proceedings of the VI International Symposium (Trieste, Italy, 9-12 July, 1985).
- [2] E. Veliev, V. Onufriyenko. Fractal Electrical and Magnetic Radiators // Symposium Proceedings, MSMW-98.-Kharkov, Ukraine (September 15-17, 1998).-1998. V.1, pp.357-359.
- [3] V.M.Onufriyenko. Physical and Geometric Interpretation of Electromagnetic Field's  $\alpha$ -Characteristics // Telecommunications and Radio Engineering, Vol. 53(4-5), 1999, pp. 136-139.
- [4] N. Engheta. On the Role of Fractional Calculus in Electromagnetic Theory // IEEE Antennas & Propagation Magazine. Vol. 39, No4, 1997, pp.35-46.
- [5] V.M.Onufriyenko, I.G.Prohoda, V.P.Chumachenko. Numerical solution of the problem on a waveguide transformer with a coupling cavity of complex geometry // Izv. vuzov.Radiofizika.-1975.-V.18, №4. PP.584-587.
- [6] V.M.Onufrienko. Absorption of the Plane Electromagnetic Wave Energy by a Fractal Conducting Surface // Telecommunications and Radio Engineering, Vol. 55(6-7), 2001, pp. 98-103.
- [7] V.M.Onufrienko, P.A.Samolchev, and T.I.Slyusarova. Estimating the Attenuation Factor in Guiding Structures with Fractal Properties of the Boundaries // Telecommunications and Radio Engineering, Vol. 55(6-7), 2001, pp. 91-97.
- [8] V.M.Onufrienko. The Differintegral Model for Describing Fractal Coupling Between Waveguide Surfaces//Telecommunications and Radio Engineering, Vol. 57(1), 2002, pp. 30-36.



**GRATINGS  
AND  
FREQUENCY-  
SELECTIVE  
SURFACES**

## MATHEMATICAL SIMULATION OF IMPEDANCE DIFFRACTION GRATINGS

Galina A. Kalinchenko<sup>1</sup>, Alexander M. Lerer<sup>1</sup>, Alexey A. Yachmenov<sup>2</sup>

<sup>1</sup>The Rostov state university  
Rostov-on-Don, Russia  
phone: (8632) 331-320, e-mail: lerer@ip.rsu.ru

<sup>2</sup>The Rostov state university of transport communications  
Rostov-on-Don, Russia - 344038  
phone: (8632) 726-439, e-mail: kaf\_svyaz@rgups.ru

### ABSTRACT

In this paper the eigenwaves of periodic impedance diffraction grating (DG), reflection and transmittance on finite DG are under investigation. The approximate boundary conditions (ABC) were used for simulations. The refined expression for impedance dielectric strips is obtained. Singular part of approximate integral equations (IE) is extracted and analytically transformed. As the result the IE of second type with smooth kernel has been carried out and solved with collocation method (CM) and Galerkin method (GM).

### INTRODUCTION

The application of impedance boundary conditions (IBC) greatly simplifies the solution of boundary problem for structure consisted of fine dielectric layers. It became a reason of huge amount of work appearance dedicated as to IBC obtaining, as to their application for concrete electrodynamics problems solution. For example, the problem of wave reflection from dielectric grating was solved in paper [1] with IBC method. The main disadvantage of IBC for dielectric structure is narrow frameworks of application. In theory these conditions are correct if a layer thickness is rather smaller than a wavelength. In practice these conditions give satisfactory accuracy if a layer thickness is smaller than a wavelength. IBC application area may be enlarged, for example, due to modernization described in [2]. In present paper we elaborate one more type of IBC. The IE described here are obtained by means of approximate solution of a rigorous IE [3]. Our IE become more simple in the case of  $\vec{E}(0,0,E)$  wave diffraction on two-dimensional structure (Fig. 1)

$$E(x,y) = E^e(x,y) + k^2 \int_S \tau(x',y') E(x',y') g(x,x',y,y') ds', x,y \in S \quad (1)$$

where  $E^e(x,0)$  is the external field,  $\tau = \varepsilon - \varepsilon_e$ ,  $k$  - wave number,  $\varepsilon, \varepsilon_e$  - dielectric permittivity of local inhomogeneity and surrounding environment,  $S$  - cross-section of the local inhomogeneity,  $g(x,x',y,y')$  - Green function (GF), in our case the GF is one f planar DW. The GF for planar DW consisted of an arbitrary number of layers is obtained. Half-analytical solution for this IE is already described in [4]. Let's consider the solution (1) for a single inhomogeneity. Process to large quantity of inhomogeneities is evident. Let's find an approximate IE solution for rectangular inhomogeneity.

Considering  $E(x', y') \approx E(x') \exp(-ik\sqrt{\varepsilon} y')$ , where  $E(x')$  is unknown function, we have

$$\int_{-a}^a E(x', y') g(x, x', y, y') dy' \approx g(x, x', y, y) \int_{-a}^a E(x', y') dy' \approx g(x, x', y, y) 2 \frac{\sin(k\sqrt{\varepsilon} a)}{k\sqrt{\varepsilon}}$$

And as the result we arrive at following one-dimensional IE.

$$\int_{-l}^l E(x') G(x, x') dx' - E(x) / k^2 \delta = -E^v(x, 0) / k^2 \delta,$$

where  $G(x, x') = g(x, x', 0, 0)$ .

$$\delta = 2 \frac{\sin(k\sqrt{\varepsilon} a)}{k\sqrt{\varepsilon}} \tau. \quad (2)$$

At  $k\sqrt{\varepsilon} a \ll 1$  the expression for  $\delta$  is well-known

$$\delta = 2a(\varepsilon - \varepsilon_c). \quad (3)$$

It gives us an ability to write the IE as follow

$$\int_{-l}^l J(x') G(x, x') dx' - J(x) / k^2 \delta = -E^v(x, 0), \quad (4)$$

where  $J(x) = k^2 \delta E(x)$ . We would obtain the same IE if use approximate IBC from [4] with supposition  $J(x) = -i\omega \mu_0 [H(x, a) - H(x, -a)]$ . Considering  $\delta = \infty$  in (4) yields the IE for inhomogeneity as metal strip. The current  $J(x)$  has a singularity on the border of metal strip. One of the methods to avoid this singularity is to change variables as  $x = l \cos \varphi$ ,  $f(\varphi) = J l \sin \varphi$ . Numerical experiments have shown that the changing of variables gives good convergence for impedance strips too, because the current on these strips increases at the border as well. Our IE (4) in this case may be written as

$$\int_0^\pi f(\varphi') g(\varphi, \varphi') d\varphi' - f(\varphi) / k^2 \delta l \sin \varphi = -E^v(l \cos \varphi, 0), \quad (5)$$

where  $g(\varphi, \varphi') = G(l \cos \varphi, l \cos \varphi')$ . Note, that the condition  $\varphi' \rightarrow \varphi$  yields  $g(\varphi, \varphi') \approx g_0(\varphi, \varphi') = -\log |2(\cos \varphi - \cos \varphi')| / 2\pi$ . Then we extract singular part of kernel IE (5) and transform this IE as follow

$$\int_0^\pi [f(\varphi') g(\varphi, \varphi') - f(\varphi) g_0(\varphi, \varphi')] d\varphi' + f(\varphi) \int_0^\pi g_0(\varphi, \varphi') d\varphi' - f(\varphi) / k^2 \delta l \sin \varphi = -E^v(l \cos \varphi, 0) \quad (6)$$

The first integral in (6) has no singularity, the second one is equal to zero. Simplified IE (6) we solved with collocation method. To calculate the integral the highest calculation accuracy formula (formula of quadrangles) has been used. The second way to solve (6) is the Galerkin method (GM) with  $\cos j\varphi'$  functions as basical ones. Upon transfer to the  $x$  coordinate they correspond to the first kind of Chebyshev polynomials. There is a

sense to use  $\cos m\varphi$  only for metal strips, for impedance ones the function  $\sin m\varphi$  may be applied.

## RESULTS AND CONCLUSIONS

The methods elaborated have a good convergence. The number of collocation points and number of basic functions per one strip is from 3 up to 7. Therefore, the wave diffraction by high number of strips (up to 100) it is possible to investigate. The CM codes calculate ten times faster than GM ones.

Therefore, the eigenwaves of periodic impedance diffraction grating are investigated. Dispersion characteristics, the windows of transparency and phase synchronism conditions for first and second harmonics (Fig 1, 2) have been obtained as the result of the investigation. Table illustrates the comparison of waves propagation coefficients (for DG placed over planar waveguide  $h=1$ ;  $d/h=0,5$ ;  $\varepsilon=4,0$ ;  $\varepsilon_1=4,0$ ;  $\varepsilon_2=2,1$ ;  $\varepsilon_3=1,0$ ;  $a/h=0,2$ ;  $l/h=0,25$ ;  $N=1$  is a number of strips) we obtained by rigorous method (variant

Variant	$\lambda$		
	3,5	5,0	6,5
1	1,7328	1,6827	1,6064
2	1,7247	1,6996	1,6198
3	1,6873	1,7284	1,6349

1) and by approximate one described above (variants 2 and 3). Clearly seen, that the impedance we introduced gives higher accuracy for thick strips ( $k\sqrt{\varepsilon}a \leq 1$ ). Analogous results are obtained for reflection coefficient  $|S_{11}|$  from dielectric

inhomogeneity [3].

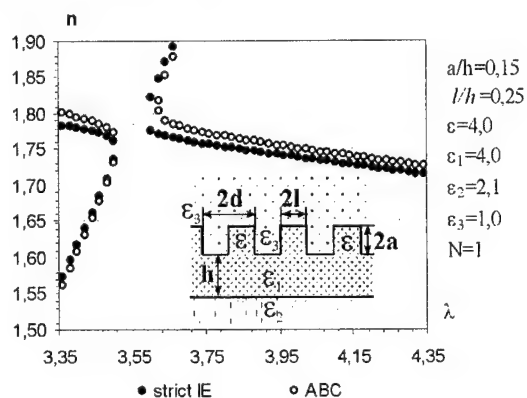


Fig.1

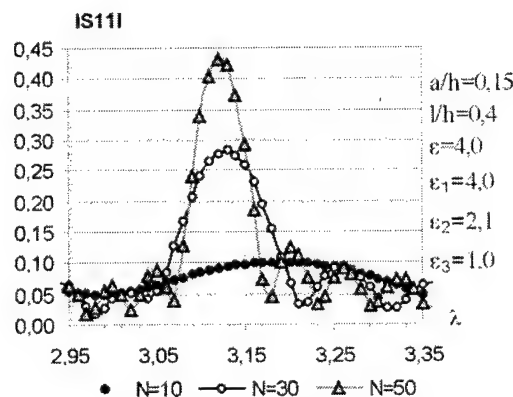


Fig. 2

## REFERENCES

- [1]. T.L. Zinenko, A.I.Nosich, Y. Okuno. IEEE Trans. AP, V.46, No10. P.1498.
- [2]. A.M. Lerer, Journal of Communications Technology and Electronics. 1991, T. 36 #10.
- [3]. G.A. Kalinchenko, A.G. Kyurkchan, A.M. Lerer, S.A. Manenkov, and A.L. Soloveichik. Journal of Communications Technology and Electronics. 2001. V. 46 # 9, P.1005.
- [4]. L.A. Vainshtein The theory of diffraction and method factorization M.: Sovetskoe radio. 1966. 432 p. (In Russian).

## ANALYSIS OF FREQUENCY SELECTIVE STRUCTURES WITH FRACTAL ELEMENTS

A.O.Kasyanov, V.A.Obukhovets

Taganrog State University of Radio Engineering  
44 Nekrasovsky street, GSP-17A, Taganrog, Russia, 347928,  
Phone (8634) 371-883, E-mail: vao@tsure.ru

### ABSTRACT

It is shown the possibility of development of multifrequency frequency selective surfaces (fss) by means of complicating of the shape of elements, for example, using elements with composite fractal shape. In the paper the method of integral equations is applied for the analysis of scattering characteristic of these gratings. In the paper the possibility of applying of ffs with elements of the composite shape at development of multifrequency fss with reduced angular sensitivity on the basis of numerical experiment is shown. The obtained results can be used for choosing the most rational version of element shape of fss at a solution of some problems in antenna engineering.

### INTRODUCTION

The frequency selective structures usually apply to ensure operation on many frequencies of reflective type antennas with several feeds [1]. The multifrequency frequency selective gratings are usually multilayer structures. However, to operate on several frequencies frequency selective gratings it is not necessary should be multilayer structures. The constructions of antennas with radiators, which have the shape of fractals, are known. Such antennas can operate at once on several frequencies [2]. In a paper [3] the frequency selective structure, which is composed from the fractal elements, is represented. The elements of this frequency selective structure have the shape of Sierpinski gasket.

The purpose of the present work is the numerical analysis of scattering characteristics of frequency selective structures as gratings of metal plates and slots in the perforated screens, which have the fractal shape.

### THEORY

The mathematical model foundation for the frequency selective structures is made in accordance with the concept of infinite periodic arrays. Such approach is reasonable because of consideration the multielement arrays with rather complicated element structure. An alternative way of modelling may be based on the basis of so called "element by element method" with taking into account mutual coupling between array elements. This way may become much more difficult because of necessity to solve large sized system of integral equations.

The frequency selective structure is excited by plane electromagnetic wave. This plane electromagnetic wave has linear polarization. We enter to Cartesian system of coordinates. We direct axis  $Oz$  along the normal vector by the plane, where printed elements of the frequency selective structure are located. We assume that these printed elements have arbitrary shape. The steps of array along axes  $Ox$  and  $Oy$  equal accordingly  $d_1$  and  $d_2$ . The permittivity of substrate is  $\epsilon$ . The substrate represents the

flat layer, on obverse surface of which (plane  $z = 0$ ) there are printed the array elements. It is necessary to determine the current distribution on the radiators of array, scattering polarizing, frequency and angular characteristic of the array.

The boundary problem was solved by integral equation method. The equation is made on the basis of Lorentz's lemma in integrated form. The application of periodicity condition has allowed to reduce the solution to search of currents within the limits of one Floquet channel. The integral equation solution is produced by moment method. The array aperture magnetic current surface density is approximated by set of subsectional current functions. In this case the rooftop functions are useful. The currents obtained from integral equations system solution allow to determine all main performances of periodic printed frequency selective structure. Therefore, one can vary the mentioned secondary parameters of the printed frequency selective structure. It is convenient to use such a procedure in the interactive mode. In a number of cases, the processes can be made automatic by means of numerical optimization of some goal function reflecting the proximity of the synthesized parameters of the frequency selective structure to the given values.

## NUMERICAL RESULTS

The first example of the numerical analysis is a solution of the diffraction problem of a plane electromagnetic wave on a periodic grating, which is composed from fractal dipoles. The dipoles are composed from two triangles. The shape of these triangles is Sierpinski triangle [2]. To create this geometric fractal the following algorithm is used. Let's take a triangular metal plate. Let middles of legs of this triangle are tops of a new triangle. This new triangle we shall delete from an initial triangle. It is clear, that the created now structure consists of three triangles. The sizes of these triangles twice are less than sizes of an initial triangle. In the further process of deleting of metal from the stayed triangular elements repeats similarly. The fractal element of  $N$  generation will be generated after a termination of  $N$  steps of this algorithm.

The unit cell of a periodic grating, which is composed from such printed dipoles, is shown in Fig.1,a. The single dipole of this frequency selective structure consists of two Sierpinski.

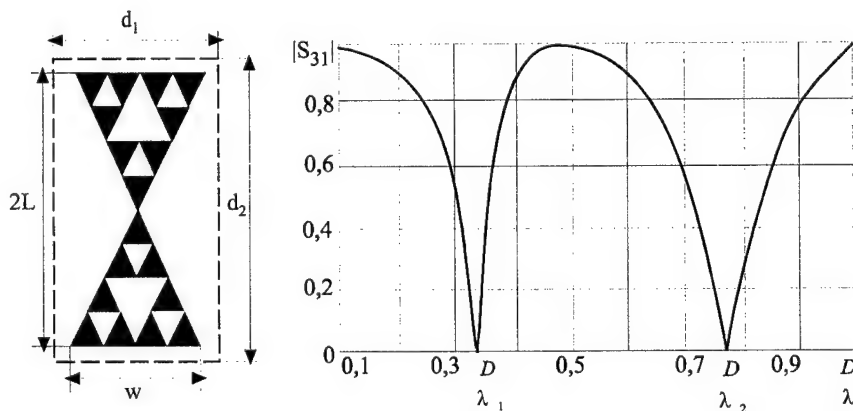


Fig. 1

triangles. These triangles are fractals of second generation. It is shown that the fractal element represents a self-similar structure, in which each triangular fragment represents a duplicate in the reduced scale of all fractal structure in whole. Here is designated:  $L =$

7 mm — length of a dipole shoulder;  $W = 13$  mm — foundation of a triangle;  $d_1 = d_2 = 15$  mm — sizes of a grating unit cell. The frequency selective structure is excited by a plane electromagnetic wave with linear polarization. The vector of polarization of an excited wave is directed along axis of printed dipoles. The calculated frequency characteristic of an electromagnetic wave transition factor by such fractal frequency selective structure in case of co-polarization is shown in a fig. 1,b. It is shown, there are two resonances of a full reflection, when  $2L/\lambda_1 = 0.32$  and  $2L/\lambda_2 = 0.72$  in a single-wave range of a grating. The ratio of upper frequency of a rejection to the lower frequency is equal  $\zeta = 2.25$ . It is important to notice, that as against [3], in the given example the dipoles are located in knots of a grid with a rectangular cell. In a paper [3] the case has been considered, when the similar fractal dipoles locate in knots of a grid with a triangular mesh. The ratio of rejection frequencies in this case is equal  $\zeta = 2.9$ .

Thus, the printed frequency selective structure composed from fractal dipoles has a property of a two-frequency rejection in a single-wave range of a grating.

In further we shall consider performances of scattering of the perforated screens. Now, as against a grating of plates, in the perforated screen on some (resonance) frequencies the phenomenon of incident electromagnetic wave full transition is observed. It is possible to create a mode of full transition of electromagnetic waves through perforated screen at once on several frequencies. The realization such slots in the perforated screen, which have shape of fractal, will allow to achieve full transition electromagnetic wave on several frequencies.

To check up a validity of this supposition such perforated screen is researched, in which slots have the shape of Sierpinski square. The perforated screen is considered, in which the slots are located so that the unit cell of a grating had the shape of Sierpinski square of second generation. The topology of a grating unit cell is shown in insertion of Fig.2.

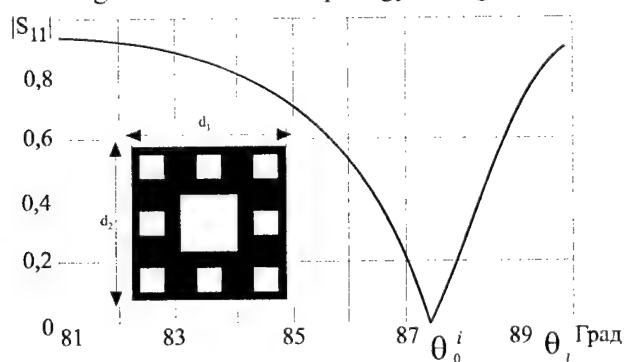


Fig. 2

The grating unit cell has following sizes:  $d_1 = d_2 = 10$  mm. If such perforated screen is excited by normal incident plane electromagnetic wave, then resonances are not present in single-wave range of an array periodicity, because the sizes of square slots in a screen are unsufficiently great. However, in case of an electromagnetic

wave sloping incidence on a grating it is possible to observe effect of full transition of electromagnetic waves through such a frequency-selective structure. The relationship of reflection factor of an electromagnetic wave with parallel polarization in a sector of incidence angle close to a "sliding" incidence is shown in Fig.2. This characteristic has been calculated in a case, when  $f = 15$  GHz. It is shown, that the resonance of full transition is observed with  $\theta'_0 = 87.4^\circ$ . Thus it is necessary to notice, that as shown in [5], the screen with identical square slots has not resonances of full transition in an angular sector from normal incidence down to a "sliding" incidence of an electromagnetic

waves.

Thus, the modification of a unit cell shape of the perforated screen has reduced to emerging scattering modes of electromagnetic waves, which are not typical for frequency selective structures composed from simple (not fractal) elements.

To achieve full transition of electromagnetic waves through the perforated screen, not only with sloping, but also with a normal electromagnetic wave incidence, it is necessary, that slots in a screen would have resonance sizes in a single-wave range of a grating. For example, the application of crosslike slots allows to create a mode of a full transition of electromagnetic waves through a screen also with a normal electromagnetic wave incidence [5]. By replacing square slots in Sierpinski fractal to crosslike slots we achieve necessary increasing of slots sizes down to resonance in a single-wave range of a grating. The size of a unit cell remains same, as in the previous example. The frequency characteristic of reflection factor of such perforated screen is shown in Fig. 3.

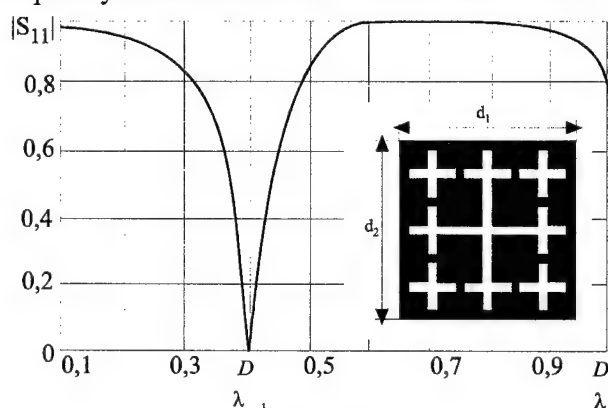


Fig. 3

It is shown, the unique resonance of full transition of electromagnetic wave through frequency-selective surface is observed in a single-wave range of wavelengths with  $D/\lambda_1$ . Two-frequency mode of an electromagnetic wave transition such frequency selective surface does not ensure, because only central crosslike slots, which have large arm length "resonate" in a single-wave range of a

grating. At the same time resonance frequencies of peripheral crosslike slots locate in a multimode range of a grating, therefore these slots do not influence to transition of an electromagnetic wave through the perforated screen in a single-wave range of an array. It is necessary to notice, that the similar result was obtained in paper [6]. In this paper the perforated screen as a periodic grating of slots was investigated. The shape of each slot of this grating is Jerusalem cross. Jerusalem cross is enclosed by simple crosslike slots, is similar to that is represented in insertion of Fig.3.

Thus, for reaching multifrequency mode of operations of the perforated screen it is necessary, that all slots were resonance in a single-wave range of a grating.

Last numerical example connects with the perforated screen, which unit cell has a topology shown in Fig.4, a. This grating has following parameters:  $L_1 = 13,4$  mm;  $L_2 = 7$  mm. The size of a unit cell is same, as well as in two previous examples. The grating is excited by a plane electromagnetic wave of linear polarization. The normal incidence of electromagnetic wave is considered. The vector of electromagnetic wave polarization is directed along a diagonal of square, which limits a unit cell of the perforated screen. The frequency characteristic of a reflection factor of this frequency selective structure is shown in Fig. 4, b. It is shown, that such grating has two resonance frequencies in a single-wave range of array. These frequencies are just those frequencies, on which the full transition of an electromagnetic wave through the perforated screen is observed. If



$D/\lambda_1$  is equal 0,37, then the long wavelength resonance is observed. It is shown, that in this case  $L_1/\lambda_1$  is equal 0,5. If  $D/\lambda_2$  is equal 0,67, then the short-wave resonance is observed. It is shown, that in this case  $L_2/\lambda_2$  is equal 0,475. So, it is possible to make a conclusion that a long wavelength resonance "ensure" longer slots (central slot of a unit cell of the perforated screen), and a short-wave resonance "ensure" more short, that is peripheral, slots.

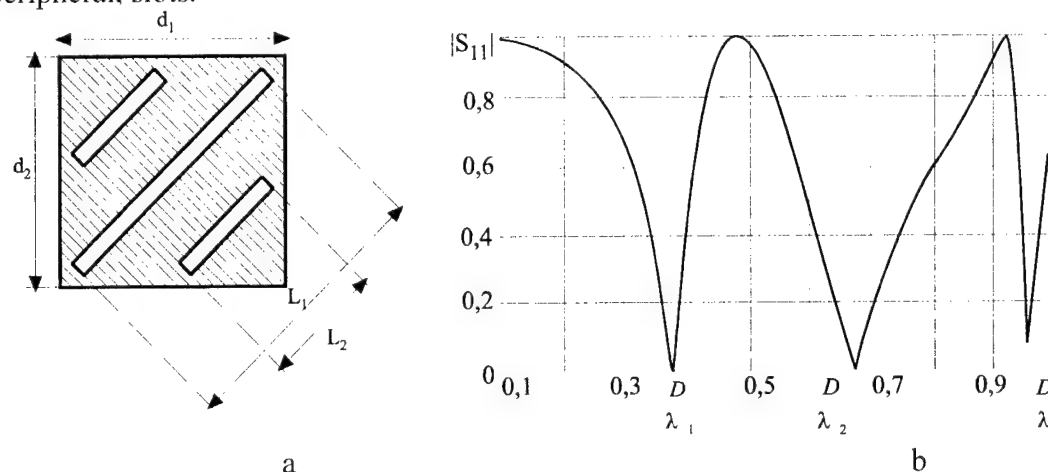


Fig. 4

Thus, if the frequency selective structure is the perforated screen, which consists of fractal slots, then this structure has a property of electromagnetic wave transition on two frequencies in a single-wave range of a grating.

## CONCLUSION

Basing on numerical experiment, in a paper it is shown the possibility to use printed arrays with the fractal elements for development of two-frequency electrodynamic frequency selective structures. These results can be used for a choice of the most rational variant of a frequency-selective structure geometry for a solution of the some problems of an antenna engineering.

## REFERENCES

- [1]. A.Yu.Kovalenko, P.V.Sokolov Two-Resonance Frequency Selective Surfaces// Proceedings of the XXXVIII Moscow International Conference on Antenna Theory and Technology, 1998. — P. 412–415.
- [2]. Puente, C., Romeu, J., Pous, R., and Cardama, A. On the behavior of the Sierpinski multiband antenna// IEEE Trans., 1998, AP-46, (4). — P. 517–524.
- [3]. Romeu, J. and Rahmat-Samii, Y. Dual band FSS with fractal elements// Electronics Letters, 29<sup>th</sup> April 1999. Vol. 35, No. 9. — P. 702–703.
- [4]. Troncet, E., Albart, G., and Allam L. Microwave characterization and modeling of the surface impedance of the fractal structure copper films// IEEE Trans., 1998, AP-46, (3). — P.434–442.
- [5]. Rubin B.J., Bertoni H.L. Reflection from a periodically perforated plane using a subsectional current approximation//IEEE Trans., 1983.- Vol. AP-31, N 6. — P.829–836.
- [6]. R.Mitra, C.H.Chan, T.Cwik, Techniques for analyzing frequency selective surfaces — A review// Proc. IEEE, vol.76, 1988, №12. — P. 1593–1615.

# ELECTROMAGNETIC WAVE DIFFRACTION BY A DOUBLE-LAYER PERIODIC GRATING OF CURVILINEAR METAL STRIPS

P.L. Mladyonov

Institute of Radio Astronomy of National Academy of Sciences of Ukraine, Kharkov, Ukraine  
Phone: (0572) 448-503; e-mail: mladyon@rian.ira.kharkov.ua.

## ABSTRACT

Reflection and transmission characteristics of double-layer two-periodic gratings of perfectly conducting infinite strips with a complex shape are considered. The structures with layers that have strips turned on 90 degrees and parallel are considered. The comparison of reflection properties of double-layer two-periodic gratings of straight-line strips with curvilinear ones is presented.

## INTRODUCTION

Recently, new applications of periodic structures are very popular to design so-called electromagnetic crystals known also as photonic band gap (PBG) crystals for microwave devices. As a result, interest to two- and even one-dimensional periodic structures is renewed. Two-periodic plane strips structures are more attractive for application because of their possess resonance properties in the frequency band of single-wave regime due to a complex shape of the array elements and their very small thickness. The artificial electromagnetic crystals could find many applications for passive microwave devices such as filters, reflectors or antenna covers. The simple PBG crystals are made with only a few layers of periodic array. These multi-layered structures have of reflection or transmission frequency bands with sharp boundaries due to Feby-Perot effects.

The reflection properties of complex layered arrays of metal strips of C-, S- and  $\Omega$ -shape placed in free space [1] and on dielectric substrates [2] were studied earlier. The main goal of this report is to study the reflected properties of two-layer periodic structures of curvilinear metal strips in free space. The element of grating is plane periodic metal strip having arbitrary shape on the grating period. The period of the grating is much greater than its width. The width of the strip can change along the strip.

## OPERATORS OF REFLECTION AND TRANSMISSION OF TWO-LAYER GRATING

Let's consider a system of two parallel gratings (Fig 1a). The parameter  $\Delta$  is the distance between layers. Matrixes of the operators of reflection and transmission of the first and second gratings are written as  $\hat{r}_1$ ,  $\hat{t}_1$  and  $\hat{r}_2$ ,  $\hat{t}_2$ . The amplitude of the partial waves between layers (Fig.1b) satisfy the following set of equations,

$$\begin{cases} \vec{A} = \hat{t}_1 \vec{q} + \hat{r}_1 e \vec{B} \\ \vec{B} = \hat{r}_2 e \vec{A} \\ \hat{R} \vec{q} = \hat{r}_1 \vec{q} + \hat{t}_1 e \vec{B} \\ \hat{T} \vec{q} = \hat{t}_2 e \vec{B} \end{cases} \quad (1)$$

where  $e$  is the plane-wave propagation operator in free space

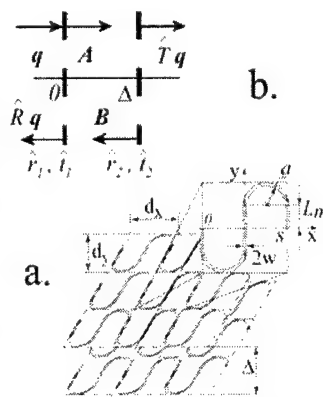


Fig. 1 The two-layer periodic grating of curvilinear metal strips.

between the surface of layers. After the eliminating vectors of  $A$  and  $B$  from equations (1) we obtain the expressions for matrixes of reflection and transmission of two-layer grating,

$$\begin{aligned}\hat{R} &= \hat{r}_1 + \hat{t}_1 \hat{e} \hat{r}_2 \hat{e} (\hat{I} - \hat{r}_1 \hat{e} \hat{r}_2 \hat{e})^{-1} \hat{t}_1, \\ \hat{T} &= \hat{t}_2 \hat{e} (\hat{I} - \hat{r}_1 \hat{e} \hat{r}_2 \hat{e})^{-1} \hat{t}_1,\end{aligned}$$

where  $\hat{I}$  is the unit matrix. Numerical analysis below was carried out without taking in to account evanescent partial waves in the case of one-mode regime.

## NUMERICAL RESULTS AND DISCUSSION

The scattering characteristics of two-layer arrays in free space for the cases of different strip shapes are presented and discussed bellow. Let us firstly pay attention to the frequency dependence of the reflection coefficients for a single array (Fig. 2). This is important for explanation the reflection properties of a two-layer structure. The reflection properties of single layer of curvilinear metal strips and all mathematical transformations have been considered in [3] more explicitly.

Now we consider the structure, which has identical layers when it is illuminated by E-polarized (along the x-axis) wave. The reflection coefficient of the straight strips is represented on Fig. 3. Coincidence of the data obtained by a rigorous numerical-analytical method described in [4] and the present method is good. The resonance of transmission due to interaction between the layers of the structure is observed of the frequency parameter  $d_y / \lambda \approx 0.6$ . A simple estimation of the interlayers resonant frequency can be made by considering the condition of equality of phases of the wave reflected by the structure's front boundary and the wave reflected by second layer taking into account a phase jump of wave propagated through a single array. The phase of the reflected by the first layer of the structure is  $\psi_1 = \arg r_1$ . The phase of the wave reflected by the second layer at the plane of structure's front boundary is  $\psi_2 = \arg r_2 + 2(\arg t_1 + \Delta k)$ . One can expect that the maximum of reflection occurs when,

$$\psi_1 - \psi_2 = 2\pi l, \quad (2)$$

and it will be minimum if,

$$\psi_1 - \psi_2 = \pi(2l + 1), \quad (3)$$

where  $l = 0, \pm 1, \pm 2, \dots$ . For a case of identical strips, if  $\Delta = d_y / 2$  the requirement equation (3) becomes  $2(\arg t_1 + \pi d_y / \lambda) = \pi(2l + 1)$ . At  $\arg t_1 = 0$ , the minimum of a reflectivity would be observed at  $d_y / \lambda = 0.5$  and for  $l=0$ , but as the  $\arg t_1 \neq 0$ , the minimum is shifted to the greater frequencies. For the structure of wavy strips one more minimum generated by properties of the single layer is observed, except for a minimum of a reflectivity because of interaction between layers (Fig 4, curve 1). These two minimums practically coincide forming the band of almost total transmission, for structure of lines having the shape of rounded meander (Fig. 5, curve 1). The band of reflection at near  $d_y / \lambda \approx 0.8$  is generated by the complex shape of strips, but it is more widely and has more steep edges than in case of single layer.

If the structure consist from identical layers and the incident wave polarized along the y-direction (H-polarization) the grating of vary narrow straight strips do not reflect (Fig 3, curve 2). This effect looks like there is the incident wave simply does not see the grating. The change of the shape of strips leads to appearance of the band of reflection, which is more widely and has more steep edges ( than in case of one layer) because interaction between layers. For structure of wavy strips this band is narrow than for the grating of strips with the shape of rounded meander narrow (Fig.4,5, curves 2), because of different magnitude of the quality factor of a resonance for single layer of such strips.

The dependence of the reflection coefficient upon polarization of the incident wave is observed, if there is identical orientation of strips in layers. This polarization influence is not desirable sometime. It is possible to decrease this dependence by rotation of the second layer on 90 degrees with respect to first one. Then the module of the reflection coefficient for normally incident waves polarized along axes of periodicity does not differ practically (curves 3 in a Fig. 3, 4, 5). If the polarization of the wave is arbitrary then the absolute value of the reflection coefficient remain about the same magnitude.

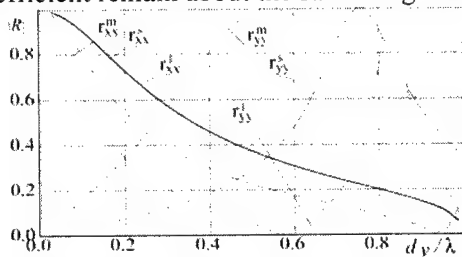


Fig. 2 Magnitudes of reflection coefficients of metal strips of variety shapes. 1 layer.  $d_x=d_y$ ,  $2w/d_y=0.05$ , straight strips-superscript i, wavy line ( $L_m=0$ )- superscript s, the rounded meander with  $L_m=0.2$ - superscript m.

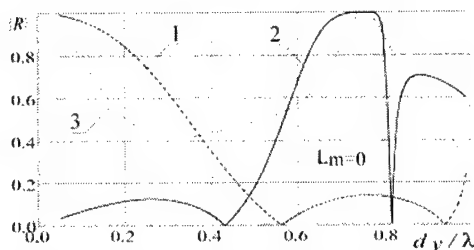


Fig4. Magnitudes of reflection coefficients of metal strips having the shape of wavy line, 2 layer.  $d_x=d_y$ ,  $2w/d_y=0.05$ , curve1 - E-polarization and identical layers, curve 2 - H-polarization and identical layers, curve 3 - layers that have crossed strips..

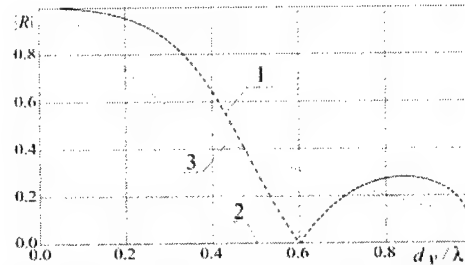


Fig3. Magnitudes of reflection coefficients of metal straight strips. 2 layer.  $d_x=d_y$ ,  $2w/d_y=0.05$ , curve1 - E-polarization and identical layers, curve 2 - H-polarization and identical layers, curve 3 - layers that have crossed strips.

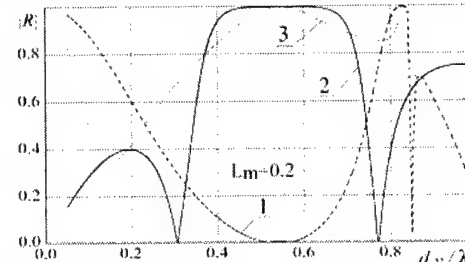


Fig5. Magnitudes of reflection coefficients of strips having the shape of rounded meander, 2 layer.  $d_x=d_y$ ,  $2w/d_y=0.05$ , curve1 - E-polarization and identical layers, curve 2 - H-polarization and identical layers, curve 3 - layers that have crossed strips.

## CONCLUSION

The electromagnetic scattering by two-layer periodic grating of curvilinear metal strips was considered. The numerical study for normal incidence wave shows the possibility of making resonant layers, polarization sensitive, having frequency bands of total reflection and transmission with very steep boundaries. In contrast to a single array, a layered structure offers the possibility to obtain sharp and wide filtering zones.

The author is grateful to S.L. Prosvirnin for the problem formulation and encouragement during the performance of this work.

## REFERENCES

- [1] S.L. Prosvirnin, A.S. Tretyakov, T.D. Vasilyeva, A. Fourier-Lamer and S. Zouhdi, Analysis of reflection and transmission of electromagnetic wave in complex layered arrays, *Journal of Electromagnetic Waves and Applications*, Vol. 14, pp. 807-826, 2000.
- [2] S.L. Prosvirnin and S. Zouhdi, Multi-layered arrays of conducting strips: switchable photonic band gap structures, *International Journal of Electronics and Communication*, pp. 260-265, 2001.
- [3] S.L. Prosvirnin, S.A. Tretyakov, P.L. Mladyonov, Electromagnetic wave diffraction by planar periodic gratings of wavy metal strips, *J. Electromagnetic Waves and Applications*, vol. 16, no. 3, pp. 421-435, 2002.
- [4] V.P. Shestopalov. The method of Rimann-Gilbert problem in theory of diffraction and propagation of electromagnetic waves. Kharkov, 1972.

# FEM AND ITS GENERALIZATION FOR THE DIFFRACTION BY POLYGONAL PROFILE GRATINGS

J. Elschner, A. Rathsfeld, and G. Schmidt

Weierstrass Institute for Applied Analysis and Stochastics  
Mohrenstr. 39, D-10117 Berlin, Germany  
E-mail: [elschner@wias-berlin.de](mailto:elschner@wias-berlin.de), [rathsfeld@wias-berlin.de](mailto:rathsfeld@wias-berlin.de),  
[schmidt@wias-berlin.de](mailto:schmidt@wias-berlin.de)

## ABSTRACT

For the numerical computation of efficiencies for optical gratings, there exists a huge variety of algorithms. Dealing with a boundary value problem for an elliptic partial differential equation, the application of finite element methods (FEM) is natural too. However, the oscillatory nature of the electromagnetic fields requires some modifications. The resulting FEM program can be used as a part of an algorithm to design optimal gratings.

## THE FINITE ELEMENT METHOD (FEM)

The variational form of the boundary problems is well known and its coerciveness is well established (cf. e.g. [6,1,3]). For example the variational equation for  $u(x, y) = v(x, y) \cdot \exp(-i\alpha x)$  with  $v$  the unknown third component of the amplitude of the scattered magnetic field in the case of TM polarization is

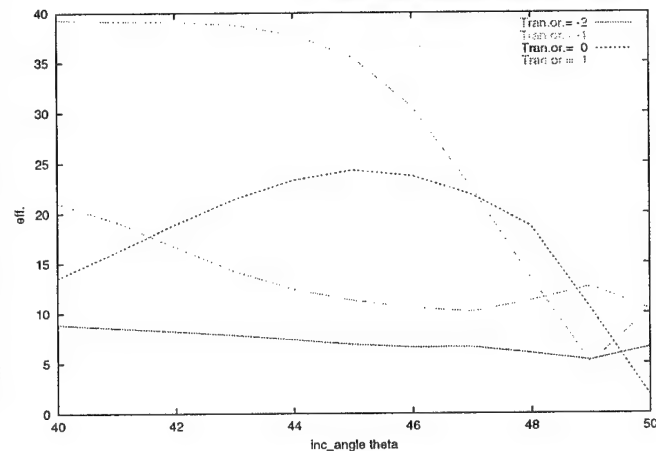
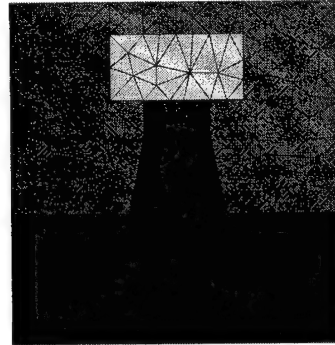
$$\begin{aligned} \int_{\Omega} \frac{1}{k^2} \{ \nabla + i(\alpha, 0) \} u \cdot \overline{\{ \nabla + i(\alpha, 0) \} \varphi} - \int_{\Omega} u \overline{\varphi} + \frac{1}{(k^+)^2} \int_{\Gamma^+} (T_{\alpha}^+ u) \overline{\varphi} \\ + \frac{1}{(k^-)^2} \int_{\Gamma^-} (T_{\alpha}^- u) \overline{\varphi} = - \frac{1}{(k^+)^2} \int_{\Gamma^+} (2i\beta e^{-i\beta b}) \overline{\varphi}, \quad \varphi \in H_p^1(\Omega). \end{aligned} \quad (1)$$

The domain  $\Omega$  is the rectangular cross section of the grating profile taken over one period and  $\Gamma^{\pm}$  stand for the upper resp. lower boundary sides. The symbol  $k$  stands for the piecewise constant refractive index taking the constant values  $k^+$  resp.  $k^-$  above resp. below the grating. The number  $\alpha$  is the product of  $k^+$  times the sine of the incidence angle,  $\nabla$  is the gradient, and  $T_{\alpha}^{\pm}$  a hypersingular boundary integral operator. The test function  $\varphi$  runs through all periodic (w.r.t. to the first variable  $x$ ) functions in the Sobolev space  $H^1(\Omega)$ . A variational equation similar to (1) holds for the TE polarization. For the case of conical diffraction (incident plane wave with direction not in the plane perpendicular to the grooves of the grating), a coupled system of two such variational equations is to be solved.

To get the FEM solution, the domain is split into triangles/rectangles. An approximation of the magnetic field is sought in form of a continuous piecewise

linear/bilinear function, and the test functions in (1) are replaced by the piecewise linears/bilinears. Substituting the numerical solutions for  $u$  over  $\Gamma^\pm$  into well-known integral representations, we get the reflected and transmitted energy and the efficiencies of the reflected and transmitted modes. In contrast to popular alternative methods, the FEM needs no Rayleigh expansion, no slicing of blaze gratings, and no solution of big dense systems of integral equations. The convergence of the method is well established.

Example : *cover material* : Air  
*coating material* : Photoresist  
*substrate material* :  $\text{SiO}_2$   
*polarization* : TM  
*period* : 588 grooves/mm  
*incidence angle* :  $47.5^\circ$



The figures show a coarse FEM grid of a coated lamellar grating profile with overetching, the isolines of the real part of the solution  $u$ , and the efficiencies of the transmitted modes of order -2, -1, 0, and 1 depending on the incidence angle in the interval  $[40^\circ, 50^\circ]$ .

## GENERALIZED FEM

Unfortunately, due to a mismatch of the frequency of the solution and the discrete frequency of the approximate solution, the FEM deteriorates with large wave numbers. Even if the function can be approximated in the space of piecewise linears with high accuracy, the error of the FEM solution of Eq. (1) may be large. To overcome this so-called "pollution effect", we have first implemented a generalized FEM for the case of lamellar (binary) gratings which is a finite difference scheme over uniform rectangular gratings (cf. [2,4]). Further, we have tested the partition of unity method together with mortar techniques (cf. [5]),

and we have implemented a new generalized FEM based on trial functions the restrictions of which to the triangles of the triangulations are solutions of the partial differential equation. These solutions are generated by an FEM over a fine uniform grid in the subtriangle. For a fixed accuracy, these methods reduce the storage requirements and, in some cases, the computing times essentially. In the table we present results for a coated echelle grating (wave length 160 nm, 166 grooves per mm, width of MgF2 coating 25 nm, blaze angle  $80^\circ$ , apex angle  $90^\circ$ , cover material Air, grating material Al, TE polarization, incidence angle  $80^\circ$ ).

degrees of freedom	memory for solver	efficiency of order 74 (refl.)
105 785	0.35 GB	37.931045
263 624	0.70 GB	67.384460
559 800	1.98 GB	68.390312

### OPTIMIZATION OF GRATINGS (SYNTHESIS PROBLEM)

The mentioned methods for the numerical solution of the direct diffraction problem can be used as a part of an algorithm to design optimal gratings. We have implemented a code (cf. [4]) to minimize several objective functions including efficiencies and phase shifts. On a set of coated lamellar grids containing a certain number of rectangular pieces with prescribed material properties, we determine an optimal grating by a gradient descent method. The latter is based on the efficient computation of the gradients by generalized FEM.

### ACKNOWLEDGEMENT

The authors gratefully acknowledge the support of the German Ministry of Education, Research and Technology under Grant No. 03-ELM3B5.

### REFERENCES

- [1] G. Bao, D.C. Dobson, and J.A. Cox, "Mathematical studies in rigorous grating theory", *J.Opt.Soc.Amer. A* 12, 1029–1042 (1995).
- [2] I. Babuška, F. Ihlenburg, E. Paik, and S. Sauter, "A generalized finite element method for solving the Helmholtz equation in two dimensions with minimal pollution", *Comp.Methods Appl.Mech.Eng.* 128 325–359 (1995).
- [3] J. Elschner, R. Hinder, F. Penzel, and G. Schmidt, "Existence, uniqueness and regularity for solutions of the conical diffraction problem", *Math.Models & Methods Appl.Sci.* 10, 317–341 (2000).
- [4] J. Elschner and G. Schmidt, "Numerical solution of optimal design problems for binary gratings", *J.Comput.Phys.* 146, 603–626 (1998).
- [5] J.M. Melenk and I. Babuška, "The partition of unity method: Basic theory and applications", *Comput.Methods Appl.Mech.Eng.* 139, 289–314 (1996).
- [6] H.P. Urbach, "Convergence of the Galerkin method for two-dimensional electromagnetic problems", *SIAM J.Numer.Anal.* 28, 697–710 (1991).

# ELECTROMAGNETIC CHARACTERISTICS OF DOUBLY-PERIODIC MAGNETODIELECTRIC LAYER BOUNDED BY TWO UNIFORM MEDIA

Natalia V. Sidorchuk, Vladimir V. Yachin and Sergey L. Prosvirnin  
 Department of Calculus Mathematics, Institute of Radio Astronomy  
 4 Krasnoznamennaya Street, 61002 Kharkov, Ukraine  
 email: yachin@rian.kharkov.ua

## ABSTRACT

The problem of electromagnetic wave propagation in a doubly-periodic magnetodielectric layer bounded by two uniform infinite media is solved by new method based on the rigorous volume integro-differential equations of electromagnetics.

The Galerkin method is applied to reduce these equations to a set of second-order differential ones with constant coefficients in field functionals which contain information about geometry of the scattering structure. The special scheme of equation set solving is introduced in the case of thick layers to overcome usual numerical difficulties associated with the undesired exponential functions in the expressions. This method unifies the treatment of both TE- and TM-waves by replacing  $\varepsilon$  by  $\mu$ ,  $\mu$  by  $\varepsilon$ , E-components by H-components, H-components by E-components.

## METHOD

Formulation of the problem is as follows: from the region 2 ( $z < -h$ ) with complex relative permittivity  $\varepsilon_2$  and permeability  $\mu_2$ , a linearly-polarized plane electromagnetic wave is incident at an arbitrary angle  $\varphi$  on the double-periodic infinite layer (region 1) bordering the region 3 ( $z > 0$ ) with complex relative permittivity  $\varepsilon_3$  and permeability  $\mu_3$  (Fig.1).

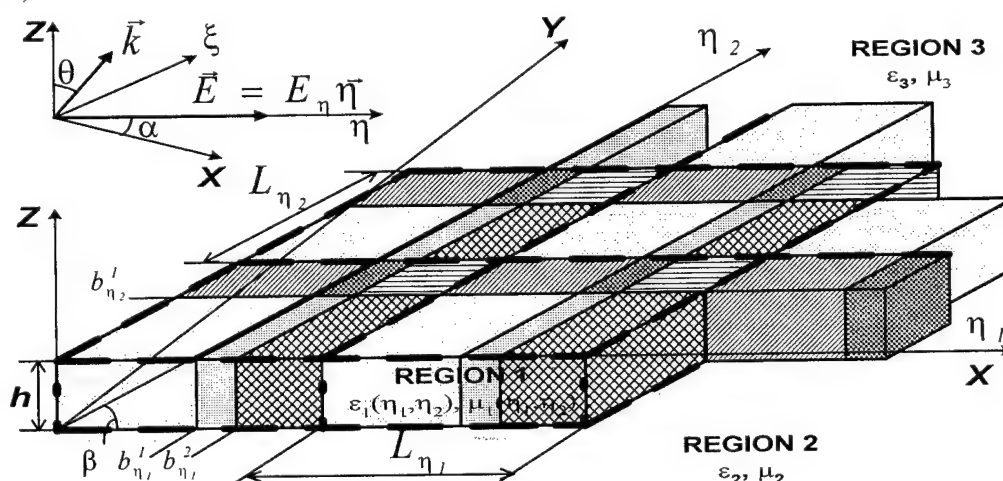


Figure 1. Geometry of the problem.



The periodic cell of the layer is an oblique-angle parallelepiped of arbitrary sizes along the  $\eta_1$  axis and the  $\eta_2$  axis,  $L_{\eta_1}$  and  $L_{\eta_2}$  are periodicities of the layer in the  $\eta_1$  and  $\eta_2$  direction, respectively. The parallelepiped is characterized by the complex relative permittivity  $\varepsilon_1(\eta_1, \eta_2)$  and permeability  $\mu_1(\eta_1, \eta_2)$  and has the thickness  $h$ . We suppose that the incident wave is TE-polarized and  $\alpha$  is the angle between the  $\eta_1$  axis and the electric field vector  $E$  lying in the plane of the layer and consider the field components in the  $(\eta, \xi, z)$  orthogonal coordinate system connected with the incident field polarization. We have to obtain the transmitted and reflected fields in the immediate vicinity of the layer. The form of the integro-differential equations for the electromagnetic field is taken from [1]:

$$\begin{aligned} E(\vec{r}) &= E_0(\vec{r}) + \frac{1}{4\pi} (\nabla\nabla + k_1^2) \int_{V'} \left( \frac{\varepsilon_1}{\varepsilon_2} - 1 \right) E(\vec{r}') G(\vec{r} - \vec{r}') d\vec{r}' + \\ &+ \frac{ik_1}{4\pi} \sqrt{\frac{\mu_2}{\varepsilon_2}} \cdot \nabla \times \int_{V'} \left( \frac{\mu_1}{\mu_2} - 1 \right) H(\vec{r}') G(\vec{r} - \vec{r}') d\vec{r}', \\ H(\vec{r}) &= H_0(\vec{r}) + \frac{1}{4\pi} (\nabla\nabla + k_1^2) \int_{V'} \left( \frac{\mu_1}{\mu_2} - 1 \right) H(\vec{r}') G(\vec{r} - \vec{r}') d\vec{r}' - \\ &- \frac{ik_1}{4\pi} \sqrt{\frac{\varepsilon_2}{\mu_2}} \cdot \nabla \times \int_{V'} \left( \frac{\varepsilon_1}{\varepsilon_2} - 1 \right) E(\vec{r}') G(\vec{r} - \vec{r}') d\vec{r}'. \end{aligned}$$

Here the Green's function is presented in the integral form,  $V$  is the scatterer volume,  $k_1 = k\sqrt{\varepsilon_2\mu_2}$  and  $k$  is a wave number. For beginning we suppose that the periods are partitioned into segments with constant material parameters. For each period segment numbered  $(k, l)$  we can write the notations  $b_{\eta_1}^{k-1} < \eta'_{1k} < b_{\eta_1}^k$ ,  $b_{\eta_2}^{l-1} < \eta'_{2l} < b_{\eta_2}^l$ ,  $\varepsilon_1(r'_{kl}) = \varepsilon_{kl}$  and  $\mu_1(r'_{kl}) = \mu_{kl}$ .

Following the algorithm given in [2] we present the field in each period segment as an expansion in terms of the spatial harmonics numbered  $(r, s)$  and act on the equation for these fields by the linear operator

$$\hat{A}_{pq}^{kl} F(\eta'_1, \eta'_2, z') = \frac{1}{L_{\eta_1} L_{\eta_2}} \int_{b_{\eta_1}^{k-1}}^{b_{\eta_1}^k} \int_{b_{\eta_2}^{l-1}}^{b_{\eta_2}^l} \left( \frac{\varepsilon_{kl}}{\varepsilon_2} - 1 \right) e^{-i(k_{\eta_1} + \frac{2\pi p}{L_{\eta_1}})\eta'_1} e^{-i(k_{\eta_2} + \frac{2\pi q}{L_{\eta_2}})\eta'_2} F(\eta'_1, \eta'_2, z') d\eta'_1 d\eta'_2.$$

Thus we can obtain the set of linear differential equations for the field functionals. By summing these equations over all segments we can express the fields and field functionals for individual segment through the ones for another segment, e.g.:

$$E_{\eta pq}^{kl} = \frac{\varepsilon_{k'l'}(\varepsilon_{kl} - 1)}{\varepsilon_{kl}(\varepsilon_{k'l'} - 1)} (ax_{p-r}^{k'} ay_{q-s}^l) (ax_{p-r}^{k'} ay_{q-s}^{l'})^{-1} E_{\eta pq}^{k'l'},$$

where

$$ax_{p-r}^k = \frac{1}{L_{\eta_1}} \int_{b_{\eta_1}^{k-1}}^{b_{\eta_1}^k} e^{-ix \frac{2\pi(p-r)}{L_{\eta_1}}} d\eta_1, \quad ay_{q-s}^l = \frac{1}{L_{\eta_2}} \int_{b_{\eta_2}^{l-1}}^{b_{\eta_2}^l} e^{-ix \frac{2\pi(q-s)}{L_{\eta_2}}} d\eta_2.$$

Next we solve the equation set for the field functionals and thus for the field components (the procedure in paper [2]). Using the extinction theorem at the last stage we express the internal fields of the structure (region 1 and 3) through the incident wave field. Upon separation the equation set to be solved onto the subsets including the exponential functions with a positive and negative real part of eigenvalues, we apply the iterative procedure developed for calculations of characteristics of scattering from a very thick lossy doubly-periodic magnetodielectric layer in a wide frequency range.

## RESULTS

Presented in Fig.2 are the results of the transmission coefficient calculation for the periodic structure composed of the array of square parallelepipeds with  $\varepsilon = 3 + 0.01i$ ,  $\mu = 1$ , lying on the half-space with  $\varepsilon_3 = 3$ ,  $\mu_3 = 1$ ,  $h/L_{\eta_1} = 10$ ,  $b_{\eta_1}/L_{\eta_1} = b_{\eta_2}/L_{\eta_2} = 0.5$ ,  $L_{\eta_1} = L_{\eta_2} = L_{\eta}$ ,  $\alpha = 25^\circ$ ,  $\varphi = 0.001^\circ$ . The example demonstrates the iterative procedure stability for very thick doubly-periodic structures.

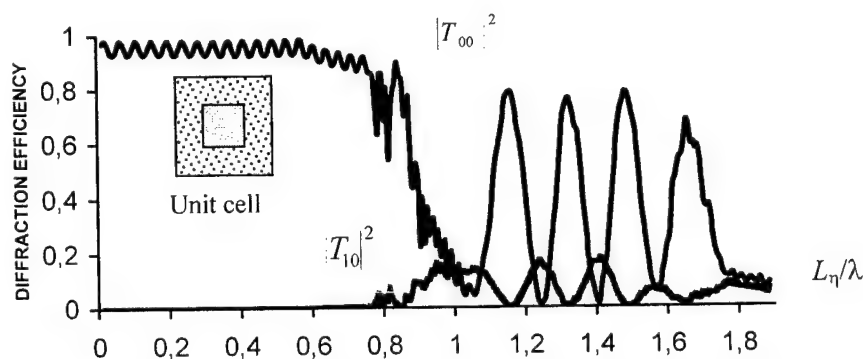


Figure 2. Transmission of the normally incident plane wave through the thick doubly-periodic array lying on the half-space.

Our results are in a good agreement with data concerned thick periodic structures and presented by other authors (see, for example, paper [3], where the one-periodic grating of rectangular rods with  $h/L = 4$  was considered).

## REFERENCES

1. N. A. Khizhnyak, "Green's function of Maxwell's equations for inhomogeneous media," Soviet Phys.-Technical Phys., Physics, vol. 28, No. 7, 1958, pp.1592-1609, (original Russian pagination).
2. V.V.Yachin and N.V.Ryazantseva, "The scattering of electromagnetic waves by rectangular-cell double-periodic magnetodielectric gratings," Microwave and Optical Technology Letters, vol.23, No. 3, 1999, pp.177-183.
3. D.M.Pai and K.A.Awada., "Analysis of dielectric gratings of arbitrary profiles and thicknesses," J. Opt. Soc. Am. A 8, 1991, pp.755-762.

# SCATTERING OF ELECTROMAGNETIC WAVES BY HOMOGENEOUS DIELECTRIC GRATINGS WITH PERFECTLY CONDUCTING STRIP

Tsuneki YAMASAKI, Takashi HINATA, and Toshio HOSONO

Department of Electrical Engineering, College of Sci. and Tech., Nihon University  
Tel. +81-3-3259-0771, Fax. +81-3-3259-0783, E-mail: yamasaki@ele.cst.nihon-u.ac.jp

## INTRODUCTION

Recently, the refractive index can easily be controlled to make the periodic structures such as optoelectronic devices, photonic bandgap crystals, frequency selective devices, and other applications by the development of manufacturing technology of optical devices<sup>[1]</sup>. Thus, the scattering and guiding problems of the inhomogeneous gratings have been considerable interest, and many analytical and numerical methods which are applicable to the dielectric gratings having an arbitrarily periodic structures combination of dielectric and metallic materials<sup>[2]</sup>.

In this paper, we proposed a new method for the scattering of electromagnetic waves by inhomogeneous dielectric gratings with perfectly conducting strip using the combination of improved Fourier series expansion method<sup>[3]</sup> and point matching method<sup>[4]</sup>.

## METHOD OF ANALYSIS

We consider inhomogeneous dielectric gratings with perfectly conducting strip as shown in Fig.1(a). The grating is uniform in the  $y$ -direction and the permittivity  $\varepsilon(x, z)$  with respect to the position  $(= w)$  is an arbitrary periodic function of  $z$  with period  $p$ . The permeability is assumed to be  $\mu_0$ . The time dependence is  $\exp(-i\omega t)$  and suppressed throughout. In the formulation, the TM wave is discussed. When the TM wave (the magnetic field has only the  $y$ -component) is assumed to be incident from  $x > 0$  at the angle  $\theta_0$ , the magnetic fields in the regions  $S_1 (x \geq 0)$  and  $S_3 (x \leq -d)$  are expressed<sup>[3]</sup> as

$$S_1 (x \geq 0) : H_y^{(1)} = e^{ik_1(z \sin \theta_0 - x \cos \theta_0)} + e^{ik_1 z \sin \theta_0} \sum_{n=-N}^N r_n^{(1)} e^{i(k_n^{(1)} x + 2\pi n z / p)}; k_1 \triangleq \omega \sqrt{\varepsilon_1 \mu_0} \quad (1)$$

$$S_3 (x \leq -d) : H_y^{(3)} = e^{ik_1 z \sin \theta_0} \sum_{n=-N}^N t_n^{(3)} e^{-i(k_n^{(3)} (x+d) - 2\pi n z / p)} \quad (2)$$

$$k_n^{(j)} \triangleq \sqrt{k_0^2 \varepsilon_j / \varepsilon_0 - \gamma_n^2}; \gamma_n \triangleq k_1 \sin \theta_0 + 2\pi n / p, k_0 \triangleq 2\pi / \lambda, j = 1, 3.$$

where  $r_n^{(1)}$  and  $t_n^{(3)}$  are unknown coefficients to be determined by boundary conditions.

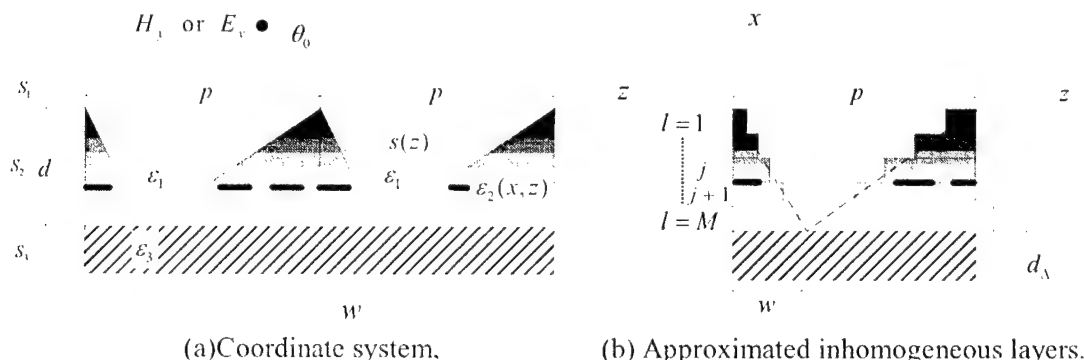


Fig.1 Structure of inhomogeneous dielectric grating with perfectly conducting strip.

Main process of our method to treat these problems is as follows (see Fig.1(b)):

(1) First, the grating layer ( $-d < x < 0$ ) is approximated by an assembly of  $M$  stratified layer of modulated index profile with step size  $d_\Delta (\triangleq d/M)$  approximated to step index profile  $\varepsilon^{(l)}(z) [\triangleq \varepsilon((l+0.5)d_\Delta, z); l=1 \sim M]$ , and the magnetic fields are expanded appropriately by a finite Fourier series.

$$S_z(-d < x < 0) : H_y^{(l,2)} = \sum_{v=1}^{2N+1} \left[ A_v^{(l)} e^{ih_v^{(l)}\{x+(l-1)d_\Delta\}} + B_v^{(l)} e^{ih_v^{(l)}(x+ld_\Delta)} \right] e^{ik_1 z \sin \theta_0} \sum_{n=-N}^N u_{n,v}^{(l)} e^{i2\pi n z/p} \quad (3)$$

where  $h_v^{(l)}$  is the propagation constant in the  $x$ -direction. We get the following eigenvalue equation in regard to  $h^{(l)}$  [3].

$$\Lambda_1 \mathbf{U}^{(l)} = \left\{ h^{(l)} \right\}^2 \Lambda_2 \mathbf{U}^{(l)} ; \Lambda_1 \triangleq [\eta_{m,n}^{(l)}], \Lambda_2 \triangleq [\zeta_{m,n}^{(l)}], l=1 \sim M, \quad (4)$$

where,  $\mathbf{U}^{(l)} \triangleq [u_{-N}^{(l)}, \dots, u_0^{(l)}, \dots, u_N^{(l)}]^T$ ,  $T$ : transpose,

$$\zeta_{n,m}^{(l)} \triangleq k_0^2 \varepsilon_{n,m}^{(l)} - \gamma_n \{ \gamma_n \eta_{n,m}^{(l)} + 2\pi(n-m)\eta_{n,m}^{(l)}/p \}, \gamma_n^{(l)} \triangleq (k_1 \sin \theta_0 + 2\pi n/p), \quad (5)$$

$$\eta_{n,m}^{(l)} \triangleq \frac{1}{p} \int_0^p \{ \varepsilon^{(l)}(z) \} e^{i2\pi(n-m)z/p} dz, \quad \xi_{n,m}^{(l)} \triangleq \frac{1}{p} \int_0^p \{ \varepsilon^{(l)}(z) \}^2 e^{i2\pi(n-m)z/p} dz, \quad m, n = -N, \dots, 0, \dots, N.$$

For the TM case, the permittivity profile approximated by a Fourier series of  $N_f$  terms<sup>[3]</sup> and  $N_f$  is related to the modal truncation number  $N (N=1.5N_f)$  [3].

(2) Second, the strip region ( $j < l < j+1$ ), see Fig.1(b), we obtain the matrix form combination of metallic region  $C$  and the dielectric region  $\bar{C}$  using boundary condition at the matching points  $z_k (= pk/(2N+1), k=0, \dots, 2N)$  on  $x = -l \cdot d_\Delta (l=j)$ . Boundary condition are as follows:

$$z_k \in C : [E_z^{(2,j)} = E_z^{(2,j+1)} = 0] \sum_{v=1}^{2N+1} h_v^{(j)} [A_v^{(j)} e^{ih_v^{(j)} d_\Delta} - B_v^{(j)}] \cdot \sum_{n=-N}^N u_{n,v}^{(j)} e^{inz_k} = 0, \quad (6)$$

$$\sum_{v=1}^{2N+1} h_v^{(j+1)} [A_v^{(j+1)} + B_v^{(j+1)} e^{ih_v^{(j+1)} d_\Delta}] \cdot \sum_{n=-N}^N u_{n,v}^{(j+1)} e^{inz_k} = 0$$

$$z_k \in \bar{C} : [H_y^{(2,j)} = H_y^{(2,j+1)}]$$

$$\sum_{v=1}^{2N+1} [A_v^{(j)} e^{ih_v^{(j)} d_\Delta} + B_v^{(j)}] \cdot \sum_{n=-N}^N u_{n,v}^{(j)} e^{inz_k} = \sum_{v=1}^{2N+1} [A_v^{(j+1)} + B_v^{(j+1)} e^{ih_v^{(j+1)} d_\Delta}] \cdot \sum_{n=-N}^N u_{n,v}^{(j+1)} e^{inz_k} \quad (7)$$

$$z_k \in \bar{C} : [E_z^{(2,j)} = E_z^{(2,j+1)}] : \frac{1}{\varepsilon^{(j)}(z)} \sum_{v=1}^{2N+1} h_v^{(j)} [A_v^{(j)} e^{ih_v^{(j)} d_\Delta} - B_v^{(j)}] \cdot \sum_{n=-N}^N u_{n,v}^{(j)} e^{inz_k} = \frac{1}{\varepsilon^{(j+1)}(z)} \sum_{v=1}^{2N+1} h_v^{(j+1)} [A_v^{(j+1)} + B_v^{(j+1)} e^{ih_v^{(j+1)} d_\Delta}] \cdot \sum_{n=-N}^N u_{n,v}^{(j+1)} e^{inz_k} \quad (8)$$

In the Eq.(8), the boundary condition at  $E_z^{(2,j)} = E_z^{(2,j+1)}$ , it is satisfied in all matching points. Therefor, rearranging after multiplying both sides  $\varepsilon_j(z) \cdot \varepsilon_{j+1}(z)$  in Eq.(8) by using the orthogonality properties of  $\{e^{i2\pi n z/p}\}$ , we get following equation.

$$\sum_{v=1}^{2N+1} h_v^{(j)} [A_v^{(j)} e^{ih_v^{(j)} d_\Delta} - B_v^{(j)}] \cdot \phi_{n,v}^{(j)} = \sum_{v=1}^{2N+1} h_v^{(j+1)} [A_v^{(j+1)} - B_v^{(j+1)} e^{ih_v^{(j+1)} d_\Delta}] \cdot \psi_{n,v}^{(j+1)}, \quad (9)$$

$$\text{where } \phi_{n,v}^{(j)} \triangleq \sum_{m=-N}^N u_{v,m}^{(j)} \eta_{m,n}^{(j)} \quad \psi_{n,v}^{(j+1)} \triangleq \sum_{m=-N}^N u_{v,m}^{(j+1)} \eta_{m,n}^{(j+1)}, \quad n = -N, \dots, 0, \dots, N.$$

By using matrix algebra in Eq.(9), we get following matrix form.

$$\Phi^{(j)} \mathbf{C}^{(j)} [\mathbf{D}^{(j)} \mathbf{A}^{(j)} - \mathbf{B}^{(j)}] = \Psi^{(j+1)} \mathbf{C}^{(j+1)} [\mathbf{A}^{(j+1)} - \mathbf{D}^{(j+1)} \mathbf{B}^{(j+1)}], \quad (10)$$

$$\text{where } \Phi^{(j)} \triangleq [\phi_{n,v}^{(j)}], \Psi^{(j+1)} \triangleq [\psi_{n,v}^{(j+1)}], \mathbf{C}^{(j)} \triangleq [h_v^{(j)} \cdot \delta_{(n+N+1),v}], \mathbf{D}^{(j)} \triangleq [e^{ih_v^{(j)} d_\Delta} \cdot \delta_{(n+N+1),v}], \delta_{(n+N+1),v} :$$

Kronecker's delta. We get following matrix form combined with Eq.(6) and Eq.(7).

$$\mathbf{H}^{(j)}[\mathbf{D}^{(j)}\mathbf{A}^{(j)} + \mathbf{D}^{(j)}\mathbf{B}^{(j)}] = \mathbf{H}^{(j+1)}[\mathbf{A}^{(j+1)} + \mathbf{D}^{(j+1)}\mathbf{B}^{(j+1)}] \quad @ \quad @ \quad @ \quad @ \quad @ \quad @ \quad @ \quad @ \quad (11)$$

$$\mathbf{H}^{(j)} = \left\{ \begin{array}{c} \left[ \begin{array}{cccc} \vdots & \vdots & \vdots & \vdots \\ e^{-iNz_k} & \dots & e^{i0z_k} & \dots & e^{iNz_k} \\ \vdots & \vdots & \vdots & \vdots \\ e^{-iNz_k} & \dots & e^{i0z_k} & \dots & e^{iNz_k} \end{array} \right] \left\{ \begin{array}{l} z_k \in C \\ z_k \in \bar{C} \end{array} \right. \cdot \mathbf{U}^{(j)} \cdot \left\{ \begin{array}{l} \mathbf{D}^{(j)} \triangleq [\eta e^{ih_v^{(j)} d_v} \cdot \delta_{(n+N+1),v}], \\ \eta = h_v^{(j)}; z_k \in C, \quad \eta = 1; z_k \in \bar{C} \\ \mathbf{D}^{(j)} \triangleq [\eta \cdot \delta_{(n+N+1),v}] \\ \eta = -h_v^{(j)}; z_k \in C, \quad \eta = 1; z_k \in \bar{C} \end{array} \right. \\ \\ \left[ \begin{array}{cccc} \vdots & \vdots & \vdots & \vdots \\ 0 & \dots & 0 & \dots & 0 \\ \vdots & \vdots & \vdots & \vdots \\ e^{-iNz_k} & \dots & e^{i0z_k} & \dots & e^{iNz_k} \end{array} \right] \left\{ \begin{array}{l} z_k \in C \\ z_k \in \bar{C} \end{array} \right. \cdot \mathbf{U}^{(j+1)} \cdot \left\{ \begin{array}{l} \mathbf{D}^{(j+1)} \triangleq [h_v^{(j+1)} e^{ih_v^{(j+1)} d_v} \cdot \delta_{(n+N+1),v}] \end{array} \right. \end{array}$$

(3) Finally, we obtain the relationship between  $\mathbf{A}^{(1)}, \mathbf{B}^{(1)}$  and  $\mathbf{A}^{(M)}, \mathbf{B}^{(M)}$ .

$$\begin{pmatrix} \mathbf{A}^{(1)} \\ \mathbf{B}^{(1)} \end{pmatrix} \triangleq \begin{pmatrix} \mathbf{S}_1^{(1)} & \mathbf{S}_2^{(1)} \\ \mathbf{S}_3^{(1)} & \mathbf{S}_4^{(1)} \end{pmatrix} \begin{pmatrix} \mathbf{S}_1^{(2)} & \mathbf{S}_2^{(2)} \\ \mathbf{S}_3^{(2)} & \mathbf{S}_4^{(2)} \end{pmatrix} \dots \begin{pmatrix} \mathbf{S}_1^{(j)} & \mathbf{S}_2^{(j)} \\ \mathbf{S}_3^{(j)} & \mathbf{S}_4^{(j)} \end{pmatrix} \dots \begin{pmatrix} \mathbf{S}_1^{(M)} & \mathbf{S}_2^{(M)} \\ \mathbf{S}_3^{(M)} & \mathbf{S}_4^{(M)} \end{pmatrix} \begin{pmatrix} \mathbf{A}^{(M)} \\ \mathbf{B}^{(M)} \end{pmatrix} = \begin{pmatrix} \mathbf{S}_1 & \mathbf{S}_2 \\ \mathbf{S}_3 & \mathbf{S}_4 \end{pmatrix} \begin{pmatrix} \mathbf{A}^{(M)} \\ \mathbf{B}^{(M)} \end{pmatrix} \quad (12)$$

where  $l \neq j$   $\mathbf{S}_k^{(l)} \triangleq \begin{bmatrix} {}^{(l)}s_{n,v}^{(k)} \end{bmatrix}$   $k=1 \sim 4$ ,  $l=1 \sim M$ ,

$${}^{(l)}s_{n,v}^{(1)} \triangleq \frac{1}{2} \left[ v_{n,v}^{(l)} + \theta_{n,v}^{(l)} h_{n+N+1}^{(l+1)} / h_v^{(l)} \right] e^{-ih_v^{(l)} d_v} {}^{(l)}s_{n,v}^{(2)} \triangleq {}^{(l)}s_{n,v}^{(3)} \cdot e^{i \{ h_{n,v}^{(l+1)} - h_v^{(l)} \} d_v},$$

$${}^{(l)}s_{n,v}^{(3)} \triangleq \left[ v_{n,v}^{(l)} - \theta_{n,v}^{(l)} h_{n+N+1}^{(l+1)} / h_v^{(l)} \right] / 2, \quad {}^{(l)}s_{n,v}^{(4)} \triangleq \frac{1}{2} \left[ v_{n,v}^{(l)} + \theta_{n,v}^{(l)} h_{n+N+1}^{(l+1)} / h_v^{(l)} \right] e^{ih_{n,v}^{(l+1)} d_v},$$

$$\mathbf{V} \triangleq [\mathbf{v}_{n,v}^{(l)}] = [\mathbf{U}^{(l)}]^{-1} \cdot [\mathbf{U}^{(l+1)}], \quad \Theta \triangleq [\theta_{n,v}^{(l)}] = [\Phi^{(l)}]^{-1} \cdot [\Psi^{(l+1)}],$$

$$l=j \quad \mathbf{FS}_k^{(j)} \triangleq \begin{bmatrix} {}^{(j)}s_{n,v}^{(k)} \end{bmatrix} \quad \mathbf{C}^{(j)} s_{n,v}^{(1)} \triangleq [v_{n,v}^{(1)} + d_{n,v}^{(1)}]^{-1} \cdot [v_{n,v}^{(2)} + \theta_{n,v}^{(1)}], \quad \mathbf{D}^{(j)} \triangleq [d_{n,v}^{(j)}],$$

$${}^{(j)}s_{n,v}^{(2)} \triangleq [v_{n,v}^{(1)} + d_{n,v}^{(1)}]^{-1} \cdot [v_{n,v}^{(3)} - \theta_{n,v}^{(1)} d_{n,v}^{(j+1)}] \quad \mathbf{C}^{(j)} s_{n,v}^{(3)} \triangleq [V_1^{-1} + \mathbf{D}^{-(j+1)}]^{-1} \cdot [V_1^{-1} V_2 - \mathbf{D}^{-(j+1)} \theta],$$

$${}^{(j)}s_{n,v}^{(4)} \triangleq [V_1^{-1} + \mathbf{D}^{-(j+1)}]^{-1} \cdot [V_1^{-1} V_3 - \mathbf{D}^{-(j+1)} \theta \mathbf{D}^{-(j+1)}] \quad \mathbf{GV}_1 \triangleq [v_{n,v}^{(1)}] = [\mathbf{H}^{(j)} \mathbf{D}^{(j)}]^{-1} \cdot [\mathbf{H}^{(j)} \mathbf{D}^{(j+1)}] \quad \mathbf{C}$$

$$\mathbf{V}_2 \triangleq [v_{n,v}^{(2)}] = [\mathbf{H}^{(j)} \mathbf{D}^{(j)}]^{-1} \cdot [\mathbf{H}^{(j+1)} \mathbf{D}^{(j+1)}], \quad \mathbf{V}_3 \triangleq [v_{n,v}^{(3)}] = [\mathbf{H}^{(j)} \mathbf{D}^{(j)}]^{-1} \cdot [\mathbf{H}^{(j+1)} \mathbf{D}^{(j+1)}]$$

$$\Theta \triangleq [\theta_{n,v}^{(j)}] = [\mathbf{C}^{(j)}]^{-1} \cdot [\Phi^{(j)}]^{-1} \cdot [\Psi^{(j+1)}] \cdot [\mathbf{C}^{(j+1)}].$$

Using Eq.(12), we get the following homogeneous matrix equation in regard to  $\mathbf{A}^{(M)}$ .

$$\mathbf{W} \cdot \mathbf{A}^{(M)} = \mathbf{F}, \quad \mathbf{W} \triangleq [\mathbf{Q}_1 \mathbf{S}_1 + \mathbf{Q}_2 \mathbf{S}_3 - (\mathbf{Q}_1 \mathbf{S}_2 + \mathbf{Q}_2 \mathbf{S}_4) \mathbf{Q}_4^{-1} \mathbf{Q}_3], \quad (13)$$

The mode power transmission coefficients  $|T_n^{(TM)}|^2$  is given by

$$|T_n^{(TM)}|^2 \triangleq \epsilon_1 \operatorname{Re} \left\{ k_n^{(3)} \right\} |t_n^{(3)}|^2 / (\epsilon_3 k_0^{(1)}) \quad (14)$$

## CONCLUSION

In this paper, we have proposed a new method for the scattering of electromagnetic waves by inhomogeneous dielectric gratings with perfectly conducting strip using the combination of improved Fourier series expansion method and point matching method.

## REFERENCES

- [1] Tamir, T., ed., Integrated Optics, Springer-Verlag, - p.110-118, 1979.
- [2] Tamir, T., M. Jiang and K. M. Leung, Modal Transmission-Line Theory of Composite Periodic Structures: I. Multilayered Lamellar Gratings, URSI International Symposium on Electromagnetic Theory, MIN-T2.25, pp.332-334, 2001.
- [3] Yamasaki, T., Tanaka, T., Hinata, T. and Hosono, T., Analysis of Electromagnetic Fields Inhomogeneous Dielectric Gratings with Periodic Surface Relief, Radio Science, Vol.31, No.6, pp.1931-1939, 1996.
- [4] Yamasaki, T., Hinata, T. and Hosono, T., Scattering of Electromagnetic waves by Plane Grating with Reflector, IECE Trans. in Japan., Vol.J61-B, No.11, p.953-961, 1978 (in Japanese). [translated Scripta Technica, INC., Vol.61, No.11 pp.52-60, 1978.

## **SIMULATION OF THE FINITE PHOTONIC CRYSTAL-BASED ADAPTIVE ANTENNA**

A.Bijamov, R.Zaridze, K.Tavzarashvili, V.Tabatadze.

Laboratory of Applied Electrodynamics, Tbilisi State University

e-mail: lae@access.sanet.ge

### **ABSTRACT**

The present work is dedicated to the FPC based adaptive antenna structure simulation. The effectiveness of the photonic crystals in such implementation is discussed. Several types of antenna devices are presented. The influence of the inaccuracy during the technical realization of the device is studied.

### **INTRODUCTION**

In the superhigh frequency band devices like mixers, separators, frequency filters, and splitter and so on are widely used. With the growth of operating frequency development of such devices also becomes complicated. In the sub-millimeter and optical frequencies range the devices of special type – so called photonic devices become efficient. The main part of such device is a crystal dielectric structure with the defects, introduced to it in special way. According to the nature of photonic crystals there are gaps in their spectrum, that causes some frequencies to be filtered out – and some – pass through. The ordinary absorbing media transforms the power of electromagnetic wave to heat. Instead, the band-gap does not dissipate power – it is accumulated and can therefore be supplied to necessary direction. The placements of defects in the crystal define its behavior towards the propagating wave – will it split, mix, or filter it. For example, one can introduce several “channels” to the crystal, that having different resonant capabilities will provide a way of exarticulation the carriers of different frequencies from the incoming signal. All these properties of the photonic crystals can be used also to develop an efficient antenna device having the specified parameters. Experimental way of developing and investigating such structures is either too time consuming and expensive, or quite impossible because some of the system’s properties can not be easily changed continuously, or the defect’s positions can not be arbitrary chosen.

In the present work several types of antenna are discussed, developed using the specially created software for the field propagation in FPC structures numerical simulation for the device’s parameters optimization

### **MODEL**

As a photonic crystal a rectangular body has been taken with the defects represented by the metallic rods, located inside it. The excitation is applied at the arbitrary point inside the crystal and is simulated by the cylindrical wire. The numerical solution of the corresponding electrodynamic problem is fulfilled using MAS [1]. By means of the created software several numerical results have been obtained, demonstrating the ability of such structure to serve as a core elements in complicated optical and SHF devices, as well as the capabilities of the software to analyze and simulate different configurations – to avoid expensive experimental development.

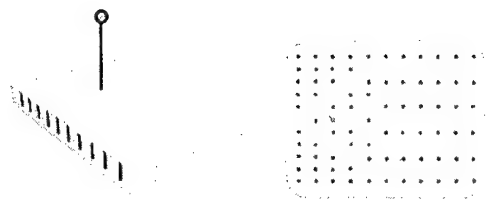


Fig 1. FPC antenna layout



Fig 2. Near field and radiation pattern

The presented sandwich-like antenna structure consists of a two metallic plates with the dielectric photonic crystal located between them (Fig.1). A periodical structure is formed by the homogeneously distributed metallic cylindrical rods inside the antenna volume. A defect is a vacancy – absence of the rod in the given cell. The antennas' feeding is supplied by a coaxial cable and is simulated by the linear current. The resonant channels are formed by the defects introducing a phase delays to the propagating in them wave, thus promoting the directed radiation behavior of the antenna. The near field distribution at the resonant frequency and the pattern of radiation is presented on Fig 2.



Fig 3. Near fields.

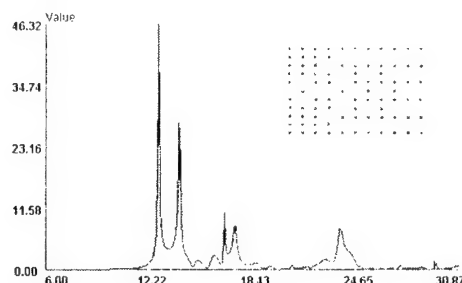


Fig 4. Frequency Response.

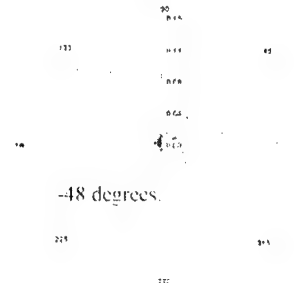


Fig 5. Patterns

In some application it is necessary for the antenna to be adaptive i.e. able to shift the beam of radiation electrically, for example, changing the phases of feeding currents. For this purpose, a slightly altered FPC structure has been developed, shown on Fig 3. The feeding is applied by the two phased sources.

On Fig. 4 the frequency response of an antenna is shown. The presented near field plot correspond to the first peak's left slope. The nearer the frequency is to the resonant one, the more effective will be radiation, but the beam shifting possibility will be decreased. This rectangular antenna may be implemented when just slight beam steering capabilities are needed.

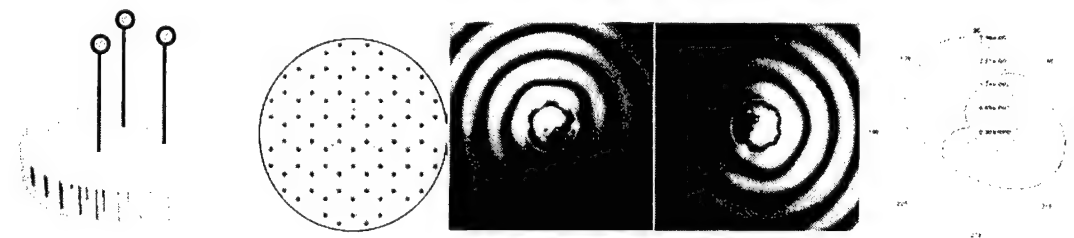


Fig 6. The hexagonal FPC structure, its near fields and Patterns at different feeding phases sets  
More flexible and omni-steerable antenna can be built up using the symmetrical hexagonal lattice as the core for the FPC (fig 6).

Here three independent sources are placed symmetrically relative to the lattice thus providing a possibility to radiate in fact, in any direction, depending on the feeding current's phases and amplitudes selection. The fig 5 show the near field distribution along with the corresponding patterns of radiation (fig 7). Such antenna can be used in some kind of radar or autotracking systems.

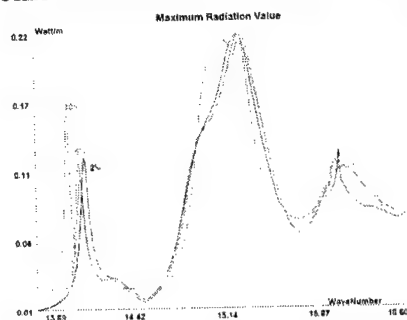


Fig. 8. Spectrum

The important thing, which must be taken into account when developing such devices, is how the inaccuracy in the real technical realization of the device may affect the position and Q-factor of the resonances and other radiation parameters. To investigate these conditions a possibility of giving the pseudo-random displacements to rod-s position and sized have been introduced and the influence on pattern, near field, and position of resonances has been studied.

As an under test problem the rectangular antenna has been chosen, as having the quite narrow resonant peak i.e. high Q-factor.

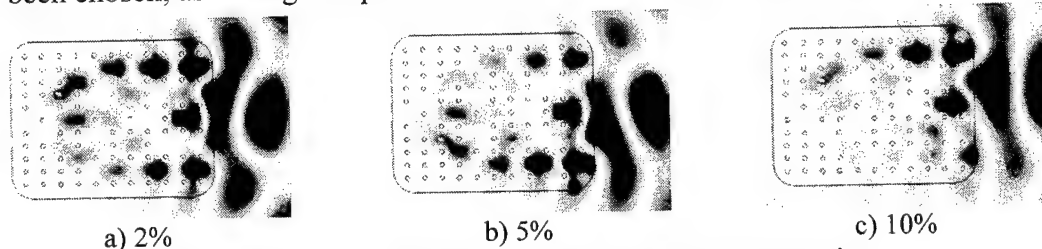


Fig. 9. Influence of inaccuracy during device implementation

The resulting frequency responses for the different assembly precision are shown on Fig 8. One can see that during realization of the device a precision of up to 5% is quite acceptable, and the lower precision lead to significant displacement of the operating frequency and completely changes the inner field distribution, leading to malfunctioning of the device Fig 9.

## CONCLUSIONS

FPC structures proved to be efficient for use as a core element in antenna devices, providing high degree of flexibility, and allowing to create complicated devices using simple core elements, such as metallic stocks, that is quite easy realizable by the modern technology. A software package has been developed allowing real time design and simulation of the FPC based devices, including the finite precision limitation of technical realization of the device, which makes it directly applicable for engineering calculations.

## REFERENCES

- [1] R. Zaridze, G. Bit-Babik, K. Tavzarashvili, N. Uzunoglu, D. Economou. "Wave Field Singularity Aspects Large-Size Scatterers and Inverse Problems." IEEE Transactions on Antennas and Propagation, vol. 50, No. 1, January 2002, p. 50-58.
- [2] J. Joannopoulos, R.Meade, J.Winn "Photonic Crystals: Modeling the flow of light", Princeton University Press, 1995



# A COMBINATION OF UP- AND DOWN-GOING PLANE WAVES USED TO DESCRIBE THE FIELD INSIDE GROOVES OF A DEEP GRATING

Yoichi Okuno, Da-Qing Zhou, Koji Yoshimoto, Akira Matsushima  
Kumamoto University, Kumamoto 860-8555, Japan  
Toyonori Matsuda

Kumamoto National College of Technology, Nishigoshi 861-1102, Japan

## INTRODUCTION

The purpose of the present research is to extend the range of application of Yasuura's method [1,2] in solving the problem of diffraction by a grating. Although alternative terminology for the method (e.g., a least-squares boundary residual method or a modified Rayleigh method) exists, we employ the name throughout this paper.

It is an accepted knowledge [3, 4] that Yasuura's method, in particular, the conventional Yasuura method with Floquet modes as basis functions does not have a wide range of application. Although the convergence of the sequence of solutions obtained by the method is proven, the rate of convergence is often so slow for deep gratings that we cannot find solutions with accuracy. Let  $D$  and  $2H$  be the period and the depth of a sinusoidal grating made of a perfectly conducting metal. The period is assumed to be comparable to the wavelength, i.e., we are working in the resonance region. For an E-wave (s polarization) problem where  $2H/D = 0.5$ , taking 71 Floquet modal functions, we can obtain a solution with 1 percent error in both energy conservation and boundary condition. Employment of additional Floquet modal functions easily causes numerical trouble in making least-squares approximation on the boundary. Hence, a practical limit in  $2H/D$  in the E-wave case is 0.5 so long as we use conventional double-precision arithmetic. Similarly, the limit in the H-wave (p polarization) case seems to be a little less than 0.4.

To accelerate the convergence of solutions, Yasuura's method is equipped with a smoothing procedure [5, 6]. It has been shown that: in the above problem, we can obtain a solution with 1 percent error using 17-41 modal functions (the number depends on the order of the smoothing procedure and on the polarization). Hence, Yasuura's method with the smoothing procedure is effective in making a systematic research that needs to handle problems with complicated boundaries, e.g., Fourier gratings.

Although Yasuura's method with the smoothing procedure solves most of the problems for commonly used gratings, the limit in  $2H/D$  has as yet been scarcely dealt with. There still is a limit at  $2H/D = 0.7$  or  $0.8$  even if we employ the smoothing procedure. This limitation can be removed practically by the following way. Here, *practically* means that we can solve the problem with a profile deep enough for our research work in the direction of our interest.

## STATEMENT OF THE PROBLEM

Let the cross section of the grating be periodic in  $X$  as shown in Fig. 1. The depth is in  $Y$  and  $y = f(x)$  represents the profile.  $f(x)$  is a sinusoidal function with a period  $D$  and a depth  $2H$ . The profile is the

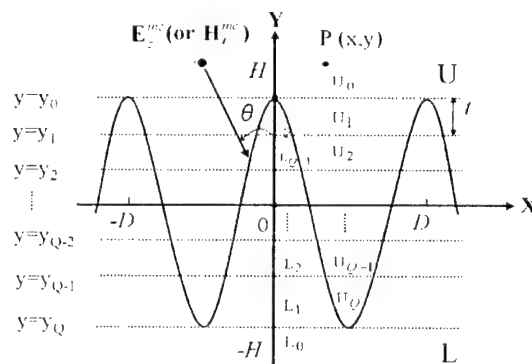


Fig. 1. Geometry of the problem.

boundary between two regions  $U(Y > f(X))$  and  $L(Y < f(x))$ .  $U$  is a vacuum and  $L$  is filled with a dielectric with a relative refractive index  $n$ . We consider the problem to seek diffracted waves in  $U$  and  $L$  assuming a plane E-wave incidence that comes from the positive  $Y$  direction.

## METHOD OF ANALYSIS

The basic idea of the present method includes two strategies. First, in constructing an approximate solution inside the grooves in  $U$  (or in  $L$ ), we employ down-going (or up-going) Floquet modes in addition to the up-going (or down-going) solutions. This would expand the function space spanned by the modal functions and make the boundary matching easy. Second, in consideration of the ill nature of higher-order evanescent modes (They strongly oscillate in  $X$  and rapidly increase or decrease in  $Y$ ), we divide the regions inside the grooves into a couple of sub-regions and define approximate solutions in each sub-region. This may be understood as a kind of normalization of the modal functions.

To do this, we first separate a groove region  $U_G$  ( $f(x) < Y < H$ ) from a free space region  $U_0$  ( $Y > H$ ).  $U_G$  and  $U_0$  are sub-regions of  $U$  having a common border at  $Y = H$ . Another groove region  $L_G$  ( $-H < Y < f(X)$ ) and a homogeneous half plane  $L_0$  ( $Y < -H$ ) are defined similarly. Approximate solutions in  $U_0$  and  $L_0$  take the form of commonly employed modal expansion satisfying the radiation condition. That is, an approximate solution in  $U_0$  (or in  $L_0$ ) is a sum of up-going (or down-going) plane waves.

Next, we slice the groove regions to have  $Q$  layers.  $U_G$  is divided into  $\{U_1, U_2, \dots, U_Q\}$  and a horizontal line  $Y = (1 \pm 2q/Q)H$  ( $q = 0, 1, \dots, Q \pm 1$ ) is the boundary between  $U_q$  and  $U_{q+1}$ . Similarly,  $L_G$  is divided into  $\{L_1, L_2, \dots, L_Q\}$  by horizontal lines  $Y = (2r/Q \pm 1)H$  ( $r = 0, 1, \dots, Q \pm 1$ ). Consequently, we have  $2Q$  sub-regions in one period ( $0 < X < D$ ). As a matter of fact, we have  $3Q$  sub-regions because either  $U_G$  or  $L_G$  should be partitioned into two. We, however, regard the groove region consists of  $2Q$  sub-regions because the latter partition is not essential. Each sub-region has its own local coordinates and modal functions are defined in each sub-region. It should be noted that: the set of modal functions in  $U_q$  includes not only up-going separated solutions but also down-going solutions. Similarly, the set in  $L_r$  includes both down- and up-going waves. An approximation in a sub-region ( $U_q$  or  $L_r$ ;  $q, r = 1, 2, \dots, Q$ ) is a finite sum of up- and down-going modal functions with unknown modal coefficients.

Now we have  $2(2N+1)(2Q+1)$  unknown coefficients in total:  $2(2N+1)$  for  $U_0$  and  $L_0$ ;  $2Q(2N+1)$  for  $U_q$ ; and  $2Q(2N+1)$  for  $L_r$ . Here,  $N$  is the number of truncation and summation should be taken from  $-N$  through  $N$ . The coefficients are determined so that the approximate solutions satisfy the boundary conditions. We employ the least-squares method noting that a sub-region is enclosed with two horizontal lines and a part of grating profile.

## NUMERICAL RESULTS AND DISCUSSIONS

Results of numerical computation and a couple of comments are itemized as follows:

- (1) If  $2H/D < 0.5$ , the result obtained by the present method agrees well with the results by the conventional Yasuura method.
- (2) Comparison with an existing data [7] shows good agreement at  $2H/D = 1.0$  for an E-wave incidence (Figs. 2 and 3 ( $Q = 4, N = 11, 0.04\%$  energy error)) and for an H-wave incidence (Figs. 4 and 5 ( $Q = 13, N = 16, 0.9\%$ )).
- (3) A personal computer (Pentium 1.7 GHz, RAM 512 MB) can handle an E-wave problem with a depth  $2H/D = 1.7$  ( $Q = 11, N = 7, 1\%$ ; or  $16, 5, 0.4\%$ ). Because this limitation in  $2H/D$  comes from memory requirement, we can employ the technique of sequential accumulation [8] to extend the range of application.
- (4) If we construct approximations in  $U_q$  (or in  $L_r$ ) employing up-going (or down-going) waves alone, we cannot obtain convergent solutions for  $2H/D > 1.0$ . This means that the normalization of the modal functions alone is not so effective as the combined strategies.

- (5) We have succeeded in establishing a method of modal-expansion that solves the problem of deep gratings. We are planning to employ the method in solving the problem of a stratified grating in which the boundaries between layers have a common period but do not have a common profile.

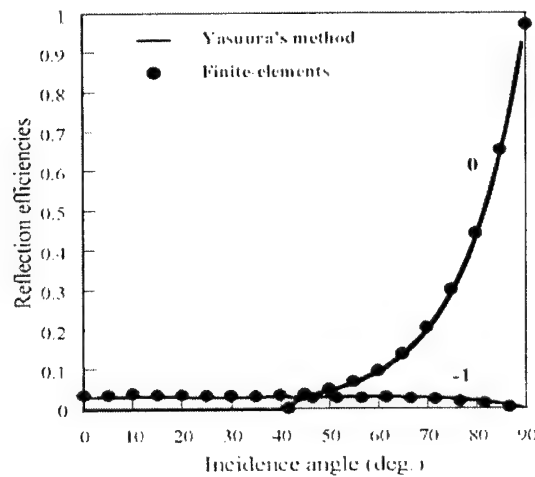


Fig. 2. Reflection efficiency (E-wave)

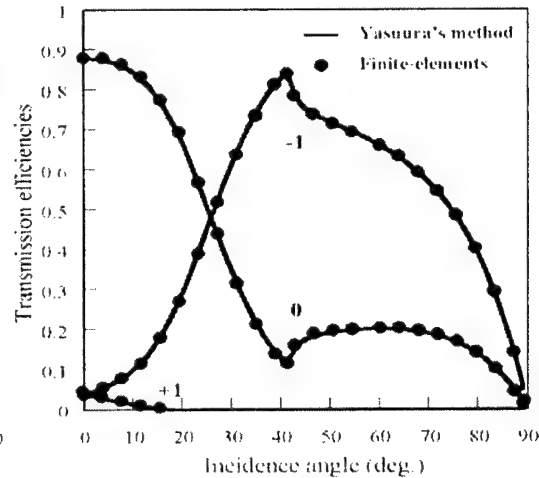


Fig. 3. Transmission efficiency (E-wave)

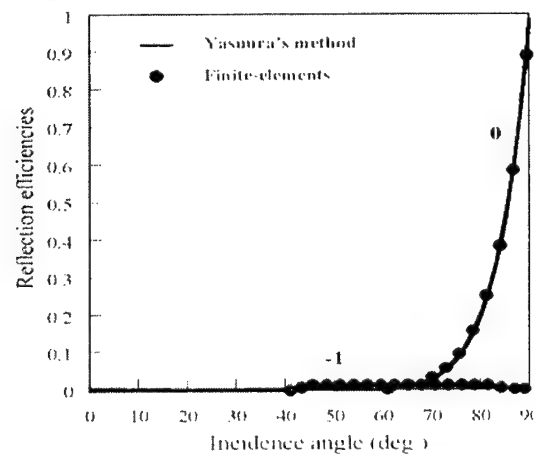


Fig. 4. Reflection efficiency (H-wave)

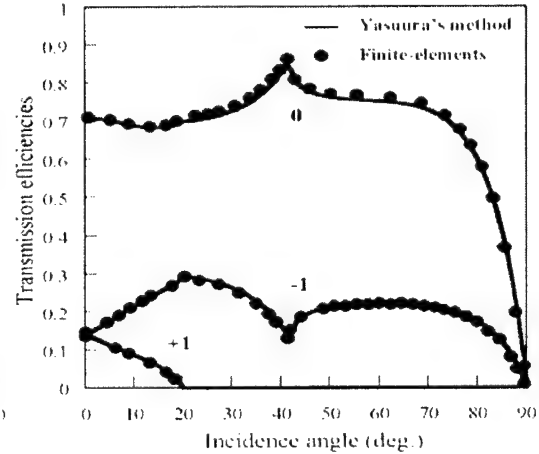


Fig. 5. Transmission efficiency (H-wave)

## REFERENCES

- [1] K. Yasuura and T. Itakura, Approximation method for wave functions (I), (II), and (III), *Kyushu Univ. Tech. Rep.*, **38**, 1, 72-77 (1965); **38**, 4, 378-385 (1966); **39**, 1, 51-56 (1966).
- [2] K. Yasuura, A view of numerical methods in diffraction problems, in *Progress in Radio Science 1966-1969* (W.V. Tilson and M. Sauzade, eds.), 257-270, URSI, Brussels (1971).
- [3] J.P. Hugonin, R. Petit, and M. Cadilhac, Plane-wave expansions used to describe the field diffracted by a grating, *J. Opt. Soc. Amer.*, **71**, 5, 593-598 (1981-05).
- [4] P.M. van den Berg, Reflection by a grating: Rayleigh methods, *J. Opt. Soc. Amer.*, **71**, 10, 1224-1229 (1981-10).
- [5] K. Yasuura and H. Ikuno, Smoothing process on the mode-matching method for solving two-dimensional scattering problems, *Mem. Fac. Eng. Kyushu Univ.*, **37**, 4, 175-192 (1977).
- [6] K. Yasuura and Y. Okuno, Singular-smoothing procedure on Fourier analysis, *Mem. Fac. Eng. Kyushu Univ.*, **41**, 2, 123-141 (1981).
- [7] Y. Nakata, M. Koshiba, and M. Suzuki, Finite-element analysis of plane wave diffraction from dielectric gratings, *Trans. IECE Jpn. C*, **J69-C**, 12, 1503-1511 (1986-12).
- [8] C.L. Lawson and R.J. Hanson, *Solving Least-Squares Problems*, Prentice-Hall, Engle-wood Cliffs, NJ (1974).

## SCATTERING AND ABSORPTION OF LIGHT BY NANO-THICKNESS NEGATIVE-DIELECTRIC STRIP GRATINGS.

T.L. Zinenko\*, A.I. Nosich,

Institute of Radiophysics & Electronics NASU, ulitsa Proskury 12, 61085 Kharkov, Ukraine,  
Email: zinenko@ire.kharkov.ua

In the innovative optoelectronics, “negative-dielectrics” (ND) are considered as promising materials. Metals, like silver and gold, are ND in visible light and near-infrared range. The goal of the present paper is to study the problems of the plane wave scattering of light by a thin flat grating made of penetrable ND strips or of impenetrable strips covered with ND from one or both sides. Strip gratings have been used in wide range of applications. Several techniques have been devised for building the numerical solutions to perfectly conducting strip gratings and also to penetrable imperfect ones, like resistive and thin dielectric strip gratings: the spectral Galerkin moment method [1], the Fourier transformation method [2], the singular integral equation method with projection to orthogonal polynomials [3], and the method of analytical regularization of dual series equations [4].

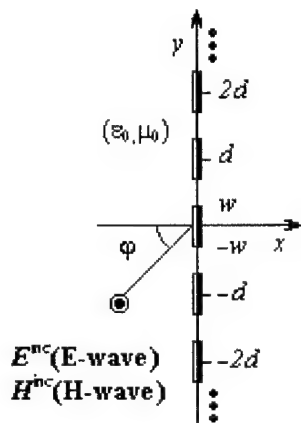


Fig.1. Geometry of the Problem

The problem formulation involves a set of generalized boundary conditions, relating tangential fields to effective electric and magnetic currents. The strip coatings are characterized by two surface impedances  $Z^\pm$  on corresponding sides. Notations can be seen in Fig.1. Accurate numerical solution is based on the Floquet-Rayleigh field expansions, which lead to the coupled pair of the dual-series equations for the series coefficients. To determine the unknown coefficients  $a_n$  and  $b_n$ , we use two dual sets of boundary conditions that hold on the complimentary subintervals (the strip and the slot) of the elementary period. Further, we make an extraction and analytical inversion of the static part of the full-wave dual-series equations that

needs combined application of the Riemann-Hilbert problem (RHP) technique and inverse Fourier transform depending on the equation features. This procedure leads to the simultaneous linear equations:

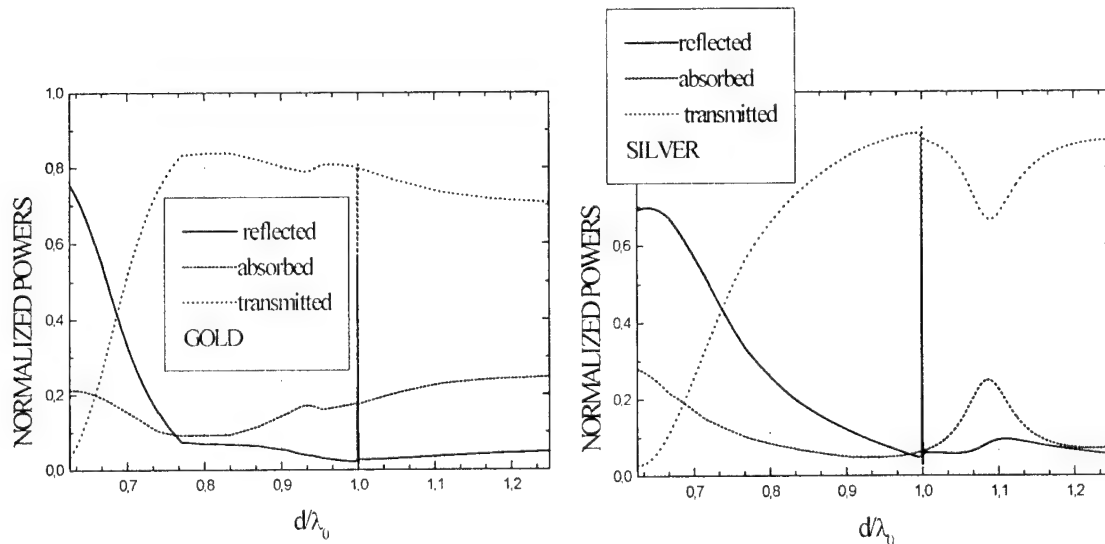
$$\begin{cases} \sum_{n=-\infty}^{\infty} \left[ \left( \delta_{mn} + A_{E(H),mn}^{11} \right) x_n + A_{E(H),mn}^{12} d_n \right] = B_{E(H),m}^1 \\ \sum_{n=-\infty}^{\infty} \left[ A_{E(H),mn}^{21} x_n + \left( \delta_{mn} + A_{E(H),mn}^{22} \right) d_n \right] = B_{E(H),m}^2 \end{cases} \quad (1)$$

With the matrix and right-hand-part elements:

$$\left\{ \begin{array}{l} A_{E,mn}^{11} = \frac{1}{2(R/\zeta_0)g_n} S_{mn}(\theta) \\ A_{E,mn}^{12} = -\frac{W}{(R/\zeta_0)} S_{mn}(\theta) \\ B_{E,m}^1 = -\frac{1}{(R/\zeta_0)} S_{m0}(\theta) \\ A_{E,mn}^{21} = 2j\kappa W T_{mn}(\theta) \\ A_{E,mn}^{22} = (2j\kappa(Q\zeta_0) - r_n) T_{mn}(\theta) \\ B_{E,m}^2 = 2r_0 T_{m0}(\theta) \end{array} \right. \quad \left\{ \begin{array}{l} A_{H,mn}^{11} = \frac{1}{2(Q\zeta_0)g_n} S_{mn}(\theta) \\ A_{H,mn}^{12} = -\frac{W}{(Q\zeta_0)} S_{mn}(\theta) \\ B_{H,m}^1 = -\frac{1}{(Q\zeta_0)} S_{m0}(\theta) \\ A_{H,mn}^{21} = -2j\kappa W T_{mn}(\theta) \\ A_{H,mn}^{22} = (2j\kappa(R/\zeta_0) - r_n) T_{mn}(\theta) \\ B_{H,m}^2 = 2r_0 T_{m0}(\theta) \end{array} \right. \quad (2)$$

where  $T_{mn}(\theta)$  and  $S_{mn}(\theta)$  can be found in [4],  $g_n = (1 - (\sin\phi + l/\kappa)^2)^{1/2}$ ,  $r_n = |n| - jg_n\kappa$ ,  $\kappa = d/\lambda_0$ , and  $\theta = 2\pi w/d$ . The unknown coefficients are  $x_n = c_n g_n$ ,  $c_n = a_n + b_n$ ,  $d_n = a_n - b_n$ . It can be shown that (1) is a Fredholm second kind equation and therefore yields stable and accurate numerical solution with accuracy controlled by the truncation number  $N$  of each block. According to [5], three complex parameters,  $R$ ,  $Q$ , and  $W$ , are electric, magnetic, and cross resistivities.  $W$  is responsible for different properties of the two faces and vanishes for a surface with two identical face impedances and for a penetrable ND strip grating.

Numerical computations have been carried out for the reflected, transmitted, and absorbed power fractions as a function of the electrical and material parameters of the ND grating. In Fig.2. we present several samples of plots of the reflected, transmitted, and absorbed powers versus the normalized period of the gratings made of gold, silver, and platinum for the H-wave case. These gratings are penetrable and  $W=0$  in this case. One can see that for the gratings made of gold and silver the reflected power prevails over transmitted and absorbed ones in the frequency range  $0.6 < d/\lambda_0 < 0.7$  whereas the transmitted power prevails over the reflected and absorbed powers for most of optical



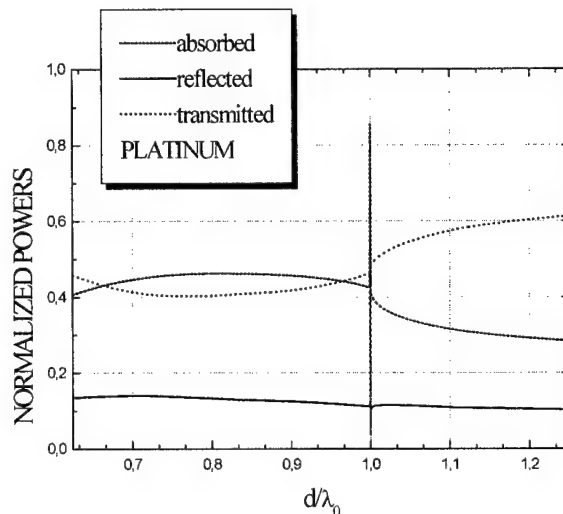


Fig.2. Normalized powers for H-wave scattering by strip gratings versus the electrical period.  
 $2w/d=0.5$ ,  $\varphi=0^0$ ,  $h/d=0.02$ ,  $d=5 \cdot 10^{-7}$  m.

range starting with  $0.7 d/\lambda_0$ . The values of transmission are quite comparable and run up to 0.9. The absorption by the grating made of platinum exceeds the transmission and reflection in the frequency range  $0.65 < d/\lambda_0 < 1$  and transmission prevails over absorption and reflection for the rest of optical range. The reflection stays low over all optical range. Fig.2 demonstrates a deep drop of transmission for all gratings and a rise of absorption for a grating made of platinum near the  $\pm$  first Wood's anomaly ( $\kappa=1$ , for the normal incidence).

We have developed accurate numerical solutions to the scattering problems concerning the ND strip gratings in free space. The computations have been carried out for the reflected, transmitted, and absorbed power fractions as a function of the electrical and material parameters of the grating.

## REFERENCES

- [1] R.C. Hall, and R.Mitra, "Scattering from a periodic array of resistive strip", *IEEE Trans. Antennas Propag.*, Vol.AP-33, pp.1009-1011, 1985.
- [2] R.Petit, and G.Tayeb, "Theoretical and numerical study of gratings consisting of periodic arrays of thin and lossy strips," *J.Opt. Soc. Am. A*, Vol.7, pp.1686-1692, 1990.
- [3] A.Matsushima, T.L.Zinenko, H.Minami and Y.Okuno, Integral Equation Analysis of Plane Wave Scattering from Multilayered Resistive Strip Gratings, *J. Electromagnetic Waves Applicat.*, Vol.12, pp.1449-1469, 1998.
- [4] T.L.Zinenko, A.I.Nosich, and Y.Okuno, "Plane wave scattering and absorption by resistive-strip and dielectric-strip grating." *IEEE Trans. Antennas Propag.*, Vol.AP-46, pp.1498-1505, 1998.
- [5] E.Bleszynski, M. Bleszynski, and T.Jaroszewicz, "Surface-integral equations for electromagnetic scattering from impenetrable and penetrable sheets," *IEEE Antennas Propagat. Mag.*, Vol.36, pp.14-25, 1993.

## RECONSTRUCTION OF PERIODIC BOUNDARY BETWEEN DIELECTRIC MEDIA

Jean Chandezon<sup>1</sup>, Anatoliy Ye. Poyedinchuk<sup>2</sup>, and Nataliya P. Yashina<sup>1,2</sup>

<sup>1</sup> Universite B. Pascal, Clermont-Ferrand, France

<sup>2</sup> IRE NASU, Kharkov 61085, Ukraine. Email: nataliya@lin.com.ua

Boundary shape analysis and reconstruction is important area of research [1-4], however there is a shortage of rigorous approaches. We propose a robust and clear modification of the known C method [5,6] for solving the wave scattering by arbitrarily shaped surface. This approach makes a reliable basis for solution of recognition problem: the reconstruction of surface profile and material parameters of media from known data on the scattered field.

For the *direct problem* solution, the C-method in combination with  $\alpha$  regularisation has been chosen [5,6]. This enables us to reduce the original 2D problem of linearly polarized plane wave diffraction by an arbitrary boundary of dielectric media to operator equation

$$\alpha X + AX = C, \quad (1)$$

where  $\alpha$  is regularizing parameter,  $A$  is a self-adjoint positively defined compact operator in corresponding Hilbert space  $H = l_2 \times l_2$ . The entries of unknown vector  $X$  are coefficients of scattered field that is expanded over eigenfunctions of C-method [5,6]. Vector  $C$  is defined by the excitation field. For boundary shape between media and given dielectric parameters the equation (1) can be solved efficiently by means of truncation method. The choice of regularising parameter  $\alpha$  may be done on the base of generalised residual principle [7,8]. The input data for correspondent *inverse problem* are complex amplitudes  $R = (R_n(\lambda))_{n=-N}^N$  of reflected propagating waves,  $\lambda$  is a wavelength. We suppose that this data are known in certain wavelength range  $[\lambda_1, \lambda_2]$ . Besides the period of boundary shape and dielectric parameters of media are also known. It is necessary do find out by these input data the function, describing the boundary of two media. Let  $a = (a_n)_{n=-\infty}^{\infty}$  be Fourier coefficients of this boundary function. The solution of operator equation (1) gives the mapping that associates set of  $a = (a_n)_{n=-\infty}^{\infty}$  with set of complex amplitudes  $R = (R_n(\lambda))_{n=-N}^N$ . Thus, on certain set of vectors  $D_F \subset l_2$  the non linear operator

$$F(a, \lambda) = R(\lambda), \quad \lambda \in [\lambda_1, \lambda_2] \quad (2)$$

is defined. Having found out from (2) the Fourier coefficients  $a = (a_n)_{n=-\infty}^{\infty}$ , we can, by summation of Fourier series with approximate in  $l_2$ -space metric coefficients [7], derive the profile function. Formally, the scheme can be outlined as follows. Let  $Y(\lambda)$ , that is the solution of (2), is the set of operator  $F$  values. Introduce on  $Y(\lambda)$  the norm according following formula  $\|R(\lambda)\|_l^2 = \sum_{n=-N}^N |R(\lambda)|^2 \frac{\cos \theta_n}{\cos \theta}$ . Here following notations are used:  $\theta_n$  are angles of diffracted field,  $\theta$  is angle of incident field. Consider the functional that is given in definitional domain  $D_F$  of operator  $F$

$$\Phi(a) = \sum_{m=1}^M \sum_{n=-P(\lambda_m)}^{P(\lambda_m)} \left| R_n^e(\lambda_m) - R_n^M(\lambda_m) \right|^2 \frac{\rho_n(\lambda_m)}{\kappa \sqrt{\varepsilon_1 \mu}} + \gamma \sum_{n=-Q}^Q |a_n|^2 (1 + n^{2R}) \quad (3)$$

where  $\gamma > 0$ , is the parameter of regularization,  $R > 0$ ,  $\rho_n = \sqrt{\kappa_m^2 \varepsilon_1 \mu - n^2}$ ,  $\kappa_m = d/\lambda_m$ ,  $d$  is a period of boundary,  $\lambda_n \in [\lambda_1, \lambda_2]$ ,  $a(v) = \sum_{n=-Q}^Q a_n e^{inv}$ . Vector  $a_\gamma^p = (a_{\gamma m})_{m=-p}^p$ , which provides the functional (3) with minimum we consider to be a solution to (2).

**Numerical experiments.** On the basis of the approach developed the numerical algorithms for the solving (1) and (2) have been implemented. The search of vector  $a_\gamma^p$  is organized by means of regularized quasi Newton's method with step adjustment, using only first derivatives. The minimum residual method is applied for the choice of regularizing parameter  $\gamma$ . Based on (1), we simulated input data  $R^e(\lambda_m) = (R_n^e(\lambda_m))_{n=-N}^N$ ,  $m=1,2,\dots,P$  for several boundaries between media characterized by profiles:

$$a_1(y) = h \left[ 0.5 + \frac{\pi^3 y}{6d} \left( \frac{2y}{d} - 1 \right) \left( 1 - \frac{y}{d} \right) \right], \quad a_2(y) = h \left[ 0.375 + 0.25 \sin\left(\frac{2\pi y}{d}\right) + 0.125 \cos\left(\frac{4\pi y}{d}\right) \right],$$

$$a_3(y) = h \left[ 0.5 - \frac{4}{\pi^2} \left( \cos\left(\frac{2\pi y}{d}\right) + \frac{1}{9} \cos\left(\frac{6\pi y}{d}\right) + \frac{1}{25} \cos\left(\frac{10\pi y}{d}\right) \right) \right]$$

periodically continued from interval  $[0, d]$  onto interval  $(-\infty, +\infty)$ . Parameters  $d$  and  $h$  satisfy the restriction  $2\pi h/d \leq 1$ . The wavelength of incident plane  $E$  polarized wave was varying within the range  $0.5 \leq d/\lambda \leq 3.5$ . Permittivity of the first medium has been chosen as  $\varepsilon_1 = 1$  and of the second one as  $\varepsilon_2 = 2.25$ . Permeability of both media is  $\mu = 1$ . Functions  $a_1(y)$ ,  $a_2(y)$  are chosen for they belong to two essentially different classes. Namely, function  $a_2(y)$  has a finite series of its Fourier coefficients. In the contrary, function  $a_1(y)$  and  $a_3(y)$  have an infinite Fourier series, which Fourier coefficients have algebraic type of decaying only. Results of numerical tests are presented in Fig. 1. Solid lines correspond to the exact functions  $a_i(y)$ ,  $i=1,2,3$ . Lines depicted as crosses are the graphs of functions  $a_1^R(y)$  and  $a_2^R(y)$  that have been defined via input data  $R^e(\lambda_m) = (R_n^e(\lambda_m))_{n=-N}^N$  according to above described algorithm. As they almost coincide with graphic accuracy, the deviations  $10h^{-1} \left| a_i(y) - a_i^R(y) \right|$ ,  $i=1,2,3$  are presented in the same figures as dotted lines. It worth to emphasize that maximum absolute value of deviation essentially decreases with value of points  $P$  increases (we remind that  $P$  is a number of values of incident plane wave wavelengths, for which the input data,  $m=1,2,\dots,P$ , have been calculated) that is in compliance with given level of noise in input data  $R(\lambda_m) = (R_n(\lambda_m))_{n=-N}^N$ . Rather good approximation used for starting values of Fourier coefficients guarantees the shape reconstruction with accuracy  $10^{-2} - 10^{-3}$ . These algorithms are efficient tools for the study of influence of input data errors on the accuracy of boundary shape reconstruction.



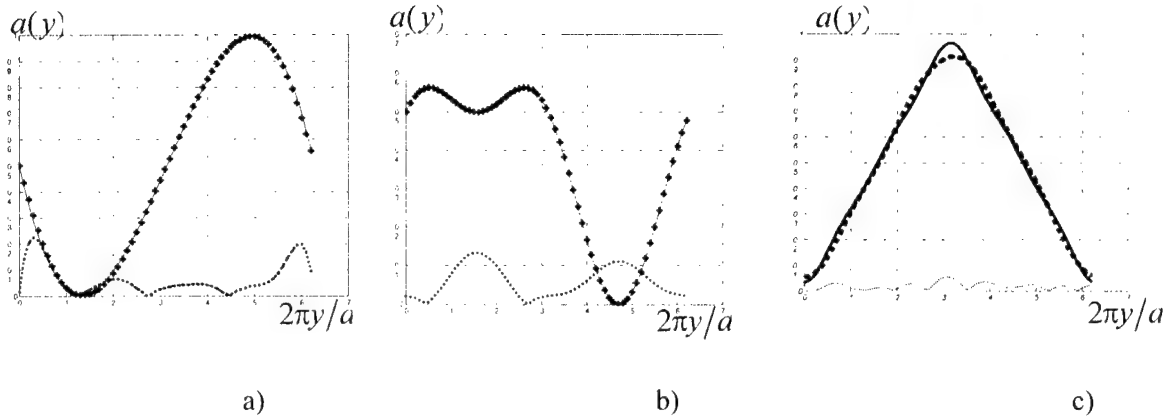


Figure 1. Reconstruction of profiles given by functions  $a_1(y)$  (a),  $a_2(y)$  (b), and  $a_3(y)$  (c) for the values  $P = 6$ ,  $\varepsilon_2 = 2.25$ ,  $0.5 \leq d/\lambda \leq 3.5$ ,  $2\pi h/d = 0.4$ .

It is well known that one of the most complicated problems in solving unstable problems of reconstruction is the problem of matching regularizing parameter  $\alpha$  with given level of errors in input data  $R_{mn}^e$ . We have demonstrated that such tradeoff can be obtained by means of residual method [7, 8]. We shall demonstrate this statement for the test problem for reconstruction shape of the surface, described by the function  $a_2(y)$ . Basing on the solution to direct problem we have calculated the input data  $R_{mn}^e = R_m^e(\lambda_n)(1 + \gamma \cdot Rand)$  for various levels of relative error  $\gamma$ . The error  $Rand$  has been simulated by the generator of random numbers with normal distribution. One of the numerical examples is presented in Fig. 2. In fragment a) you can see the characteristic behavior of relative error of profile reconstruction has been estimated according

formula 
$$\delta(\alpha) = \left( \frac{\sum_n |a_n^e - a_n^\alpha|^2 (1 + |n|^2)}{\sum_n |a_n^e|^2} \right)^{1/2}, \quad \text{calculated for numbers of}$$

$\alpha = 10^{-n}, n = 1, 2, \dots, N; N \leq 10$ . Here  $a_n^e$  are exact values of function  $a_2(y)$  Fourier coefficients. As it is clearly seen the function  $\delta(\alpha)$  has pronounced minimum, that appears for all considered levels of error  $\gamma$ . In pictures b) and c) the results of boundary shape reconstruction are presented. Relying on our numerical experiment we can conclude that reconstruction can be performed with best accuracy for that value of  $\alpha$ , that provides minimum to function  $\delta(\alpha)$ .

The residual method can provide reliable determination of optimal value of  $\alpha$  according to

relation  $\alpha_{opt} = \sup_{\alpha} (\alpha : \Delta_{\alpha}(\gamma) \leq \gamma)$ . Here 
$$\Delta_{\alpha} = \left( \frac{\sum_n |R_{mn}^e - R_{mn}^{\alpha}|^2}{\sum_n |R_{mn}^e|^2} \right)^{1/2}$$
 is a relative residual of

input data  $R_{mn}^e$  and  $R_{mn}^{\alpha}$ , that are the results of the solution of direct problem, calculated for function  $a_2^{\alpha}(y)$  found out from minimization of (3) for given  $\gamma$ . From the results of numerical experiments we can see, that  $\Delta_{\alpha}(\gamma)$  depends on  $\alpha$  monotonically, and, thus  $\alpha_{opt}$  is unique for each level of input data errors. The suggested algorithm, which performs reconstruction of shape of periodic boundary between two dielectric media relying on information about

diffraction harmonics that are known within certain interval of wavelength, requires certain starting approximation for Fourier coefficients of function  $a(y)$  describing boundary. Such an approximation can be constructed by generalizing results of [10].

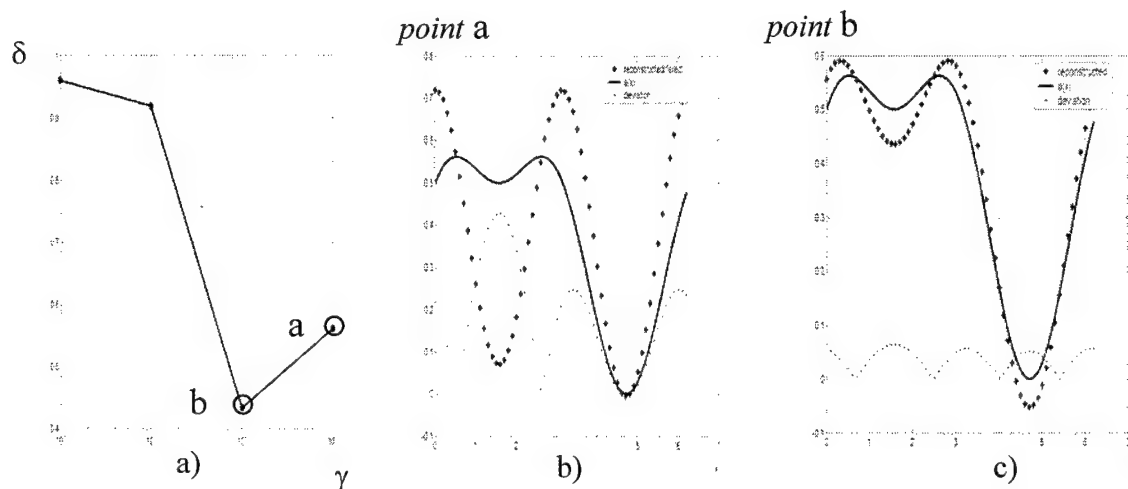


Fig.2

## REFERENCES

- [1] P. van Oevelen, D. Hoekman, Radar backscatter inversion technique for estimation of surface soil moisture: EFEDA-Spain and HAPEX-Sahel case Studies, *IEEE Trans. Geoscience Remote Sensing*, 1999, vol. GE-37, pt. I, no 1.
- [2] E. G. Njoku, *et al.*, Evaluation of an inflatable antenna concept for microwave sensing of soil moisture and ocean salinity. *IEEE Trans. Geo. Rem. Sens.*, 1999, vol. 37, pt. I, no 1.
- [3] E. G. Njoku, L. Li, Retrieval of land surface parameters using passive micro wave measurements at 6-18 GHz, *IEEE Trans. Geosci. Remote Sens.*, 1999, vol. GE-37, pt. I, no 1.
- [4] D. N. Ostrov. Boundary conditions and fast algorithms for surface reconstruction from Synthetic aperture radar data, *IEEE Trans. Geosci. Remote Sens.*, 1999, vol. 3, pt. II, no 1.
- [5] L. Li, J. Chandezon, G. Granet, J-P. Plumey, A rigorous and efficient grating analysis method made easy for optical engineers, *J. Optical Society of America*, 1999, no 1.
- [6] J. Chandezon, A. Poyedinchuk, N. Yashina, Diffraction of electromagnetic waves by periodic boundary between two media: C method and Tikhonov's regularization." *Proc. URSI Int. Symp. EM Theory*, Victoria, 2000, pp.241-242.
- [7] A.N. Tikhonov, V.Y. Arsenin, *Methods of Solution of Ill Posed Problems*, Moscow, Nauka, 1986 (in Russian).
- [8] V.K. Ivanov, V.V. Vasin, V.P. Talanov, *Theory of Linear Ill Posed Problems and its Applications*, Moscow, Nauka, 1978 (in Russian).
- [9] J. Chandezon, A. Y. Poyedinchuk, N. P. Yashina. Study of dielectrics' electromagnetic properties: resonant scattering and parameter reconstruction, *J. Europeennes sur les Methodes Numeriques en Electromagnetisme*. (JEE'02), Toulouse, 2002.
- [10] V. Hadson, J. Pim, *Application of Functional Analysis in Operator Theory*. Moscow, Mir, 1987 (translated from English).

## REFLECTIVE PROPERTIES OF GRID STRUCTURES WITH DIELECTRIC COATING

Mikalai U. Sitsko, Valerij I. Demidchik.

Belarusian State University, Department of Radiophysics, Minsk, Belarus.

E-mail: demidvi@bsu.by

### ABSTRACT

The based on the solution of an integral equation method for calculating electrodynamic characteristics of a half-wave dipole located above the grid screen with dielectric coating is considered in the article. The acquired analysis results allow to estimate the influence of geometric parameters of the screen and dielectric parameters on radiation characteristics.

Grid screens are widely used in antenna techniques. They are used in various devices for electromagnetic protection, as reflectors of mirror and dipole antennas, as screens of passive retranslation. Depending on the function of antenna system application of a grid screen allows to solve such problems as mass reduction, wind impact reduction etc. While exploiting these systems quite possible is the formation of different kinds of thin coating, ice for instance, that can be approximated to an ideal dielectric. That is the practical importance of the research work concerned with modeling of electrodynamic properties of grid structures.

Usually the reflective properties of grid screens are considered using the results of solving the task of a plane electromagnetic wave incident on the grid of infinite dimensions [1]. But in practice we deal with systems of finite dimensions.

The purpose of this work is to model the radiation characteristics of half-wave dipole located above the grid screen covered with dielectric and to determine the dependence of these characteristics on dielectric permittivity and dielectric layer thickness.

The solution of this task was found within the limits of thin-wire approximation using an integral equation which is an analogue of Pocklington's equation for thin ideal conductors [2]:

$$\int_L I(s') K(s, s') ds' = i\omega\epsilon_0 E'_\tau \quad (1)$$

$$K(s, s') = -k^2 \overline{ss'} G_a(s, s') + \frac{1}{\epsilon_r} \frac{\partial^2}{\partial s \partial s'} G_a(s, s') + \frac{\epsilon_r - 1}{\epsilon_r} \frac{\partial^2}{\partial s \partial s'} G_b(s, s') \quad (2)$$

$$G_{a,b} = \frac{e^{-ikr_{a,b}}}{2\pi r_{a,b}}, \quad r_a = \sqrt{\sum_{i=1}^3 (x_i - x'_i)^2 + a^2}, \quad r_b = \sqrt{\sum_{i=1}^3 (x_i - x'_i)^2 + b^2};$$

where  $s, s'$  - the curvilinear coordinates counted along the conductor,  $x_i, x'_i$  - cartesian coordinates of observation and source points,  $\epsilon_r$  - relative dielectric permittivity of the layer,  $k$  - wave number,  $\omega$  - cyclic frequency,  $2a$  - conductor diameter,  $d = b - a$  - thickness of the dielectric layer,  $L$  - general length of the vibrator and all conductors of the grid,

$I(s)$  – the sought function of current distribution,  $E_t^i$  – tangential component of an electric fields.

The solution of IE (1) is found by the method of moments transforming it to a matrix equation, choosing step-function as the basis function and delta-function as the weight function [3, 4].

$$E_m = \sum_{n=1}^N K_{mn} I_n, K_{mn} = \int_{\Delta s_m} K(s_n, s') ds' \quad m, n = 1 \dots N \quad (3)$$

To provide solution convergence it is necessary to choose the optimal length of segments of conductor fragmentation, the side of the cell should be covered with an integer number of segments [5]. The choice of wavelength is determined by the IE core behaviour. In this connection the analysis of IE core dependence on dielectric parameters for thin-wire structures of different configuration covered with a layer of dielectric was carried out. It is found out that the optimal fragmentation for electrically long rectilinear structures is  $\Delta s/\lambda = 0.04 \dots 0.05$ .

The calculation of amplitude-phase current distribution for dielectric permittivity  $\varepsilon = 2 \dots 9$  and the thickness of conductor dielectric coating  $d/\lambda = 0.05 \dots 0.4$  was made. By the known current distribution the radiation field in far zone in 2 mutually perpendicular planes  $\mathbf{E}$  and  $\mathbf{H}$  was calculated. Using the results of calculation of orientation characteristic the width of the main lobe of half-power, the level of back radiation were determined. That allows to estimate the reflective properties of grid screens. The square screen was considered, its geometric parameters varied within the following limitations: side length  $L_s/\lambda = 0.8 \dots 2.4$ , square cell dimensions  $l/\lambda = 0.08 \dots 0.3$ , conductor radius  $a/\lambda = 0.005; 0.01$ . The half-wave dipole was located at the height  $h/\lambda = 0.25$  in parallel with grid plane.

Calculation results for the grid screen with parameters  $L_s/\lambda = 2.4$ ,  $l/\lambda = 0.15$ ,  $a/\lambda = 0.005$  are shown on fig. 1- fig. 4.

On fig. 1 as an example the dependence of maximal level of back lobe (MLBL)  $\mathbf{p}$  in planes  $\mathbf{H}$  (curve  $\mathbf{a}$ ) and  $\mathbf{E}$  (curve  $\mathbf{b}$ ) on dielectric permittivity  $\varepsilon$  is shown. MLBL is normalized on the radiation maximum of the main lobe. On fig. 1 also shown is the dependence of mean level of back lobe (mean LBL) in planes  $\mathbf{H}$  (curve  $\mathbf{c}$ ) and  $\mathbf{E}$  (curve  $\mathbf{d}$ ) on dielectric permittivity  $\varepsilon$ . (mean LBL – the ratio of rear lobe area and the main lobe area). On fig. 2 the dependence of MLBL and mean LBL on dielectric layer thickness  $d/\lambda$  is shown. On fig. 3 – 4 the change of the main lobe width of half power  $2\theta_{0.5}$  in planes  $\mathbf{H}$  (curve  $\mathbf{a}$ ) and  $\mathbf{E}$  (curve  $\mathbf{b}$ ) from dielectric permittivity (fig. 3) and dielectric layer thickness (fig. 4) is shown.

The numerical investigation allows to make the conclusion that for a grid screen of finite dimensions the increase of dielectric permittivity and dielectric layer thickness leads to decrease of shielding effect. This is found to be in good agreement with similar structures of infinite dimensions [1].

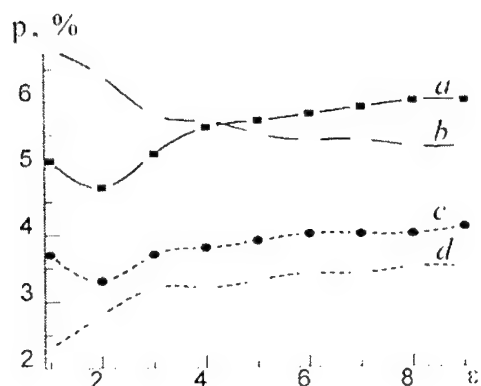


Fig. 1.

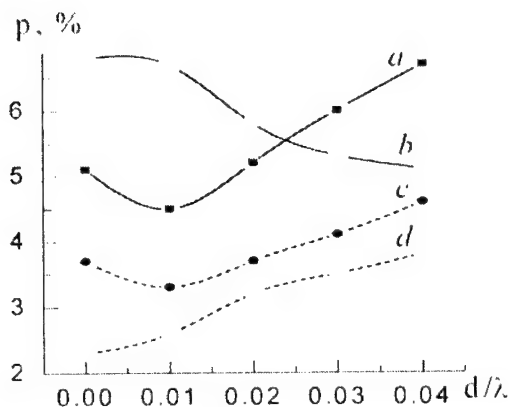


Fig. 2.

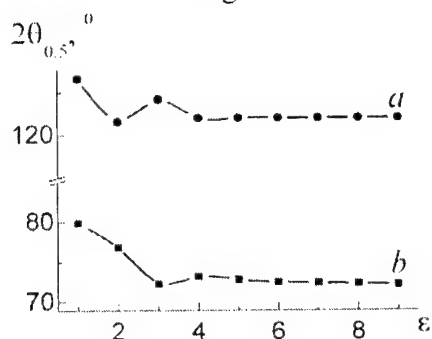


Fig. 3.

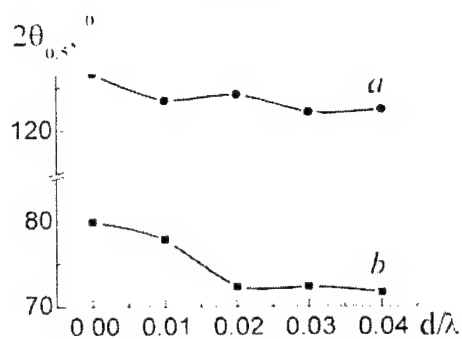


Fig. 4.

The offered methods allow to estimate reflective properties of a grid screen of finite dimensions covered with dielectric in dependence on geometric parameters, dielectric permittivity and dielectric layer thickness.

## REFERENCES

- [1] Electrodynamics of grid structures / Edited by Kontorovich M.I. – M.: Radio i svyaz, (Russian), 1987. – 133 p.
- [2] Demitchik V.I. Integral equation for thin-wire conductors with coating dielectric // Vestnik BSU. Ser. 1., (Russian), 2000. №3. pp. 29-31.
- [3] Demitchik V.I., Kalashnikov N.V., Runov A.V. The algorithm of current distribution computation for electric-long curvilinear conductors.- Izvestia Vuzov, Radioelektronika, (Russian), 1983, v.26, №3, pp. 82-84.
- [4] Computer techniques for electromagnetics. / Edited by Mittra R. – M.: Mir, (Russian), 1977. – 485 p.
- [5] Volynec N.A., Demitchik V.I. Reflective properties of a finite grid screen // Vestnik BSU. Ser. 1., (Russian), 1999. №2. pp. 33-36.

## COMPARATIVE STUDY OF INTEGRATION SCHEMES USED ON DIFFERENTIAL THEORY OF GRATINGS

Koki WATANABE

Department of Information and Communication Engineering  
Faculty of Information Engineering  
Fukuoka Institute of Technology  
3-30-1 Wajirohigashi, Higashi-ku, Fukuoka 811-0295, Japan  
E-mail: koki@fit.ac.jp

### ABSTRACT

Several integration schemes are applied to the differential method for a sinusoidal-profiled surface-relief grating made of an anisotropic and conducting material. The numerical results show the importance of the numerical stability and the advantage of the implicit integration schemes.

### DIFFERENTIAL THEORY OF GRATINGS

We investigate the diffraction problem on a surface-relief grating ruled on an anisotropic and homogeneous substrate schematically shown in Fig.1. The grating grooves are parallel to the  $z$ -axis and the equation of the grating surface is  $y = p(x)$  where  $p(x)$  is a known periodic function with the period  $d$  and the depth  $h$ . The region  $y > p(x)$  is filled with a homogeneous and isotropic material described by the relative permittivity  $\epsilon_1$  and the relative permeability  $\mu_1$ , and the homogeneous and anisotropic material that fills the region  $y < p(x)$  is described by the relative permittivity matrix  $\overline{\epsilon}_2$  and the relative permeability matrix  $\overline{\mu}_2$ . We consider only time harmonic fields assuming a time-dependence in  $\exp(-i\omega t)$ , and deal with the plane incident wave propagating in the direction of polar angle  $\theta$  and azimuth angle  $\phi$ .

The differential theory [1,2] is one of the most commonly used approaches in the analyses of such gratings. Thanks to the periodic structure, the electromagnetic field compo

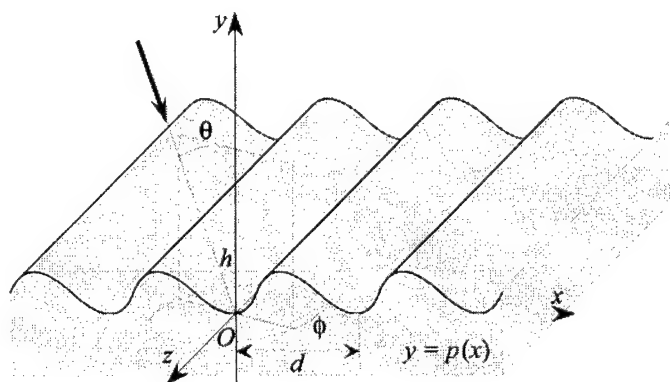


Figure 1: Geometry of the surface-relief grating under consideration.

nents can be approximately expanded in the truncated generalized Fourier series [2]; for example the  $x$ -component of  $\mathbf{E}$  field can be written as

$$E_x(x, y, z) = \sum_{n=-N}^N E_{x,n}(y) \exp[i(\alpha_n x + \gamma z)] \quad (1)$$

with

$$\alpha_n = k_1 \sin \theta \cos \phi + n \frac{2\pi}{d}, \quad \gamma = k_1 \sin \theta \sin \phi \quad (2)$$

where  $N$  is the truncation order,  $k_1$  is the wavenumber in the region  $y > p(x)$ , and  $E_{x,n}(y)$  are the  $n$ th-order generalized Fourier coefficients which are functions of  $y$  only. Replacing all the periodic and the pseudo-periodic functions by their Fourier series and using the Fourier factorization rules [3], Maxwell's curl equations are transformed into a coupled differential equation set in the form of

$$\frac{d}{dy} \begin{pmatrix} \mathbf{e}_x(y) \\ \mathbf{e}_z(y) \\ \mathbf{h}_x(y) \\ \mathbf{h}_z(y) \end{pmatrix} = \mathbf{M}(y) \begin{pmatrix} \mathbf{e}_x(y) \\ \mathbf{e}_z(y) \\ \mathbf{h}_x(y) \\ \mathbf{h}_z(y) \end{pmatrix} \quad (3)$$

where, for example,  $\mathbf{e}_x(y)$  denotes a  $(2N+1) \times 1$  column matrix generated by the Fourier coefficients of  $E_x$  and  $\mathbf{M}(y)$  is the coupling coefficient matrix. Then, the scattering problem of grating is reduced to an integration problem of the coupled differential equation set with boundary conditions at the top and the bottom of the groove region.

## NUMERICAL RESULTS OF VARIOUS INTEGRATION SCHEMES

One method for integrating the coupled differential equation set (3) is the rigorous coupled-wave method, which introduces the staircase approximation to describe arbitrary profiled gratings. The real profile in each step is replaced by the structure uniform in the  $y$ -direction, and then the boundary-value problem can easily be turned into an eigenvalue problem because of the absence of the  $y$ -dependence. Another approach is based on the shooting method, which can transform the boundary-value problem into the initial-value one. The initial-value problem can be solved by usual numerical integration schemes. In the narrow sense, this approach is called the differential method. In the method, the Runge-Kutta or the predictor-corrector Adams schemes are suggested for integration [2,4].

Here, several numerical integration schemes are applied to the differential method for a sinusoidal grating made of conducting material and the convergences of the TM diffraction efficiencies in  $-1$ st-order with respect to the number of the integration steps are compared in Fig.2. The grating parameters are chosen as follows:  $\lambda_0 = 0.6328 \mu\text{m}$ ,  $\theta = 30^\circ$ ,  $\phi = 20^\circ$ ,  $d = 0.6 \mu\text{m}$ ,  $h = 0.5 \mu\text{m}$ ,  $p(x) = (h/2)[1 + \cos(2\pi x/d)]$ ,  $\epsilon_1 = \mu_1 = 1$ ,  $\epsilon_{2,xx} = \epsilon_{2,yy} = \epsilon_{2,zz} = -8.19 + i16.38$ ,  $\epsilon_{2,xz} = -\epsilon_{2,zx} = -0.495 - i0.106$ ,  $\epsilon_{2,xy} = \epsilon_{2,yx} = \epsilon_{2,yz} = \epsilon_{2,zy} = 0$ ,  $\mu_2 = \mathbf{I}$ , and TM ( $H_y = 0$ ) polarized incident plane wave. To avoid the numerical difficulty for deep gratings, we used the scattering matrix propagation al

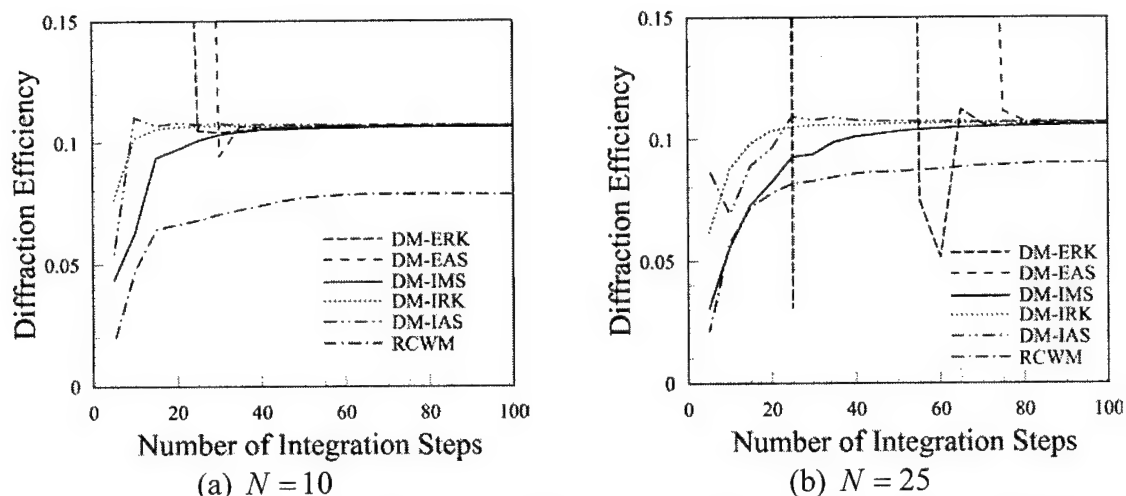


Figure 2: Convergences of diffraction efficiencies computed using various integration schemes (DM: differential method, RCWM: rigorous coupled-wave method, ERK: classical fourth-order Runge-Kutta scheme, EAS: predictor-corrector Adams scheme, IMS implicit midpoint scheme, IRK: implicit fourth-order Runge-Kutta scheme, IAS: implicit Adams-Moulton scheme).

gorithm [5]. The rigorous coupled-wave method shows stable convergence but does not give reliable solutions for such a conductive grating as reported in Ref.[4,6]. The explicit schemes (ERK, EAS) show serious numerical instabilities and require large number of integration steps for reliable solutions. On the other hand, the implicit schemes (IMS, IRK, IAS) are numerically stable even when the number of integration steps is small. Consequently, the use of implicit schemes reduces greatly the computation time and is highly suggested.

## REFERENCES

- [1] R. Petit, "Diffraction d'une onde plane par un réseau métallique," *Rev. Opt.*, Vol.45, pp.353-370, 1966.
- [2] P. Vincent, "Differential method," in *Electromagnetic Theory of Gratings*, R. Petit, ed. (Springer-Verlag, Berlin, 1980), Chap.4, pp.101-121.
- [3] L. Li, "Use of Fourier series in the analysis of discontinuous periodic structures," *J. Opt. Soc. Am. A*, Vol.13, pp.1870-1876, 1996.
- [4] E. Popov, M. Nevière, B. Gralak, and G. Tayeb, "Staircase approximation validity for arbitrary shaped gratings," *J. Opt. Soc. Am. A*, Vol.19, pp.33-42, 2002.
- [5] L. Li, "Formulation and comparison of two recursive matrix algorithms for modeling layered diffraction gratings," *J. Opt. Soc. Am. A*, Vol.13, pp.1024-1035, 1996.
- [6] K. Watanabe, "Numerical integration schemes used on differential theory for anisotropic gratings," *J. Opt. Soc. Am. A* (to be published).



## EIGENWAVES IN THE LAYERED MEDIUM OF BIPERIODIC STRIP ARRAYS

Sergey L. Prosvirnin<sup>(1)</sup>, Dmitry O. Tyrnov<sup>(2)</sup>

(1), (2) Institute of Radio Astronomy of National Academy of Sciences of Ukraine, Krasnoznamennaya str. 4, 61002 Kharkov, Ukraine.

E-mail: prosvirn@rian.ira.kharkov.ua, tyrnov@rian.ira.kharkov.ua

Periodic layered structures are considered. Each layer of the structure is an array of plane metal strips of complex shape placed on a dielectric substrate. The frequency dependencies of eigenwave propagation constants have been obtained. The reflection coefficients from the half-space filled by such medium have been studied. The results for structures made of identical layers and for structures composed of pairs of different layers are presented.

1. Let each layer be constructed by using the plane C-shaped elements oriented in one direction (see Fig. 1a). In this case, on the array period small compared with the incident wavelength, the first or even the second current resonances are possible on the element. The periods of all layers along the  $OX$  and  $OY$  axes are identical. The layers are positioned perpendicularly to the  $OZ$  axis (see Fig. 1b). The field near this array may be presented as the sum of an incident field and the field reflected by the array. The reflected field may be presented as the sum of spatial harmonics (see [1]). We shall consider the case when only one spatial harmonic is propagating. Its propagation constant is equal to  $k$ .

The matrix elements of the reflection and transmission operators ( $r$  and  $t$ ) for

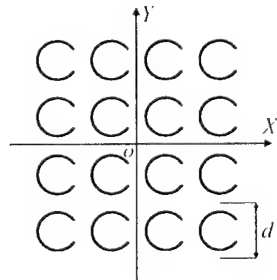


Fig. 1a.

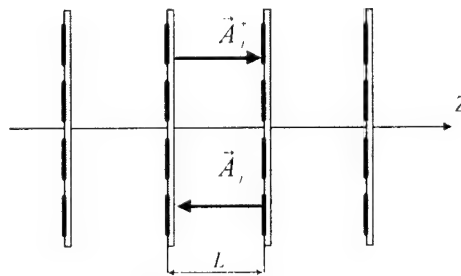


Fig. 2a

one layer can be obtained by using the method of moments. As we take into account only a one harmonic and consider two orthogonal polarizations, the reflection and transmission operators look like square  $2 \times 2$  matrixes. And as the chosen structure of the layer is symmetric, there will be no transformation of polarization of the reflected and transmitted field. Thus the matrixes  $r$  and  $t$  will be diagonal. The operator equations describing the eigen waves in such medium is possible to derive in the same manner as in [2]. They are:

$$(I - e^{-i\beta L} t^- e) \vec{A}_j^+ - r^- e \vec{A}_j^- = 0 \quad (1a)$$

$$r^+ e \vec{A}_j^+ - (I - e^{i\beta L} t^- e) \vec{A}_j^- = 0 \quad (1b)$$

where  $e$  is the operator describing change of a field propagated from any layer to the neighboring one;  $\bar{A}_j^\pm$  are the amplitudes of eigenwave partial constituents in the interval between  $j$  and  $j+1$  layers (hereinafter the "+" and "-" superscripts refer to propagation of the wave from left to right and from right to left, respectively);  $L$  is the period of the structure;  $\beta$  is the propagation constant of an eigenwave.

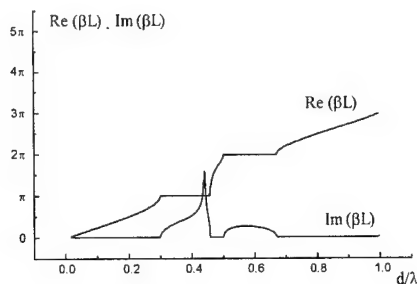


Fig. 2a.

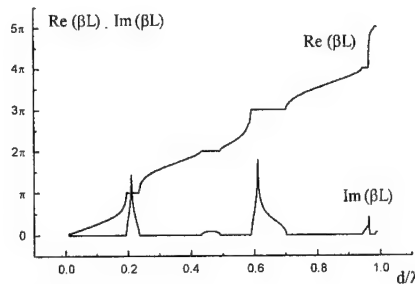


Fig. 2b.

The dispersion dependencies for the eigenwaves propagation constants are solved numerically. They are presented in Fig. 2a (the eigenwave is polarized in the  $OX$  plane) and Fig. 2b (the eigenwave is polarized in the  $OY$  plane).

Consider semi-infinite structure of layers described above. The reflection operator for such a structure may be obtained in the same manner as in [3] as a solution of equation

$$R_\infty^+ = r^+ + t^- e R_\infty^+ e (I - r^- e R_\infty^+ e)^{-1} t^+. \quad (2)$$

Equation (2) is solved numerically by an iterative method. As an initial approximation it is possible to take, for example, the reflection operator of a positive partial constituent of eigen wave for semi-infinite structure. This operator is possible to find from (1a) and (1b) in the form

$$R_e^+ = (I - t^- e e^{i\beta L})^{-1} r^+. \quad (3)$$

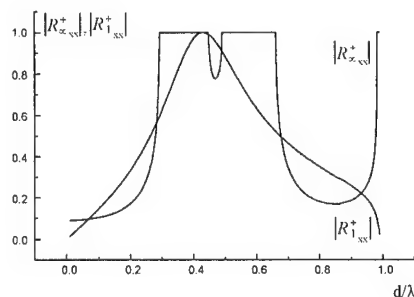


Fig. 3a.

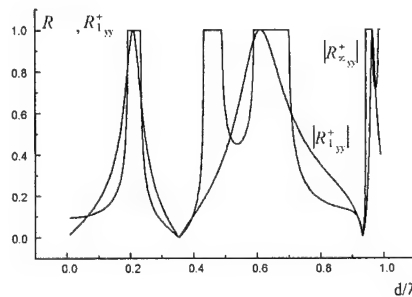


Fig. 3b.

Frequency dependencies of the matrix elements  $R_{\infty xx}^+$  and  $R_{\infty yy}^+$  are represented in Fig. 3a and 3b. Curve I in both figures refers to the reflection coefficient for a semi-infinite structure, a curve II - for the reflection coefficient of one layer. Comparing dependencies in Fig. 2 and Fig. 3, we can see, that the zones of total reflection from this artificial medium refer to the cutoff zones for eigenwaves in this medium. It can be seen

that in those areas where the reflection factor for one layer is close to unity, a sharp increase is observed in the imaginary part value of the propagation constant. This increase can be explained by the total reflection of the incident field from each layer, and therefore the eigen wave cannot be excited as a propagating wave. Thus, the imaginary part of its wave number tends to infinity.

2. The difference between the reflection coefficients for different polarizations may be undesirable in creating of microwave devices. To avoid this strong polarization dependence, we shall rotate each second layer through  $90^\circ$  around the  $OZ$  axis. Consider a new layered medium constructed from pairs of layers, one of which is rotated through  $90^\circ$ . Let the distance between layers in pair be equal to  $h$ ,  $h < L$ . Reflection and transmission operators for a pair of layers ( $R$  and  $T$ ) is possible to obtain in the same manner as in [4].

The 1 subscript refers to a layer oriented, as in Fig. 1a. and the subscript 2 to the layer rotated through  $90^\circ$ . The equations governing the eigenwaves in this medium looks analogously to (1). And the equations (2) and (3) can be rewritten too.

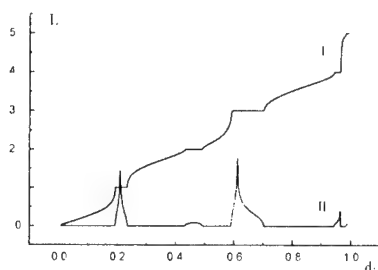


Fig. 4a

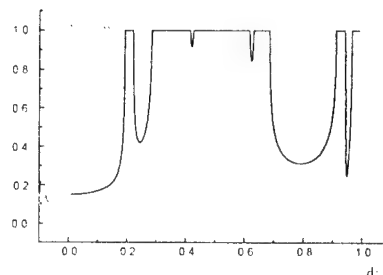


Fig. 4b

Now the solutions for the dispersion equation coincide for both polarizations. The reflection coefficient for this medium also will be identical to both polarizations. Its frequency dependence is presented in Fig. 4b.

## REFERENCES

- [1] S. L. Prosvirnin and S. Zouhdi, "Multi-layered arrays of conducting strips: switchable photonic band gap structures," *International Journal of Electronics and Communications, Special Issue: Bianisotropics 2000*, vol. 55, no. 4, p. 260, 2001.
- [2] S. L. Prosvirnin and T. D. Vasilyeva, "Eigen waves of periodic layered structure of complex arrays," *8-th Int Conf on Electromagnetics of Complex Media*, Lisbon, Portugal, Proceedings, p.241, September 27–29, 2000.
- [3] L. M. Lytvynenko and Prosvirnin S. L., "Analysis of wave diffraction by a sequence of identical strip gratings. Multi-wave conditions," *Radio Physics and Radio Astronomy*, vol.4, no. 3, pp. 276–286, 1999 (in Russian).
- [4] D. Kokody and S. L. Prosvirnin, "Analysis of electromagnetic characteristics of multi-layered periodic structures with turning layers," *Proceedings of 8-th Int. Conf. on Mathematical Methods in Electromagnetic Theory (MMET2000)*, Kharkov, vol. 1, p. 256, September 12–15, 2000.

# MATHEMATICAL MODELS OF ELECTROMAGNETIC WAVE SCATTERING BY TWO-ELEMENT STRIP GRATING WITH A PERPENDICULARLY MAGNETIZED GYROTROPIC MEDIUM

Y.V. Gandel, V.V. Khoroshun  
Kharkov National University  
Pl. Svobody 4, Kharkov 61077, Ukraine  
E-mail: gandel@ilt.kharkov.ua

## ABSTRACT

Two mathematical models are proposed for analyzing a linearly polarized plane wave scattering by a strip grating placed on isotropic-gyrotropic media interface in the case of oblique incidence. The first mathematical model is based on reducing the original boundary value problem to the Riemann-Hilbert problem. The second model is based on reducing the same problem to a singular integral equation of the first kind with Cauchy kernel and its numerical solving by the discrete singularities method.

In this paper, the results obtained in [1-3] are generalized for the case of periodic structure consisting of two strips of different widths per period (two-element grating). This results in richer diffraction phenomena in comparison to simple grating because of additional control parameters. Moreover, unlike papers [1-3] here the case of oblique incidence of an H-polarized plane wave on a two-element grating is considered. The center of coordinate system is chosen in the middle of one of the strips.

The following set of dual series equations is mathematical model of a structure

$$\sum_n A_n \gamma_{n1} e^{in\varphi} = \gamma_{01}, \quad \theta_m < \varphi < \theta_m^{(1)}; \quad (1)$$

$$\sum_n A_n r_n e^{in\varphi} = -p_0, \quad \theta_m^{(1)} < \varphi < \theta_{m+1}^{(1)}, \quad (2)$$

where  $\gamma_{n1} = \sqrt{k_0^2 n_1^2 - h_n^2}$ ,  $n_1 = \sqrt{\epsilon_1 \mu_1}$ ,  $h_n = k_0 n_1 \sin \zeta + \frac{2\pi}{l} n$ ,

$$r_n = 1 + \frac{\gamma_{n1}}{\epsilon_1 (R \gamma_{n2} - i L h_n)}, \quad \gamma_{n2} = \sqrt{k_0^2 \epsilon_\perp \mu_\parallel - h_n^2}, \quad \epsilon_\perp = \frac{\epsilon^2 - \epsilon_a^2}{\epsilon}$$

$$R = \epsilon_\perp^{-1}, \quad L = -\frac{\epsilon_a}{\epsilon^2 - \epsilon_a^2}, \quad k_0 = \frac{2\pi}{\lambda},$$

$$p_0 = 1 - \frac{\gamma_{01}}{\epsilon_1 (R \gamma_{02} - i L h_0)}, \quad \varphi = \frac{2\pi}{l} y, \quad \theta_m = 2\pi \frac{y_m}{l}, \quad (m=1,2),$$

$l$  is the grating period,  $d$  is the slot width,  $\lambda$  is the wavelength,  $\zeta$  is the incidence angle.

Denote  $\tilde{A}_n = A_n r_n + p_0 \delta_{0n}$ , and  $\delta_{0n}$  for the Kronecker symbol.

Then initial set of dual series equations takes the form:

$$\sum_n \tilde{A}_n e^{in\varphi} = 0, \quad \theta_m < \varphi < \theta_m^{(1)}; \quad (3)$$

$$\sum_{n>0} n \tilde{A}_n \frac{\eta_{n1}}{r_n^+} e^{m\varphi} + \sum_{n<0} n \tilde{A}_n \frac{\eta_{n1}}{r_n^-} e^{m\varphi} = (1 - \frac{\tilde{A}_0 - p_0}{r_0}) \kappa_1 \cos \zeta, \quad \theta_m^{(1)} < \varphi < \theta_{m+1}^{(1)}, \quad (4)$$

$$\sum_{n \neq 0} \tilde{A}_n e^{m\delta_m} = -\tilde{A}_0, \quad \theta_m^{(1)} < \delta_m < \theta_{m+1}^{(1)}, \quad (5)$$

The set of equations (3)-(5) can be reduced to non-homogeneous conjugation problem (Riemann-Hilbert's problem) with a complex-valued coefficient in the case of account of dissipative losses.

To calculate matrix elements of final matrix equation, it is necessary to introduce polynomials  $Q_n(u_m, \rho)$  [3], where  $\rho = \frac{\ln|G|}{2\pi}$ ,  $u_m = \cos \theta_m$ , ( $m=1,2$ ).

In the case of multi-element gratings, an efficient numerical-analytical method for solving these dual series equations was suggested in [4]. The method consists in reducing them to a singular integral equation of the first kind with the Cauchy kernel on the set of segments, and its following solution by the method of discrete singularities [4,5]. Integral equation is of the following form

$$\frac{1}{\pi} \int_L \frac{F(\xi)}{\xi - x} d\xi + \frac{1}{\pi} \int_L K(x, \xi) F(\xi) d\xi = f(x), \quad x \in L \quad (6)$$

where  $L = \bigcup_{q=1}^m (a_q, b_q)$ ,  $-\infty < a_1 < b_1 < \dots < a_m < b_m < +\infty$ ;

$f(x)$ ,  $x \in \bar{L}$ ;  $K(x, \xi)$ ,  $x \in \bar{L}$ ,  $\xi \in \bar{L}$  are known smooth functions, and function  $F(\xi)$ ,  $\xi \in L$  is sought in the functional class whose restriction on interval  $(a_q, b_q)$ :

$$F_q(\xi) = F(\xi), \quad a_q < \xi < b_q, \quad q = 1, \dots, m$$

can be represented in the form

$$F_q(\xi) = \frac{v_q(\xi)}{\sqrt{(\xi - a_q)(b_q - \xi)}}, \quad a_q < \xi < b_q,$$

where  $v_q(\xi)$ ,  $\xi \in [a_q, b_q]$  is a smooth function.

The sought function  $F(\xi)$ ,  $\xi \in L$  satisfies additional conditions, which in general case are of the following form:

$$\frac{1}{\pi} \int_L S_p(\xi) F(\xi) d\xi = C_p, \quad p = 1, \dots, m, \quad (7)$$

where  $S_p(\xi)$ ,  $\xi \in [a_p, b_p]$  is a known smooth function, and  $C_p$  is a known constant.

In conclusion we shall present the discrete mathematical model that is a set of linear algebraic equations for numerical solution of the integral equation (6) with additional condition (7).

Denote

$$t_i^n = \cos \frac{2i-1}{2n} \pi, \quad i = 1, \dots, n; \quad t_{0,j}^n = \cos \frac{j}{n} \pi, \quad j = 1, \dots, n-1;$$

$$g_k(\tau) = \frac{b_k - a_k}{2}\tau + \frac{b_k + a_k}{2}; \quad \xi_{qi}^{n_q} = g_q(t_i^{n_q}), \quad i = 1, \dots, n_q; q = 1, \dots, m$$

$$\chi_{pj}^{n_p} = g_p(t_{0j}^{n_p}), \quad j = 1, \dots, n_p - 1; p = 1, \dots, m$$

To calculate approximate values  $\{v_{qn_q}(\xi)\}_{q=1}^m$  of the desired functions  $v_q(\xi)$ ,  $q = 1, \dots, m$  in principal points  $\{t_i^{n_q}\}_{i=1}^{n_q}$ , we have a set of linear algebraic equations (where  $R(x, \xi) = \frac{1}{\xi - x} + K(x, \xi)$ )

$$\sum_{q=1}^m \sum_{i=1}^{n_q} R(\chi_{pj}^{n_p}, \xi_{qi}^{n_q}) v_{qn_q}(\xi_{qi}^{n_q}) \frac{1}{n_q} = f(\chi_{pj}^{n_p}), \quad j = 1, \dots, n_p - 1; \quad p = 1, \dots, m,$$

$$\sum_{i=1}^{n_p} S_p(\xi_{pi}^{n_p}) v_{pn_p}(\xi_{pi}^{n_p}) \frac{1}{n_p} = C_p, \quad (j = n_p), \quad p = 1, \dots, m$$

The values of the physical characteristic of scattered field,

$$H = \int_L H(\xi) F(\xi) d\xi = \sum_{q=1}^m \int_{a_q}^{b_q} H_q(\xi) v_q(\xi) \frac{d\xi}{\sqrt{(\xi - a_q)(b_q - \xi)}}.$$

are expressed in terms of the functions  $v_q(\xi)$ ,  $\xi \in [a_q, b_q]$ ,  $q = 1, \dots, m$ ,

where  $H_q(\xi)$ ,  $\xi \in [a_q, b_q]$  are known functions.

Approximate values of

$$H_{\bar{n}} = \sum_{q=1}^m \sum_{i=1}^{n_q} H_q(\xi_{qi}^{n_q}) v_{qn_q}(\xi_{qi}^{n_q}) \frac{1}{n_q}, \quad \bar{n} = (n_1, \dots, n_m)$$

are calculated in numerical experiments.

Obtained results can be applied in the design and elaboration of various devices containing periodic structures with ferrite substrates or in plasma.

## REFERENCES

- [1] Y.V. Gandel, V.V. Khoroshun. Singular integral equations of the problem of electromagnetic wave diffraction by grating with a cross-magnetized ferrite, *Proc. Int. Symp. "Methods of Discrete Singularities in the Problems of Mathematical Physics"*, Kharkov, 1993, pp.123-124 (in Russian).
- [2] Y.V. Gandel, V.V. Khoroshun. The vortex lattice method in the electromagnetic wave diffraction on the method grating with gyrotropic layer, *Proc. Int. Conf. on Mathematical Methods in Electromagnetic Theory*, Kharkov, 2000, pp.578-580.
- [3] Y.V. Gandel, A.V. Litvinov, V.V. Khoroshun. Solution of the problem of electromagnetic wave diffraction by a strip grating with a cross-magnetized bigyrotropic medium, *Proc. Int. Symp. "Methods of Discrete Singularities in the Problems of Math. Phys."*, Orel, 2000, pp.128-132.
- [4] Y.V. Gandel. Method of discrete singularities in electromagnetic problems, *Cybernetics Problems*, M.: AN SSSR Publ., 1986, pp.166-183 (in Russian).
- [5] S.M. Belocerkovskiy, I.K. Lifanov. *Numerical Methods in Singular Integral Equations*, M.: Nauka, 1985 (in Russian).

## DISPERSIVE AND DIFFRACTION ANALYSIS OF INTEGRATED PERIODIC WAVEGUIDE STRUCTURE

T. I. Bugrova

Radio Engineering Department of Zaporozhye National Technical University

Bildg.64, Zhukovsky Street, Zaporozhye 69063, Ukraine

Tel.+38 (0612) 643281 fax 642141 e-mail: bugrova@zstu.edu.ua

### ABSTRACT

A semi - infinite homogenous nonmagnetic shielded slab with grating of thin metallic strips that are printed symmetrically on both sides of the slab was considered. The main wave of the dielectric slab falls under arbitrary angle on the boundary between slab and grating. The dispersive equation of periodic structure was obtained and solved by numerical-analytical method. The diffraction problem was formulated and solved by Wiener-Hopf technique.

### THE EIGENWAVE PROBLEM

Let us consider a homogeneous nonmagnetic dielectric shielded slab of thickness  $2d$ . Gratings of thin metallic strips with  $2l \ll \lambda$  width, where  $\lambda$  is a wavelength in slab medium, are printed symmetrically on both sides of the slab. Coordinates are assumed as shown in Fig.1. The eigenwaves of the structure considered in our case are assumed to be solutions of a boundary value problem for an electromagnetic field. These solutions exhibit a harmonic dependence on the  $x$  axis of  $\exp(-j\chi x)$  and quasiperiodic dependence on the  $z$  axis of type  $E(z)=E(z+nP)\exp(j\beta nP)$ , where  $\chi$  and  $\beta$  are spectral parameters determining the wave propagation direction, and  $n$  is the strip number. The electric field amplitude time dependence  $\exp(j\omega t)$  is omitted for simplification. An electric or magnetic wall can be placed in the structure symmetry plane  $y=0$ . In the present article we shall limit ourselves to analysis of waves corresponding to the magnetic wall case. Because of thinness of the grating strips, the longitudinal components of currents are much more than cross components. So we can use only one boundary condition for the formulation of the problem. It is assumed that  $E_x=0$  for perfectly conducting metallic strips.

Let us obtain the approximate dispersion equation. This equation couples the structure spectral parameters  $\chi$  and  $\beta$  with nonspectral ones:  $P/\lambda$ ,  $2d/\lambda$ ,  $2l/\lambda$ , and  $\epsilon_r$  – relative dielectric permittivity of the slab. Keeping in mind the equal spacing of the grating, let us set periodic conditions for the strip currents at  $I_{xn}=I_0\exp(-j\beta nP)$ , where  $I_0$  – current density on zero strip. It is known that the cross-strip current distribution is given by the Maxwell function  $(1-(z'/l)^2)^{1/2}$  [1]. Taking into account the above approximation and using the boundary conditions, we shall formulate the integral equation as

$$\int_{-\infty}^{\infty} \int_{-l}^l G(x, x'; z, z') I(x) \exp(-j\beta nP) (1 - (z'/l)^2)^{-1/2} dx' dz' = 0, \quad (1)$$

where

$n=0, \pm 1, \pm 2, \dots$  - the strip number. The function  $G$  can be obtained by the Fourier integral

$$G(x, x'; z, z') = \int_{-\infty}^{\infty} g(\xi, \alpha) \exp(-j\xi(x - x') - j\alpha(z - z')) d\xi d\alpha, \quad (2)$$

where  $g(\xi, \alpha)$  is a known function. Let us evaluate an integral on  $\alpha$  in (2) according to Cauchy theorem. An integral on  $x'$  in (1) is evaluated trivially, assuming the current variability along the strip to be  $I(x') = \exp(-j\chi x')$ . It is equal to  $2\pi\delta(\xi - \chi)$ , where the symbol  $\delta$  denotes the Dirac delta function. To avoid a  $z'$  dependence in (1) let us use the Galerkin method. As a rule in a slab two modes are propagating ones. They are the  $TE_1$  and  $TM_2$  modes with  $\alpha_1 = \alpha_h$  and  $\alpha_2 = \alpha_e$ . The term with  $n=0$  is calculated numerically. As a result we obtain a rather simple relationship reducing the integrals on  $z'$  and  $n$   $\alpha$  in (1) and (2) to a double series. Evaluating an integral on  $\xi$  we obtain

$$ZD_e D_h + j\chi_e k_0 \beta_h^{-1} \sin(\chi_h P) D_e + j\chi \beta_e^2 k_0^{-2} \eta_s^2 \chi_e^{-1} \sin(\chi_e P) D_h = 0, \quad (3)$$

where  $D_{e,h} = \cos(\chi_{e,h} P) - \cos(\beta P)$ ,  $\eta_s$ ,  $Z$  are definite functions of  $\chi$ , and  $\chi_{e,h} = (\beta_{e,h}^2 - \chi^2)^{1/2}$ . For the grating considered, as a rule, single - mode conditions are not satisfied because even in a shielded slab without a grating  $TE_1$  and  $TM_2$  waves exist. In the grating they are converted into  $HE_{11}$  and  $EH_{21}$  modes with similar structure. However, by proper selection of structure parameters, we can create the situation where only the main  $HE_{11}$  mode propagates. Cutoff conditions for  $HE_{12}$  and  $EH_{21}$  modes were obtained from the dispersion equation

$$\beta_{HE_{12}}^{cut} = P^{-1} \arccos \left[ \frac{k_0}{\beta_h Z(0)} \sin(\beta_h P) + \cos(\beta_h P) \right]; \beta_{EH_{21}}^{cut} = \beta_e.$$

## THE DIFFRACTION PROBLEM

The diffraction problem was solved by Wiener-Hopf technique. A semi-infinite homogeneous nonmagnetic shielded slab with grating of thin metallic strips that are printed symmetrically on both sides of the slab was considered. The main wave of the dielectric slab falls under arbitrary angle on the boundary between slab and grating. The transfer strip current approximation was taken as Maxwell function. The longitudinal component of strip current was found from the integral equation formulated for boundary conditions. Using the field expression through the Green's function  $G$  and using zero boundary conditions we obtain an integral equation:

$$\int I_t(s') Z(s-s') ds' + E_t(s) = 0, \quad (4)$$

where  $E_t$  and  $I_t$  are the electrical field and current components that are tangential to the strip axes. The function  $Z(s-s')$  can be defined from the function  $G$ . The evaluation of an integral in (4) is carried out along the strip axes. Using the Galerkin technique and the transfer current approximation by the Maxwell function, we succeeded in obtaining a one-dimensional equation from the two-dimensional one. It is convenient to solve equations like (4) by using the Wiener-Hopf technique [1]. Hence, we can obtain an expression for  $I_t(s)$  in the Fourier integral form. Evaluating the residue of the integrand at the point  $\alpha = \chi_h$ , coincides with the root corresponding to the  $HE_{11}$  wave, and describes the current component of our interest ( $I_{THE11}$ ).



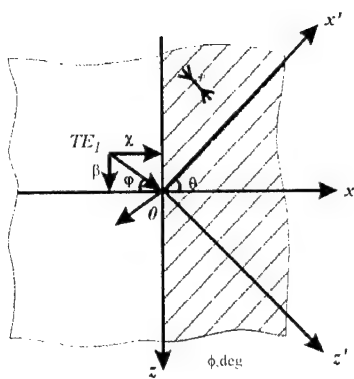


Fig.1

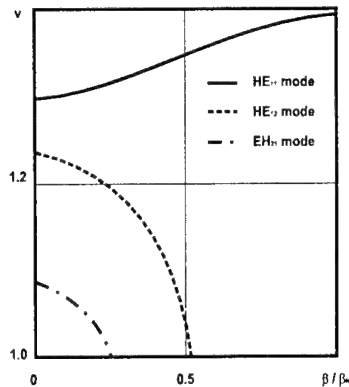


Fig.2

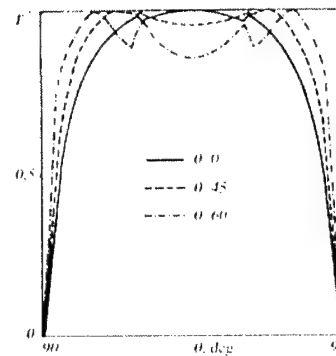


Fig.3

## NUMERICAL RESULTS

Dispersive equation (3) was solved numerically. Figure 3 shows variation of the  $HE_{11}$ -wave longitudinal normalized propagation constant  $v = \chi_0/k_0$  versus cross-strip normalized transverse propagating constant  $\beta/\beta_h$  for relative dielectric permittivity  $\epsilon_r = 9.8$ . It is shown that when  $\beta = 0$  (longitudinal wave propagation) the retardation factor is equal to that of a dielectric slab  $H_1$  - wave for any structure parameters, because in this case an electric field has no longitudinal components ( $E_x = 0$ ) and is not perturbed by thin grating strips. If the direction of wave propagation varies ( $\beta \neq 0$ ), the retardation factor increases. It is characteristic for the dependence of  $HE_{12}$  and  $EH_{21}$  - wave factors on  $\beta/\beta_h$  for various structure periods that from the onset of some critical  $P$  value, the  $HE_{12}$  - wave retardation factor decreases rapidly.

Due to solving the diffraction problem we can obtain the conversion factor  $T^2$  of an  $H_1$  wave into an  $HE_{11}$  wave as a ratio of wave powers transmitted normally to boundary. In Figure 2 the dependences of  $T^2(\phi)$  for various  $\theta$  angles and the period  $P/\lambda = 0.45$  are shown. High values of  $T^2$  is seen in the range of angles  $\phi$  from  $-45^\circ$  to  $+45^\circ$ . At some angular points  $T^2(\phi)$  is equal to unity. It takes place when the incidence angle  $\phi$  is equal to the angle between the direction normal to an array boundary and strip axes  $\theta$ . The main-mode incident wave does not interact with the grating. We observe complete transmission for  $\phi = -\theta$ . In this case the transmitted wave is perturbed by the grating strips. This effect is similar to the whole transmission with the Brewster angle in the case of wave diffraction on the boundary between the two dielectric media. In some angles the  $T^2(\phi)$  dependence has sharp breaks. They appear when  $E_2$  and  $EH_{21}$  waves become nonpropagating ones, turning into an attenuating mode from a propagating one. This is characteristic for so-called Wood's anomalies, when the derivative on  $\theta$  for transmission factor and for reflectivity is striving to infinity at some points.

The proposed structure can be used as a basis for integrated beam-forming networks for multibeam antennas.

## REFERENCES

- [1] R. Mittra, S. W. Lee, Analytical Techniques in the Theory of Guided Waves. McMillan, New York, London, 1971.

**ANTENNA  
ANALYSIS  
AND  
SYNTHESIS**

# CALCULATION OF ELECTROMAGNETIC FIELD IN NEAR FIELD ZONE OF REFLECTOR ANTENNA WITH EDGE RADAR ABSORBING COATING

S.V. Nechitaylo, A.Z. Sazonov, O.I. Sukharevsky

Kharkov Military University, Kharkov, Ukraine  
E-mail: sukharevsky@euro.dinos.net

## ABSTRACT

In the paper technique of electromagnetic field calculation in near-field zone of parabolic antenna with reflector edges covered by toroidal radar absorbing coating is presented. The calculation technique is based on the applying of the integral representations obtained using Lorentz lemma. For calculation of the reflector edge parts contribution to the total antenna field the solution of model scattering problem for half-plane with radar absorbing cylinder on the edge, sounded by plane electromagnetic wave, is used. Calculation results for different values of radius of radar absorbing coatings are presented.

## INTRODUCTION

In a number of situations the radar systems antennas may be positioned nearly one to another. In this connection the problem of electromagnetic compatibility and interference immunity of such systems is of importance. One way of improvement of antennas interference immunity in back half-space is the reflector edge coating by radar absorbing materials. Therefore the problem of calculation of electromagnetic field in near-field zone of antennas with radar absorbing coating on the edges is of interest.

## THE TECHNIQUE OF SOLUTION

The parabolic-reflector antenna with reflector edges covered by toroidal radar absorbing coating is located in the free space (Fig. 1). Let's consider a case, when the antenna feed is the pyramidal horn located in antenna focal point.

Near the reflector surface antenna feed creates the following field:

$$\vec{E}(\vec{X}) = \frac{jk_0}{4\pi} \vec{p}' \frac{\exp[jk_0 \vec{R}^0(\vec{X} + \vec{\rho})]}{\vec{R}^0(\vec{X} + \vec{\rho})} F(\theta, \varphi). \quad (1)$$

Here, according to Fig. 1  $\vec{R}^0$  is unit vector sounding direction from antenna feed to the point  $A$  on the reflector surface, the angel  $\theta$  characterizes a direction of a vector  $\vec{R}^0$  concerning an antenna axis, and angel  $\varphi$  characterizes position of the point  $A$  with reference to the plane  $xOz$ ,  $\vec{\rho}$  is the radius-vector, directed from the focal point to vertex of reflector,  $\vec{p}' = \frac{\vec{R}^0 \times (\vec{\rho} \times \vec{R}^0)}{|\vec{R}^0 \times (\vec{\rho} \times \vec{R}^0)|}$  is the polarization of wave incident in direction

$\vec{R}^0$  ( $\vec{p}$  is the vector antenna feed polarization),  $\mu_0$ ,  $\varepsilon_0$  are permeability and permittivity

of free space,  $k_0 = \omega\sqrt{\varepsilon_0\mu_0}$ . The function  $F(\theta, \varphi)$  defines dependence of antenna feed

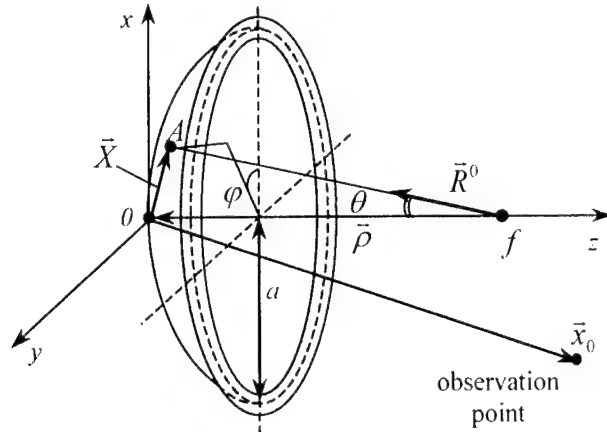


Fig.1

field amplitude and phase in a far-field zone for angular coordinates  $\theta$  and  $\varphi$ .

The field of the antenna in observation point can be represented as the sum of the feed field  $\vec{E}'(\vec{x}_0)$  and field scattered by antenna reflector  $\vec{E}^s(\vec{x}_0)$ :

$$\vec{E}(\vec{x}_0) = \vec{E}'(\vec{x}_0) + \vec{E}^s(\vec{x}_0). \quad (2)$$

As a main calculation formula for determination of scattered by reflector field we shall use an

integral representation of a field obtained using Lorentz lemma

$$\begin{aligned} \vec{p}\vec{E}^s(\vec{x}_0) = & \frac{1}{4\pi} \int_S \frac{e^{jk_0r}}{r} \sqrt{\frac{\mu_0}{\varepsilon_0}} \left( \frac{2-2jk_0r}{jk_0r^2} \vec{p} + \left( \frac{jk_0r-1}{jk_0r^2} - jk_0 \right) \vec{p}^\perp \right) \vec{H}^\perp ds + \\ & + \frac{1}{4\pi} \int_S \frac{e^{jk_0r}}{r} \left( \frac{1-jk_0r}{r} \right) \vec{p} (\vec{r}_0 \times \vec{E}^\perp) ds \end{aligned} \quad (3)$$

where  $S$  is arbitrary closed surface which encloses the antenna reflector.  $\vec{E}^\perp = \vec{n} \times \vec{E}$ ,  $\vec{H}^\perp = \vec{n} \times \vec{H}$ ,  $\vec{n}$  is the internal normal unit vector,  $\vec{p}$  is the receiver polarization,  $\vec{r}_0$  is the unit vector of the direction from a point on the surface  $S$  to the observation point.  $\vec{p} = (\vec{p} \cdot \vec{r}_0) \vec{r}_0$ ,  $\vec{p}^\perp = \vec{p} - (\vec{p} \cdot \vec{r}_0) \vec{r}_0$ ,  $r$  is the distance between the point on the surface  $S$  and the observation point. Let's select the surface of integration as a surface coinciding with reflector surface everywhere except the some neighborhood of the edge. Then the integral in (3) (we shall denote it as  $I(\vec{x}_0)$ ) it is possible to represent as the sum of integrals on the reflector surface  $S_1$ , not including a neighbourhood edge, and surface  $S_0$ , enclosing edge neighborhood

$$I(\vec{x}_0) = I_{S_1}(\vec{x}_0) + I_{S_0}(\vec{x}_0). \quad (4)$$

$I_{S_1}(\vec{x}_0)$  we shall calculate using the solution of the model scattering problem for half-plane with radar absorbing cylinder on the edge, sounded by plane electromagnetic wave [1]. Since the electrical sizes of the antenna reflector are great, the contribution of the surface  $S_1$  in total field we shall carry out in Kirchhoff approximation.

## RESULTS OF NUMERICAL CALCULATION

Using described technique the calculations were carry out for a case when  $k_0a = 30$  ( $a$  is aperture reflector radius),  $k_0f = 26$  ( $f$  is the reflector focus distance), the feed created distribution of field amplitude reducing to antenna edge on 15 dB, the observation point located on the plane  $yOz$ , the absorber is made of the material with

relative electrical parameters  $\mu = 1.35 + j0.8$  and  $\varepsilon = 20 + j0.1$ . In figures 2 and 3 the dependences of normalized amplitude of antenna field from the angle  $\psi$  between a direction of observation point and axis  $Oz$  are presented. Distance from the origin of coordinate system to the observation point was  $17\lambda$  ( $\lambda$  is the wavelength). The figure 2 corresponds to the case, when the vector of feed polarization is parallel to axis  $Ox$ , in the figure 3 the feed polarization vector is parallel to axes  $Oy$ . In figures 2 and 3 bold solid lines correspond to a case, when the absorber on the edge is absent, a thin solid line corresponds to a case when the absorber radius is equal to  $0.2\lambda$ , dashed line corresponds to the case when the absorber radius is equal to  $0.4\lambda$ .

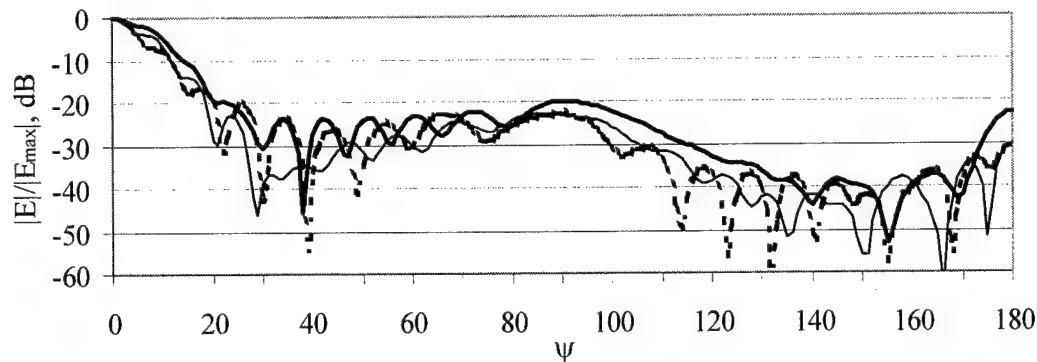


Fig. 2

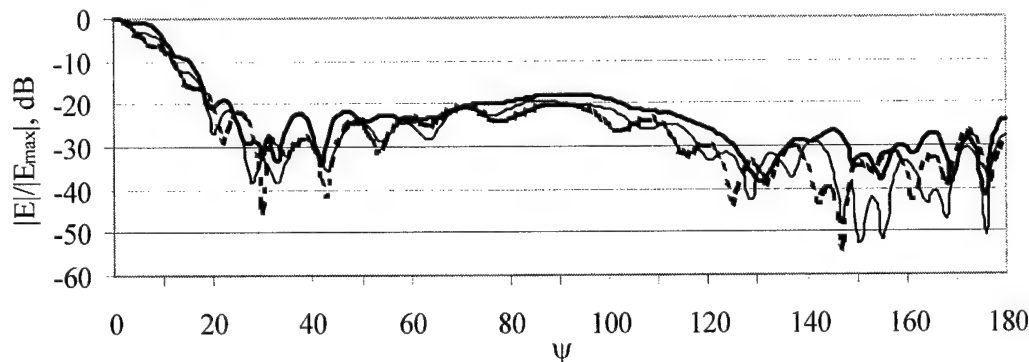


Fig. 3

The analysis of simulation results has shown, that the using of the absorber with radii  $0.2\lambda$  and  $0.4\lambda$  reduces the antenna radiation at  $\psi = 177^\circ..180^\circ$  at the average on 7 dB. For different polarizations the value of lowering antenna lateral radiation is also different. So for  $\psi = 140^\circ..170^\circ$  at the figure 3 we can see rather strong radiation reduction for the antenna with radius absorber equal to  $0.2\lambda$ .

It is necessary to denote that choosing of absorber parameters should be carried out for each specified construction of antenna.

## REFERENCES

- [1]. Y.K. Sirenko, I.V. Sukharevsky, O.I. Sukharevsky, and N.P. Yashina.  
Ed. by Y.K. Sirenko. Fundamental and applied problems of the electromagnetic wave scattering theory. -Kharkiv: Krok, 2000. (In Russian).

## ANALYSIS OF REFLECTOR PATTERN IN DIFFERENT FREQUENCY RANGES IN THE BACKWARD HEMISPHERE

G. V. Yermakov

Kharkov Military University, p. O. 9063. Kharkov 61204, Ukraine

E-mail: promk@vlink.kharkov.ua

### ABSTRACT.

The reflector directional characteristics determination method grounded on the usage of the second kind Fredholm integral equations for "jumping" of the current surface density is offered.

When using the thin absolutely conductive unenclosed shield as an antenna, the exact calculation of the distant side and backward radiation is possible if we use the Fredholm first kind integral equations. The solution of the second kind integral equations for the diffraction problems on unenclosed shields with boundary conditions the Dirichlet and Neumann types are considered in [1, 2]. However it is difficult to algorithm the obtained three-dimensional problems solutions in the special functions class. This limits the feasibilities of the numerical method usage when calculating real unenclosed constructions. The purpose of this article is the development of the Fredholm second kind integral representations operation theory for calculation of reflector spatial characteristics as a paraboloid of rotation in quasi-optical range ( $D/\lambda=10$ ). When calculating exactly it is necessary to bear in mind that the behavior character of surface currents in the central part of a reflector and in the boundary zone can considerably differ from each other [4]. The calculation and registration of "edge" currents allow to calculate exactly the intensity of the distant side and back radiation.

If we enter a concept of the current surface density "jumping" [1] on a surface, defined as  $\vec{K} = (\vec{H}_\perp)^+ - (\vec{H}_\perp)^- = \vec{J}_S^+ - \vec{J}_S^-$ , the solution of the delivered problem outside an ideally conductive surface S can be expressed through tangent components of electrical and magnetic vectors on the surface S

$$\vec{H}(M) = \vec{H}_0(M) + \frac{1}{4\pi} \oint_S \left\{ \text{grad}_P \frac{\exp(-ikR_{MP})}{R_{MP}} \times \vec{K}(P) \right\} dS. \quad (1)$$

Where  $R_{MP}$  - the distance between the M and P points (P - a point on a surface S, M - a view point),  $(\vec{H}_\perp)^+, (\vec{H}_\perp)^-$  - the normal to a surface of a component of a magnetic intensity on the internal (lighted) and external (shadow) mirror surface sides,  $\vec{J}_S^+, \vec{J}_S^-$  - the area current density on the internal and external reflector sides.

If we multiply (1) by  $\vec{n}_{P_0}$  and to aim on a normal the M point to the  $P_0$  point of the surface S, then, using the properties of a simple stratum potential normal derivative, we shall receive the Fredholm second kind representation:

$$\frac{1}{2}(\bar{J}_S^+(P_0) + \bar{J}_S^-(P_0)) = \bar{J}_S^0(P_0) - \frac{1}{2\pi} \int_S \bar{n}_{P_0} \times \left[ (\bar{J}_S^+(P) - \bar{J}_S^-(P)) \times \text{grad}_P \frac{\exp(-ikR_{PP_0})}{R_{PP_0}} \right] dS \quad (2)$$

The task of determining the volumetric current density distribution is reduced to a repetitive process, at each stage of which the Fredholm second kind integral equation concerning the area current density on the lighted  $\bar{J}_S^+$  or on the shadow  $\bar{J}_S^-$  side of the reflector with an updated right side, is solved. The iterative procedure application allows to update the area current density value on both sides of a reflector in the boundary area essentially influencing the distant side and back radiation. It allows to reduce the integration area and to reduce the run time. For implement a numerical algorithm determining the area current density  $\bar{J}_S^-(P_0)$  or  $\bar{J}_S^+(P_0)$  on the surface S, it is dissected into N of not intersected cells. The sizes of the cells can be selected  $0,1\lambda$  ( $\lambda$  - wavelength) [3]. The Focks equation for the surface current density, for example, on the external side of S, will look like

$$\begin{aligned} \bar{J}_S^-(P_0) - \frac{1}{2\pi} \int_S \bar{n}^e(P_0) \times \left[ \bar{J}_S^-(P) \times \text{grad}_P \frac{\exp(-ikR_{PP_0})}{R_{PP_0}} \right] dS = \\ = 2\bar{J}_S^0(P_0) - \bar{J}_S^+(P_0) - \frac{1}{2\pi} \int_S \bar{n}^e(P_0) \times \left[ \bar{J}_S^+(P) \times \text{grad}_P \frac{\exp(-ikR_{PP_0})}{R_{PP_0}} \right] dS \end{aligned} \quad (3)$$

Because of the boundary conditions the Meixner conditions for the surface current density will be as follows: components which are orthogonal to the edge will have the feature of the aspect  $\rho^{-1/2}$ , and components which are parallel to the edge will have the aspect  $\rho^{1/2}$  [4]. Then the solution is searched as

$$j_x^{-/+} = \rho^{1/2} \sum_{n=1}^N \dot{A}_n \Psi_n, \quad j_y^{-/+} = \rho^{-1/2} \sum_{n=1}^N \dot{B}_n \Psi_n, \quad j_z^{-/+} = \rho^{1/2} \sum_{n=1}^N \dot{C}_n \Psi_n, \quad (4)$$

where  $\rho$  is the distance to the edges of a mirror,  $\dot{A}_n, \dot{B}_n, \dot{C}_n$  are unknown factors,

$\Psi_n$  is known system of functions, N is amount of surface segments.

When we hold numerical calculations a collocation method is used. The Haar system of characteristic functions was selected as  $\Psi_n$  [3]. If the integration points coincide the kernel has a feature, to eliminate which, it is excised by a circle with the radius  $\varepsilon = 10^{-6}\lambda$  [3]. The presence of the feature allows to generate a system of linear algebraic equations with a dominant principal diagonal. In fig. 1 the relation of the  $K_y$  component of the surface current density for  $f=1\text{GHz}$  is shown. Curve 1 corresponds to the physical optics approximation, curve 2 - current density obtained on the basis of the integral equations solution considering the boundary conditions. From fig. 1 we make an important conclusion that when we determine the currents it is necessary to carefully calculate the

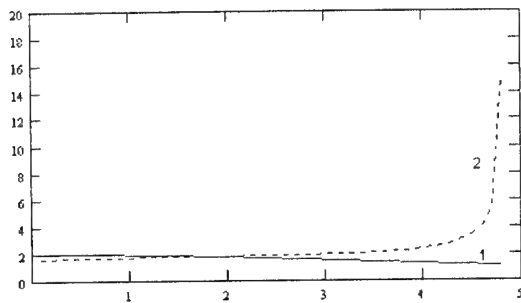


Fig. 1. The  $K_y$  component

boundary area making approximately  $0,5\lambda$  from the mirror edge, and we can use a physical optics approximation for the rest.

Knowing the distribution of currents on a surface, we can determine the directivity diagram in a far-field region (fig. 2).

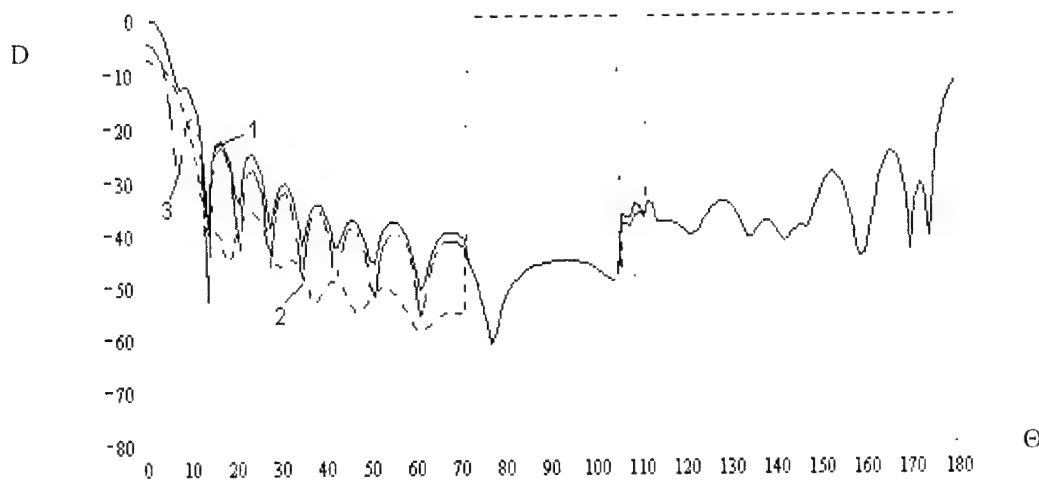


Fig. 2. The pattern of a reflector ( $f=1$  a GHz)

( 1 - total field, 2 - field created by a boundary part, 3 - field created by a central part)

From the data, shown in the figures, it is possible to make some more important practical conclusions concerning reflector characteristics calculation: 1. The basic contribution to distant side lobes is given by the edge, which at angles more than  $15^\circ$  determines the shape of the whole pattern: 2. The registration of "becoming numb" currents allows to determine the level of the reflector back radiation - it diminishes with the increase of frequency and makes about -40 dB for this construction.

## REFERENCES

- [1]. Feld Ya.N., Sukharevsky I.V. About integral equations of the tasks of a diffraction on unenclosed shields // Radio engineering and electronics engineering. -1966. -T.11. -Вып.7. -С.1159-1168.
- [2]. Feld Ya.N., Sukharevsky I.V. About integral equations of the tasks of a diffraction on unenclosed shields // Radio engineering and electronics engineering. -1967. -T.12. -Вып.10. -С.1713-1720.
- [3]. Dmitriev V.I., Zaharov Ye.V. Integral equations in boundary value problems of an electrodynamics: studies. A manual. - M.: Moscow, 1987. - 167 P.
- [4]. Henl H., Maue A., Vestphal To. The theory of a diffraction: Tr. With it. M.: Mir, 1961. - 428 P.



## TO A PROBLEM OF THE ANALYSIS OF DIELECTRIC ROD ANTENNAS

Buharov S.V.

Dnepropetrovsk National University, Ukraine 49050, Dnepropetrovsk, Naykovy lane 9,  
korp. 12, ph. + 380 (56) 776-90-92; e-mail: buser@ap1.net-rff.dsu.dp.ua

### ABSTRACT.

A number of problems arising at designing and the analysis of dielectric rod antennas is reviewed. The complex propagation constants for the  $HE_{11}$  wave in a dielectric rod are obtained. The field distribution along the rod of finite length with allowance for reflections from the rod ends is analyzed.

### INTRODUCTION

At present time decimeter and centimeter bands are widely used by different telecommunication systems. Requirements to antennas depend on their field of application. To protect antennas against climatic factors different covers are put on the open surfaces or the streamer is mounted, that can result in changes of an input resistance, distortion of antennas patterns, rereflections of a signal etc. The dielectric rod antennas, exciter of which is completely submerged in a dielectric rod from polystyrene or ceramics less depend on aggressive environmental factors and can be widely used by different telecommunication systems.

### THE WAVE PROPAGATION ALONG THE ROD

The hybrid wave  $HE_{11}$  is the main wave of dielectric rod of circular cross section. It has both magnetic and electrical longitudinal components of an electromagnetic field. From a condition of continuity the tangent components on a surface of a rod it is possible to receive the following equation:

$$4 \cdot \pi^2 \cdot f^2 \cdot g^2 \cdot n^2 \cdot (\varepsilon - 1)^2 / c^2 = [\varepsilon \cdot \psi_2^2 \cdot (\frac{\psi_1 \cdot J_{n-1}(\psi_1)}{R \cdot J_n(\psi_1)} - \frac{n}{R}) - \psi_1^2 \cdot (\frac{\psi_2 \cdot K_{n-1}(\psi_2)}{R \cdot K_n(\psi_2)} - \frac{n}{R})] \cdot$$

$$\cdot [\psi_2^2 \cdot (\frac{\psi_1 \cdot J_{n-1}(\psi_1)}{R \cdot J_n(\psi_1)} - \frac{n}{R}) - \psi_1^2 \cdot (\frac{\psi_2 \cdot K_{n-1}(\psi_2)}{R \cdot K_n(\psi_2)} - \frac{n}{R})];$$

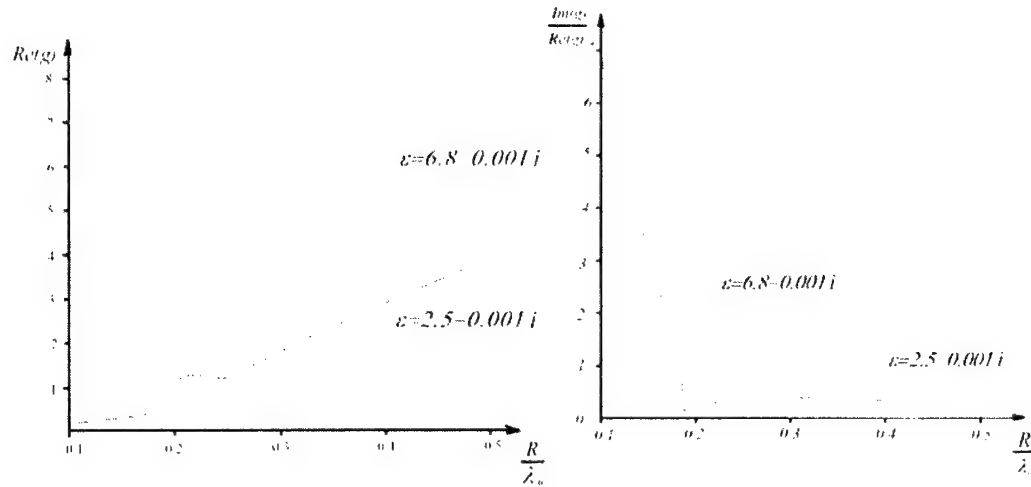
Where:  $\psi_1^2 = \frac{4 \cdot \pi^2 \cdot f^2 \cdot \varepsilon \cdot R^2}{c^2} - g^2 = (\chi_1 \cdot R)^2$ ,  $\chi_1$  transversal wave number in a rod,

$\psi_2^2 = \frac{4 \cdot \pi^2 \cdot f^2 \cdot R^2}{c^2} - g^2 = (\chi_2 \cdot R)^2$ ,  $\chi_2$  transversal wave number outside of a

rod,  $g = hR = \text{Re}(g) - i \cdot \text{Im}(g)$ ,  $h$  is a longitudinal wave number.

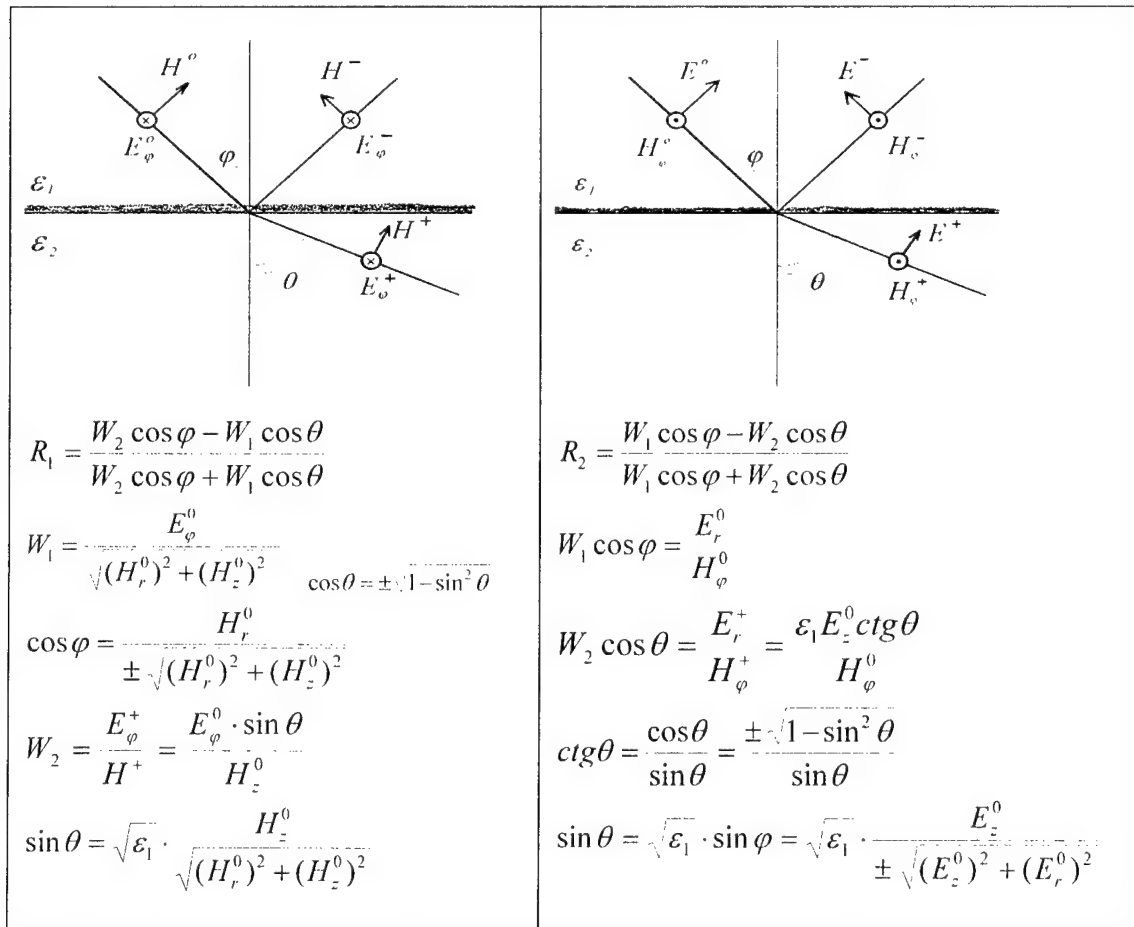
Numerical solution of the given transcendental equation rather  $g$  at known  $f, R, \varepsilon, n$  allows to find required propagation coefficients of an interesting type of wave.

The obtained results for two materials are shown in the fig.1

Fig.1. The  $HE_{11}$  longitudinal wave numbers

### REFLECTION FROM THE ROD END

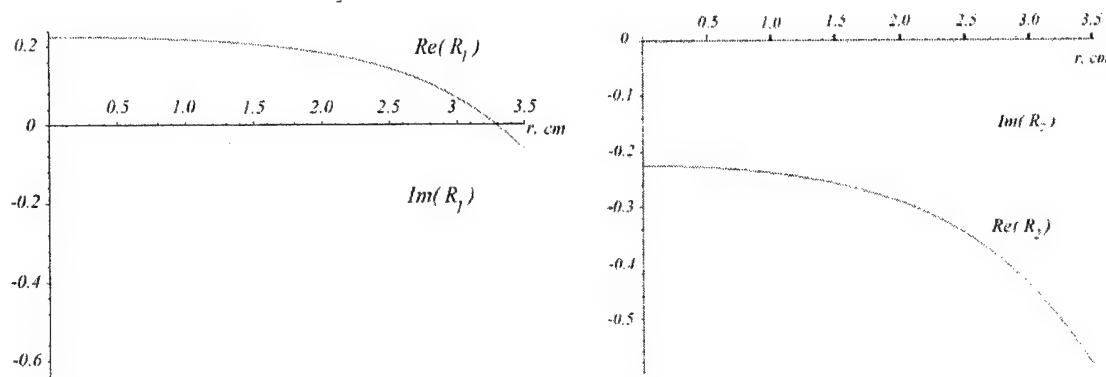
As the first approach the hybrid wave reflection from the rod end can be considered as the sum of reflections of different polarization inhomogeneous waves.[1]



When the square radix sign is chosen, it is necessary to take in to account that  $abs(R_{1,2}) \leq 1$

The obtained results for the reflection coefficients depend on distance from the rod axis. The antennas pattern calculation uses the rod surface field distribution, that's why the reflection coefficient values when  $r = R$  are used mostly.

Thus for  $\varepsilon = 2.5 - 0.001i$ ,  $f = 2.5GHz$ ,  $R = 3.5cm$  following results were obtained:



$$R_{1, r=R} = -0.064 - 0.637i$$

$$R_{2, r=R} = -0.587 - 0.317i$$

Fig. 2. The reflection coefficients for the different polarizations

Usually one end of the rod is leaned against waveguide metal wall. In this case the reflection coefficient is equal  $-1$  or  $+1$  (depend on polarization of the falling wave). Thus for the components  $E_\varphi, H_r, H_z$  the reflection coefficient from first (metallized) end is equal  $R_0 = -1$  from the second end (in free space) is equal  $R_1$ . For the components  $H_\varphi, E_r, E_z$  the reflection coefficient from the first end is equal  $R_0 = 1$ , from the second one is equal  $R_2$ .

The field distribution along the rod of the finite length  $L$  can be obtained as superposition of multiply wave reflections from the rod ends. In the general case the each component distribution along the rod can be presented as

$$U(\alpha, z) = U_0(\alpha) \cdot e^{-ihz + \phi_0} \cdot \frac{1 + R_{1,2} \cdot e^{-2ih(L-z)}}{1 - R_0 \cdot R_{1,2} \cdot e^{-2ihL}}$$

where  $h$  is a longitudinal wave number,  $\phi_0$  is an initial phase,  $U_0(\alpha)$  is the angle component distribution (variety  $\sin(\alpha)$  or  $\cos(\alpha)$ ).

## REFERENCES

- [1] V.V. Nicolskiy. Theory of electromagnetic field. Moskow: Vis. Shkola, 1961. (in Russian)

## STATISTICAL ANALYSIS OF INTERNAL PARAMETERS OF RADIATING SYSTEMS WITH REACTANCE ELEMENTS

V.V. Ovsyanikov

Dnipropetrovsk National University, Ukraine 49050, Dnipropetrovsk,  
Naykovy lane 9, korp. 12, ph. + 380 (56) 776-90-92; e-mail: root@ap1.net-rff.dsu.dp.ua

### ABSTRACT

The mathematical model of the statistical analysis of a standing-wave ratio of a voltage on an input of the radiator is offered depending on small random fluctuations of values of reactive elements, included into the radiator and from coordinates of their inclusion. From the results of a statistical estimation it follows, that minor random deviations of parameters of reactive loads of the short vibrators from design values result in essential changes of a standing-wave ratio, that must be taken into consideration at designing and using of similar radiating systems

One of the important internal radio parameters of radiating systems (RS) with impedance elements is the standing-wave ratio of voltage ( $K_s$ ) on input connectors RS, which as is known is expressed through active ( $R_{in}$ ) and reactive ( $X_{in}$ ) components of input impedance at given frequency as follows [1]:

$$K_s = \left\{ 1 + \sqrt{1 - 4R_{in}^n \left[ (1 + R_{in}^n)^2 + X_{in}^{n2} \right]} \right\} : \left\{ 1 - \sqrt{1 - 4R_{in}^n \left[ (1 + R_{in}^n)^2 + X_{in}^{n2} \right]} \right\}, \quad (1)$$

where  $R_{in}^n$ ,  $X_{in}^n$  are normalized on a wave impedance of a feeding channel ( $W_{fd}$ ) components of input resistance of a radiating system.

In their turn components  $R_{in}^n$  and  $X_{in}^n$  are functions of values ( $x_i$ ) of geometrical parameters RS ( $d, r_d$ ), included in it of impedances ( $Z$ ) and coordinates of their inclusion ( $h_Z$ ), operational frequency ( $f$ ) of an exciting source  $U$ , wave impedance  $W_{fd}$  etc (see fig.1). These relations can be presented as:

$$\begin{aligned} R_{in}^n &= R(x_1, x_2, \dots, x_N) = R(x_i), \quad i = 1, 2, \dots, N; \\ X_{in}^n &= X(x_1, x_2, \dots, x_N) = X(x_i), \quad i = 1, 2, \dots, N; \end{aligned} \quad (2)$$

Taking into account, that  $R_{in}^n$ ,  $X_{in}^n$ ,  $x_i$  are random quantities and regarding systematic components of errors of values  $R_{in}^n$ ,  $X_{in}^n$  and parameters  $x_i$ , which can be defined and

eliminated, we consider expressions (2) with the account of only random errors ( $\Delta_{x_i}$ ), the estimation of which is fulfilled below.

Let's expansion (2) in a Taylor's series near to average values of  $x_i$  or their mathematical expectations [2]:

$$\begin{aligned} R_{in}^n + \Delta_{R_{in}^n} &= R(x_i) + \sum_{i=1}^N \frac{\partial R_{in}^n}{\partial x_i} \Delta_{x_i} + \frac{1}{2} \sum_{i=1}^N \frac{\partial^2 R_{in}^n}{\partial x_i^2} \Delta_{x_i}^2 + \dots; \\ X_{in}^n + \Delta_{X_{in}^n} &= X(x_i) + \sum_{i=1}^N \frac{\partial X_{in}^n}{\partial x_i} \Delta_{x_i} + \frac{1}{2} \sum_{i=1}^N \frac{\partial^2 X_{in}^n}{\partial x_i^2} \Delta_{x_i}^2 + \dots \end{aligned} \quad (3)$$

Provided that the random errors  $\Delta_{x_i}$  are small in comparison with values  $x_i$  we neglect addends containing hqwrs of  $\Delta_{x_i}$  above the first. Further, subtracting (2) from (3) we receive values of random errors as:

$$\Delta_{R_{in}^n} = \sum_{i=1}^N \frac{\partial R_{in}^n}{\partial x_i} \Delta_{x_i}; \quad \Delta_{X_{in}^n} = \sum_{i=1}^N \frac{\partial X_{in}^n}{\partial x_i} \Delta_{x_i}. \quad (4)$$

Powering both parts of expressions (4) in a square and taking into account absence of a correlation between parameters  $x_i$ , we determine dispersions of components  $R_{in}^n$  and  $X_{in}^n$ :

$$\sigma^2(R_{in}^n) = \sum_{i=1}^N \left( \frac{\partial R_{in}^n}{\partial x_i} \right)^2 \sigma^2(x_i); \quad \sigma^2(X_{in}^n) = \sum_{i=1}^N \left( \frac{\partial X_{in}^n}{\partial x_i} \right)^2 \sigma^2(x_i). \quad (5)$$

At known dispersions (5) we determine a dispersion  $K_s$ , considering similarly to the previous making of expressions (5) provided that the random errors  $\Delta_{R_{in}^n}$  and  $\Delta_{X_{in}^n}$  are small in comparison with values of the relevant components  $R_{in}^n$  and  $X_{in}^n$ :

$$\sigma^2(K_s) = \left( \frac{\partial K_s}{\partial R_{in}^n} + \frac{\partial K_s}{\partial X_{in}^n} \right)^2 \cdot \sigma^2(R_{in}^n) \cdot \sigma^2(X_{in}^n). \quad (6)$$

Derivatives from  $K_s$  for expression (6) is determined from (1) as:

$$\frac{\partial K_s}{\partial R_{in}^n} = \frac{4(R_{in}^{n^2} - X_{in}^{n^2} - 1)}{\left[ (1 + R_{in}^n)^2 + X_{in}^{n^2} \right]^2 \sqrt{1 - \frac{4R_{in}^n}{(1 + R_{in}^n)^2 + X_{in}^{n^2}}} \left[ 1 - \sqrt{1 - \frac{4R_{in}^n}{(1 + R_{in}^n)^2 + X_{in}^{n^2}}} \right]^2} \quad (7)$$

$$\frac{\partial K_s}{\partial X_{in}^n} = \frac{8R_{in}^n X_{in}^n}{\left[ \left( 1 + R_{in}^n \right)^2 + X_{in}^{n^2} \right]^2} \left[ 1 - \frac{4R_{in}^n}{\left( 1 + R_{in}^n \right)^2 + X_{in}^{n^2}} \left[ 1 - \frac{4R_{in}^n}{\left( 1 + R_{in}^n \right)^2 + X_{in}^{n^2}} \right] \right]^2, \quad (8)$$

and dispersions of expressions  $R_{in}^n$  and  $X_{in}^n$  for the studied radiator we shall find from the formulas (5).

Thus, with the help of expressions (4) - (8) it is possible to design a statistical estimation any RS with included reactive elements. Thus, it is necessary to know particular relations such as (2) for  $R_{in}^n$  and  $X_{in}^n$  and derivatives from them on the conforming parameters  $x_i$ .

Let's put the results of a statistical estimation  $K_s$  on an input shortened twice ( $d=0,12\lambda$ ) concerning resonant length of the symmetrical vibrator with included in radiating branches the inductive loads depending on random fluctuations of values of these loads and places of their connection (fig. 1). An estimation is designed by method with usage of the theory of an equivalent long line.

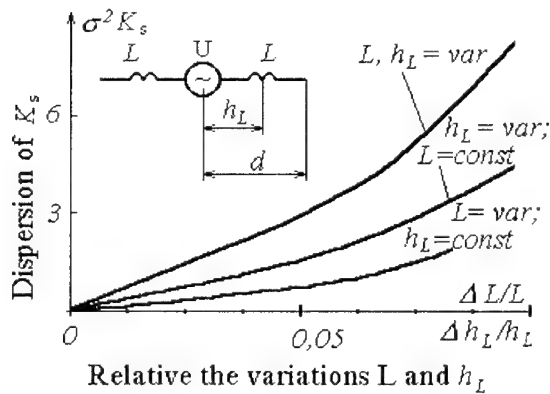


Fig.1. Dispersion  $K_s$  versus the random errors  $L$  and  $h_L$ .

with the purpose, for example, dilating of frequency range or the correction of the directional diagrams do not result in such sharp of variations the input characteristics.

The results of research are shown in a fig. 1. As follows from the charts of a fig. 1 random changes of parameters of included reactances result in essential oscillations  $K_s$ .

For small-sized radiators of such type it is possible to explain this phenomenon by narrowing of their bandwidth because of linear shrinkage of length.

Let's mark, that in the not shortened radiators of a fluctuation of reactances, included for correction distribution of a current in them

## REFERENCES

- [1] V.V. Ovsyanikov. Wire Antennas with Reactive Loads.- Moscow: Radio i Svyaz, 1985.- 120 p. (in Russian).
- [2] Ya. S. Shifrin. Statistical theory of the antennas // Chapt.IX in the boock: Reference book on the antenna technics.-V.1.-Moscow: Radiotechnics,1997.-P.148-205.(in Russian).

## AN ALGORITHM OF THE SIDELobe LEVEL OPTIMIZATION FOR THE DUAL SHAPED SYMMETRIC REFLECTOR ANTENNA

Marina V. Romanenko

State Design Bureau of Instrument and Program Systems "Svyaz"  
of the All-Russia Scientific Research Institute "Gradient",  
96 Sokolov av., Rostov-on-Don, 344010, Russia  
Email: [gkbsviaz@don.sitek.net](mailto:gkbsviaz@don.sitek.net), [mvrom@icomm.ru](mailto:mvrom@icomm.ru).

### ABSTRACT

The algorithm of the sidelobe level optimization for the dual shaped symmetric reflector antenna with the aperture diameter  $D > 20\lambda$  is presented. It is based on the method of the far-field pattern estimation by the aperture distribution. The maximal aperture efficiency is the criterion of the aperture distribution optimization on the condition that the far-field pattern estimation answers to recommendations ITU-R. Optimization parameters are defined by the function of the aperture distribution that is described as analytical function with shadow area at the center aperture, uniform area and transition regions.

### INTRODUCTION

Modern communication reflector antennas with the high aperture efficiency for ground stations are to comply with international norms and parameters. If antenna for ground station operating with geostationary satellites put into commission after 1995 then its radiation diagram must satisfy to ITU-R recommendations.

Traditionally such antennas are designed by using of the geometrical optics technique to synthesize the reflector surfaces [1]. The resulting surfaces  $S_0$  and  $S_{sr}$  (Fig.1) are determined by the solution of the system of differential equations when functions of the aperture power density  $I(r) = f^2(r)$  and the primary feed pattern  $F(\theta)$  are chosen. As a rule the ensuring of maximum aperture efficiency is the main requirement for the choice of the function described the aperture power density. Execution of ITU-R recommendations for the sidelobe level supposes a finding of amplitude distribution function  $f(r)$  as a result of decisions of the pattern synthesis problem.

In this paper the choosing of the form of the amplitude distribution function is discussed and possibility of its parameters optimization for providing the specified sidelobe level without essential reduction of aperture efficiency is analyzed.

### A DESCRIPTION OF THE METHOD

As known, the physical optic technique for the far-field calculations becomes equivalent to the aperture distribution method when the aperture diameter of the reflector antennas is  $D > 20\lambda$ . Therefore in this paper the sidelobe level evaluation is fulfilled valued by the aperture method, and the antenna gain is determined on the base of the aperture efficiency  $\eta_a(f(r))$  calculation.

The amplitude distribution in the aperture of the axially symmetric dual reflector antenna may be expressed as the difference of analytical functions:

$$f(r) = f_1(r) - f_2(r), \quad (1)$$

where

$$f_1(r) = \begin{cases} 1, & r \leq a_2 \\ \exp\left(-b\left((a_2 - r)/(a_2 - 1)\right)^2\right), & a_2 \leq r < 1 \end{cases}, \quad (2)$$

$$f_2(r) = \begin{cases} 1, & r < a_{\min} \\ \cos\left(\frac{\pi}{2}\left((r - a_{\min})/(a_1 - a_{\min})\right)^2\right), & a_{\min} \leq r < a_1 \\ 0, & a_1 \leq r < 1 \end{cases}$$

$r = R/R_{\max}$  is the normalized coordinate of the amplitude distribution function,

$r_{\min} = R_{\min}/R_{\max}$  is the relative radius of the shadowed central area,  $a_1$ ,  $a_2$  are relative radii of intermediate areas, the coefficient  $b = -\ln(f(1))$  define the field level at the edge of the aperture (Fig. 2). This type of analytical function is suitable for problem decision of the aperture efficiency optimization:

$$\eta_{a\max} = \max(\eta_a(a_1, a_2, b)). \quad (3)$$

However the expression (2) can't be used for the analytical calculation of the radiation integral  $\mathbf{K}^A(\theta, \varphi) = \int_{S_1} \mathbf{E}^A \exp(jk\mathbf{p} \cdot \mathbf{i}_R) dS_1$ , which is required for the estimation of the reflector antenna far field:

$$\mathbf{E}(R, \theta, \varphi) = -\frac{jk}{4\pi R} \exp(-jkR) \mathbf{i}_R \times (\mathbf{i}_z + \mathbf{i}_R) \cdot \mathbf{K}^A. \quad (4)$$

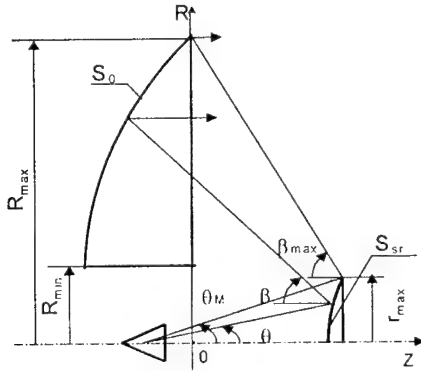


Fig. 1. Shaped feed system for the reflector

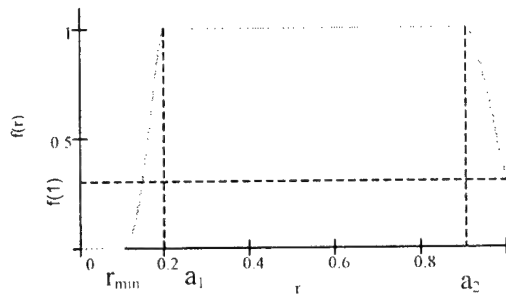


Fig. 2. Amplitude distribution at the aperture

So the amplitude distribution function (1) is approximated as difference of series:

$$f_{ann}(r) = \sum_{l=0}^{l_1} A_l (1-r^2)^l - \begin{cases} \sum_{l=0}^{l_2} B_l \left(1 - (r/a_1)^2\right)^l, & 0 \leq r < a_1 \\ 0, & a_1 \leq r < 1 \end{cases}, \quad (5)$$



where  $A_l$ ,  $B_l$  are approximation coefficients of functions  $f_1(r)$ ,  $f_2(r)$ , accordingly. Matching points along radial line of the aperture coincide with zeros of Chebyshev polynomials  $T_L(1-2r^2)$ . This choice of match points allows minimizing the maximum error.

Substituting (5) into (4) and carrying out the integration using the properties of the Bessel function [2] we have the resulting expression for  $\mathbf{K}^A$ :

$$\begin{aligned} \mathbf{K}^A(\theta, \varphi) &= \mathbf{K}_1^A(\theta, \varphi) - \mathbf{K}_2^A(\theta, \varphi), \\ K_{11}^A(\theta, \varphi) &= 2\pi R_{\max}^2 \exp(ju \cos \varphi) \sum_{l=0}^{L_1} A_l 2^l \Gamma(l+1) \frac{J_{l+1}(u)}{u^{l+1}}, \\ K_{12}^A(\theta, \varphi) &= 2\pi (a_1 R_{\max})^2 \exp(ju_1 \cos \varphi) \sum_{l=0}^{L_1} B_l \Gamma(l+1) \frac{J_{l+1}(u_1)}{u_1^{l+1}}. \end{aligned} \quad (6)$$

where  $u = kR_{\max} \sin \theta$  and  $u_1 = a_1 u$ .

When the geometrical optics syntheses of antenna surfaces is fulfilled for the amplitude distribution given by function (5), the expression (6) describes the far field without the loss of accuracy.

Resulting dependencies are presented on Fig. 3

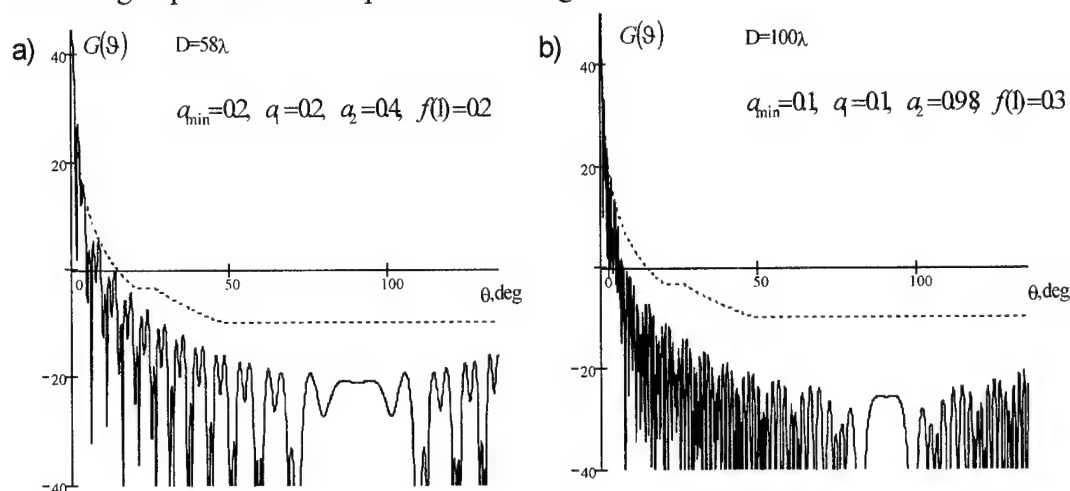


Fig. 3. Radiation pattern of the dual symmetric reflector antenna

## REFERENCES

- [1] G.Z. Azenberg, V.G. Iampolski, O.N. Tereshin. Antennas of USW. – M: "Svyaz" V. 2. – 1997. – Pp. 58-74. (In Russian).
- [2] K. Hongo, H. Matsuura. Simplified Technique for Evaluating the Radiation Integrals. – IEEE Trans. Antennas Propagat. – V. AP-34. – Pp. 732-737. – No. 5. – May. – 1986.

## FITNESS FUNCTION CALCULATION TECHNIQUE IN YAGI – UDA ANTENNAS EVOLUTIONARY DESIGN

Sergey N. Sorokin, Vladimir V. Savelyev, Elena V. Ivanchenko, Maxim P. Oleynik

Taganrog State University of Radioengineering,  
Taganrog, Nekrasovsky, 44, GSP-17A, Russia, 347928  
+7-863-4-371733, airpu@tsure.ru

### ABSTRACT.

Yagi – Uda antennas is the one of most simple type of wire antennas in different applications. A design of these antennas turned out to be the complex problem. It is connected with complexity of definition of current distributions on antenna's vibrators. This currents distribution can be used for account of external and internal antenna parameters. These parameters are used for fitness function calculation, which allowing finding the optimum decision of designing problem. The chosen fitness function should include both external, and internal antennas parameters. Hallen's integral equation application for current distribution definition on Yagi – Uda antennas vibrators is considered in this paper. It is shown, that the examination of frequency dependences of input resistance and currents amplitudes distributions can in addition simplify a design of the antenna.

### INTRODUCTION

Modern computer-aided modeling tools permit to calculate external and internal antennas parameters. Most popular tool is NEC2 [1, 2]. The application of this software allows to simplify the decision of tasks of antenna design optimization. The main role in reduction of time of the optimization task decision is defined by a choice of fitness function. The large reduction of decision time can be achieved in a case, when fitness function includes parameters, which reflecting basic physical processes proceeding in the antenna. At a choice of such parameters it is desirable to use integrated antenna's parameters. Such parameters are antenna's complex input resistance, pattern width, side lobe level and so on. Besides at generation of an initial population it is necessary to take into account the theoretical and experimental results received earlier for a chosen antennas type. In another case received solution may be very far from optimal solution, or can not be realized. It can occur because the considered software uses the approximated laws of currents distribution in antennas vibrators. Thus the put task can overstep the bounds of methods applicability used at creation of this tool. Other reason of similar mistakes can become not enough detailed structure of fitness function. It can occur when fitness function includes only external or internal parameters.

As example of such fitness function can be considered function, which was used at the decision of optimization of the Yagi – Uda antennas construction problem, considered in [3]. In the given paper the design of the antennas from 14 elements ensuring work in a frequencies bandwidth near 12 percents is developed. Thus the thickness of antennas vibrators relied identical and equal 3 mms. But the analysis of experimental researches of such antennas shows, what even for the five-element antenna it is difficult to receive a pass band

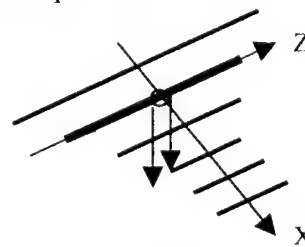


Fig. 1

Antennas construction

in 10 per cents [4]. It is necessary to use active vibrators of the special form or to increase their thickness for expansion of such antennas passband.

Besides it is necessary to note, that at such disorder of the vibrators sizes some vibrators will have the large complex part of entrance resistance. It will result that the current amplitude in them will be much less, than in vibrators, which length is close to half of working wavelength. Hence they will not influence to antennas pattern formation and can be excluded from the antenna construction.

### APPROACH DESCRIPTION

Let's consider a task in the following statement. There is the Yagi – Uda antenna in the free space, which consisting of  $N$  linear elements (fig. 1). Its active vibrator is coincided by a dot source, which located at its centre. The vibrators thickness is much less, than working wavelength. It is required to choose a method of currents distribution calculation on the antennas vibrators, which permit to have an opportunity to define its external and internal parameters.

The opportunity of two types integral equations application for the decision of the put task was investigated. It was shown, that the poklington's system of the integral equations does not permit to receive the steady solution of a considered problem. The current distribution on antennas vibrators was received on the basis of the decision of hallen's integral equations system:

$$\sum_{n=1}^N \int_{-l_n}^{l_n} J_{nz}(z') \frac{e^{-ikR_{pq}}}{R_{pq}} dz' = C_m \cos(\beta z) - \frac{iU_m}{60} \sin(\beta|z|), \quad (1)$$

Where  $z$  - arrangement coordinate of an auxiliary source

$z'$  - coordinate of integration point on the vibrator surface with number  $m$ ;

$L_n$  - length of the vibrator with number  $n$ ,

$U_m$  - the voltage amplitude stimulating in a backlash of the active vibrator,

$$R_{pq} = \begin{cases} \sqrt{(z'_n - z_m)^2 + D_{nm}^2}, & \text{if } z_m \notin L_n; \\ \sqrt{(z'_n - z_m)^2 + a^2}, & \text{if } z_m \in L_n; \end{cases}$$

$R_{pq0}$  - distance between a point of an auxiliary source and middle of the active vibrator.

The constant  $C_m$  can be found directly from (1) when  $z$  is equal to the 0. Using a designation

$$K_{mn} = \frac{e^{-ikR_{pq}}}{R_{pq}} - \cos(\beta z) \frac{e^{-ikR_{pq0}}}{R_{pq0}},$$

Transform expression (1) to the following

$$\sum_{n=1}^N \int_{-l_n}^{l_n} J_{nz}(z') K_{mn}(z, z') dz' = -\frac{iU_m}{60} \sin(\beta|z|)$$

decomposition of series:

$$J_{mz}(z') = \sum_{p=1}^P J_{mp} \left(1 - \frac{|z'|}{l_m}\right)^p \quad (2)$$

The input resistance of antenna is calculat

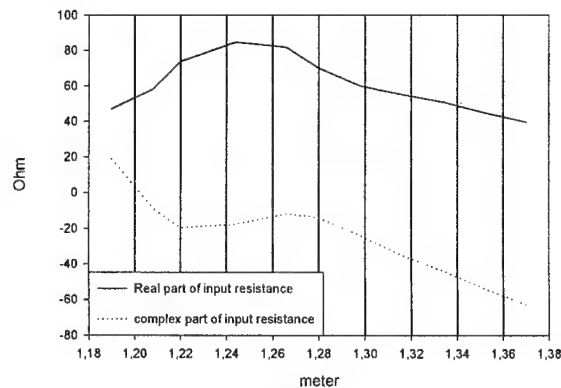


Fig. 2

$$Z_{entr} = U_m / J_m(0)$$

## EXPERIMENTAL RESULTS.

For the decision of the put task three harmonics in series (2) were used. The received currents distribution was used for calculate of antennas entrance resistance and its pattern in main planes. It was shown, that the pattern's form in E- plane changes insignificantly in the specified frequency range. But in the H- plane there are large changes of the pattern's form and side lobe levels. Also the large changes are tested by input resistance in the working frequency bandwidth. It is equal to the 39,7-j63,9 Ohm at the frequency 219 MHz, 70-j17 Ohm at frequency 235 MHz, and 49,3+j6 Ohm at frequency 250 MHz. Dependences of an active and complex components of antennas input resistance from working wavelength are shown in figure 2. Such character of entrance resistance changing specifies to resonant character of processes, which proceeding in the antenna. The abrupts of active and complex components of antennas input resistance in a working strip complicate its connection with feed line. These abrupts can be eliminated by introduction of the additional agreeing device into antennas construction. It will complicate a design of the antenna and can decries the working bandwidth.

Distribution of currents amplitudes at the centers of vibrators in a working frequencies bandwidth was investigated. It is shown, that the currents amplitudes on short vibrators of the considered antenna can be in fifty ore one hundred times less, than currents amplitudes in resonant vibrators in working frequency range. It allows making the conclusion that such vibrators can be excluded from antenna's construction.

Change of behavior of antenna entrance resistance in frequency range also was examined at increasing of vibrators thickness. To not leave from borders of applicability of a using method the vibrators by thickness of 6 mm were considered. The analysis of results shows, that in this case it is possible to reduce jumps of a complex component of antenna entrance resistance.

## CONCLUSION

Thus is shown, that the introduction in fitness function in [3] input resistance of the antenna would allow essentially changing a construction of the developed antenna. After examining the antennas construction, developed in [3], we can say that this antenna is not Yagi – Uda antenna, because the classic phase relationships between the vibrators currents are not required in this construction. In additional we note, that application of classic relationships between antennas elements sizes and distances between vibrators provided the reduction of calculation efforts.

## REFERENCES

- [1]. G. J. Burke Recent improvements to the model for wire antennas in the code NEC,1989, IEEE
- [2].S. Chakrabarti, R. Ravichender, E. K. Miller, J.R. Auton, G.J. Burke Applications of Model-based parameter estimation in electromagnetic computations, 1990, IEEE
- [3]. Evolutionary Optimization of Yagi – Uda antennas. Jason D. Lohn, William F. Kraus, Derek S. Linden and Silvano P. Colombano, 2001, Proc. ICECS
- [4]. Sorokin S.N., Savelyev V.V. Types of communication antennas Taganrog, 1999

## EVALUATION OF UNCERTAINTY BUDGET FOR ANTENNA CALIBRATIONS

B. Türetken<sup>1</sup> S. E. San<sup>2</sup> M. Yazıcı<sup>1</sup> İ. Araz<sup>1</sup> A.İ. Yürekli<sup>1</sup> M. Hekim<sup>3</sup>

<sup>1</sup>TÜBİTAK-UEKAE, P.K.74, Gebze, 41470 Kocaeli TURKEY bahattin@uekae.tubitak.gov.tr

<sup>2</sup>TÜBİTAK-UME, P.K.54, Gebze, 41470 Kocaeli TURKEY

<sup>3</sup>GAZİOSMANPASA UNIVERSITY, Tokat MYO, Tokat TURKEY

### ABSTRACT

Accurate field strength measurements for EMC conformance testing can be obtained by using antennas which have reliable antenna factors (AF). AF is a major component in calculating the uncertainty budget of an EMC test. So AF must be highly accurate and the equipment used for measurement must be traceable to a national standard. In a calibration process, it is important to obtain reliable data on two important characteristics : traceability and uncertainty. In this study, we report the evaluation of uncertainty budget in antenna calibrations. Parameters acting in this budget are explicitly presented. Apart from providing precise information about the characteristic uncertainty of device, such a budget permits the overall evaluation of the system so that one could think about possible innovations for reduction of measurement uncertainty [1].

### INTRODUCTION

A measurement could be distinguished as a calibration under appropriate circumstances, if and only if, traceability and uncertainty information are included as a part of this measurement. In this study, we present the evaluation of uncertainty of antenna calibrations in the frame of conventional uncertainty estimation where partial derivatives of the fundamental formula constitute the basis of uncertainty budget [2,4]. Both A and B type factors, coming from random effects and known uncertainty values of devices respectively, are concerned in the evaluation process.

### THEORY

Those equations that can be concerned as the starting point are listed below:

$$AF_1 = 10\log f_M - 24.46 + 1/2 [E_{Dmax} + A_1 + A_2 - A_3] \quad (1)$$

$$AF_2 = 10\log f_M - 24.46 + 1/2 [E_{Dmax} + A_1 + A_3 - A_2] \quad (2)$$

$$AF_3 = 10\log f_M - 24.46 + 1/2 [E_{Dmax} + A_2 + A_3 - A_1] \quad (3)$$

where;  $E_D^{max}$  is the maximum received field at separation distance R from the transmitting antenna,  $AF_{1,2,3}$  are the antenna factors of antennas 1,2 and 3 in dB(1/m),  $A_{1,2,3}$  are the measured site attenuation results in dB.  $f$  is the frequency in MHz [3].

In the scope of the uncertainty evaluation, partial derivatives of the starting equation with respect to the included parameters are constituted in the following manner:

$$D_1 = \frac{\partial}{\partial f_M}(AF_1) + \frac{\partial}{\partial E_{Dmax}}(AF_1) + \frac{\partial}{\partial A_1}(AF_1) + \frac{\partial}{\partial A_2}(AF_1) + \frac{\partial}{\partial A_3}(AF_1) \quad (4)$$

Absolute values of these partial derivatives yield,  $10/f_M$ ,  $1/2$ ,  $1/2$ ,  $1/2$ ,  $1/2$  respectively, and the uncertainty of the system could be established on this basis as follows:

$$U = \sqrt{(10/f_M)^2 \Delta f_M^2 + (1/2)^2 \Delta E_{Dmax}^2 + (1/2)^2 \Delta A_1^2 + (1/2)^2 \Delta A_2^2 + (1/2)^2 \Delta A_3^2} \quad (5)$$

where U is the total uncertainty and  $\Delta$  terms represent the individual uncertainty values of the corresponding quantities. In the numerical step, evaluation all terms inside the square root are expressed either by certificate values of the devices in use (i.e. B type), or statistical evaluation of the data of the measurement (i.e. A type). In the case of A type uncertainty, repeatability of

the measurement plays an important role and reliability of this factor increases as the number of measurements increase. It is a convenient preference to multiply the obtained uncertainty value  $U$  by 2 so that an extended uncertainty is concerned and this situation is generally denoted as uncertainty at  $k=2$ .

## EXPERIMENTAL RESULTS

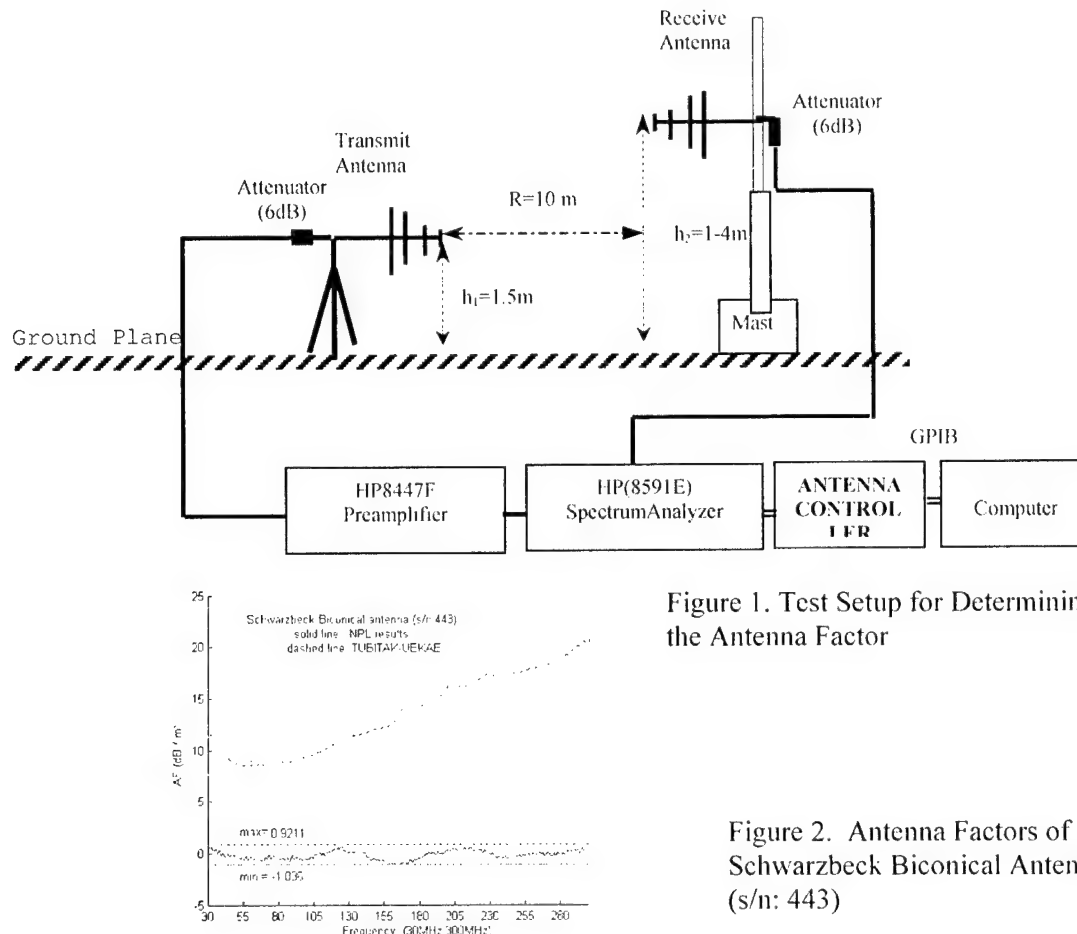
We have applied ANSI C63.5-1998 Standard Site Method (SSM) in an Open Area Test Site (OATS) [3]. UEKAE has a large flat outdoor ground plane which has been shown to act as a near-perfect mirror at VHF frequencies. The SSM, based solely on horizontally polarized measurements, provides antenna factor measurements from 30 MHz to 1000 MHz. The measurement distances are 3m and 10 m, transmitting antenna heights are 1m and 2m, and receiving antenna search heights are from 1m to 4m. The methods are used for horizontal polarization on a standard antenna calibration site. The SSM requires three site attenuation measurements under identical geometries using three identical antennas taken in pairs, as shown Figure 1.

$$AF_1 + AF_2 = A_1 + 20 \log(f_{\text{MHz}}) - 48.92 + E_{\text{Dmax}} \quad (6)$$

$$AF_1 + AF_3 = A_2 + 20 \log(f_{\text{MHz}}) - 48.92 + E_{\text{Dmax}} \quad (7)$$

$$AF_2 + AF_3 = A_3 + 20 \log(f_{\text{MHz}}) - 48.92 + E_{\text{Dmax}} \quad (8)$$

There are two measurement procedures that may be used to determine site attenuation: *discrete frequency method* and *swept frequency method*. We have used *swept frequency method* controlling the test equipment by using a computer interface (Figure 1).



We have obtained the antenna factors of Schwarzbeck biconical antenna (s/n:443) with a very good agreement between the NPL measurement results (Figure 2).

Table 1. Estimated Uncertainties (30MHz-1000MHz)

Description of uncertainty	Coverage factor	Biconic Antenna		Log-Per Antenna	
		3m	10m	3m	10m
Cable Attenuation	Normal k=2	± 0.3	±0.3	±0.3	±0.3
Receiver Specifications	Rectangular $k=\sqrt{3}$	± 0.2	±0.2	±0.2	±0.2
Preamplifier	Rectangular $k=\sqrt{3}$	± 0.4	±0.4	±0.4	±0.4
Attenuator	Rectangular $k=\sqrt{3}$	± 0.3	±0.3	±0.3	±0.3
Height Measurement	Rectangular $k=\sqrt{3}$	± 0.6	± 0.4	± 0.6	± 0.4
Distance Measurement	Rectangular $k=\sqrt{3}$	± 0.6	± 0.4	± 0.6	± 0.4
Site imperfections	Rectangular $k=\sqrt{3}$	± 0.04	± 0.04	± 0.05	± 0.05
Maximum measured	Standard deviation	± 0.6	± 0.6	± 0.8	± 0.8
<b>Combined standard</b>	<b>Normal k=2</b>	<b>0.84</b>	<b>0.765</b>	<b>1</b>	<b>0.93</b>
<b>Expanded uncertainty</b>	<b>Normal k=2</b>	<b>1.69</b>	<b>1.53</b>	<b>2</b>	<b>1.86</b>

By using equation (5) combined standard uncertainty can be calculated as follow:

$$U = \sqrt{\frac{0.3^2}{4} + \frac{0.2^2 + 0.4^2 + 0.3^2 + 0.6^2 + 0.6^2 + 0.04^2}{3} + 0.6^2} = 0.84$$

## CONCLUSION AND DISCUSSION

The antennas were identical biconic and log periodic antennas covering the frequency range of 30 MHz to 1GHz. The data were measured at 800 frequency points using spectrum analyzer, low loss cables, and a positioning with 1cm. The test was performed at 3 and 10-meter separation, 1.5-meter transmit height, and 1-to 4-meter scan height per ANSI C.63.5 on an open area test site (OATS). The standard deviation of 12 (biconic and log periodic) antenna factors and their maximum deviations from the average are calculated. Another systematic error contribution is the max-hold height step. For continuous height scanning, this is a function of sweep time versus tower speed. The final and most troubling contribution is site imperfections. For this purpose, scattering objects nearby are cleaned, measurement site is wiped with sandpaper and painted. Directivity of antennas are positioning of the cables are adjusted so as to minimize reflections. Recording of the measurement results are performed automatically in order to overcome uncertainty due to personnel failure in reading. The estimated uncertainties in the measured antenna factors are listed Table 1.

## REFERENCES

- [1] M.J. Alexander, M.J. Salter, D.G. Gentle, K.P. Holland "Advances in measurement methods and reduction of measurement uncertainties associated with antenna calibration" IEE Proc. -Sci Meas. Technol., Vol.141, No.4, July 1994
- [2] International Organisation for Standardisation 1993-Guide to the expression of uncertainty in measurement,
- [3] ANSI C63.5-1998 American National Standard for Electromagnetic Compatibility-Radiated Emission Measurements in Electromagnetic Interference (EMI) Control-Calibration of Antennas (9kHz-40 GHz)
- [4] M. D. Foegelle, "A statistical Approach to Measurement Uncertainty" Antenna Catalog Essential Equipment for EMC Testing-EMCO 1998.

# ANTENNA ARRAYS SYNTHESIS ACCORDING TO THE SECTOR PATTERN BY MULTIPARAMETRIC METHOD OF REGULARIZATION

N.N. Gorobets, O.N. Nosenko

Kharkov National University, 4, Svobody Sq., Kharkov, 61077, Ukraine

E-mail: Olga.N.Nosenko@univer.kharkov.ua

## ABSTRACT

The synthesis problem of linear antenna arrays has been solved numerically by multiparametric regularization method (MRM). The synthesis power directivity pattern was given by a sector pattern with prescribed width and direction of pattern main lobe, low level of side lobes. The investigations of the synthesis problem quasi-solutions and their properties have been carried out.

## PROBLEM STATEMENT AND METHOD OF SOLUTION

As known, the nonlinear synthesis problems of radiation systems according to the prescribed amplitude or power directivity pattern (PDP) are the most complicated. These problems belong to the set of ill-posed inverse problems [1]. The field directivity pattern of radiation system with linear polarized radiators has the following view:

$$G(\theta, \varphi) = \sum_{m=1}^N a_m f_m(\theta, \varphi) e^{-ikr_m(\theta, \varphi)}, \quad (1)$$

where  $f_m(\theta, \varphi)$  is the partial directivity pattern of radiator with Cartesian co-ordinates  $(x_m, y_m, z_m)$  of its phased center (with unit current on it). To registrate the mutual coupling we must calculate or measure directivity pattern, when other radiators are passive.  $N$  is the quantity of radiators,  $k = 2\pi/\lambda$  is the wave number,  $r_m(\theta, \varphi) = x_m \sin \theta \cos \varphi + y_m \sin \theta \sin \varphi + z_m \cos \theta$ ,  $\mathbf{a} = (a_1, a_2, \dots, a_N)$  is the excitation vector of radiation system,  $(\theta, \varphi) \in W = \{(\theta, \varphi) : 0 \leq \theta \leq \pi, 0 \leq \varphi \leq 2\pi\}$ . The PDP of radiation system is determined by the expression  $F(\theta, \varphi) = |G(\theta, \varphi)|^2$ . The sector

function  $S(\vartheta, \varphi, \varphi_{\max}, h) = \begin{cases} 1, & \varphi_{\max} - h \leq \varphi \leq \varphi_{\max} + h \\ 0, & \varphi \in [-90^\circ, \varphi_{\max} - h) \cup (\varphi_{\max} + h, 90^\circ] \end{cases}$  defines the

directivity pattern in the plane  $\theta = \pi/2$ , where  $2h(^\circ)$  is the width of sector and  $\varphi_{\max}$  is the direction of the pattern main lobe.

According to the MRM we consider a system of control directions  $\psi_i = (\theta_i, \varphi_i)$ ,  $i=1, 2, \dots, L$ . In our case all of the points are located in the plane  $\theta = \pi/2$ . Some of the points  $\psi_i$ ,  $i=1, 2, \dots, M$  ( $M < L$ ) are in the region of main lobe  $V_1$  ( $|\varphi_i - \varphi_{\max}| \leq h$ ), and  $\psi_i = (\theta_i, \varphi_i)$  for  $i=M+1, \dots, L$  are in the region of side lobes  $V_2$  ( $\varphi_i \in [-90^\circ, \varphi_{\max} - h) \cup (\varphi_{\max} + h, 90^\circ]$ ). The tolerant values of PDP are given by the inequalities in the region of main lobe  $V_1$ :

$$d_i \leq F_i(\mathbf{a}) \leq c_i \quad \text{for } i=1, 2, \dots, M, \quad (2)$$



and in the region of side lobes  $V_2$

$$F_i(\mathbf{a}) \leq c_i \quad \text{for } i=M+1, \dots, L, \quad (3)$$

$c_i, d_i$  are positive numbers,  $F_i(\mathbf{a}) = F(\theta_i, \varphi_i) = (\mathbf{B}_i \mathbf{a}, \mathbf{a})$ ,  $\mathbf{B}_i$  is a complex  $N$ -dimension Erermite matrix with elements  $(\mathbf{B}_i)_{m,l} = \tilde{f}_m^*(\theta_i, \varphi_i) \cdot \tilde{f}_l(\theta_i, \varphi_i)$ , where  $\tilde{f}_m(\theta_i, \varphi_i) = f_m(\theta_i, \varphi_i) \cdot e^{-k r_m(\theta_i, \varphi_i)}$ . Inequalities (2) and (3) define the tolerant set  $D$  of vectors  $\mathbf{a} \in X_N$ . The synthesis problem according to the prescribed PDP of the antenna array is formulated as minimization problem of smoothing functional:

$$R(\mathbf{a}, \mathbf{u}) = Q(\mathbf{a}) + \sum_{i=1}^L u_i F_i(\mathbf{a}), \quad (4)$$

where  $Q(\mathbf{a}) = (\mathbf{A}(\mathbf{a} - \mathbf{a}_0), (\mathbf{a} - \mathbf{a}_0))$  is quadratic functional,  $u_i$ ,  $i=1, \dots, L$ , are some real weight parameters,  $\mathbf{a}_0$  is the given vector. We consider the next minimization problem

$$\min_{\mathbf{a} \in X_N} R(\mathbf{a}, \mathbf{u}) \quad \text{for } \mathbf{u} \in U. \quad (5)$$

$R(\mathbf{a}, \mathbf{u})$  is the positive definite quadratic functional with respect to excitation vector  $\mathbf{a}$  for all  $\mathbf{u} \in U$ .

The quasi-optimal synthesis problem for antenna array is formulated in the next form:

$$\min_K P(\mathbf{a}), \quad \text{where } K = \bar{K}_0, K_0 = \bigcup_{\mathbf{u} \in U} \arg \min_{\mathbf{a} \in X_N} \{R(\mathbf{a}, \mathbf{u})\}, \quad (6)$$

$P(\mathbf{a}) = \sum_{i=1}^M \max \{0, d_i - F_i(\mathbf{a}), F_i(\mathbf{a}) - c_i\} + \sum_{i=M+1}^L \max \{0, F_i(\mathbf{a}) - c_i\}$ . It is proved [2], that

the problem (6) has solution even in the case, when tolerant set  $D$  is empty. Hence, there is a vector  $\mathbf{a} \in K$ , which minimizes the function  $P(\mathbf{a})$ . We have convergent iterative process with respect to  $\mathbf{u}$  [2], which minimizes errors of synthesis PDP in the control directions. On each step we may choose vector  $\mathbf{u} \in U$  by making use of well-grounded special way and must solve the minimization problem (5). As the synthesis PDP the sector directivity pattern  $S(\theta, \varphi, \varphi_{\max}, h)$  is chosen. Inequalities (2) and (3) are given with the next parameters:  $c_i = 1 + 0.01$ ,  $d_i = 1 - 0.01$  for  $\varphi_i \in V_1$ ,  $c_i = 0.01$  for  $\varphi_i \in V_2$ .

## NUMERICAL RESULTS AND DISCUSSION

The synthesis problems were solved for antenna arrays, which had different parameters. In particular, we considered various radiators, linear antenna arrays with different quantity of elements  $N$  and radiators distance. We changed the width of the sector and direction of the main lobe of PDP. As an example, the synthesis problem of antenna arrays with several isotropic radiators, where  $f_i(\theta, \varphi) = 1$ , was considered. In this case the gotten excitation vector  $\mathbf{a}$  had the constant amplitude distribution and the linear phased distribution. The condition of existence of single main lobe with low level of side lobes fulfilled for sector of angles  $\varphi \in [-40^\circ, 40^\circ]$ . The maximum level of side lobes was equal to  $-25$  dB.

Also, we considered antenna arrays when the distance between radiators was  $d/\lambda = 0.2 < 0.5$ . For some values of the scanning angles of main lobe the iterative process

didn't converge to the single point in  $X_N$ . We got several quasi-solutions for different parts of this process. This example corresponded to the case, when the period  $T=2\pi/d$  of array directivity pattern is greater than interval of real angles  $[-k, k]$ , where PDP was defined.

Directivity pattern with the narrowest main lobe for antenna arrays with parameters  $d/\lambda=0.6$ ,  $f_i(\theta, \varphi) = (\cos \varphi)^{5/2}$ ,  $N=21$  is described in Figure 1(a). In Figure 1(b) the result of the PDP synthesis is represented for antenna arrays with parameters  $d/\lambda=0.6$ ,  $f_i(\theta, \varphi) = (\cos \varphi)^{5/2}$ ,  $N=20$ ,  $h=0.14\text{rad}$ .

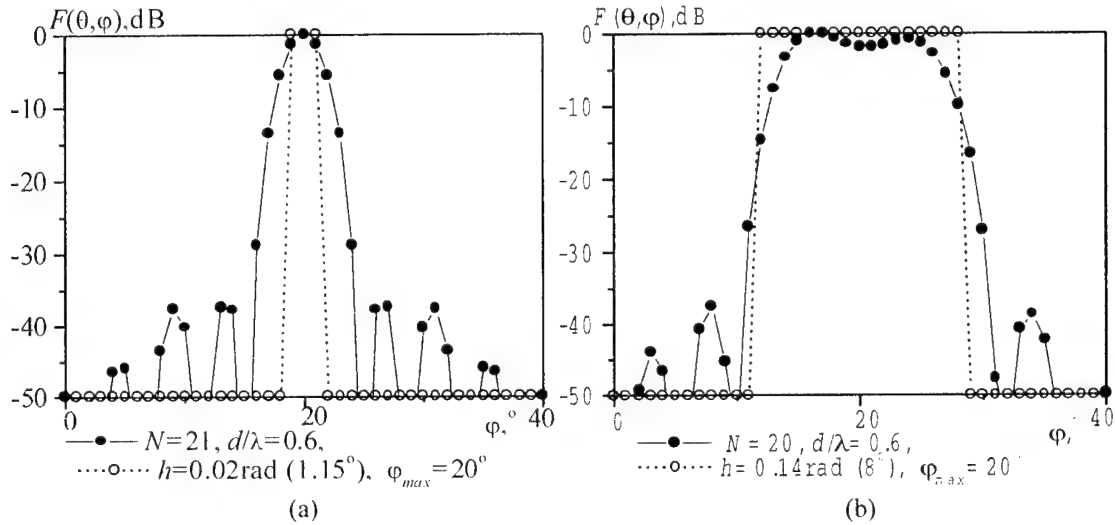


Figure 1. Sector PDP with the width of sector  $2h$  in the plane  $\theta=\pi/2$  with direction of the main lobe  $\varphi_{max}=20^\circ$  and synthesis PDP for the equidistant antenna arrays.

## CONCLUSIONS

Computer codes for solving antenna array synthesis according to the prescribed PDP have been developed using multiparametric regularization method. These codes enable to find quasi-solutions of the synthesis problems for different types of antenna arrays with the given partial directivity patterns of radiators and the given geometry of the antenna arrays.

In spite of complication of the MRM for creating program codes we marked convenience in the application of this method and good convergence of the algorithm, especially, for the given sector patterns. We analyzed the class of quasi-solutions according to the sector power directivity patterns with different width and directions of main lobe. It was shown, that the synthesis problem had nonunique solution in the case, when radiators distance  $d/\lambda \leq 0.5$ . The examples of the synthesis will be presented. The arrived results prove high effectiveness of multiparametric regularization method.

## REFERENCES

- [1] A.N.Tichonov, B.Y.Arsenin, Methods of Solution of Incorrect Problems, Nauka Publ., Moscow, 1979 (in Russian).
- [2] V.I.Dmitriev, N.I.Berezina, Numerical Methods of Synthesis Problems Solution of Radiation Systems, Moscow, Moscow State University, 1986 (in Russian).

# **NUMERICAL TECHNIQUES**

## A STUDY FOR THE FAST SOLUTION OF ELECTROMAGNETIC SCATTERING PROBLEMS: A WAVELET BASED APPROACH

M. Bahattin Kurt, Niyazi Ari\* and Osman Cerezci\*\*

Institute of Sciences and Technology, University of Sakarya, Sakarya, Turkey

E-mail: [mbkurt70@hotmail.com](mailto:mbkurt70@hotmail.com)

\*University of Applied Sciences, Zürich, Switzerland

E-mail: [nari@fhzh.ch](mailto:nari@fhzh.ch)

\*\* Institute of Sciences and Technology, University of Sakarya, Sakarya, Turkey

E-mail: [cerezci@sakarya.edu.tr](mailto:cerezci@sakarya.edu.tr)

### ABSTRACT

Conventional method of moments (MoM), when directly applied to integral equations arising in numerical solution of electromagnetic(EM) scattering problems, leads to a dense( fully populated) matrix which often becomes computationally ungovernable even for supercomputers, especially when the electrical size of the scatterer becomes large. To overcome this difficulty, wavelet bases have been used recently which lead to a sparse matrix that can be solved easily by an efficient sparse solver. Using wavelet in solving EM integral equations has been widely studied. The purpose of this paper is to develop a strategy for efficient wavelet solution of integral equations by connecting and using efficient studies have been done in this area. Numerical results are provided to illustrate the validity of the proposed approach.

### INTRODUCTION

A large class of EM scattering problems can be formulated by the following integral equation

$$\int f(s')G(s,s')ds' = g(s) \quad (1)$$

where  $f(s)$  stands for the induced surface current,  $G(s,s')$  is the Green's function, and  $g(s)$  stands for the excitation source. Generally, equation (1) has no closed-form solutions and the MoM is used to solve it numerically. As well known, the use of traditional basis and testing functions for solving in the MoM results in a dense matrix equation. A direct solution of a dense matrix equations needs  $O(N^3)$  operations, and an iterative solutions requires  $O(N^2)$  operations per dense matrix-vector multiplication, where  $N$  is the number of unknowns in the discretized integral equations. Therefore, traditional MoM is not of practical use, as the number of unknowns increases, due to the large memory requirement and high computation time necessary to solve matrix equation.

To overcome these difficulties, recently, EM researchers used wavelets, primarily because of their local supports and vanishing moment properties, to solve EM integral equations. There are currently two approaches to introducing wavelets in the MoM: In the first, the integral equation has been directly expanded and tested with wavelet bases

functions [1]-[2]. However, since few kinds of wavelets can be solved in closed form, this approach requires considerable numerical effort to efficiently evaluate the integrals, which dims the use of wavelets in the MoM. The other approach is to use a conventional basis and testing functions to convert integral equation into matrix equation and then perform a discrete wavelet transform on the resultant matrix equation [3]. More recently, the authors have proposed an effective circulant wavelet transform method, which can be adaptively used to solve efficiently a wide range of EM problems [4]. In this study, therefore, we use the approach used in [4].

## FORMULATION

By using the MoM, we obtain the matrix equation

$$ZI = V \quad (2)$$

where  $Z$  is a dense impedance matrix. Introducing a wavelet matrix  $W$ , the matrix equation in (2) then transformed as

$$Z'T' = V' \quad (3)$$

where

$$Z' = WZW^T, \quad I' = (W^T)^{-1}I, \quad V' = WV. \quad (4)$$

Here  $T$  stands for the transpose of a matrix. For a given threshold value  $\tau$  ( $0 < \tau < 1$ ), (3) becomes a sparse matrix equation which can be efficiently solved by a sparse solver. Once  $I'$  is solved, the desired solution is obtained as

$$I = W^T I' \quad (5)$$

The construction of the wavelet matrix  $W$  can be found in [4]. In constructing  $W$ , among the wavelet types, Daubechies' wavelet is chosen, because of its compactness and orthogonality properties, to effectively construct sparse wavelet matrix, which reduces the computational cost [5]. Finally, an appropriate choice of the number of vanishing moments of wavelets is made as 8 from [4] to obtain fast and accurate solution in the numerical experiments.

## NUMERICAL RESULTS

In this section, the results of a study of matrix sparsity as a function of the problem size are presented. Scattering of plane wave from 2-D rectangular cylinder is computed numerically using a constant number of test functions (20 pulse) per wavelength. The system sizes studied ranged from  $N = 64$  (contour length of  $3.2\lambda$ ) to  $N = 2048$  (contour length of  $102.4\lambda$ ). The sparsity of truncated  $Z'$  and the associated relative error of current distribution on the contour surface for several thresholds is shown in Fig. 1. Here the percent sparsity is  $S = ((N_0 - N_\tau)/N_0) \times 100$  where  $N_0$  is the total number of elements and  $N_\tau$  is the number of remaining element after the truncation. The relative error caused by the truncation is  $\epsilon = \|I_0 - I_w\|_2 / \|I_0\|_2$  where  $I_0$  is the solution obtained by the MoM and  $I_w$  is that obtained from the wavelet method.

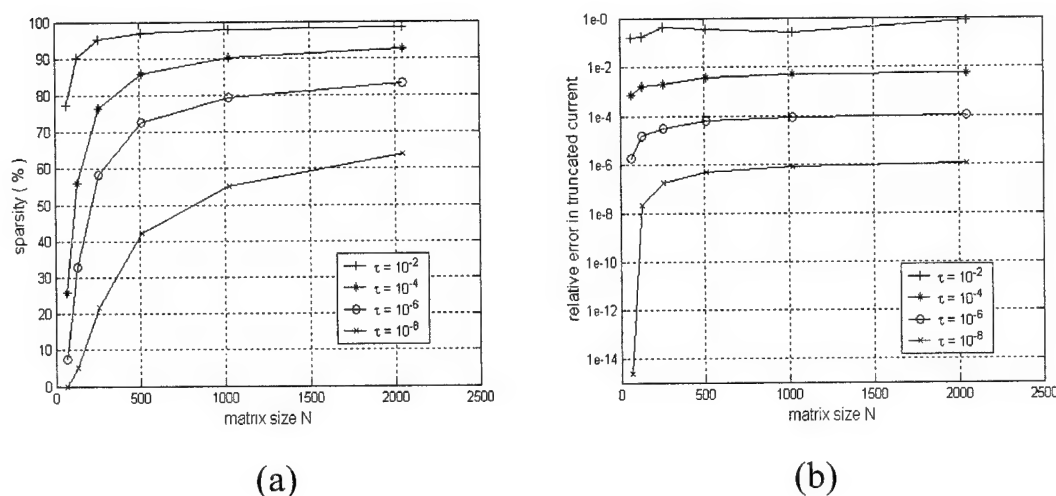


Fig. 1 Matrix Sparsity(a) and Relative Error in Current(b) as a Function of Size  $N$

## CONCLUSION

The EM scattering from a 2-D rectangular cylinder has been successfully analyzed by using the wavelet matrix transform approach. Numerical results have shown that the present approach does highly sparsify MoM matrices, especially as the problem size increases, and hence dramatically reduces the computation time by an efficient sparse solver without causing much error in the solutions.

## REFERENCES

- [1] B.Z. Steinberg and Y. Leviatan, "On the Use of Wavelet Expansions in the Method of Moments", IEEE Trans. Antennas and Propagation, Vol. AP-41, pp.610-619, May 1993.
- [2] J.C. Goswami, A.K. Chan, and C.K. Chui, "On Solving First-Kind Integral Equations Using Wavelets on a Bounded Interval", IEEE Trans. Antennas and Propagation, Vol. AP-43, pp.614-622, June 1995.
- [3] H. Kim and H. Ling, "On the Application of Fast Wavelet Transform to the Integral Equation solution of Electromagnetic Scattering Problems", Micro.Opt.Tech.Lett., vol.6, no.3, pp.168-173, March 1993.
- [4] Z. Xiang and Y. Lu, "An Effective Wavelet Matrix Transform Approach for Efficient Solution of Electromagnetic Integral Equations", IEEE Trans. Antennas and Propagation, Vol. 45, no.8, pp. 1205-1213, August 1997.
- [5] N. Guan, K. Yashiro, and S. Ohkawa, "On a Choice of Wavelet Bases in the Wavelet Transform Approach", IEEE Trans. Antennas and Propagation, Vol. 48, no.8, pp.1186-1190, August 2000.

## SYMBOLIC COMPUTATION TECHNIQUES FOR APERTURE ANTENNAS

Niyazi Ari, Ahmet Y. Tesneli\*, S. Selim Seker\*\*, Osman Cerezci\*

University of Applied Sciences Zurich, Dept. of Applied R&D,  
Technoparkstr 1 CH-8005, Zurich, E-mail: [nari@fhzh.ch](mailto:nari@fhzh.ch)

\*Sakarya University, Dept. of El-Electr. Eng, 54187 Esentepe, Sakarya, Turkey  
E-mail: [atesneli@sakarya.edu.tr](mailto:atesneli@sakarya.edu.tr), E-mail: [cerezci@sakarya.edu.tr](mailto:cerezci@sakarya.edu.tr)

\*\*Bogazici University, Dept. of El-Electr. Eng, 80815 Bebek, İstanbul, Turkey  
E-mail: [seker@boun.edu.tr](mailto:seker@boun.edu.tr)

### ABSTRACT

Symbolic Computations are very important since to get closed formula solutions in many applications. One of the computer code is MACSYMA that is written in program language LISP for the performing symbolic and numeric mathematical manipulations. The purpose of this paper is to present a number of MACSYMA applications that show how the new MACSYMA possibilities can be used in electromagnetics. To understand the procedure easily, rectangular aperture antenna analysis has been studied and the results have been illustrated.

### SYMBOLIC COMPUTATION OF A RECTANGULAR APERTURE

The analysis of apertures begins by considering the radiation from the elemental area oriented in the  $x=0$  plane as shown in Figure 1. The elemental area is part of some arbitrary aperture bounded by the curve  $C$ . The spherical coordinates of the elemental area is  $(r', \pi/2, \theta')$  and the fields are to be evaluated at the point  $P(r, \phi, \theta)$ .



Figure 1. Elemental area

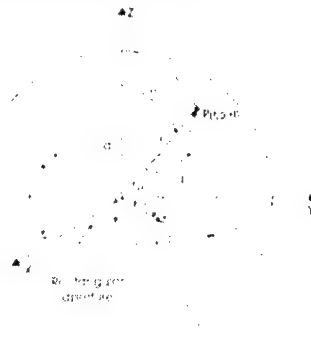


Figure 2. Rectangular aperture

Since the elemental area being analyzed can be excited by both electric and magnetic fields, It is convenient to use both the magnetic and electric vector potentials[2]. Therefore, the magnetic (**A**) and electric (**F**) vector potentials become, respectively

(c1) `{declare({a,f,y,m,n,v,le,n,le1,h1}, nonscalar), depends({n,v}, {rp,phi,theta})}`

(c2) `la:vect_express(mu*exp(-%f*k*r)*n/(4*pi*r),spherical);`

(d2)

$$\left[ \frac{\mu e^{-ikr} N_r}{4\pi r}, \frac{\mu N_\phi e^{-ikr}}{4\pi r}, \frac{\mu e^{-ikr} N_\theta}{4\pi r} \right]$$

(c3) `lf:vect_express(epsilon*exp(-%f*k*r)*W/(4*pi*r));`

(d3)

$$\left[ \frac{\epsilon e^{-ikr} L_r}{4\pi r}, \frac{\epsilon L_\phi e^{-ikr}}{4\pi r}, \frac{\epsilon e^{-ikr} L_\theta}{4\pi r} \right]$$

where **N** and **L** are the radiation vectors. The far electric field from the electric and magnetic vector potentials becomes

(c4) `le:vect_express(-%f*w*la-%f*w/k^2*grad(div(la))+curl(lf/epsilon))`

(c5) `(le:ev(le.diff),le:expand(le));`

(d5)

$$\left[ \begin{aligned} & \frac{\mu e^{-ikr} N_\theta \cos(\theta) w}{4\pi k^2 r^2 \sin(\theta)} + \frac{i\mu e^{-ikr} N_\theta \cos(\theta) w}{2\pi k^2 r^3 \sin(\theta)} + \frac{i\mu e^{-ikr} N_r w}{2\pi k^2 r^3} - \frac{L_\phi e^{-ikr} \cos(\theta)}{4\pi r^2 \sin(\theta)} \\ & \frac{ik e^{-ikr} L_\theta}{4\pi r} - \frac{i\mu N_\phi e^{-ikr} w}{4\pi r} \\ & \frac{i\mu e^{-ikr} N_\theta \cos^2(\theta) w}{4\pi k^2 r^3 \sin^2(\theta)} - \frac{i\mu e^{-ikr} N_\theta w}{4\pi r} + \frac{i\mu e^{-ikr} N_\theta w}{4\pi k^2 r^3} - \frac{ik L_\phi e^{-ikr}}{4\pi r} \end{aligned} \right]$$

Since the far field distance is large, terms which vary inversely with the distance can be ignored compared to the other terms so that for the far electric field

(c6) `(le:{0,le[2],part(le,3,[2,4])},le:subst(mu=k^2*Z0/w,le),le:undistrib(le));`

(d6)

$$\left[ 0, \frac{ik e^{-ikr} (L_\theta - N_\phi Z_0)}{4\pi r}, -\frac{ik e^{-ikr} (N_\theta Z_0 + L_\phi)}{4\pi r} \right]$$

A rectangular aperture of finite dimensions can be analyzed in terms of the elemental area. Consider an aperture in the  $x=0$  plane with sides of lengths  $a$  and  $b$  in the  $y$  and  $z$  directions, respectively, as shown in Figure 2. Let the electric field be aligned with the  $y$  axis and the magnetic field be aligned with the  $z$  axis to give a plane wave traveling in the  $x$  direction. If the aperture is uniformly illuminated, the electric field is constant in amplitude and phase over the aperture. For this case, the electric and the magnetic surface current densities are

(c7) `(n:{1,0,0},le1:{0,le0,0},h1:{0,0,le0/Z0},lf:vect_express(n-h1),lm:vect_express(-n-le1))`

The radiation vectors for the rectangular aperture become

(c8) `{rp:{0,yp,zp},ar:{sin(theta)*cos(phi),sin(theta)*sin(phi),cos(theta)}}`

(c9) `ln:integrate(integrate(y*exp(%f*k*vect_express(ar,rp)),yp,-a/2,a/2),zp,-b/2,b/2)`

Is  $k \sin(\phi) \sin(\theta)$  zero or nonzero?

nonzero

(c10) `lf:integrate(integrate(lm*exp(%f*k*vect_express(ar,rp)),yp,-a/2,a/2),zp,-b/2,b/2)`

Is  $k \sin(\phi) \sin(\theta)$  zero or nonzero?

n

(c11) `t:{sin(theta)*cos(phi),-sin(phi),cos(theta)*cos(phi);sin(theta)*sin(phi),cos(phi),sin(phi)*cos(theta);cos(theta),0,-sin(theta)}`

(c12) `{ln:ln,t,lf:lf}`

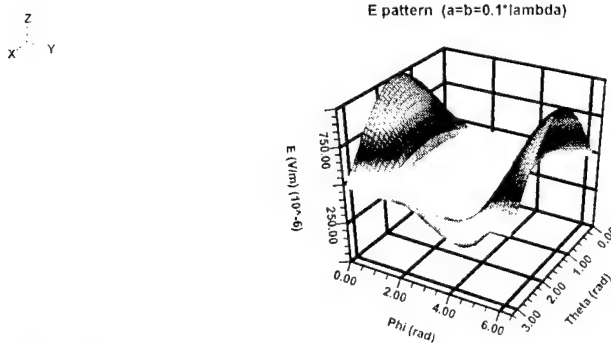


The far electric field vector is obtained as

$$\begin{aligned} \text{(c13)} \quad & \text{The far electric field vector is obtained as} \\ \text{(c14)} \quad & \text{The far electric field vector is obtained as} \\ \text{(d14)} \quad & \left[ \begin{array}{l} i e^{-i k r} \left( \frac{\cos(\phi)}{\sin(\theta)} + 1 \right) \sin\left(\frac{b k \cos(\theta)}{2}\right) \sin\left(\frac{a k \sin(\phi) \sin(\theta)}{2}\right) E_0 \\ 0, \frac{\pi k \sin(\phi) r \cos(\theta)}{\pi k r \sin(\theta)} \\ i e^{-i k r} \sin\left(\frac{b k \cos(\theta)}{2}\right) \sin\left(\frac{a k \sin(\phi) \sin(\theta)}{2}\right) E_0 \\ \frac{\pi k r \sin(\theta)}{\pi k r \sin(\theta)} \end{array} \right] \end{aligned}$$

The electric field pattern is

$$\begin{aligned} \text{(c15)} \quad & \text{The electric field pattern is} \\ \text{(c16)} \quad & \text{The electric field pattern is} \\ \text{(c17)} \quad & \text{The electric field pattern is} \\ \text{(c18)} \quad & \text{The electric field pattern is} \end{aligned}$$



## CONCLUSION

Symbolic computation results of a uniformly illuminated rectangular aperture have been obtained and the electric field pattern have been illustrated as a numerical example. So, how the symbolic computation techniques can be applied to electromagnetics has been shown.

## REFERENCES

- [1] "Macysma Mathematics and System Reference Manual", 16<sup>th</sup> ed., Macysma, Inc., USA, 1996.
- [2] WOLFF, Edward A., "Antenna Analysis", John Wiley & Sons, Inc., USA, 1966.

## THE 2,5D ELECTROMAGNETIC ANALYSIS IN TIME DOMAIN MODE

Timothey V. Kamichev, Constantin N. Klimov,  
Boris V. Sestroretsky\* and Sergey A. Ivanov\*

Moscow State Institute of Electronics and Mathematics, Bolshoy Trechsvytitelsky lane  
3/12, Moscow 109028, Russia, ph. (095)-916-88-17, E-mail: const0@online.ru

\* Lavochkin Association, Leningradskay st. 24, Chimki-2 Moscow Area 141400,  
Russia, ph. (095)-575-50-69, E-mail: const0@online.ru

### ABSTRACT

The expressions are submitted, allowing to make transformation E-plane waveguide the tasks containing 5 component of an electromagnetic field (for example  $H_x, H_y, H_z, E_y, E_z$ ), to the scalar 2D task containing to 3 unequal zero components of an electromagnetic field ( $H_x, E_y, E_z$ ). At such transformation the magnitude appropriate to magnetic permeability it becomes frequency dependent. It corresponds to dielectric permeability of plasma, if plasma frequency corresponds to cutoff frequency of a wave  $H_{m0}$ . This fact has allowed to use for the analysis in time domain E plane waveguide facility earlier developed effective programs 2D the electromagnetic analysis. The example of the analysis in time domain of the filter constructed on the basis of a rectangular waveguide with variations of the geometrical sizes in E plane is given.

### INTRODUCTION

In engineering practice are frequently used E-plane waveguide devices. For the electrodynamics analysis of such devices in frequency domain were developed effective procedures [1-3]. Now all greater attention is given investigations directly in time domain: tasks of a location supershort impulse and signals with a wide spectrum. In view there was a task of development of the technique used usually in frequency domain to have an opportunity to investigate characteristics of devices directly in time domain. The historical moment is interesting also. During absence of computing device for analog modeling plasma were used waveguide devices, and in the present work it is offered for the analysis in time domain waveguide devices to use the developed effective programs for the analysis of non-uniform plasma.

### STATEMENT E-PLANE PROBLEM IN THE RECTANGULAR WAVEGUIDE

Let's consider the structure were the E-plane device on the basis of a rectangular waveguide with metal walls, which is represented on fig. 1. Inputs of the device are rectangular waveguides, which are raised by a wave  $H_{m0}$ .

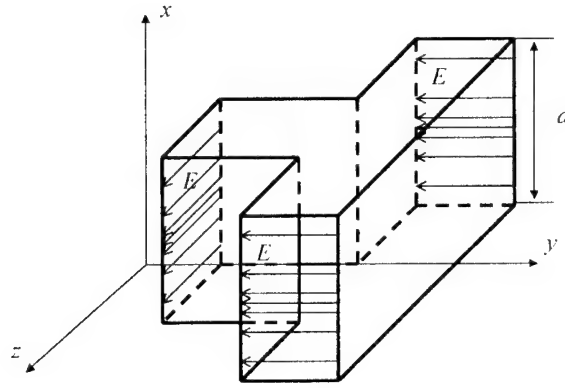


Fig. 1. Geometry  $E$  - plane device on the basis of a rectangular waveguide.

Devices of such type refer to E-plane, as all changes of geometry occur only in a plane of a vector of intensity of electric field  $E$  (plane  $ZOY$  see Fig. 1.), and the width of the device remains to a constant and is equal  $a$ . From the mentioned above conditions follows, that should the following ratio will be executed [4]:

$$E_x = 0 \quad (1)$$

$$E_y(x, y, z) = \sin \frac{m\pi x}{a} E_y(y, z) \quad (2)$$

$$E_z(x, y, z) = \sin \frac{m\pi x}{a} E_z(y, z) \quad (3)$$

$$H_x(x, y, z) = \sin \frac{m\pi x}{a} H_x(y, z) \quad (4)$$

For the decision of a problem it is necessary to write down Maxwell's equations in the chosen Cartesian system of coordinates (see fig. 1) and to substitute in the received system of the equations of a condition (1) - (4) in view of that foreign electric and magnetic currents inside analyzed area are equal to zero

By virtue of that ratio should will be executed at any values  $x$ , we receive the equations, not dependent on it. Analyzing these equations, we shall find final system of the differential equations which after use of properties of a permutable duality [4], can be written down in the following kind:

$$\frac{\partial E_x(y, z)}{\partial z} = i\omega\mu_a H_y(y, z) \quad (5)$$

$$-\frac{\partial E_x(y, z)}{\partial y} = i\omega\mu_a H_z(y, z) \quad (6)$$

$$\frac{\partial H_z(y, z)}{\partial y} - \frac{\partial H_y(y, z)}{\partial z} = -i\omega\epsilon_a(\omega) E_x(y, z) \quad (7)$$

The fact of concurrence frequency dependences permittivity is interesting in case of plasma and at the decision waveguide tasks that allows to investigate directly in time domain mode non-stationary processes for  $E$  Plane waveguide devices, using effective algorithms and the programs developed for the decision of bidimensional problems of

dispersion from non-uniform plasma formations in time domain mode on the basis of a method of impedance analogue of electromagnetic space [6]. As an example of similar research we shall result analysis  $E$  plane rejector the filter.

### RESEARCH $E$ PLANE REJECTOR THE FILTER

As an example we shall investigate characteristics  $E$  plane rejector the filter submitted on (fig. 2.)

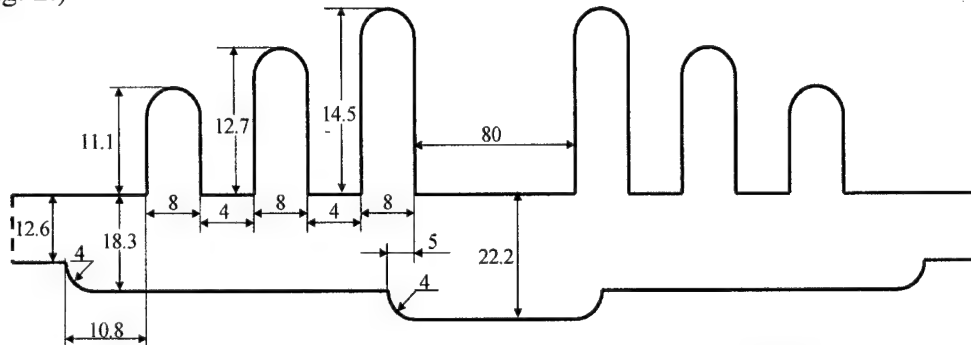


Fig. 2. Geometry  $E$  plane device on the basis of a rectangular waveguide.

All sizes of topology designed waveguide the filter, width  $28.5\text{ mm}$ , represented on (fig. 2.) in a plane of a vector  $E$ , specified in millimeters. On (fig. 3 and 4) time dependences of amplitudes reflected (it is designated square) and past (it is designated cross) waves suppressed frequency band on frequency  $f=7.170\text{ GHz}$  and in a passband on frequency  $f=8.425\text{ GHz}$  are shown.

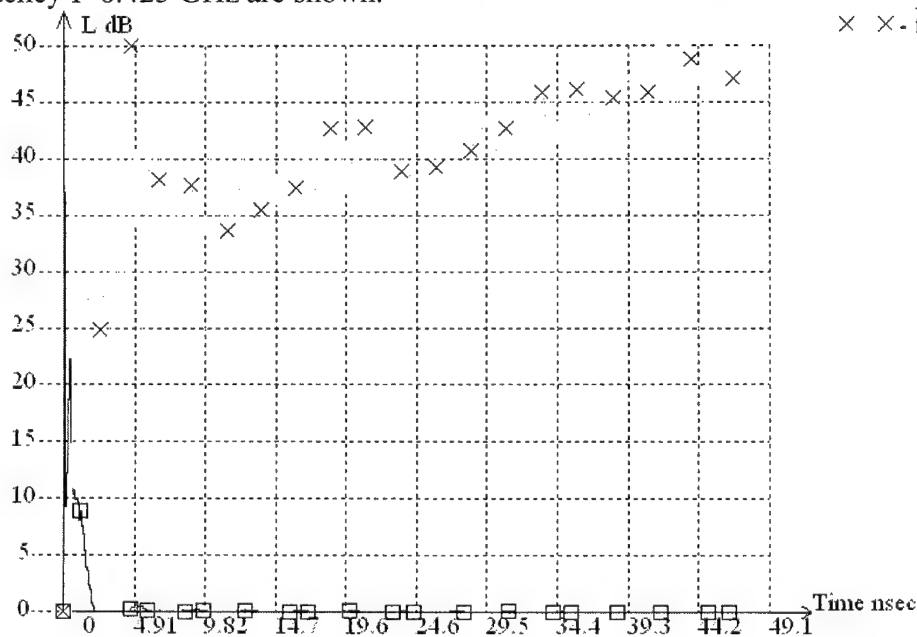


Fig. 3. Dependence on time of amplitude of the reflected and past wave at inclusion of a sinusoid with frequency of filling  $7.170\text{ GHz}$ .

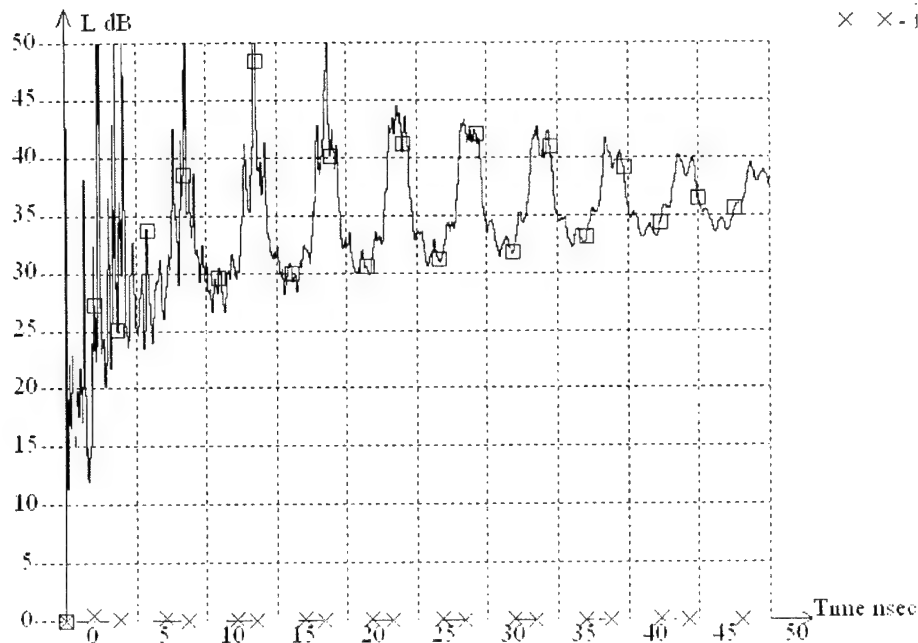


Fig. 4. Dependence on time of amplitude of the reflected and past wave at inclusion of a sinusoid with frequency of filling 8.425 GHz.

In the present work the expressions which are carrying out transformation E-plane waveguide of problems to a scalar 2D problem with permeability, having frequency dispersion that has allowed to use for the analysis in time domain mode E plane waveguide devices earlier developed effective programs 2D the electromagnetic analysis are given.

## REFERENCES

- [1] *Kustov V.Y.* Impedance's interpretation of a method of finite elements for the electrodynamic analysis planar waveguide devices // the Dissertation. M. MFTI. 1988. p. 210.
- [2] *Sestroretskij B.V., Zinovev A.V.* Electrodynamics the analysis and optimization of geometry E plane waveguide devices // Questions of radio electronics. Series. The general questions of radio electronics.-1988.- Part.12.- p. 43.
- [3] *Fedorov N.N.* Decision's of some problems of electrodynamics in non-uniform environments methods finite-difference elements // the Dissertation. M. MPEI. 1969. p. 472.
- [4] *Fedorov N.N.* Foundations of electrodynamics. the Higher School 1980. With. 399.
- [5] *Klimov K.N., Sestroretskij B.V.* // Radiotechnique and electronics. T. 46. 2001. N10. p. 1223.
- [6] *Klimov K.N.* Application of a method of impedance grids to the electrodynamics analysis in time area of bidimensional models non-uniform, including plasma // the Dissertation. M. MPEI. 2002. p. 245.

## CALCULATION OF LEAKAGE THROUGH APERTURES ON COAXIAL CABLE BRAIDED SCREENS

Bektaş ÇOLAK<sup>1,2</sup> Osman ÇEREZCİ<sup>2</sup> Zafer DEMİR<sup>2</sup> Mehmet YAZICI<sup>1</sup> Bahattin TÜRETKEN<sup>1</sup> İsa ARAZ<sup>1,2</sup>

<sup>1</sup>TÜBİTAK UEKAE, EMC Laboratory, PO.Box:74 Gebze Tel:+90 262 6481235

<sup>2</sup>Sakarya University, SAKARYA, bektas@uekae.tubitak.gov.tr

**ABSTRACT:** In this paper the more accurate calculation of the direct leakage of magnetic field through the diamond shaped holes is shown by using an early work [1] on the planar mesh surfaces. The exact geometry of the diamond shaped holes is taken into account. The details of the calculation are shown step by step.

### INTRODUCTION

The braid structure made by strands of helically interwoven wires and there are diamond shaped holes at the crossing point of the strands. Since the braid structure includes diamond shaped apertures, some of the magnetic flux lines penetrate from these apertures through to the interior conductor. Leakage from the apertures on the braid surface is calculated in literature by making some assumptions on the hole geometry [2]. The most famous one is assuming the diamond shaped geometry as an elliptical aperture. With this assumption it is possible to use the elliptical functions on the calculation. On the other hand, Ikrath [1] done a detailed calculation on the exact geometry of the diamond shaped apertures. But it is assumed that the cable surface is unlimited and planar. In real geometry, the geometry of the screen surface is cylindrical and in limited size. We modified the results of Ikrath by taking into account the exact geometry of the cable.

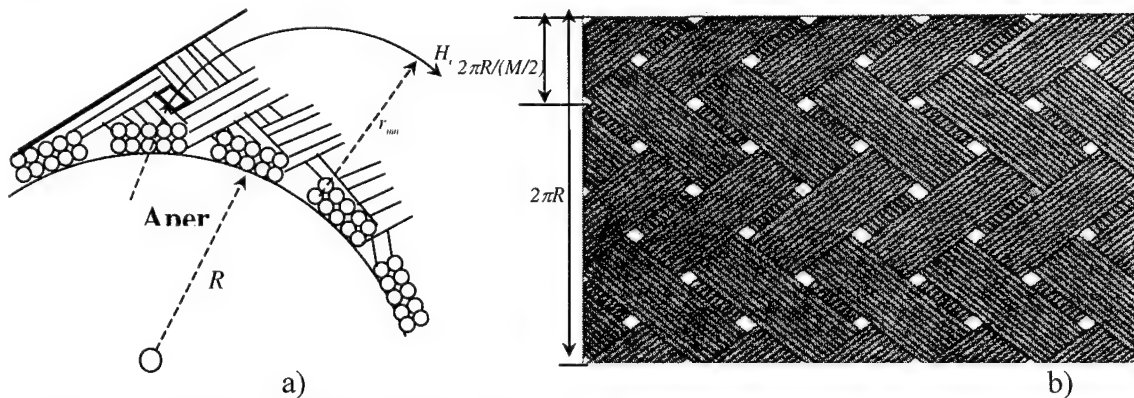


Fig.1. a) H field on aperture from single wire. b) Braid geometry on planar form

### Magnetic Field Leakage on Cylindrical Braid Geometry

Coaxial braid structure includes  $M$  carriers and in each carrier there are  $N$  wires (Fig.1). It is assumed that the total disturbing current,  $I$ , flows from each wires equally ( $i=I/MN$ ). The normal component of surface magnetic field to the hole surface is calculated by superposition of each single wire to the hole center. As a first step we consider only the effect of the nearest wires to the hole center. (Fig.2).

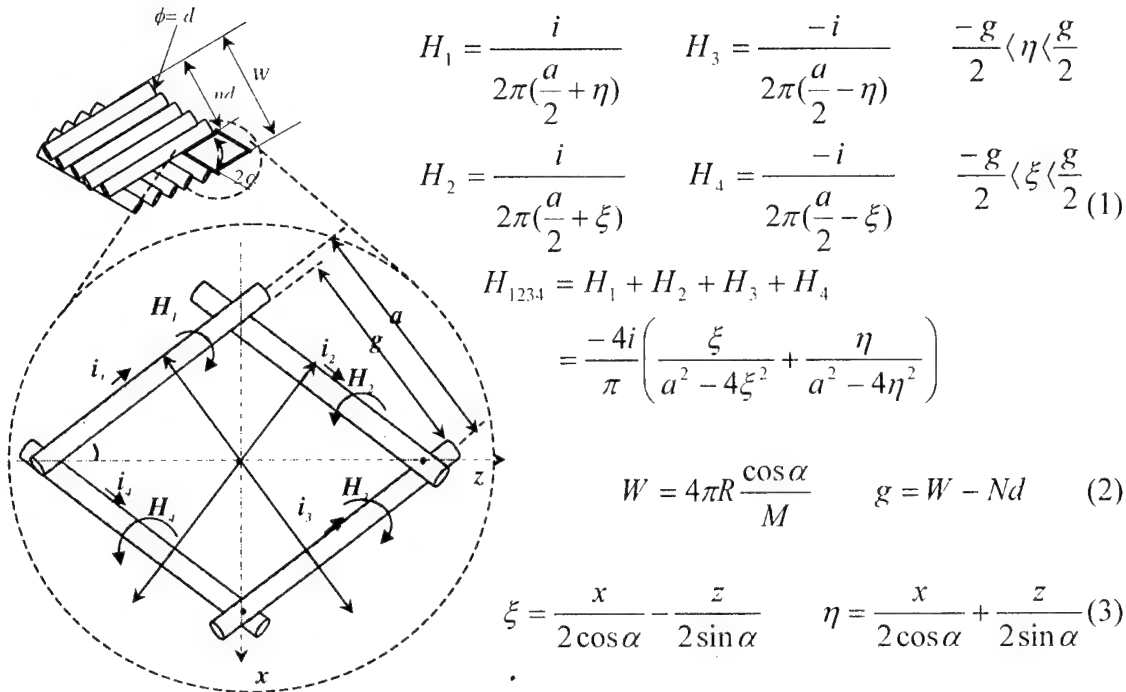


Fig.2. H field near the diamond shaped aperture

On the z-axis, the total magnetic field distribution is zero. In the diamond-shaped aperture, the total H-field can be calculated by summing up the four H-fields originating from the nearest wires (1). Since the H field is normal to the current direction, we have to define new axis as  $\xi$  and  $\eta$  normal to the each wire direction. Aperture size is related with braid geometry (2) and perpendicular axis to the wires could be transformed from x-z plane by (3). In order to find the whole wire's H field to the aperture center, it is necessary to formulate the distance from the any wires to the aperture center (Fig.3) (4). At the center along the z-axis, each H fields cancel each other. By the way the magnetic field lines enter to the inside of the interior layer from the upper triangular part of the z axis and go out from the lower part. Since the H fields must close around themselves a rotation occurs around the z-axis. Therefore, there is an e.m.f. produced per unit length of the z axis [1]. In Fig.4, the more detailed geometry for the circular form is given. The radial distance on the circular surface of the braid from any wire to the aperture center should be converted to the shortest distance as in (7). The radial distance is equal to the  $r_{mn}$  and shortest distance is equal to the  $R_{mn}$ .

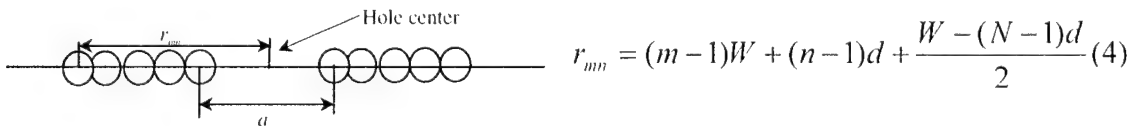
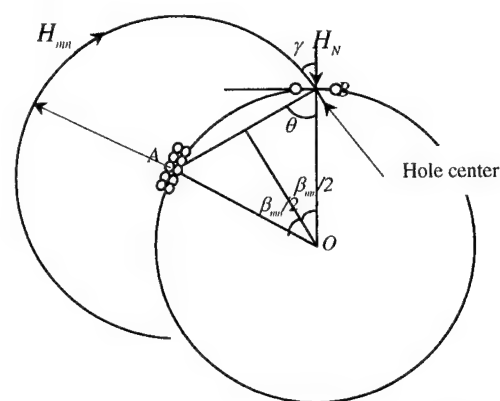


Fig.3. Distance from any wire to the aperture center in planar form.

For the total H field distribution in any point on the diamond shaped aperture, the effects from the all wires should be summed referred to the circular geometry (8). This

total term can be simulated via numerical calculation for digitized  $\eta$  and  $\xi$  axis points (Fig.5).

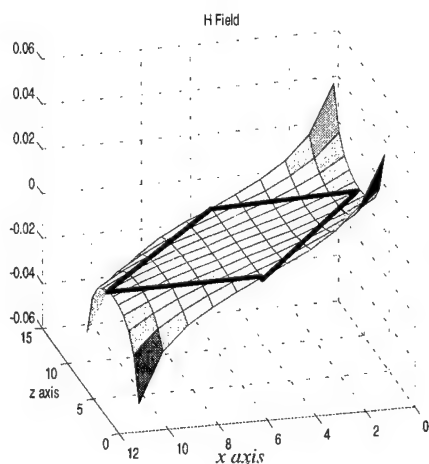


$$\gamma = \frac{\pi}{2} - \theta, \quad \theta = \frac{\pi}{2} - \frac{\beta}{2} \Rightarrow \gamma = \frac{\beta}{2} \quad (5)$$

$$\vec{H}_N = \vec{H}_{mn} \cdot ds \Rightarrow H_N = H_{mn} \cos \gamma \quad (6)$$

$$R_{mn} = |AB| = 2R \sin \frac{\beta_{mn}}{2} \quad \beta_{mn} = \frac{r_{mn}}{R} \quad (\text{in radian}) \quad (7)$$

Fig.4.Distance from any wire to the aperture center in circular form.



$$H_{\eta, \xi} = \frac{1}{2\pi} \cos \left( \frac{r_{mn}}{2R} \right) \sum_{m=1}^{M/4} \sum_{n=1}^N \left[ \frac{1}{R_{mn} + \eta} - \frac{1}{R_{mn} - \eta} + \frac{1}{R_{mn} + \xi} - \frac{1}{R_{mn} - \xi} \right] \quad (8)$$

Fig.5. Simulated value of H field. The values out of the border of the diamond shall be omitted. (M=24, N=8, d=0.15mm, i= 1Amp  $\alpha=\pi/6$ )

## CONCLUSION

The direct magnetic leakage term of the diamond shaped apertures of the coaxial braided screen are modified for the real geometric conditions of the cylindrical shield structure as if including the curvature and the limited number of the wires. One can calculate the total H field leakage by using this field distribution on one aperture, multiplying the hole number in unit length.

## REFERENCES

- [1] K. Ikrath, *Leakage of Electromagnetic Energy from Coaxial Cable Structures*, US Army and Signalling Engineering Laboratories, Fort Monmouth, NJ, December 1957.
- [2] H. Kaden, *Wirbelströme und Schirmwirkung in der Nachrichtentechnik*, Berlin, Springer, 1959.



## EFFICIENT CFIE-MOM ANALYSIS OF 3-D PEC SCATTERERS IN LAYERED MEDIA

Oleksiy S. Kim, Erik Jørgensen, Peter Meincke, and Olav Breinbjerg

Ørsted•DTU, Electromagnetic Systems, Technical University of Denmark,  
Building 348, Ørsted's Plads, DK-2800 Kgs. Lyngby, Denmark  
Tel: +45 4525 3800, Fax: +45 4593 1634, E-mail: osk@oersted.dtu.dk

### ABSTRACT

This paper presents an efficient technique for analysis of arbitrary closed perfectly conducting (PEC) scatterers in layered media. The technique is based on a method of moments (MoM) solution of the combined field integral equation (CFIE). The high efficiency is obtained by employing an accurate expansion of the multilayer dyadic Green's function along with a higher order hierarchical discretization scheme and a rapidly converging iterative solver with preconditioner.

### INTRODUCTION

Numerical analysis of electromagnetic scattering by PEC objects has attracted great attention for many years. Naturally, available computational resources limit the size of objects that can be analysed by numerical techniques. The situation becomes even worse when layered medium is considered. Furthermore, for objects penetrating the interface (interfaces) between the layers, conventional methods can not efficiently handle the different wavelength in different media.

In this paper, a new efficient MoM scheme, combining fast calculation of dyadic Green's functions for multilayered media with higher order hierarchical basis functions, is presented. This technique allows the number of unknowns to be decreased in comparison with conventional techniques employing low-order discretization schemes. The relaxation of memory requirements is especially pronounced when the scatterer is located in two or more layers. Further improvement in computational efficiency is achieved by employing a rapidly converging iterative solver with preconditioner. The technique is validated with examples available in the literature.

### INTEGRAL EQUATION TO BE SOLVED

The electric field integral equation (EFIE) and the magnetic field integral equation (MFIE) each fail at a set of discrete frequencies for closed PEC objects. Being a linear combination of EFIE and MFIE, CFIE provides stable and reliable solutions at all frequencies. EFIE is a well-known and quite elaborated technique for analysis of scattering by PEC objects both in free space and in layered media. At the same time, MFIE is usually applied for scatterers in homogeneous media. There are very few papers devoted to MFIE in layered media and only conducting bodies of revolution have been treated thoroughly by MFIE [1] (the MFIE-BOR method). In this paper, we apply the MFIE (as an essential part of CFIE) to arbitrary closed PEC objects in layered media.

## DYADIC GREEN'S FUNCTIONS FOR MULTILAYERED MEDIA

The dyadic Green's functions for multilayered media are implemented using the Formulation C for the mixed potential integral equation [2]. Under this formulation, only three different Sommerfeld integrals arise in the solution. They are computed in a very efficient way using the discrete complex image method (DCIM) [3] which allows spatial Green's functions to be represented in closed form in terms of complex images. If the scatterer is confined to one layer, the coefficients of the complex image expansion are invariant with respect to the coordinates of the source and observation points. Otherwise, the coefficients depend only on the z-coordinate of the source point and the layer the observation point belongs to. It is worth noting that the coefficients of the complex image expansion are reused in both EFIE and MFIE.

## DISCRETIZATION TECHNIQUES

Higher order hierarchical basis functions [4] based on orthogonal Legendre polynomials are employed for discretizing the CFIE. The hierarchical property of the functions provides a very efficient discretization scheme especially when the scatterer is not confined to one layer. The order of the polynomial expansion can be selected separately on each patch depending on the wavelength of the layer in which the patch is located. This allows a very low number of unknowns and a uniform mesh despite the different wavelengths. In contrast to this, conventional low-order methods are forced to use a patch size based on the shortest wavelength, which introduces unnecessary unknowns and leads to a poor condition number of the resulting MoM matrix. Alternatively, conventional methods may employ a highly non-uniform mesh that is difficult to construct and also leads to a poor condition number. The higher order hierarchical basis functions are here employed on second-order curved patches that provide accurate geometrical modeling of smooth surfaces.

## IMPLEMENTATION AND NUMERICAL RESULTS

The described technique has been implemented in an efficient computer code that is well parallelized on both shared and distributed memory multiprocessor systems. The most time consuming part of the analysis is the calculation of the dyadic Green's functions for multilayered media. On a multiprocessor workstation, it can be done in parallel for different pairs of source and observation points. Furthermore, due to reusing of the Green's function expansion in both EFIE and MFIE, the CFIE matrix filling time increases only by 10% with respect to MFIE alone.

The presented technique was validated by comparison with the results obtained by the MFIE-BOR method [1] for scattering by a PEC sphere in the presence of the interface between two contiguous half-spaces. For instance, Fig. 1 shows the currents on a half-buried metallic sphere illuminated by a plane wave. It is observed that the results of the new technique are in excellent agreement with those of [1]. Fig. 2 presents a new result for a geometry that can not be treated by the MFIE-BOR method [1]. Both a first-order discretization scheme (rooftops on a uniform mesh) and a hierarchical discretization scheme are used. In the first case, significant overdiscretization in the free space is observed (709 unknowns per square wavelength, see Table 1). In the second case, the

hierarchical discretization allows the total number of unknowns to be reduced by more than a factor of three while the accuracy is maintained (Fig. 2).

## REFERENCES

- [1] A.A.K. Mohsen et al., *Progress In Electromag. Research*, PIER 24, pp. 19-37, 1999.
- [2] K.A. Michalski et al., *IEEE Trans.*, vol. AP-38, pp. 335-344, 1990.
- [3] Y.L. Chow et al., *IEEE Trans.*, vol. MTT-39, pp. 588-592, 1991.
- [4] E. Jørgensen et al., *Proc. of IEEE AP-S*, San Antonio, USA, 2002, pp. 618-621.

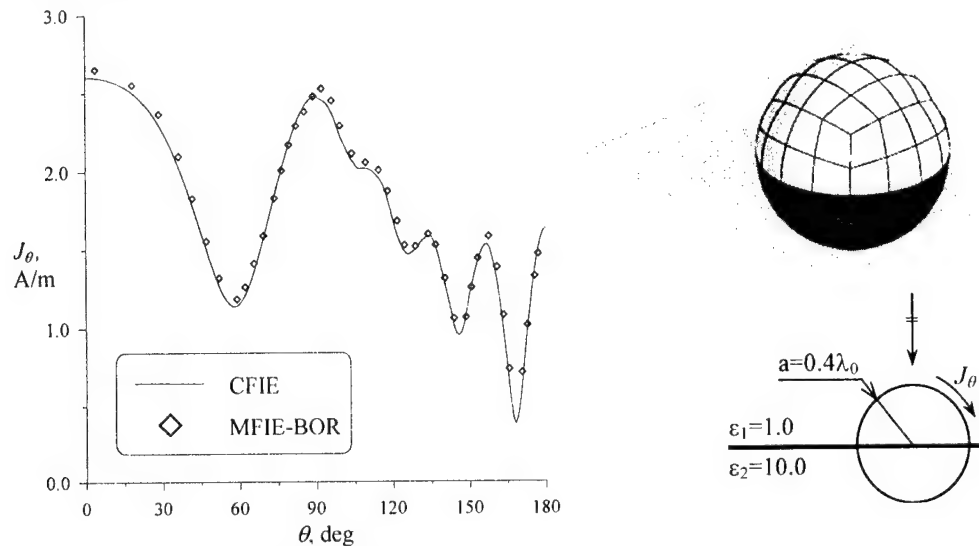


Fig. 1. Current on the half-buried PEC sphere illuminated by a plane wave.

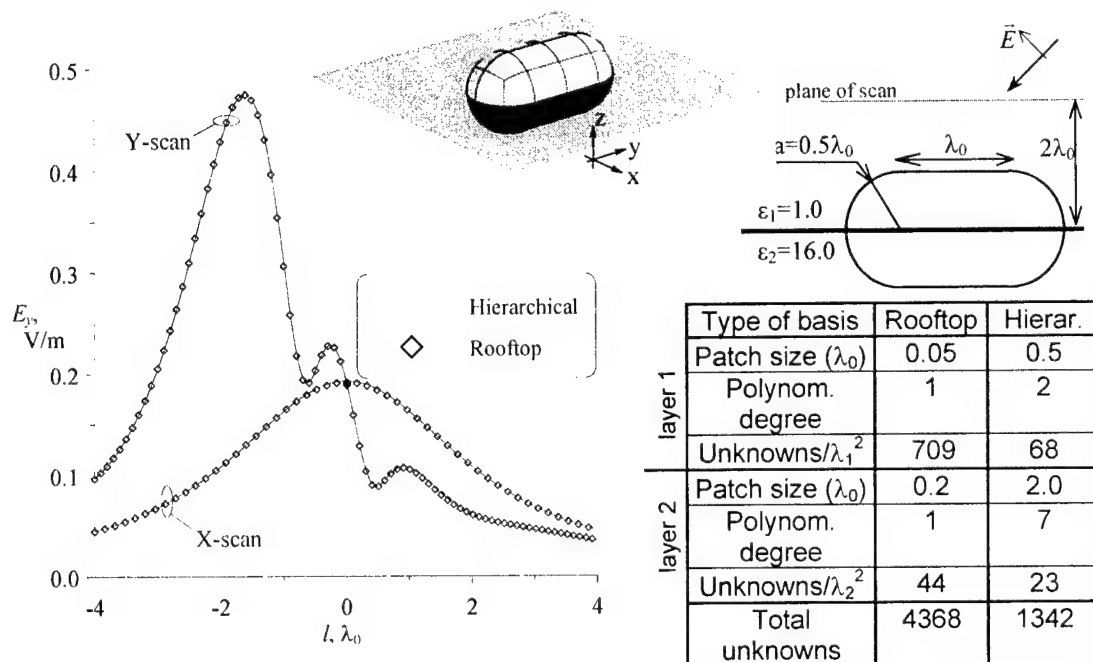


Fig. 2. Scattered near-field from the half-buried PEC tube illuminated by a plane wave.

## THE PARTIAL REGION METHOD IN 2-D ELECTROMAGNETIC AND ACOUSTIC PROBLEMS

Tihomir Trifonov

Faculty of Mathematics and Informatics,  
Veliko Turnovo University "St.St. Cyril and Methodius",  
2 Teodosij Turnovski Str., 5003 Veliko Turnovo, Bulgaria  
Tel: +359 62 39412 Email: TihomirTrifonov@ieee.org

### ABSTRACT

The mathematical methods, used for solving acoustic and electromagnetic wave problems, defined in two dimensions, are analogous in many cases. The analytical and numerical results of a field in the outside domain of curvilinear rectangle are presented in this paper. Based on the wave equation, boundary conditions and radiation condition the structure of the field is determined. The method of the partial regions is used. For the acceptability criterion of the quantity of the members by which the field is calculated, the fulfillment of boundary conditions on the radiating surfaces and the fulfillment of conjunction conditions between the partial regions were observed. The results are applicable to the optimum design of acoustic and electromagnetic antennas.

### INTRODUCTION

It is known that in the 2-D case the Maxwell equations can be transformed in two independent equations for the vectors of electrical and magnetic fields [1]. By this reason in 2-D the solutions of acoustic and electromagnetic problems coincide. Using the technique of partial region [2,3], many interesting problems can be solved and results can be implemented in the two areas.

### BOUNDARY-VALUE ANALYSIS AND ANALYTICAL RESULTS

The geometry of the problem is shown in **Fig. 1**. This is an outside boundary value problem, i.e. a problem in the infinite domain. The curvilinear rectangle is limited by the arcs with radii  $r_1$  and  $r_2 = a$ , and the segments  $AD$  and  $BC$ . It is assumed that the surfaces  $\theta = \pm\theta_0$ ,  $r_1 \leq r \leq a$  are acoustically rigid. Sound field is generated by the surfaces  $r = r_1$  and  $r = r_2$ ,  $\theta_0 < |\theta| \leq \pi$ , on which the distribution of particle velocity is assigned:

$$-\frac{\partial F}{\partial r} = f_1(\theta), r = r_1 \quad (1)$$

$$-\frac{\partial F}{\partial r} = f_2(\theta), r = r_2 \quad (2)$$

where  $F$  - velocity potential. In order to analyze a sound field with time dependence factor  $\exp(-i\omega t)$ , which is created by the radiating body, shown in Fig., the boundary value problem for the Helmholtz equation in cylindrical coordinates must be solved:

$$\Delta F(r, \theta) + k^2 F(r, \theta) = 0 \quad (3)$$

where:  $F(r, \theta)$  - velocity potential;  $\Delta \equiv \nabla^2$  - Laplace's operator;  $k$  - wave number.

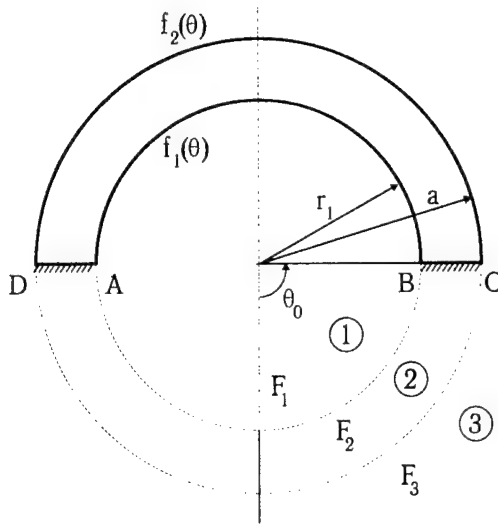


Fig. 1. Geometry of the problem

The whole field is divided in parts. In each partial region there must exist a solution of the Helmholtz equation (3), which satisfies the boundary conditions of some part of the whole surface and the conjunction conditions of the boundaries of the neighboring partial regions [2]. Using the orthogonal properties on the corresponding segments of the functions, which describe the field in regions 1, 2 and 3, the functional equations can be transformed into the following infinite simultaneous linear algebraic set of equations for the complex coefficients,  $A_n$ ,  $B_m$ ,  $C_m$ , and  $D_l$ :

$$\left\{ \begin{array}{l} \delta_n J'_n(k\rho a) A_n - \sum_{m=0}^{\infty} \gamma_{\alpha_m n} J'_{\alpha_m n}(k\rho a) B_m - \sum_{m=0}^{\infty} \gamma_{\alpha_m n} N'_{\alpha_m n}(k\rho a) C_m = -\frac{\beta_n}{k} \\ -\sum_{n=0}^{\infty} \gamma_{\alpha_m n} J_n(k\rho a) A_n + \delta_m J_{\alpha_m}(k\rho a) B_m + \delta_m N_{\alpha_m}(k\rho a) C_m = 0 \\ \delta_m J_{\alpha_m}(ka) B_m + \delta_m N_{\alpha_m}(ka) C_m - \sum_{l=0}^{\infty} \gamma_{\alpha_m l} H_l^{(1)}(ka) D_l = 0 \\ \sum_{m=0}^{\infty} \gamma_{\alpha_m l} J'_{\alpha_m}(ka) B_m + \sum_{m=0}^{\infty} \gamma_{\alpha_m l} N'_{\alpha_m}(ka) C_m - \delta_l H_l^{(1)'}(ka) D_l = \frac{\beta_l}{k} \end{array} \right. \quad (4)$$

where  $n = m = l = 0, 1, 2, \dots, N, \dots$ ;  $\alpha_m = \frac{m\pi}{\theta_0}$ ;

$$\delta_n = \begin{cases} 2\pi, & n = 0 \\ \pi, & n > 0 \end{cases}; \delta_m = \begin{cases} 2\theta_0, & m = 0 \\ \theta_0, & m > 0 \end{cases}; \delta_l = \begin{cases} 2\pi, & l = 0 \\ \pi, & l > 0 \end{cases}$$

$$\beta_n = -\frac{2 \sin(n\theta_0)}{n}; \beta_l = -\frac{2 \sin(l\theta_0)}{l}$$

$$\gamma_{\alpha_m n} = \frac{2\alpha_m}{\alpha_m^2 - n^2} \sin(\alpha_m \theta_0) \cos(n\theta_0) - \frac{2n}{\alpha_m^2 - n^2} \sin(\alpha_m \theta_0) \cos(n\theta_0)$$

$$\gamma_{\alpha_m l} = \frac{2\alpha_m}{\alpha_m^2 - l^2} \sin(\alpha_m \theta_0) \cos(l\theta_0) - \frac{2l}{\alpha_m^2 - l^2} \sin(\alpha_m \theta_0) \cos(l\theta_0)$$

The prime (') means a derivative of the whole argument. Except this, it is accepted that  $f_1(\theta) = f_2(\theta) = 1$ . This simplification has not meaning of a principle [4].

Solving the set, the complex coefficients  $A_n$ ,  $B_m$ ,  $C_m$ , and  $D_l$  can be obtained. The velocity potential of the field  $F(r, \theta)$  in each point of the outside domain of the curvilinear rectangle can be found.

## NUMERICAL RESULTS

In **Fig. 2** the modulus of the potential  $F_1$  for determined wave parameters near the geometric focus is shown. As can be seen, the structure of the field is complex and optimization of the main parameters ( $\theta_0, \rho, a$ ) is recommended to obtain the necessary intensity and focus spot. In **Fig. 3** the equipotential curves are drawn. It is clear that real focus spot is shifted ( $\theta = 0$ ,  $r = 0.3$ ). This effect can be explained with edge points diffraction and radiation of the surface  $CD$ .

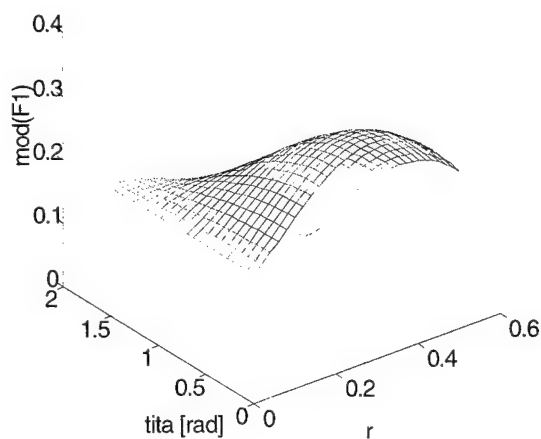


**Fig.2.** Modulus of potential  $F_1$

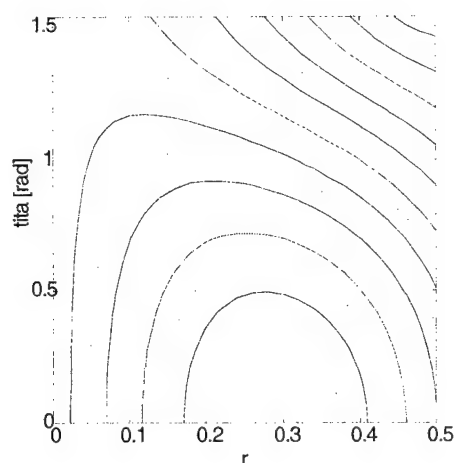


**Fig.3.** Equipotential curves

## CONCLUSION

The results, obtained above, can be used to the optimum design of acoustic and electromagnetic antennas in 2-D space.

## REFERENCES

- [1] Shenderov E.L., Radiation and diffraction of sound, Sudostroenie, Leningrad, 1989, in Russian.
- [2] Grinchenko V.T. and I.V. Vovk, Wave Problems of Sound Diffraction on Elastic Shells, Naukova Dumka, Kiev, 1989, in Russian.
- [3] Shestopalov V.P., Summation Equations in the Modern Diffraction Theory, Naukova Dumka, Kiev, 1983, in Russian.
- [4] Grinchenko V., Trifonov T., Y. Syderov, On the Acoustic Field of a Cylindrical Focusing Projector, Journal of Theoretical and Applied Mechanics, Sofia, Year XXVII, No3, pp.80-89.

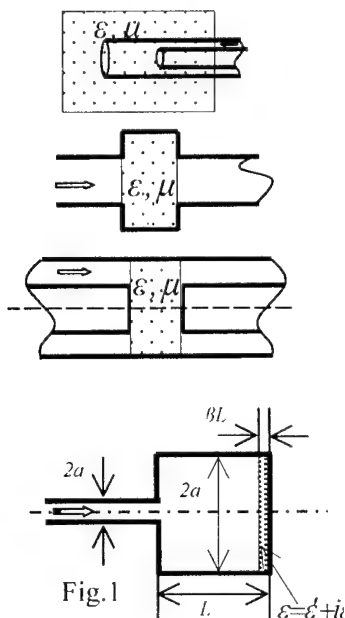
## DIELECTRIC PARAMETERS RECOGNITION BY USING A WAVEGUIDE CAVITY AND A RIGOROUS PROCESSING ALGORITHM

Anatoliy Ye. Poyedinchuk, Anatoliy A. Kirilenko and Nataliya P. Yashina

IRE NASU, Kharkov 61085, Ukraine. E-mail: nataliya@lin.com.ua

### INTRODUCTION

Measurement of scattered electromagnetic field and further permittivity or permeability reconstruction based on experimental data and adequate mathematical model is the key issue in dielectric materials study [1, 2]. Here, accuracy of measurements and adequacy of mathematical model is of principal importance. Today, special attention is attracted to the study of thin dielectric films with  $tg(\delta) \sim 10^{-3} \div 10^{-6}$ . In this paper we consider a resonator that can be used for a thin film study, its electromagnetic model, and advantages and capacities of corresponding numerical algorithm.



### DESCRIPTION OF THE ALGORITHM

Our solution to inverse problem is based on accurate and efficient solution to direct problem. Suppose that the diffraction of one of the modes of small circular waveguide by the chamber (Fig.1) is reduced to a functional relation  $Y = f(X)$ . Here  $X = (x_1, x_2, x_3, \dots, x_m)$  is the set of input data (frequency,  $\epsilon$ , geometry, amplitude of incident wave  $A$ , etc.) and  $Y = (y_1, y_2, \dots, y_n)$  is the set of output data - reflection coefficients  $R_1, R_2, \dots, R_n$ , normalized by  $A$ . Assume that a part of input data is known (frequency and geometry) and given by the values  $x_l^0, x_2^0, \dots, x_l^0$  ( $l < m$ ) from the set  $X$  of all input variables. Suppose also that values  $Y^0 = (y_1^0, y_2^0, \dots, y_n^0)$  of output variables are known. The problem of the model identification is reduced to a necessity of finding  $x_{l+1}, \dots, x_m$  from equation

$$Y^0 = f(x_1^0, \dots, x_l^0, x_{l+1}, \dots, x_m) \quad (1)$$

In our case, we have to find unknown dielectric constant  $\epsilon = \epsilon' + i\epsilon''$ . The accuracy of the parameter evaluation depends on several factors:

1. The error of reproduction of the relation between output data  $Y$ , known input data  $x_1, x_2, x_3, \dots, x_m$ , and unknown parameters in the form of equation (1), that is called inadequacy of the model to the phenomena simulated.
2. Errors of measuring the known parameter values, that is  $Y^0, x_1^0, x_2^0, \dots, x_l^0$ .
3. Errors of the numerical algorithm applied to solving equation (1).

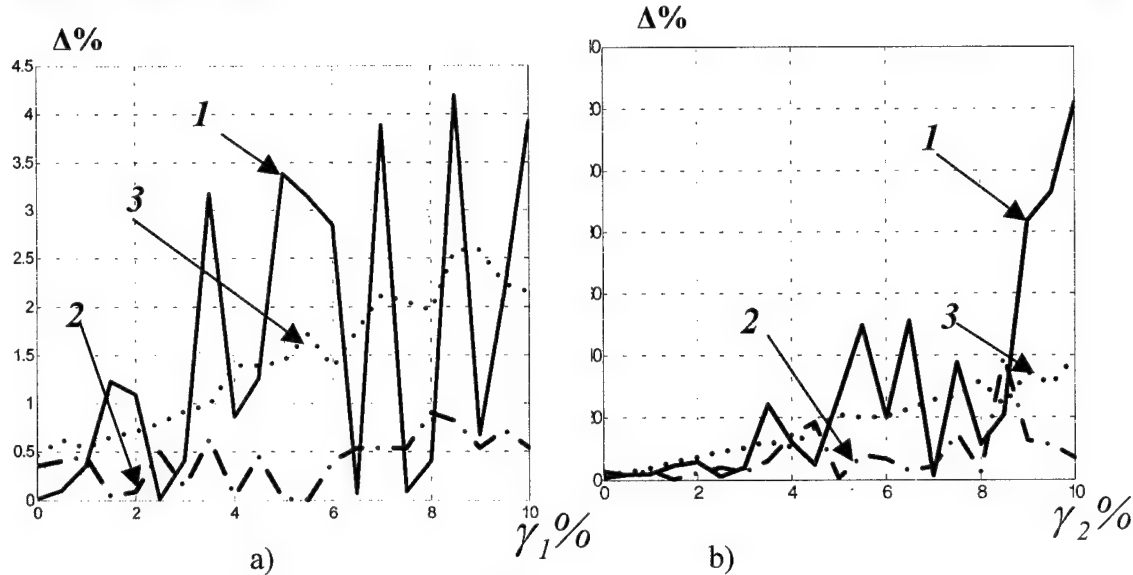


Fig.2

As a functional relation we choose the solution of the considered problem obtained by the semi-inversion method [4, 6]. Here, we reduce it to numerical solution of a matrix equation of the second kind  $R^M - HR^M = B$  with exponential convergence. This approach allows us to find out with given accuracy the amplitudes of reflected modes  $R_1^M, R_2^M, \dots, R_N^M$  if the frequency, geometry, and dielectric constant  $\varepsilon = \varepsilon' + i\varepsilon''$  are known, so that  $R_n^M = f_n(\kappa, \varepsilon, A)$  depends on geometry, frequency parameter  $\kappa = a/\lambda$  ( $a$  is characteristic dimension, see Fig.1), and  $\varepsilon$ . The accuracy of calculation of  $R_n$  is limited by the capacity of the computer utilized. For the solution of direct and inverse problems we used the ideas of [7, 3-5]. We pose the inverse problem as a minimization one, see [6,3,4]. After carrying out numerical investigation of various types of functionals according the scheme of [4], we arrive at the conclusion that the most efficient is

$$\Phi(\varepsilon) = \sum_{m=1}^P \sum_{n=1}^N F(R_{nm}^e - R_n^M(\kappa_m, \varepsilon)) + \alpha Q(\varepsilon) \quad (2)$$

where  $F(u) = |u|^2$ . Due to analyticity of functions  $R_n^M(\kappa, \varepsilon, A)$  in  $\kappa$  and  $\varepsilon$ , the functional in (2) (within the considered level of input errors) does not require regularization and we can put (2)  $\alpha = 0$ .

## NUMERICAL EXPERIMENTS

In the parameter reconstruction of thin films,  $\beta L < \lambda$ , with small  $tg(\delta)$  there are two most important criteria:

- influence of the error of input data on the accuracy of parameter reconstruction, and
- range of parameters, within which accuracy of the algorithm is sufficient.

To simulate experimental input data we used (see also [3, 4]) a generator of random numbers with normal distribution:

$$R_n^e(\kappa, \varepsilon) = |R_n^M(\kappa, \varepsilon)| (1 + \gamma_1 \text{Random}) \exp(\arg(R_n^M(\kappa, \varepsilon)) (1 + \gamma_2 \text{Random})),$$



where  $-1 < \text{Random} < 1$ . We studied the relative errors of reconstructed parameters and algorithm properties according to the formulas:

$$\Delta_g = \frac{|tg(\delta)_R - tg(\delta)_M|}{tg(\delta)_M} \% ; \quad \Delta_e = \frac{|\varepsilon'_R - \varepsilon'_M|}{\varepsilon'_M} \% ; \quad \text{and} \quad \Delta = \left( \frac{\sum_j R_n^e(\kappa_j) - R_n^M(\varepsilon_R, \kappa_j)^2}{\sum_j R_n^e(\kappa_j)^2} \right)^{1/2}$$

as functions of input data errors. Relevant curves are marked as 1,2,3 in Fig.2, respectively. In all experiments we accounted 21 frequency points in functional (2).

Fig. 2 presents the variations of relative errors when input data errors for amplitudes  $\gamma_1$  and arguments  $\gamma_2$  change from 0% to 10%. In Fig.2-a we fixed  $\gamma_2 = 3\%$  and in Fig.2-b it was  $\gamma_1 = 5\%$ . Here we had to present curves 2 corresponding to the values of  $\Delta_e \cdot 100$  in order to be visible within the common scale. The errors change randomly, however around certain increasing with rise of errors level mean values. The input errors in arguments influence the accuracy more crucially, and it is clear that better to accept errors less than 5%. Due to the high accuracy of the algorithm of direct problem solution, there is no restriction on reconstructed parameters if one has "hypothetical" situation with accurate input data, i.e. if  $\gamma_1 = \gamma_2 = 0$ . However, from numerical experiments we conclude that if the error in input data is  $\gamma_1 \geq 10\%$  (for normalized amplitude that is deviation of 0.1) and  $\gamma_2 \geq 5\%$  (that is  $18^\circ$ ) it is necessary to apply regularization to (2).

## REFERENCES

- [1]. Sucher M., Fox J. *Handbook of Microwave Measurements*. NY: Wiley, 1993.
- [2]. Takur K.P. and Holmes W.S., An inverse technique to evaluate permittivity of material in cavity. *IEEE Trans. MTT* 49, 2001.
- [3]. Poyedinchuk A.Ye., Yashina N. P. Mathematical modeling for reconstruction electromagnetic characteristics of various media. *Proc. URSI Int. Symp. on Electromagnetic Theory*. Victoria, 2001.
- [4]. Kirilenko A. A., Poyedinchuk A.Ye., and Yashina N.P. Non-destructive control of dielectrics: mathematical models based on analytical regularization. *Proc. IV ISAAC Congress*, Berlin, 2001.
- [5]. Yashina N.P. Accurate analysis of coaxial waveguide slot bridge. *Microwave and Optical Technology Letters*. **20**, 1999.
- [6]. Tikhonov A.N., and Arsenin V.Y. *Methods for the solution of ill posed problems*. Moscow, 1986.
- [7]. Press W.H., Teukolsky S.A., Vetterling W.T., Flannery B.P. *Numerical Recipes in C. The Art of Scientific Computing*. Cambridge University Press, 1992.

## DROP-SHAPED MONOPOLE ANTENNA AND ITS INTERACTION WITH THE USER'S HEAD

G. Ghvedashvili, R. Zaridze, K. Tavzarashvili, G. Sapparishvili, A. Bijamov  
 Laboratory of Applied Electrodynamics, Tbilisi State University, Georgia  
 e-mail: lae@access.sanet.ge

### ABSTRACT

This paper is dedicated to the EMC/EMI problems from the standpoint of the efficient and safe mobile equipment antenna structures development and to investigation of the influence of such antennas on the user's head. The dielectric monopole drop-shaped antenna has been proposed and the numerical investigations of its behavior taking into account its interaction with the feeding cable and user's head have been carried out. The corresponding EM problem is solved using Method of Auxiliary Sources (MAS) [1].

### INTRODUCTION

For the antennas used in the modern personal communicational systems it is necessary to be small in size and have wideband radiation. For the real radiating systems simulation in the framework of EMC problems it is very important to take into account the interaction of the under study subsystem with the surrounding objects – in case of antenna these are the user's head, free space and the feeding cable.

In this paper we consider a drop shaped monopole antenna fed by the coaxial cable located in the close proximity of the user's head. The head is simulated by the IEEE Standard Head Model. The problem of obtaining a good matching of the antenna both with the feeding cable and free space has been resolved throughout the proper choice of the antenna shape. Also an attention was paid to the SAR distribution in the user's tissues. Based on MAS [1] the engineer-oriented software package has been created to perform the necessary numerical experiments.

### NUMERICAL RESULTS

In the [2,3] the drop shaped antenna covered with thin dielectric layer has been introduced and its diffraction properties have been investigated. The next stage of such type of an antenna development is a real antenna-cable structure simulation (Fig.1). In this paper the antenna of a certain type has been investigated and its properties versus its shape and material



Fig.1 Antenna geometry

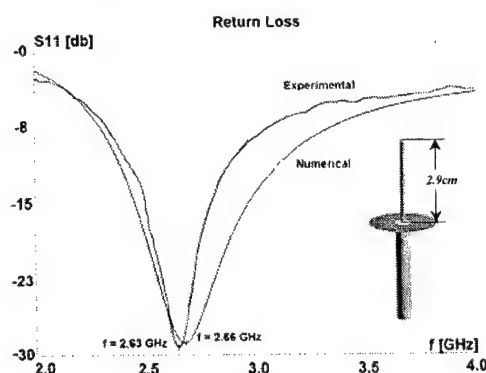


Fig. 2. Comparison of the numerical and experimental measurements

parameters have been investigated. Varying the antenna shape one can control the Q-factor, while the dielectric layer of high permittivity helps to keep the antenna size small and shift the resonant frequency down.

The first step was investigation of a simplified flagpole antenna and comparison of the calculated data with that measured experimentally. Fig.2 shows the return loss versus

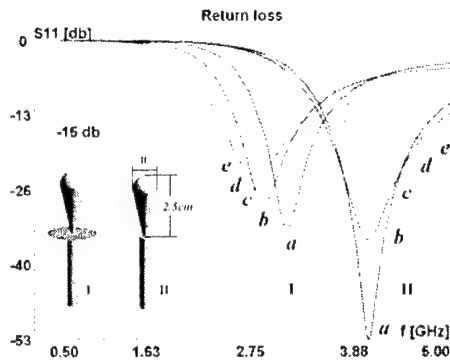


Fig. 3 Return loss versus frequency for different antenna's width  
a)0.13cm b)0.4cm c)0.6cm d)0.8cm  
e)1.0cm



Fig.4 Near field distribution at the resonance frequency

frequency for this antenna.

Next, the numerical investigation of the given drop shaped antenna structure dependence on the various material and geometrical parameters have been performed. Fig.3 shows antenna return loss versus frequency for different antenna's width having its height fixed. In this

figure there are two curve families corresponding to the two presented geometries of antennas. The leftmost and rightmost families correspond to the geometry I and II respectively. In the first case the cable is separated from the antenna by the metallic disk while in the second case antenna is directly connected to the cable. The numerical experiment shows that in the first case the resonance frequencies are shifted to the left compared to the second one. With the increase of antenna width the radiation band also increases and the radiation efficiency diminishes. In Fig.4 the near field at the resonance frequency for the case II is presented. Analysis of the near field structure have shown the absence of the reactive component in it that means that the antenna is well matched with the cable and free space.

Under the certain optimal choice of antenna's shape it is possible to increase the radiation frequency band. From the obtained results one can see that the resonance frequencies for the presented antenna (3.0-4.0 GHz) do not fit into to the current standards for mobile communications (0.9-2.8 GHz). In order to conform to them the electrical size of the antenna should be enlarged. This is possible by covering the antenna with the thin dielectric layer of high permittivity. In order to obtain good matching between the dielectric layer and the free space it is necessary for the corresponding wave impedance at the antenna surface to be equal to that of the free space. This can be achieved by the suitable choice of the layer's material parameters. Modern technology is able to provide a material with the negative permittivity. The created software allows for such media to be simulated.

The next aim of the investigations was to study the influence of the antenna on the user's head. The one of the main demands antenna must satisfy is the safety to the user -



Fig.5 SAR distribution inside head at 1.0GHz

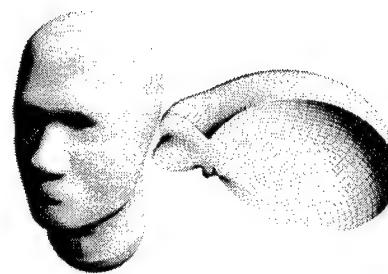


Fig.6 Radiation pattern

i.e. the SAR in the user's tissues must conform existing standards and be as low as possible. As a head model an IEEE Standard Head has been taken. Its averaged material parameters are  $\epsilon=45$ ,  $\sigma=0.9\text{S/m}$ . The Fig.5 and Fig.6 show the SAR distribution in different sections and radiated pattern when using a conventional monopole-style antenna at 1.0GHz. The absorbed energy in the head is approximately 70% of the feeding power. An optimized antenna structure for the SAR minimization has been developed. The corresponding results will be also presented.

## CONCLUSION

The presented antenna configuration allows one development of the desired antenna structure, conforming to the EMC demands and possibly other restrictions applied. The radiating capabilities of the presented antenna prototype on its material and geometrical properties dependence have been studied. The real antenna-cable-head system has been investigated and EMC and SAR issues considered.

## REFERENCES

- [1]. R. Zaridze, G. Bit-Babik, K. Tavzarashvili, N. Uzunoglu, D. Economou. "Wave Field Singularity Aspects Large-Size Scatterers and Inverse Problems." IEEE Transactions on Antennas and Propagation, vol. 50, No. 1, January 2002, p. 50-58.
- [2]. R. Zaridze, G. Bit-Babik, K. Tavzarashvili, A. Bijamov, G. Ghvedashvili "Analyses of Voluminous Metallic Antenna Covered with Dielectric Layer" 2001 IEEE Antenna & Propagation Society International Symposium, July 8-13, 2001, Boston, Massachusetts, USA. IEEE Catalogue Number: 01CH37229, ISBNB 0-7803-7070-8. pp. 472-475.
- [3]. R. Zaridze, G. Ghvedashvili, K. Tavzarashvili, G. Sapparishvili, A. Bijamov, G. Bit-Babik. "Radiation Characteristics of Pear-Shaped Metal-Dielectric Antenna With Cable Excitation". Proceedings of VI-th International Seminar/Workshop on Direct and Inverse Problems of Electromagnetic and Acoustic Wave Theory (DIPED-2001), Lviv, Ukraine, September 18-20, 2001, pp. 49-53.

## BUILDING TREFFTZ FINITE ELEMENTS FOR ELECTROMAGNETIC PROBLEMS

Yuriy Olegovich Shlepnev

Innoveda, Inc., 1369 Del Norte Road, Camarillo, CA, 93010, USA  
e-mail: shlepnev@ieee.org

Generalized algorithm to build descriptor matrices of convex polytope Trefftz finite elements is introduced in the paper. A finite number of plane waves is used to expand electromagnetic field inside the elements. Projections of the intra-element field on an additional set of basis functions defined on the element surface are used to build admittance matrix descriptors of the element.

### INTRODUCTION

As a generalization of the method of minimum autonomous blocks, introduced by V.V. Nikol'skii and T.I. Lavrova in the late 70s [1], Trefftz Finite Element method (TFEM) has been recently introduced into the computational electromagnetics [2], [3]. As the conventional finite element method (FEM), the TFEM is based on a division or decomposition of a boundary value problem for Maxwell's equations into a set of elements. Though, instead of polynomial functions, plane-wave solutions of the Maxwell's equations are used as the intra-element basis functions to expand electric and magnetic fields inside the elements. Though, the basic concepts of the method are quite general and are outlined in [2], [3], there is no formalized procedure to build descriptors of complex polytope structures such as polygonal prisms, tetrahedrons and so on. This paper introduces such formalized procedure to build the admittance matrices of convex polytope elements.

### BUILDING DESCRIPTORS OF 3-D ELEMENTS

Let us consider a 3-D boundary value electromagnetic problem in the frequency domain. The problem is described by the Maxwell's equations and boundary conditions in a Cartesian coordinate system. The problem is subdivided into a set of small convex polytope elements. All external and internal boundaries of the problem are mapped on the boundaries of the elements. An element can be represented as a convex polytope  $\Omega_p$  in three-dimensional Euclidian space with  $N_{face}$  polygonal faces  $F_n$ ,  $n = 1, \dots, N_{face}$ . The element is uniformly filled with an isotropic medium. Let us expand the polytope element interior field using  $N_{int}$  pairs of plane wave solutions of the Maxwell's equations. The field distribution inside the element can be expressed as

$$\begin{pmatrix} \vec{E}(\vec{r}) \\ \vec{H}(\vec{r}) \end{pmatrix} = \sum_{m=1}^{N_{int}} \left[ A_m^+ \cdot \begin{pmatrix} \vec{E}_{0m} \\ \vec{H}_{0m} \end{pmatrix} \cdot e^{ik_0 \vec{k}_m \cdot \vec{r}} + A_m^- \cdot \begin{pmatrix} \vec{E}_{0m} \\ \vec{H}_{0m} \end{pmatrix} \cdot e^{-ik_0 \vec{k}_m \cdot \vec{r}} \right], \quad \vec{r} \in \Omega_p, \quad \vec{k}_m \cdot \vec{E}_{0m} = 0, \quad \vec{H}_{0m} = \frac{\vec{k}_m \times \vec{E}_{0m}}{Z_0} \quad (1)$$

where symbol  $\cdot$  denotes scalar products, symbol  $\times$  denotes vector product,  $\vec{k}_m$  is the unit vector of propagation direction of the plane wave number  $m$ ,  $\vec{r}$  is a radius vector of a point inside the polytope or on its boundary,  $\vec{E}_{0m}$  is the unit electric field vector of the plane wave,  $\vec{H}_{0m}$  is the magnetic field vector of the wave,  $A_m^+$  and  $A_m^-$  are unknown magnitudes of the waves or expansion coefficients,  $k_0$  is a propagation constant of the plane wave, and  $Z_0$  is a characteristic impedance of the plane wave:

$$k = \omega\sqrt{\epsilon\mu}, Z_0 = \sqrt{\mu/\epsilon}. \quad (2)$$

$N_{\text{int}}$  magnitudes of the plane waves in (1) are considered to be linearly independent.

To provide connectivity of the element interior with the surrounding elements and to impose the inter-element boundary conditions, an additional set of basis functions is defined on the faces of the polytope element. Let us choose  $L_n$  vector basis functions defined on the polygonal face  $F_n$  for the electric field expansion and  $L_n$  basis functions on the same face to expand the magnetic field. The total number of pairs of the surface field expansion functions is

$$N_{\text{surf}} = \sum_{n=1}^{N_{\text{face}}} L_n \quad (3)$$

Designating the surface basis functions defined on the face  $F_n$  as  $\bar{e}_{n(l)}$  and  $\bar{h}_{n(l)}$ , the electric and magnetic fields on the surface of the polytope element can be expressed as follows:

$$\bar{E}_{\text{surf}} = \sum_{n=1}^{N_{\text{face}}} \sum_{l=1}^{L_n} v_{n(l)} \cdot \bar{e}_{n(l)}, \quad \bar{H}_{\text{surf}} = \sum_{n=1}^{N_{\text{face}}} \sum_{l=1}^{L_n} i_{n(l)} \cdot \bar{h}_{n(l)} \quad (4)$$

where  $v_{n(l)}, i_{n(l)}$  are unknown expansion coefficients. The total number of the boundary field expansion coefficients in (4) is  $2N_{\text{surf}}$ . It is in addition to the  $N_{\text{int}}$  independent interior expansion coefficients (1). The number of the interior basis functions  $N_{\text{int}}$  can be chosen equal to the number of the electric or magnetic field surface basis functions  $N_{\text{surf}}$ . It provides a possibility to uniquely define a matrix descriptor of the element. To do so, we can project the interior field on the surface basis functions [2], [3]:

$$v_{n(l)} = P_n \{ \bar{E}, \bar{e}_{n(l)} \}, \quad i_{n(l)} = P_n \{ \bar{H}, \bar{h}_{n(l)} \}, \quad l=1, \dots, L_n, \quad n=1, \dots, N_{\text{face}} \quad (5)$$

where  $\bar{E}$  and  $\bar{H}$  are values of the electric and magnetic fields defined by (1) taken on the face  $F_n$  where basis functions  $\bar{e}_{n(l)}$  and  $\bar{h}_{n(l)}$  are defined. Either point matching or Galerkin projectors can be used in (5). Constant vector basis functions may be used with the point matching projectors defined as

$$P_n \{ \bar{D}, \bar{b}_{n(l)} \} = \bar{D}(\bar{r}_{n(l)}) * \bar{b}_{n(l)}(\bar{r}_{n(l)}), \quad l=1, \dots, L_n, \quad n=1, \dots, N_{\text{face}} \quad (6)$$

where  $\bar{D}$  is either  $\bar{E}$  or  $\bar{H}$ ,  $\bar{b}_{n(l)}$  is either  $\bar{e}_{n(l)}$  or  $\bar{h}_{n(l)}$ ,  $\bar{r}_{n(l)}$  is the radius vector of a matching point on the face  $F_n$  for the basis function  $l$ . The matching points can be defined as centroids of the polygonal areas where the corresponding face basis functions are defined. Galerkin or averaging projectors can be defined as

$$P_n \{ \bar{D}, \bar{b}_{n(l)} \} = \frac{1}{|N_{n(l)}|} \int_{F_n} \bar{D} * \bar{b}_{n(l)}^* \cdot ds, \quad l=1, \dots, L_n, \quad n=1, \dots, N_{\text{face}} \quad (7)$$

where the integral is taken over the surface of  $F_n$ , and  $|N_{n(l)}|$  are the norms of the expansion functions. Substituting (1) into (5) we can obtain the following relations between the interior field expansion coefficients and the surface expansion coefficients:

$$\bar{v} = M_e^+ \cdot \bar{A}^+ + M_e^- \cdot \bar{A}^-, \quad \bar{i} = M_h^+ \cdot \bar{A}^+ + M_h^- \cdot \bar{A}^-, \quad (8)$$

where  $\bar{A}^+$  and  $\bar{A}^-$  are vectors with  $N_{\text{int}}$  coefficients  $A_m^+$  and  $A_m^-$  (1),  $\bar{i}$  and  $\bar{v}$  are vectors with  $N_{\text{surf}}$  components defined as

$$\bar{i} = [\bar{i}_1, \dots, \bar{i}_{N_{\text{face}}}]^T, \bar{i}_n = [i_{n(1)}, \dots, i_{n(L_n)}]^T, \bar{v} = [\bar{v}_1, \dots, \bar{v}_{N_{\text{face}}}]^T, \bar{v}_n = [v_{n(1)}, \dots, v_{n(L_n)}]^T, \quad (9)$$

where symbol  $'$  denotes transposition.

Matrices  $M_e^\pm$  and  $M_h^\pm$  are  $N_{\text{surf}}$  by  $N_{\text{int}}$  complex matrices of projections of the interior basis functions (1) on the boundary basis functions with the elements defined with either projectors (6) or (7) as

$$\begin{aligned} (M_e^\pm)_{n(l),m} &= P_n \left\{ \bar{E}_{0m}^\pm \cdot e^{\pm i k_0 \bar{k}_m \cdot \bar{r}}, \bar{e}_{n(l)} \right\}, \quad (M_h^\pm)_{n(l),m} = P_n \left\{ \bar{H}_{0m}^\pm \cdot e^{\pm i k_0 \bar{k}_m \cdot \bar{r}}, \bar{h}_{n(l)} \right\} \\ m &= 1, \dots, N_{\text{int}}, \quad l = 1, \dots, L_n, \quad n = 1, \dots, N_{\text{face}} \end{aligned} \quad (10)$$

A descriptor matrix of the polygonal element can be deduced by eliminating unknown interior field expansion coefficients  $\bar{A}^\pm$  from (8). From here on we assume that  $N_{\text{int}} = N_{\text{surf}} = N$ , which leads to square  $N$  by  $N$  matrices  $M_e^\pm$  and  $M_h^\pm$ . An assumption of the equality of two terms in the magnetic field projection sum or alternatively in the electric field projection sum (8) leads to two alternative additional expressions to construct the descriptor matrix:

$$\bar{A}^- = T_h \cdot \bar{A}^+, \quad T_h = (M_h^-)^{-1} \cdot M_h^+ \quad (11)$$

$$\bar{A}^- = T_e \cdot \bar{A}^+, \quad T_e = (M_e^-)^{-1} \cdot M_e^+ \quad (12)$$

Now, an admittance matrix descriptor of the element relating the unknown boundary expansion coefficients can be defined as

$$\bar{i} = Y \cdot \bar{v}, \quad Y = M_h \cdot M_e^{-1}, \quad Y \in C^{N \times N}, \quad (13)$$

where  $M_e = M_e^+ + M_e^- \cdot T_{e/h}$ ,  $M_h = M_h^+ + M_h^- \cdot T_{e/h}$ .

The linear independency of the element interior basis functions is the necessary condition of existence of a non-degenerate descriptor of a polytope element. Plane waves propagating in the directions perpendicular to the sides of a convex polytope provide such a system of functions. Assembling of the admittance matrices (13) into a global admittance matrix is a simple and straightforward procedure and is described in [2].

## CONCLUSION

Trefftz finite element method has been generalized in the paper on the problems subdivided into a set of convex polytope elements. The boundary value problem has been reduced to a building and re-composition of admittance matrices of the polytope elements. Generalized matrix formulas are derived to build the admittance matrix descriptors of the elements.

## REFERENCES

- [1] V.V. Nikol'skii, T. I. Lavrova, *Radio Engineering & Electronic Physics*, vol. 23, no. 2, pp. 1-10, 1978.
- [2] Y. O. Shlepnev, *IEEE Trans. Microwave Theory Tech.*, vol. MTT-50, pp. 1328-1339, May, 2002.
- [3] Y. O. Shlepnev, in *Proc. of the 18th Annual Review of Progress in Applied Computational Electromagnetics*, Monterey, CA, pp. 327-334, March, 2002.

**SCATTERING  
AND  
RADAR CROSS  
SECTION**



# CALCULATION OF NEAR-ZONE ELECTROMAGNETIC FIELDS SCATTERED BY COMPLEX SHAPE AIRBORNE OBJECTS AND ESTIMATION OF THEIR ANGULAR COORDINATES BY ONBOARD ANTENNA SYSTEMS

N.V. Barkhudaryan, A.Z. Sazonov, O.I. Sukharevsky

Kharkov Military University, Kharkov, Ukraine

E-mail: sukharevsky@euro.dinos.net

The technique of calculation of near-zone electromagnetic fields scattered by complex shape airborne objects is present. It is shown that the direction line defined by a direction finder differs from true one and depends on geometry of the object, its electrical sizes and also on mutual location of the transmitting antenna, object and receiving antenna. The results of numerical calculations for the object such as "airplane" are represented. Calculation was carried out in a centimeter band, separately in a plane of course and pitches one, radiation – monochromatic. The angle of object elevation is constant and it is equal to three degrees.

Most of modern airborne objects have complex geometrical shape of its surface. The character of reflections depends from orientation of object with reference to the direction of sounding. The scattered field incident on the antenna aperture is the result of interference of waves reflected from separate units of object surface. The contribution to the resulting field of components with different amplitudes and phases results in the not plane phase front of the scattered electromagnetic wave. The distortion

of phase front causes to deflection of the measured target angular position from true one as the direction line is defined as a normal to a phase front [1]. The calculation technique includes simulation of the object surface by the system of triangular facets [2]. In a Figure 1 the model of a standard airplane with a wings span of 20 meters is represented. The calculations of scattered field consist of a numerical integration of surface current densities for each facet in barycentric coordinates. The calculations were carried out by means of special cubature formulas permitting to evaluate integrals of high-oscillatory functions [2].

The electrical dimensions of the object are large. In this case acceptable

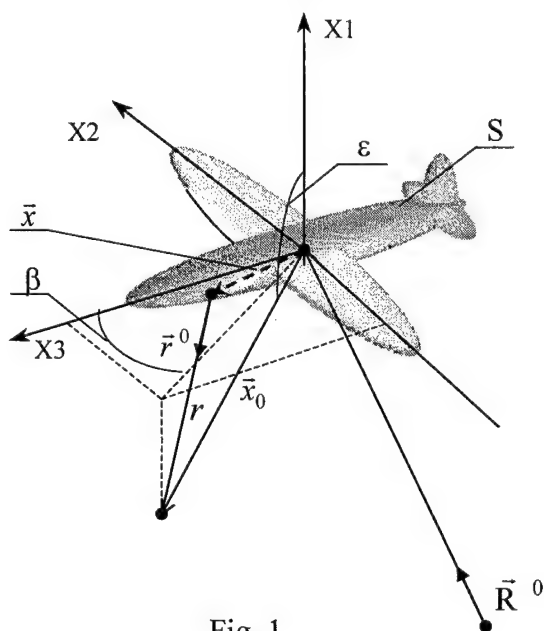


Fig. 1

Kirchhoff approximation. Let a plane electromagnetic wave incidents on perfectly conducting scatterer with surface  $S$  located in the free space

$$\vec{E}^0(\vec{x}) = \vec{p} \exp(-jk_0(\vec{R}^0 \vec{x})), \quad \vec{H}^0(\vec{x}) = (\vec{p} \times \vec{R}^0) \sqrt{\frac{\epsilon_0}{\mu_0}} \exp(-jk_0(\vec{R}^0 \vec{x})), \quad (1)$$

where  $\vec{R}^0$  is the unit vector of sounding direction;  $\vec{p}$  is the vector of polarization;  $k_0$  is the wave number of free space;  $\epsilon_0, \mu_0$  are permittivity and permeability of free space accordingly;  $\vec{x}$  is the position vector of object surface point (Figure 1).

If  $\vec{E}(\vec{x}), \vec{H}(\vec{x})$  are vectors of total field then scattered field will be defined by formula  $\vec{E}^s(\vec{x}) = \vec{E}(\vec{x}) - \vec{E}^0(\vec{x})$ . Let in some point  $\vec{x}_0$  somewhere outside of  $S$  the electric dipole with the vector-moment  $\vec{p}$  is located. Vector  $\vec{p}$  is arbitrary on the value and direction. This dipole creates a field. Applying a Lorentz lemma, we have

$$j\omega \vec{p} \vec{E}^s(\vec{x}_0) = \int_S \vec{H}^\perp(\vec{x}) \vec{E}_0^{eT}(\vec{x}/\vec{x}_0, \vec{p}) - \vec{E}^T(\vec{x}) \vec{H}_0^{e\perp}(\vec{x}/\vec{x}_0, \vec{p}) ds, \quad (2)$$

where

$$\vec{H}^\perp = \vec{n} \times \vec{H} \quad \vec{E}^T = \vec{E} - \vec{n}(\vec{n} \cdot \vec{E}) \quad \vec{E}_0^{eT} = \vec{E}_0 - \vec{n}(\vec{n} \cdot \vec{E}) \quad \vec{H}_0^{e\perp} = \vec{n} \times \vec{H}_0 \quad - \quad (3)$$

the tangential components of electrical and magnetic fields,  $\vec{n}$  – is the unit normal vector to the object surface. For the perfectly conducting scatterer  $\vec{E}^T|_S = 0$  and consequently the integrand function is zero.

The field of an electric dipole can be represented in the form

$$\vec{E}_0^{eT}(\vec{x}/\vec{x}_0, \vec{p}) = \frac{1}{\epsilon_0} [\vec{\nabla}(\vec{p} \cdot \vec{\nabla}) \dot{G} + k_0^2 \vec{p} \dot{G}], \quad (4)$$

where  $\dot{G} = e^{jk_0 r} / 4\pi r$ ;  $\vec{r}^0 = (\vec{x}_0 - \vec{x})/r$ ;  $r = |\vec{x}_0 - \vec{x}|$  – the distance between object and receiving antenna;  $\vec{p} = \vec{p}^\parallel + \vec{p}^\perp$  are longitudinal and tangential component of polarization vector. Taking into account that in Kirchhoff approximation formula (2) for a scattered field

$$\vec{p} \vec{E}^s(\vec{x}_0) = \frac{1}{2\pi j k_0} \oint_{S_s} \left[ \vec{R}^0(\vec{p} \cdot \vec{n}) - \vec{p}(\vec{R}^0 \cdot \vec{n}) \right] \left[ \left( k_0^2 + \frac{j k_0 r - 1}{r^2} \right) \vec{p}^\perp - \frac{2(j k_0 r - 1)}{r^2} \vec{p}^\parallel \right] e^{jk_0(r + \vec{R}^0 \cdot \vec{x})} ds_s, \quad (5)$$

where  $S_s$  is "illuminated" part of object surface. Using the representation (5) calculations of scattered field were carry out for  $\beta = 0 \dots 90^\circ$  and  $\epsilon = 75^\circ, 85^\circ, 95^\circ$ . For example, in Fig. 2 results of calculation for  $\epsilon = 75^\circ$  and  $r = 200m$  are presented. Direction finding accuracy depends on the type of angle discriminator and amplitude-phase distribution (APD) in antenna aperture. In this paper we simulated combined calculation accuracy is given by the antenna: in  $\beta$ -plane – amplitude method of

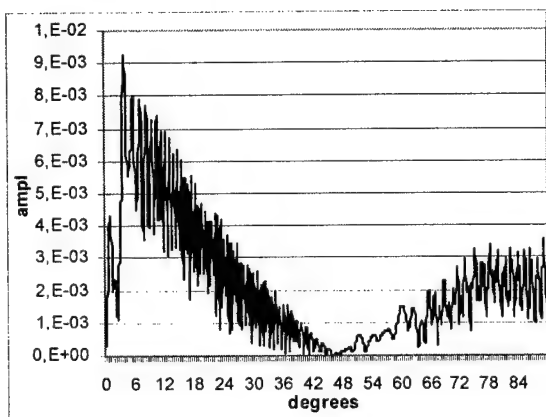


Fig. 2

$r(p) = \text{Re}[U_s U_d^* \exp(j\pi/2)] / U_s U_s^*$  – for pitch-plane, where  $U_s = U_1 + U_2$ ,  $U_d = U_1 - U_2$ . For example dependences of  $r(c)$  and  $r(p)$  from angle  $\beta$  are shown in Figures 3, 4.

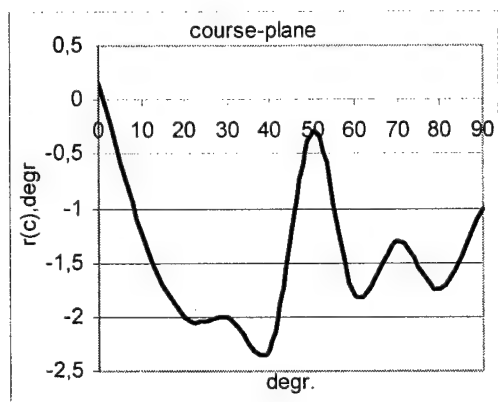


Fig. 3

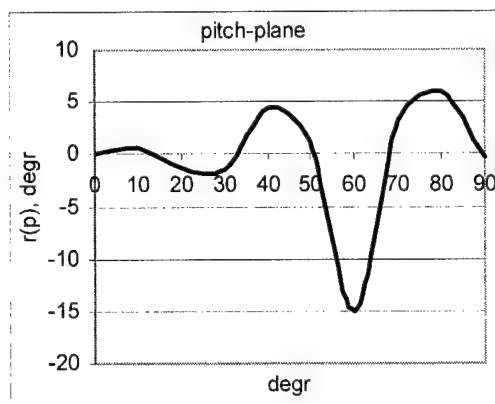


Fig. 4

The analysis of Figures 3, 4 have shown that in the course-plane the deviation can be obtained the values 1,7-2,3 degrees. In the pitch-plane it possible to obtain 15 degrees. For azimuth  $60^\circ$  in the  $\varepsilon$ -plane the angular deviation is more than object angular size.

By using proposed technique one can efficiently calculate the errors in airborne object direction finding appearing in short-range radar.

## REFERENCE

- [1] Ostrovityanov R.V., Basalov F.A. Statistical theory of lengthy targets radiolocation. – Moscow: Radio i Svyaz, 1982. – 232 p. (in Russian).
- [2] Sukharevsky O.I., Vasilets V.A., Sazonov A.Z., Tkachuk K.I. Calculation of scattering of electromagnetic wave by perfectly conducting object partly covered with radar absorbing material using triangulation cubature formulas, Radiofizika i Radioastronomiya. – 2000. – Vol.5, №1 – P. 47–54. (in Russian).

direction finding; in  $\varepsilon$ -plane – phase one. Such finding direction functioning is described by expression

$$U_{1,2}(\vec{x}_0) = \oint_{S_{ap}} \vec{E}^s(\vec{x}_0) \vec{A}_{1,2}(\vec{x}_0) dS_{ap},$$

where  $\vec{A}_{1,2}(\vec{x}_0)$  is APD in antenna aperture for two channels of receiving antenna,  $S_{ap}$  is aperture area. Deviation of measured object bearing from true one is determined by expressions  $r(c) = \text{Re}[U_s U_d^*] / U_s U_s^*$  – for course-plane and

## MATHEMATICAL METHODS IN SOME DIFFRACTION PROBLEMS FOR DOMAINS WITH DEFECTS

Alla A. Gousenkova

Department of Applied Mathematics, Kazan State University  
18, Kremlyovskaya, Kazan, 420008, Russia  
e-mail: gaa@ksu.ru

Mathematical methods in diffraction problems for elastic time-harmonic waves on defects are considered. It is assumed that the body forces are absent and the defect may be disposed on the plane in the homogeneous isotropic space or on the media interface of two homogeneous isotropic half-spaces. It is obtained systems of singular integral equations equivalent to the problems. Considered mathematical methods may be useful for solving some form researched in [1] diffraction problems for electromagnetic time-harmonic waves on defects. Some approaches to elastodynamic problems in the case of the anisotropic elastic medium are considered too. It is get analogues of the Lopatinskii condition and boundary conditions of an elliptic boundary value problem in the half-space. It is shown that both approaches are equivalent.

To solve these problems *the classes of outgoing from a plane solutions* are introduced. The Fourier transformation in the class of generalized functions of the slow growth at infinity and presentations of solutions of the problems by *potential functions* are used.

### SOME ANISOTROPIC ELASTODYNAMIC PROBLEMS.

One considered harmonic oscillations of the anisotropic elastic half-space  $\{x_3 > 0\}$ . Assume that the body forces are absent. In this case we have the equations

$$\sum_{k,l,j=1}^3 C_{ijkl} \frac{\partial^2 u_k}{\partial x_i \partial x_j} + \rho v^2 u_i = 0, \quad i = 1, 2, 3$$

where  $u(u_1, u_2, u_3)$  is the complex displacement vector,  $\tilde{u}(x, t) = \text{Re}\{u(x)e^{-i\omega t}\}$ ,  $\tilde{u}(\tilde{u}_1, \tilde{u}_2, \tilde{u}_3)$  is the displacement vector,  $\rho$  is the density of the body,  $C_{ijkl}$  ( $i, j, k, l = 1, 2, 3$ ) are the elastic constants,  $C_{ijkl} = C_{jkl i} = C_{klij}$ .

A solution  $u(u_1, u_2, u_3)$  of the equation for  $x_3 > 0$  we will to call *outgoing from the plane*  $\{x_3 = 0\}$  to the half-space  $\{x_3 > 0\}$  [2], if  $u_i(x_1, x_2, x_3)$  ( $i = 1, 2, 3$ ) are distributions of the slow growth and

$$\text{supp } u_i(x_1, x_2, x_3) \subset \{x_3 > 0\}, \quad i = 1, 2, 3$$

$$\text{sing supp } U_i(\xi_1, \xi_2, \xi_3) \cap \{\xi_3 < 0\} = \emptyset, \quad i = 1, 2, 3$$

where the Fourier transforms of the unknown functions are denoted by capital letters.

For solving this problem with some boundary conditions on the plane  $\{x_3 = 0\}$  the Fourier transformation with respect to all variables in the space of distributions one used. Therefore one get some auxiliary conditions. One can show that the boundary and auxiliary conditions at this approach for solving of the problem are analogous to the Lopatinskii condition and the boundary conditions at the considered in [3] approach for solving of the elliptic boundary value problem for the half-space. In [3] the Fourier

transformation does not take with respect to all variables. Therefore one get a system of ordinary differential equations for the Fourier transforms of unknown functions. But we get the system of linear algebraic equations for the Fourier transforms of  $u_i(\cdot, \cdot)$  ( $i = 1, 2, 3$ ).

If the roots with the positive imaginary part of some equation are known, then the solution of the boundary value problem for the half-space can be written in the obvious form. In this case one can obtain presentations of solutions of the boundary value problems by stress and displacement jumps on the plane  $\{x_3 = 0\}$ . And it is convenient to research, for example, diffraction problems for the elastic time-harmonic wave on a defect disposed on the plane  $\{x_3 = 0\}$ .

**SOME ISOTROPIC ELASTO- AND ELECTRODYNAMIC PROBLEMS.** Let  $\Omega$  be an infinitely thin defect disposed on the plane  $\{x_3 = 0\}$  in an isotropic elastic medium. Assume that the dependence from the time is harmonic for the components of the stress vector and for the components of the displacement vector, the body forces are absent. One searched the complex amplitudes of the functions, the time factor  $e^{-ikt}$  one omitted.

It is well known that by made assumptions the elastodynamic equations have the form

$$(\lambda + \mu) \operatorname{grad} \operatorname{div} u + \mu \Delta u + \rho k^2 u = 0 \quad \text{in } R^3 \setminus \overline{\Omega}$$

where  $\Delta = \partial^2 / \partial x_1^2 + \partial^2 / \partial x_2^2 + \partial^2 / \partial x_3^2$  is the Laplace operator,  $\lambda, \mu$  are the Lamé constants,  $\rho$  is the density of the body.

In the case of a soldered hard screen, for example, the boundary conditions have the form

$$u_i|_{\Omega} = -u_i^0(x_1, x_2), \quad i = 1, 2, 3 \quad \text{on } \Omega$$

where  $u_i^0(\cdot, \cdot)$  ( $i = 1, 2, 3$ ) are the known functions.

For solving this problem it is convenient to consider an auxiliary jump problem. One searched solutions of the Lamé equations for  $\{x_3 > 0\}$  and for  $\{x_3 < 0\}$  in the class of solutions outgoing from the plane  $\{x_3 = 0\}$ . On the plane  $\{x_3 = 0\}$  the stress and displacement jumps are given

$$[u_i]|_{\Lambda} = a_{u_i}(x_1, x_2), \quad [\sigma_{i3}]|_{\Lambda} = a_{\sigma_{i3}}(x_1, x_2), \quad i = 1, 2, 3 \quad \text{on } \Lambda$$

where  $\Lambda$  is the plane  $\{x_3 = 0\}$ ,  $[f]|_{\Lambda} = f(x_1, x_2, 0+0) - f(x_1, x_2, 0-0)$ . Functions in the right-hand sides of the conditions are the given functions on the plane  $\{x_3 = 0\}$ ; we will to call its *the potential functions*.

For solving the jump problem it is convenient to use the longitudinal and lateral potentials  $\varphi(\cdot, \cdot)$  and  $\psi = (\psi_1(\cdot, \cdot), \psi_2(\cdot, \cdot), \psi_3(\cdot, \cdot))$

$$u = \operatorname{grad} \varphi + \operatorname{rot} \psi, \quad \operatorname{div} \psi = 0$$

and the Fourier transformation with respect to all variables in the space of distributions. For the functions  $\varphi(\cdot, \cdot)$ ,  $\psi_i(\cdot, \cdot)$  ( $i = 1, 2, 3$ ) we have the Helmholtz equations

$$\Delta \varphi + k^2 \varphi = 0, \quad \Delta \psi_i + k^2 \psi_i = 0, \quad i = 1, 2, 3 \quad \text{in } R^3 \setminus \overline{\Omega}$$

where  $k_i = k/c_i$  ( $i = 1, 2$ )  $c_1 = \sqrt{(\lambda + 2\mu)/\rho}$ ,  $c_2 = \sqrt{\mu/\rho}$  are the velocities of spreading of longitudinal and lateral waves in the isotropic elastic medium.

In some electrodynamic boundary value problems systems of Helmholtz equations may be obtained too, when boundary conditions for unknown functions do not separate. In these cases solutions of Helmholtz equations we will search independently, if the Fourier transformation in the class of distributions one used.

Boundary conditions for the potentials  $\varphi(\cdot, \cdot)$  and  $\psi$  do not separate in boundary value problems for an isotropic space with the defect  $\Omega$  on the plane  $\{x_3 = 0\}$ . But the problems for the Fourier transforms of the functions  $\varphi(\cdot, \cdot)$  and  $\psi_i(\cdot, \cdot)$  ( $i = 1, 2, 3$ ) in the auxiliary jump problem one can consider independently, if we will take the Fourier transformation in the space of distributions.

For solving the jump problem we take the Fourier transformation with respect to all variables in the Helmholtz equations. One can to obtain presentations of solutions of the diffraction problems for the elastic time-harmonic wave on a defect  $\Omega$  by the potential functions. One obtained systems of singular integral equations (SSIE) equivalent to the boundary value problems in cases of some defects  $\Omega$ . For example, one can shown that in the case of a soldered hard screen in presentations of solutions of the boundary value problems the functions  $a_{u_i}(\cdot, \cdot)$  ( $i = 1, 2, 3$ ) are equal to zero identically and the functions  $a_{\sigma_{i3}}(\cdot, \cdot)$  ( $i = 1, 2, 3$ ) are non-zero on  $\Omega$  only. One obtained SSIE for defining the functions  $a_{\sigma_{i3}}(\cdot, \cdot)$  ( $i = 1, 2, 3$ ) on the screen. Equations of the system have the logarithmic singularity with respect to all variables.

In the considered in Sec.1, 2 dynamic problems longitudinal and lateral potentials are used in the auxiliary jump problem only. It is convenient, because to take the Fourier transformation to the independent Helmholtz equations is more easy than to the system of the connected Lamé equations. And the problems for the Fourier transforms of functions  $\varphi(\cdot, \cdot)$  and  $\psi_i(\cdot, \cdot)$  ( $i = 1, 2, 3$ ) are separated in the jump problem, if one used the Fourier transformation in the space of distributions. Usually in analogous elastodynamic problems the Fourier transformation does not take with respect to all variables. And problems for longitudinal and lateral potentials do not can to consider independently.

## REFERENCES

- [1] A.S. Ilyinsky, Yu.G. Smirnov, Electromagnetic wave diffraction by conducting screens (Pseudodifferential operators in diffraction problems), VSP, Zeist, 1998
- [2] A.A. Gousenkova, The potential functions method in the problems of the elasticity theory for bodies with a defect, Prikl. Mat. i Mekh. (3) **66**, 470-480 (2002); English transl. in J. Appl. Maths Mechs (3) **66** (2002)
- [3] Yu.V. Egorov, Linear differential equations of the principal type, Nauka, Moscow, 1984 (in Russian)
- [4] A.A. Gousenkova, Diffraction problems for electromagnetic wave on a strip and for elastic wave on a defect in comparison, Proc. Int. Conf. Mathematical Methods in Electromagnetic Theory MMET 2000, Kharkov, Ukraine, Sept. 12-15, 2000, vol. 2, 426-428

# APPLICATION OF THE METHOD OF AUXILIARY SOURCES FOR THE ANALYSIS OF PLANE-WAVE SCATTERING BY IMPEDANCE SPHERES

Mirza Karamahmedović, Olav Breinbjerg

Ørsted•DTU, Electromagnetic Systems, Technical University of Denmark

Ørsted's Plads, building 348, DK-2800 Kgs. Lyngby, Denmark

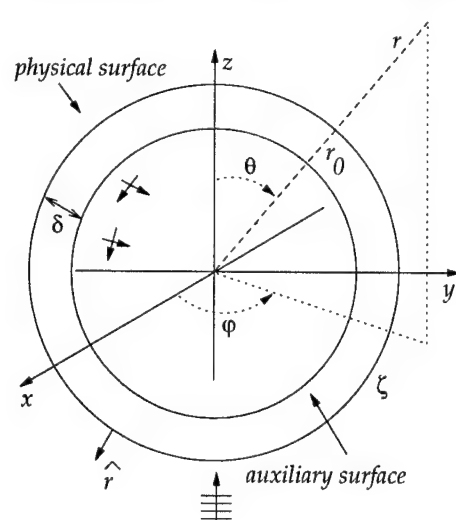
e-mail: mirza@ieee.org, ob@oersted.dtu.dk

## ABSTRACT

The Method of Auxiliary Sources (MAS) is applied to 3D scattering problems involving spherical impedance scatterers. The MAS results are compared with the reference spherical wave expansion (SWE) solution. It is demonstrated that good agreement is achieved between the MAS and SWE results.

## INTRODUCTION

The Method of Auxiliary Sources (MAS) is a numerical technique applicable to electromagnetic scattering problems. In the general case, a set of spatially impulsive electric and/or magnetic sources is introduced to radiate an approximation to the unknown scattered field. These so-called auxiliary sources are located on an auxiliary surface, typically conformal to, and enclosed within, the physical surface of the scatterer. Point matching of the boundary condition on the physical surface is enforced to determine the complex amplitudes of the auxiliary sources. The MAS originates from an application of a special case of the Method of Moments (MoM), utilising spatially impulsive expansion and testing functions, to a generalised surface integral equation formulation [1]. An overview of MAS is given in [2]. Utilisation of MAS for numerical solution of various 2D scattering problems and 3D PEC and dielectric scattering problems has been reported earlier [3], [4], [5]. The purpose of this work is to investigate the performance of MAS when the method is applied to scattering problems involving spherical impedance scatterers. The spherical wave expansion (SWE) solution is developed and used as a reference. The scattering problem under investigation is



illustrated in Figure 1, together with the introduced Cartesian and spherical co-ordinate systems. The spherical scatterer of radius  $r_0$  is illuminated by an  $x$ -polarised uniform plane wave ( $\mathbf{E}^i, \mathbf{H}^i$ ) of wavelength  $\lambda$  and propagating in the  $z$ -direction. The Standard Impedance Boundary Condition (SIBC) holds on the physical surface of the scatterer,  $\hat{\mathbf{r}} \times (\mathbf{E} \times \hat{\mathbf{r}}) = \zeta \hat{\mathbf{r}} \times \mathbf{H}$ . The chosen auxiliary sources are pairs of crossed  $\hat{\theta}$ - and  $\hat{\phi}$ -directed electric Hertzian dipoles located on a sphere of radius  $r_0 - \delta$ . The auxiliary source pairs, as well as the matching points, are placed equidistantly in the angular co-ordinates  $(\theta, \phi)$ . The total number of source pairs is denoted by  $N$ .

Figure 1: The scattering problem geometry

The SWE solution is given by (see [6, Chapter 2] for definitions of symbols)

$$\mathbf{E}^S = k/\sqrt{\eta} \sum_{s,m,n} Q_{s,m,n}^{(3)} \mathbf{F}_{s,m,n}^{(3)}, \mathbf{H}^S = -ik\sqrt{\eta} \sum_{s,m,n} Q_{s,m,n}^{(3)} \mathbf{F}_{3-s,m,n}^{(3)}, Q_{s,m,n}^{(3)} = E^i a/b,$$

$$a = i^{n+1} \sqrt{\pi(2n+1)} (-1)^{4-s-m} R_{3-s,n}^{(3)} R_{s,n}^{(1)} (-\delta_{s,1}(\delta_{m,1} + \delta_{m,-1}) + \delta_{s,2}(\delta_{m,-1} - \delta_{m,1})) -$$

$$i^{n+2} \zeta \eta \sqrt{\pi(2n+1)} (-\delta_{s,1} R_{2,n}^{(1)} R_{2,n}^{(3)} (\delta_{m,1} + \delta_{m,-1}) + \delta_{s,2} R_{1,n}^{(1)} R_{1,n}^{(3)} (\delta_{m,-1} - \delta_{m,1})),$$

$$b = -k/\sqrt{\eta} (-1)^{3-m-s} R_{3-s,n}^{(3)} R_{s,n}^{(3)} + \zeta ik \sqrt{\eta} (-1)^m (R_{3-s,n}^{(3)})^2,$$

$$R_{1,n}^{(3)} \equiv h_n^{(1)}(kr_0), R_{2,n}^{(1)} \equiv j_n'(kr_0), R_{2,n}^{(3)} \equiv h_n^{(1)'}(kr_0).$$

## NUMERICAL RESULTS

We define the boundary condition error (BCE) by

$$BCE \equiv \frac{1}{MN} \sum_{m,n} |\hat{\mathbf{r}}_{m,n} \times (\mathbf{E}_{m,n} \times \hat{\mathbf{r}}_{m,n}) - \zeta \hat{\mathbf{r}}_{m,n} \times \mathbf{H}_{m,n}| \quad (1)$$

The summation is performed over the scatterer physical surface. Figure 2 shows the BCE as a function of  $N$  for four different scatterer surface impedances  $\zeta$  and three values of  $\delta$  ( $\blacklozenge$ :  $\delta/\lambda=0.2$ ,  $\blacksquare$ :  $\delta/\lambda=0.5$ ,  $\blacktriangledown$ :  $\delta/\lambda=0.8$ ). In all cases,  $r_0/\lambda=1$  is chosen. It is observed that the BCE attained for  $\delta/\lambda=0.5$  is the lowest, and that it starts with a rapid decrease, whereafter it attains a constant level.

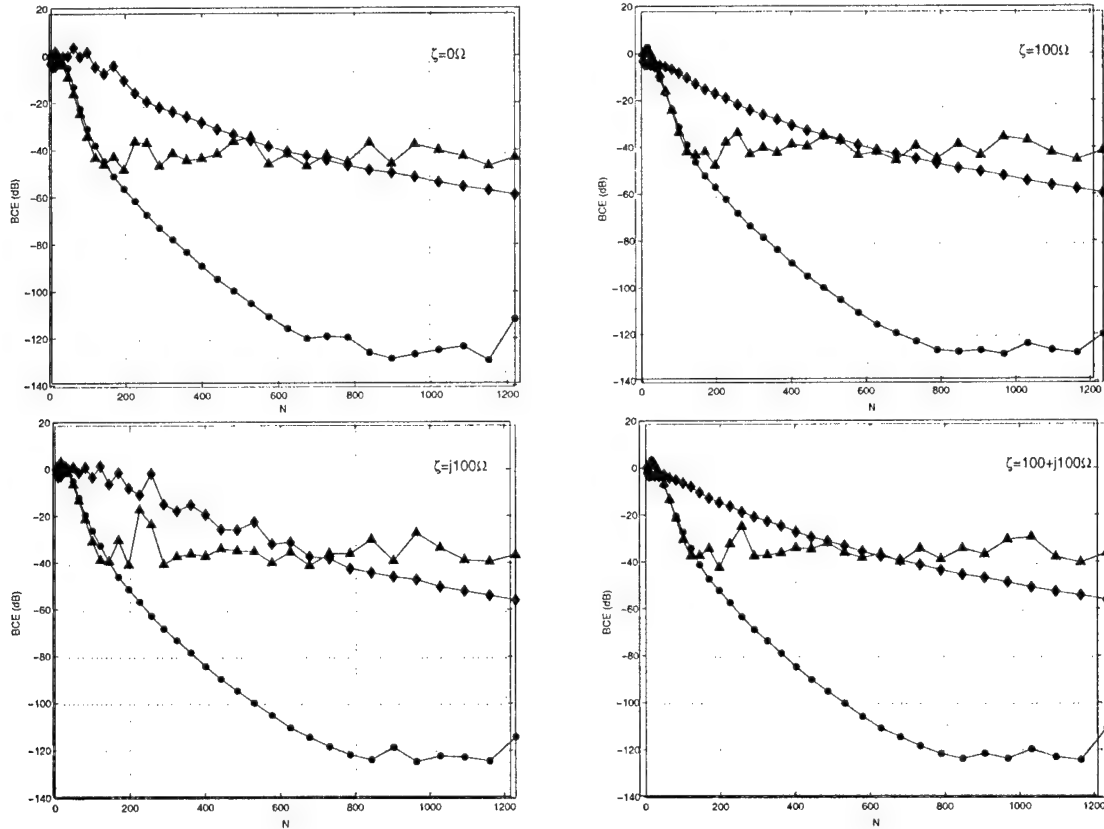


Figure 2



In Figure 3, the normalised bistatic radar cross section (BRCS) results obtained using MAS for four different scatterers and for two different planes of observation ( $\phi=0$  and  $\phi=\pi/2$ ) are compared with the corresponding SWE results. In all cases,  $\zeta=100+j100\Omega$  is chosen. There is a very good correspondence between the MAS and SWE results. The small discrepancies can be diminished further if  $N$  is increased.

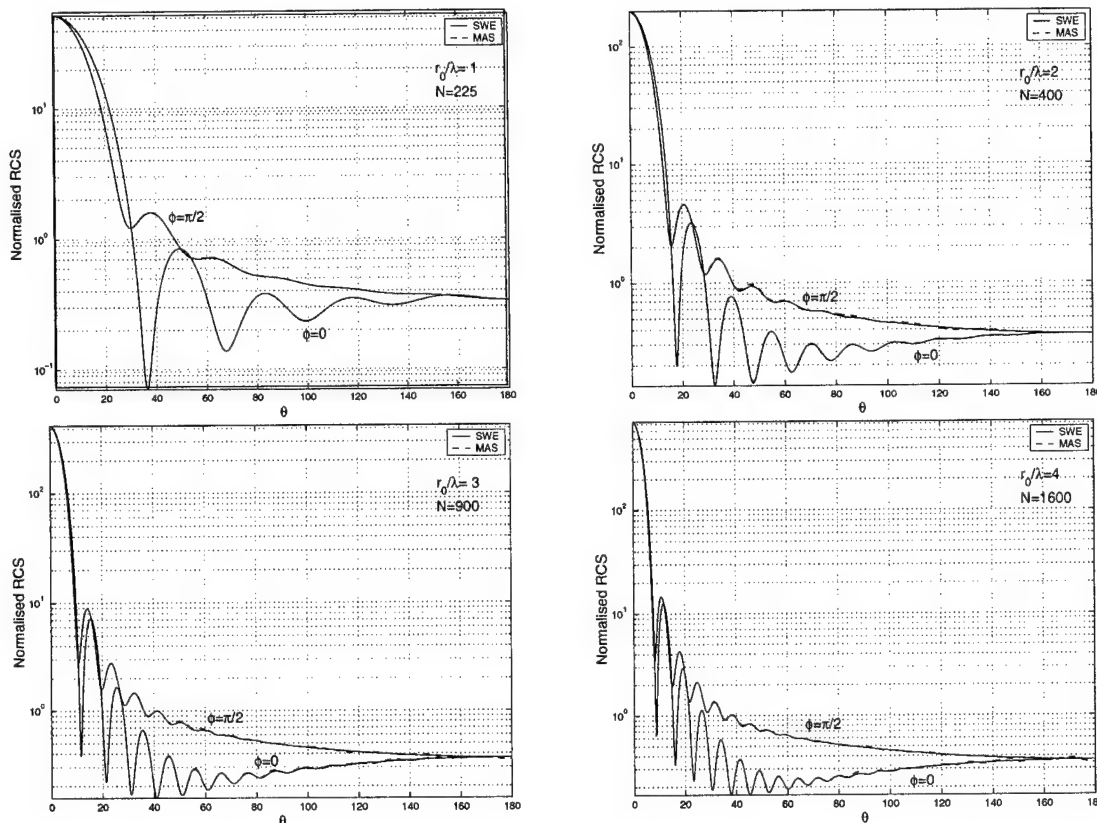


Figure 3

## CONCLUSION

It is seen that the initial decrease in the boundary condition error of the MAS numerical solution is relatively fast. Also, the limiting error level achieved is small enough for the MAS to be able to produce good approximations to exact results at a relatively small computational cost. However, the existence of a finite limit level for the MAS boundary condition error indicates that the present numerical implementation of the method is not convergent. Bistatic radar cross section results obtained by MAS are found to be in good agreement with the reference spherical wave expansion (SWE) solution.

## REFERENCES

- [1] Y. Leviatan et al., IEEE Trans. Antennas Propagat., vol. 36, 1722-1734, Dec. 1988
- [2] D. I. Kaklamani, European Congress on Computational Methods in Applied Sciences and Engineering, Barcelona 11-14 Sep. 2000
- [3] S. Eisler et al., IEE Proceedings, vol. 136, 431-438, Dec. 1989
- [4] H. T. Anastassiou et al., IEEE Trans. Antennas Propagat., vol. 50, 59-66, Jan. 2002
- [5] Y. Leviatan et al., IEEE Trans. Antennas Propagat., vol. 38, 1259-1263, Aug. 1990
- [6] J. E. Hansen, *Spherical Near-Field Antenna Measurements*, Peter Peregrinus 1988

# Galerkin Method for Solving of Singular Integral Equation of Diffraction Problem\*

Smirnov Yu.G., Tsupak A.A.

## 1 The statement of the diffraction problem

Let  $P = \{x : 0 \leq x_1 \leq a, 0 \leq x_2 \leq b, 0 \leq x_3 \leq c\}$  be a resonator with perfectly conducting boundary. Let  $Q$  be a three-dimensional body, located in  $P$ .  $Q$  is characterized by tensor permittivity  $\hat{\epsilon}$  and constant permeability  $\mu_0$ . We suppose that components of  $\hat{\epsilon}$  are smooth functions in  $\bar{Q}$  and  $(\frac{\hat{\epsilon}}{\epsilon_0} - \hat{I})$  is invertible in  $\bar{Q}$ ;  $Q \cap \partial P = \emptyset$ . Let  $P/\bar{Q}$  be homogeneous and isotropic medium. Incident and diffraction fields depend on time variable as  $e^{-i\omega t}$ .

We will find electromagnetic diffraction fields  $E$  and  $H$ , satisfying Maxwell's equations in  $P \setminus \partial Q$ :

$$\begin{aligned} \text{rot } \vec{H} &= -i\omega \hat{\epsilon} \vec{E} + \vec{j}_E^0 \\ \text{rot } \vec{E} &= i\omega \mu_0 \vec{H} - \vec{j}_H^0 \end{aligned} \quad (1)$$

The complete field should have continuous tangent components at  $\partial Q$ :

$$\left[ \vec{n} \times \vec{E}^c \right] \Big|_{\partial Q} = \left[ \vec{n} \times \vec{H}^c \right] \Big|_{\partial Q} = 0$$

and must satisfy the following boundary condition:

$$\vec{E}_\tau^c|_{\partial P} = 0. \quad (2)$$

## 2 Integro-differential equations for the diffraction problem

We will express the solution of the stated problem in terms of vector potentials  $\vec{A}_E$  and  $\vec{A}_H$  [4]:

$$\begin{aligned} \vec{A}_E &= \int_Q \hat{G}_E(x, y) \vec{j}_E(y) dy, \quad \vec{A}_H = \int_Q \hat{G}_H(x, y) \vec{j}_H(y) dy, \\ \vec{E} &= i\omega \mu_0 \vec{A}_E - \frac{1}{i\omega \epsilon_0} \text{grad div } \vec{A}_E - \text{rot } \vec{A}_H, \\ \vec{H} &= i\omega \epsilon_0 \vec{A}_H - \frac{1}{i\omega \mu_0} \text{grad div } \vec{A}_H + \text{rot } \vec{A}_E. \end{aligned} \quad (3)$$

Here  $\vec{j}_E = \vec{j}_E^0 + \vec{j}_E^p$ ,  $\vec{j}_H = \vec{j}_H^0 + \vec{j}_H^p$ , ( $\vec{j}_E^p, \vec{j}_H^p$  are polarization currents).  $\hat{G}_E, \hat{G}_H$  are Green functions for Helmholtz equation, conforming to the arbitrary currents  $\vec{j}_E^0, \vec{j}_H^0$ .

$\hat{G}_E, \hat{G}_H$  are known [3] to have the form of diagonal tensors (the components of  $\hat{G}_E$  are written out below):

$$\begin{aligned} G_E^1 &= \sum_{n=0}^{\infty} \sum_{m=1}^{\infty} \frac{2\epsilon_n}{ab\gamma \text{sh}\gamma c} \cos\left(\frac{\pi n}{a} x_1\right) \sin\left(\frac{\pi m}{b} x_2\right) \cos\left(\frac{\pi n}{a} y_1\right) \sin\left(\frac{\pi m}{b} y_2\right) \begin{cases} \text{sh}\gamma x_3 \text{sh}\gamma(c - y_3), & x_3 < y_3 \\ \text{sh}\gamma y_3 \text{sh}\gamma(c - x_3), & x_3 > y_3 \end{cases} \\ G_E^2 &= \sum_{n=1}^{\infty} \sum_{m=0}^{\infty} \frac{2\epsilon_m}{ab\gamma \text{sh}\gamma c} \sin\left(\frac{\pi n}{a} x_1\right) \cos\left(\frac{\pi m}{b} x_2\right) \sin\left(\frac{\pi n}{a} y_1\right) \cos\left(\frac{\pi m}{b} y_2\right) \begin{cases} \text{sh}\gamma x_3 \text{sh}\gamma(c - y_3), & x_3 < y_3 \\ \text{sh}\gamma y_3 \text{sh}\gamma(c - x_3), & x_3 > y_3 \end{cases} \\ G_E^3 &= \sum_{n=1}^{\infty} \sum_{m=1}^{\infty} \frac{4}{ab\gamma \text{sh}\gamma c} \sin\left(\frac{\pi n}{a} x_1\right) \sin\left(\frac{\pi m}{b} x_2\right) \sin\left(\frac{\pi n}{a} y_1\right) \sin\left(\frac{\pi m}{b} y_2\right) \begin{cases} \text{ch}\gamma x_3 \text{ch}\gamma(c - y_3), & x_3 < y_3 \\ \text{ch}\gamma y_3 \text{ch}\gamma(c - x_3), & x_3 > y_3 \end{cases} \end{aligned} \quad (4)$$

\*supported by Russian Foundation for Basic Research, grant 01-01-00053

Here  $\gamma = \sqrt{\left(\frac{\pi n}{a}\right)^2 + \left(\frac{\pi m}{b}\right)^2 - k_0^2}$  (the proper branch for square root is chosen as in [2], §2.3),  $\varepsilon_0 = 1$  and  $\varepsilon_n = 2$  for  $n = 1, 2, 3, \dots$ .

We can obtain the following integro-differential equations (under the condition  $\hat{\mu} = \mu_0 \hat{I}$  in  $P$ ):

$$\begin{aligned} \vec{E}(x) &= \vec{E}^0(x) + k_0^2 \int_Q \hat{G}_E \left[ \frac{\hat{\varepsilon}(y)}{\varepsilon_0} - \hat{I} \right] \vec{E}(y) dy + \text{grad div} \int_Q \hat{G}_E \left[ \frac{\hat{\varepsilon}(y)}{\varepsilon_0} - \hat{I} \right] \vec{E}(y) dy, \\ \text{and we have} \\ \vec{H}(x) &= \vec{H}^0(x) - i\omega \varepsilon_0 \text{rot} \int_Q \hat{G}_E \left[ \frac{\hat{\varepsilon}(y)}{\varepsilon_0} - \hat{I} \right] \vec{E}(y) dy, \quad x \in Q. \end{aligned} \quad (5)$$

We can extract singularity of Green function  $\hat{G}$ . Using Fourier transformation and interpolation polynomials we can obtain:

$$\hat{G}_E(x, y) = \frac{1}{4\pi} \frac{e^{ik_0|x-y|}}{|x-y|} \cdot \hat{I} + \text{diag}\{g_1(x, y), g_2(x, y), g_3(x, y)\},$$

where  $g_k$  are smooth functions.

### 3 Galerkin method

Let us introduce the following auxiliary function

$$\begin{aligned} \tilde{G}(x, y) &= - \sum_{n=1}^{\infty} \sum_{m=1}^{\infty} \frac{4}{ab\gamma \text{sh} \gamma c} \sin\left(\frac{\pi n}{a} x_1\right) \sin\left(\frac{\pi m}{b} x_2\right) \sin\left(\frac{\pi n}{a} y_1\right) \sin\left(\frac{\pi m}{b} y_2\right) \times \\ &\quad \times \begin{cases} \text{sh} \gamma x_3 \text{sh} \gamma(c - y_3), & x_3 < y_3 \\ \text{sh} \gamma y_3 \text{sh} \gamma(c - x_3), & x_3 > y_3 \end{cases}. \end{aligned} \quad (6)$$

The derivatives of  $\tilde{G}$  are connected to the derivatives of  $G_E^i$  through the equalities:

$$\frac{\partial G_E^i}{\partial x_i} = \frac{\partial \tilde{G}}{\partial y_i}, \quad i = 1, 2, 3. \quad (7)$$

Before describing the method itself we should make some transformations of equation (5). Denoting  $\left(\frac{\hat{\varepsilon}(x)}{\varepsilon_0} - \hat{I}\right)^{-1}$  as  $\hat{\xi}$  and  $\left(\frac{\hat{\varepsilon}(x)}{\varepsilon_0} - \hat{I}\right) \vec{E}$  as  $\vec{J}$  we obtain the following equation

$$A\vec{J} := \hat{\xi} \vec{J}(x) - k_0^2 \int_Q \hat{G}_E \vec{J}(y) dy - \text{grad div} \int_Q \hat{G}_E \vec{J}(y) dy = \vec{E}_0(x) \quad (8)$$

We can write vector equation (8) as a system of three scalar equations:

$$\sum_{i=1}^3 \xi_{li} J^i(x) - k_0^2 \int_Q G_E^l(x, y) J^l(y) dy - \frac{\partial}{\partial x_l} \text{div}_x \int_Q \hat{G}(x, y) \vec{J}(y) dy = E_0^l(x), \quad l = 1, 2, 3. \quad (9)$$

We will determine the components of approximate solution  $\vec{J}$  in the following way:

$$\vec{J}^1 = \sum_{k=1}^N a_k f_k^1(x), \quad \vec{J}^2 = \sum_{k=1}^N b_k f_k^2(x), \quad \vec{J}^3 = \sum_{k=1}^N c_k f_k^3(x), \quad (10)$$

where  $f_k^i$  are basis "hat"-functions dependent essentially on  $x^i$ . The explicit form of  $f_k^1$  is given below.

Let  $Q$  be a parallelepiped:  $Q = \{x : a_1 \leq x^1 \leq a_2, b_1 \leq x^2 \leq b_2, c_1 \leq x^3 \leq c_2\}$ ,  $Q \subset P$ . We will cover  $Q$  with smaller parallelepipeds

$$\begin{aligned} \Pi_{klm}^1 &= \{x : x_{k-1}^1 \leq x^1 \leq x_{k+1}^1, x_l^2 \leq x^2 \leq x_{l+1}^2, x_m^3 \leq x^3 \leq x_{m+1}^3\} \\ x_k^1 &= a_1 + \frac{a_2 - a_1}{n} k, \quad x_l^2 = b_1 + 2 \frac{b_2 - b_1}{n} l, \quad x_m^3 = c_1 + 2 \frac{c_2 - c_1}{n} m; \end{aligned} \quad (11)$$

where  $k = 1, \dots, n-1$ ;  $l, m = 0, 1, \dots, \frac{n}{2} - 1$ .

Denoting  $(x_k - x_{k-1})$  as  $h^1$  we get the formulas for  $f_{klm}^1$ :

$$f_{klm}^1 = \begin{cases} \frac{x^1 - x_{k-1}^1}{x_k^1 - x_{k-1}^1}, & \text{if } x^1 \in [x_{k-1}^1; x_k^1] \text{ and } x \in \Pi_{klm}^1 \\ \frac{x_{k+1}^1 - x^1}{x_{k+1}^1 - x_k^1}, & \text{if } x^1 \in [x_k^1; x_{k+1}^1] \text{ and } x \in \Pi_{klm}^1 \\ 0, & \text{if } x \notin \Pi_{klm}^1 \end{cases} \quad (12)$$

or

$$f_{klm}^1 = \begin{cases} 1 - \frac{1}{h^1} |x^1 - x_k^1|, & \text{if } x \in \Pi_{klm}^1 \\ 0, & \text{if } x \notin \Pi_{klm}^1 \end{cases} \quad (13)$$

Functions  $f_{klm}^2$  and  $f_{klm}^3$  should be determined by similar formulas. Since

$$f_{klm}^1|_{x^1 \in \{x_{k-1}^1, x_{k+1}^1\}} = 0, \quad f_{klm}^2|_{x^2 \in \{x_{l-1}^2, x_{l+1}^2\}} = 0, \quad f_{klm}^3|_{x^3 \in \{x_{m-1}^3, x_{m+1}^3\}} = 0, \quad (14)$$

every component of approximate vector solution vanishes at some side of  $Q$ . However the constructed set of basis functions does satisfy the necessary approximation condition.

Introducing total enumeration for basis functions we get

$$f_k^1, f_k^2, f_k^3; \quad k = 1, \dots, N,$$

where  $N = \frac{1}{4}(n^3 - n^2)$ .

It is convenient to represent the augmented matrix for determining unknown coefficients  $a_k, b_k, c_k$  in block form:

$$\left( \begin{array}{ccc|c} A_{11} & A_{12} & A_{13} & B_1 \\ A_{21} & A_{22} & A_{23} & B_1 \\ A_{31} & A_{32} & A_{33} & B_1 \end{array} \right) \quad (15)$$

where columns  $B_k$  and matrices  $A_{kl}$  are determined by formulas:

$$B_k^i = (E_0^k, f_i^k); \quad (16)$$

$$A_{kl}^{ij} = (\xi_{kl} f_j^l, f_i^k) - \delta_{kl} k_0^2 \left( \int_Q G_E^k(x, y) f_j^l(y) dy, f_i^k(x) \right) - \left( \frac{\partial}{\partial x_k} \int_Q \frac{\partial}{\partial x_l} G_E^k(x, y) f_j^l(y) dy, f_i^k(x) \right), \quad (17)$$

$k = 1, 2, 3$ ;  $i = 1, \dots, N$ .  $(f, g)$  determines the scalar product in  $L_2$ ,  $(f, g) = \int_Q f(x)g(x)dx$ .

Applying the formulas of integration by parts to both internal and external integrals and taking into account (7) and (14) we obtain:

$$A_{kl}^{ij} = \int_{\Pi_j^l \cap \Pi_i^k} \xi_{kl} f_j^l(x) f_i^k(x) dx - \delta_{kl} k_0^2 \int_{\Pi_i^k} \int_{\Pi_j^l} G_E^k(x, y) f_j^l(y) f_i^k(x) dy dx - \int_{\Pi_i^k} \int_{\Pi_j^l} \tilde{G}(x, y) \frac{\partial}{\partial x_l} f_j^l(y) \frac{\partial}{\partial x_k} f_i^k(x) dy dx. \quad (18)$$

## References

- [1] Ilinski, A.S., Smirnov, Yu.G., "Electromagnetic Wave diffraction by Conducting Screens", VSP, The Netherlands, Utrecht, 1998
- [2] Markov, G.T., Panchenko, B.A., "Tensor Green functions of rectangular resonators", Izvestiya Vuzov, Radiotekhnika, Moscow, 1964, V. 7, pp. 34-41. (in Russian)
- [3] Samohin, A.B., "Integral Equations and Iteration Methods in Electromagnetic Scattering", Radio & Sviaz, Moscow, 1998. (in Russian)

# **RADAR CROSS SECTION OF A PERFECTLY CONDUCTING, FLAT, POLYGONAL PLATE OVER A DIELECTRIC, LOSSY HALF SPACE: A CLOSED FORM, PHYSICAL OPTICS EXPRESSION**

Hristos T. Anastassiou

Institute of Communication and Computer Systems, Department of Electrical and  
Computer Engineering, National Technical University of Athens,  
Iroon Polytechniou 9, GR-15780 Zografou, GREECE  
e-mail: [hristosa@esd.ece.ntua.gr](mailto:hristosa@esd.ece.ntua.gr) Tel.: +3010 7722466 FAX: +3010 7723557

## **ABSTRACT**

The Physical Optics approximation is employed in the derivation of a closed form expression for the Radar Cross Section (RCS) of a flat, polygonal, perfectly conducting (PEC) plate, located over a dielectric, possibly lossy half space. The well-known "four-path model" is invoked in a first order approximation of the half space contribution to the scattering mechanisms. Numerical results are successfully compared to a reference, Moment Method solution. The analytical expressions derived can facilitate very fast RCS calculations for realistic scatterers, such as ships in a sea environment, or aircraft flying low over the ground.

## **INTRODUCTION**

Radar Cross Section (RCS) estimation of electrically large, complex targets is usually performed via high frequency techniques, such as Physical Optics (PO). A target of complex geometry is routinely decomposed into an aggregate of elementary surfaces, and the total scattered field is computed as a superposition of the elementary scattering contributions. Since the simplest possible shape of an elementary patch is a flat polygon, accurate RCS calculation for such a geometry is extremely important. Most papers in the literature are related to RCS calculations in free space, which is not a realistic situation in several cases, such as a floating ship, or a low – flying aircraft. RCS analysis in the presence of a half space can be performed via use of the "four-path model" [1]-[3], yielding good results for special geometries, e.g. [4]. The purpose of this paper is to extend Gordon's [5] important PO analytical expressions for the RCS of a flat, PEC, polygonal plate, so that they are valid in the presence of a dielectric, possibly lossy half space. The objective of such a work is the reduction of the computational cost associated with RCS calculations of electrically large, complex targets in the presence of sea or ground, since utilization of a closed form PO expression implies avoidance of time-consuming, numerical, surface integrations.

## **MATHEMATICAL ANALYSIS**

The geometry of the problem to be analyzed (Fig.1) consists of a PEC, polygonal, flat plate with  $Q$  vertices, vanishing thickness, located over a half space, which is filled with a dielectric, possibly lossy material of relative electric permittivity  $\epsilon_r$  and conductivity

$\sigma$ . The half space is assumed to lie in the far field region of the polygonal plate. The interface between free space and dielectric is assumed to lie at the  $z=0$  plane. A spherical coordinate system  $(r, \theta, \phi)$  is defined as shown in the figure. The images of the associated unit vectors with respect to the half space boundary are denoted by subscript “ $r$ ” in Fig. 1. A plane wave illuminates the plate target, impinging from an elevation angle  $\theta$ . In order to simulate the half space effects in a simple fashion, the well-known “four-path model” [1]-[3] is invoked. Assuming ray optical behaviour of the fields, the total backscattered field can be expressed as a cumulative result of four separate mechanisms (see Fig.2). Although the four-path model is not exact, it yields accurate results under certain limitations [3]. To apply the four-path model in the problem, the general, far field expression for the PO scattered field is utilized four times. Summing all contributions, the monostatic RCS  $\sigma_{HH,VV}$  of the flat plate is finally expressed as

$$\left\{ \begin{array}{l} \sigma_{HH} \\ \sigma_{VV} \end{array} \right\} = \frac{k^2}{\pi} \left| \hat{\mathbf{r}} \cdot \hat{\mathbf{n}} I(2\hat{\mathbf{r}}) + (\hat{\mathbf{r}} + \hat{\mathbf{r}}_r) \cdot \hat{\mathbf{n}} I(\hat{\mathbf{r}} + \hat{\mathbf{r}}_r) \left\{ \begin{array}{l} R_H \\ R_V \end{array} \right\} + \hat{\mathbf{r}}_r \cdot \hat{\mathbf{n}} I(2\hat{\mathbf{r}}_r) \left\{ \begin{array}{l} R_H^2 \\ R_V^2 \end{array} \right\} \right|^2 \quad (1)$$

where the upper line is valid for horizontal, and the lower for vertical polarization,  $R_H$  and  $R_V$  are the respective Fresnel reflection coefficients for the half space and  $\hat{\mathbf{n}}$  is the unit vector normal to the plate, whereas

$$I(\mathbf{v}) = \frac{j}{k(\mathbf{v} - \mathbf{v} \cdot \hat{\mathbf{n}}\hat{\mathbf{n}})^2} \sum_{q=1}^Q \mathbf{v} \times \hat{\mathbf{n}} \cdot (\mathbf{r}_{q+1} - \mathbf{r}_q) \text{sinc} \left[ \frac{k}{2} \mathbf{v} \cdot (\mathbf{r}_{q+1} - \mathbf{r}_q) \right] \exp \left\{ \frac{jk}{2} \mathbf{v} \cdot (\mathbf{r}_{q+1} + \mathbf{r}_q) \right\} \quad (2)$$

where, by definition,  $\mathbf{r}_q$  is the location of the  $q^{\text{th}}$  vertex,  $\mathbf{r}_{Q+1} \equiv \mathbf{r}_1$  and  $\mathbf{v}$ ,  $\hat{\mathbf{n}}$  are not parallel to each other. If  $\mathbf{v}$ ,  $\hat{\mathbf{n}}$  are parallel to each other, (2) is not valid, but reduces to

$$I(\mathbf{v}) = A \exp \{ jk \mathbf{v} \cdot \mathbf{r}_0 \} \quad (3)$$

where  $A$  is the area of the polygon and  $\mathbf{r}_0$  is an arbitrary point on its surface. It should be pointed out that (1) was derived under the PO assumption that both sides of the plate can be illuminated, either by the direct or by the reflected wave.

## NUMERICAL RESULTS

The expression in (1) was validated via comparisons with reference Moment Method (MoM) results [6]. A square, PEC,  $2\lambda$  by  $2\lambda$  flat plate was located vertically, in the  $yz$  plane, over a half space (Fig. 3), with relative permittivity  $\epsilon_r=80-j70$  (simulating sea water). The center of the plate was located at a distance  $d=10\lambda$  from the interface. The RCS results at the  $\phi=0$  cut, as a function of the  $\theta$  angle, and for horizontal polarization are depicted in Fig. 4, showing excellent agreement, for a wide range of elevation angles. For  $\theta$  angles closer to 0, the agreement is expectedly not as good, since the PO approximation fails in the region of grazing incidence.

## REFERENCES

- [1] Knott, E. F., J. F. Schaeffer and M. T. Tuley, *Radar Cross Section*, Artech House, Boston/London, 1993.
- [2] Fabbro, V., “Three-dimensional backscattering by a target above the sea surface”, *Electromagnetics*, 21(6), pp. 451-466, Sep. 2001.
- [3] Johnson, J. T., “A study of the four-path model for scattering from an object above a half space”, *Microwave and Optical Technology Letters*, 30(2), pp. 130-134, July 2001.

- [4] Sarkar, T. K. and R. F. Harrington, "RCS of conducting bodies over a lossy half space", *Radio Science*, vol. 15, no. 3, pp. 581-585, May-June 1980.
- [5] Gordon, W. B., "Far - field approximations to the Kirchhoff - Helmholtz representations of scattered fields", *IEEE Transactions on Antennas and Propagation*, vol. 23, pp. 590-592, 1975.
- [6] Burkholder, R. J., personal communication, Feb. 2002.

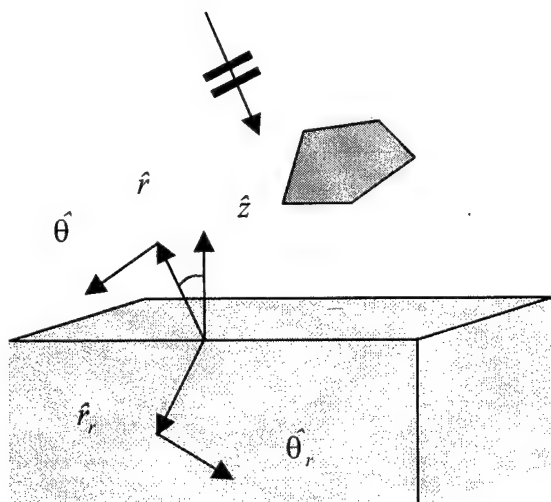


Fig. 1. Geometry of the problem

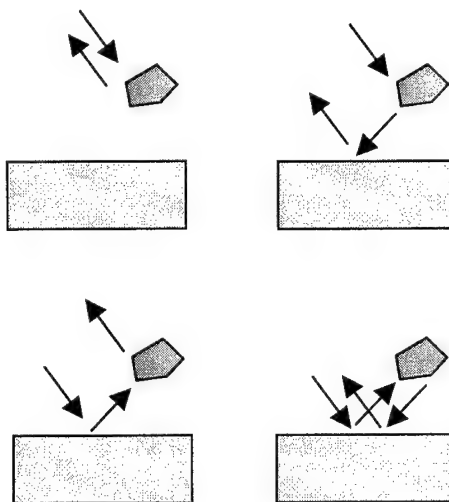


Fig. 2. The four path model

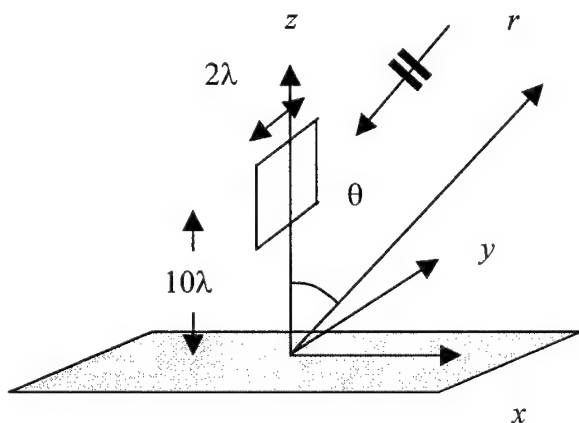
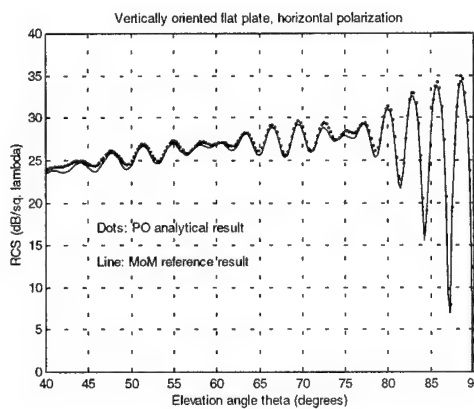


Fig. 3. A vertically oriented PEC square plate

Fig. 4. Monostatic RCS plot for the configuration of Fig. 3 ( $\phi=0$  cut, horizontal polarization)

## **ELECTROMAGNETIC MODELING OF THE JET AIRCRAFT INTAKE WITH THE INTERIOR IMPELLER**

V.N. Kisel', A.I. Fedorenko

Russian Academy of Sciences, Institute for Theoretical and Applied Electromagnetics,  
125412, ITAE, Izhorskaya 13/19, Moscow, Russia  
E-mail: kis\_v@mail.ru, kis@eldyn.msk.ru, fed@eldyn.msk.ru

### **ABSTRACT**

The 3D electromagnetic model of the aircraft intake terminated with blade structure is based on the utilization of equivalence theorem and integral expressions for electromagnetic fields. Acceptable numerical efficiency is achieved due to implementation of the special algorithm of successive electromagnetic field calculation through the sectioned air duct from inlet aperture to the termination section and backwards. The equivalent surface currents over the apertures separating the sections and conducting walls are calculated iteratively in separate processes for each section, wall smoothness and large dimensions of the duct are taken into account to reduce computational cost. Rigorous integral equation technique exploiting rotational periodicity of the impeller is employed to treat the termination. Far field is evaluated via integrating currents over the intake aperture. Computed data are close to reference results (including experimental ones).

### **ELECTROMAGNETIC MODEL DESCRIPTION**

It is well known that scattering from engine intake of modern jet aircraft constitutes a main contribution to the total backscattered field at the front illumination aspects. The specific feature of the scattering is its dependence upon the properties of the intake loading to be the blade structure. Our previously reported results [1] referred to the developed 3D model based on the utilization of equivalence theorem and integral expressions for electromagnetic fields. Corresponding numerical techniques are highly time and computer memory consuming. To achieve sufficient computational efficiency the special algorithm of successive electromagnetic field calculation through the sectioned air duct from inlet aperture to the termination section was developed and applied. Recently we found in literature analogous technique of duct subdivision [2], the main difference is that in our approach we have no need in evaluation scattering matrices of the duct sections. The surface currents over the apertures separating the sections, on the conducting walls and termination blades were calculated in the iteration processes. But further investigations revealed that when treating especially complex realistic termination sections (like impeller discussed below) the iterative physical optics (IPO) technique [3] tend to be divergent. So we turned to the rigorous integral equation (IE) approach in order to investigate the blade structure with the high precision. To make IE computer implementation suitable for the large (in terms of wavelength) real-sized blades we have exploited the rotational periodicity of the

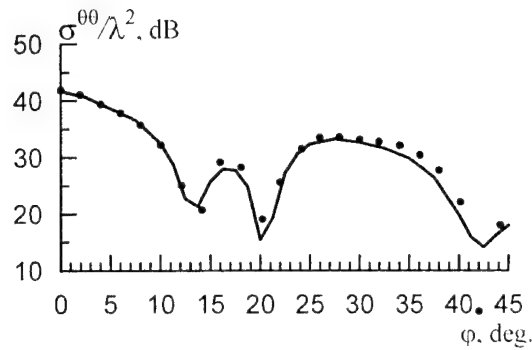


scatterer resulting in the reduction of the computational domain to a single blade according to Prof. E.N. Vasiliev's ideas [4]. Similar approach was also discussed in literature (see, e.g. [5], where Green's function of the PEC circular waveguide was used). We applied Green's function of the free space that enabled us to solve corresponding electric field IE for a single blade  $N$  times ( $N$  being the number of blades rather than the number of circular waveguide modes) with respect to the unknown Fourier-harmonics of the surface currents. Besides, we preserved opportunity to account for presence of coating on the termination section walls. Galerkin's technique (moment method with the roof-top basis and testing functions defined on the rectangular cell grid) was used to convert IEs into the linear algebraic equation systems. Having defined scattering by the blades, the total scattered field was evaluated via the similar successive calculation of waves propagation through the sections of the duct from the termination to the inlet aperture. The reciprocity principle (see, e.g. [2]) was not applied since we took in mind the possibility of treating some other objects that might be placed into the duct, or cope with the specific properties of coating. Besides, while processing backwards, the contribution of wall current defined earlier (at "forward" propagation calculation) may be used to refine Kirchhoff's approximation. Far field is evaluated via integrating currents over the intake aperture. Possible coating of the interior walls was taken into account via its equivalent impedance and corresponding spatial, polarization and angular dependencies.

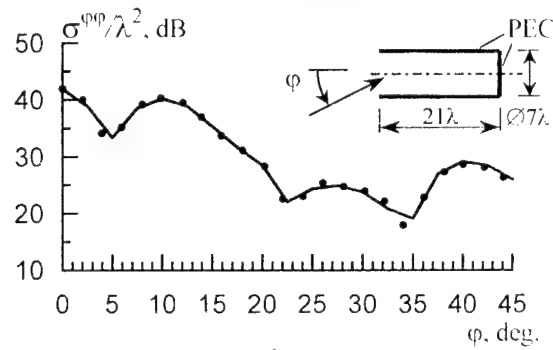
The communication discusses the accuracy and numerical efficiency of the approach comparing to IPO and pure PO treatment of the termination. Selected examples illustrating features of the technique are presented in Fig. 1 (comparison to modal expansion solution, [2]) and Fig. 2 (comparison to our experimental investigations of the model shown in Fig. 3); here calculated data are shown with solid curves. Example of numerical evaluation of the coating influence is depicted in Fig. 4 ( $Z/W_0=0.4-i0.3$ ,  $W_0=120\pi$ , Ohms; note, section 4 remained uncoated).

## REFERENCES

- [1] V.N. Kisel', A.I. Fedorenko. Electromagnetic scattering from cavities with complex objects inside// Conf. Proc.: 2000 Int. Conf. on Math. Methods in Electromagn. Theory MMET2000, Sept. 12-15, 2000, Kharkov. Ukraine. V. 2. P.447-449.
- [2] F. Obelleiro, J. Campos-Nino, J.L. Rodriguez, A.G. Pino. A segmented approach for computing the electromagnetic scattering of large and deep cavities// *Progress in Electromagnetic Research*, PIER 19, 1998. P.129-145.
- [3] F. Obelleiro-Basteiro, J.L. Rodrigues, R.J. Burkholder. An iterative physical optics approach for analyzing the electromagnetic scattering by large open-ended cavities// *IEEE Trans. Antennas and Propag.* V.AP-43. No.4. P.356-361. 1995.
- [4] E.N. Vasiliev. Excitation of the bodies of rotation (*Vozbuzhdeniye tel vrascheniya*) – in Russian. - Moscow, Radio I Svyas', 1987. 272 p.
- [5] H.T. Anastassiou, J.L. Volakis, D.S. Filipovic. Integral equation modeling of cylindrically periodic scatterers in the interior of a cylindrical waveguide// *IEEE Trans. Microwave Theory Tech.*, V.MTT-46. No.11. P.1713-1720. 1998.

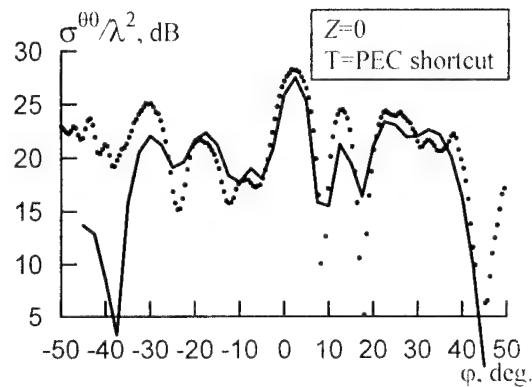


a)

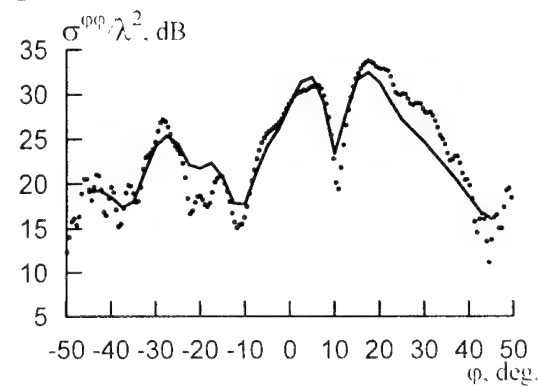


b)

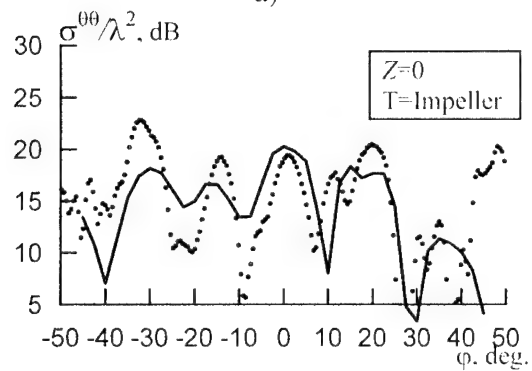
Fig. 1



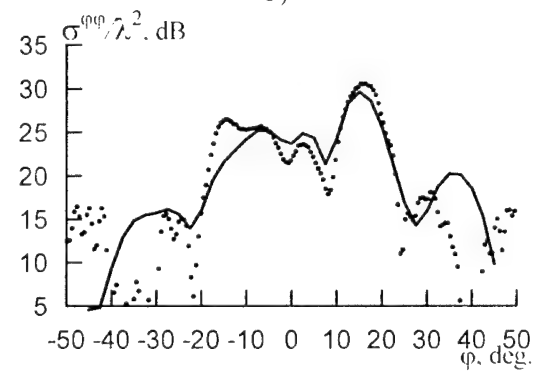
a)



b)



c)



d)

Fig. 2

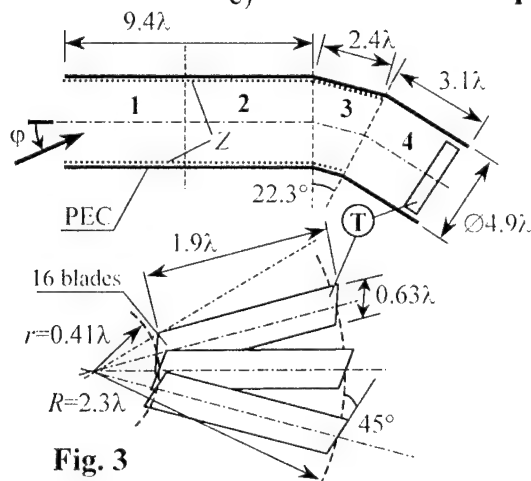


Fig. 3

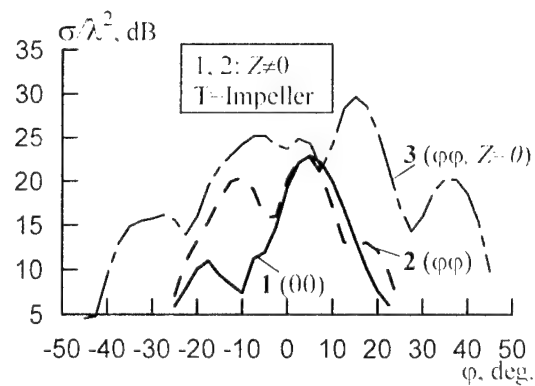


Fig. 4

## FINITE ELEMENT ANALYSIS OF SCATTERING FROM 2D-OBJECTS OF ARBITRARY COMPOSITION

A.M. Lebedev

Russian Academy of Sciences, Institute for Theoretical and Applied Electromagnetics,  
125412, ITAE, Izhorskaya 13/19, Moscow, Russia  
E-mail: lebedev\_am@mail.ru, lebedev@eldyn.msk.ru

### ABSTRACT

A number of techniques suggested for numerical analysis of scattering from 2D-objects with complex border shape and/or arbitrarily changing electromagnetic parameters (for brevity, from 2D-objects of arbitrary composition) is very large indeed, even if to take into account only the approaches based on finite element method (MFE). Nevertheless, some methodological and "technological" questions of MFE application have been under consideration ever since first implementations of the method. The task of correct field behavior description near the border, where the electromagnetic parameters change abruptly, belongs to the first group of questions. The convenient means of problem statement, such as specification of scattering object geometry and its electromagnetic parameters variation, is an important "technological" task.

The aim of this paper is to present the MFE-based numerical procedure to evaluate the RCS signature of 2D-objects of arbitrary composition, including dielectric, metal and plasma-like objects. The scattering of waves of two polarizations (H-wave with  $E_z$ ,  $H_{r,\varphi}$  components, and E-wave with  $H_z$ ,  $E_{r,\varphi}$  components) is calculated. The original variants of solutions to the two above-mentioned questions were implemented: the weighted residual minimization type condition is implemented on the border of scattering object in order to achieve the continuity of tangential to the border field components, and AutoCAD is used for data input.

### CHARACTERISTIC FEATURES OF THE NUMERICAL PROCEDURE

Wave equations for  $E_z$  or  $H_z$  components are solved with the nodal FE. The objects with arbitrary cross sections are placed inside the rectangular region, where the MFE is used. The rectangularity permits a simple adjustment of the mesh with respect to the objects' borders.

The AutoCAD possesses the convenient user's interface; it is widely used in industry. That is why AutoCAD was chosen for inputting data on the geometry of the problem and electromagnetic parameters distribution. The borders of objects are outlined with

cubic spline  $\vec{r}(u) = \vec{\alpha}_0 + \vec{\alpha}_1 \cdot u + \vec{\alpha}_2 \cdot u^2 + \vec{\alpha}_3 \cdot u^3$ , where  $\vec{\alpha}_i = \begin{pmatrix} \alpha_{ix} \\ \alpha_{iy} \end{pmatrix}$ ,  $i = 0 \div 3$ ; the

electromagnetic parameters can either be set analytically or as a surface  $z(x, y)$  above the cross section. The data are read from AutoCAD output file, and then the mesh is

adjusted with the use of parametrical object's border representation. see the examples of AutoCAD drawing and automatically generated mesh in Fig1 a.b).

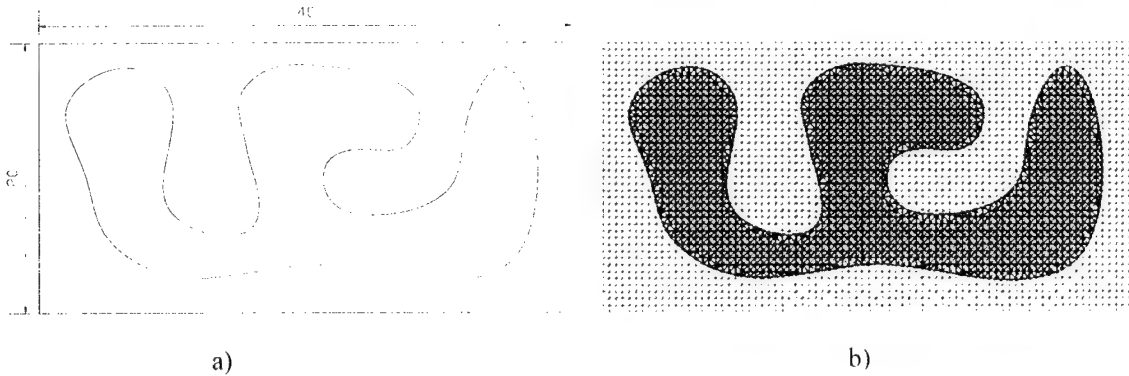


Fig.1

The distribution of  $E_z$  or  $H_z$  is found as a solution of the problem. In comparison with the known edge-based finite element technique [1] the reduction of resulting SLAE order is achieved, while the process of SLAE creation is simpler.

The question of the tangential field component ( $H_t$  for H-wave or  $E_t$  for E-wave) on the border of two media is solved by the corresponding boundary condition imposition, analogously to [2], but again with respect to the only z-component of the field. Generally the equation of SLAE has the form  $R_1 + \alpha \cdot R_2 = 0$ , where  $R_1$  and  $R_2$  are the weighted residuals, corresponding to satisfying wave equation and tangential field component continuity on the border of two media,  $\alpha$  is a coefficient. The calculated field distributions for plane H and E-wave diffraction by dielectric cylinder with  $\epsilon = 4$ ,  $k_0 r = 3$  are shown in Fig.2, where the direction of incidence is indicated with arrows. The solution very close to reference eigen function solution can be obtained in wide range of  $\alpha$  here - in case of E-wave. The criterion of the best choosing  $\alpha$  is under investigation now.

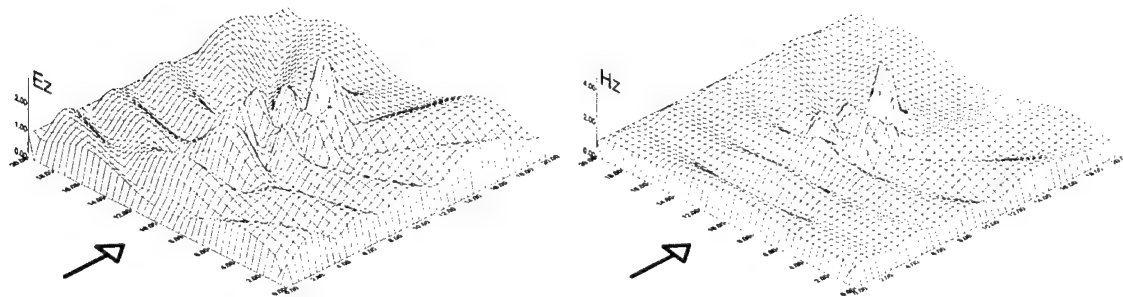


Fig. 2

The other features of the procedure are quite traditional for finite methods: the absorbing boundary conditions are imposed upon the scattered field at the mesh border, the scattering diagram is calculated with the Kirchhoff's formula and from the assumption of far zone observation point location [3].

There exists an opportunity of immediate visualization of field distribution within the calculation area, because such a distribution is just the output of wave equation solution.

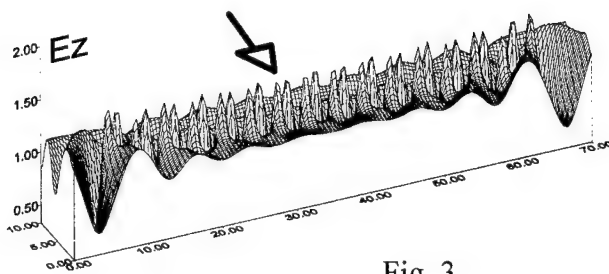


Fig. 3

distribution within the slab resulting from interaction between going through and transversal standing waves, can be seen.

The backscattering RCS pattern of  $k_0 l = 60$  ( $\approx 10\lambda_0$ ) metal plate, calculated in H-wave case, is presented in Fig.4.

The advantages of the above-described procedure are its universality, the simplicity of interface, the opportunity to introduce the inhomogeneous media.

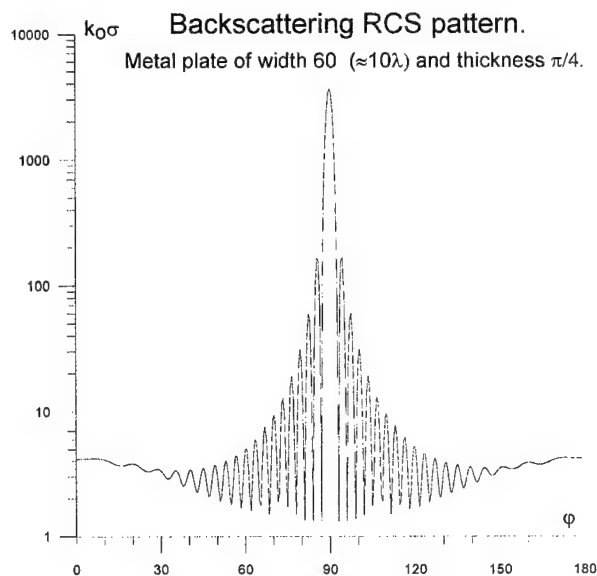


Fig. 4

## REFERENCES

- [1] J.L. Volakis, A. Chatterjee, L.C. Kempel. Finite element method for electromagnetics. Antennas, microwave circuits and scattering applications. – IEEE PRESS, N.Y., 1998. 344p.
- [2] X.Yuan, D.R. Lynch, K. Paulsen. Importance of normal field continuity in inhomogeneous scattering calculations// *IEEE Trans. Microwave Theory Tech.*, April 1991. P. 638-642.
- [3] A. Taflov, S.C. Hagness. Computational electrodynamics: the finite-difference time-domain method. – Artech House, Boston, , London, 2nd edition, 2000. 854p.

## RADIOABSORBING MATERIAL OPTIMAL USING IN THE REDUCTION OF AIRCRAFT RADAR CROSS-SECTION

Vitaliy A. Vasilets, Stanislav A. Gorelyshev, Konstantin I. Tkachuk  
Kharkov military university, Kharkov, Ukraine  
E-mail: vasilets@euro.dinos.net

### ABSTRACT

It's well known, local scattering parts on a smooth convex object elements make the most important contribution to reflected signal energy. So these surface parts of complex shape objects are coated by radioabsorbing materials (RM) in camouflage purpose. As a rule, the radioabsorbing coating (RC) has the sizeable weight and the cost. In this case the problem of optimal using of RM on the object surface has been occurred. The optimal coating method for the reduction of radar cross-section (RCS) has been obtained for a certain illumination and reception directions in limitation conditions for a quantity of the RC using. Optimal coating has been realized due to decision of some integer linear programming problem. Using this method we have had RCS numerical results for reductive aircraft model partly coated by RM.

### BASE CALCULATION RELATIONS

The object construction and coating technology determine the surface fragmentation on some parts. These ones may be have RC or may be perfectly conducting. In this case object RCS is approximately represented as sum of RCS of these parts

$$\sigma(\theta) = \sum_{i=1}^N \sigma_i(\theta), \quad (1)$$

where  $N$  is the number of object surface parts.  $\theta$  is an illumination or reception angle and RCS is a function of this angle. Finally, the values of object RCS averaged in some range of illumination or reception angles will be interested by us and RCS representation by (1) is reasonably for calculation. The method offered in [1] may be used for calculation of RCS separate object parts. Let a mean RCS for whole object and a mean RCS for  $i$ -th surface part for angle range  $\theta_1 \leq \theta \leq \theta_2$ :

$$\bar{\sigma} = \frac{1}{|\theta_2 - \theta_1|} \int_{\theta_1}^{\theta_2} \sigma(\theta) d\theta, \quad \bar{\sigma}_i = \frac{1}{|\theta_2 - \theta_1|} \int_{\theta_1}^{\theta_2} \sigma_i(\theta) d\theta. \quad (2)$$

Calculating the range averaging for (1), we obtain

$$\bar{\sigma} = \sum_{i=1}^N \bar{\sigma}_i. \quad (3)$$

We'll minimize the sum (3) of separate part RCS averaged in a finite range of illumination or reception angles. Let  $\bar{\sigma}_{i1}$  is a mean RCS of  $i$ -th part with perfectly conducting surface,  $\bar{\sigma}_{i2}$  is a mean RCS of the same part in case of using RC on a surface of this part. The RCS of completely coated object is

$$\bar{\sigma}_2 = \sum_{i=1}^N \bar{\sigma}_{i2}. \quad (4)$$

If subtract (4) from (3), we'll obtain

$$\bar{\sigma} - \bar{\sigma}_2 = \sum_{i=1}^N (\bar{\sigma}_i - \bar{\sigma}_{i2}) = \sum_{i=1}^N \kappa_i (\bar{\sigma}_{i1} - \bar{\sigma}_{i2}) = \sum_{i=1}^N \kappa_i \Delta \sigma_i. \quad (5)$$

Here  $\kappa_i$  is binary factor, which equals zero if  $i$ -th part uses RC and equal one if this surface part is perfectly conducting. Let  $S_0$  is as much as a possible square of RM on an object surface,  $S$  is the total square of an object surface and

$$S = \sum_{i=1}^N S_i. \quad (6)$$

The RC square limitation using  $\kappa_i (i=1, \dots, N)$  can be written as

$$\sum_{i=1}^N \kappa_i S_i \geq S - S_0. \quad (7)$$

The problem of RM optimal distribution on an object surface comes to problem of integer linear programming – determination of binary factors  $\kappa_i$  series, that minimize representation (5) and satisfy the limitation condition (7). The solution of this problem may be obtain by any standard method, for example, additive method or method of branches and boundaries [2].

## NUMERICAL RESULTS

The reductive aircraft model (Fig.1) has been used for numerical calculation. The model includes the surfaces of 4 ellipsoids. The model length is 18m, width is 22m, height is 4.25m. The model RCS has been calculated for sounding frequency 10GGz. The RC parameters are: thickness 1.3mm, permittivity  $\epsilon'_1 = 20 + i0.1$ , permeability  $\mu'_1 = 1.35 + i0.8$ .

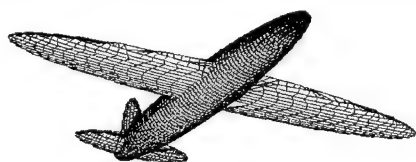


Fig. 1.

This material reduces plate RCS by 15dB for a normal incidence of sounding signal with

given frequency. The object surface has been broken into 140 parts  $N=140$ . The dependence of aircraft averaged RCS on optimal used RM square has been represented on Fig.2 for azimuth range  $-10^\circ \dots +10^\circ$  relatively aircraft axis and elevation angle (range  $0^\circ \dots -8^\circ$ ) relatively wing plane (monostatic case and illumination from a lower

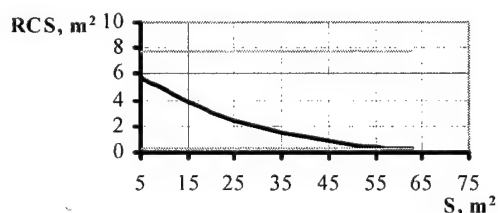


Fig.2.

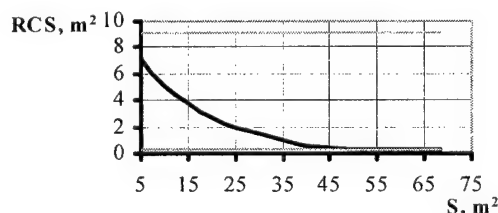


Fig.3.

half-space). The similar dependence for bistatic case for front sounding and bistatic angle by azimuth  $-10^\circ \dots +10^\circ$  and by elevation  $0^\circ \dots -8^\circ$  has been represented on Fig.3. In bistatic case the averaged RCS decreases quicker than in monostatic case. This is determined by lesser displacements of local scattering centers on object surface in bistatic case and, therefore, by different optimal distribution of RM. The acceptable

RCS values have been obtained by RM optimal using on 20-25% of object surface. The similar results have been represented on Fig.4 (monostatic case) and Fig.5 (bistatic case) for bigger average angle range (azimuth  $-20^\circ \dots +20^\circ$ , elevation angle  $0^\circ \dots -20^\circ$ ).

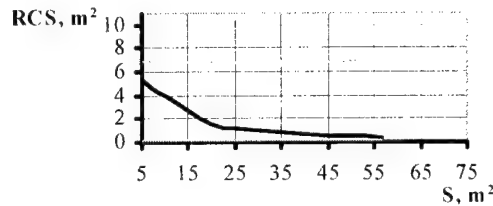


Fig.4.

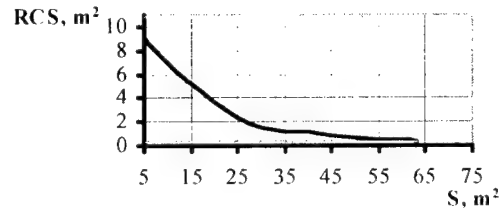


Fig.5.

The RC optimal distribution for averaged RCS in azimuth range  $-5^\circ \dots +5^\circ$  and elevation range  $-3^\circ \dots +3^\circ$  has been represented on Fig.6 (Fig.6a is the model view from upper half-space and Fig.6b – the same model from lower one. RC places pointed by gray color and frames. RC square is  $40\text{m}^2$ . Averaged RCS for this model is  $0.68\text{m}^2$ . RCS for perfectly coated model is  $0.26\text{m}^2$  and for completely conducting one is  $8.11\text{m}^2$ .

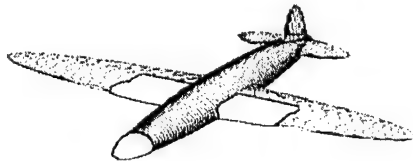


Fig.6a

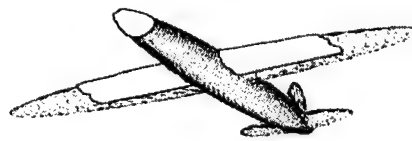


Fig.6b

The RC optimal distribution for averaged RCS in azimuth range  $-20^\circ \dots +20^\circ$  and elevation range  $0^\circ \dots +20^\circ$  has been represented on Fig.7. RC square is  $40\text{m}^2$ . RCS for this case is  $0.74\text{m}^2$ . RCS for completely coated model is  $0.23\text{m}^2$  and perfectly conducting one is  $6.81\text{m}^2$ . The picture analysis shows the visible difference between optimal distributions of RM limited quantity for two mentioned ranges of illumination and reception angles.

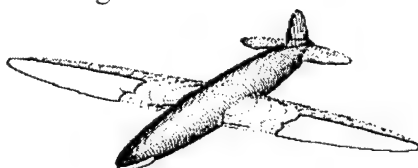


Fig.7a

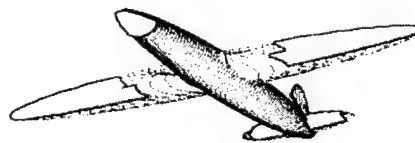


Fig.7b

The RCS reduction estimation in finite range of illumination and reception angles has been proposed in RM optimal using on the part of object surface. It can conclude that the essential and actually complete reduction of RCS has been obtained for wide range of fighting angles at using RM only 20-25% of an aircraft model surface.

## REFERENCES

- [1] O.Sukharevsky, V.Vasilets, S.Gorelyshev, A.Sazonov. Electromagnetic Scattering By Complex Shape Objects Partly Coated With Absorbing Materials. //MMET-2000 Proceedings, Kharkov, Ukraine, 2000, v.1, pp. 94-101
- [2] Romanovskiy V.O. Solution algorithms for extremum problem. – Moscow.: Nauka, 1977, 352p. (in Russian)



## MINIMIZATION OF THE FIELD DIFFRACTED FROM A CONVEX IMPEDANCE BODY TO THE SHADOW REGION

A.A. Zvyagintsev, A.I. Ivanov

V.N.Karazin Kharkiv National University  
Svoboda sq., 4, Kharkov, 61077, Ukraine

mladyon@rian.ira.kharkov.ua

### INTRODUCTION

Modern means of transport, such as aircrafts, can contain several dozens transmitting and receiving antennas aboard. Each of these antennas is the potential source of the interference for the others. That is why the developers have to take appropriate steps to decrease the undesirable reciprocal effects. This can be made, for example, by means of the optimal positional relationship, or directional patterns correction, or by means of the various coverings.

This work presents a method of the body impedance (or covering) distribution determination, under which the field of the first antenna is the lowest on the second one. It is based on the well-known asymptotic methods of field determination - Geometrical Theory of Diffraction (GTD), Uniform Asymptotic Theory (UAT) [1] and Ritz method for functional minimization [2].

### PROBLEM SETTING

Let us consider the following problem: The point of observation  $M$  is situated in the shadow region relative to point source  $M_0$  (fig. 1). The body is bounded by the smooth curve  $l$ .

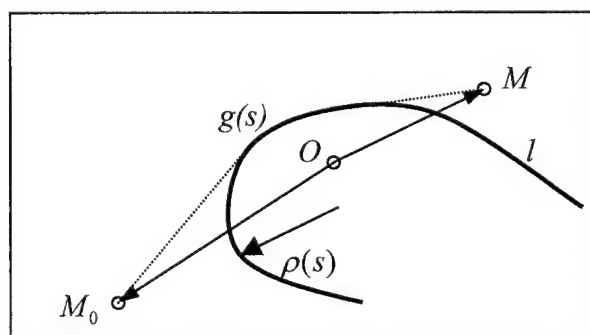


Fig.

The curvature radius of  $l$  is  $\rho(s)$ , where  $s$  is the natural parameter of  $l$ . The impedance of the body  $g(s)$  can be any smooth complex function of  $s$  with the only restriction  $|g(s)| = O(1)$ . This restriction will be explained later. Enter the coordinates  $(s, n)$  where  $n$  is the length of the perpendicular dropped to the body from a point, and  $s$  is the natural parameter of the meet point of the body and the perpendicular. The field at the point  $M$  can be calculated using GTD formulas for the creeping waves if both the point source and the observation point are far enough from the body. If the points are close to the

body, the asymptotic formulas of V.M. Babich and V.S. Buldyrev [1] should be used:

$$\begin{aligned}
 U(M) &= \sum_{n=-\infty}^{\infty} \sum_{p=0}^{\infty} \Gamma_p(r_0, \varphi_0; r, \varphi + 2\pi n; k); \\
 \Gamma_p(r_0, \varphi_0; r, \varphi; k) &= \frac{1}{2i} \left( \frac{2}{k} \right)^{1/3} [\rho(s)\rho(s_0)]^{-1/6} \left[ w_1'(\xi_p) \right]^{-2} e^{ik(s-s_0)} * \dots \\
 \exp \left( i\xi_p \left( \frac{k}{2} \right)^{1/3} \int_{s_0}^s \frac{ds}{\rho^{2/3}(s)} + \int_{s_0}^s \frac{ds}{\rho(s)g(s)} + \frac{i}{6k^{1/3}} \left[ \frac{\rho'(s)}{\rho(s)} \nu^2 - \frac{\rho'(s_0)}{\rho(s_0)} \nu_0^2 \right] \right) * \dots \\
 \exp \left( i \frac{\alpha_{10}(s) - \alpha_{10}(s_0)}{k^{1/3}} + O(k^{-2/3}) \right) w_1(T(\xi_p, M_0)) w_1(T(\xi_p, M))
 \end{aligned} \quad (1)$$

where  $w_1(x), w_1'(x)$  are the Airy function of first order and its derivative ( $w_1(z) = 2e^{i\frac{\pi}{6}} \frac{\sqrt{\pi}}{2} Ai(ze^{2\pi i/3})$ );  $\xi_p$  is the  $p$ -th root of the equation  $w_1(\xi_p) = 0$ ;  $\nu = nk^{2/3}$ , and  $\alpha_{10}, T(\xi, M)$  are defined by the following formulas:

$$\begin{aligned}
 \alpha_{10}(s) &= 2^{1/3} \xi_p^2 \int_0^s \rho^{-4/3}(s) \left[ \frac{1}{60} + \frac{4}{135} \rho'^2(s) - \frac{2}{45} \rho(s) \rho''(s) \right] ds \\
 T(\xi, M) &= \xi - \nu \left( \frac{2}{\rho(s)} \right)^{1/3} - \frac{i}{\left( \frac{k}{2} \right)^{1/3} \rho^{1/3}(s) g(s)} + O(k^{-2/3})
 \end{aligned}$$

It is evident that the formula (1) can't be used if the impedance becomes too small by absolute value. That is why the present method doesn't allow the passage to the limit  $g(s) \rightarrow 0$ .

We are interested in the function  $g(s)$ , which minimizes one of the following functionals:

$$\begin{aligned}
 F_1(g(s)) &= |U(g(s); M, M_0, k)| \\
 F_2(g(s)) &= \max_i |U(g(s); M + \delta M_i, M_0, k)| \\
 F_3(g(s)) &= \max_i |U(g(s); M, M_0 + \delta M_0^i, k)| \\
 F_4(g(s)) &= \max_i |U(g(s); M, M_0, k + \delta k_i)|
 \end{aligned}$$

The functionals  $F_{2,3,4}$  can be used if the source, the observation point or the frequency varies within the defined limits. They also allow estimating the stability of the results to the deviations of the initial conditions.

The problem of functional minimization can be reduced to problem of function minimization if we assume that  $g(s) = \sum_p^N a_p f_p(s) + R_N(s)$  where  $f_p(s)$  are the members

of a set of orthogonal functions that is complete on the defined space, and  $R_N(s)$  is the remainder [2]. There is a great variety of function minimization methods. In the present work the method of Nelder and Mead [3] has been used, though the other methods, for

example [4], are also applicable.

## NUMERICAL RESULTS

In order to test the present method, it was applied to the problems of scattering on circular, elliptic and parabolic cylinders.

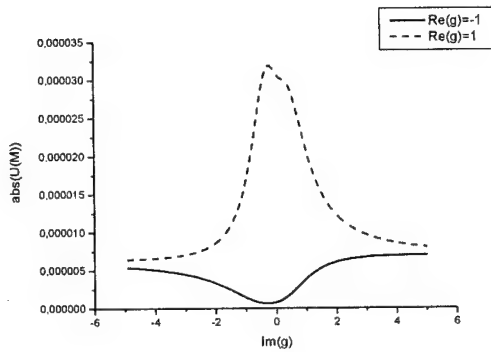


Fig. 2

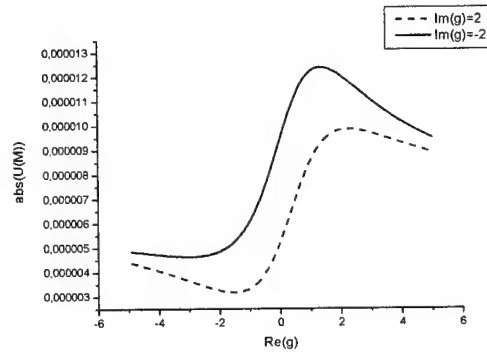


Fig. 3

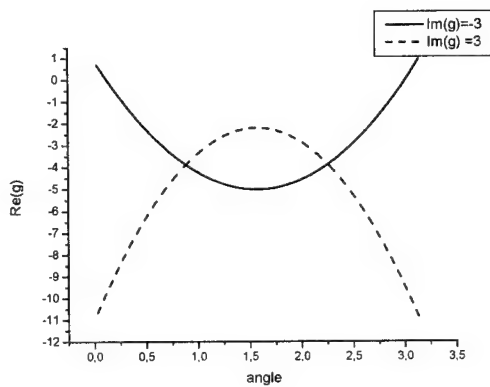


Fig. 4

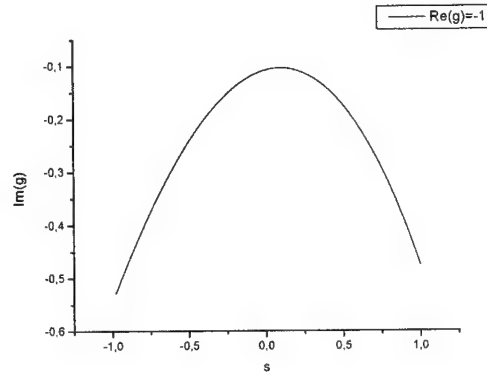


Fig. 5

The fig. 2,3 shows the field amplitude dependencies in the point M on the real and imaginary parts of the impedance ( $s_0 = 0; s = \pi; n = n_0 = 0.1; \rho = 1; k\rho = 10$ ). On the fig. 2  $\text{Re}(g(s)) = \text{const} = \pm 1$ , and on the fig. 3  $\text{Im}(g(s)) = \text{const} = \pm 2$ . The dependencies have extremums at small real (imaginary) parts of the impedance, and have the common limit if  $\text{Re}(g) \rightarrow \pm\infty$  ( $\text{Im}(g) \rightarrow \pm\infty$ ). This allows to solve both the problem for minimization and maximization of the field. It is evidently from fig. 2,3 that the minimum of the field for the circle can be reached only if the real part of the impedance becomes negative at least in a small sector, and the maximum – only if the real part becomes positive at least in a small sector. The fig. 4 shows the impedances that minimize the functional  $F_1(g(s))$  (the geometry is the same as in the previous example). Both distributions are symmetrical relative to the point  $\pi/2$  accordingly to the reciprocity principle. The optimal imaginary part of the impedance for the parabolic cylinder is shown on fig.5 ( $kF=10$  where  $F$  is the focal distance;

$s_0 = -F; s = F; n_0 = 0.05F; n = 0.1F; \operatorname{Re}(g(s)) = -1$ ). The minimum of the field is still observed only for the negative real parts, but the distribution is no longer symmetrical and parabolical.

## CONCLUSIONS

The proposed method of field minimization in the shadow region has shown that it can be used for various optimization procedures provided that  $ka \sim 10$  or larger, where  $a$  is the typical dimension of the scatterer. It can also be generalized to the 3-dimensional case and improved by accounting surface waves in the case  $\operatorname{Im} g(s) < 0; \operatorname{Re} g(s) > 0$ . As the formula (1) actually presents the Green's function, the method can be easily modified to deal with distant sources.

## REFERENCES

- [1] V.M. Babich, V.S. Buldyrev, Asymptotic methods in problems of short waves diffraction. Moscow, Nauka, 1972.
- [2] S.K. Godunov, V.S. Ryabenky, Finite difference schemes. Moscow, Nauka, 1977.
- [3] J.A. Nelder, R. Mead. A Simplex Method for Function Minimization. Computer Journal. Vol. 7. P. 308-313.
- [4] G. Antonini, A. Orlandi. Gradient Evaluation for Neural-Networks-Based Electromagnetic Optimization Procedures. IEEE Trans. on MTT vol. 48, N 5, May 2000.

# **WAVEGUIDE CIRCUITS**

# INFLUENCE OF DEFECTS ON ELECTRODYNAMIC PROPERTIES OF A SEMI-INFINITE PERIODIC SEQUENCE OF THE METAL-DIELECTRIC SCATTERERS

Vyacheslav.V. Khardikov, Vadim.B. Kazanskiy

Kharkov National University, 4 Svobody sq., Kharkov, 61077, Ukraine

E-mail: Vyacheslav.V.Khardikov@univer.kharkov.ua

## ABSTRACT

A semi-infinite periodic sequence of the metal-dielectric scatterers with defect in  $N$  basic element is investigated. The analysis of the dynamic of electromagnetic properties of investigated structure was carried out for different polarization of the exciting field and degree of the electrodynamic connection between resonance volume.

## OBJECT OF RESEARCH

The dynamic of the monochromatic ( $\exp(-i\omega t)$ ) fields of the scattering of the symmetric  $TE_{0n}$ -,  $TM_{0n}$ - waves of the circular waveguide on a semi-infinite periodic sequence of the metal-dielectric scatterers, if the geometric and electric parameters of the  $N$  basic element are changing, is investigated. The structure and the coordinate system is depicted schematically in Fig. 1. The base element, which has length  $L$  (period), consist of the two dielectric layers, which characterized by the thickness'  $d_j$ , the wave conductivities  $Y_j$ , permittivities  $\epsilon_j$  and permeabilities  $\mu_j$  ( $j = 1, 2$ ). Between the layers is placed the resistive film (it has conductivity  $Y_\sigma$ ) (fig. 1.a) or the ring

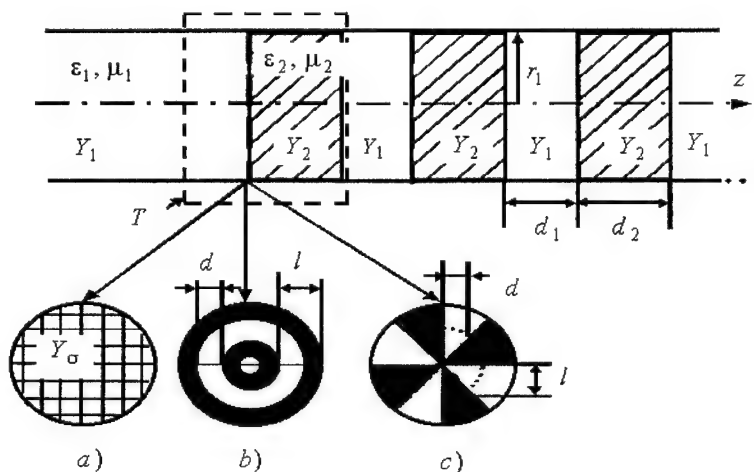


Fig. 1. Geometry of studding structure

(fig. 1.b) or radial (fig. 1.c) diaphragms. The diaphragms are infinitely thin and perfectly conducting and have a period  $l$  and a separation between conducting tape  $d$

( $u = \cos(\pi d/l)$  is the filling parameter of diaphragm). The characteristic dimension of the diaphragms is supposed to be significantly smaller than the wave length ( $\kappa = l/\lambda \ll 1$ ), therefore the phenomena of the transformation of the wave types are absence. In this approaching the transfer matrix of the basic elements ( $T$ ) was defined in [1].

The reflection coefficient ( $R_\infty$ ) from the perfect semi-infinite periodic sequence can be defined as the root of equation

$$t_{12}R_\infty^2 + (t_{11} - t_{22})R_\infty - t_{21} = 0, \quad (1)$$

which less then 1 ( $|R_\infty| \leq 1$ ).  $t_{ij}$  is the elements of transfer matrix of basic elements.

The reflection coefficient  $R$  from the defect semi-infinite periodic sequence (the parameters of the  $N$  basic element is changed) can be found from operator equation:

$$\begin{pmatrix} A_0 \\ RA_0 \end{pmatrix} = T^{N-1} T' \begin{pmatrix} A_{N+1} \\ R_\infty A_{N+1} \end{pmatrix}. \quad (2)$$

Where  $T'$  is transfer matrix of defect basic element, the elements of the degree of the transfer matrix ( $T^{N-1}$ ) were presented in [1] by the analytical formulas through the Mauguin polynomials  $P_{N-1}(X)$ , where  $X = (t_{11} + t_{22})/2$ .

## RESULTS

There are a two type zones on the dependencies of the reflection coefficient of perfectly semi-infinite sequence of diaphragms on the frequency (fig. 2-3). The one of them has a relatively high value of reflection coefficient (stop band) and the second has a relatively small value of  $R_\infty$  (pass band). The value of the  $R_\infty$  in pass band depends on degree of electromagnetic connection between the basic elements. For the low degree connection

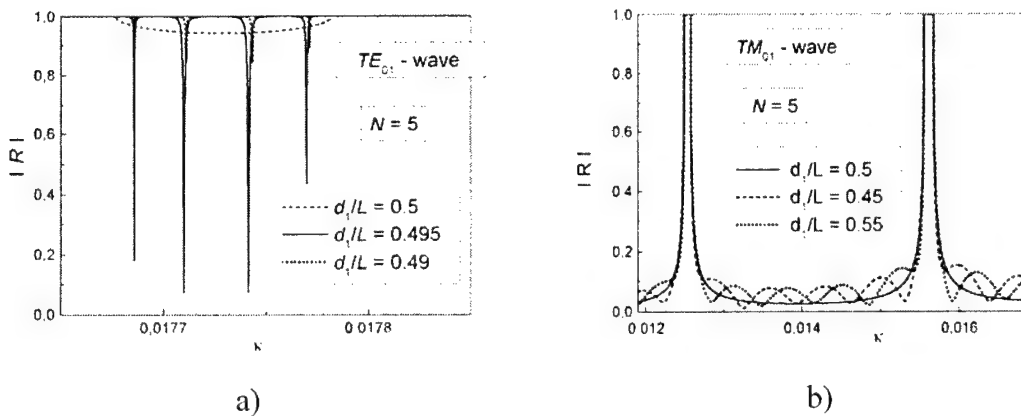


Fig. 2. The dependencies of the reflection coefficient from sequence of ring diaphragms on frequency.  $\varepsilon_j = 2$ ,  $\mu_j = 1$ ,  $L/l = 100$ ,  $r_1/l = 40$ ,  $d_1/L = 0.5$ .

a)  $u = -0.9$ ; b)  $u = 0.9$

( $TE_{01}$ -wave for ring and  $TM_{01}$ -wave for radial diaphragms) the value  $R_\infty \sim 1$ , in other case  $R_\infty \sim 0$ .

The resistive film is the active local conductivity. As its volume  $Y_\sigma$  is much less of the wave conductivity of the waveguide channels, then the changes of the relative volume  $\Delta Y_\sigma / Y_\sigma$  on the 10% or less result to the minor change of the average level of the reflection coefficient in the pass band. These changes does not depend from the type of the exciting field and position of the defect.

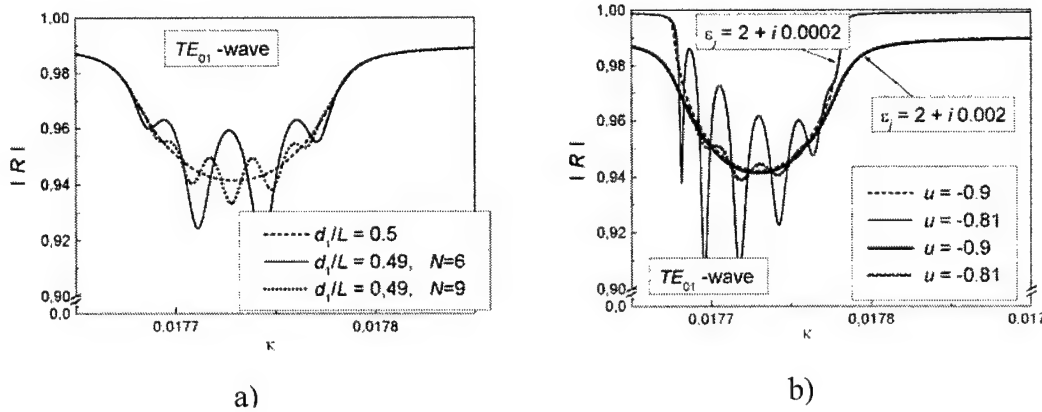


Fig. 3. The dependencies of  $R$  from the semi-infinite sequence of ring diaphragms on frequency.  $\mu_j = 1$ ,  $L/l = 100$ ,  $r_1/l = 40$ ,  $u = -0.9$ ,  $d_1/L = 0.5$ . a)  $\varepsilon_j = 2 + i0.0002$ ; b)  $N = 7$ .

The reactivity of the diaphragms and the thickness of the layer determine the phase properties of the system. The changes one of these parameters in the  $N$  basic element result in the appearance of the high frequency oscillations in the pass bands (fig. 2). This fact is explained by exciting eigen oscillations of the set from  $N - 1$  identical elements loaded by the defect. The amplitude and number of high frequency oscillations is depended to the value of the defect and its number ( $N$ ) (fig. 2-3).

The system with low electromagnetic connection between the basic elements is very sensitive to the phase defect (fig 2.a). The degree of influence of the defects can be decreased by the using in such system of the dielectric with low dissipative loses (fig. 3). The degree of the influence is decreased if the dissipative loses or number of defect elements increasing.

## CONCLUSIONS

The dynamic of the dependencies amplitude characteristics on the frequency with the change of the composition or geometric and material parameters in one of the base elements was determined in long wave region. The analysis of this dynamic was carried out for different polarization of the exciting field and degree of the electrodynamic connection between resonance volume.

## REFERENCE

- [1]. Kazanskiy V.B., Podlozny V.V., Khardikov V.V. // *Electromagnetic Waves and Electronic System*, 1999, V. 4, № 3.



## WAVEGUIDE FILTERS ON THE LUMPED ELEMENTS

A.R. Sorkin

Krasnoyarsk State Technical University, Krasnoyarsk, Russia

E-mail: sorkin@fromru.com

In mobile microwaves systems traditional waveguide filters appear to be too big. A way out is the application of structures on the lumped elements. The ways of realization of this idea are below described.

*Filters with quarter wave couplings.* The improvement of selective properties can be received when replacing a parallel resonant circuit by a pair of rejection circuits (fig. 1a).

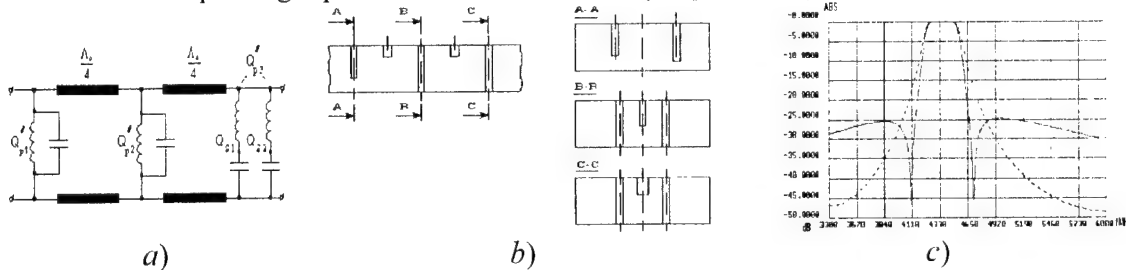


Fig. 1. Three-section filter with quarter wave couplings when replacing one resonant circuit by a pair of rejection circuits: a) circuit, b) a design, c) frequency response

At the allocation of two resonators on the distance less than  $90^\circ$  the characteristic turns out to be double-humped (fig. 2b). At the replacement of one passing circuit by a pair of rejection circuits the characteristics on Cauchy type are received.

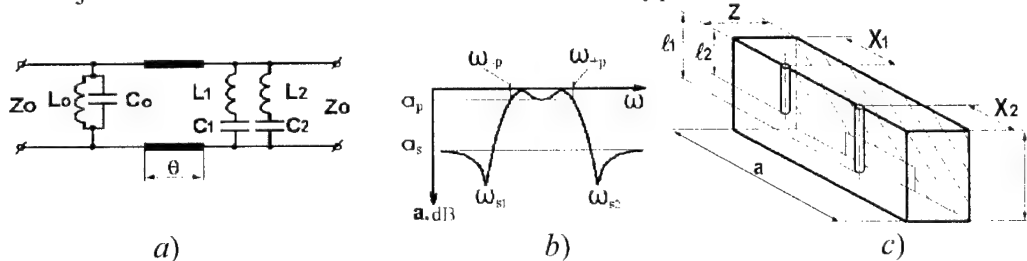


Fig. 2. A passing cascade section at the replacement of one passing circuit by a pair of rejection circuits (a), its frequency response (b) and design (c)

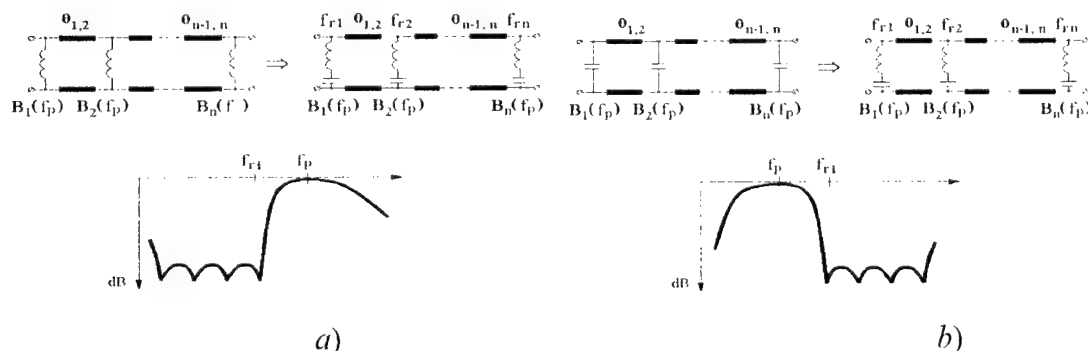


Fig. 3. Transformation of a polynomial filter into the filter with poles: a) in the bottom stopband (quasi-high-pass filter); b) in the top stopband (quasi-low-pass filter)

Practically such a filter is carried out as a short waveguide insertion (fig.2c). The original filter – a flange with the electric length  $60-70^\circ$  ( $\approx \lambda/5 - \lambda/6$ ) is received. Its characteristic is shown on fig.2b.

Passband filters with direct couplings. If in the filter with direct couplings the jet irregularity is replaced with a rejection circuit we shall receive the filter with the asymmetrical characteristics (fig.3). The method of synthesis of such filters - prototypes is developed. On fig. 4 the design of a similar filter and its frequency characteristics is shown.

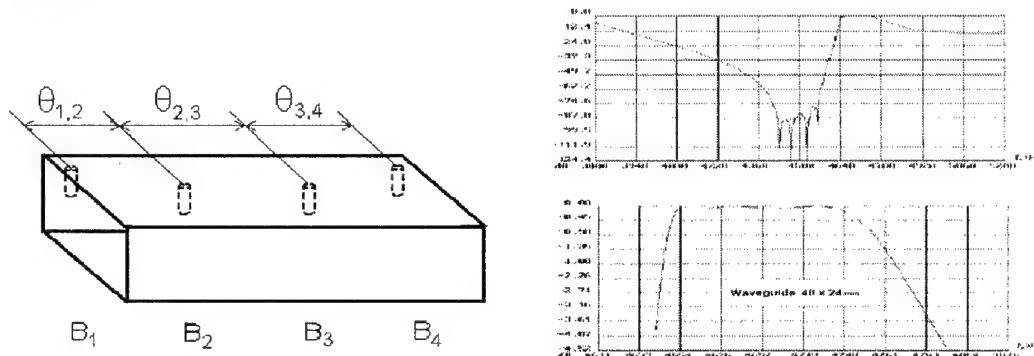


Fig. 4. The design of three-section filter and. frequency characteristics of a quasi- high-pass filter

Waveguide filters with a ladder structure. It is experimentally proved, that in waveguides it is possible to realize a ladder circuit without introduction of inverters of immittances. Two circuits of a five-section filter (fig.5) have been examined.

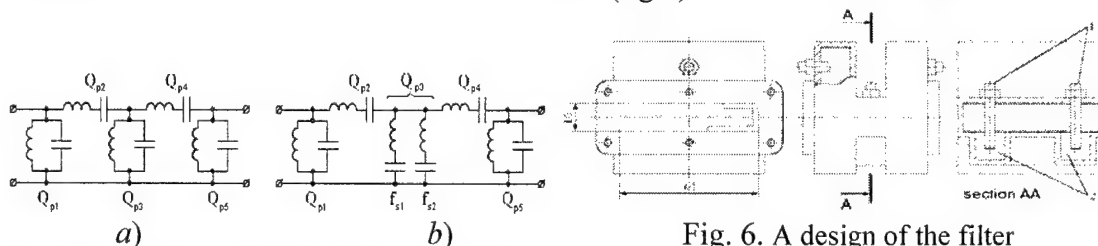


Fig. 5. Ladder circuits of five-section filters

Fig. 6. A design of the filter under the circuit fig.5b

The filter design according to the scheme of fig. 5b, is shown on fig. 6. Here quality  $Q_3$  is formed by a pair of rejection circuits. On fig.6 these rejection circuits are executed as resonant posts 1. Parallel circuits realized as a resonant diaphragm with the U-shaped aperture. Q-factor is determined by the size of shift of the ends of a slot. The length of a slot is made a little bit shorter than that of the resonant one. The tuning screw, located near a longer horizontal part of a slot, is shifted along a waveguide with regard to a plane of a diaphragm. Series circuits represent two short-circuited stubs included into the opposite wide walls. The filter is executed from two identical units between the flanges of which central diaphragm  $Q_{p3}$  is inserted. Two filters executed according to the schemes of fig. 5a and 5b have been experimentally investigated. In a passband the loss of both filters does not exceed 0.2 dB. The length of filters: according to the

scheme of fig. 5a - 48 mm, according to the scheme of fig. 5b - 44 mm, that is a bit less than half of a wave length in a waveguide.

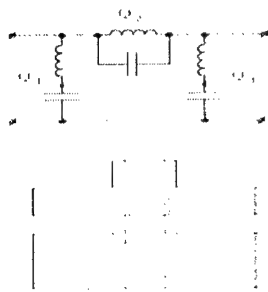


Fig. 7. Rejection filters of a smaller section with direct couplings

Rejection filters with direct coupling. At low requirements to a slope steepness it is possible to build a stopband filter on circuits with direct coupling (fig. 7). Resonant posts are placed in reference planes T of the E-plane junction. As the experience shows, at such connection the equivalent qualities of a stub and especially posts are reduced due to the additional coupling. To reduce this coupling it is possible to use diaphragms or – which is easier structurally - to carry out a stub on a waveguide

Filters with a low-pass filter structure. Capacitor elements are carried out as flat capacitor diaphragms. The opportunity to reduce sizes of series inductances follows from the expression for wave resistance of a waveguide:  $Z_{\text{ш}} = bA/a\sqrt{1 - (\lambda/2a)^2}$ , where  $A$  – is a constant dependent on a method of wave resistance definition.

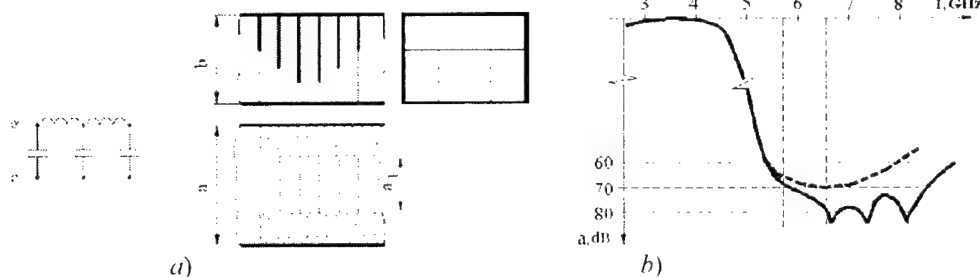


Fig. 8. The low-pass filter on capacitor diaphragms

Hence it is clear, that for the wave resistance increase the height  $b$  is increased or the wide wall  $a$  is narrowed. It allows to make the inductive elements length much smaller than the wave length i.e. to receive practically lumped elements. This idea is used when creating LPF (fig. 8) and the transformer for connection of waveguides with different height.

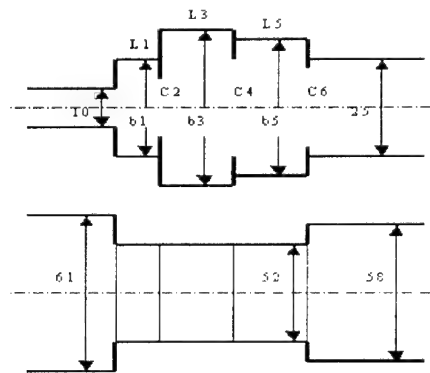


Fig.9. The design of transformer

In the latter case the filter from [1] was a low-frequency prototype. The transformer connects waveguides with the section 58x25 and 61x10 mm. The quarter wave transformer similar in parameters contains three links and has length  $3A/4$ . Thus, the transformer considered gives a gain in a length approximately 4.5 times. In the band of frequencies 3.2–4.2 GHz VSWR did not exceed the value 1.16. The transformer has 6 reactive elements. Structurally it represents a package of linings in which windows of different section (fig.9) are cut out. The full length of the transformer is 20 mm.

## REFERENCE

- [1] Matthaei G.L. Tables of Chebyshev impedance transforming networks of low-pass filter form. – Proc. IEEE, 1964, v.52, №8. pp.939-963

## WAVE SCATTERING BY CYLINDRICAL OBSTACLE IN GENERALISED WAVEGUIDE

Vitaliy P. Chumachenko and Igor V. Petrusenko \*

Gebze Institute of Technology, 41400, Gebze, Kocaeli, Turkey and  
Zaporizhzhia National Technical University, 64 Zhukovsky Str.,  
Zaporizhzhia, 69063 Ukraine  
E-mail: chumac@penta.gyte.edu.tr

\*Gebze Institute of Technology, 41400, Gebze, Kocaeli, Turkey  
E-mail: petrus@penta.gyte.edu.tr

### ABSTRACT

A novel full-wave solution of the problem of electromagnetic wave scattering by a circular post in a straight or continuously curved rectangular waveguide is presented. A rigorous mathematical model is based on the domain-product technique. It allows to construct an efficient series representation for the field in the interaction region. As a result, the initial boundary value formulation is reduced to a matrix equation with the fredholm operator. The last has the form of a sum of several products of the hilbert-schmidt operators provided the post does not touch the boundaries of the interaction region. The kernel matrix operator predetermines the fast convergence of the numerical approximations for a wide range of curvature variation, any possible radius of the cylinder and arbitrary location of the obstacle in the interior of the guide.

### INTRODUCTION

A variety of techniques has been applied to the problem of electromagnetic wave scattering by cylindrical obstacles in the straight rectangular waveguides, which has been examined for many years (see, for instance, [1-4, 6]). The well known works deal exclusively with the special situation of relatively thin and centered posts [1, 2]. Recently these tight constraints have been overcome [3, 4], but, as a rule, the data obtained are validated by computational experiment in the form of "practical convergence" and comparative checks. Rigorous analysis of a post in continuously curved rectangular waveguide did not carry out at all.

We present an alternative rigorous analytical approach for solving the outlined class of problems that is quite straightforward, effective and well substantiated. The method of analysis is the domain-product technique (DPT) [5]. We consider the region of field determination as a common part of several auxiliary domains with separable geometry. After projective procedure the initial formulation is reduced to a matrix operator equation with respect to expansion coefficients that are associated with the auxiliary region related to the post. Functional properties of the matrix operator obtained are a subject of our investigation. The approach is described for a circular perfectly conducting post in a common 2-D waveguide structure, which is a generalisation of both straight and continuously curved rectangular waveguide.

### DPT MODEL OF INDUCTIVE POST

The configuration of interest and the co-ordinate systems used are shown in Fig.1a. The circular post of a radius  $r$  placed across the guide parallel to the narrow wall and arbitrary centered. The mode incident upon the post is  $LM_{10}$ . To take the advantage of the physical symmetry plane the problem has been partitioned into two sub-problems corresponding to the symmetric and anti-symmetric excitations.

The interior of the guide is divided into the interaction region and two regular semi-infinite waveguides. Their fields are bound by the matching conditions on the common boundary lines. According with DPT, a field inside the interaction region can be represented in the form

$$u = u^{(r)} + \sum_{j=1}^4 u^{(j)} \quad (1)$$

as a superposition of partial solutions of the Helmholtz equation for five specially constructed intersecting domains [6]. In the expression (1)

$$u^{(r)}(\rho', \theta') = \sum_{n=-\infty}^{\infty} x_n \exp(in\theta') \frac{H_n^{(2)}(k\rho')}{H_n^{(2)}(kr)}, \quad \rho' \geq r, -\pi < \theta' \leq \pi$$

is a solution in the exterior to the post, which meets the condition at infinity. The expansion coefficients  $\{x_n\}$  are sought in the Hilbert space

$$h_1 = \left\{ \mathbf{x} : \sum_{n=-\infty}^{\infty} (|n|+1) |x_n|^2 < \infty \right\}$$

Using continuity of the tangential electric and magnetic fields inside of guide and homogeneous boundary conditions on the conducting parts of the boundaries of the interaction region we obtain the matrix equation

$$\mathbf{x} + \mathbf{A}\mathbf{x} = \mathbf{b}, \mathbf{b} \in h_1 \quad (2)$$

after familiar algebraisation.

### PROPERTIES OF MATRIX OPERATOR

The matrix operator  $\mathbf{A} : h_1 \rightarrow h_1$  from (2) has the form

$$\mathbf{A} = (\mathbf{T}_1 \mp \frac{1}{2} \mathbf{T}_2 \mathbf{F}_1) \mathbf{D}_1 + (\mathbf{T}_3 \mp \frac{1}{2} \mathbf{T}_2 \mathbf{F}_3) \mathbf{D}_3 \mp \frac{1}{2} \mathbf{T}_2 (\mathbf{F}_2 - \mathbf{G}) \quad (3)$$

It compactness follows from asymptotic estimates of some integrals, which are Fourier's coefficients of the functions being differentiable infinitely many times. For the elements of matrix operators  $\mathbf{T}_j$  from (3) we have relations

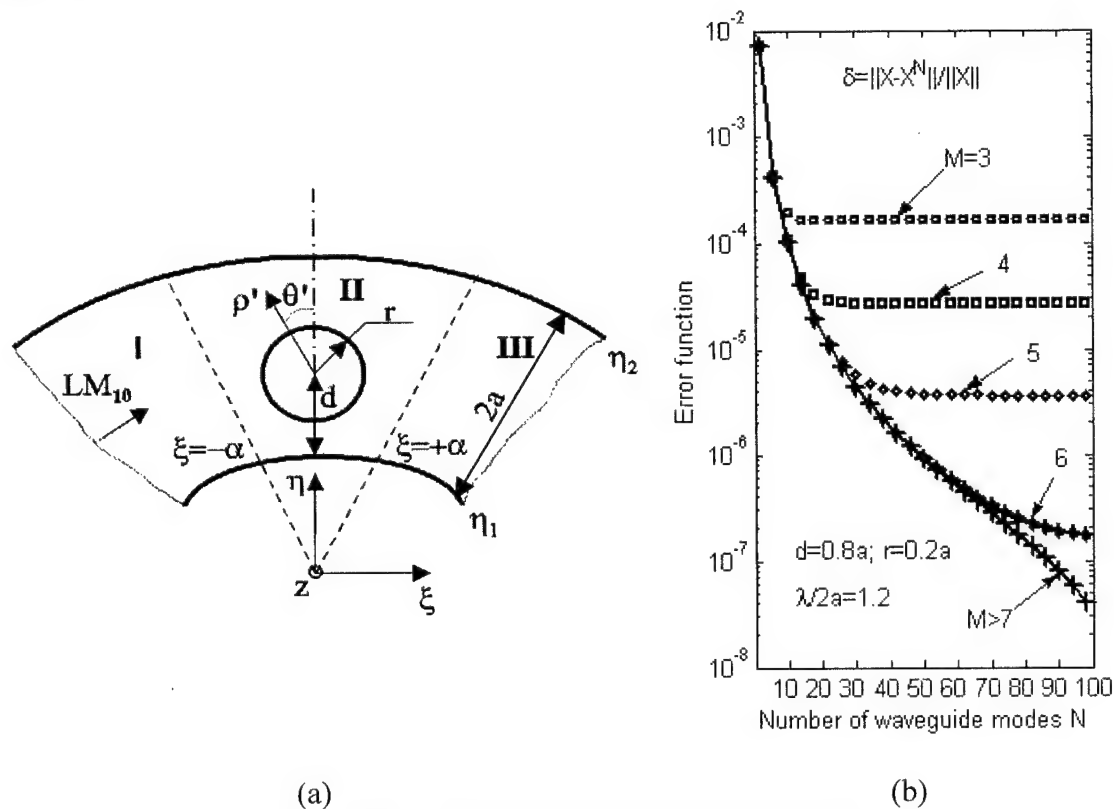
$$\sum_{m,n} m |t_{mn}^{(j)}|^2 = O\left[(1 - \zeta_j)^{-\tau}\right], \tau > 0, j = \overline{1,3}$$

The conditions  $\zeta_j < 1, j = \overline{1,3}$ , mean that the post does not touch the boundaries of the interaction region. Under the same condition, we get

$$\sum_{m,n} |f_{mn}^{(1,3)}|^2 < \infty, \sum_{m,n} \frac{1}{n} |\beta_j^{(m,n)}|^2 < \infty, j = \overline{1,3}$$

where  $\beta^{(m,n)} = (f_{mn}^{(2)}, g_{mn}, d_{mn}^{(1,3)})$ . It proves that  $\mathbf{A} : h_1 \rightarrow h_1$  is the kernel operator.

Let  $\mathbf{x}^{N,M}$  be the solution of a "truncated" counterpart of the matrix equation, then in the sense of the  $h_1$ -norm the relative errors of approximation tend to zero with  $M, N \rightarrow \infty$ , Fig. 1b.



(a) (b)  
Fig.1. Geometry of the problem (a) and convergence of approximate solution in norm (b)

## REFERENCES

- [1] Schwinger, J., and Saxon, D.S., Discontinuities in Waveguide, New York: Gordon and Breach, 1968.
- [2] Collin, R.E., Field theory of guided waves, Oxford: Oxford University Press, 1991.
- [3] Leviatan, Y., Li, P.G., Adams, A.T. and Perini, J., 'Single-post inductive obstacle in rectangular waveguide,' IEEE Trans. Microwave Theory Tech., vol. MTT-31, pp. 806-812, October 1983.
- [4] Toyama, T., and Sawado, E., 'Functionals in the variational method applied to equivalent impedance matrix of metallic posts unsymmetrically positioned in a rectangular waveguide,' IEEE Trans. Microwave Theory Tech., vol. MTT-40, pp.1655-1660, August 1992.
- [5] Chumachenko, V.P., 'The use of integral equation method for solving one class of electrodynamics problems,' (in Russian), Izvestiya VUZ. Radiofizika, vol. 21, pp. 1004-1010, July 1978.
- [6] Chumachenko, V.P., and Petrusenko, I.V., 'Domain-product technique solution for scattering by cylindrical obstacle in rectangular waveguide', Electromagnetics, vol.22, 6/2002.

## CAPACITIVE IRIS BANDPASS FILTERS WITH SPURIOUS HARMONIC MODES SUPPRESSION

A. Kirilenko, L. Mospan, V. Tkachenko

Institute of Radiophysics and Electronics of the National Academy of Sciences of Ukraine,  
12, Ak. Proskury Str., 61085, Kharkov, Ukraine  
phone: 380 572 448518, fax: 380 572 441105, E-mail: kirilenko@ire.kharkov.ua

### ABSTRACT

A new design of capacitively coupled bandpass filter, that provides suppression of spurious passbands for the dominant and the second waveguide modes without any extension of the filter dimensions, keeping the same return loss within the passband, is presented. Spurious passbands suppression is provided by cutting in iris strips additional pair of slots. Cutting the additional slots leads to the appearance of attenuation poles, which are placed in the spurious passbands. The  $k$ -inverter of corresponding two-side double-slot iris changes slightly and may be easily fine-tuned. Numerical examples are presented for the three-section 5% filter in wr90 waveguide.

### INTRODUCTION

Directly coupled bandpass filters are widely used structures in practical design of space and ground-based microwave systems. However it was found in practice [1] that if a bandpass filter is used in a complex microwave system, the spurious second harmonic mode appears in supposed attenuation band. This may cause a serious interference problem, leading to a degradation of the filter frequency response. As it was proposed in [1] one should use asymmetric filters with improved attenuation band or ridged filters, in which the second harmonic mode cannot propagate through the filter.

In this report we propose a new design of capacitively coupled bandpass filters that provides effective suppression of the spurious harmonic passbands for both the dominant and the second waveguide modes. It is achieved due to the cutting additional horizontal slots in the strips of coupling irises (see Fig. 1). In contrast to ridged filters the second waveguide mode can propagate through the filter under consideration. Although we failed to suppress it's the main passband, we succeeded in suppression of its spurious passband, the dominant mode spurious passband and in increasing the attenuation level of the dominant mode in the frequency range corresponding to the main passband of the second waveguide mode. Moreover, we succeeded in significant reduction of electric field strength magnitude within the coupling irises.

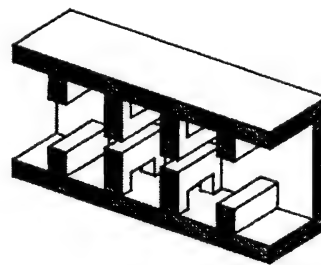


Fig. 1. Draft of the bandpass filter based on the two-side double-slot capacitive irises

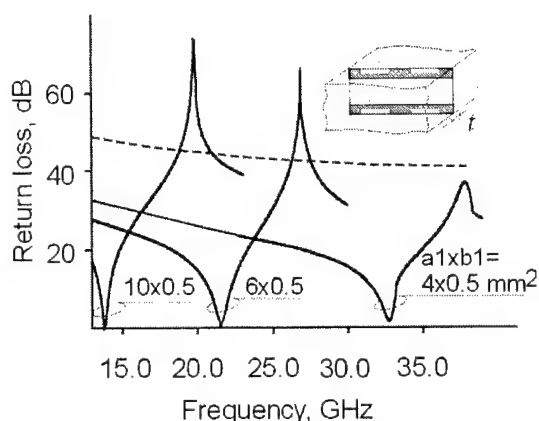


Fig. 2. The modification of return loss response for the double-slot two-side strip in WR90 with decreasing the slot width,  $t=0.5$  mm.

sections that form the parasitic passband. Moreover, as it is demonstrated in [2] the multislot configurations are able to reject simultaneously not only the dominant mode but also the higher ones in the two- or three-mode frequency bands. Four configurations of the slotted strip that is able to reject the dominant mode are shown in Fig. 3. Two-side double-slot strip has the richest properties as to a frequency harmonic mode suppressor of the resonance type. There is a quadruplet of eigen-oscillations symmetrical and asymmetrical in the  $OX$  or  $OY$  directions with very close real and imaginary parts of their complex eigen-frequencies. This fact makes possible to reject three modes simultaneously:  $TE_{10}$ ,  $TE_{20}$ , and  $TM_{11}$ . This configuration has been chosen as a modified coupling section for the filter under consideration.

Numerical results are demonstrated by two examples of a 5% third order filter in WR90 (Fig. 4). Left-hand side and right-hand side responses from the Fig. 4 correspond to the classic BPF and the BPF with two identically modified (two-side and double-slot) interior coupling irises, respectively. Black solid and dashed curves correspond to the insertion loss for the dominant mode and the second mode, respectively. Modified interior sections of the latter filter provide attenuation poles in the spurious passband for the dominant mode. As a consequence, the spurious passband is shifted with

## RESULTS

The salient feature of the slotted strips to reject waveguide modes is on the base of achieved results. It was shown in [2] that cutting additional slot(s) in the iris strips (symmetrical central-placed or two-side) provides a resonance of total rejection in the response. The location of this resonance is mainly determined by the slot width  $a_1$  (see Fig. 2), whereas its quality depends primarily on the thickness of the metal "bridge(s)", separating the main iris slot and the new ones, and on the resonant slot height  $b_1$ . Note a rejection can be provided in the whole operating range of rectangular waveguide up to the frequency band of the second longitudinal resonances of the filter

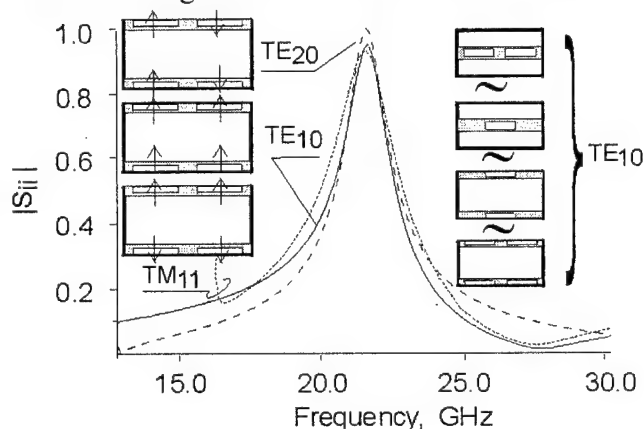


Fig. 3. Reflection coefficients of the dominant and higher modes from double-slot two-side-strips with  $a_1 \times b_1 = 6.0 \times 0.5$  mm<sup>2</sup> in WR90,  $t=0.5$  mm



simultaneous improvement of stopband attenuation in general. It is clear that the filter configuration shows an excellent opportunity to suppress the main part of the spurious passband for the second waveguide mode. Notice that the frequency responses are almost identical within the passband. Besides, the electric field strength magnitude in modified iris sections is approximately equal to the one for the corresponding inductively coupled filters.

## CONCLUSIONS

A new design of the bandpass filters provides the improvement of frequency response regarding to the bandstop attenuation for both the dominant mode and the second modes as well. By choosing the appropriate set of slots it is easy to implement several attenuation poles, suppress the parasitic passbands and to achieve the better passband separation. Moreover cutting the slots in the iris strips provides a considerably lower magnitude of the electric field strength within basic of the slot iris. For all the filters the new properties are achieved without increasing both the transversal and longitudinal filter dimensions.

## REFERENCES

- [1]. Wu K.-L., McDonald G., "Coping with hidden Spurious Harmonic Modes in the Design of Low Pass Corrugated Waveguide Filters," *Microwave journal*, V.44, №11, 2001, pp. 180-186.
- [2]. Kirilenko A.A., Mospan L.P., "Harmonic Rejection Filters For The Dominant and Higher Waveguide Modes Based On The Slotted Strips", 2002 IEEE MTT Symposium, pp.373-376.

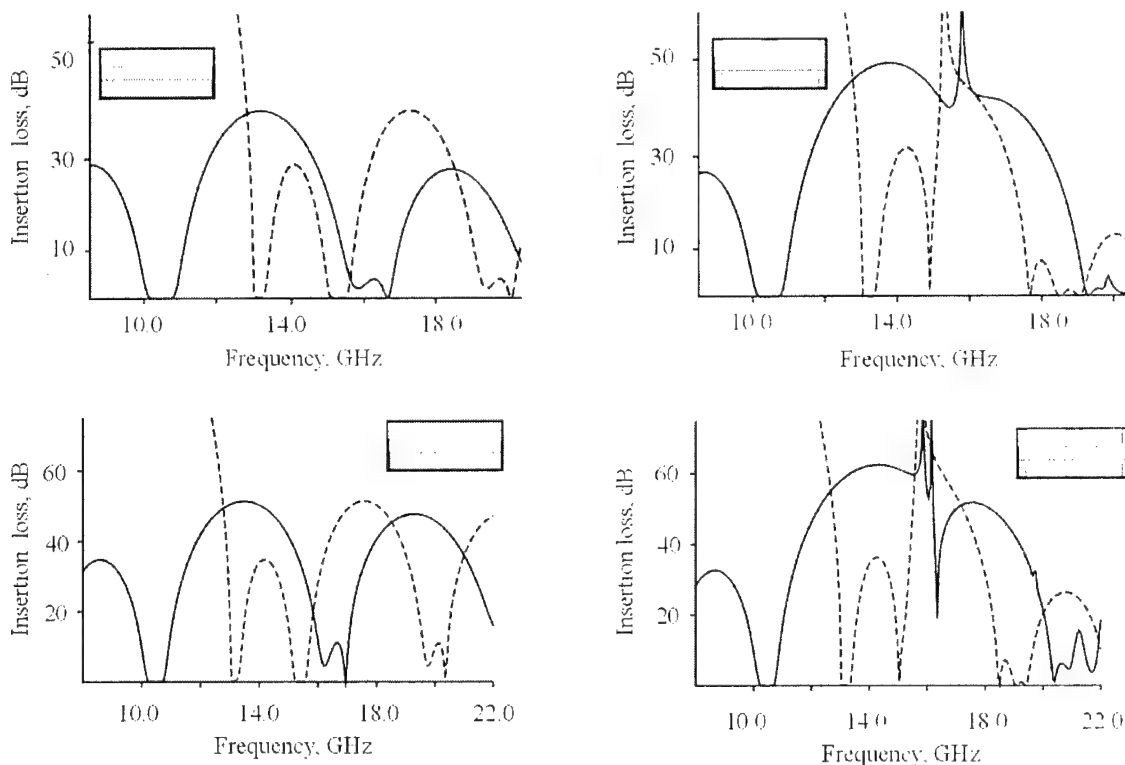


Fig. 4. The frequency responses of 5% classic bandpass filters and the filters with two identically modified internal irises that provide suppression of the spurious passbands for both the dominant and the second waveguide modes

## DATA PREPROCESSING FOR GENERALIZED MODE-MATCHING METHOD

Anatoly Kirilenko, Dmitry Kulik

Institute of Radio Physics and Electronics National Academy of Sciences of Ukraine  
12 Akad. Proskury St., Kharkov, 61085, Ukraine; E-Mail: kirilenko@ire.kharkov.ua

### ABSTRACT

The paper goal is to describe a geometrical data preprocessor, which is used at realization of the generalized mode-matching technique (GMMT). Its destination consists in processing of the geometry specification of the cross-section a complicated waveguide line by the manner that allows the unificate the process of the matrix operators required to find the mode basis.

In spite of widespread using of finite difference and other lattice methods the MMT [0,0] is still the most attractive procedure of the waveguide problem solution regarding to common efficiency-universality estimation. Nevertheless the drawback of this method is an individual approach to each of problem under consideration. This makes MMT algorithms relatively time-consuming ones both at analytical and numerical consideration of the solutions and at testing and tuning as well. Really this reason increases the time of waiting of the final results and hampers somewhat the practical usage of MMT.

The goal of our work was to generalize the MMT, making it possible to unificate the process of the numerical algorithm development for initially unpredetermined geometries of a wide class. Saving the well-known efficiency and accuracy of MMT algorithms this brings such GMMT solutions to lattice methods [0] regarding to both the easiness of usage and the universality of approach as well.

We consider such a generalization of MMT as a procedure that creates the MMT-algorithms without any preliminary analytical consideration. Here we describe the part of this algorithm that responsible for processing of a geometrical data. We named it "preprocessor" by analogy with corresponding parts of the software based on the lattice methods. Its function here consists in the data preparing for implementation of MMT matrix equation at calculation of the full mode bases for a waveguide line with arbitrary cross-section having the coordinate piecewise-linear boundary.

A waveguide line that may be considered as a rough approximation of the coaxial line is presented in Fig. 1. The line cross-section has to be divided into a set of nonoverlapping rectangular subregions. This fragmentation may be performed in Y or in X directions meaning that all such the subregions have metallized sidewalls parallel to Y or X axis (Fig. 1 demonstrates typical Y-fragmentation). The sidewalls of these subregions are metallized and the upper and low walls may be open or closed by electrical (PEW) or magnetic (PMW) walls. They may appear at consideration of the lines with symmetrical cross-section. In other words the cross-section will be presented as a set of peaces of plane-parallel waveguides that make it possible using the transverse resonance method to obtain the mode basis.

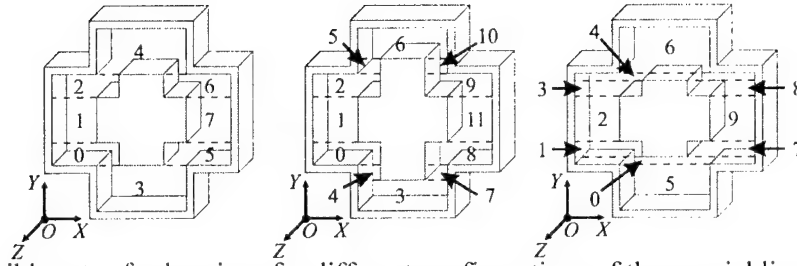


Fig. 1 The possible sets of subregions for different configurations of the coaxial line formed by a cross internal conductor within the crossed waveguide.

The number and coordinates of the rectangular subregions forming the line cross-sections provides really the full information required to calculate the mode basis. Naturally the situations exist when a weak geometry varying may require not only corresponding changing the geometrical parameters but also rearranging the set of subregions and even their total number as well. Such a situation is illustrated by the left and right pictures of Fig. 1. This is a reason of the necessity of the preprocessor operations not only at the initial stage of calculation but at any variations of the geometrical parameters as well.

The main purpose of the preprocessor consists in fragmentation the cross-section specified by a simple and easy in use manner into the set of subregions. Initial specification may consists, for example, of several contours specified by arranged sets of vertex points. Fig. 2 illustrates successive steps of preprocessing procedure.

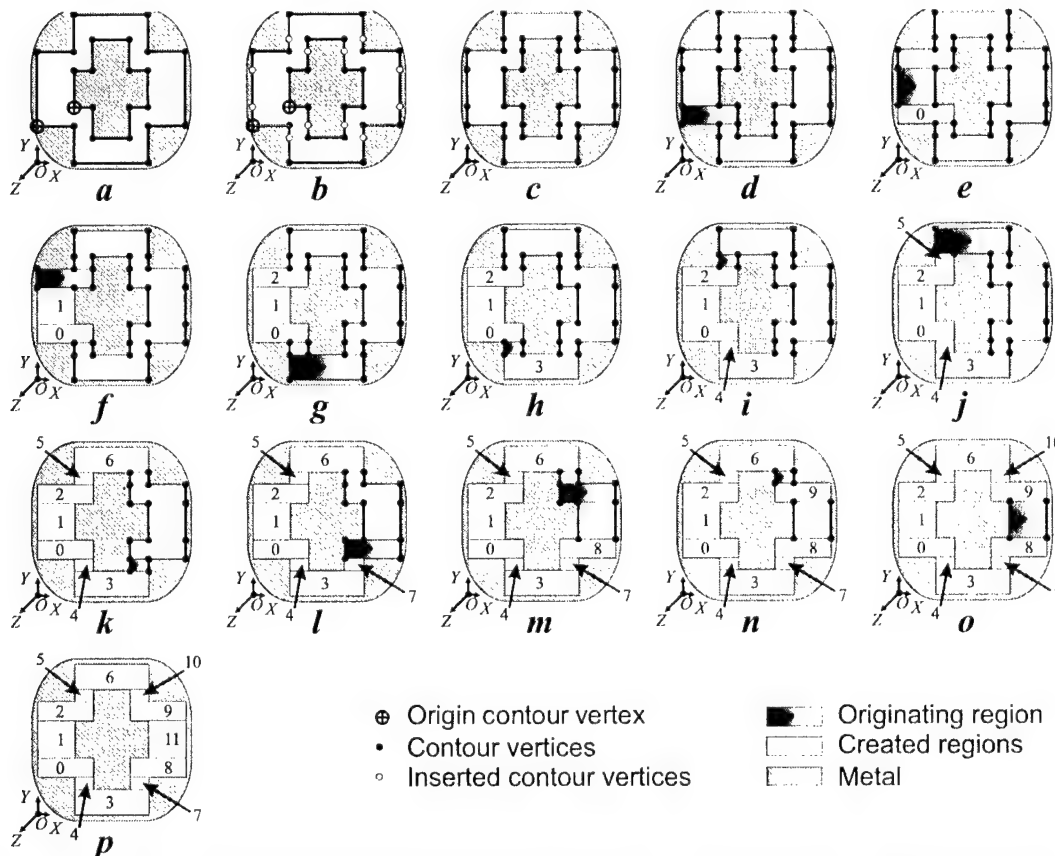


Fig. 2 The stages of the subregions set forming according to specified piece-wise coordinate contours which describe the cross-section.

Fig. 2a shows two initial contours forming the cross-section. The dark circles mark the vertices. At the first step the ensemble  $U$  of the  $y$ -coordinates, which characterize the points of the uniformity breakdown in vertical direction have to be found. After that the corresponding to  $U$  additional vertices are inserted in all contours. The light circles in Fig. 2b mark them.

Using the all set of vertices the set of vertical line pieces are formed. They represent the sidewalls of the future subregions (Fig. 2c).

The next steps of subregion ensemble forming presented in Fig. 2d-Fig. 2o. They are the following:

- The found pieces set is successfully looked through to find the “pairs”. The pair is two pieces with the same height and placed at the same coordinates.
- The pair of the nearest on horizontal pieces forms the subregion. The pieces generative it are moved away of the set of pieces.
- The process is continued until the pieces set is not empty. In principle this step finished the stage of cross-sections segmentation.

The following steps are aimed to prepare the data for MMT matrix operators:

- The matrix of the subregion couplings is formed. Each geometrical coupling matrix element is a data structure that determine : a) if the subregion  $I$  is coupled by an open aperture with subregion  $j$ ; b) if “Yes”, the what are the coordinates and the placement peculiarities of a common aperture. The determination of the geometrical subregion coupling matrix is performed by successive looking through all set of subregions and analyzing the type of subregions' contact.
- After that it is possible to extract the subsets of noncontacting subregions that describe possible separate waveguides (for example a hollow waveguide within the hollow waveguide). This accelerates the computational process in times.

At the calculation of a TEM mode field distribution it is required to know the potentials of the subregions sidewalls. The equipotential contour to which a sidewall belongs is determined according to the number of contour to which the wall belonged initially.

To facilitate the mode basis search for the lines with symmetrical cross section the dividing the problems into two or four ones is foreseen. These subproblems are the boundary value problems relative the halves or the quarters of initial cross-section with PEW or PMW in the planes of symmetry. Sometimes these subproblems have to be divided in its turn etc. Except of rarefying the roots of dispersion equation this enables to avoid the root omission for twinned cutoffs of the TM-modes, when the field is totally concentrated in the left part or in the right one of a cross-section.

Above discussed steps of preprocessing provides all required data to create the matrix operators of generalized mode-matching technique. One way to create dispersion equation is to use the matching operations immediately for the subregions fields at their common boundaries defined by the coupling matrix. The role of unknowns here play the amplitudes of the field space harmonics within subregions. Though it is the simplest approach, however it is immediately applicable to the situations when all subregion couplings may be described as a contact a “big” subregion with a “small” one. In the opposite case the intermediate zero-length virtual subregion has to be implemented.

Another way is to use the matching procedure basing on the unknown field distributions on the subregion coupling apertures. Except of a possibility to reduce

somewhat the number of unknown amplitude vectors there is essential advantage to use special bases for the field distribution expansion. They may take into account all types of the fields behavior near coupling aperture ends: rectangular or sharp edge, electrical wall or magnetic wall. Such algorithms have shown very good convergence on a range of partial configurations [0,0]. Last time they came to attention again [0].

The above-described preprocessor and the electromagnetic solver corresponding to first of MMT approaches was realized in the frames of AutoCAD based electromagnetic software for analysis and synthesis of waveguide devices *MWD01*. Detailed description of the solver background, realization and numerical peculiarities are the subject of a separate message. See, for example [0].

Here we present a set of the field distribution of the main and high modes of the waveguides with complicated cross-sections.

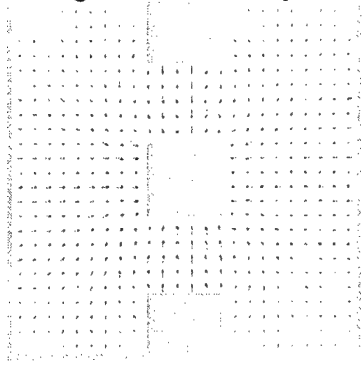


Fig. 3

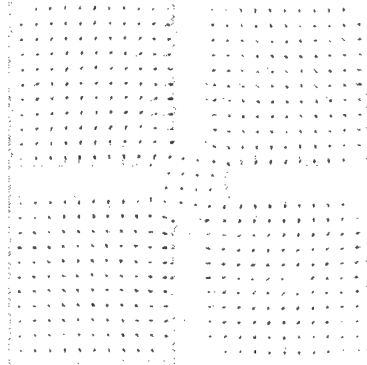


Fig. 4

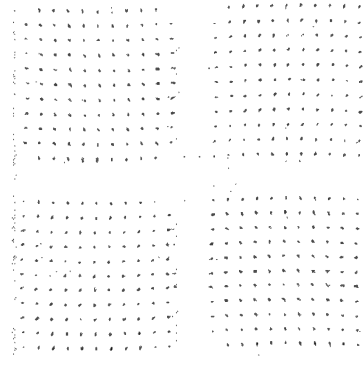


Fig. 5

The Fig. 3 presents the field of the dominant TEM-mode of a ridged rectangular bar line that used in special types of the bandpass filters. The Fig. 4 demonstrates a like to TE01-mode of circular waveguide distribution of a higher TE4 mode of the rectangular quadruple ridged waveguide. The origin of this mode may be treated as a difference of the TE20 and the TE02 modes of the square waveguide. By the same manner the origin of the higher TE5 mode of the rectangular quadruple ridged waveguide (Fig. 5) may be explained as the sum of the TE20 and the TE02 modes.

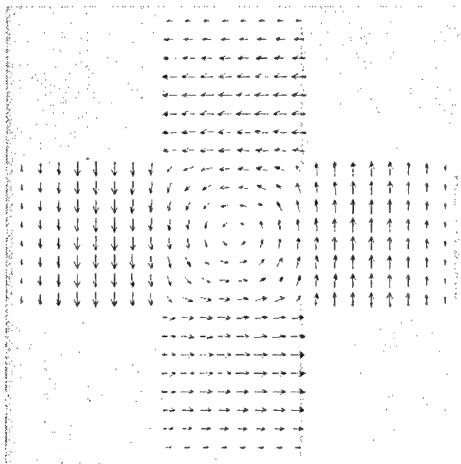


Fig. 6

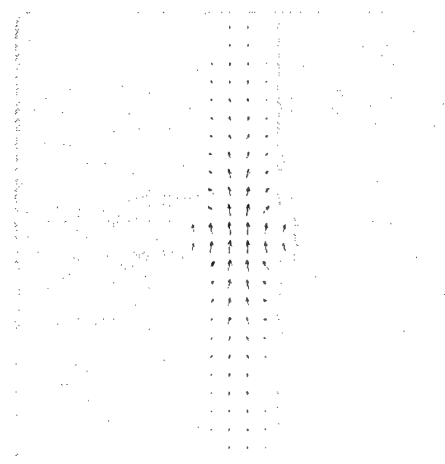


Fig. 7

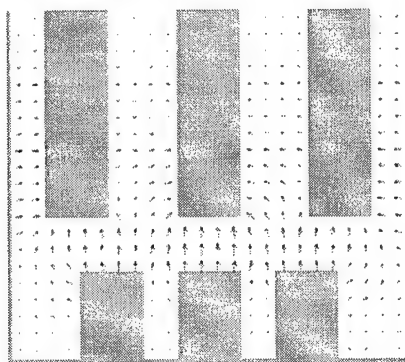


Fig. 6

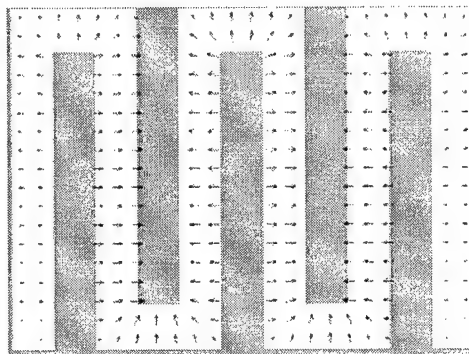


Fig. 7

Fig. 6 demonstrates the TE<sub>4</sub> mode of the crossed rectangular waveguide with the axially symmetrical distribution of the transversal electrical field as well. Fig. 7 presents the field of the main mode of the grooved waveguide. It confirms the possibility to calculate the groove mode a mode of crossed waveguide (TE<sub>3</sub>). The cross-sections similar to shown in Fig. 8 are used at design of the waffle-iron low-pass filters. Finally the Fig. 9 presents the dominant mode field of the waveguide with a serpentine cross-section. Due to such type of the cross-section it has a very low cutoff.

## REFERENCES

- [1] G.V. Kisunko, *Electrodynamics of the Hollow Systems*, VKAS Publ., Leningrad, 1949 (in Russian).
- [2] A. Wexler, "Solution of Waveguide Discontinuities by Modal Analysis", IEEE Trans. on MTT, vol. 15, #9, 1967, pp. 508-517.
- [3] T. Itoh (ed), *Numerical Techniques for Microwave and Millimeter-Wave Passive Structures*, New York: J. Wiley, 1989.
- [4] G.I. Veselov, N.I. Platonov, E.S. Slesarev, "Taking into account the field singularities near edges and mode-matching", Radiotekhnika, vol. 35, #5, 1980, pp. 27-34, (in Russian).
- [5] G.F. Zargano, V.P. Lyapin and others, *The Waveguides of Complicated Cross-sections*, Radio i Svyaz', Moskow, 1986, (in Russian).
- [6] S. Amari, J. Borneman, R. Vahldieck, Application of Coupled -Integral-Equation Technique to Ridged Waveguides, IEEE Trans. on MTT, vol. 44, #12, 1996, pp.2256-2264.
- [7] A. Kirilenko, D. Kulik, Yu. Parkhomenko, L. Rud, V. Tkachenko, "Automatic electromagnetic solvers based on mode-matching, transverse resonance, and S-matrix techniques", MICON-2002 Conf. Proc. Gdansk, Poland, May 20-22, 2002, vol. 3 pp.815-824.

## MODE-MATCHING APPROACH FOR THE CALCULATION OF A WAVEGUIDE TEE DISTORTED BY SEMI-PLATES IN THE BRANCHING REGION

Sergey Kulishenko, Anatoly Kirilenko, Sergey Senkevich.

IRE NASU, ul. Proskury 12, Kharkov 61085, Ukraine; E-Mail: ksf@krla.ire.kharkov.ua

One of configurations of OMT is a tee with metal plates in one of the straight arms. These plates form a system of cutoff waveguides and reflect the mode of one of the polarizations. The simplest example is a waveguide tee with one plate within the direct port and no overlapping of the plate and the branching region (Fig. 1a). This configuration, as shown in [1], provides a good matching of side arm in a narrow frequency band only and has increased dimensions. These facts limit OMT application. The authors have pointed that MMT can be used *only* if there is no overlapping of plate and branching region ([1], p. 388).

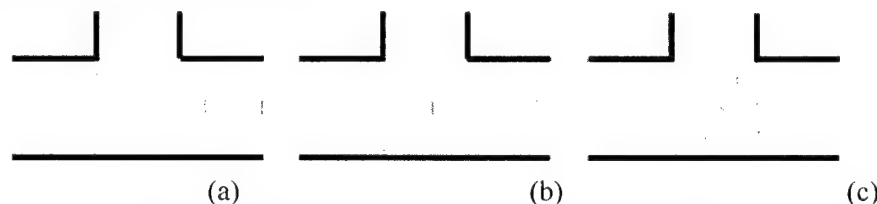


Fig. 1. OMTs based on the tee with metal plates

As it turned out later, one can solve the of mode diffraction on a tee with coordinate discontinuities in branching region by using MMT (see [2] for configuration in Fig. 1b). However the calculations have shown that a low return loss can be obtained in direct arm for the single-plate case only in the beginning of operating frequency range. This is caused by too deep penetration of the electromagnetic field into the cutoff regions. Due to this fact the plate and below-cutoff waveguides cannot "imitate" the mitered bend. It is obvious that increasing the number of plates can facilitate the problem solution.

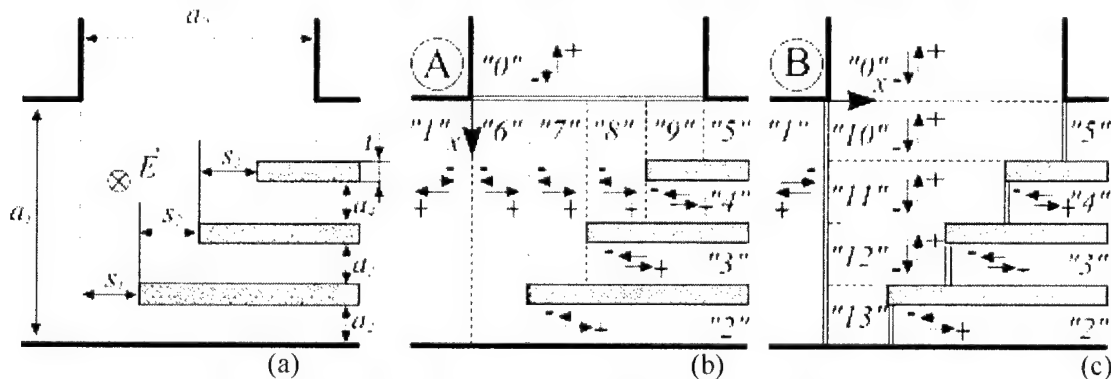


Fig. 2. Tee with three plates and its division to subregions

In this paper we use the modification of MTT published in [2]. The field in branching region (Fig. 2a) is represented as a superposition of two fields: a) horizontal configuration with PEW on the top and b) vertical configuration with PEWs on right and left side waveguides. We consider the case of E-field parallel to semi-plate edges. The field matching for the inner regions of the subproblem geometries can be performed independently for both subproblems A and B.

Fig. 3 shows some elementary cell formed by subregions "6", "7" and "2" belonging to subproblem A (Fig. 3a) and subregions "13", "2" of subproblem B (Fig. 3b).

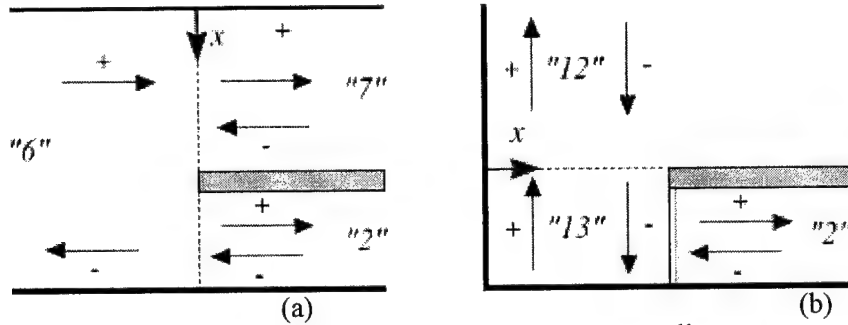


Fig. 3. Field matching in the elementary cell

Transverse field in subregions can be expressed as a superposition of eigen waves of parallel-plate waveguide:

$$E_y^{(p)} = \sum_{n=1}^{\infty} \left[ p_n^+ \cdot e^{i\gamma_n^{(p)} z^{(p)}} + p_n^- \cdot e^{-i\gamma_n^{(p)} (z^{(p)} - h^{(p)})} \right] \cdot \sin(\beta_n^{(p)} x^{(p)}),$$

$$H_x^{(p)} = \sum_{n=1}^{\infty} i\gamma_n^{(p)} \cdot \left[ p_n^+ \cdot e^{i\gamma_n^{(p)} z^{(p)}} - p_n^- \cdot e^{-i\gamma_n^{(p)} (z^{(p)} - h^{(p)})} \right] \cdot \sin(\beta_n^{(p)} x^{(p)}),$$

where  $p$  is the subregion number,  $p_n^+$  and  $p_n^-$  are the mode amplitudes,  $\beta_n^{(p)} = n\pi/a^{(p)}$  and  $\gamma_n^{(p)} = \sqrt{k^2 - (\beta_n^{(p)})^2}$  are transverse and longitudinal wave numbers. The field must satisfy the following boundary conditions:

$$\begin{cases} E_y^{(6)} = E_y^{(7)} \text{ on aperture "6"-"7"} \\ E_y^{(6)} = 0 \text{ on metall} \\ E_y^{(6)} = E_y^{(2)} \text{ on aperture "6"-"2"} \end{cases} \quad \begin{cases} H_x^{(6)} = H_x^{(7)} \text{ on aperture "6"-"7"} \\ H_x^{(6)} + H_z^{(13)} = H_x^{(2)} \text{ on aperture "6"-"2"} \end{cases}$$

Now we can perform field matching and project it on the basis functions of corresponding subregions. Resulting equations are presented in matrix form as follows:

$$\begin{aligned} N^{(6)} E^{(6)} \vec{\mathbf{6}}^+ + N^{(6)} \vec{\mathbf{6}}^- &= M^{(67)} \vec{\mathbf{7}}^+ + M^{(67)} E^{(7)} \vec{\mathbf{7}}^+ + M^{(62)} \vec{\mathbf{2}}^+ + M^{(62)} \vec{\mathbf{2}}^-, \\ M^{(76)} \gamma^{(6)} E^{(6)} \vec{\mathbf{6}}^+ - M^{(76)} \gamma^{(6)} \vec{\mathbf{6}}^- &= N^{(7)} \gamma^{(7)} \vec{\mathbf{7}}^+ - N^{(7)} \gamma^{(7)} E^{(7)} \vec{\mathbf{7}}^-, \\ iM^{(26)} \gamma^{(6)} E^{(6)} \vec{\mathbf{6}}^+ - iM^{(26)} \gamma^{(6)} \vec{\mathbf{6}}^- &+ Me_{-}^{(2-13)} \beta^{(13)} J^{(13)} \vec{\mathbf{13}}^+ + \\ &+ Me_{+}^{(2-13)} \beta^{(13)} J^{(13)} \vec{\mathbf{13}}^- = iN^{(2)} \gamma^{(2)} \vec{\mathbf{2}}^+ - iN^{(2)} \gamma^{(2)} \vec{\mathbf{2}}^-, \end{aligned}$$

where  $\vec{\mathbf{p}}^{\pm} = \{p_n^{\pm}\}$ ,  $N^{(p)} = \text{diag} \left\{ \frac{a^{(p)}}{2} \right\}$ ,  $E^{(p)} = \text{diag} \left\{ e^{i\gamma_n^{(p)} h^{(p)}} \right\}$ ,  $\gamma^{(p)} = \text{diag} \left\{ \gamma_n^{(p)} \right\}$ ,  $\beta^{(p)} = \text{diag} \left\{ \beta_n^{(p)} \right\}$ ,  $J^{(p)} = \text{diag} \left\{ (-1)^n \right\}$ ,  $n = 1, 2, 3, \dots$

Here  $M^{(pq)}$  are the matrices of conventional coupling integrals and the elements of matrices  $Me_{\pm}^{(pq)}$  are the following integrals:



$\{Me_+^{(pq)}\}_{m,n} = \int_S \sin(\beta_m^{(p)} x) \cdot \exp(i\gamma_n^{(q)} x) \cdot dx$ . Note, that the electric field has been

matched on the wide cross-section (subregion "6"), and the magnetic field has been matched on the two narrow ones (subregions "7" and "2").

The field matching on each of apertures results in 21 equations with 21 unknown vectors of field expansion amplitudes. This allows us to form the matrix equation of the 2nd kind with a block type operator. By solving it we obtain the  $S$ -matrix of full circuit and also the internal field. A study of the obtained solution numerical convergence shows that it has non-monotonous character. Nevertheless, taking into account 40 modes in port "0" (number of modes in the each of other regions is proportional to its width according to Mittra's rule [3]) is quite enough for rather good accuracy. Power disbalance between incoming and outgoing modes is less than  $10^{-4}$ . Under these conditions the calculation of  $S$ -matrix per frequency point takes about 2 sec on 1100 MHz PC. In examination of the algorithm certain instabilities were revealed. They are accompanied with a sudden change of the matrix operator condition number

$cond(A) = \frac{\|A\| \cdot \|A^{-1}\|}{\det(A)}$  (by several orders). Simultaneously the power conservation law fails. This phenomenon causes sharp spikes on frequency response curves. The spike width decreases with increasing the matrix dimension. It is determined that the positions of spikes coincides with the eigen frequencies of the branching region (the resonator formed by assuming PEWs of subproblems A and B simultaneously).

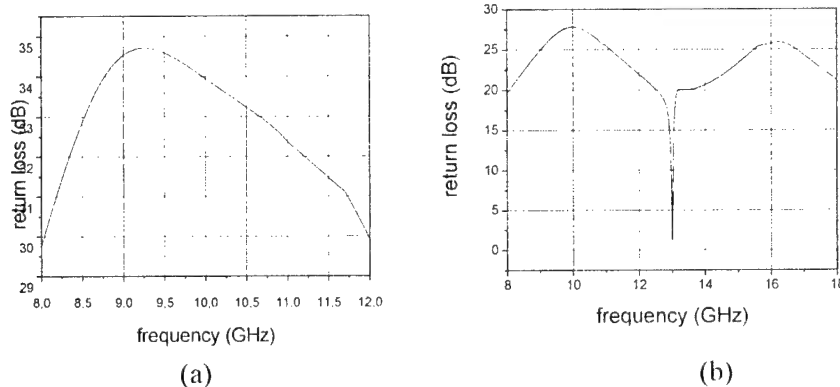


Fig. 4. Frequency response of optimized construction

In order to obtain a good matching of the device under consideration, optimization procedure was applied in two frequency bands. Corresponding results are shown in Fig 4. In the optimization within operating range of the waveguide (8-12 GHz) it is possible to ensure the return loss less than 28 dB (Fig. 4a). For a wider band (8-18 GHz) the return loss is about 22 dB except of the resonance area near 13 GHz (Fig. 4b). This resonance is caused by the appearance of the second mode and has the same nature as discussed in [4].

#### REFERENCES.

- [1]. Uher J., Bornemann J., Rosenberg U., Waveguide Component for Antenna Feed Systems: Theory and CAD, Norwood, MA, -Artech House, 1993.
- [2]. Kirilenko A.A., Kulik D.Yu., Tkachenko V.I., Kulishenko S.F., Generalization of the Mode-Matching Technique for the Waveguide T-junction with Inner Metallic Insert, Radiophysics and Electronics, 2001, vol. 6, №2-3, pp.181-186 (in Russian).
- [3]. Mittra R., Lee S., Analytical Methods of Waveguide Theory, Moscow, "Mir", 1974.
- [4]. Shestopalov V.P., Kirilenko A.A., Rud' L.A., Waveguide Discontinuities, Kyiv, "Naukova Dumka", 1986 (in Russian).

# THE EFFECTS OF RESONANCE ENERGY ABSORPTION IN LOSSY WAVEGUIDE-DIELECTRIC RESONATORS

Lyudmila B. Minakova, Leonid A. Rud

IRE NASU, ul. Proskury 12, Kharkov 61085, Ukraine;

E-mail: rud@ire.kharkov.ua

## ABSTRACT

The effects of a half and total resonance absorption of the input power are studied with the developed qualitative theory and exact numerical models for the case of waveguide-dielectric resonators built on  $e$ -plane rectangular lossy-dielectric posts in a rectangular waveguide.

## THEORY AND RESULTS

A qualitative theory of the microwave power resonance absorption is developed for lossy waveguide-dielectric resonators (wdrs) operating on a first higher oscillation and loaded with two identical waveguides. The theory is based on the assumption that the  $s$ -th natural oscillation of a lossless resonator is characterized by a complex-valued natural frequency,  $\omega_s = \omega'_s - i\omega''_s$ . The imaginary part  $\omega''_s$  determines the resonator radiation  $q$ -factor,  $Q_{s,rad} = \omega'_s / 2\omega''_s$ . Assuming that due to introducing the filling losses, the natural frequency of the above-mentioned oscillation changes as

$$\tilde{\omega}_s = \tilde{\omega}'_s - i\tilde{\omega}''_s = (1 + \alpha_s)\omega'_s - i(1 + \beta_s)\omega''_s. \quad (1)$$

Similar to [1], we succeeded in finding the following formula for calculating the absorption power input with the dominant mode incident from one of the resonator waveguide ports

$$W_L^{(s)} = \frac{2\beta_s}{(1 + \beta_s)^2 (\xi_s^2 + 1)}. \quad (2)$$

In (1),  $\alpha_s\omega'_s$  is the frequency shift and  $\beta_s\omega''_s$  is the additional attenuation caused by the absorption,  $\xi_s = 2\tilde{Q}_s(\omega - \tilde{\omega}'_s)/\tilde{\omega}'_s$  is the resonator detuning parameter. The following expressions for the reflected and transmitted powers of the incident mode have been derived as well:

$$W_R^{(s)} = \frac{\beta_s^2}{(1 + \beta_s)^2 (\xi_s^2 + 1)}, \quad W_T^{(s)} = \frac{\xi_s^2 (1 + \beta_s)^2 + 1}{(1 + \beta_s)^2 (\xi_s^2 + 1)} \quad (3)$$

The parameter  $\beta_s$  can be interpreted as a loss coefficient and the value  $\beta_s = 1$  as a critical loss for which the equality of the radiation and intrinsic  $q$ -factors is fulfilled. In this case, from (2) – (3) it follows that the maximum absorption  $W_L^{(s)} = 0.5$  and the equality  $W_R^{(s)} = W_T^{(s)} = 0.25$  are reached at the resonance frequency,  $\xi_s = 0$ .

The qualitative theory conclusions are confirmed by the results of the exact numerical calculations for the WDRs formed by  $E$ -plane rectangular dielectric posts in a rectangular waveguide. It is considered as a section of a partially filled waveguide included into a hollow rectangular waveguide. Three exact algorithms are worked out that allow 1) to synthesize the post geometry according to the required complex-valued natural frequency, 2) to calculate the natural frequency spectrum for the post-resonator with a fixed geometry, and 3) to calculate the full-wave scattering matrix in the  $TE_{m0}$  mode basis. These algorithms are based on the mode-matching technique [2].

The special investigations have been carried out for the WDRs operating on the first higher  $TE_{201}$  oscillation and providing a single resonance of the 50% absorption of the incident  $TE_{10}$  mode power. At first, the lossless WDR geometry providing the given values of the  $Q$ -factor and the resonance frequency is searched for using the first above-listed algorithm. Further with the aid of the second algorithm, the value of  $\tan \delta$  corresponding to the desired coefficient  $\beta_{201}$  is obtained. The comparative analysis of the exact and approximate WDR responses, illustrated by Fig. 1(a) for the case of the critical loss, shows their good agreement. In Fig. 1 and further,  $\kappa = \omega a / 2\pi c$  is the frequency parameter where  $c$  is the free-space light velocity,  $a$  is the waveguide width. An evident total absorption phenomenon should be waited when two in-phase  $TE_{10}$  modes are incident simultaneously from both of waveguide ports. In this case, the structure with the magnetic-wall symmetry occurs. According to [1], the absorption losses in such a structure has to be determined as  $W_L^{++} = 2W_L$  where  $W_L$  is calculated after the formula (2). The responses in Fig. 1(b) confirm this conclusion. We have found that the loss additivity principle in the form of

$$W_\Sigma = \sum_{s=1}^N W_L^{(s)} \quad (4)$$

Is valid if a wdr maintains  $n$  natural oscillations in the considered frequency range.

Fig. 1. Rectangular dielectric post responses calculated with the exact (solid curves) and approximate (dotted curves) models in the case of the critical loss,  $\beta = 1$ . (a) Excitation from one port. (b) Excitation from two ports simultaneously ( $t/a = 0.084$ ,  $r/a = 0.051$ ,  $\varepsilon = 50(1 + i0.0285)$ ).

To realize the condition for the total resonance absorption, one has to operate with degenerated natural oscillations having equal  $q$ -factors and the different symmetry along the wdr longitudinal axis.

As an example of a multimode wdr, we will consider the lossless dielectric post with  $t/a = 0.217$ ,  $r/a = 0.514$ , and  $\varepsilon' = 15$ . The location of the complex-valued eigenfrequencies of its  $TE_{m0n}$  natural oscillations is shown in fig. 3(a) by empty circles. We see that  $TE_{301}$  and  $TE_{204}$  oscillations of the different symmetry have the coincide eigenfrequencies  $\kappa'_{301} \approx \kappa'_{204} = 0.941$ . In the vicinity of this point, a total transmission is observed in the scattering problem (see the dashed-dotted curve in fig. 3(b)).

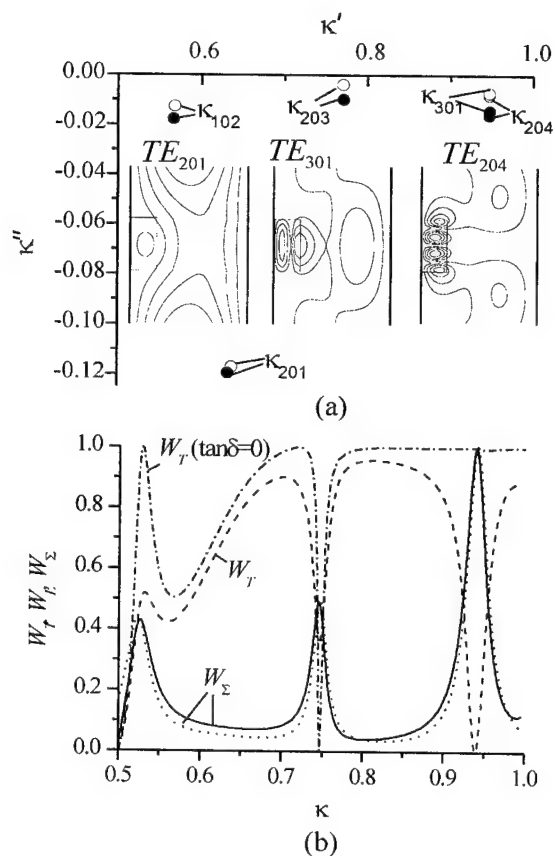


Fig. 3. (a) Location of the eigen-frequencies in the complex plane  $\kappa$  for the lossless and lossy dielectric posts. (b) Frequency responses of the lossless and lossy posts.

## REFERENCES

- [1] L.A. Vainshtein, *Electromagnetic Waves*, Moscow, Radio i Svyaz Publ., 1988 (in Russian).
- [2] L.B. Minakova and L.A. Rud', "A spectral approach to the synthesis of dielectric waveguiderejection resonators," *Journ. Telecommun. Techn. Electronics*, V. 47, No 5, 2002, pp. 507-512.

Further, we have found the value of  $\tan \delta = 0.0183$  providing the critical loss for the above-mentioned oscillations. The eigen-frequency location for the lossy dielectric post is presented in Fig. 3(a) by black circles. The exact responses of the transmitted and absorbed power for the lossy post are shown in Fig. 3(b) by the dashed and solid curves, respectively. The effect of a practically total absorption is realized at the point  $\kappa = 0.940$ .

To verify the validity of the loss additivity principle (4), we have calculated the loss coefficients  $\beta_{m0n}$  for all the oscillations from Fig. 3(a) and have used them in calculating the dependence  $W_\Sigma(\kappa)$  with using (2) and (4) (see the dotted curve in Fig. 3(b)).

We can conclude that the representation (4) gives very exact results elsewhere over the single-mode waveguide range if the values of  $\beta_{m0n}$  and  $\xi_{m0n}$  are exactly defined for all the natural oscillations taken into account during the calculations.

# DIFFRACTION ON THE EIGEN WAVES ON AN INCLINED MEDIUM INTERFACE IN THE WAVEGUIDES WITH METALLIC BOUNDS

Pleshchinskii I.N., Pleshchinskii N.B.

Kazan State University

P.O.Box 234 Kazan, 420111, Russia e-mai: pnb@ksu.ru. pnb@kzn.ru

## ABSTRACTS

The electromagnetic wave diffraction problems on an inclined medium interface with a metallic plate and without it in the plane waveguide and in the rectangular waveguide are considered. It is shown that these problems can be reduced to boundary value problems for the Helmholtz equation or for the Maxwell system in a bounded rectangular domain.

## INTRODUCTION

Let the infinite cylindrical waveguide with metallic bounds be separated by some surface into two parts filled up by the dielectric with different dielectric indexes. Let the eigen electromagnetic wave run on the medium interface (from the left, for example). It is necessary to calculate the scattered field.

The main idea of our method is to isolate some bounded domain containing the medium interface and to replace the rejected semi-infinity parts of waveguide by boundary conditions of special form. These conditions can be obtained by solving over-determined Cauchy type problems [1] for the Helmholtz equation or for the Maxwell system.

## SEMI-INFINITE PLANE WAVEGUIDES

Consider the auxiliary boundary value problems. It is necessary to seek in the semi-strips  $S_1 : -\infty < x < 0, 0 < z < h$  and  $S_2 : g < x < +\infty, 0 < z < h$  of the plane  $(x, z)$  solutions of the Helmholtz equation

$$\frac{\partial^2 u}{\partial x^2} + \frac{\partial^2 u}{\partial z^2} + k^2 u(x, z) = 0 \quad (1)$$

belonging to the classes of outgoing into infinity solutions satisfying the conditions

$$u(x, 0+0) = 0, \quad u(x, h-0) = 0. \quad (2)$$

It is shown in [2] (see also [1]) that

**Lemma 1** *The solvability conditions for these problems can be written down in the non-local integral form*

$$u(0-0, z) = -i \int_0^h \frac{\partial u}{\partial x}(0-0, t) K_1(t, z) dt, \quad 0 < z < h, \quad (3)$$

$$u(g+0, z) = i \int_0^h \frac{\partial u}{\partial x}(g+0, t) K_2(t, z) dt, \quad 0 < z < h, \quad (4)$$

$$K_j(t, z) = \frac{2}{h} \sum_{m=1}^{\infty} \frac{1}{\gamma_{j,m}} \sin \frac{m\pi t}{h} \sin \frac{m\pi z}{h}, \quad \gamma_{j,m} = \sqrt{k_0^2 \varepsilon_j - (m\pi/h)^2}.$$

The boundary value problems (1), (2) and

$$u(0-0, z) = u_{00}(z), \quad \frac{\partial u}{\partial x}(0-0, z) = u_{01}(z) \quad \text{or} \quad u(g+0, z) = u_{g0}(z), \quad \frac{\partial u}{\partial x}(g+0, z) = u_{g1}(z)$$

define all eigen waves of semi-limited waveguides outgoing into infinity.

### INCLINED BARRIER IN THE PLANE WAVEGUIDE

Let  $I: z = x \tan \theta$ ,  $\tan \theta = g/h$ ,  $0 < x < g$  be the inclined medium interface in the plane waveguide. We give the typical conjunction conditions on the  $I$

$$u(x+0, hx/g) = u(x-0, hx/g), \quad \frac{\partial u}{\partial n}(x+0, hx/g) = \frac{\partial u}{\partial n}(x-0, hx/g), \quad 0 < x < g, \quad (5)$$

here  $\partial/\partial n = \partial/\partial x \sin \theta - \partial/\partial z \cos \theta$ . We denote  $u^0(x, z)$  the potential function of the external wave and  $u(x, z)$  the unknown potential function.

**Theorem 1** *The diffraction problem for TE-wave on the inclined interface medium is equivalent to the boundary value problem for the Helmholtz equation (1) in the classes of outgoing into infinity solutions with boundary conditions (2), (5) and*

$$u(0+0, z) = -i \int_0^h \frac{\partial u}{\partial x}(0+0, t) K_1(t, z) dt + 2u^0(0-0, z), \quad 0 < z < h, \quad (6)$$

$$u(g-0, z) = i \int_0^h \frac{\partial u}{\partial x}(g-0, t) K_2(t, z) dt, \quad 0 < z < h. \quad (7)$$

In [3] the numerical method for solving this boundary value problem is constructed and is investigated by abstract approximate scheme [4].

### SEMI-INFINITE RECTANGLE WAVEGUIDES

Let  $W_1: 0 < x < a$ ,  $0 < y < b$ ,  $-\infty < z < 0$  and  $W_2: 0 < x < a$ ,  $0 < y < b$ ,  $0 < z < +\infty$  be two semi-infinity rectangular domains (semi-beams). We consider the Cauchy type problem for the Maxwell system

$$\text{rot} H = i\omega \varepsilon_0 \varepsilon E, \quad \text{rot} E = i\omega \mu_0 \mu H \quad (8)$$

in the domain  $W_1$  with boundary conditions

$$E_x = 0, \quad E_z = 0 \quad \text{for} \quad x = 0, \quad x = a; \quad E_y = 0, \quad E_z = 0 \quad \text{for} \quad y = 0, \quad y = b; \quad (9)$$

$$E_\tau(x, y, 0) = e(x, y), \quad H_\tau(x, y, 0) = h(x, y), \quad (10)$$

here  $E_\tau, H_\tau$  are the tangential components of vectors  $E, H$ .

**Lemma 2** *The Cauchy type problem (8) – (10) has a solution in the class of outgoing into infinity solutions if and only if*

$$e(x, y) = \int_0^a \int_0^b K(s, t; x, y) h(s, t) ds dt, \quad (11)$$

here  $K(s, t; x, y)$  is the functional matrix  $2 \times 2$  with elements of the form

$$\text{const} \sum_n \sum_m \frac{nm}{\gamma_{nm}} \varphi_{nm}(s, t) \psi_{nm}(x, y),$$

$$\varphi_{nm}(s, t), \psi_{nm}(x, y) = \sin \frac{\pi ns}{a} \cos \frac{\pi mt}{b} \quad \text{or} \quad \cos \frac{\pi ns}{a} \sin \frac{\pi mt}{b},$$

$$\gamma_{nm} = \sqrt{k_0^2 \varepsilon_1 - (\pi n / a)^2 - (\pi m / b)^2}.$$

## INCLINED MEDIUM INTERFACE IN THE RECTANGULAR WAVEGUIDE

Let the planes  $x = 0$ ,  $x = a$ ,  $y = 0$ ,  $y = b$  be the walls of rectangular waveguides and let the rectangle  $P: z = x \tan \theta_1 + y \tan \theta_2$  separate the waveguide into two parts with different dielectric indexes.

**Theorem 2** *The diffraction problem of electromagnetic wave on the inclined interface medium is equivalent to the boundary value problem for the Maxwell system (8) with boundary conditions (9), non-homogeneous boundary condition of the form (11) on the sides  $z = 0$ ,  $z = c$  and conjunction conditions on the rectangle  $P$ .*

## METALLIC PLATE ON THE MEDIUM INTERFACE

If the metallic plate  $M$  is placed on the medium interface, then the conjunction conditions are to be replaced by the following ones: the tangential components of vector  $E$  are equal to zero on  $M$  and the tangential components of vectors  $E$  and  $H$  are continuous on the other part of the barrier. This fact is insignificant for the formulations of Theorem 1 and Theorem 2, but the calculation scheme will be more complicate. New unknown variables are added to the set of variables during the direct action of calculation for every node placed on the metallic plate, and size of linear algebraic system will increase.

The numerical method for solving this boundary value problem is constructed and is investigated by abstract approximate scheme also.

## REFERENCES

- [1] Pleshchinskaya I.E., Pleshchinskii N.B., The Cauchy problem and potentials for elliptic partial differential equations and some of their applications. Advances in Equations and Inequalities (A.E.I.) (ed. J.M. Rassias), Athens, Greece, 1999.
- [2] Pleshchinskii N.B., Tumakov D.N. Partially domain method for scalar coordinate problems of electromagnetic waves diffraction in the spaces of distributions // Preprint 2000-1. Kazan Math. Soc. – Kazan, 2000. – 50 pp.
- [3] Pleshchinskii I.N. Numerical method of solving of electromagnetic wave diffraction problem on an inclined metallic plate in place waveguide // Proc. Math. Lobachevsky Center. V.13. Kazan Math. Soc. – Kazan: DAS, 2001. – P.197-204.
- [4] Pleshchinskii N.B. On the abstract theory of approximate methods for solving linear operator equations // Izv. Vuzov. Matematika. – 2000. – No. 3. – P.39-47.

# **COMPOSITE MEDIA AND METAMATERIALS**



## THE SECOND OR THE THIRD HARMONIC GENERATION ON A NONLINEAR FILM IN A BRAGG RESONATOR

V. F. Borulko

Dept. of Radiophysics, Dnipropetrovsk National University, 13 Naukova St.,  
Dnipropetrovsk 49050 Ukraine

Tel: 38 056 7254592, E-mail: borulko@hotmail.com

### ABSTRACT

A resonator formed by nonperiodic Bragg structure and nonlinear film is considered. Effects of the second or the third harmonic generation are theoretically investigated. System of nonlinear equations for amplitudes of time harmonics is obtained. Phenomenon of resonant increasing of amplitude of the higher harmonic caused by combination of nonlinear and Bragg effects is discovered. Reason of instability of numeric algorithm for "optimal" case is revealed. Ways for overcoming this instability are found. Bistable behavior of scattered waves is observed for cubic nonlinearity.

### INTRODUCTION

If a harmonic plane wave falls on a nonlinear film scattered field contains higher harmonics (the second harmonic for quadratic non-linearity or the third one for cubic non-linearity). As a rule values of non-linearity and amplitude of fundamental harmonic is not very large so that amplitudes of generating higher harmonics are usually small [1]. Higher-harmonic amplitude is increased under phase-matching condition that can be achieved more easily in nonlinear spatially periodic waveguiding structure [2]. Amplitude of wave falling onto nonlinear film can be increased also by situating nonlinear film into resonator. Non-periodic Bragg structures used as resonator reflector [3] have flexible frequency characteristics so that they can be useful for devices operating on some frequencies simultaneously.

### METHOD OF ANALYSIS

In the paper physical effects in a resonator formed by non-periodic Bragg reflector and non-linear film situated on metal plane are theoretically considered. The boundary-value problem for  $H_x$  contains spatial inhomogeneity in wave equation and non-linearity in quasiimpedance boundary condition

$$\frac{\partial^2 H}{\partial y^2} - \frac{1}{\varepsilon} \frac{\partial \varepsilon}{\partial y} \frac{\partial H}{\partial y} - \frac{\varepsilon(y)}{c^2} \frac{\partial^2 H}{\partial t^2} = 0, \quad (1)$$

$$\left[ \frac{\partial H}{\partial y} - \frac{1}{c^2} \frac{\partial^2}{\partial t^2} (w_0 H + w_N H^q) \right]_{y=0} = 0. \quad (2)$$

where  $w_0$  is unperturbed values of impedance parameter,  $w_N$  is parameter describing non-linearity of film,  $q = 2$  (quadratic non-linearity) or  $q = 3$  (cubic non-linearity). For quasiperiodic Bragg structure permittivity as function of coordinate  $y$  has form:

$$\varepsilon(y) = \varepsilon_a + \beta \sum_j \varepsilon_j(\beta y) \exp[i\psi_j(y)], \quad (0 < y < y_b) \quad (3)$$

$\psi_j(y) = \int \chi_j(\beta y) dy$ ,  $y_b$  is coordinate of Bragg-structure beginning,  $\beta$  is small parameter [3]. If the non-linearity is very small, undepleted pump approximation could be used [4].

This approach is easy for implementation, but it does not allow one to take into account changing energy of fundamental harmonic. We suppose that plane time-periodic wave ( $T = 2\pi/\omega$  is time period) falls on the structure. Along with real function  $H(y, t)$  we consider complex function  $H_c(y, t)$ . The solution of the boundary-value problem (1), (2) for  $H(y, t)$  and  $H_c(y, t)$  will be searched as a sum of monochromatic waves

$$H_c(y, t) = \sum_{n=1}^N a_{cn}(y) \exp(in\omega t), \quad a_{cn}(y) = a_m(y) + ia_m(y), \quad (4)$$

$$H(y, t) = \text{Re}[H_c(y, t)] = \sum_{n=1}^N [a_m(y) \cos(n\omega t) - a_m(y) \sin(n\omega t)], \quad (5)$$

A linear spatial problem must be solved for each frequency harmonic to obtain transmission matrices of Bragg structure.

$$\frac{d^2 a_{cn}}{dy^2} - \frac{1}{\varepsilon} \frac{d\varepsilon}{dy} \frac{da_{cn}}{dy} + \varepsilon(y) n^2 k_0^2 a_{cn} = 0, \quad k_0 = \omega/c, \quad (6)$$

If  $y > y_b$  functions  $a_{cn}(y)$  express propagation of direct and opposite plane waves

$$a_{cn}(y) = a_{bdn} \exp[i(y - y_b)k_b] + a_{bon} \exp[-i(y - y_b)k_b],$$

where  $k_b = k_0 \sqrt{\varepsilon(y_b)}$ ,  $a_{bdn}$  and  $a_{bon}$  are complex amplitudes of direct and opposite plane waves in beginning of Bragg-structure ( $y = y_b$ ).

Result of solving equations (6) is transmission matrices  $T_n$ , that couple amplitudes of direct and opposite waves in beginning and end of Bragg structure

$$a_{edn} = T_{n11} a_{bdn} + T_{n12} a_{bon}, \quad a_{eon} = T_{n21} a_{bdn} + T_{n22} a_{bon}, \quad (7)$$

where  $a_{edn}$  and  $a_{eon}$  are amplitudes of direct and opposite waves on surface of nonlinear

film ( $y = 0$ ). They are connected with values  $a_{cn0} \equiv a_{cn}(0)$  and  $a'_{cn0} = \left. \frac{da_{cn}}{dy} \right|_{y=0}$  by

following relations:

$$a_{cn0} = a_{edn} + a_{eon}, \quad a'_{cn0} = ik_e(a_{edn} - a_{eon}), \quad k_e = k_0 \sqrt{\varepsilon(0)}. \quad (8)$$

Granting nonlinearity of boundary condition it is more convenient to operate with real function  $H(y, t)$  and real spatial functions  $a_{rn}(y)$  and  $a_{in}(y)$  in (2). Taking into account expression (5), boundary condition (2) can be written in the form

$$F(t) \equiv H_d - k^2 w_0 H_u - k^2 w_n q H_0^{q-2} [(q-1)H_i^2 + H_0 H_u] = 0, \quad (9)$$

where  $H_d, H_0, H_i, H_u$  are auxiliary functions of time coordinate  $t$

$$H_d = \sum_{n=1}^N [a'_{r0n} \cos(n\omega t) - a'_{i0n} \sin(n\omega t)], \quad H_0 = \sum_{n=1}^N [a_{r0n} \cos(n\omega t) - a_{i0n} \sin(n\omega t)],$$

$$H_i = -\sum_{n=1}^N n [a_{r0n} \sin(n\omega t) + a_{i0n} \cos(n\omega t)], \quad H_u = -\sum_{n=1}^N n^2 [a_{r0n} \cos(n\omega t) - a_{i0n} \sin(n\omega t)].$$

Real parameters  $a'_{rn0}, a_{rn0}, a'_{in0}, a_{in0}$  are expressed in terms of complex parameters  $a'_{cn0}$  and  $a_{cn0}$

$$a_{rn0} = \text{Re}(a_{cn0}), \quad a_{in0} = \text{Im}(a_{cn0}), \quad a'_{rn0} = \text{Re}(a'_{cn0}), \quad a'_{in0} = \text{Im}(a'_{cn0}).$$

Introducing frequency-harmonic expansion into boundary condition (9) in discrete time points on time period we get system of non-linear equations with respect to harmonic

amplitudes on output from Bragg structure. Here we consider that amplitude of falling fundamental wave is specified on outer interface of Bragg reflector. Obtained non-linear system has been solved by numerical method based on Newton method with finite-difference approximation of derivatives.

### THE PHYSICAL EFFECTS

The most interesting phenomena occur at resonance and middle values (close to optimal ones) of non-linearity. In this case amplitude of fundamental harmonic near the film multiply exceeds the amplitude of falling wave, the amplitude of the reflected fundamental wave on outer interface of the resonator is close to zero, energy of falling wave almost completely transforms to energy of higher harmonics. Unfortunately near optimal values of parameters quasi-Newton method collapses. To overcome difficulty of algorithm convergence we describe the fundamental harmonic not by the wave amplitudes on outer boundary of the Bragg structure but by the amplitudes of the direct and reflected waves on the surface of the non-linear film.

Obtained solutions essentially depend on from type of non-linearity. For cubic non-linearity the amplitude of the wave falling onto the resonator as function of the amplitude of fundamental harmonic on the film is not monotonic thus dependences of amplitudes of all scattered waves have hysteretic character.

### CONCLUSIONS

Physical effects of scattering of a monochromatic plane wave on non-linear films situated in Bragg resonator are theoretically considered. Mathematical model of processes of higher-harmonic generation are derived. Influence of phase and amplitude parameters of Bragg reflection on amplitudes of scattered waves is investigated. Conditions of appearance of bistable regime are found. Obtained results can be used for designing generator, transformer and digital devices.

### REFERENCES

- [1] R. W. Boyd, *Nonlinear Optics* (Academic Press, San Diego, 1992).
- [2] X. Liu, H. Zhang, and M. Zhang, "Exact analytical solutions and their applications for interacting waves in quadratic nonlinear medium," *Opt. Express* **2**, pp. 83-97 (2002), <http://www.opticsexpress.org/abstract.cfm?URI=OPEX-10-1-83>
- [3] V.F. Borulko "Asymptotic method for Bragg reflection from media with nonperiodic perturbation of gyrotropy," in *Proceeding of the Fourth International Kharkov Symposium "Physics and Engineering of Millimeter and Sub-Millimeter Waves"* June 4-9, 2001, Kharkov, Ukraine, pp. 223-225.
- [4] M.Neviere, E.Popov, R.Reinisch, "Enhanced and reduced second harmonic generation in nonlinear corrugated waveguides," in *Proc. of the 1995 URSI Intern. Symposium on Electromagnetic Theory* (St. Petersburg, Russia) May, 1995, pp.547-549.

## ANALYTICAL INVESTIGATION OF PERIODIC MEDIA WITH NEGATIVE PARAMETERS

K. Vytovtov

Radiophysics Department, Dnepropetrovsk National University, Dnepropetrovsk-50, Ukraine  
49050, e-mail: vytovtov@mailru.com

### ABSTRACT

The electromagnetic properties of an artificial layered material with negative permittivity and permeability are studied analytically. To analyse the translation matrix method is employed. The translation matrix for multilayered structure is found in analytical form. The reflection and propagation coefficients of multilayered plate are written in analytical form. The propagation conditions of a wave within periodic layered structure with negative parameters are obtained in analytical form.

### INTRODUCTION

Materials with negative permittivity and permeability are very interesting at last time for theoretical and experimental investigation. The wave behavior within homogeneous material has been described in [1] at first. The experimental research proofing of existence of such media has been presented in [2]. The possible kinds of different material with negative parameters have been described in [2,3,4]. Probable applications of such material have been considered in [5]. Possibility of having negative permittivity and permeability in omega media for certain range of frequencies has been shown in [6].

However the periodic structures with negative parameters have not been considered. The problem of propagation and reflection by an inhomogeneous (layered) plate is also interesting for our consideration.

### STATEMENT OF THE PROBLEM

The layered medium with negative parameters  $\mu$  and  $\epsilon$  of the layers is considered in this work. Our purpose is investigation of the propagation conditions of the wave within an infinite periodic layered medium with arbitrary number of layers and the propagation and reflection coefficients of a multilayered plate. The translation matrix method is used for analysis. The translation matrix relates the field components and derivations at end of the period to these at beginning of this period. The propagation conditions will have been found in the analytical form also. Using the translation matrix the expressions of the propagation and reflection coefficients will have been written in analytical form.

### TRANSLATION MATRIX

Translation matrix of a layer with negative permittivity and permeability is

$$\mathbf{M}_l = \begin{pmatrix} \cos k_l z & j k_l \sin k_l z \\ j \sin k_l z & \cos k_l z \\ k_l & 0 \\ 0 & k_l \end{pmatrix}$$

The translation matrix for a multilayered structure is found as production of matrices of the layers and after mathematical transformations we can write

$$\mathbf{L}(\Lambda) = \sum_{q=1}^{2^{N-1}} \left\{ \frac{1}{2^{N-1}} f_{q,N} \sqrt{k_N/k_1} \times e^{\sum_{i=1}^{N-1} \text{Ln} \left( 1 + \frac{k_{i+1} f_{q,i+1}}{k_i f_{q,i}} \right)} \times \mathbf{L}_q \right\},$$

where

$$\mathbf{L}_q = \begin{vmatrix} \sqrt{\frac{k_1}{k_N}} \cos \left[ \sum_{i=1}^N (\varphi_i f_{q,i}) \right] & -j \sqrt{k_1 k_N} \sin \left[ \sum_{i=1}^N (\varphi_i f_{q,i}) \right] \\ -\frac{j}{\sqrt{k_1 k_N}} \sin \left[ \sum_{i=1}^N (\varphi_i f_{q,i}) \right] & \sqrt{\frac{k_N}{k_1}} \cos \left[ \sum_{i=1}^N (\varphi_i f_{q,i}) \right] \end{vmatrix},$$

$$f_{q,i} = \text{sign} \left\{ \sin \left[ \frac{\pi}{2^{N+1-i}} (2q-1) \right] \right\}.$$

is the optical thickness of the  $i$ -th wave.  $f_{q,i}$  is the function introduced in [7].

According with the stable theory the propagation conditions in an infinite medium is determined by the expression  $\text{tr} \mathbf{L} = \pm 2$ . Thus for the considered case we have

$$\left| \sum_{q=1}^{2^{N-1}} \frac{1}{2^{N-1}} f_{q,N} \left( \frac{k_N}{k_1} + \frac{k_1}{k_N} \right) \times e^{\sum_{i=1}^{N-1} \text{Ln} \left( 1 + \frac{k_{i+1} f_{q,i+1}}{k_i f_{q,i}} \right)} \cos \left[ \sum_{i=1}^N (\varphi_i f_{q,i}) \right] \right| = 2.$$

## PROPAGATION AND REFLECTION COEFFICIENTS

The propagation and reflection coefficients of multilayered plate are written in the form analogous to ones for an isotropic layered plate

$$R = \frac{(M_{11} + M_{12}\sigma_2)\sigma_1 - (M_{21} + M_{22}\sigma_2)}{(M_{11} + M_{12}\sigma_2)\sigma_1 + (M_{21} + M_{22}\sigma_2)} \quad T = \frac{2\sigma_1}{(M_{11} + M_{12}\sigma_2)\sigma_1 + (M_{21} + M_{22}\sigma_2)}$$

Here  $\sigma_{1,2}$  is the wavenumbers in first and second medium accordingly,  $M_{kl}$  is the element of the translation matrix.

## NUMERICAL EXAMPLE

For example the two-layered medium with the parameters  $\varepsilon_1 = -1.1$   $\varepsilon_2 = 12$   $\mu_1 = -1$   $\mu_2 = -1$   $d_1 = 7 \times 10^{-6}$   $d_2 = 0.1$  is considered. Wave propagation normal to the interfaces is studied.

The dependence of the module of the eigennumber of the translation matrix on frequency is shown in Fig.1 and Fig.2. As it is seen that in low frequency region there are propagation regions, but in high-frequency region there only points of propagation instead regions.

The dependence of the reflection coefficient on frequency is presented in Fig.3. In region to 5 GHz the reflection coefficient has resonances. The physical reason of this is the fact that the wave is not extinguished completely in the layer with negative parameters.

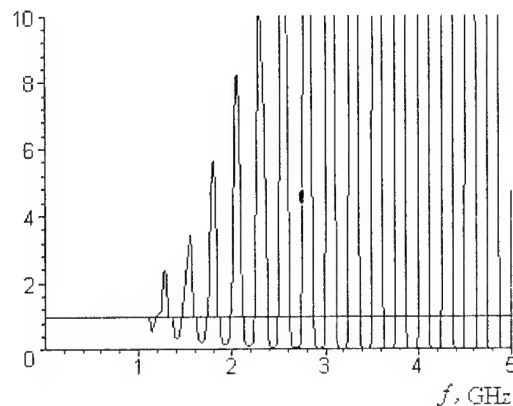


Fig.1. The dependence of the eigennumber of the translation matrix on frequency

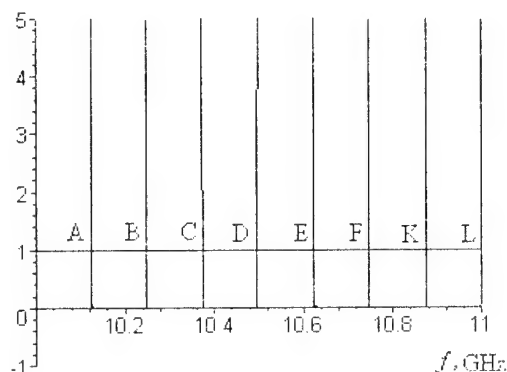


Fig.2. The dependence of the eigennumber of the translation matrix on frequency

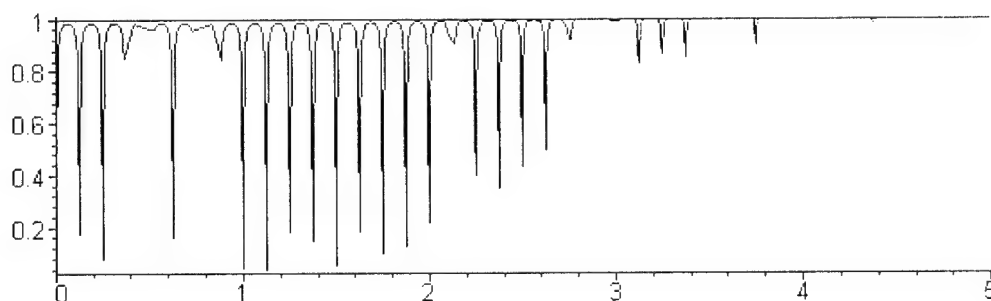


Fig.3. The dependence of the reflection coefficient on frequency

## REFERENCES

- [1] Veselago V. G. The electrodynamics of substances with simultaneously negative values of epsilon and mu. Soviet Physics Uspekhi v.10 N.4, pp.509-514, 1968.
- [2] Shelby R. A., et. al. Experimental verification of a negative index of refraction. Science, v.292, N. 5514, pp.77-79, 2001.
- [3] Ziolkowski R. W., Auzanneau F., Artificial molecule realisations of a magnetic wall, J. Appl. Phys., v. 82, N.7, pp. 3192-3194, 1997.
- [4] Smith D. R., Padilla W. J., et. al. A composite medium with simultaneously negative permeability and permittivity.-Appl.Phys. Lett., 2000.
- [5] Tretyakov S. A. Nefedov I. S., Maslovski S. I. et. al. Modelling and microwave properties of artificial materials with negative parameters.-NATO Adv. Research Workshop Bianisotropy 2002, p.34.
- [6] Saadoun M. M. I., Engeta N. Theoretical study of electromagnetic properties of non-local omega media.- Progress in Electromagnetic research, v.9.A. 1994, pp.351-397.

# INVESTIGATION OF COMPOSITE MATERIALS WITH CONTROLLABLE ELECTRODYNAMIC PROPERTIES

Ruslan. V. Kornev, Valerij. I. Demidchik.

Belarussian State University, Department of Radiophysics, Minsk, Belarus

E-mail: demidvi@bsu.by

## ABSTRACT

The method of electrodynamic analysis of single conducting fibres having various configuration is offered. Numerical experiments on studying the influence of wire elements geometry on properties of a scattered field are carried out and the possibility to control these properties is shown.

In recent time much attention of researchers is given to creation of various types of artificial composite materials having gyrotropic and anisotropic properties in microwave range. Such materials allow to project various waveguide microwave devices that can transform polarization of electromagnetic waves. Generally composite materials are a collection of particles of arbitrary geometry and internal structure embedded in a dielectric. Thus the main task is to define the effective material parameters of artificial medium knowing the sizes of separate inclusions and the nature of particle distribution in a dielectric.

The composite materials on the basis of conductive fibres are of interest for creating media with controllable properties. In this work the method for analyzing the properties of single fibre scattering is offered. This method can be used for later reconstruction of material parameters of a composite material. The analysis is based on the numerical solution of Poklington's integral equations for current distribution in a thin conductor (the so-called thin-wire approximation) by the collocation method with step basis function application [1]. Knowing the current makes it possible to define the field parameters scattered by the particle.

The wire structures that are widely used for constructing composite materials were

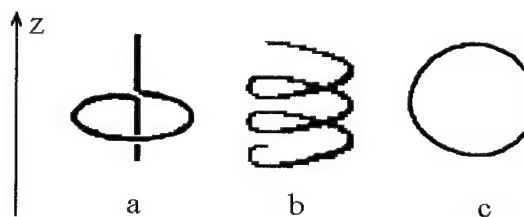


Fig. 1.

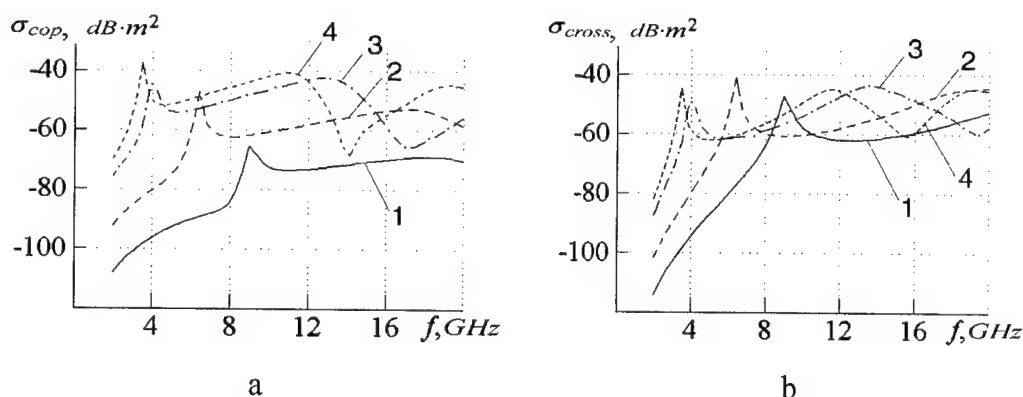


Fig. 2.

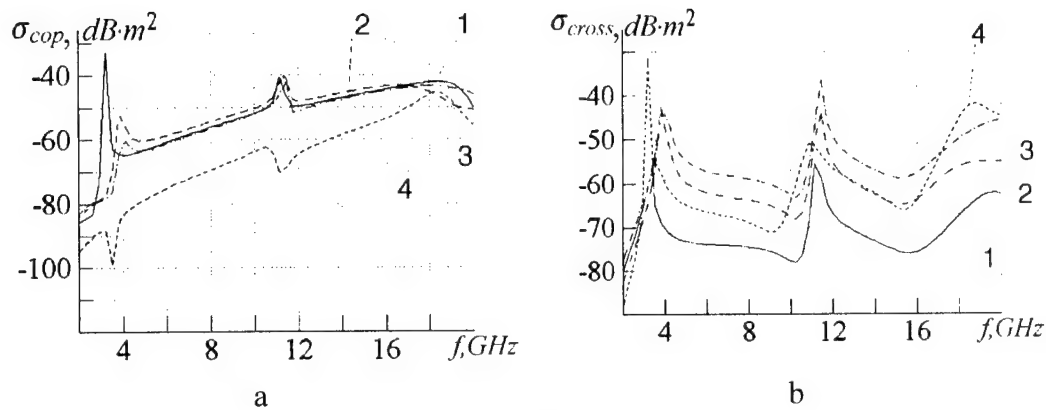


Fig. 3.

considered: a spiral particle with attached conductors, few-coil helix and omega-particles (fig. 1). The estimation of electrodynamic properties was carried out on the basis of analysis results of the radar cross section  $\sigma$  (RCS).

On fig. 2 the frequency dependences of co-polarized (fig. 2a) and cross-polarized (fig. 2b) RCS components for back-scattered radiation are shown at various vibrator lengths  $l$  of a particle represented on fig. 1a ( $l$ : 1 - 0; 2 - 2mm; 3 - 4mm; 4 - 8mm). The direction and polarization of the incident wave are chosen so that the  $\mathbf{H}$  vector was polarized along the axis  $Z$ . In this case the most effective interaction between an incident electromagnetic field and a particle is provided. The spiral radius is  $a=5\text{mm}$ , wire width is  $r_0=0.2\text{mm}$ . The spiral loop works as a receiver providing particle excitation, and vibrators of the particle are the source of the field parallel to axis  $Z$ . On fig. 2a one can see that the increase of vibrator length leads to little changes of copolarized RCS. It is the result of the vibrators being perpendicular to the copolarized field and not contributing to its production. At the same time the value of crosspolarized RCS (fig. 2b) is greatly increased when the vibrators length rises.

Similar dependences can be received by varying the spiral radius. In this case the variation of spiral radius  $a$  gives the considerable changes of copolarized RCS only at  $2\pi a < \lambda$ . Change of radius almost does not influence the crosspolarized RCS. In work [2] the research of interaction between similar particles was also carried out.

At the analysis of few-coil helices (fig. 1b) the direction of an incident wave is chosen

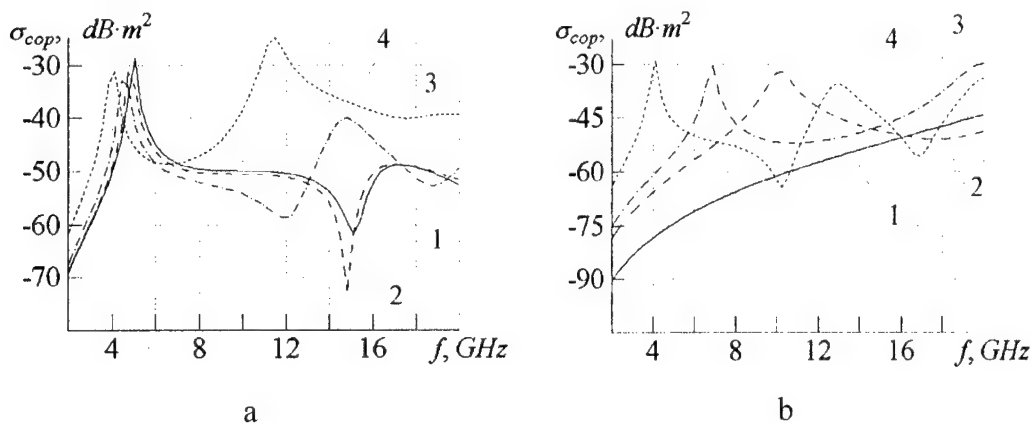


Fig. 4.



so that the  $\mathbf{H}$  vector was polarized along the axis  $Z$ . On fig. 3 the frequency dependences of the back-scattered RCS from a winding angle  $\alpha$  of the three-coil helix are given ( $\alpha$ : 1 – 5°; 2 – 15°; 3 – 30°; 4 – 60°). The total length of a helix  $l_{SP}$  is constant and equal  $l_{SP}=40\text{mm}$ . The results of calculation have shown, that the variation of the angle is effective up to the certain value (up to 30°) and essentially influences only crosspolarized RCS. The general features of dependence are determined only by the total helix length, not by the number of coils.

In case of an omega-particle (fig. 1c) the  $\mathbf{E}$  vector was along the vibrators and the  $\mathbf{H}$  vector was perpendicular to the planes of a particle loop. On fig. 4 the frequency dependences of back-scattered RCS on various length of vibrators  $l$  (fig. 4a.  $a=5\text{mm}$ ; length of vibrators  $l$ : 1 – 0; 2 – 2mm; 3 – 4mm; 3 – 8mm) and various loop radius  $a$  of the omega-particle (fig. 4b.  $l=5\text{mm}$ ; loop radius  $a$ : 1 – 0; 2 – 1mm; 3 – 2mm; 3 – 5mm). are shown. Apparently, the change of wire element geometry does not lead to considerable changes of scattered radiation power.

The results of calculations also show that RCS dependence from frequency has oscillatory feature that is caused by the resonance phenomena when the total length of a conductor is approximately equal to the whole number of half-waves. The empirical results and other authors' data [3] verify the similar character of frequency dependence RCS for chiral elements as few-coil helices.

In paper [4] the method for calculating effective material parameters of composites with known scattering characteristics of a single particle and the information about the whole structure is given. On this basis within the scope of thin-wire approximation the method for computing the effective dielectric permittivity and magnetic permeability of the composite materials containing conducting particles considered above is developed.

## REFERENCES

- [1] Demidchik V.I., Runov A.V., Kalashnikov N.V. // *Izvestia Vuzov, Radioelektronika*, (Russian) 1983. v. 26. №3. p.82-84.
- [2] Demidchik V.I., Kucharchik P.D., Kornev R.V. // *Izvestia GSU, (Gomel)*, (Russian), 2001, №5(8), p.63-66.
- [3] Marriotte F., Tretjakov S. A. // *IEEE Antennas and Propagation Magazin*. 1996. vol.38. №2. p.22-25.
- [4] Hizhnjak N.A. *The integrated equations of macroscopical electrodynamics*. Kiev, (Russian), 1986.

# SIMPLIFIED ANALYSIS OF SPLIT RING RESONATOR USED IN BACKWARD META-MATERIAL

Silvio Hrabar, Juraj Bartolic

Department of Radiocommunications and Microwave Engineering, University of Zagreb,  
Unska 17, Zagreb, HR-10000, Croatia, e-mail: Silvio.Hrabar@fer.hr

## ABSTRACT

A simple equivalent circuit of recently introduced split ring resonator (SRR) is proposed in this paper. It is shown that in the vicinity of resonant frequency, the SRR can be thought of electrically small, capacitively loaded loop antenna. Due to resonant behaviour of the antenna current, intensity of the magnetic field of the incoming plane wave may be locally decreased yielding a stop-band with negative effective permeability. Theoretical analysis was verified by measurements of the transmission coefficient of experimental structures in rectangular waveguide, in 10 GHz frequency band.

## INTRODUCTION

Recent introduction of 'left-handed' (or 'backward') meta-material (material with both  $\epsilon < 0$  and  $\mu < 0$ ) [1] has attracted a lot of attention. In such a material, the wave vector  $\mathbf{k}$  and Poynting vector  $\mathbf{P}$  are anti-parallel, causing reversal of some basic electromagnetic phenomena such as Snell law and Doppler effect. In original design [1], the negative permittivity was achieved with an array of thin wires, for which is well known to have dielectric function similar to that from dilute plasma. Negative permeability was achieved by a new type of inclusion coined 'split ring resonator', (SRR). So far, properties of SRR have been analysed numerically [1] and literature is sparse of simple engineering model.

## ANALYSIS OF SPLIT RING RESONATOR

The split ring resonator used in design of the first backward meta-material [1] is sketched in Fig.1.

The SRR comprises two concentric rings printed on a thin dielectric substrate and separated by

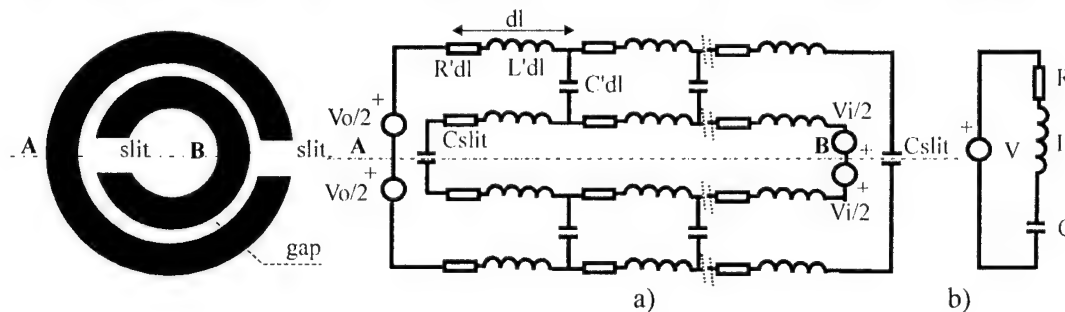


Fig. 1 The split ring resonator (SRR)

Fig. 2 a) The complete equivalent circuit of the SRR  
b) The simplified approximate equivalent circuit

a narrow gap. Each ring has a slit, and rings are oriented in such a way that slits are on the opposite sides of line of symmetry. The electrical dimensions of the SRR are much smaller than a wavelength of the impinging plane wave. Bearing this fact in mind, one can think of the SRR as two mutually coupled small loop antennas. The voltage induced in each antenna can be simply calculated from Faraday law:

$$V = -j\omega \mu_0 A H_i \quad (1)$$

Here,  $V$  stands for induced voltage,  $\omega$  stands for radial frequency,  $A$  and  $\mu_0$  stand for the loop area and free-space permeability, respectively. The symbol  $H_i$  stands for incident magnetic field,

which is assumed being perpendicular to the loop. The induced voltages are modelled as simple voltages sources located at point A (the source  $V_0$  - outer ring) and point B (the source  $V_i$  - inner ring). The complete equivalent circuit is sketched in Fig. 2a. The symbols  $R'$  and  $L'$  stand for distributed resistance and inductance respectively,  $C_{slit}$  stands for capacitance of the slits and  $C'$  stands for distributed capacitance of the gap between rings. In circuit from Fig. 2a one identifies two main loops (inner and outer ring) which are connected across the gap via distributed capacitance  $C'$ . It is important to notice that voltage  $V_0$  is always higher than voltage  $V_i$  by the ratio of areas formed by outer and inner ring, respectively (square of the ratio of radii of outer and inner rings). In SRR developed in [1], voltage  $V_0$  is approximately two times higher than voltage  $V_i$ . Thus, current essentially flows from the outer ring into inner ring across the gap. It flows through many branches formed by distributed capacitance  $C'$ . Due to this branching, current in outer ring changes with the location at the ring. It is maximal at point A, then decreases along the ring and reaches minimal value at the slit. All the currents, which flow from the outer ring into the inner ring, of course, contribute to the net current in inner ring. Therefore, the current in inner ring exhibits maximum at the location of voltage source  $V_i$  (point B), then decreases along the ring and reaches minimum at the slit. Contribution of the current which flows across the slit (through the  $C_{slit}$ ) to the net ring current is negligible, thus one can actually consider that  $C_{slit} = 0$ . Now, taking into account fact that currents flow predominantly across the gap, one can approximate the whole circuit with a much simpler circuit sketched in Fig. 2b. It comprises a single voltage source and a serial tank circuit. It actually means that a single, electrically small loop antenna loaded with a capacitor should behave very similarly to the SRR.

The simple analysis published elsewhere [3] shows that the magnetic field across the capacitively loaded loop antenna illuminated by a plane wave exhibits resonant behaviour:

$$H = H_i \left( 1 - j \frac{K\omega\mu_0 A}{R + j\omega L - j/\omega C} \right) \quad (2)$$

Here,  $R$  and  $L$  stand for intrinsic resistance and inductance of the loop, respectively,  $K$  is a constant, which describes geometry, and  $C$  denotes capacitance of the load. Alteration of the local magnetic field by the scattered field given by (2) is behaviour analogues to the magnetization of the magnetic material. Calculated intensity of the resultant local magnetic field (normalised on the incident field) is sketched in Fig. 3.

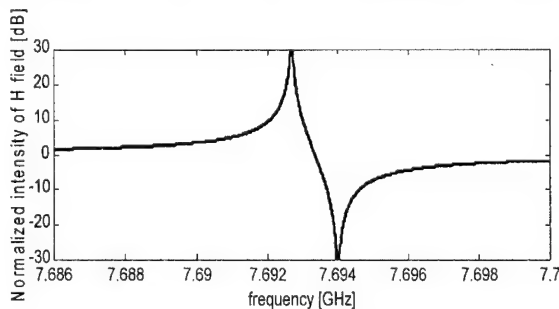


**Fig. 3** Calculated local magnetic field  
**Loop parameters:**  $K=1\text{m}^{-1}$ ,  $R=0.1\ \Omega$ ,  
 $L=26\ \text{nH}$ ,  $C=0.016\ \text{pF}$ ,  $S=0.07\ \text{cm}^2$

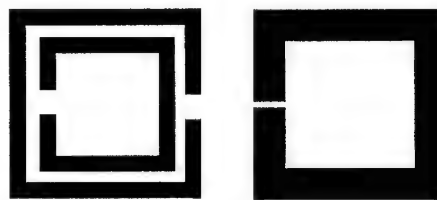


**Fig. 4** Left Experimental SRR  
 Right Experimental capacitively loaded loop

It can be seen that intensity of the resultant local magnetic field can be either higher or lower than intensity of the incident field. Thus, it is possible to achieve both paramagnetic ( $\mu > 0$ ) and diamagnetic ( $\mu < 0$ ) behaviour. Please note that curve in Fig. 3 is analogues to the curve of relative permeability of the SRR published in [2].

## EXPERIMENT

Two experimental structures have been fabricated on the ComClad substrate (thickness 0.5 mm,  $\epsilon_r=2.6$ ). The first structure (Fig. 4 - left) is the SRR, dimensions of which were scaled from those in [1] in order to achieve resonance around 9 GHz. The second structure (Fig. 4 - right) is a single loop loaded with a capacitor (narrow gap). The capacitance and inductance were calculated using approximate equations from the standard handbook [4]. Each structure was inserted into standard rectangular X-band waveguide. The structures were always oriented in such a way that there is a component of the magnetic field perpendicular to the loop (or rings), i.e., the substrate was perpendicular to the waveguide walls. The waveguide was excited in dominant TE 01 mode and  $S_{21}$  parameter was measured by HP 8720B network analyzer. The measurement results are given in Fig.5 and Fig 6.

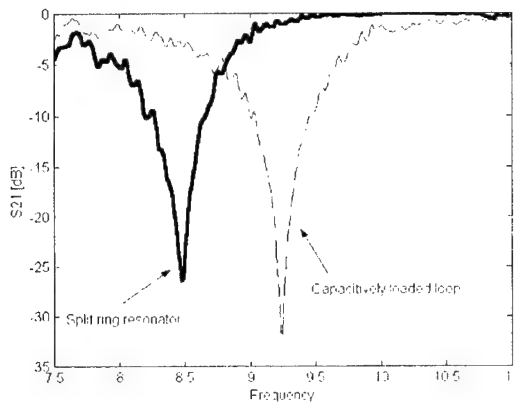


**Fig 5.** Magnitude of measured  $S_{21}$  parameter

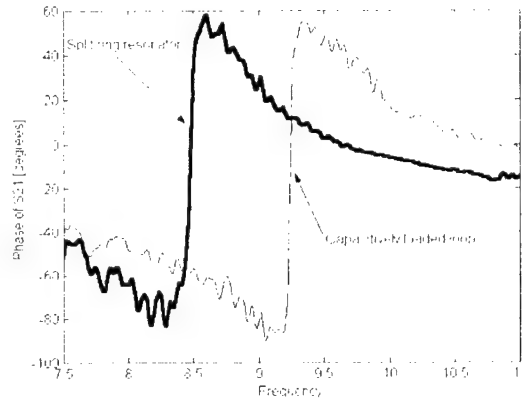


**Fig 6.** Phase of measured  $S_{21}$  parameter

One can notice that resonant frequencies of SRR and loaded loop are different, which is consequence of approximate equations used for design of the loop. Apart from this, behaviour of these two structures are very similar. Both structures exhibit a notch in transmission characteristic (Fig. 5) which corresponds with the serial resonance. Also, the curves of phase of  $S_{21}$  parameter (Fig.6) are very similar. It proves that SRR can indeed be thought of a small capacitively loaded loop antenna and background physics is essentially the same. By extension of above analysis, the approximate equation for effective permeability of an array of capacitively loaded loop antennas was derived. Also, the appropriate negative permeability meta-material was designed, fabricated and successfully tested. Details of this research can be found elsewhere [3].

## CONCLUSIONS

It is shown that SRR can be thought of capacitively loaded loop antenna. Such an antenna may increase or decrease local intensity of magnetic field of the incoming plane wave yielding both paramagnetic ( $\mu>0$ ) and diamagnetic ( $\mu<0$ ) behaviour.

## REFERENCES

- [1] D.R. Smith, et. al., 'A Composite Medium with Simultaneously Negative Permeability and Permittivity', *Appl. Phys. Letters*, Vol 84, No 18, pp 4184-4187, May 2000
- [2] J.B. Pendry, et. al., 'Magnetism from Conductors and Enhanced Nonlinear Phenomena', *IEEE Transactions on MTT*, Vol 47, No 11, pp 2075-2081, November 1999
- [3] S. Hrabar, Z. Eres, J. Bartolic, 'Capacitively Loaded Loop as Basic Element of Negative Permeability Meta-material', to be presented at European Microwave, Milan, 2002
- [4] C. R. Paul, 'Introduction to EMC', Wiley, New York 1992.

# THE ANALYTICAL METHOD OF INVESTIGATION OF FARADAY CHIRAL MEDIA

K. Vytovtov

Radiophysics Department, Dnepropetrovsk National University, Dnepropetrovsk-50,  
Ukraine 49050, e-mail: vytovtov@mailru.com

## ABSTRACT

A plane-parallel homogeneous bianisotropic plate under an oblique incidence of a plane harmonic wave is considered. The bianisotropy axis is not coincide with a normal to a plate. The propagation and reflection coefficients are found in the analytical form.

## INTRODUCTION

Electromagnetic of chiral and bianisotropic media is developing very extensively.. Wave behavior within infinite bianisotropic media have been analyzed in [1]. The phenomena at an interface between isotropic achiral and isotropic chiral materials have been studied in [2]. In that paper reflection and transmission by a chiral slab have been considered. Waves refracted by interface between an isotropic achiral and a bianisotropic materials have been investigated in [3]. The problem of reflection and propagation for an omega-slab has been considered in [4]. The problem of realization of soft-and-hard surfaces have been studied in [5]. Analogous problem has been studied in [6]. A bianisotropic slab under a normal incidence of a plane harmonic wave is investigated analytically in [7]. In this paper a bianisotropic slab under an oblique incidence of a plane harmonic wave is studied analytically. It is assumed also that the bianisotropy axis is not co-inside with a normal to a slab.

## STATEMENT OF THE PROBLEM

The homogeneous lossless bianisotropic medium described by the constitutive relations

$$\vec{D} = \epsilon \vec{E} + \zeta \vec{B} \quad \vec{H} = \xi \vec{E} + \mu^{-1} \vec{B} \quad (1)$$

is considered in this paper. The constitutive relations (eqn.1) contain four constitutive dyadics,  $\epsilon$ ,  $\xi$ ,  $\zeta$ ,  $\mu$ , in gyrotropic form:

$$a = \begin{bmatrix} a_{xx} & -ja_{xy} & 0 \\ ja_{xy} & a_{xx} & 0 \\ 0 & 0 & a_{zz} \end{bmatrix} \quad (2)$$

Our purpose here is to find the propagation and reflection coefficients of the homogeneous plane-parallel plate under an oblique incidence of a plane harmonic wave. It is assumed also that the bianisotropy axis is not coincide with a normal to the plate. For this it is necessary to obtained the wavenumbers of the refracted waves, to write the translation matrix for a plate, and to express the reflected and propagating fields as functions of the incident field.

## METHOD

The wavenumbers of the refracted waves are obtained by using the dispersion relation for the infinite bianisotropic medium and Snell's law taking into account the geometry

of the problem:

$$\begin{cases} a_4 k_{\text{refr } i}^4 + a_3 k_{\text{refr } i}^3 a_2 k_{\text{refr } i}^2 + a_1 k_{\text{refr } i} + a_0 = 0 \\ \cos \alpha = \frac{1}{k_{\text{refr } i}} \left( \cos \beta \sqrt{k_{\text{refr } i}^2 - k_{\text{inc}}^2 \sin^2 \alpha_{\text{inc}}} + k_{\text{inc}} \sin \beta \sin \alpha_{\text{inc}} \cos \psi \right) \end{cases} \quad (3)$$

where  $\beta$  is the angle between the bianisotropy axis and a normal to the interface,  $\psi$  is the angle between the incidence plane and the plane including the bianisotropy axis and a normal to the interface, the coefficients in the first equation (3) are:

$$\begin{aligned} a_4 &= A_{44} \cos^4 \alpha + A_{42} \cos^2 \alpha + A_{40} ; a_3 = A_{33} \cos^3 \alpha + A_{31} \cos \alpha ; \\ a_2 &= A_{22} \cos^2 \alpha + A_{20} ; a_1 = A_{11} \cos \alpha ; a_0 = A_{40} . \end{aligned} \quad (4)$$

$A_{kl}$  are the coefficients expressed in terms of the constitutive dyadic.

After algebraic transformations we obtain the dispersion relation for refracted waves in the form:

$$c_8 k^8 + c_6 k^6 + c_4 k^4 + c_2 k^2 + c_0 = 0 . \quad (5)$$

The translation matrix can be written using the well-known technique [8]:

$$\mathbf{L}(d) = \sum_{i=1}^4 \begin{pmatrix} \gamma_{11}^i \mathbf{M}_i & \gamma_{12}^i \mathbf{M}_i & \gamma_{13}^i \mathbf{M}_i & \gamma_{14}^i \mathbf{M}_i \\ \gamma_{21}^i \mathbf{M}_i & \gamma_{22}^i \mathbf{M}_i & \gamma_{23}^i \mathbf{M}_i & \gamma_{24}^i \mathbf{M}_i \\ \gamma_{31}^i \mathbf{M}_i & \gamma_{32}^i \mathbf{M}_i & \gamma_{33}^i \mathbf{M}_i & \gamma_{34}^i \mathbf{M}_i \\ \gamma_{41}^i \mathbf{M}_i & \gamma_{42}^i \mathbf{M}_i & \gamma_{43}^i \mathbf{M}_i & \gamma_{44}^i \mathbf{M}_i \end{pmatrix} , \quad (6)$$

where

$$\mathbf{M}_i = \begin{pmatrix} \cos(k_{z \ i} d) & -j \sin(k_{z \ i} d) \\ -jk_{z \ i} \sin(k_{z \ i} d) & \cos(k_{z \ i} d) \end{pmatrix} ; \gamma_{m,l}^i = 2h_{2m+1,2i+1} \frac{\det(\mathbf{B}_{2l+1,2i+1})}{\det(\mathbf{B})} . \quad (7)$$

$\mathbf{B}$  is the  $8 \times 8$  matrix obtained directly from Maxwell's equations.  $\mathbf{B}_{2l+1,2i+1}$  is the minor of the element with the indices  $2l+1, 2i+1$  of the matrix  $\mathbf{B}$ .  $\mathbf{M}_i$  is the  $2 \times 2$  matrix analogous to the one for an isotropic medium.

$\mathbf{L}(d)$  is  $8 \times 8$  in general case, but considering the particular cases it is possible to obtain  $4 \times 4$  translation matrix. This matrix (6) relates the field components and them derivations at both surfaces of the bianisotropic plate. The tangential field components are continuos at an interface, but for them derivations it is necessary to write the surface matrix. One must relate the field components and them derivations at both sites of an interface. Such matrix can be found directly from Maxwell's equations

$$\mathbf{U}_{\text{bianis}} = \mathbf{I} \mathbf{U}_{\text{isotr}} \quad (8)$$

$\mathbf{U}$  is the column-matrix including the tangential field components and them derivations. Therefore it is possible to write

$$\begin{pmatrix} E_{xm}^{\text{prop}}(d) \\ -j\sigma_2 E_{xm}^{\text{prop}}(d) \\ E_{ym}^{\text{prop}}(d) \\ -j\sigma_2 E_{ym}^{\text{prop}}(d) \\ -E_{ym}^{\text{prop}}(d)/\rho_2 \\ j\sigma_2 E_{ym}^{\text{prop}}(d)/\rho_2 \\ E_{xm}^{\text{prop}}(d)/\rho_2 \\ -j\sigma_2 E_{xm}^{\text{prop}}(d)/\rho_2 \end{pmatrix} = \mathbf{L}_1(d) \begin{pmatrix} E_{xm}^{\text{inc}}(0) + E_{xm}^{\text{refl}}(0) \\ -j\sigma_1 (E_{xm}^{\text{inc}}(0) - E_{xm}^{\text{refl}}(0)) \\ E_{ym}^{\text{inc}}(0) + E_{ym}^{\text{refl}}(0) \\ -j\sigma_1 (E_{ym}^{\text{inc}}(0) - E_{ym}^{\text{refl}}(0)) \\ -(E_{xm}^{\text{inc}}(0) - E_{xm}^{\text{refl}}(0))/\rho_1 \\ j\sigma_1 (E_{xm}^{\text{inc}}(0) + E_{xm}^{\text{refl}}(0))/\rho_1 \\ (E_{xm}^{\text{inc}}(0) - E_{xm}^{\text{refl}}(0))/\rho_1 \\ -j\sigma_1 (E_{xm}^{\text{inc}}(0) + E_{xm}^{\text{refl}}(0))/\rho_1 \end{pmatrix} \quad (9)$$

where  $\mathbf{L}_1(d) = \mathbf{I}^{-1} \mathbf{L} \mathbf{I}$ . After algebraic transformations the  $2 \times 2$  matrices relating incident, refracted and propagating fields are written as following:

$$\begin{pmatrix} E_x^{\text{refl}} \\ E_y^{\text{refl}} \end{pmatrix} = \mathbf{R} \begin{pmatrix} E_x^{\text{inc}} \\ E_y^{\text{inc}} \end{pmatrix}, \quad \begin{pmatrix} E_x^{\text{prop}} \\ E_y^{\text{prop}} \end{pmatrix} = \mathbf{T} \begin{pmatrix} E_x^{\text{inc}} \\ E_y^{\text{inc}} \end{pmatrix} \quad (10)$$

## CONCLUSIONS

The bianisotropic plate described by the constitutive relations (1) with all dyadic in gyrotropic under an oblique incidence of a plane harmonic wave is studied. The translation matrix of a homogeneous bianisotropic slab is written in analytical form. The reflection and propagation matrix of plane-parallel plate under an oblique incidence of a plane harmonic wave is found in analytical form.

## REFERENCES

- [1] Vytovtov K. A. Analytical investigation of electromagnetic waves in bianisotropic media.— IEE prociding microwave antennas and propagation v.148, N.4, pp.257–260, 2001.
- [2] Bassiri S., Papas C. H., Engeta N. Electromagnetic wave propagation through a dielectric-chiral interface and through a chiral slab.—J. Opt. Soc. Am. v. 5, pp.1450–1459, 1988.
- [3] Vytovtov K.A. The wavenumber of the electromagnetic waves in a bianisotropic medium.— J. Communications Technology and Electronics.—v.41.—№4.—2002
- [4] Mariote F., Sauviac B., Tretyakov S. Artificial bianisotropic composites.—Frontiers in electromagnetics, Inc. New York, 2000.
- [5] Viitanen A. J., Tretyakov S. A., Lindell I. V. On realization of generalizad soft-and-hard surface. — Radio Science, v. 35, N. 6, pp. 1257–1264, 2000.
- [6] Norgen M., He S. On the possibility of reflectionless coating of a homogeneous bianisotropic layer on a perfect conductor.—Electromagnetics, v.17, N. 4, pp. 295–307, 1997.
- [7] Semchenko I. V., Khakomov S. A., Tretyakov S. A., Sihvola A. H., Fedosenko E. A. Reflection and transmission by a uniaxially bi-anisotropic slab under normal incidence of plane waves.—J. Phys. D.: Appl. Phys. N.31, pp.2458–2464, 1998.
- [8] Gantmaher F. R. Theory of matrix.—M.: Nauka.—1967.

## SCATTERING OF A WAVE BEAM BY INHOMOGENEOUS ANISOTROPIC CHIRAL LAYER

A.V. Malyuskin, D. N. Goryushko, A.A. Shmat'ko, S.N. Shulga  
Kharkiv National University, Svobody Sq., 4, Kharkiv 61077, Ukraine  
E-mail: Alexander.V.Malyuskin@univer.kharkov.ua

### ABSTRACT

Wave beam scattering from uniaxial unidirectionally inhomogeneous lossy chiral layer is studied using Fourier spectral method. As an example reflection of the H-polarized Gaussian beam is analyzed and distinctive features of the reflected beam field distribution is revealed and graphically illustrated.

### INTRODUCTION

Layered chiral media with unidirectionally inhomogeneous parameters are potentially attractive for optoelectronic and microwave device design, e.g. for the fabrication of matching layers, which simultaneously transform the EM wave polarization. Plane wave scattering from layered chiral structures has been investigated in detail by many authors [1, 2]. In practice, however, electromagnetic fields of real sources and apertures substantially differ from plane waves but as a rule can be represented as partial plane waves continual superposition – wave beams [3, 4]. In the present study we consider the problem of the H-polarized Gaussian wave beam scattering from unidirectionally inhomogeneous anisotropic chiral layer.

### FORMULATION OF THE PROBLEM

Let us consider H-polarized Gaussian beam obliquely impinges on uniaxial chiral layer with material parameters varying with depth (Figure 1). The axis  $z$  of the global Cartesian coordinate system  $xyz$  is coincident with the axis of layer stratification. Material parameters of the slab are described by the second rank tensors  $\hat{\epsilon}, \hat{\mu}, \hat{\kappa}$ , that relate the components of the time harmonic,  $\exp(-i\omega t)$ , plane wave electric displacement  $\vec{D}$  and magnetic induction  $\vec{B}$  with fields  $\vec{E}, \vec{H}$

$$\vec{D} = \hat{\epsilon} \cdot \vec{E} + \hat{\kappa} \cdot \vec{H}, \quad \vec{B} = -\hat{\kappa} \cdot \vec{E} + \hat{\mu} \cdot \vec{H}. \quad (1)$$

Due to the uniaxial symmetry material tensors can be written in the form

$$\hat{\eta} = \eta_{\perp} \hat{I}_{\perp} + \eta_{\parallel} \vec{z}_0 \vec{z}_0,$$

where  $\hat{I}_{\perp} = \vec{x}_0 \vec{x}_0 + \vec{y}_0 \vec{y}_0$ , and

$$\eta_{\perp, \parallel}(z) = \eta_{\perp, \parallel} f(z), \quad \eta = \epsilon, \mu, \kappa.$$

Function  $f(z)$  specifies inhomogeneity profile of the slab. Magnetic field of the incident wave beam is polarized along the  $x$  direction,  $\vec{H}^{inc} = H_x^{inc} \vec{x}_0$ , with spatial magnetic field distribution represented as a continual sum of partial plane waves over spectral

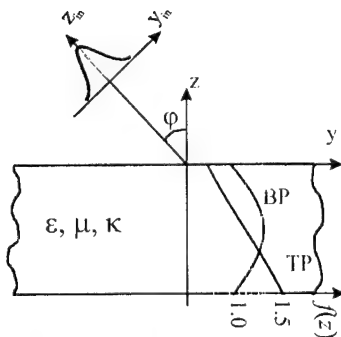


Fig. 1. Geometry of the problem



parameter  $k_{in}$ ,

$$H_x^{inc} = \int_{-\infty}^{\infty} U(k_{in}) \exp i(k_{in} y_{in} - \gamma_{in} z_{in}) dk_{in}. \quad (2)$$

In Eq. (2)  $\gamma_{in} = \sqrt{k_0^2 - k_{in}^2}$ ,  $k_0 = \omega/c$ . Physically  $k_{in}$  and  $\gamma_{in}$  determine the components of a partial plane wave vector in the local basis set  $x_{in} y_{in} z_{in}$ . The spectral density  $U(k_{in})$  is assumed to be  $U(k_{in}) = \exp(-b^2 k_{in}^2 / 4) H_n(k_{in} b / \sqrt{2})$ , where  $2b$  is a beam width,  $H_n(\cdot)$  is Hermite polynomial of the  $n$ -th order [5]. In the frames of spectral method the scattering beam field distribution is represented in the Fourier integral form

$$H_x^r = \int_{-\infty}^{\infty} R_{ss}(k) U(k_{in}) \exp i(ky + \gamma z) dk_{in}, \quad (3)$$

$$E_x^r = \int_{-\infty}^{\infty} R_{ps}(k) U(k_{in}) \exp i(ky + \gamma z) dk_{in}, \quad (4)$$

where  $k$  and  $\gamma$  determine the components of a partial plane wave vector in the global coordinate system,  $R_{ss}$  and  $R_{ps}$  are the partial plane wave reflection coefficients. The  $R_{ps}$  term describes EM wave polarization transformation due to chirality of the slab. The reflection coefficients  $R_{ss}$  and  $R_{ps}$  are obtained numerically using the finite-difference algorithm [2].

## NUMERICAL RESULTS AND DISCUSSION

As an example we consider the slab with material parameters  $\varepsilon_{\perp} = 2.1 + 0.2i$ ,  $\varepsilon_{\parallel} = 5.6 + 0.2i$ ,  $\mu_{\perp} = 1.10 + 0.1i$ ,  $\mu_{\parallel} = 1.22 + 0.1i$ ,  $\kappa_{\perp} = -0.01 + 0.2i$ ,  $\kappa_{\parallel} = -0.01 + 0.2i$ , homogeneous and inhomogeneous with barrier and transitional profiles  $f(z)$ , which are schematically indicated in figure 1 as "BP" and "TP" respectively.

Figure 2 delineates how the changes of the material inhomogeneity profile affect the partial plane wave reflection coefficient module and phase. The main interesting feature is the Brewster angle and phase steepness behavior. It should be noted that the crucial role plays chirality parameter  $\kappa_{\perp}$ : increasing of  $\kappa_{\perp}$  leads to smoothing of the sharp variation of the reflection coefficient phase and module and to shifting of the Brewster angle position in the incidence angles scale. Scattering beam field distribution in the near zone ( $z = 0$ ) is shown in the Figures 2b and 2c. Gaussian beam of the width  $4\lambda$  with spectral density described by the first order Hermite polynomial incident on the slab at the angle  $\varphi = 46.8^\circ$ . Fig. 2b illustrates strong distortions of the beam shape – reflected beam splitting (occurred in the copolarized component) and the beam axis displacement. These distortions are caused by sharp variations of the partial plane wave reflection coefficient module and phase near the critical angle. In the case of inhomogeneous slab with described profiles reflected beam splitting is absent, but beams axial displacement, proportional to the first derivative of the reflection coefficient phase, is still substantial. In the far field zone the reflected beam spatial distribution becomes smoother.

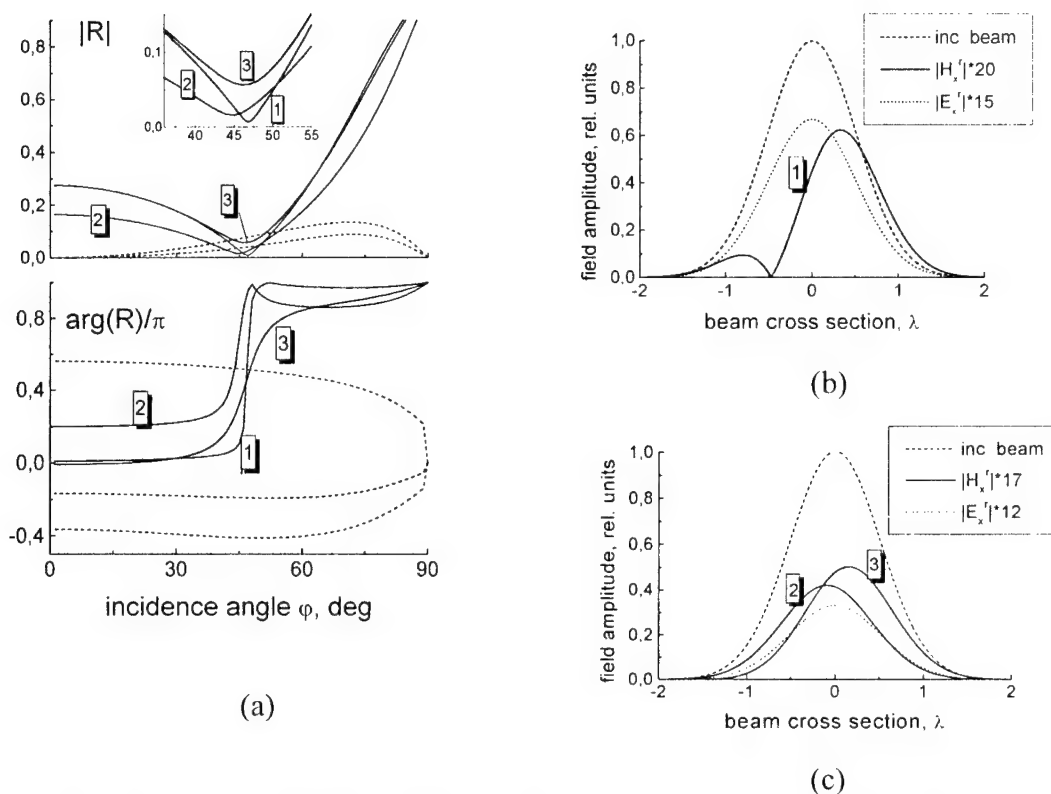


Fig.2. Partial plane wave reflection coefficients (2a) and scattering beam field distribution (b,c) in the near zone. Curve 1 – homogeneous layer, 2 – inhomogeneous layer, barrier profile, 3 – transitional profile. For fig. 2a solid curves –  $R_{ss}$ , dashed curves –  $R_{ps}$

## CONCLUSION

The problem of Gaussian wave beam scattering from anisotropic lossy inhomogeneous chiral layer is solved using spectral Fourier method. It has been shown that for the case of H-polarized beams strong distortions – reflected beam splitting and beam axis displacement – dependent on the material parameters inhomogeneity are occurred. Results of the undertaken investigation can be applied in the theory of the wave beam shaping control and remote sensing of chiral media.

## REFERENCES

- [1] Lindell I. V., Sihvola A.H. // IEEE Trans. Antennas Propagat. – 1995. – Vol. 43, № 12. – P. 1397 – 1404.
- [2] Zhuck N. P., Malyuskin A.V., Shulga S. N. // Radiotekhnika i Elektronika. – 2000. – V. 45, № 6. – P. 654 – 661.
- [3] Arnaud J.A. Beam and Fiber Optics. N.Y.: Academic, 1976.
- [4] Brekhovskih L. M. Waves in Layered Media. Moscow, 1957.
- [5] Goncharenko A. M. Gaussian Light Beams. Minsk, 1977.

## MODELING OF ELECTROMAGNETIC FIELD FROM MOBILE PHONE DISTRIBUTED IN THE HUMAN HEAD PHANTOM

Victor Goblyk, Yevheniya Yakovenko

Lviv National University "Lvivska Polytechnica", Lviv, Ukraine

This work is a development of ideas originally presented in [1, 2]. In the work [1], a general equation for the modeling of electromagnetic field in a inhomogeneous dielectric environment was given. In the work [2], this approach was used for the hyperthermia problems solution. In our work the modeling of electromagnetic field from a mobile phone distributed in the human head phantom was carried out. The modeling was done by the integral equation method with unknown polarization currents induced by the mobile phone antenna. The induced current distribution was determined in inhomogeneous environment with complex-valued dielectric permittivity.

Existing EMC standards take into consideration thermal influence of EM fields and restrict the average specific absorption rate (SAR) in the human body. But in the case when the wavelength in biological environment is smaller then the body size, the EM-field distribution becomes irregular and its level can be higher than limit value. With increasing of mobile phone frequencies this problem becomes more and more actual.

For investigations of EM field from mobile phone distributed in the human head, a mathematical model has been elaborated. In this model development, we have modified the approach used by authors of [2] for solving hyperthermia problems.

The model used in [1] and [2], was changed according to specific radiation source. The human body electromagnetic properties were characterized by complex-valued dielectric permittivity varying from point to point. After that the problem of dielectric inhomogeneous body heating by radiation source was solved. When solving integral equation with unknown polarization currents, we used a numerical method.

As initial one, the following integral equation was taken:

$$\frac{-1}{i \cdot \omega \cdot \varepsilon} \cdot (\text{grad div} + k^2) \cdot \int_V \bar{J}(\bar{r}') \cdot G(\bar{r} - \bar{r}') dV + \frac{\bar{J}(\bar{r})}{i \cdot \omega \cdot [\varepsilon'_a(\bar{r}) - \varepsilon]} = E^{\text{in}}(\bar{r}), \quad (1)$$

where  $J = i \cdot \omega \cdot (\varepsilon'_a - \varepsilon) \cdot E$  is the polarization current,  $G$  is the Green's function,  $E^{\text{in}}$  is the incident EM-field amplitude.

The use of the grid method and by presenting the polarization currents as a superposition of trial functions enables us to transform integral equation (1) into linear equations system. At the first stage of the model elaboration the case of a body with constant shape and electromagnetic parameters along the Z-axis was studied. Polarization currents in every cell were characterized by piecewise-linear functions. Special features of EM field distributed in human phantom were obtained and analyzed.

## REFERENCES

- [1]. Y.N. Vasiliev, *Applied Electromagnetics*, 1976, no 1, p. 94 (in Russian).
- [2]. A. Khzmalyan, A. Chaplin, *Electromagnetic Model of Hyperthermia*, Moscow, Nauka, series Radio Engineering and Electronics, 1989 (in Russian).

## THE MECHANISMS OF GRAVITO-PHOTO-PHORESIS FOR AEROSOL AGGREGATES IN THE FREE-MOLECULAR REGIME

A.A. Cheremisin, Yu .V. Vassilyev

Research Institute of Physics & Engineering  
Krasnoyarsk State University,  
P.O.Box 8678, Akademgorodok, Krasnoyarsk, 660036, Russia  
Fax: (3912) 49-41-68, e-mail: cheremisin@nifti.krasnoyarsk.ru  
Krasnoyarsk State Technical University  
Kirensky str. 26, Krasnoyarsk, 660074, Russia

The gravito-photophoretic forces in the free-molecular regime are calculated for the some types of aerosol particles by using the Monte-Carlo method to estimate molecular transfer. The absorption cross sections of aggregate components are calculated according to the results of the light scattering theory for fractal systems obtained within the framework of Berry-Percival's method and in the work by S.D. Andreev.

It is shown that two types of gravito-photophoresis can contribute to the levitation of aerosol particles absorbing the Sun and the Earth's radiation. There is a well-known  $\Delta\alpha$ -gravito-photophoresis [1] caused by a difference in the thermal accommodation coefficient, and there is a  $\Delta T$ -gravito-photophoresis, when the aerosol aggregate consists of individual particles differing in temperature due to a difference in the physical properties and the radiation absorption power.

Both mechanisms can induce large-value lifting forces able to provide a vertical transport of aerosol particles into the upper atmosphere. A connection between the existence of aerosol layers at the altitudes near 20, 50, 70-100 km in the real Earth's atmosphere, according to the results of our space observations in the ultraviolet range [2], and a condition of the balance of photophoretic and gravity forces is shown.

### REFERENCE

- [1] R.F. Pueshel, S. Verma, H. Rohatschek, G.V. Ferry, N. Boiadjieva, S.D. Howard, A.W. Strawa. Vertical transport of anthropogenic soot aerosol into the middle atmosphere. *J. Geophys. Res.*, 2000, vol. 105, No. D3, pp. 3727-3736.
- [2] A. Cheremisin, L. Granitskii, V. Myasnikov, N. Vetchinkin. Improved aerosol scattering in the upper atmosphere according to data of ultraviolet observations from space, with instrumental smoothing taken into account, *SPIE*, 2000, vol. 4341, pp. 383-389.

# **ANALYTICAL REGULARIZATION**

# THE PLANE H-POLARIZED WAVE DIFFRACTION BY A METAL GRATING WITH A MAGNETOACTIVE PLASMA

A.V. Brovenko, P.N. Melezhik, and A.Ye. Poyedinchuk

Institute of Radiophysics and Electronics, NAS of Ukraine  
12 Academic Proskury Str., 61085, Kharkov, Ukraine  
E-mail: chuk@ire.kharkov.ua

A periodic grating of infinitely thin, perfectly conducting metal strips is considered in the  $yOz$  plane. The  $d$ -spaced strips are extending along the  $oZ$  axis, the grating period is  $l$ . The subspace  $x < 0$  is occupied by a magnetoactive plasma with the magnetic field having the  $oZ$  direction. The plasma is characterized by the tensor

$$\hat{\varepsilon} = \begin{pmatrix} \varepsilon_1 & i\varepsilon_2 & 0 \\ -i\varepsilon_2 & \varepsilon_1 & 0 \\ 0 & 0 & \varepsilon_3 \end{pmatrix},$$

where  $\varepsilon_1 = 1 - \frac{\chi_p^2}{\chi^2 - \chi_c^2}$ ,  $\varepsilon_2 = -\frac{\chi_p^2 \chi_c}{\chi(\chi^2 - \chi_c^2)}$ ,  $\varepsilon_3 = 1 - \frac{\chi_p^2}{\chi^2}$ , and  $\chi = \frac{\omega l}{2\pi c}$ ,  $\chi_p = \frac{\omega_p l}{2\pi c}$ ,

$\chi_c = \frac{\omega_c l}{2\pi c}$ ;  $\omega = kc$  is the incident field frequency,  $\omega_p$  and  $\omega_c$  are, respectively, the

plasma and electron cyclotron frequencies,  $c$  is the velocity of light in vacuum.

From above ( $x > 0$ ), a plane  $H$ -polarized electromagnetic wave  $e^{-ikx}$  is normally incident on the grating plate. The time dependence is chosen to be  $e^{-i\omega t}$ . The field of the wave diffraction by the grating-plasma structure is necessary to find.

The diffraction field (function  $V_1(x, y)$  and  $V_2(x, y)$ ) sought in terms of the boundary value problem:

$$\varepsilon_1 \Delta V_2(x, y) + k^2 (\varepsilon_1^2 - \varepsilon_2^2) V_2(x, y) = 0, \quad x < 0; \quad (1)$$

$$\Delta V_1(x, y) + k^2 V_1(x, y) = 0, \quad x > 0;$$

$$V_j(x, y \pm l) = V_j(x, y), \quad j = 1, 2; \quad (2)$$

$$\left( \frac{\partial V_2(0, y)}{\partial x} - i\tau \frac{\partial V_2(0, y)}{\partial y} \right) = 0, \text{ on metal,} \quad (3.a)$$

$$\frac{\partial V_1(0, y)}{\partial x} = ik, \text{ on metal,} \quad (3.b)$$

$$\left( \lambda \frac{\partial V_1(0, y)}{\partial x} - \frac{\partial V_2(0, y)}{\partial x} + i\tau \frac{\partial V_2(0, y)}{\partial y} + i\lambda k \right) = 0, \text{ over grating period,} \quad (4)$$

$$(V_2(0, y) - V_1(0, y)) = 1, \text{ in slot.} \quad (5)$$

In addition, functions  $V_1(x, y)$  and  $V_2(x, y)$  must fit the Meixner and radiation conditions on any compact set in the  $xOy$  plane. Here  $\lambda = \frac{\varepsilon_1^2 - \varepsilon_2^2}{\varepsilon_1}$ ,  $\tau = \frac{\varepsilon_2}{\varepsilon_1}$ , and functions  $V_1(x, y)$  and  $V_2(x, y)$  are related to the scattered field component  $H_z(x, y)$  as follows

$$H_z(x, y) = \begin{cases} V_1(x, y); & x > 0, \\ \left(\varepsilon_1^2 - \varepsilon_2^2\right) V_2(x, y); & x < 0. \end{cases}$$

Satisfying boundary conditions (3)-(5) gives the system of dual series equations

$$\begin{cases} \sum_{(n, n \neq 0)} \frac{1 + \tau_n}{1 + \tau_n + \lambda} |n| x_n e^{\frac{2\pi}{l} i n y} = \frac{\chi i}{1 + \sqrt{\lambda}} (x_0 + 2) + \sum_{(n, n \neq 0)} \frac{1 + \tau_n}{1 + \tau_n + \lambda} |n| x_n \delta_n e^{\frac{2\pi}{l} i n y}, & \text{on metal,} \\ \sum_{(n)} x_n e^{\frac{2\pi}{l} i n y} = 0, & \text{in slot,} \end{cases} \quad (6)$$

with  $x_0 = b_0 \left(1 + \frac{1}{\sqrt{\lambda}}\right) - 2$ , where  $b_0 = \sqrt{\lambda} (1 - a_0)$ ,  $\tau_n = \text{sign}(n)$ .

For all  $n \neq 0$ ,  $x_n = \left(1 + \frac{\xi'_n + i\tau_n}{\lambda \xi_n}\right) b_n$ ,  $\xi_n = \sqrt{\frac{\chi^2}{n^2} - 1}$ ,  $\xi'_n = \sqrt{\lambda \frac{\chi^2}{n^2} - 1}$ ,  $a_n = -\frac{\xi'_n + i\tau_n}{\lambda \xi_n} b_n$ .

The values to find are amplitudes  $a_n$  and  $b_n$  of the diffraction spectra:  $a_0$  and  $b_0$  are, respectively, the reflection and transmission coefficients.

The authors' analytical regularization procedure suggested in [1] makes it possible to convert (6) into the infinite system of linear algebraic equations of the type

$$x_n = \sum_{m=-\infty}^{+\infty} B_{nm} x_m + w_n. \quad (7)$$

The matrix elements look like

$$B_{nm} = \begin{cases} \frac{\chi i (1 + \varepsilon_1 - \varepsilon_2)}{1 + \sqrt{\lambda}} A_{00}; & n = 0, m = 0, \\ (-1)^n A_{n0} \frac{\chi i (1 + \varepsilon_1 - \varepsilon_2)}{1 + \sqrt{\lambda}}; & n \neq 0, m = 0, \\ (-1)^m |m| \delta_m \Lambda_m A_{0m}; & n = 0, m \neq 0, \\ (-1)^{n+m} |m| \delta_m \Lambda_m A_{nm}; & n \neq 0, m \neq 0, \end{cases} \quad w_n = \begin{cases} \frac{2\chi i (1 + \varepsilon_1 - \varepsilon_2)}{1 + \sqrt{\lambda}} A_{00}; & n = 0 \\ \frac{2\chi i (1 + \varepsilon_1 - \varepsilon_2)}{1 + \sqrt{\lambda}} (-1)^n A_{n0}; & n \neq 0. \end{cases}$$

The  $A_{nm}$  expressions can be found in [1] and  $\Lambda_n = \begin{cases} 1; & n > 0, \\ \frac{1 + \varepsilon_1 - \varepsilon_2}{1 + \varepsilon_1 + \varepsilon_2}; & n < 0. \end{cases}$  For large  $m$ ,

the smallness parameter  $\delta_m \approx \left(\frac{\chi}{2m}\right)^2 \times \begin{cases} 1 + \varepsilon_1 - \varepsilon_2; & m > 0 \\ 1 + \varepsilon_1 + \varepsilon_2; & m < 0. \end{cases}$

So, it has been shown that matrix  $\|B_{mn}\|_{m,n=-\infty}^{+\infty}$  generates the Hilbert-Schmidt operator in  $l_2$ , and  $w_n \in l_2$ . Hence the solution of (7) can be obtained by truncation with any preassigned accuracy.

No wave transmission is found if  $\chi = \sqrt{\chi_c^2 + \chi_p^2}$  and  $\chi = \frac{1}{2}(\sqrt{\chi_c^2 + 4\chi_p^2} \pm \chi_c)$  because at these frequencies the plasma acts as a perfect reflector.

In the long-wave region, the reflection and transmission coefficients take the form

$$a_0 \approx \frac{\chi i A_{00}(1 + \varepsilon_1 - \varepsilon_2) + 1 - \sqrt{\lambda}}{\chi i A_{00}(1 + \varepsilon_1 - \varepsilon_2) - 1 - \sqrt{\lambda}}, \quad b_0 \approx \frac{2\sqrt{\lambda}}{1 + \sqrt{\lambda} - \chi i A_{00}(1 + \varepsilon_1 - \varepsilon_2)}. \quad (8)$$

$$\text{For } \frac{1 + \varepsilon_1 - \varepsilon_2}{1 + \varepsilon_1 + \varepsilon_2} > 0, \quad A_{00} = \frac{e^{-2\beta\theta}}{\pi} R_{\sigma}(\beta, \theta) \frac{2\theta\varepsilon_2}{1 + \varepsilon_1 - \varepsilon_2} - \frac{e^{-\pi\beta}}{2ch(\pi\beta)} (e^{-2\beta\theta} R_{\sigma}(\beta, \theta) + e^{2\beta\theta} R_{\sigma}(-\beta, \theta)),$$

$$\text{where } \beta = \frac{1}{2\pi} \ln \frac{1 + \varepsilon_1 - \varepsilon_2}{1 + \varepsilon_1 + \varepsilon_2}, \quad \theta = \pi \left(1 - \frac{d}{l}\right); \quad R_{\sigma}(\beta, \theta) = \sum_{n=-\infty, n \neq 0}^{+\infty} \frac{(-1)^n}{n} P_{n-1}(-\beta, \theta) \quad \text{with}$$

$P_n(\beta, \theta)$  being the Pollachek polynomials. Notice that if  $\chi_p$  and  $\chi_c$  are both zero together, expressions (8) turn into the standard Lamb formulae for a grating at no plasma medium.

$$\text{For } \frac{1 + \varepsilon_1 - \varepsilon_2}{1 + \varepsilon_1 + \varepsilon_2} < 0,$$

$$A_{00} = \frac{e^{-\pi\tilde{\beta}}}{2sh(\pi\tilde{\beta})} (1 - e^{2\tilde{\beta}\theta}) - \frac{2\varepsilon_2}{\varepsilon_2 - \varepsilon_1 - 1} \frac{\theta}{\pi} + \frac{e^{\tilde{\beta}(\theta - \pi)\theta}}{\pi} \int_0^{\theta} \sin(\tilde{\beta} \ln \frac{\sin \frac{\theta + \varphi}{2}}{\sin \frac{\theta - \varphi}{2}}) d\varphi,$$

where  $\tilde{\beta} = \frac{1}{2\pi} \ln \frac{\varepsilon_2 - \varepsilon_1 - 1}{\varepsilon_2 + \varepsilon_1 + 1}$ . The integral in  $A_{00}$  presents no calculation problems since

it can be represented as a well convergent series expansion in the polynomials  $B_n$  given

$$\text{in [1]. For } \tilde{\beta} = 0, \quad A_{00} = -\frac{\theta}{\pi}.$$

## REFERENCES

- [1] A.V. Brovenko, P.N. Melezhik, and A.Ye. Poyedinchuk, The regularization method to a class of dual series equations, *Ukrainian Math. Zh.*, 2001, v.53, no.10, pp.1320-1327 (in Ukrainian).



## WAVE DIFFRACTION BY AXIALLY SYMMETRICAL SYSTEM OF FINITE SOFT CYLINDERS

Eylem Özkan<sup>1</sup>, Fatih Dikmen<sup>1</sup>, Yury A. Tuchkin<sup>1,2</sup> Sergey I. Tarapov<sup>1,2</sup>

1. Gebze Institute of Technology, PK. 141, 41400 Gebze - Kocaeli, Turkey.

2. Institute of Radiophysics and Electronics, NAS of the Ukraine, 12 Ac. Proscura St.,  
Kharkov 61085, Ukraine.

### ABSTRACT

A new strong mathematically rigorous and numerically efficient method for solving the boundary value problem of scalar wave diffraction by a system of infinitely thin circular cylindrical screens is proposed. The method is based on a combination of Orthogonal Polynomials Method [1-2] and Analytical Regularization Method as used in [3,4,5]. The solution is generalization of the investigation done for one cylinder [6] and the method has been demonstrated on flat soft circular ring [6,7,8]. As a result of the suggested regularization procedure, the initial boundary value problem was equivalently reduced to the infinite system of the linear algebraic equations of the second kind, i.e. to an equation of the type  $(I + H)x = b$ ,  $x, b \in l_2$  - in the space  $l_2$  of square summable sequences. This equation can be solved numerically by means of truncation method with, in principle, any required accuracy. Pilot experiments show good perspective of such cylindrical reflector for development of individual antenna tag for rescue radar or broadcast systems in mm waveband.

Let surface  $S$  have the following property,

$$S = \bigcup_{j=1}^N S_j, S_j \cap S_{j+1} = \emptyset \quad (1)$$

$S$  is a system of finite circular cylinders located on  $z$ -axis defining, (Figure 1)

$$S_j = \{(z, \rho, \varphi) : z \in [\zeta_j - L_j, \zeta_j + L_j], \rho = a_j, \varphi \in [-\pi, \pi]\}, j = 1, 2, \dots, N. \quad (2)$$

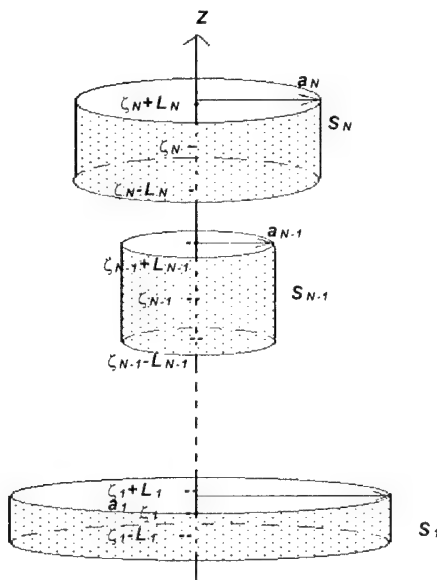


Figure 1

The following integral equation of the first kind is equivalent to the diffraction problem posed.

$$\int_S J_D(p) \cdot G(q, p) ds_p = -u^i(q); q \in S \quad (3)$$

where,  $u^i(q)$  is known incident wave,  $J_D(p)$  is unknown function i.e. current density like,  $J_D(p) = [d(p)]^{1/2} H(p)$ ,  $p \in S$ , where  $H(p)$  is a smooth function on surface  $S$ ,  $d(p)$  is the distance to the nearest edge of a ring,  $G(q, p)$  is the Green's function of free space.

The axially symmetry of the system of obstacles leads to an infinite system of one dimensional, non-interacting integral equations of the first kind below,

$$2\pi \sum_{j=1}^N a_j \int_{\zeta_j-L_j}^{\zeta_j+L_j} Z_m^j(z_p) G_m^{j,l}(|z_p - z_q|) dz_p = g_m^l(z_q), \quad z_q \in [L_l, L_l], \quad l=1,2,\dots,N, \quad (4)$$

in terms of Fourier coefficients.

Proper parametrization of the variable in the equation is required to use the Fourier-Chebyshev expansions defined on the interval  $[-1,1]$ . The parametrization to reduce the points on each  $S_j$  surface to such an interval is the following:

$$z_p^j = \eta^j(v) = \zeta_j + L_j v, \quad v \in [-1,1]; \quad (5)$$

$$z_q^l = \eta^l(u) = \zeta_l + L_l u, \quad u \in [-1,1]. \quad (6)$$

Then we have (4) reduced to:

$$\int_{-1}^1 \left\{ -\frac{1}{\pi} \ln|u-v| + K_m^{l,l}(u,v) \right\} \tilde{Z}_m^l(v) dv + \sum_{\substack{j=1 \\ j \neq l}}^N \int_{-1}^1 \tilde{G}_m^{j,l}(u,v) \tilde{Z}_m^j(v) dv = \tilde{g}_m^l(u);$$

$$u \in [-1,1], \quad l=1,2,\dots,N \quad (7)$$

Here  $K_m^{l,l}$  are sufficiently and  $\tilde{G}_m^{j,l}$  are infinitely smooth functions and it is possible to express those functions and the unknown function  $\tilde{Z}_m^j(v)$  using Fourier-Chebyshev series.

Therefore the final algebraic system of the first kind that (5) will be reduced to is

$$\gamma_n^{-2} z_n^l + \sum_{s=0}^{\infty} \left[ k_{ns}^{l,l} z_s^l + \sum_{\substack{j=1 \\ j \neq l}}^N k_{ns}^{j,l} z_s^j \right] = b_n^l, \quad n=0,1,2,\dots \quad l=1,2,3,\dots,N \quad (8)$$

and will be subject to analytical regularization in the same manner done for single obstacles (as done in [6-7-8]), easily by introducing new variables  $\hat{z}_n^l = z_n^l / \gamma_n$  and multiplying each term in (8) by  $\gamma_q$ . Here,  $\gamma_0 = (\ln 2)^{-1/2}$ ;  $\gamma_n = |n|^{1/2}$ ,  $n \neq 0$ , for every  $m=0, \pm 1, \pm 2, \pm 3, \dots$   $z_n^l$  and  $z_n^j$  are the Fourier - Chebyshev coefficients of the unknown function,  $b_n^l$  is Fourier - Chebyshev coefficients of the excitation term,  $k_{ns}^{j,l}$  and  $k_{ns}^{l,l}$  are Fourier - Chebyshev coefficients of the smooth kernels in (7).

Numerical results of the system  $ka_1=2$ ,  $ka_2=6$ ,  $ka_3=10$ ,  $kL_1=kL_2=kL_3=4$  in case of a normally incident plane wave, are following. In figure 4 the approximate locations of the surfaces are indicated.

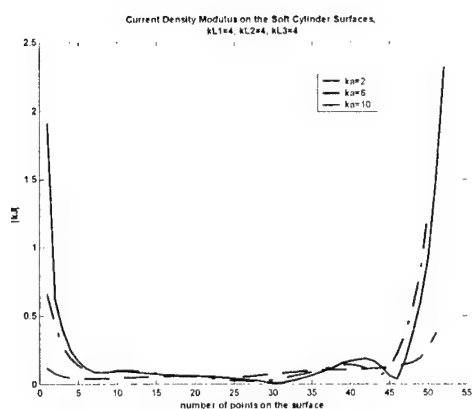


Figure 2: Current Density

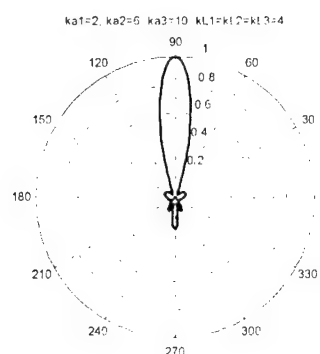


Figure 3: Far Field



Figure 4: Near Field

- [1] G.Ya.Popov. On one approximate method for solving the integral equation of wave diffraction by finite width strip - Zhurnal tekhnicheskoy fiziki, 1965. v. 35, n. 3. p.p. 381-389 (in Russian).
- [2] G.Ya.Popov. On Orthogonal polynomials method in contact problem of the elasticity theory - Prikladnaya matematika i. mekhanika, 1969, V. 33, N3 (in Russian)
- [3] Yu.A.Tuchkin. Wave scattering by unclosed cylindrical screen of arbitrary profile with Dirichlet boundary condition. - Soviet Physics Doclady, 1985, v. 30. p.p. 1027-1030
- [4] Yu.A.Tuchkin. Wave scattering by unclosed cylindrical screen of arbitrary profile with Neumann boundary condition. - Soviet Physics Doclady, 1987, v. 32, p.p. 213-216
- [5] Yu.A.Tuchkin. Regularization of boundary value problem of wave diffraction by toroidal screen of arbitrary profile - in the book: Electrodynamics of open structure of millimetre and sub-millimetre wave range. - Publishing house of IRE Acad. Sci. The Ukr. SSSR.Kharkov, 1990 (in Russian)
- [6] Fatih Dikmen, Eylem Özkan, Yury A. Tuchkin. Scalar Wave Diffraction from infinitely thin perfectly soft finite-length circular cylinder. Day On Diffraction 2001, International Seminar, St. Petersburg, May 29-31, 2001.
- [7] F. Dikmen, E. Karacuha, Yu.A. Tuchkin. Scalar Wave Diffraction by a Perfectly Soft Infinitely Thin Circular Ring. Turkish Journal of Electrical Engineering and Computer Sciences "Elektrik", Vol:9 No:21, 2001.
- [8] Yu.A. Tuchkin, E. Karacuha, F. Dikmen. Scalar Wave Diffraction from Infinitely Thin Circular Ring, Proc. of International Symposium on Mathematical Methods in Electromagnetic Theory - MMET'98, Kharkov, Ukraine.
- [9] E. Özkan, Fatih Dikmen, Eylem Özkan, Yury A. Tuchkin. Scalar Wave Diffraction by Perfectly Soft Thin Circular Cylinder of Finite Length ; Analytical Regularization. Turkish Journal of Electrical Engineering and Computer Sciences "Elektrik"(accepted, will be published).

## DIFFRACTION BY A SCREENED CHIRAL LAYER WITH A GRATING

Sergey B. Panin and Anatoly Ye. Poyedinchuk

Institute of Radiophysics and Electronics, NAS of the Ukraine,  
12 Academic Proskura Str., 61085, Kharkov, Ukraine,  
E-mail: panin@ire.kharkov.ua; chuk@ire.kharkov.ua

### ABSTRACT

Polarization characteristics of the reflecting structure like a chiral layer combined with a dielectric layer, both in between a diffraction grating and a screen, are considered. Due to the analytical regularization procedure derived from the Riemann-Hilbert problem method, the correspondent diffraction vector problem is solved in the form available for effective numerical treatment. The numerical investigation shows a number of the new diffraction features caused by the chiral medium presence.

### INTRODUCTION

A chiral inclusion can do more than vary one or another characteristic of the system, which takes it in. In cases, it imparts novel properties even to well-known structures, for example a cross-polarized component in the reflected field of a linearly polarized wave incident normally on an ordinary strip grating, attached to the isotropic chiral half space [1]. In view of the circular polarization of the chiral medium eigenwaves and due to the boundary conditions, the chiral medium binds both linear polarizations. On the one hand, this gives rise to the new interesting effects, but on the other hand it complicates the problem, which becomes then a vector one.

### PROBLEM FORMULATION AND SOLUTION

The structure of interest is shown in Fig.1. A half-space  $h_1 < z$  is a dielectric characterized by permittivity  $\varepsilon_1$  and permeability  $\mu_1$ . The dielectric layer ( $0 < z < h_1$ ) with the constitutive parameters  $\varepsilon_2, \mu_2$  and the chiral one ( $-h_2 < z < 0$ ) with  $\varepsilon_3, \mu_3$  and the chirality parameter  $\gamma$  are placed between the perfectly conducting screen ( $z = -h_2$ ) and the grating ( $z = h_1$ ) composed by infinitely thin and perfectly conducting strips parallel to the  $OX$  axis. The grating period is  $l$ , the slot width is  $d$ .

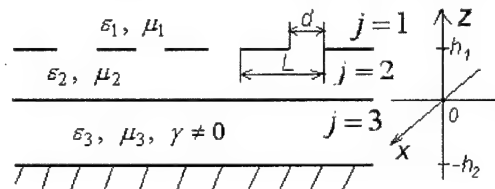


Fig.1. The structure profile.

The wave  $\mathbf{E}^i = \mathbf{E}_0 \exp(i(\mathbf{k}^i \mathbf{r} - \omega t))$ ,  $\mathbf{H}^i = \mathbf{H}_0 \exp(i(\mathbf{k}^i \mathbf{r} - \omega t))$  with  $\mathbf{E}_0 = (\tilde{e}, 0, 0)$  and  $\mathbf{H}_0 = (\tilde{h}, 0, 0)$  ( $\tilde{e}, \tilde{h}$  are complex) is obliquely incident on the grating so that

$\mathbf{k}^i = -2\pi\sqrt{\varepsilon_1\mu_1}/\lambda_0 \times (0, \sin\alpha, \cos\alpha)$ , where  $\alpha$  is the angle between the incident wave vector  $\mathbf{k}^i$  and the  $OZ$  axis. We seek to find the diffracted field.

In so far as the incident field is  $x$ -independent and the grating extends infinitely in the  $x$  direction, the problem can be solved in two-dimensional terms ( $\partial/\partial x \equiv 0$ ). For existence and uniqueness of the solution, the conditions [2] to satisfy are: Maxwell's equations; radiation condition; boundary conditions; quasiperiodicity condition, and condition of the field energy finiteness. For the considered two-dimensional problem, the field in the homogeneous chiral medium looks like [3]

$$\mathbf{E} = \mathbf{E}^+ + \mathbf{E}^-, \quad \mathbf{H} = \mathbf{H}^+ + \mathbf{H}^- = -i(\mathbf{E}^+ - \mathbf{E}^-)/\rho_3,$$

$$\Delta_{yz}u^\pm + k^\pm u^\pm = 0, \quad E_x^\pm = u^\pm(y, z), \quad k^\pm E_y^\pm = \mp \partial u^\pm / \partial z, \quad k^\pm E_z^\pm = \pm \partial u^\pm / \partial y,$$

where  $k^\pm = -k_3(1 \pm \eta)$ ,  $k_j = \omega\sqrt{\varepsilon_0\varepsilon_j\mu_0\mu_j}$ ,  $\eta = \gamma/\sqrt{\varepsilon_3\mu_3}$ ,  $\rho_j = \sqrt{\mu_0\mu_j/\varepsilon_0\varepsilon_j}$ . Thus all the field components are expressed through the  $E_x^\pm$ . The eigenwaves are right and left

circularly polarized waves with the propagation constants  $k^\pm$ . The discussed problem requires vector approach because the sought fields have all the components.

In view of that the medium interfaces coincide with the coordinate planes, our approach to this boundary problem solution is by the method of separation of variables. Anticipating existence of the solution, the grating periodicity along the  $OY$  axis enables the problem solution to be expanded into Fourier series for each structural region.

Substitution the series in Helmholtz equation ( $\Delta_{yz}u + k_j^2u = 0$  for the  $j=1,2$  domains and  $\Delta_{yz}u^\pm + k^{\pm 2}u^\pm = 0$  for  $j=3$ ) gives the field representation, which coincides with

the Rayleigh expansion of the diffracted field as an infinite series of partial waves of spatial spectrum. The wave propagation character is clear from the obtained field representation: the propagation constants of the  $n$ -harmonic are  $\xi_n = 2\pi n/l - k_1 \sin\alpha$  along

the  $OY$  axis and  $\zeta_n^j|_{j \neq 3} = \sqrt{(k_j)^2 - (\xi_n)^2}$ ,  $\zeta_n^\pm|_{j=3} = \sqrt{(k^\pm)^2 - (\xi_n)^2}$ ,  $(\text{Im}\zeta_n^{j,\pm} \geq 0)$  along

$OZ$ . The wave complex amplitudes are unknown Fourier coefficients.

Applying the boundary conditions to each surface one can relate the sought Fourier coefficients in the partial domains and obtain the two coupled systems of dual series equations involving trigonometric functions. The obtained systems are equivalent to an operator equation of the first kind in the Hilbert space given by the Meixner condition [2]. These systems are ill-conditioned, therefore the truncation technique is generally unappreciable. The analytical regularization can help us to get rid of this ill-conditioning and arrive at the form admitting effective numerical and analytical treatment [2,4].

## NUMERICAL RESULTS

Introduce the structure efficiency in the  $n$ -order of spectrum  $R_n^x, R_n^y$ , which determines the relative part of scattered energy spread from the structure to the upper half-space by

the traveling  $n$ -harmonic ( $\zeta_n^1 > 0$ ) with the wave vector  $\mathbf{k}_n^1 = (0, \xi_n, \zeta_n^1)$ . The upper indexes respectively relate to the field of E- and H- polarizations (E-polarization when  $\mathbf{E} \parallel OX$  and H-polarization when  $\mathbf{H} \parallel OX$ ). Let us call major polarization that of incidence, then the cross one is that normal to it. The values  $R_0^x, R_0^y$  as a functions of  $\chi = l/\lambda_0$  and  $H_2 = h_2/l$  are represented in Fig.2.

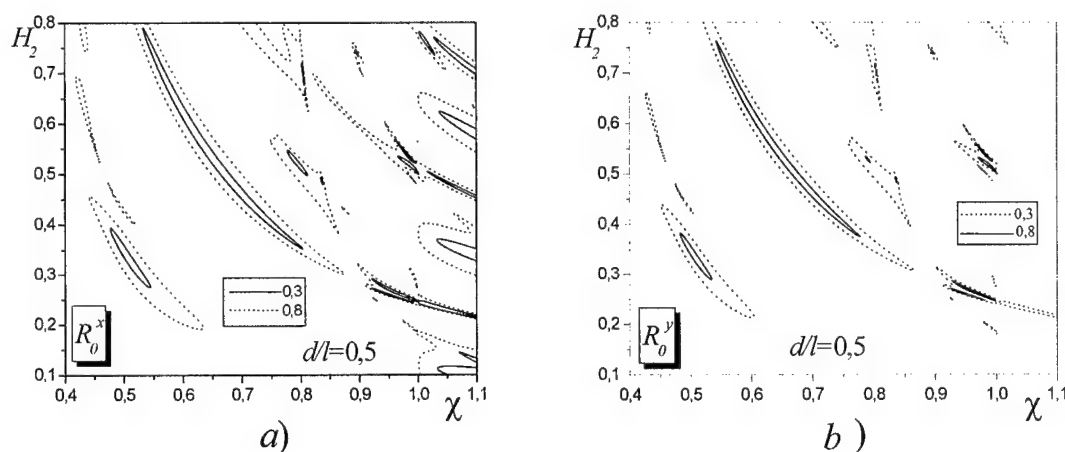


Fig.2 Efficiency in the 0-order of spectrum:  
a-main polarization; b-cross polarization

( $\tilde{e} = 1, \tilde{h} = 0, \alpha = 0^\circ, h_1/l = 0.03, \varepsilon_1 = 1, \varepsilon_2 = \varepsilon_3 = 4, \mu_j = 1, \gamma = 0.3$ ).

## CONCLUSION

The analytical regularization procedure for solving the vector problem considered has been constructed. Our approach based on the Riemann-Hilbert problem method lends as a reliable and effective tool. An incident plane-polarized field can be totally converted into the regularly reflected cross-polarized field. The character of the polarization conversion is influenced by the grating and by the resonance properties of the grating-screen volume. The laws of the polarization conversion have been established as well as the possibilities for the enhancement of the structure efficiency and broadbandness.

## REFERENCES

- [1] S.B. Panin and A.Ye. Poyedinchuk, "The Plane Wave Diffraction by a Grating over a Chiral Medium," *Telecommunications & Radio Engineering*, vol. 53, N 4-5, pp. 98-109, 1999.
- [2] A.Ye. Poyedinchuk, Yu.A. Tuchkin, Yu.K. Sirenko and V.P. Shestopalov, *New solution method of direct and inverse problems in diffraction theory*, Kharkov: Osnova, 285 pp., 1997. (In Russian)
- [3] A.H. Sihvola, *Electromagnetic mixing formulas and applications*, London: Institution of Electrical Engineers, 350 pp., 1999.
- [4] S.B. Panin and A.Ye. Poyedinchuk, "Polarization properties of a screened chiral layer with a diffraction grating," *Radiophysics & Electronics*, IRE of NASU, Kharkov, Ukraine, vol. 7, N 1, pp.45-57, 2002. (In Russian)

## RESONANT COUPLING OF CAVITY-BACKED SLOTS

Aleksandr V. Sulima

Institute of Radio Astronomy of National Academy of Sciences of Ukraine,  
4 Krasnoznamennaja, Kharkov 61002, Ukraine  
sulima@rian.kharkov.ua

### ABSTRACT

A rigorous solution of the problem of a TE wave scattering by a finite number of slots in a PEC plane backed by resonant cavities is given. The scattering problem formulated in terms of system of singular integral equations has been solved by the method of analytical regularization. Application of the regularization procedure allowed obtaining an accurate and numerically efficient solution.

### INTRODUCTION

The problem of scattering of a TE wave by a slot in a PEC plane, backed by a resonant cavity, or by a trough in a plane, has been discussed by many authors [1]-[2] in the context of the method of moments and the mode matching method. A numerically efficient solution of the problem, which works well on resonant and non-resonant frequencies, can be obtained, if a procedure of regularization is applied to an initial integral equation or a system of linear algebraic equations. As, there is no a "standard" procedure of regularization [3], for each problem a regularization algorithm, if exists, must be derived independently. The regularization algorithm employed in this paper originally was designed for elasto-dynamic problems and described in [4]. Lately it was used in different scattering problems [5], [6]. Application of the regularization algorithm [4] to the problem of a TE wave scattering by a cavity backed slot allows the transformation of initial integral equation into infinite system of linear algebraic equations. As the system of equations is well conditioned its solution can be found numerically, with desired accuracy, from a truncated system of equations. In the case of a narrow slot, slot width doesn't exceed one tenth of wavelength, the solution of the problem can be obtained in an analytical form. An efficient solution of the single slot problem provides a possibility to obtain solutions for more complicated structures, such as a collection of a finite number of cavity-backed slots, with the same high accuracy and numerical efficiency.

### PROBLEM FORMULATION

Consider N cavity backed slots as shown in Fig.1. The problem of a TE wave scattering by slots loaded on resonant cavities is formulated by using Green function formalism. Green functions of the upper half-space and of a rectangular cavity for the Neuman boundary condition under assumption that  $y = y' = 0$  are defined as follows:

$$G_H(x, x') = -\frac{k}{2W} H_0^{(2)}(k|x - x'|), \quad (1)$$

$$G_m(x, x') = -\frac{ik}{2Wa_m} \sum_{n=0}^{\infty} \frac{\varepsilon_n}{\gamma_n^m} \coth(\gamma_n^m b) \cos\left(\frac{n\pi}{2a_m}(x + d_m)\right) \cos\left(\frac{n\pi}{2a_m}(x' + d_m)\right) \quad (2)$$

where  $k = 2\pi/\lambda$ ,  $H_0^{(2)}(z)$  - Hankel function of zero order of the second kind,  $W$  - free space impedance,  $\varepsilon_m = 1$ ,  $m \neq 0$ ,  $\varepsilon_0 = 2$ ,  $\gamma_m = \sqrt{(\frac{n\pi}{2a_m})^2 + k^2}$ . The subscript  $m$  in (2) corresponds to the cavity number. The cavity parameters -  $a_m$ ,  $b_m$ ,  $c_m$ , and  $d_m$  are defined as shown in the Fig.2, where  $2a_m$  - cavity width in the X direction,  $b_m$  - cavity depth,  $2c_m$  - slot width and  $d_m$  - defines slot position with respect to the upper left corner

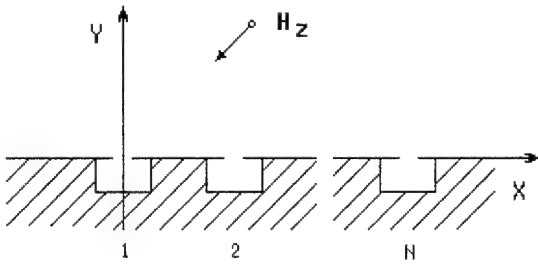


Fig.1 The original problem.

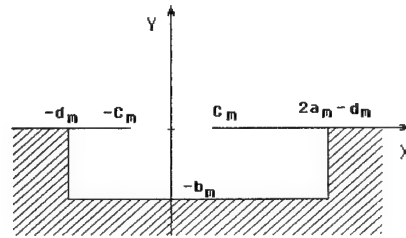


Fig.2 Geometry of the cavity-backed slot.

of the cavity ( $d_m = a_m$  corresponds to the case when slot center is positioned at the midpoint of the interval  $[-a_m, a_m]$ ). If the system of  $N$  slots is excited by a TE wave, a system of  $N$  integral equations for the problem can be formulated as

$$\int_{-c_m}^{+c_m} E_m(x') [G_H(x, x') + G_m(x, x')] dx' = -2f(x) - 2 \sum_{\substack{i=1 \\ i \neq m}}^N H_i(x), \quad (3)$$

where  $E_m(x)$  - is an unknown magnetic current on the slot  $m$ ,  $f(x)$  - the incident field,  $H_i(x)$  - is a secondary incident field produced by the magnetic current on the slot  $i$ . The system of singular integral equations (3) can be reduced, by the method of analytical regularization, to a system of linear algebraic equations of the form

$$z_m^k A_m^k + \sum_{l=0}^M z_l^k B_{m,l}^k + \sum_{\substack{i=1 \\ i \neq m}}^N \sum_{l=0}^M z_l^i D_{m,i}^l = f_m^k, \quad (4)$$

where  $Z_m^l$  are unknown Tchebyshev coefficients of magnetic current on the slot  $i$ . The system of equations (4) allows us to calculate  $M$  unknown coefficients in the unknown magnetic current expansion for each slot, once these coefficients are calculated the scattered field is determined at any point in the upper half-space and inside resonant cavities.



## NUMERICAL RESULTS

The far field diagram of  $N$  slots is defined as

$$H = \sum_{n=1}^N kc_n e^{ikx_n \cos(\varphi)} \sum_{j=0}^M z_j'' \int_{-1}^1 \frac{e^{ikc_n \cos(\varphi)x} T_j(x) dx}{\sqrt{1-x^2}}, \quad (5)$$

where the polar angle  $\varphi$  is counted counterclockwise of the OX axis. Fig.3,4,5 presents graphs of the scattered field at the point  $\varphi = \pi/2$ , versus the frequency parameter  $ka$  calculated by the formula (5). The incident field is a plane wave normally incident on slots. Fig.3 presents scattered field of a single slot, and Fig.4,5 present graphs of scattered field by two slots. In the case of two slots both of them have the same slot width and cavity size, here  $a = a_1 = a_2$ . Fig.3 presents graph of  $|H|$  for a single slot with the following cavity parameters  $b_1 = 2a_1$ ,  $c_1 = 0.2a_1$ ,  $d_1 = a_1$ . Maximums in the scattered field occurs at resonant frequencies of cavity, coupled through the slot with the upper half-space. Fig. 4 presents graph of scattered field by two slots for the case of an optimum coupling between slots on the  $H_{00}$  mode, the distance between slots is defined by the formula  $kx_2 = 2ka + 0.95$ . Fig.5 shows the effect of the resonant coupling between slots on the  $TE_{10}$  mode, in this case the distance between slots is defined by  $kx_2 = 2ka + 2.5$ . Presented numerical results demonstrates, that the mutual coupling effect can drastically change the scattering properties of cavity-backed slots at resonant frequencies

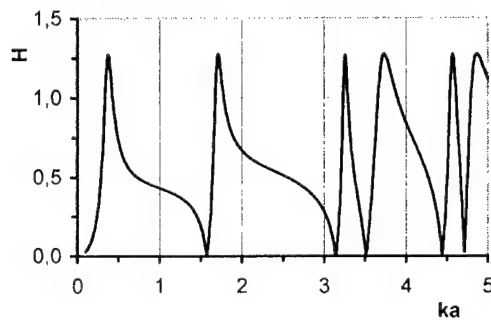


Fig. 3 Scattered field at  $\varphi = \pi/2$ , one slot,  $kb=2ka$ ,  $kc=0.2ka$ ,  $kd=ka$ .

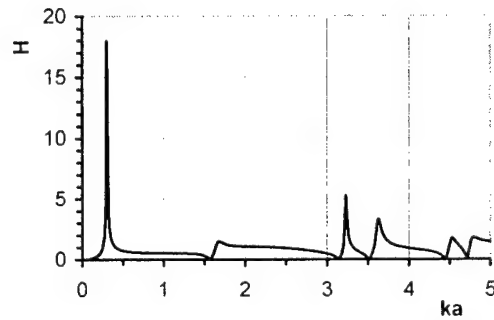


Fig.4 The effect of the resonance coupling on the  $H_{00}$  mode.

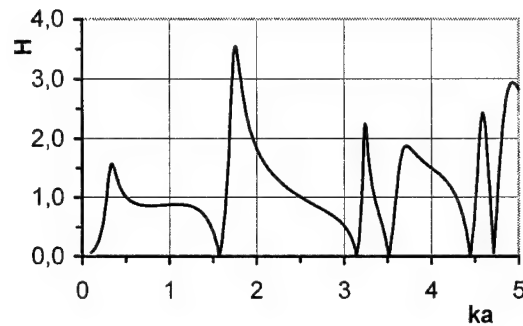


Fig. 5 The effect of resonance coupling on the  $TE_{10}$  mode

## CONCLUSION

In this paper the exact solution of the problem of a TE wave scattering by a collection of finite number of cavity- backed slots is given. The method automatically includes the effect of singular behavior of a tangent component of the electric field on slot aperture. The solution has no limitations on cavity size and is numerically efficient. The examples presented in the paper demonstrate the coupling effect on the scattering properties of cavity- backed slots. It has been shown that the method works with the same efficiency on resonant and non-resonant frequencies.

## REFERENCES

- [1] T. Wang, R.F. Harrington and J.D. Moutz, "Electromagnetic scattering from and transmission through arbitrary apertures in conducting bodies," IEEE Trans. Antennas and Propagation, vol. 38, pp. 1805-1814, November, 1990.
- [2] H.H. Park, H.J. Eom, "Electromagnetic penetration into 2-D multiple slotted rectangular cavity: TM -wave," IEEE Trans. Antennas and Propagation, vol. 48, February, 2000.
- [3] A.I. Nosich, "The method of analytical regularization in wave scattering and eigenvalue problems: foundations and review of solutions" IEEE Antennas and Propagation Magazine, vol. 41, June, pp. 34-49, 1995.
- [4] V.M. Aleksandrov, V.A. Kucharov, "The Method of orthogonal polynomials in mixed problems of the theory of elasticity," Journal of Applied Mathematics and Mechanics (Moscow ) vol. 34, N 4, 1970.
- [5] N.S. Mikhalevsky, Transmission lines of complex cross section, Rostov: Rostov State University Publishing House, 1983.
- [6] J. Tsalamengas, "Direct singular integral equation methods in scattering and propagation in strip- or slot - loaded structures," IEEE Trans. Antennas and Propagation, vol. 46, October, 1998.
- [7] P.I. Klubin, "Beams and round slabs on an elastic base," Engineering Proceedings of the Institute of Mechanics, vol. 12, pp. 95-107, 1952.

## RADIATION CHARACTERISTICS OF A 2D PARABOLIC REFLECTOR ANTENNA EXCITED BY THE H-POLARIZED COMPLEX SOURCE

Taner Oguzer, Alexander I. Nosich\*, Ayhan Altıntaş\*\*

Dokuz Eylül University, Electrical and Electronics Eng. Dept., Buca 35160, İzmir, Turkey

\* Institute of Radio-Physics and Electronics, National Academy of Sciences, Kharkov 61085, Ukraine

\*\* Bilkent University, Electrical and Electronics Eng. Dept., Bilkent 06533 Ankara, TURKEY

**ABSTRACT:** The aim of this paper is to obtain accurate reference data for the relatively large and realistic reflector antenna systems. Previously it has been done for a parabolic reflector antenna in E-case and now it is similarly performed for the H-polarization case. Directive primary feed is modeled by the complex source point method and the relative accuracy of the results is verified.

**INTRODUCTION:** Reflector antennas play an important role in the modern communication systems, and hence attract research efforts for efficient numerical analysis and optimization. Although two-dimensional (2D) modeling relates only to cylindrical reflectors, it is still interesting in terms of advanced solutions and some practical applications. The scattering from a 2D reflector can be very accurately simulated by analytical-numerical techniques. One of them is the Riemann-Hilbert Problem (RHP) technique, which reduces the canonical circularly curved screen problem to a Fredholm 2<sup>nd</sup> kind matrix equation after explicit inversion of the static part [1]. In [2], we had combined this solution with the complex source-point (CSP) method that enabled us to model realistic feed patterns in the both polarizations. However most of the realistic reflector surfaces are parabolic ones. This necessitates a modification of RHP technique to arbitrarily curved strips. In [3] we performed the analysis of 2D reflectors of conical-section profiles in the E-polarization case. Here we used a dynamic singularity extraction and inversion, as proposed in [4], to convert a logarithmic-singularity integral equation to the Fredholm 2<sup>nd</sup> kind matrix equation. Furthermore the application of the FFT algorithms enabled us to treat electrically large geometries. In the H-polarization case, the basic integral equation has a strong singularity. It is worth to mention that similar problem was considered in [5]. Here, the integral equation was reformulated into a dual series equation (DSE) with trigonometric kernel. Then it was regularized by using a specialized method developed earlier for the equations with Jacobi polynomials. Later on, in [6] it was proposed to regularize the same DSE by the RHP technique. In the both studies, although a method was outlined, no numerical data were given for arbitrary profiles.

In this study, we regularize Electric Field Integral Equation (EFIE) obtained for the parabolic reflector antenna in the H-polarization case. EFIE is discretized by transforming it into the spectral domain and also written as DSE. To make regularization the static part is inverted analytically by the RHP technique since the static part of DSE constitutes a proper canonical form. Furthermore we can say that this is equivalent to the semi-inversion of the original IE containing hyper-type singularity in the kernel static part. In the details we used the FFT algorithm to perform computations of the double Fourier Series (FS) coefficients more rapidly. All these provide us to solve relatively large reflector antennas compared to the previous results with the semi-inversion techniques. This is the continuation of the work in [2,3] and the results can be used to check the accuracy of the asymptotic and numerical techniques.

**FORMULATION:** The geometry of the problem can be defined so that infinitely thin PEC curved reflector surface having parabolic profile is illuminated by a directive feed (Figure 1). Parabola is a special case of an arbitrary profile. In the real space, the feed is located at the geometrical focus of the parabola. To perform regularization, parabolic reflector surface is completed to the closed contour  $C$  by a circle having its origin on the  $x$ -axis. Its radius,  $a$ , is chosen so that, at the connection points, the slopes of the parabola and circle are matched. So the contour first derivatives are continuous and the discontinuities in the second derivatives are finite. The boundary value problem can be stated as the satisfaction of the Helmholtz equation, Sommerfeld radiation condition, and PEC boundary condition on reflector surface  $M$ . By using the free-space Green's functions in 2D, i.e.  $G^t_o = G^p_o = i/4 H^{(1)}_0(k_o r(\varphi) - r'(\varphi'))$ , the tangential electric field can be written in terms of auxiliary vector and scalar potentials depending on tangential surface current ( $J_t$ ) and surface charge ( $\rho$ ) densities.

$$\vec{E}^{sc} \cdot \hat{t} = i\omega \vec{A} \cdot \hat{t} - \nabla \phi \cdot \hat{t} = i\omega \mu \int_C (\hat{t} \cdot \hat{t}') J_r(\vec{r}') G_o^A(\vec{r}, \vec{r}') dl' - \hat{t} \cdot \nabla \int_C \left( \frac{1}{\epsilon} \right) \rho(\vec{r}') G_o^\phi(\vec{r}, \vec{r}') dl' \quad (1)$$

Then by applying equation of charge conservation, i.e.,  $\nabla \cdot \vec{J} = i\omega \rho$ , and PEC boundary condition to the above equation and after manipulations the following integral equation is obtained:

$$-E_i^{inc}(s) \beta(s) = i\omega \mu \int_0^{2\pi} J_r(s') \cos(\xi(s) - \xi(s')) \beta(s) \beta(s') G_o^A(s, s') ds' - \left( \frac{1}{i\omega \epsilon} \right) \frac{\partial}{\partial s} \int_0^{2\pi} \left( \frac{\partial}{\partial s'} J_r(s') \right) G_o^\phi(s, s') ds' \quad (2)$$

where  $\beta(s) = r(s)/\cos(\gamma(s))$ ,  $\xi(s)$  is the angle between the contour normal and the x-direction, and  $\gamma(s)$  is the angle between the contour normal and the radial direction. Besides the closed contour  $C$  is characterized by parametric equations  $x=x(s)$ ,  $y=y(s)$ ,  $0 < s < 2\pi$  and the current density function  $J_r$  is assumed zero on the part of  $C$  complementary to  $M$ . The above IE is defined on  $M$ . On the slot part the current density is zero. The spectral versions of these two equations constitute a DSE. However a special care is needed for the Green's functions to find a regularized solution. Therefore we define the following new auxiliary regular functions,

$$H(s, s') = H_o^{(1)}(k|\vec{r}(s) - \vec{r}(s')|) - H_o^{(1)}(2ka|\sin(s-s')/2|) \quad (3)$$

$$G(s, s') = \cos(\xi(s) - \xi(s')) \beta(s) \beta(s') H_o^{(1)}(k|\vec{r}(s) - \vec{r}(s')|) - \beta^2(s) H_o^{(1)}(2ka|\sin(s-s')/2|) \quad (4)$$

These functions  $H(s, s')$  and  $G(s, s')$  have continuous first derivatives and second derivatives with respect to  $s$  and  $s'$  and belong to  $L_2$ . For regularization these functions are expanded into double FS and the corresponding expansion coefficients rapidly decay like  $O(1/(|n||m|)^{3/2+\epsilon})$ . Then by using (3) and (4), DSE is written in certain canonical form and solved by RHP technique. The main problem in this process is an efficient computation of the double FS coefficients. We perform this by using FFT algorithms and exploit the fact that the second terms in (3) and (4) are expanded into FS analytically. All this provides us to handle larger problems than can be treated with earlier methods.

**NUMERICAL RESULTS:** Firstly the convergent nature of our algorithm is shown in Figure 2. The relative error in the computed surface current is  $\max|x_n^{N_{irr}-1} - x_n^{N_{irr}}|/\max|x_n^{N_{irr}}|$ , that decreases quite rapidly with larger  $N_{irr}$ . It can be said that 0.1% accuracy can be obtained with  $N_{irr} = 2ka + 15$ . Figure 3 presents a comparison of the radiation patterns obtained by the presented method and Physical Optics solution. It shows that excluding the back lobes the two methods show quite similar patterns but still some disappearances are observed in the penumbra region.

**CONCLUSION:** Two-dimensional parabolic reflector antenna illuminated with directive feed is solved by the analytical regularization in the H-polarization case. Presented numerical results have uniform 3-digit accuracy although the algorithm can generate them with machine precision. Application of the FFT codes provides us to solve larger problems, and our data can be used as a reference to validate purely numerical or asymptotic methods.

#### REFERENCES:

- [1] A.I. Nosich, "Green's function - dual series approach in wave scattering from combined resonant scatterers", in M. Hashimoto et al. (Eds.), *Analytical and Numerical Methods in Electromagnetic Wave Theory*, Tokyo: Science House, 1993, pp. 419-469.
- [2] T. Oğuzer, A. Altıntaş A.I. Nosich, "Accurate simulation of reflector antennas by the complex source - dual series approach", *IEEE Trans. Antennas Propagat.*, 1995, vol. AP-43, no 8, pp. 793-802.
- [3] T. Oğuzer, A.I. Nosich and A. Altıntaş, "E-polarized beam scattering by an open cylindrical PEC strip having arbitrary conical-section profile", *Microwave Optical Tech. Lett.*, 2001, vol. 31 no. 6, pp 480-484.

- [4] A.I. Nosich, S.V. Boriskina, "Economic and accurate in resonances solution to the wave scattering by arbitrary smooth dielectric cylinders, based on the canonical-shape inversion", *IEEE Trans. Antennas Propagat.*, submitted in 2001.
- [5] Y.A. Tuchkin, "Wave scattering by an open cylindrical screen of arbitrary profile with the Neumann boundary condition", *Soviet Physics Doklady*, vol. 32, pp. 213-214, 1987.
- [6] V. Veremey, A. Poyedinchuk, "Two-dimensional scattering from a cavity-backed aperture with resonant loading", *IEEE APS-URSI Int. Symp. Digest*, Chicago, 1994, pp.1090-1093.

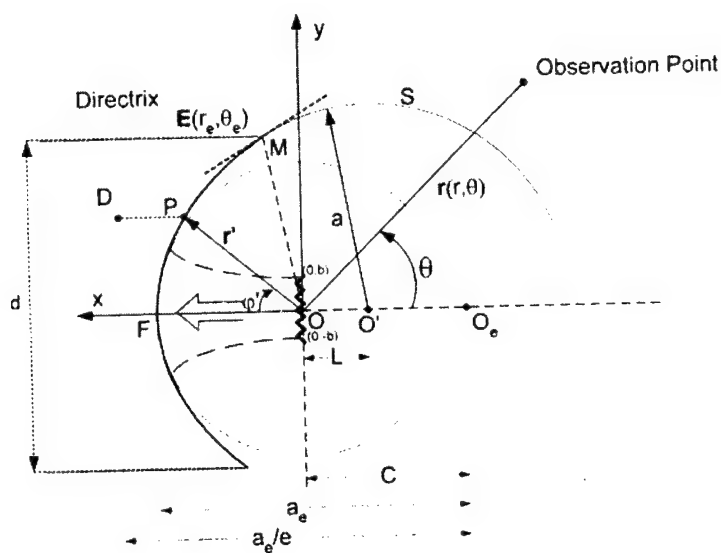


Figure 1: Geometry of 2D reflector antenna system

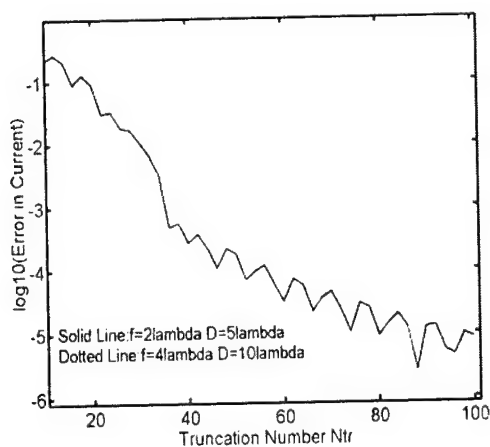


Figure 2: Truncation Error in the current coefficients. Feed directivity factor is  $kb=2.6$

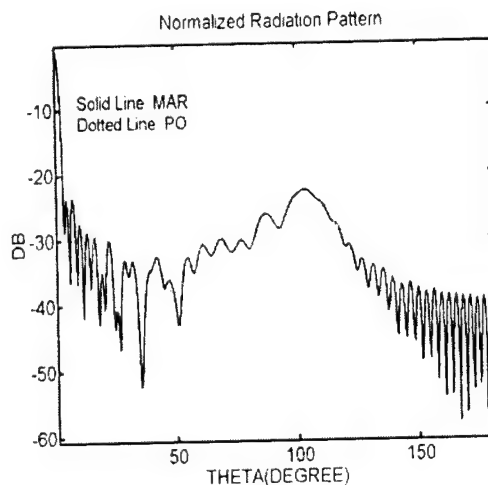


Figure 3: Comparison of radiation patterns for MAR and PO solutions.  $f=8\lambda$ ,  $D=20\lambda$ . Feed directivity factor is  $kb=1.5$ .

## ELECTROMAGNETIC WAVES SCATTERING ON AN UNCLOSED CONE WITH AN ISOTROPIC ONE INSIDE

Vladimir A. Doroshenko, Elena K. Semenova

Kharkov National University of Radioelectronics

14, Lenin av., Kharkov, 61166, Ukraine

Email: h\_semenova@yahoo.com

### ABSTRACT

The problem of electromagnetic wave scattering by a perfectly conducting thin long bicone is considered. The bicone consists of a slotted cone and an isotropic one. The solution method is based on using the Kontorovich-Lebedev integral transforms and the semi-inversion method. Both analytical and numerical results are presented.

### INTRODUCTION

Cones and bicones are omnidirectional and super-wide band in radiation pattern and matching. The structure under consideration is a model of a specific bicone reflector and a slotted cone antenna. The task of this work is to study effects of slots and isotropic cone on scattering characteristics.

### FORMULATION AND SOLUTION METHOD

Let us consider the scattering of incident electromagnetic waves from a thin perfectly conducting long circular slotted bicone. The geometry of the bicone configuration is shown in Fig.1;  $(r, \theta, \varphi)$  are spherical coordinates with the origin at the bicone tip. The bicone structure  $\Sigma$  consists of a semi-infinite cone with periodical longitudinal slots  $\Sigma_2: \theta = \gamma_2$  and an isotropic one  $\Sigma_1: \theta = \gamma_1$  ( $\Sigma = \Sigma_1 \cup \Sigma_2$ ). The period  $l = 2\pi/N$  and the slot width  $d$  are angular values. The source of an incident field is a magnetic radial dipole (the time dependence is assumed to be  $\exp(i\omega t)$ ) that is located at the point  $B_0(r_0, \theta_0, \varphi_0)$ ,  $\gamma_2 < \theta_0$ . The vectors  $\vec{E}$  and  $\vec{H}$  of total fields satisfy the system of Maxwell equations, the boundary condition on the bicone:  $\vec{E}_{\tan}|_{\Sigma} = 0$ , the condition of finite stored energy and the infinity condition. The conditions mentioned above guarantee the uniqueness of solution. In order to find it, it is convenient to use Debye potential  $\vartheta$ , which satisfies the three-dimensional homogeneous Helmholtz equation outside the bicone and the source, the Neumann boundary condition on the bicone, the principle of ultimate absorption, and the edge condition in the proximity of boundary singularities. In accordance with the structure of the total fields  $\vec{E} = \vec{E}^{(i)} + \vec{E}^{(s)}$ ,  $\vec{H} = \vec{H}^{(i)} + \vec{H}^{(s)}$ , we represent  $\vartheta$  in the form  $\vartheta = \vartheta^{(i)} + \vartheta^{(s)}$ , where indices  $(i)$  and  $(s)$  correspondence to dipole fields and fields scattered by the bicone respectively. We look for the solution in the form

$$\vartheta^{(s)}(r, \theta, \varphi) = -\frac{1}{2} \int_0^{+\infty} \tau \sinh \pi \tau e^{\pi \tau} \hat{\vartheta}_{\tau}^{(s)}(\theta, \varphi) \frac{H_{\pi}^{(2)}(kr)}{\sqrt{r}} dr,$$

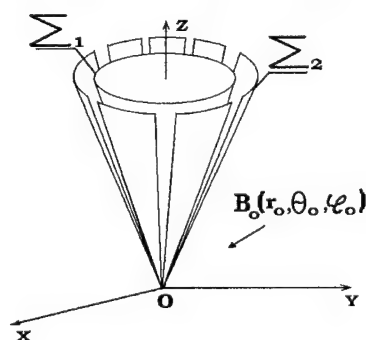


Fig.1 Bicone structure

$$\hat{g}_\tau^{(s)} = - \sum_{m=-\infty}^{+\infty} a_{m\pi} \frac{d}{d\gamma_2} P_{-1/2+\pi}^m(\cos\gamma_2) P_{-1/2+\pi}^m(\cos\theta_0) V_{m\pi}(\theta, \varphi),$$

$$V_{m\pi} = \begin{cases} \sum_{n=-\infty}^{+\infty} [\beta_{mn} P_{-1/2+\pi}^{m+nN}(\cos\theta) + \xi_{mn} P_{-1/2+\pi}^{m+nN}(-\cos\theta)] e^{i(m+nN)\varphi}, & \gamma_1 < \theta < \gamma_2, \\ \sum_{n=-\infty}^{+\infty} \eta_{mn} P_{-1/2+\pi}^{m+nN}(-\cos\theta) e^{i(m+nN)\varphi}, & \gamma_2 < \theta < \pi; \end{cases}$$

where  $H_\pi^{(2)}(kr)$  is the Hankel function,  $P_\mu^m(\cos\theta)$  is the associated Legendre function,  $a_{m\pi}$  are given;  $\beta_{mn}$ ,  $\xi_{mn}$ ,  $\eta_{mn}$  are unknown coefficients and expressed via  $y_n$ . The boundary condition imposed on the bicone and the field continuity condition on the slots yield the dual series equations those are reduced to the matrix equation of the Fredholm second kind [1] like  $(I - A)Y = B$ ,  $Y = \{y_n\}$ . Coefficients  $y_n$  are independent of the wave-number  $k$ ; it is convenient for finding the field both near the vertex ( $kr \ll 1$ ) and far from it ( $kr \gg 1$ ). The solution of the matrix equation exists, is unique, and can be approximated by solving a truncated matrix equation. For a cone with narrow slots ( $d_2/l \ll 1$ ) one can solve the equation by method of successive approximations.

## ANALYTICAL RESULTS

For a cone with narrow slots we obtain the asymptotic expansion of potential  $\mathfrak{g}^{(s)}$  at a large distance from the slots in terms of parameter  $(1-u) \ll 1$ ,

$u = \cos(\pi d_2/l)$  in the following form ( $\varphi_0 = 0, \theta_0 = \pi, m = 0$ )

$$\mathfrak{g}^{(s)} = \int_0^{+\infty} b_\tau \frac{H_\pi^{(2)}(kr)}{\sqrt{r}} \frac{F_\pi}{F_\pi + \zeta} \cdot \frac{P_{-1/2+\pi}(-\cos\theta)}{\frac{d}{d\gamma_2} P_{-1/2+\pi}(-\cos\gamma_2)} d\tau - \zeta \int_0^{+\infty} b_\tau \frac{H_\pi^{(2)}(kr)}{\sqrt{r}} \frac{F_\pi}{F_\pi + \zeta} \times$$

$$\times \sum_{p \neq 0} \frac{1}{|p|} \varepsilon_p \frac{P_{-1/2+\pi}(-\cos\theta)}{\frac{d}{d\gamma_2} P_{-1/2+\pi}(-\cos\gamma_2)} d\tau + \zeta \int_0^{+\infty} b_\tau \frac{H_\pi^{(2)}(kr)}{\sqrt{r}} \frac{A_\pi F_\pi}{F_\pi + \zeta} \sum_{n \neq 0} \frac{P_{-1/2+\pi}^{nN}(-\cos\theta)}{\frac{d}{d\gamma_2} P_{-1/2+\pi}^{nN}(-\cos\gamma_2)} e^{inN\varphi} d\tau +$$

$$+ O((1-u)), \gamma_2 < \theta < \pi; \quad C_\tau^M = \frac{\frac{d}{d\gamma_1} P_{-1/2+\pi}^M(\cos\gamma_1) \frac{d}{d\gamma_2} P_{-1/2+\pi}^M(-\cos\gamma_2)}{\frac{d}{d\gamma_1} P_{-1/2+\pi}^M(-\cos\gamma_1) \frac{d}{d\gamma_2} P_{-1/2+\pi}^M(\cos\gamma_2)}$$

$$A_\pi = \frac{ch\pi\tau}{\pi \sin^2 \gamma_2} \frac{1}{(\tau^2 + \frac{1}{4}) P_{-1/2+\pi}^{-1}(\cos\gamma_2) P_{-1/2+\pi}^{-1}(-\cos\gamma_2)} \frac{1}{1 - C_\pi^M|_{M=0}}, \quad F_\pi = \frac{1}{A_\pi - \frac{1}{N} \sum_{p \neq 0} \frac{1}{|p|} \varepsilon_p},$$

$$\zeta = -\frac{N}{\ln((1-u)/2)}, \quad \varepsilon_n = O(N^{-1}(n+\nu)^{-2}), \quad nN \gg 1, -1/2 \leq \nu < 1/2, \quad b_\tau \text{ is given.}$$

## NUMERICAL RESULTS

We'll discuss the far field scattering characteristics of the bicone based on numerical examples of  $\varphi$ -plane scattering patterns. Let the source be at the  $z$ -axis ( $\varphi_0 = 0, \theta_0 = \pi, m = 0$ ) and  $N = 1$ . Thus Fig.2 depicts the dependence of the far field scattering

on the angle  $\gamma_2$  for an alone slotted cone (the isotropic cone is absent). The ray  $\varphi = 0^\circ$  coincides with the slot axis. The slot lobe is symmetrical with respect to the slot axis; the main lobe of the slot radiation is centered in the direction  $\varphi = 0^\circ$ . The effects of the isotropic cone on the scattered far field are shown in the Fig.3 - Fig.5.

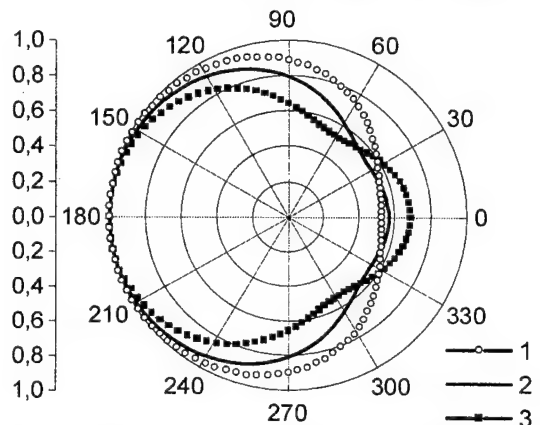


Fig.2  $\varphi$ -plane scattering patterns for the alone slotted

cone  $\Sigma_2 (\gamma_1 = 0)$   $d_2 = 60^\circ$  for different values of  $\gamma_2$ .  
1. -  $\gamma_2 = \pi/6$ , 2. -  $\gamma_2 = \pi/8$ , 3. -  $\gamma_2 = \pi/16$ .

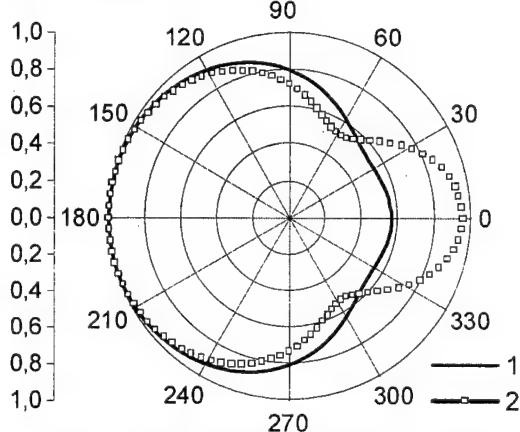


Fig.3  $\varphi$ -plane scattering patterns for the alone

cone (1) and the bicone (2)  $\gamma_1 = \pi/16$ ,  
 $\gamma_2 = \pi/8$ ,  $d_2 = 60^\circ$ .

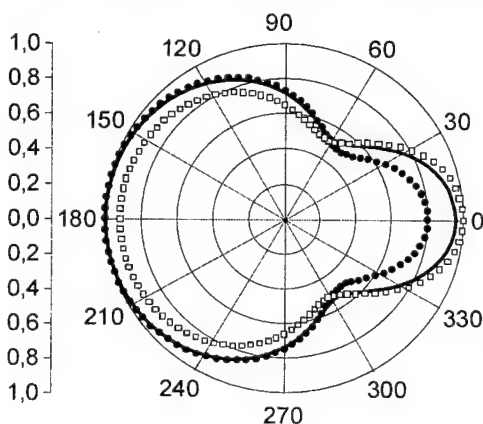


Fig.4  $\varphi$ -plane scattering patterns. Scattered far field dependence on the angle  $\gamma_1$ .

1. -  $\gamma_1 = \pi/14$ , 2. -  $\gamma_1 = \pi/16$ , 3. -  $\gamma_1 = \pi/20$ .

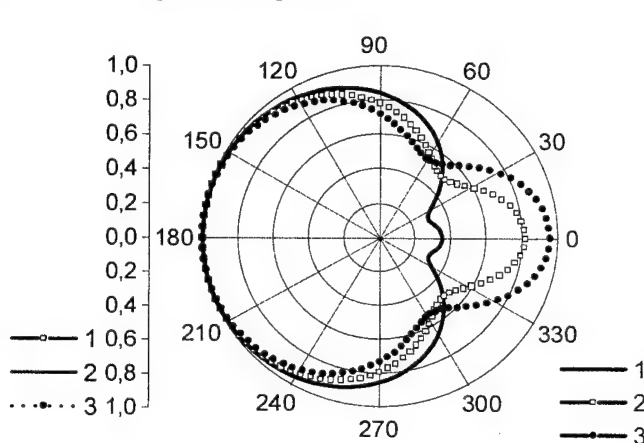


Fig.5  $\varphi$ -plane scattering patterns. Scattered far field dependence on the slot width  $d_2$ .

1. -  $d_2 = 5^\circ$ , 2. -  $d_2 = 30^\circ$ , 3. -  $d_2 = 60^\circ$

## CONCLUSIONS

The problem of exciting the slotted cone with the isotropic one inside by the magnetic radial dipole has been considered. The analytical solution for narrow slots is analyzed. The scattered field structure contains the isotropic cone contribution and the narrow slots one. Scattered field patterns are given to investigate slots effects and the isotropic cone presence both.



# ELECTROMAGNETIC BACKSCATTERING FROM A TRIANGULAR DIELECTRIC CYLINDER

Lyudmila N. Ilyashenko

IRE NASU, ul. Proskury 12, Kharkov 61085, Ukraine. E-mail: lyusi@vil.com.ua

## INTRODUCTION

Boundary integral equations (IEs) are an accurate and versatile tool in the electromagnetic scattering by smooth cylinder [1], especially when it is combined with analytical preconditioning [2]. An original approach to the E-wave scattering by PEC polygons was developed in [3] to study a triangular prism. Here the boundary of the scatterer was conformally mapped on a circular cylinder [4], and a log-singular IE was treated by a simple moment method. We combine this idea with the method of analytical regularization (MAR) and study the scattering by triangular dielectric cylinders. Applications of this analysis are expected in the design of microwave and optoelectronic prism sensors and couplers.

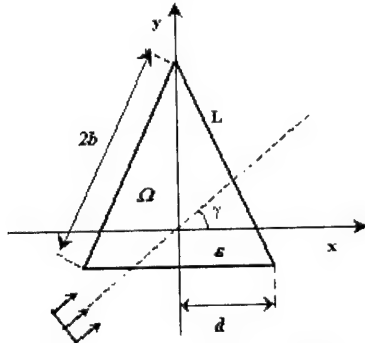


Fig. 1: Scattering geometry and notations

## FORMULATION AND INTEGRAL EQUATIONS

The geometry of the problem is shown in Fig.1. A plane electromagnetic wave  $H^i = e^{ik \cos \gamma x + ik \sin \gamma y}$  is incident on a uniform dielectric cylinder whose cross-section is an isosceles triangle of the base  $2d$  and height  $h$ , having relative permittivity  $\epsilon$ . The field functions have to satisfy the Helmholtz equation in free space and in dielectric, for  $r \notin \Omega$  ( $r \in \text{ext } \Omega$ ) and  $r \in \Omega$ , respectively. On the contour  $L$  the transmission conditions should be satisfied. The scattered field must also satisfy the Sommerfeld radiation condition at infinity and condition of local power finiteness. We will seek the solution of the problem in the form of a

pair of single-layer potentials with unknown densities  $\varphi \in C(\partial\Omega)$  and  $\psi \in C(\partial\Omega)$ . By using the conditions on  $L$  and the properties of the normal derivative of a single-layer potential when crossing the contour of integration [1], the following set of singular IEs is obtained:

$$\begin{cases} \int_L \varphi(r') G_\epsilon(r, r') ds' - \int_L \psi(r') G(r, r') ds' = H^i(r) \\ \left\{ \frac{\varphi(r)}{2\epsilon} + \frac{1}{\epsilon} \int_L \varphi(r') \frac{\partial}{\partial n} G_\epsilon(r, r') ds' + \frac{\psi(r)}{2} - \int_L \psi(r') \frac{\partial}{\partial n} G(r, r') ds' = \frac{\partial}{\partial n} H^i(r) \right\} \end{cases} \quad (2)$$

To facilitate building a fast algorithm, which is able to solve the scattering by cylinder with a contour arbitrarily close to triangle, we shall use the following continuous parametric approximation of curve  $L$ :

$$x(t) = \frac{d}{M} \left( \sin t + \sum_{k=1}^N a_k \sin(3k-1)t \right), \quad y(t) = \frac{b}{M} \left( -\cos t + \sum_{k=1}^N a_k \cos(3k-1)t \right), \quad (3)$$

$$a_k = \frac{\prod_{j=1}^k (5-3j)}{3^k (3k-1)k!} \quad (4)$$

One can obtain these formulas by conformal mapping of the region outside a regular polygon from  $Z$ -plane ( $Z=x+iy$ ) to the  $(t,s)$  plane, where  $0 \leq t \leq 2\pi$ , and by using the transformation formula first derived in [5]:  $\partial Z / \partial t = C(\cos(3t/2))^{2/3}$ , where  $C$  is a complex coefficient depending on the size and orientation of the polygon. If  $K \rightarrow \infty$  then the curve given by (3) tends to a triangle, however by truncating the series in (3) at the  $K$ -th terms a smoothed contour is obtained having the corner radius of curvature  $b$  inverse proportional to  $K$ . By changing the variables in (1) to  $t$  and  $t'$ , we arrive at IEs as follows (see also [2]):

$$\begin{cases} \int_0^{2\pi} p(t') K^\varepsilon(t, t') dt' - \int_0^{2\pi} q(t') K(t, t') dt' = f(t) \\ \frac{1}{\varepsilon} \frac{p(t)}{2} + \frac{q(t)}{2} + \int_0^{2\pi} p(t') M^\varepsilon(t, t') dt' - \int_0^{2\pi} q(t') M(t, t') dt' = \tilde{f}(t) \end{cases} \quad (5)$$

Here the following notations have been used:

$$K^\varepsilon(t, t') = \frac{i\varepsilon}{4} H_0^{(1)}(k\sqrt{\varepsilon} R(t, t')), \quad K(t, t') = \frac{i}{4} H_0^{(1)}(kR(t, t')), \quad (6)$$

$$M^\varepsilon(t, t') = \frac{ik}{4} \sqrt{\varepsilon} H_1^{(1)}(k\sqrt{\varepsilon} R(t, t')) \left( \frac{x(t) - x(t')}{R(t, t')} y'(t') - \frac{y(t) - y(t')}{R(t, t')} x'(t') \right), \quad (7)$$

$$M(t, t') = \frac{ik}{4} H_1^{(1)}(kR(t, t')) \left( \frac{x(t) - x(t')}{R(t, t')} y'(t') - \frac{y(t) - y(t')}{R(t, t')} x'(t') \right), \quad (8)$$

$R(t, t') = \sqrt{(x(t) - x(t'))^2 + (y(t) - y(t'))^2}$  is the distance between two points on  $L$ . Besides, in the right-hand parts we have:

$$f(t) = \exp(ik(x(t) \cos \gamma + y(t) \sin \gamma)) \quad (9)$$

$$\tilde{f}(t) = k(y'(t) \cos \gamma - x'(t) \sin \gamma) \exp(k(x(t) \cos \gamma + y(t) \sin \gamma)) \quad (10)$$

## REGULARIZATION AND DISCRETIZATION

As a curve given by (3) is smooth, we can solve (5) by projecting them onto the set of global basis and testing functions  $\{e^{im\theta}\}_{m=-\infty}^{+\infty}$ . Here the key step is to split the IE kernels by adding and subtracting the terms corresponding to canonical scatterer, i.e., a circular cylinder [2]. Thanks to the fact that the singularities of actual kernels are the same as of canonical ones, and that angular exponents form a complete set of orthogonal eigenfunctions of the canonical operators, the resultant infinite-matrix equation is of the Fredholm second kind. It has a (2x2) block structure generated by (5) in obvious manner. Therefore this specialized Galerkin projection procedure can be regarded as an analytical preconditioner, which leads to an always-stable numerical solution whose accuracy is easily understood and controlled. Namely, if the intermediate computations have been done with superior accuracy, then the error in matrix inversion is controlled by the size  $N$  of each block, so that large enough  $N$  guarantees a uniform accuracy. An important point of the MAR-algorithm efficiency is fast computation of the matrix elements, which are the double Fourier transform coefficients of the twice-continuous functions formed by the differences of actual and canonical kernels of IEs. Here various versions of FFT and the like numerical algorithms can be successfully implemented. We shall demonstrate the features of the developed method by presenting the dependences of the matrix condition number and inversion error as a function of the matrix block size  $N$  for various triangle sizes, dielectric constants, peak curvatures of smoothing parameterization, and frequencies.

## REFERENCES

- [1] D. Colton, R. Kress, *Integral Equation Methods in Scattering Theory*, Wiley, NY, 1983.
- [2] A.I. Nosich, S.V. Boriskina, "Economic and accurate in resonances solution to the scattering by arbitrary smooth dielectric cylinders based on canonical-shape inversion", *IEEE Trans. Antennas Propagat.*, 2002, submitted.
- [3] L. Shafai, "Surface currents on conducting triangular prisms", *Electron. Lett.*, 1971, vol.7, pp. 32-34.
- [4] W.G. Bickley, "Two-dimension potential problems concerning a single closed boundary", *Phil. Trans.*, 1929, Vol. 228, pp. 235-273.

## SIMULATION OF A DISCRETE LUNEBURG LENS FED BY A CONFORMAL PRINTED ANTENNA

S. Rondineau, A. I. Nosich\*, M. Himdi, J.-P. Daniel

IETR, UMR-CNRS 6164, Université de Rennes 1, Rennes Cédex 35042, France

\* Institute of Radio-Physics and Electronics NASU, Kharkov 61085, Ukraine

### INTRODUCTION

Communications and information technology stimulate a development of various antennas. Because of their simplicity, slot fed circular microstrip antennas (MA) [1] seem to be attractive. Even more attractive are MAs conformally printed on curved surfaces, such as spherical-circular MA (SCMA) because of their higher degree of freedom. However, conventional numerical methods, such as Moment-Method (MM) or FDTD need very high computer resources and do not guarantee a convergence because of ill-conditioned matrices, numerical instabilities, and vulnerability to high-Q resonances. Besides, many applications need special properties: agile scanning beam, multibeam capability, scanning in a large field of view, etc. Here, a very attractive candidate is a discrete Luneburg lens (LL) [2,3,4], which is a layered dielectric sphere. Spherical geometry of both SCMA and LL enables one to simulate them with the same method. Here, we shall use the Method of Analytical Regularization (MAR) [5-7], sometimes called semi-inversion method. Generally, it converts a first-kind singular integral or series equation to a well-conditioned second-kind Fredholm matrix equation, and therefore serves as a perfect pre-conditioner of an ill-posed problem. Then both numerical convergence and efficiency is achieved and matrix-truncation error is controlled.

### ELECTROMAGNETIC MODELING

Suppose that the layer # $i$  is characterized by its material properties  $\epsilon_i$  and  $\mu_i$ , outside radius  $r_i$ , and the size of corresponding PEC spherical disk,  $\theta_i$ , like in Fig. 1. The used excitation is a tangential magnetic dipole (TMD). Spherical geometry offers to expand electromagnetic field in terms of vector spherical modes involving  $P_n^l$ , associated Legendre functions, with coefficients  $a_n^{s,i}$  and  $b_n^{s,i}$ .

The first step concerns the application of so-called dual boundary conditions. This yields a set of  $4N_{shell}$  coupled dual series equations (DSE): for  $0 \leq \theta < \theta_i, i = 1 \dots N_{shell}, \sigma = e, o$ ,

$$\sum_{n \geq 1} \left( C_{an}^Z \cdot X_{an}^\sigma - X_{an}^{\sigma Z, feed} \right) \cdot P_n^1(\cos \theta) = \sigma(-1) \cdot C_1^\sigma \tan \theta / 2$$

$$\sum_{n \geq 1} \left( C_{bn}^K \cdot X_{bn}^\sigma - X_{bn}^{\sigma K, feed} \right) \cdot P_n^1(\cos \theta) = -C_1^\sigma \tan \theta / 2,$$

and also, for  $\theta_i < \theta \leq \pi, i = 1 \dots N_{shell}, \sigma = e, o$ ,

$$\sum_{n \geq 1} \left( C_{an}^K \cdot X_{an}^\sigma - X_{an}^{\sigma K, feed} \right) \cdot P_n^1(\cos \theta) = \bar{\sigma}(-1) \cdot C_2^\sigma \cot \theta / 2$$

$$\sum_{n \geq 1} \left( C_{bn}^Z \cdot X_{bn}^\sigma - X_{bn}^{\sigma Z, feed} \right) \cdot P_n^1(\cos \theta) = C_2^\sigma \cot \theta / 2,$$

where  $X_n^{feed}$  are vectors corresponding to the slot feed field modal description,  $C_n^Z$  and  $C_n^K$  are matrices related to the structure without metallic elements. The unknowns are the vectors  $X_n$ ,  $n \geq 1$ ,  $X_{an}^\sigma = [a_n^{4,2} \dots a_n^{4,N_{shell}-1}]^T$ ,  $X_{bn}^\sigma = [b_n^{4,2} \dots b_n^{4,N_{shell}-1}]^T$ .  $C_1^\sigma$  and  $C_2^\sigma$  correspond to auxiliary constants to be determined.  $\sigma(-1) = +1$  if  $\sigma = o$  and  $\sigma(-1) = -1$  otherwise. Besides, the power boundedness condition determines the allowable class of the unknowns as

$$\sum_{n \geq 1} \|C_{an}^Z \cdot X_{an}^\sigma / n\|^2 < +\infty \quad \sum_{n \geq 1} \|n \cdot C_{bn}^K \cdot X_{bn}^\sigma\|^2 < +\infty.$$

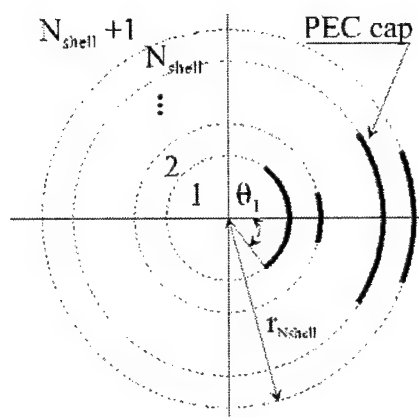
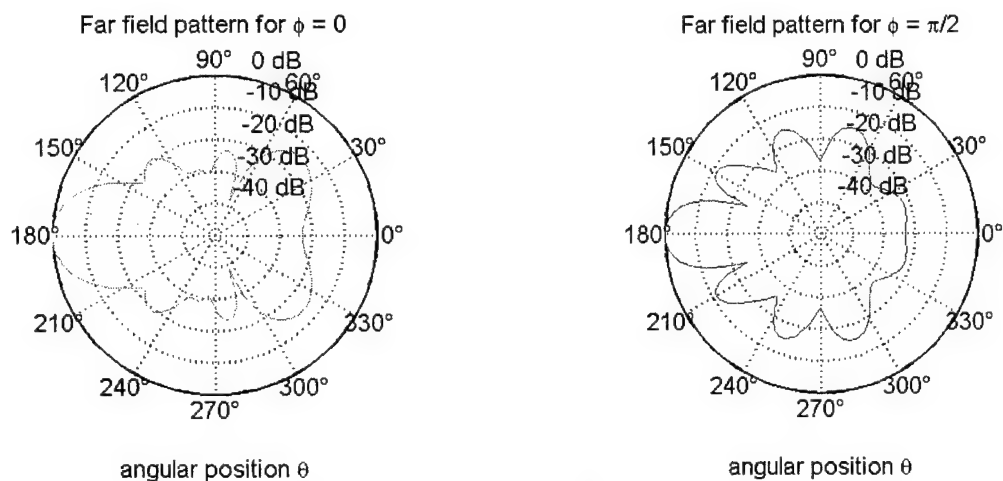
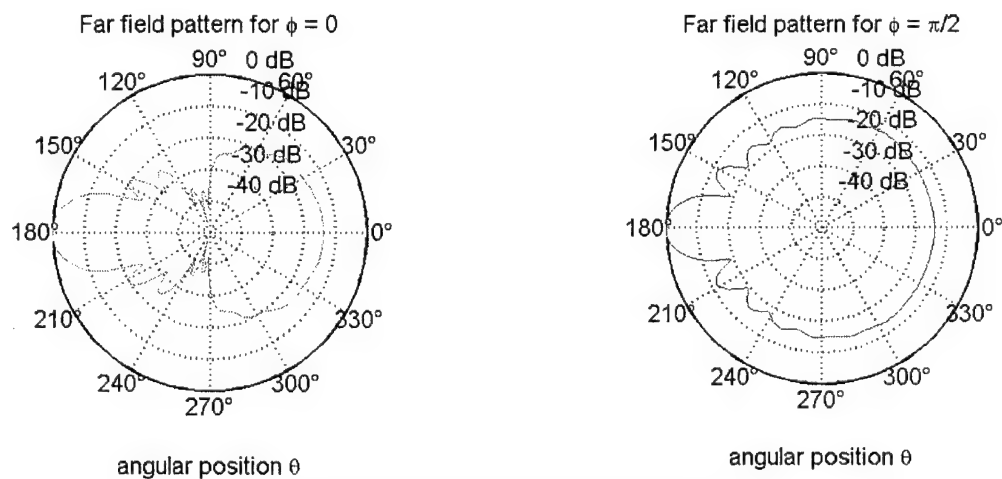


Fig. 1: Definition of the structure.

Fig. 2. Far field pattern for a SCMA fed LL with  $k_0 r_{\text{outside}} = 10.0$ .Fig. 3. Far field pattern for a TMD fed 40-layer LL with  $k_0 r_{\text{lens}} = 10.0$ .

## MAR TREATMENT

Mentioned above DSEs are collectively the 1<sup>st</sup> kind equation which can be written as  $CX = Y$  in terms of operators. Unfortunately,  $C$  is not directly invertible and its numerical inversion is not convergent. According to [6,7],  $C$  can be cut in such a way that  $C = (C_1 + C_2)C_0$ , with  $C_1^{-1}$  a known operator. Then, the 1<sup>st</sup> kind problem becomes the 2<sup>nd</sup> kind problem  $Z + AZ = Z_0$ , where  $Z_0 = C_1^{-1}Y$ ,  $Z = C_0X$  and also  $A = C_1^{-1}C_2$ .  $A$  is a Fredholm operator provided that  $\|A\|_L < +\infty$ . In our problem, MAR technique is easily applied thanks to some simple variable changes:  $\Omega_a(I - G_{aa})Z_{aa}^\sigma = n(n+1)C_{aa}^Z X_{aa}^\sigma$ , and  $(2n+1)\Omega_b(I - G_{bb})Z_{bb}^\sigma = n(n+1)C_{bb}^K X_{bb}^\sigma$ , for  $0 \leq \theta < \theta_i, i=1 \dots N_{shell}$ , with  $\Omega_a$  and  $\Omega_b$  two constant matrices, and,  $(2n+1)Z_{aa}^\sigma = n(n+1)C_{aa}^Z X_{aa}^\sigma$ , and  $Z_{bb}^\sigma = n(n+1)C_{bb}^Z X_{bb}^\sigma$ , for  $\theta_i < \theta \leq \pi, i=1 \dots N_{shell}$ . By the use of the Mehler-Dirichlet expressions, the set of  $4N_{shell}$  coupled linear equations reduces to a set of 2<sup>nd</sup> kind equations:

$$Z_m^\sigma + \sum_{n \geq 1} A_{m,n} \cdot Z_n^\sigma = Z_m^{\sigma, feed}, \quad \forall m \geq 1.$$

By collecting the unknowns into a double infinite vector  $Z^\sigma = [Z_{a0}^{\sigma T}, Z_{b0}^{\sigma T}, Z_{a1}^{\sigma T}, Z_{b1}^{\sigma T}, Z_{a2}^{\sigma T}, Z_{b2}^{\sigma T}, \dots]^T$ , and also  $Z_0^\sigma = [Z_{a0}^{feed T}, Z_{b0}^{feed T}, Z_{a1}^{feed T}, Z_{b1}^{feed T}, Z_{a2}^{feed T}, Z_{b2}^{feed T}, \dots]^T$ , and by defining an infinite matrix  $A$  having  $(2N_{shell} + 2) \times (2N_{shell} + 2)$  infinite blocks composed of the  $A_{m,n}$  matrices, the whole set of the 2<sup>nd</sup> kind can be written as  $Z^\sigma + AZ^\sigma = Z_0^\sigma$ . Each  $A_{m,n}$  is a product of two terms,  $A_{m,n} = A_n^s A_{m,n}^d$ , where  $A_n^s$  depend on the shells characteristics ( $r_n, \epsilon_{rn}, \mu_{rn}, i=1 \dots N_{shell}$ ) and  $A_{m,n}^d$  on the disk ones ( $\theta_i, i=1 \dots N_{shell}$ ). Moreover,  $A_n^s$  behave as  $O(1/n)$ , and  $A_{m,n}^d$  as  $O(1/(n-m))$  if  $m \neq n$ , and like  $O(1)$  otherwise. As a consequence,  $A$  is compact as  $\|Z_0\| < +\infty$  that ensures the existence of unique solution, which can be approached as closely as wanted thanks to point-wise convergence.

## RESULTS

In order to ensure a 3-digits accuracy in solving the matrix all the computations were done with  $N = 120$ . Figs. 2 and 3 present far field patterns of LL fed by SCMA+TMD and a simple TMD feeds, respectively. Here, the patch is the inner (smaller:  $\theta_{inside} = 1.3^\circ$ ) conductor, and the ground surface is formed by the outer (larger) metallic cap ( $\theta_{outside} = 3.0^\circ$ ). The focusing effect is clearly seen, as well as the shadowing by SCMA. MAR technique is a very powerful and economic method to study complete SCMA-LL radiation problem. It enables one to highlight with controlled accuracy the effects of finite ground size, curvature, several types of resonances connected with SCMA, ground and coating, and LL focusing, etc.

## REFERENCES

- [1] M. Pozar, *A Review of Aperture Coupled Microstrip Antennas: History, Operation, Development and Applications*, University of Massachusetts Press, 1996.
- [2] R.K. Luneburg, *The Mathematical Theory of Optics*, University of California Press, 1944.
- [3] H. Mieras, Radiation Pattern Computation of a Spherical Lens Using Mie Series, *IEEE Trans. Antennas Propagat.*, vol. AP-30, no. 6, 1982.
- [4] Y. Rahmat-Samii, et al. Luneburg Lens Antennas Revisited: Design, Optimization, and Measurements, *AP 2000 Symposium Proceedings*, 5A7, Davos, 2000.
- [5] S.S. Vinogradov, Reflectivity of a spherical shield, *Radiophysics Quantum Electronics*, vol. 26, no 1, pp. 78-88, 1983.
- [6] S.S. Vinogradov, A.V. Sulima, Calculation of the absorption cross-section of a partially shielded dielectric sphere, *Radiophysics Quantum Electronics*, v. 26, no 10, pp. 927-931, 1983.
- [7] A.I. Nosich, The Method of Analytical Regularization in wave-scattering and eigenvalue problems, *IEEE Antennas Propagat. Magazine*, vol. 43, no 3, pp. 34-49, 1999.

**PROPAGATION  
AND  
SIGNAL  
PROCESSING**

## THE FILTER FOR HORN ANTENNA MULTIFREQUENCY DATA PROCESSING

Yevgueny V. Kondratyev, Oleg O. Drobakhin\*

Dnepropetrovsk National University, Ukraine

Mailing address: 119b Kirova Avenue, apt. 83, Dnepropetrovsk 49061, Ukraine

E-mail: ce@ua.fm

\* Dnepropetrovsk National University, Ukraine; e-mail: odr@ua.fm

### ABSTRACT

The transceiver horn antenna used in multifrequency microwave measurements for probing the structure under the test and receiving reflected power has two reference discontinuities. This causes obtained reflectivity dependency to be a superposition of two similar echoing characteristics, so that clear discerning reflectivity signal peaks and estimating their parameters is impossible in the most part of uniqueness range of Fourier transform, which is used for viewing the dependency in spatial area. The Filter for Horn Antenna Multifrequency Data Processing is designed for extracting single echoing characteristic from said dependency. This allows productive using almost all the uniqueness range provided that in the far-field region the reflectivity ratio of reference discontinuities and electric length of the horn do not depend on distance to structure under the test.

### INTRODUCTION

The multifrequency reflectometers [1] implement the principle of synthesising radio pulse envelope [2] using data of reflectivity module measurements carried out in free space on a discrete frequency grid with the presence of reference discontinuity. Reflectivity is obtained as ratio of incident and reflected wave power, which is respectively irradiated and gathered by the transceiver antenna serving also as reference discontinuity (-ies). Complex-valued spatial echoing characteristic is obtained by inverse Fourier transform of measured frequency response.

### GROUND FOR DEVELOPING THE FILTER

Practical usage of horn antennas in multifrequency reflectometer looks more preferable in comparison with simpler antennas like the open-ended waveguide (OEW), especially when remote testing is necessary (in industrial conditions, for example) because of their high gain (of about 25 dB). However, analysis of reflectivity dependencies derived with horn antennas in their primal view leaves unused the greater part of distance range of uniqueness of Fourier transform. The main difficulty is that direct measurement data represents a superposition of echoing characteristics corresponding to cross-correlation functions (CCFs) of reflectivity of structure under the test with that of throat and aperture of the horn. Thus for structure with electric width exceeding the electric length of the horn the clear interpreting of synthesised signal peaks is impossible. Removing

one of the characteristics (by some method) would allow using practically all the range of a uniqueness of measurements, only limiting the aperture-structure distance by structure's electric width.

## MATHEMATICAL DESCRIPTION

We have researched the simplest of possible processings (further – horn antenna data filter) extracting a unique echoing characteristic. It is built using the following statements. The echoing characteristic  $F(\omega)$  obtained with horn antenna is a superposition of three functions:  $F_1(\omega) + F_2(\omega) + F_3(\omega)$  (typical look is shown on fig. 1a). The first of them corresponds to correlation of structure's echoing characteristic with that of the first reference discontinuity (horn's throat, for example), the second – similarly with the second (accordingly, aperture). The third is attributed all the rest, in particular auto-correlation functions of discontinuities, CCF of reference discontinuities and other (possibly unexpected) components. Further, in spatial domain it is possible to consider the function  $F_2(z)$  as  $kF_1(z + \Delta z)$ , where  $\Delta z$  is the shift along the measurement axis (equal to electric length of the horn),  $k$  is a complex multiplier taking into account the amplitude ratio and phase difference of reflection signals corresponding to CCF structure-aperture and structure-horn's throat. It is supposed that  $k = \text{const}$  in the far-field region. Specified parameters are subject for experimental determination, because of their individuality for each horn in concrete frequency band and measurement installation calibrations being in use.

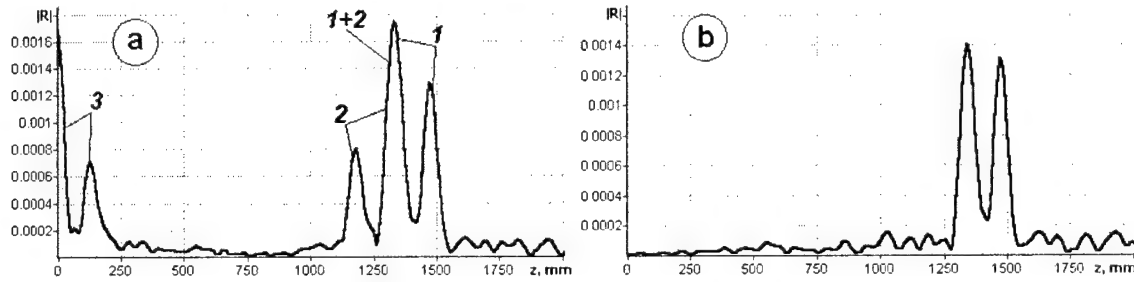


Fig 1: a – typical view of raw synthesised spatial signal for single-layer structure (1, 2, 3 – components of  $F_1$ ,  $F_2$ ,  $F_3$  respectively, 1+2 – a case of superposition of  $F_1$  and  $F_2$ ); b – single echoing characteristic  $F_1$ , derived with the filter

Thus, in frequency area  $F_2(\omega) = kF_1(\omega) \exp(j\omega \cdot \Delta t)$  where  $\Delta t = \frac{2\Delta z}{c}$ ,  $c$  is the speed of

light in vacuum, and 2 is the multiplier taking into account forward wave propagation up to the structure and backwards after reflection. To use this relation we delete the component  $F_3$  in spatial area (in working realisation of the filter it is done by applying trapezoidal window with transition width, which equals to 0.5% of the uniqueness range, but is not less than 3 discrete spatial samples). Now in frequency area the echoing characteristic appears as  $(1 + k \cdot \exp(j\omega \cdot \Delta t)) \cdot F_1(\omega)$ , so the desired echoing characteristic may be obtained by dividing by the expression  $1 + k \cdot \exp(j\omega \cdot \Delta t)$ . Treating the result of division with Fourier transform, we gain the unique spatial echoing characteristic (fig. 1b).



In real conditions the most of assertions, on which the filter is based, are disturbed a little by random factors: unreproducibility of measurements, dispersion in experimentally determined filter parameters and their light nonconstancy conditioned by properties of and distance to structure under the test. Some of them may be compensated, for example, non-linear distortions and modulation of frequency response, other may not, for example, inexact concurrence of reflection signal shapes and levels for horn's aperture and throat causing either under- or over- or improper compensation of  $F_2$ . These effects may be considered as additional component  $F_4$ , which cannot be deleted by spatial window for  $F_3$  or in other known ways. Dividing  $F_4$  by  $1 + k \cdot \exp(j\omega \cdot \Delta t)$  produces in a spatial domain the characteristics looking as  $k' F_4(z + i\Delta z)$ , where  $i = 1, 2, 3, \dots$ . Thus any uncompensated parasitic peak will give a series of peaks with the increasing (on  $|k| > 1$ ) or decreasing (on  $|k| < 1$ ) amplitude. So limiting  $|k|$  by value close to one (for example 0.9) and extracting the greater of two echoing characteristics and also using the horn with as possible lower  $|k|$  is necessary for the exception of "spawning" the parasitic components. Ideally, as well as in the case of OEW, absence of the second reference discontinuity makes the filtering unnecessary.

### APPLICABILITY OF THE FILTER

Considered filter takes plenty of computational resources (it thrice uses the Fourier transform – first before applying spatial window, further returning to frequency area with subsequent dividing by  $1 + k \cdot \exp(j\omega \cdot \Delta t)$ , and at last obtaining the final spatial echoing characteristic). Nevertheless, this is not a serious problem for modern computer technology – the most part of the computer time is still spent on the obtained characteristics visualisation, so real-time measurements are anyway possible.

The results of applying the filter to actual reflectivity data give the basis for recommending its usage in reflectometers with a horn probe. For example, the measurements in 8-12.5 GHz range with the purpose of determining the dielectric constant ( $\varepsilon$ ) for single-layer structures showed that the variation of filter parameters (separately) by  $\pm 6$  mm for  $\Delta z$  (at the wave length of 30 mm!),  $\pm 0.1$  for  $|k|$ , and  $\pm 0.3$  rad for  $\arg(k)$  results in  $\varepsilon$  estimation deviation not greater than 0.11 for  $\varepsilon$  of about 3. The actual deviation of  $\Delta z$ ,  $|k|$  and  $\arg(k)$  at different distances to the structure in far-field region measurements makes correspondingly  $\pm 0.7$  mm,  $\pm 0.02$ ,  $\pm 0.07$  rad, that results in the  $\varepsilon$  estimation error imported by the filter not greater than 0.02. It must be marked that the most preferable is applying the filter with the antenna of such a construction, which minimises  $|k|$  maintaining its independence from the distance.

### REFERENCES

- [1] Drobakhin O. O. Realisation of the method of synthesising radio pulse envelope using amplitude measurement data derived with a horn antenna. // Russian Non-destructive Testing Journal. – 1999. – #7. – P. 67-74.
- [2] Drobakhin O. O., Kondratyev Y. V., Korotkaya V. G. Computerised measurement installation for non-destructive testing of dielectric products: hardware and software // System Technologies. – 2001. – #5(16). – P. 29-32. (in Russian).

## ON UNIQUE ESTIMATION OF AZIMUTH-ELEVATION-CARRIERS BY VOLUME ARRAYS

I. Urazghildiiev\*, C. Carlemalm Logothetis\*, A. Rydberg\*, K. Wallin\*\*

\*Signals and Systems Group, Uppsala University, Box 528, 75237, Uppsala, Sweden  
E-mail: ildar.urazghildiiev@ieee.org

\*\*Sensys Traffic AB, Dag Hammarskjöldsväg 10A, 75153, Uppsala, Sweden  
E-mail: kjell.wallin@sensystraffic.se

### ABSTRACT

The necessary and sufficient conditions in terms of antenna array geometry for unique estimation of azimuth-elevation-carriers (AEC) of narrow-band signals are introduced. These conditions make it possible to solve the problem of joint AEC estimation based on spatial samples taken by the volume array without using the large number of temporal samples.

### INTRODUCTION

The problem of joint azimuth-elevation-carriers (AEC) estimation of narrow-band signals arises in communication, radar, radio astronomy, sonar and many other applications. An important issue related to this problem is the unique estimation of signal AECs via array of given geometry. This issue called also as the identifiability problem (see [1]-[3] and references herein). The standard formulation of this problem involves determination of the number of harmonics that can be resolved for a given total sample size. The solutions to be proposed are obtained under conditions of equispaced samples, existence of all samples along all the array dimensions and difference of all harmonics to be resolved. These conditions significantly restrict the practical implementation of the theory. In this paper we present the necessary and sufficient conditions for unique AEC estimation by volume array those are given in terms of the number of the antenna array sensors and array geometry.

### DATA MODEL AND PROBLEM FORMULATION

We assume that there are  $M$  point sources that are emitting the unknown narrow-band complex deterministic signals  $s_m(t)$ ,  $m=1...M$  in the direction of the measurement system. For every signal the parameters of interest are the azimuth  $\beta_m$ , the elevation  $\varepsilon_m$  and the carrier  $f_m$ . To describe the signal parameters let us introduce a vector  $\boldsymbol{\mu}_m = f_m \mathbf{e}_m / f_{max} \in R^3$ ,  $\boldsymbol{\mu}_m \in U_\mu = \{\boldsymbol{\mu} : \beta \in [0, \pi], \varepsilon \in [0, \pi], f \in [f_{min}, f_{max}]\}$ , where  $\mathbf{e}_m = [\cos\beta_m \cos\varepsilon_m, \sin\beta_m \cos\varepsilon_m, \sin\varepsilon_m]^T$  is the unit vector in the Cartesian coordinate system and  $(\cdot)^T$  denotes transpose. It is assumed that the measurement system consists of  $N$  omnidirectional point sensors. Then the model of antenna array output in noiseless case can be represented as follows:

$$\mathbf{z}(t) = \mathbf{A}\mathbf{s}(t) \in C^{N \times 1}, \quad t = 1...L, \quad (1)$$

where  $\mathbf{A}=[\mathbf{a}(\mu_1)\dots \mathbf{a}(\mu_M)]\in C^{N\times M}$  is a matrix of steering vectors,  $\mathbf{a}(\mu_m)=[1, \exp\{j2\pi \mathbf{d}_2^T \mu_m\}, \dots, \exp\{j2\pi \mathbf{d}_N^T \mu_m\}]^T$  is a steering vector,  $\mathbf{d}_n = d_n \mathbf{i}_n c / f_{max}$  is a vector of the  $n$ th sensor position ( $\mathbf{d}_1=\mathbf{0}$ ),  $d_n$  is a distance to the  $n$ th sensor,  $\mathbf{i}_n$  is a unit vector toward the  $n$ th sensor position,  $\mathbf{D}=[\mathbf{d}_1\dots \mathbf{d}_N]\in R^{3\times N}$  is a matrix that specify the antenna array geometry,  $\mathbf{s}(t)\in C^{M\times L}$  is a vector of the signal waveforms,  $L$  denotes the number of data snapshots available. We assume, that the sampled covariance matrix of signal waveforms  $\hat{\mathbf{P}}=(L)^{-1}\sum_{t=1}^L \mathbf{s}(t)\mathbf{s}^H(t)\in C^{M\times M}$  has full rank, that is  $rank(\hat{\mathbf{P}})=M$ , and the number of signals  $M$  is known.

The problem to be solved is formulated as follows: to determine the basic requirements for the number  $N$  and positions  $\mathbf{D}$  of array sensors, that guarantee the unique estimation of any distinct set  $\mu_1 \neq \dots \neq \mu_M \in U_\mu$  of signal parameters.

### IDENTIFIABILITY OF AEC ESTIMATES

The necessary and sufficient conditions for identifiability of  $U_\mu$  are [1] NSC1: the set of steering vectors  $\mathbf{a}(\mu)$  is known; NSC2: for any  $\mu_1 \neq \dots \neq \mu_M \in U_\mu$  the matrix  $\mathbf{A}$  has full rank  $rank[\mathbf{a}(\mu_1)\dots \mathbf{a}(\mu_M)]=\min(N, M)=M < N$ ; NSC3: the number of sensors  $N$ , the rank  $R$  of matrix  $\mathbf{P}$  and the number  $Q$  of parameters per signal satisfy to the following inequality  $N \geq R+Q=M+3$ . The NSC1 and NSC3 hold if the antenna array is calibrated and its geometry  $\mathbf{D}$  is known, and the maximum number of impinging signals  $M \leq N-3$ . Therefore, the problem to be solved can be reduced to the determination of the requirements for the sensor positions  $\mathbf{D}$  that guarantee the implementation of the NSC2.

*Theorem:* For any  $\mu_1 \neq \dots \neq \mu_M \in U_\mu$  the matrix  $\mathbf{A}$  has full rank if: i) the array has a subarray with  $K \leq N$  sensors, such that the number  $N_p$  of the parallel planes that can be passed through the points  $\mathbf{d}_1, \dots, \mathbf{d}_K$  satisfy the conditions  $N_p = K-2 > M$ , and ii) the maximum distance  $d_{max}$  between any nearest sensors of subarray is less then half of minimum wavelength  $d_{max} \leq \lambda_{min} / 2 = c / (2f_{max})$ .

*Proof:* The proof is based on the fact that the rank of matrix  $\mathbf{A}$  is defined as follows  $rank(\mathbf{A})=\min(N-K_r, M-K_c)$ , where  $K_r$  is the number of rows and  $K_c$  is the number of columns that are coincident to any other row or column respectively. Condition ii) means, that the maximum sampling frequency in spatial domain is higher then the Nyquist rate, therefore the vectors  $\mu$  giving  $K_c > 0$  columns that are coincident to the column  $\mathbf{a}(\mu_1)$  are the roots of the following set of equations

$$\mathbf{i}_n^T \mu = c_n, \quad n=2\dots K, \quad (2)$$

where  $c_n = \mathbf{i}_n^T \mu_1$ . The vectors  $\mu^{(n)}$  that satisfy to the  $n$ th equation of (2) represent the set of points lying on a plane  $\Xi(\mathbf{i}_n, c_n) \in R^2$  that is orthogonal to the vector  $\mathbf{i}_n$  and located on the distances  $|c_n| \leq 1$  from the origin. Therefore the set  $U'_\mu$  of roots of (2)

are the intersection between  $U_\mu$  and the planes  $\Xi(\mathbf{i}_n, c_n)$ :  
 $U'_\mu(\mathbf{i}_2 \dots \mathbf{i}_K) = U_\mu \cap_{n=2}^K \Xi(\mathbf{i}_n, c_n)$ .

Observe, that the set  $U_\mu$  is a space between two hemispheres of radiuses  $f_{\min}/f_{\max}$  and 1. Therefore, if the vectors  $\mathbf{d}_1 \dots \mathbf{d}_K$  do not lie on the same plane, i.e.  $\text{rank}([\mathbf{d}_1 \dots \mathbf{d}_K]) = 3$ , then the set  $U'_\mu$  is a point and only point  $U'_\mu = \{\mu_1\}$ . It means, that if the subarray is a volume, then for any  $\mu_1 \neq \dots \neq \mu_M \in U_\mu$  the inequality  $\mathbf{a}(\mu_1) \neq \dots \neq \mathbf{a}(\mu_M)$  holds true and  $K_c = 0$ . Observe also, that if  $K_1 \leq K$  sensors lie on a plane, then the set  $U'_\mu(\mathbf{i}_2 \dots \mathbf{i}_{K_1})$  is a section and consists of infinite number of elements. Hence, for any distinct  $\mu_1 \neq \dots \neq \mu_M \in U'_\mu(\mathbf{i}_2 \dots \mathbf{i}_{K_1})$ ,  $K_1$  equations of (2) hold and  $K_1$  rows of the matrix  $[\mathbf{a}(\mu_1) \dots \mathbf{a}(\mu_M)]$  are equal, i.e.  $K_r = K_1$ . The  $K_r - 1$  rows can be rejected without loss of information. Therefore, to ensure the full rank of the matrix  $\mathbf{A}$  the number of sensors lying in nonparallel planes has to satisfy the condition  $N_p > M$ . Since the plane can be passed through any three sensors, the minimum size of the subarray is  $K = N_p + 2$ .

## CONCLUSION

An important corollary of the theorem is that the joint AEC estimation of narrow-band signals can be performed by means of spatial samples taken by volume antenna array. The temporal averaging is needed to ensure a full rank of the covariance matrix of signal waveforms as well as to increase the signal-to-noise ratio. In practice analogue tools can successfully carry out this procedure that is very important for the MW measurements systems. Another conclusion is that the arrays with irregular geometry have advantages in comparison with the periodic arrays from the identifiability point of view.

The possible applications of the considered theory could include the wide-range spectrum monitoring direction finders, Doppler radar systems, wireless communication systems and other.

## REFERENCES

- [1] M. Wax, I. Ziskind, "On unique localization of multiple sources by passive sensor arrays", *IEEE Trans. Acoust., Speech, Signal Processing*, vol. ASSP-37, pp. 996-1000, July 1989.
- [2] J. Tao, N.D. Sidiropoulos, J.M.F. Berge, "Almost-sure identifiability of multidimensional harmonic retrieval," *IEEE Trans. Signal Processing*, vol. 49, pp. 1849-1859, September 2001.
- [3] K.-C. Tan, S.S. Goh, E.-C. Tan, "A study of the rank-ambiguity issues in direction-of-arrival estimation," *IEEE Trans. Signal Processing*, vol. 44, pp. 880-887, April 1996.

## COMPARING TECHNIQUES FOR PROVING UNSATISFIABILITY

Olga Tveretina, Hans Zantema

Department of Computer Science  
Technical University of Eindhoven  
P.O. Box 513, 5600 MB Eindhoven, The Netherlands  
Email: o.tveretina@tue.nl, h.zantema@tue.nl

### ABSTRACT

We compare two standard techniques for satisfiability (SAT), which are basic for verification of microprocessor systems. We propose an approach for construction of shorter resolution refutations based on a standard approach called DPLL.

### INTRODUCTION

Many problems in different fields, including software verification, electronic design automation, verification and diagnosis of faults in hardware can be naturally encoded into the satisfiability problem for propositional logic(SAT) and then solved by a SAT-solver.

A digital signal processor is a special type of microprocessor chip. The design of increasingly complex digital circuits includes many levels of model transformation starting from high design level where device is presented as a model specification (description) to circuit layout (realization) moving through many intermediate design levels. Each circuit design level has to be verified before production can take place. If it can be proven that an implementation satisfies the given specifications then the chip design is functionally correct (Fig.1).

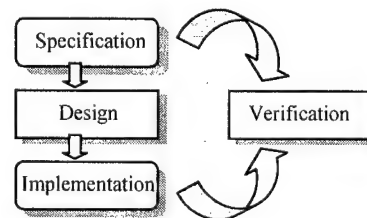


Fig.1. Equivalence checking

Various techniques to formally verify discrete systems have been developed within last decade. These techniques can be roughly divided into theorem proving and model checking. Last ones are restricted to systems with a small number of variables due to a large computational effort.

Methods of propositional logic are applied for formal verification of discrete systems with large number of variables.

In our paper we consider some aspects of formal verification based on propositional formulas validity. This provides a formal mathematical proof that the functional behavior of the specification and the implementation coincides by means of proving of equivalence of two propositional formulas.

It is well-known that the satisfiability problem for the propositional calculus is NP-complete. Roughly speaking, it means that any algorithm to the satisfiability problem will have exponential worst case complexity.

## PROPOSITIONAL FORMULAS AND SATISFIABILITY

A propositional formula  $F$  is a combination of propositional variables  $x_1, \dots, x_n$ , where each variable intended to get a value *false* or *true*, in a meaningful way with symbol  $\vee$  (or, disjunction),  $\wedge$  (and, conjunction),  $\neg$  (negation),  $\rightarrow$  (implication),  $\leftrightarrow$  (iff). Verifying a property  $P$  and  $Q$  are equivalent means proving that  $P \leftrightarrow Q$  is always *true*, which is equivalent to  $\neg(P \leftrightarrow Q)$  is not satisfiable.

Here satisfiability means that there is an interpretation for the variables such that the formula becomes *true*, otherwise the formula is unsatisfiable.

We consider methods for formulas in conjunctive normal form (CNF), being a conjunction of clauses, where a clause is a disjunction of literals, and a literal is a variable or the negation of a variable. A particular case of a clause is the empty clause, which can be considered as a representation of *false*. Any formula in propositional logic can be converted to a formula in Conjunctive Normal Form (CNF).

## SOME TECHNIQUES FOR PROVING UNSATISFIABILITY

One of the simplest and widely investigated method for proving unsatisfiability of propositional formulas is resolution [5]. Essentially, this method consists of a single rule stating that from knowing  $x \vee C$  and  $\neg x \vee D$  one may conclude  $C \vee D$ . An application of this rule is called a resolution step. The particular case of resolution when  $C$  or  $D$  is empty is called a unit resolution.

A CNF is unsatisfiable if and only if the empty clause can be derived by resolution. Such a sequence of resolution steps ending in the empty clause called a resolution refutation.

The original resolution based algorithm was DP procedure [1]. Unfortunately, it consumes a large amount of space.

A related method is the DPLL procedure [2]. DPLL based procedures are basis for almost all complete SAT solvers, including the fastest ones. This method consists of a combination of unit resolution, doing case analysis upon  $x$  and  $\neg x$ , and going on recursively.

## TRANSFORMING DPLL TO RESOLUTION

In [6] we have analyzed the relation between DPLL and resolution in detail. We have proved that if in the arbitrary DPLL procedure  $s$  unit resolution steps are executed and  $r$  recursive calls are done then there exists a resolution refutation of length at most  $s - r/2$ .

Adding the restriction that all possible unit resolution steps have to be done after every recursive call we get the stronger upper bound  $s - r$ .

We have proved for suitable formulas that the second upper bound is tight and no shorter resolution refutation exists than we give by our transformation.

Based on this theoretical result we give a construction of resolution refutation of length less than number of unit resolution steps executed during DPLL.

## CONCLUSIONS

Recently there has been interest in using resolution in combination with DPLL search [4]. It is shown that algorithms combining resolution and search are more efficient than DPLL.

We have proved that if in the DPLL procedure  $s$  unit resolution steps are executed and  $r$  recursive calls are done then the resolution refutation of length at most  $s - r$  can be constructed. We implemented this procedure in C. Since DPLL allows freedom of choosing branching variable it is difficult to draw general conclusions from a one particular choice. For examples we have made experiments it turned out that for some formulas had length less than presented upper bound.

## REFERENCES

- [1] M. Davis, H. Putnam. A computing procedure for quantification theory. Journal of the ACM, 7:201-215, 1960.
- [2] M. Davis, G. Logemann, and D. Loveland. A machine program for theorem proving. C.ACM5/1962.
- [3] A. Van Gelder. Satisfiability testing with more reasoning and less guessing. In D.S. Johnson and M. Trick, editors, Clique, Coloring, and Satisfiability: Second DIMACS Implementation Challenge, DIMACS Series in Discrete Mathematics and Theoretical Computer Science. American Mathematical Society, 1995.
- [4] I. Rish, R. Dechter. Resolution versus search: Two strategies for SAT. IOS Press, 2000.
- [5] J. A. Robinson. A machine oriented logic based on resolution principle. JACM12/1965.
- [6] O. Tveretina, H. Zantema. Transforming DPLL to resolution. Eindhoven technical university. Technical report. To appear. <http://www.win.tue.nl/~hzantema/other.html>

# MODIFIED METHOD OF GEOMETRIC ELECTROMAGNETICS FOR THE ANALYSIS OF RADIO FIELD IN MARINE TROPOSPHERIC WAVEGUIDES

Anatoly Bychkov, Alexei Bychkov

Dept. Radio Engineering, Sebastopol Navy Institute, Sebastopol, Ukraine

The interest for practical use of tropospheric waveguides (TWG) above the sea surface is still high. This is because there are many new tools for remote sensing of the atmosphere boundary layer and efficient methods for calculation of radiowave fields. Those TWG often form over the Black Sea.

An efficient method for calculation of radiofields is the method of geometric electromagnetics (GE) based on the Brillouin conception. It has been used to determine radiofields and parameters of dielectrics waveguides and microwave devices [1]. The method GE had been developed for waveguiding systems with "rigid" boundaries of layered environment. However, a sea TWG is not a system with "rigid" boundaries. The first "wall" of TWG is the surface of the sea with parameters  $\varepsilon_3, \mu_3, \sigma_3$  that reflects incident radiowaves. The layer of atmosphere having a lower value of the relative dielectric permittivity  $\varepsilon_2$  will be the second "wall". At the same time in the TWG, up to the height,  $h_1$ , the permittivity  $\varepsilon_1$  varies to  $\varepsilon_2$  smoothly. If a superposition of plane waves (e.g., incident and reflected waves) satisfies the boundary conditions, then guided-wave propagation is possible. The equation for the resulting field in TWG accounts for this circumstance.

The Poynting vector  $\vec{\Pi}$  of a plane radio wave propagating in TWG (Fig.1) forms angles  $\theta_x, \theta_y, \theta_z$  with the axes of coordinates:

$$\cos^2 \theta_x + \cos^2 \theta_y + \cos^2 \theta_z = 1. \quad (1)$$

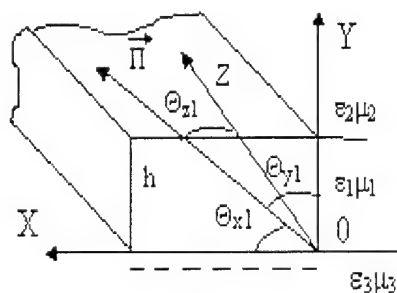


Fig. 1

At the height of TWG  $h_1$  the dielectric permittivity  $\varepsilon_1$  starts changing smoothly and reaches  $\varepsilon_2$  at the height  $h_2$ , hence to characterize the plane radio wave in the environment with a variable index of refraction we can use the equation,



$$E = E_m e^{j[\omega t - k(\cos\theta_x \cdot x + \cos\theta_y \cdot y + \cos\theta_z \cdot z)]} = E_m e^{j\left[\omega t - \frac{\omega}{c} n W_0(x, y, z)\right]}, \quad (2)$$

where  $\cos\theta_x$ ,  $\cos\theta_y$ ,  $\cos\theta_z$  are projections of the unit normal to wave's front, and

$n = \sqrt{\varepsilon}$  is the index of refraction. Equation for a smoothly varying environment is

$$W(x, y, z) = n W_0(x, y, z) = \text{const}, \quad (3)$$

where function  $W(x, y, z)$  is the eikonal:

$$\text{grad}(W) = n \text{ or } \left(\frac{\partial W}{\partial x}\right)^2 + \left(\frac{\partial W}{\partial y}\right)^2 + \left(\frac{\partial W}{\partial z}\right)^2 = n^2. \quad (4)$$

For TWG under consideration, the function  $W(x, y, z)$  can be simplified because  $\cos\theta_x = 0$ . The function  $W(y, z)$  might be presented as minimum of the linear integral  $\int n(S) dS$  taken from  $S = 0$  to  $S = h_1$ . The minimum is reached if the curve  $S$  coincides with the ray trajectory in troposphere:

$$\min \frac{1}{h_1} \int_0^{h_1} n(S) dS = \frac{1}{h_1} \int_0^{h_1} n(y) dy = \frac{W}{h_1}. \quad (5)$$

The equation (5) is used for determining the phase of radio waves reflected from the "upper wall" of TWG. A superposition of the incident wave and the reflected from the media interface yields the following electric field amplitude:

$$\begin{aligned} E &= E_m [\cos(\omega t + k_{y1} \cdot y - k_{z1} \cdot z) + \cos(\omega t - k_{y1} \cdot y - k_{z1} \cdot z + \varphi_h)] = \\ &= 2E_m \left[ \cos\left(k_{y1} \cdot y - \frac{\varphi_h}{2}\right) \cdot \cos\left(\omega t - k_{z1} \cdot z + \frac{\varphi_h}{2}\right) \right], \end{aligned} \quad (6)$$

where  $k_{y1} = k_1 \cdot \cos\theta_y$ ,  $k_{z1} = k_1 \cdot \cos\theta_z$ ,  $\varphi_h/2$  is the phase of the coefficient of reflection from the "upper wall" of TWG.

The equation (6) is valid under the conditions of total interior reflection of radio waves. As far as "upper wall" of TWG is "soft" (no "rigid" boundary between layers with  $\varepsilon_1$  and  $\varepsilon_2$ ), the current phase of the coefficient of reflection depends on the angles of incidence of radio waves and on the variation of the relative index of refraction:

$$M(y) = (\sqrt{\varepsilon(y)} - 1) \cdot 10^6 + \frac{y}{R_E} = [n(y) - 1] \cdot 10^6 + \frac{y}{R_E}, \quad (7)$$

where  $R_E$  is the radius of Earth,  $y$  is a current height of TWG for the waves with horizontal or vertical polarization, and the proper phase of the coefficient of reflection.

To account for the vector structure of the field it should be transformed to new system of coordinates,  $OX'$ ,  $OY'$ , and  $OZ'$ . This transformation is characterized with the Euler angles. If a radio wave has vertical polarization and  $\mu_1 = \mu_2 = 1$ ,  $\sigma_1 = \sigma_2 = 0$ , then we can write the final equation for  $\varphi_h/2$ :

$$\begin{aligned}\varphi_b = \frac{\varphi_h}{2} &= \arctg \left[ \frac{\varepsilon_1(y)}{\varepsilon_2(y) \cos \theta_{y1}} \cdot \sqrt{\sin^2 \theta_{y1} - \frac{\varepsilon_2(y)}{\varepsilon_1(y)}} \right] = \\ &= \arctg \left[ \frac{\frac{1}{h_1} \int_0^{h_1} n^2(y) dy}{\frac{1}{h_2} \int_{h_1}^{h_2} n^2(y) dy \cos \theta_{y1}} \times \sqrt{\sin^2 \theta_{y1} - \frac{\frac{1}{h_2} \int_{h_1}^{h_2} n^2(y) dy}{\frac{1}{h_1} \int_0^{h_1} n^2(y) dy}} \right], \quad (8)\end{aligned}$$

where  $n(y)$  is calculated after (7). The coordinate  $y$  varies from 0 through the inflection point of the profile  $M(y)$ , i.e.  $y = h_1$ , then to height  $h_2$  that is the coordinate of curve  $M(y)$  where the atmosphere is standard.

The value of  $\varphi_h/2$  obtained from (8) can be used in (6) to calculate the field both inside TWG and outside it at the heights from  $h_1$  to  $h_2$ . If dielectric permittivity of troposphere is complex-valued (conductance  $\sigma \neq 0$ ), then the equations (5)-(8) derived in this work can be used to calculate the energy losses in marine TWG.

The modified GE method that has been discussed in this work enables a more complete account of TWG effects during the waving. The evaluation of a frontier conditions by the "low wall" TWG above the Black Sea shows that radio waves with length about 10 cm experience almost specular reflection. The absolute value of the reflection coefficient is in the range of 0.87 to 0.95. The phase of reflection is  $\pi$  for the vertical and horizontal polarizations for "weak" and "strong" waveguides of evaporation having  $h_1 = 10$  m and near-surface TWG having  $h_1$  up to 500 m when the sea waving reaches 2 to 3 units [2].

Modification of the GE method allows estimation of important parameters of wave propagation in the TWG: wavelength, maximum phase and group velocities, critical angle  $\theta_{cr}$  limiting the range of wave propagation. The radiation patterns of radio devices must be oriented into angular sector that is determined by  $\theta_{cr}$ , therefore knowledge of  $\theta_{cr}$  has great practical value for proper feeding of TWG. Our theoretical results have been confirmed in radar experiments.

## REFERENCES

- [1] I.K. Bondarenko, A.I. Burya, V.V. Salamatina, *Electromagnetics Foundations of CAD of Microwave Integrated Circuits*, Moscow, IRE AN SSR Press, 1981, pp. 159-173.
- [2] A.A. Bychkov, Justification of the method of geometric electromagnetics for evaluation of parameters of marine tropospheric waveguides under the sea waving, *Proc. Int. Symp. "Radio Electronics and Youth"*, Kharkov, 2002, pp. 249-250 (in Russian).

## NONLINEAR STAGE OF PROPAGATION OF WAVE DISTURBANCES IN THE TOPSIDE IONOSPHERE

V. B. Ivanov, M. V. Tolstikov

Irkutsk State University, Irkutsk, Russia

664047, Irkutsk, Russia, Deputatskaya Str.10, 123. Phone 8 295 227 05 42.

e-mail : ivb@Ivb.baikal.ru

### ABSTRACT

This paper is continued investigations of propagation of disturbances of plasma concentration in the topside ionosphere. A mathematical modeling of the nonlinear stage of instability development has been carried out. It is shown that in the region of a maximum enhancement of perturbations, the relative fluctuations of plasma density can make up several tens of percent.

In [1,2,3] these authors showed the possibility of an enhancement of plasma density wave disturbances during their downward propagation in the topside ionosphere. The physical setting of the problem was as follows. A harmonic disturbance of plasma density with a typical period of tens to hundreds of seconds was specified on a certain upper boundary (700-800 km). Sources for such disturbances can be provided, in particular, by different types of oscillations of the neutral atmosphere, such as AGW and IGW, and effects of magnetospheric origin. The propagation of this disturbance along geomagnetic field lines was considered. It was shown that as the disturbances propagate downward, their amplitude can increase significantly, so that a region of strong plasma density fluctuations with the vertical size of the disturbances on the order of several tens of kilometres can be produced at about 500-600 km altitudes. Because the spatial growth rates of enhancement of the disturbances were quite significant, it is of interest to evaluate the range of validity of the linear approach and examine nonlinear questions arising in the case of the propagation of intense disturbances.

In previous work the basic equation describing the dynamics of small disturbances of electron density in plasma  $n$ , for the case of the ambipolar motion of charges along geomagnetic field lines, was derived from linearized equations of motion and continuity for electron-ion gas in conditions of the nightside mid-latitude ionosphere. In carrying out the linearization, the plasma density and hydrodynamic velocity were represented as the sum of the time-independent background part and a small, harmonically time-dependent addition:  $N = N_0 + n * e^{i\omega t}$ ,  $V = V_0 + v * e^{i\omega t}$ , and terms of second order of smallness were  $n*v$  discarded. In accordance with the character of the phenomenon under study, a nonlinearity of the form  $n*v$  will manifest itself in the generation of higher frequency harmonics of external action  $\omega$ . In order to take the higher harmonics into account, the following mathematical description of the nonlinear processes was developed. Let the plasma density and hydrodynamic velocity be represented as the sum:

$$N = N_0 + \sum_{j=1}^m n_j * e^{i * j \omega t}, V = V_0 + \sum_{j=1}^m v_j * e^{i * j \omega t}. \quad (1)$$

next, we substitute (1) into the equation of motion and continuity of electron-ion gas:

$$N \frac{\partial V}{\partial t} = -gN - vNV - c^2 \frac{\partial N}{\partial z} \quad (2)$$

$$\frac{\partial N}{\partial t} + \frac{\partial NV}{\partial z} + \beta N = 0 \quad (3)$$

By combining terms with identical exponentials, we obtain the equation for background density and  $m$  equations describing harmonics with the fundamental in  $m$  respectively. A natural assumption is made that harmonic amplitudes decrease with the harmonic number. Furthermore, higher harmonics are generated by lower harmonics like forcing actions. Equations for the fundamental (4) and second (5) harmonics are given below, and we may limit our consideration to them.

$$\frac{d^2 n_1}{dz^2} - \frac{dn_1}{dz} \left( \frac{1}{H_p} + \frac{1}{H} \frac{v}{v+i\omega} + \frac{i\omega V_0}{c^2} \right) + n_1 \left[ \left( \frac{1}{HH_p} + \frac{i\omega V_0}{c^2 H} \right) \frac{v}{v+i\omega} - \frac{i\omega \frac{dN_0}{dz} + (\beta + i\omega)(v + i\omega)}{c^2} \right] = 0. \quad (4)$$

$$\frac{d^2 n_2}{dz^2} - \frac{dn_2}{dz} \left( \frac{1}{H_p} + \frac{1}{H} \frac{v}{v+2i\omega} + \frac{2i\omega V_0}{c^2} \right) + n_2 \left[ \left( \frac{1}{HH_p} + \frac{2i\omega V_0}{c^2 H} \right) \frac{v}{v+2i\omega} - \frac{2i\omega \frac{dN_0}{dz} + (\beta + 2i\omega)(v + 2i\omega)}{c^2} \right] = \frac{i\omega}{c^2} \left( \frac{\partial n_1 V_1}{\partial z} - \frac{v}{(2i\omega + v)H} n_1 V_1 \right) \quad (5)$$

In the above equations the axis  $z$  is pointing down, and the origin of coordinates lies at 800 km,  $H$  is the height scale of the main component of the neutral atmosphere, atomic oxygen,  $H_p$  is the plasma height scale,  $v$  is the collision frequency of ions with neutral atoms,  $V_0$  is the hydrodynamic velocity of plasma (vertical component),  $c$  is the ion sound velocity, and  $\beta$  is the linear recombination coefficient. The quantities  $v$  and  $\beta$  were assumed to be exponentially dependent on the height, and the velocity  $V_0$  was calculated in terms of a numerical model of the ionosphere and is also a function of height. The other parameters were taken to be constant. The conditions of the nightside ionosphere of middle and moderately high latitudes were considered and modeled.

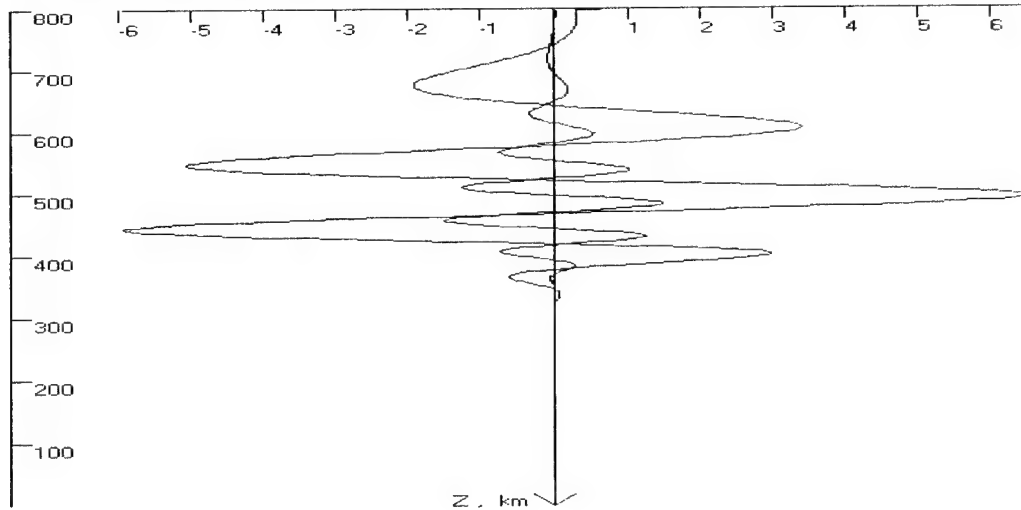


Figure 1.

Fig. 1 presents the fundamental (with the frequency  $\omega=0.05 c^{-1}$ ) and second harmonics in the linear regime. An essentially nonlinear regime in a state of saturation will occur whenever the second harmonic becomes comparable with the fundamental harmonic - the initial assumption about decreasing amplitudes does not hold. It is the estimates of this state that are of the greatest interest.

Fig. 2 plots the dependence of a maximum of the ratio of the second harmonic to the fundamental versus ratio of the fundamental to the background for the frequencies  $\omega=0.1 c^{-1}$  и  $\omega=0.01 c^{-1}$ .

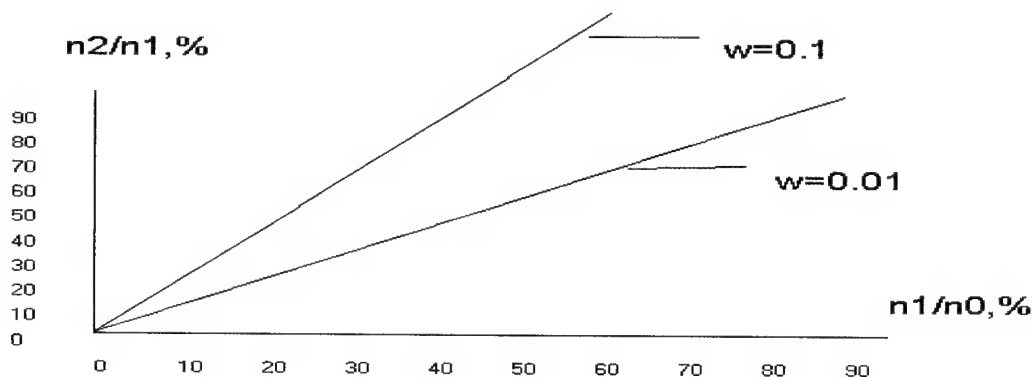


Figure 2.

As can be seen from the figure, a developed nonlinearity in the saturation regime will occur in the case of disturbances of the fundamental harmonic in the region of its maximum on the order of 20-30% of the background. Such strong disturbances can penetrate below the F2-layer peak and, hence, the results obtained in this study can be used to explain the well-known F-spread phenomenon at vertical-incidence radio soundings of the mid-latitude ionosphere.

## ACKNOWLEDGMENTS

This work was done with support from Russian Foundation FOR BASIC RESERCH under grant of leading scientific schools of Russian Federation № 00-15-98509

## REFERENCES

- [1] Izv. VUZov. RADIOFIZIKA v. XLI, No. 4, pp. 432-437., Ivanov V.B., Polyakov V.M., The evolution of wave disturbances in the topside ionosphere.
- [2] Izv. VUZov. RADIOFIZIKA v. XLI, No. 9, pp. 1086-1092., Ivanov V.B., Polyakov V.M. The evolution of wave disturbances in the topside ionosphere. Pt. 2.
- [3] Researches on a geomagnetism, aeronomy and solar physics., №111, Ivanov V.B., Polyakov V.M., Tolstikov M.V., On the propagation of perturbation of a gases medium in the gravitational field with the inertia taken into account : ionospheric applications.

## THE TECHNIQUE FOR CALCULATING OF HF-SIGNALS CHARACTERISTICS TAKING INTO CONSIDERATION IONOSPHERE WAVEGUIDE PROPAGATION

Alexey V. Oinats, Vladimir I. Kurkin, Sergey N. Ponomarchuk

Institute of Solar-Terrestrial Physics  
of Russian Academy of Science Siberian Division  
E-mail: oinats@iszf.irk.ru

### ABSTRACT

The technique based on waveguide approach for calculating of ionosphere oblique-incidence sounding signal characteristics taking account of ionosphere waveguide excitation is offered. The comparison of given technique calculation results and experimental ionograms on the path Alice-Springs (Australia) - Irkutsk (Russia) is given.

### INTRODUCTION

Within the framework of waveguide approach in ISTP SD RAS the technique for calculating of characteristics of signals that propagate on an inhomogeneous path in any of the existing Earth-ionosphere waveguides (for example, waveguide between the ground and E-layer of the ionosphere or waveguide between the ground and F-layer of the ionosphere) was designed. The stationary condition that allows defining interference properties of a series of normal modes and the structure of a field in waveguide is the basis of this technique. It is equivalent to a requirement:

$$L_n^{\pm}(\vec{r}, f) = \frac{1}{2\pi} (\Phi_n^{\pm} - \Phi_{n+1}^{\pm}) = l^{\pm} \quad (1)$$

- the phase difference of the neighboring normal modes is multiple  $2\pi$ . Here  $f$  is a frequency,  $n$  is a number of normal mode,  $\Phi_n^{\pm}$  is its phase in a point  $\vec{r}$ ,  $l^{\pm}$  is an integral nonnegative numbers (number of hops). For given number of normal mode the stationary condition determines the geometric localization of a field of group of normal modes with this central number, i.e. propagation trajectory of packet of phased normal modes.

Really there are cases, in which the modes of propagation spreading at first in one waveguides, and then transferring in other one. In particular there are the ionosphere propagation modes, i.e. which propagate in the ionosphere waveguide on a part of a path.

To calculate the characteristics of the ionosphere propagation modes, it is necessary to take into account transitive groups of the normal modes, which were not considered in the standard scheme. Those are such groups of normal modes, which propagate in one waveguide on a part of the path, and in other waveguide on another part of the path. Such an account is possible, if we introduce the continuity condition for propagation trajectory of packet of phased normal modes as is in geometric optics.

In the report the approximate scheme of the calculation of the ionosphere propagation mode characteristics based on such hybrid approach is given. All characteristics of a signal field in the Earth-ionosphere and ionosphere waveguides are calculated using the above-mentioned standard technique. In points of transition from one waveguide to other one weaving is made, based on continuity condition for propagation trajectory of packet of phased normal modes.

### THE SCHEME OF CALCULATION

The scheme of calculation is as follows. First, the group of normal modes, which is effectively incited by receiver and weakly penetrates through the ionosphere, is selected. From this group the subgroup is separated, which propagate in the Earth-ionosphere waveguide on all path. For this group of modes the calculation of the signal characteristics is carried out using a standard technique.

Further the rest group of normal modes, which participates in transitions between waveguides, is considered. The number of normal modes in this group is determined by variation of maximum and minimum waveguide numbers along a path of propagation and can reach several thousand for equatorial paths.

The calculation is carried out in a cycle on central numbers with some step. Central number of a packet of phased normal modes is adiabatic invariant and does not vary at propagation in the waveguide except for transition points. Therefore for each of them the transition point from one waveguide to other one is determined using dependences of maximum and minimum waveguide numbers on the longitudinal coordinate. Using (1) in the transition point, the height of localization and propagation delay of the normal mode packet in this waveguide is calculated. On these data the waveguide is defined, in which this packet of normal modes transfers. The condition of the propagation trajectory continuity actually means that the angle  $\alpha$  between tangent to a trajectory of the packet and horizontal should vary continuously. As it is follows from equation

$$\alpha = \arccos \left( \frac{\gamma_n}{y\sqrt{\varepsilon(y, \theta)}} \right), \quad (2)$$

where  $\gamma_n$  - spectral parameter,  $y$  relative radial and  $\theta$  angular - spherical coordinates,  $\varepsilon(y, \theta)$  - permittivity of the ionosphere, the dependence of spectral parameter on coordinate along the path  $\gamma_n(\theta)$  should be continuous too. This requirement in view of the normal modes spectral equation gives that central number of the packet at transition from one waveguide in other one changes by bound. The value of this bound is determined by volume of adjacent waveguides (for example, ionosphere waveguide will be an adjacent waveguide at transition from E to F waveguide).

After central number of the packet in the new waveguide is obtained, the new transition point is determined and the calculation for the new waveguide is iterated or, if the end of the path achieves, the characteristics are calculated using standard scheme.

In a point of the receiver arrangement the resulting interference function and resulting propagation delay of the normal mode packet are determined by the formulas

$$L_n(\theta, y) = \sum_k \Delta L_{n_k}, \quad (3)$$

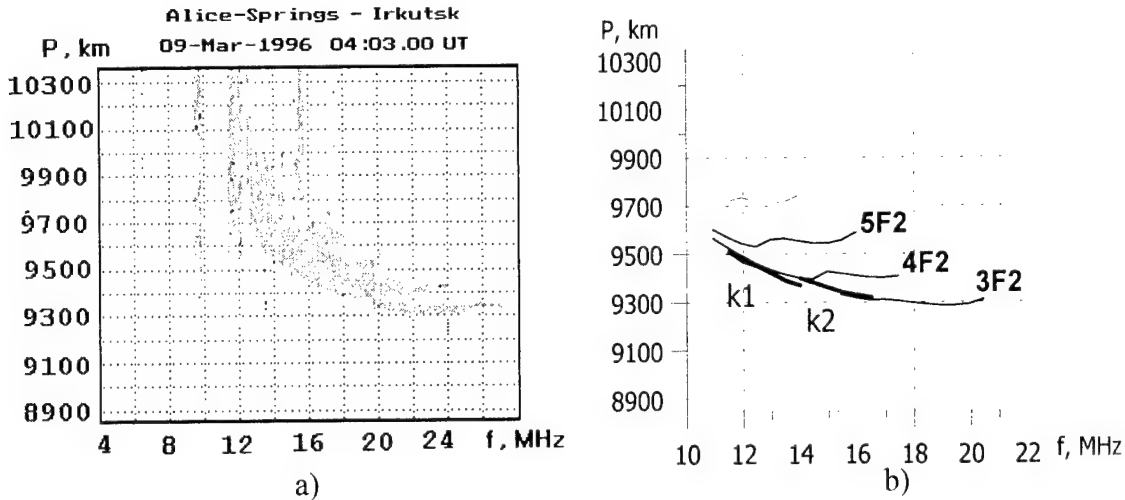


Fig.1. Experimental ionogram (a) and results of the calculation (b).

$$\tau_n(\theta, y) = \sum_k \Delta\tau_{n_k}. \quad (4)$$

Here  $\Delta L_{n_k}$ ,  $\Delta\tau_{n_k}$  are additives to interference function and delay at propagation of the packet in  $k$  waveguide under the account along the path.

The obtained dependence of interference function on central numbers in the point of the receiver arrangement (3) is approximated by splines, and using the stationary condition central numbers of packets giving the contribution to a signal field near the ground are determined.

Making similar calculation for a series of frequencies, we obtain a standard ionogram with distance-frequency dependences of transition modes of propagation.

## RESULTS OF CALCULATION

As an illustration on figure 1 the results of the calculation (b), which has been, carried out using the designed approximate scheme, and experimental ionogram (a) for equatorial path Alice-Springs (Australia) - Irkutsk (Russia) 04 UT on March 9, 1996 are shown.

The frequency range of the experimental ionogram and of the calculation results don't coincide. It is possible to explain this by the underestimated maximum F-layer frequency along the propagation path of the used ionospheric model.

On the figure 1b one can see two transition propagation modes (k2 - three-hop and k1 - four-hop), which propagate a part of the path in the ionosphere waveguide. They qualitatively explain a bend of 3F2 mode curve in the low-frequency area, which we can see on the experimental ionogram.

## REFERENCES

- [1] V.I. Kurkin, I.I. Orlov, and V.M. Popov. Normal-mode approach in the problem of HF radio communication. Moscow: Nauka, 1981.
- [2] A.V. Gurevich, E.E. Ceditina. Superdistant radiowave propagation. Moscow: Nauka, 1979.



## ELECTRODYNAMIC MODEL OF THE RECEIVING ANTENNA IN TERMS OF A WAVEGUIDE REPRESENTATION OF THE HF FIELD

Vitaly V. Khakhinov

Institute of Solar-Terrestrial Physics SD RAS  
Russia, 664033, Irkutsk, P.O.Box 4026  
E-mail: khakhin@iszf.irk.ru

### ABSTRACT

This paper is concerned with the problem of the current excitation in the receiving antenna in the HF field. The solution of the problem is performed in terms of a waveguide representation of the HF field in the spherical Earth-ionosphere waveguide. Structurally, the antenna is treated in the form of a conductor of a finite length and arbitrary configuration.

### INTRODUCTION

A variety of research problems require creating a structural physical model of the radio channel. By a radio channel is meant here the portion of the communication link in which the information signal acquires a spatial distribution. The structure of the HF radio channel consists of receive-transmit antenna-feeder systems and the Earth-ionosphere waveguide. The receiving antenna is an important element of the radio channel that requires an electrodynamic approach in a mathematical simulation. The researchers' attention to receiving antennas is inversely proportional to the factor by which their number exceeds the number of radiating antennas.

### FORMULATION OF THE PROBLEM

The electrodynamic model of the receiving antenna is determined by the representation of the incident electromagnetic field. The representation of the field, in turn, is determined by the method of solving the electrodynamic problem for radio wave propagation. The model was constructed in terms of a waveguide representation of the HF field in the spherically symmetric Earth-ionosphere waveguide. It was assumed that the receiving antenna does not disturb the structure of the incident field. Use was made of the geocentric coordinate system with the polar axis passing through the phase center of the radiating element (the radius-vector is  $\mathbf{r}_s = (r_s, 0, \varphi_s)$ ). The field was calculated on the basis of the method of normal waves [1-3].

The antenna is regarded as a conductor of finite length with an arbitrary configuration, and when treated electrostatically, it represents a long uniform line with the distributed (along it) electromotive force (EMF). Current is excited by the electric field component  $E_r$  along the conductor axis. In calculations,  $E_r$  is taken at points infinitely close to the conductor surface.

In the spherically symmetric waveguide the incident electromagnetic field breaks into the field of TM waves (with the symbol "e") containing the  $E_r$  and  $E_\theta$  components of the electric field, and the field of type TE waves (with the symbol "m") containing the  $E_\varphi$

component. An expression for EMF induced at the element  $dl$  of the antenna may be written as:

$$d\varepsilon = d\varepsilon^e + d\varepsilon^m = [(\mathbf{e}_r \mathbf{e}_l) E_r(\mathbf{r}_l) + (\mathbf{e}_\theta \mathbf{e}_l) E_\theta(\mathbf{r}_l)] dl + (\mathbf{e}_\varphi \mathbf{e}_l) E_\varphi(\mathbf{r}_l) dl. \quad (1)$$

Here  $\mathbf{e}_r$ ,  $\mathbf{e}_\theta$  and  $\mathbf{e}_\varphi$  are unit vectors of the coordinate system;  $\mathbf{r}_l = (r_l, \theta_l, \varphi_l)$  is the radius-vector of the antenna element; and  $\mathbf{e}_l$  is the unit vector along  $dl$ . In the general case the expression for the  $j$  component of the field is a series for normal waves:

$$E_j(\mathbf{r}_l) = \frac{1}{r_l} \sum_n A_n R_n(r_l) D_{jn}(\mathbf{l}, \varphi) e^{i(v_n \theta_l - \pi/4)} \quad (2)$$

Here  $A_n$  is the amplitude factor;  $D_{jn}$  stands for the coefficients of excitation of normal waves by the radiator with a given distribution of current  $\mathbf{l}$  which characterize the distribution of radiated energy in normal waves; and  $R_n$  and  $v_n$  are the eigenfunctions and the eigenvalues of the respective boundary-value problems for TM and TE waves.

### COEFFICIENTS OF RECEPTION OF NORMAL WAVES

The induced EMF generates two running current waves: from  $dl$  to the receiving end of the antenna and to the end of the antenna with load resistance  $Z_R$ . At the ends of the antenna the waves are partially reflected and partially absorbed in load resistance or escape via the feeder line to the receiver. To calculate the current we used the method of superposition of running waves [4]. By summing all components of the running and reflected waves, it is possible (according to [4](p.189)) to obtain the expression for the current at an arbitrary point of the antenna. The value of the current at the receiving end of the antenna may be written as:

$$dJ_0 = \frac{Y(l)}{W} d\varepsilon \quad (3)$$

Here:  $Y(l) = \frac{e^{ikl} + p_F e^{ikl} + p_R e^{ik(2L-l)} + p_F p_R e^{ik(2L-l)}}{2(1 - p_F p_R e^{i2kl})}$ ;  $W$  is the wave resistance of the

conductor;  $L$  is the antenna length;  $p_F = (W - Z_F)/(W + Z_F)$  and  $p_R = (W - Z_R)/(W + Z_R)$  are the coefficients of reflection of current from the ends of the antenna; and  $Z_F$  is the input resistance of the feeder line loaded by the receiving device. The function  $Y(l)$  defines the distribution of current in the antenna with regard for the load conditions at both ends. Substitute (1) into (3) by using the expressions (2) for the components of the field. The value of total output current is determined by integrating along the length of the receiving antenna:

$$J_0 = \sum_n A_n \left( D_n^e P_n^e e^{i v_n^e \theta_l} + D_n^m P_n^m e^{i v_n^m \theta_l} \right) \quad (4)$$

The integration used the condition of the smallness of the antenna's linear size compared with the distance to the radiator. The functions:

$$P_n^e = \int_l \frac{Y(l)}{W r_l} \left[ (\mathbf{e}_r \mathbf{e}_l) \frac{v_n}{k r_l} R_n^e(r_l) - (\mathbf{e}_\theta \mathbf{e}_l) \frac{dR_n^e(r_l)}{ik \varepsilon' dr} \right] e^{-i v_n^e \theta_l \cos(\varphi_s - \varphi_l)} dl \quad (5)$$

$$P_n^m = \int_l (\mathbf{e}_\varphi \mathbf{e}_l) \frac{Y(l)}{W r_l} R_n^m(r_l) e^{-i v_n^m \theta_l \cos(\varphi_s - \varphi_l)} dl$$

constitute the essence of the electrodynamic model of the receiving antenna in terms of a waveguide representation of the exciting HF field. They characterise the level of induced current by the components of the TM and TE field of a separate normal wave and are determined by the parameters of the receiving antenna. It is therefore logical to call  $P_n^{e,m}$  the coefficients of reception of normal waves of corresponding polarisation.

### RECEIVING ANTENNA EFFECTIVE LENGTH

A key characteristic of the receiving antenna is believed to be the effective length defined as the ratio of the current strength at the receiving end to the value of the incident field strength at the phase center of the antenna. It is natural to select, as the phase center of the antenna, its receiving end with the radius-vector  $\mathbf{r}_F$ . If the expression for  $Y(l)$  is transformed to the form [4](p.194):  $Y(l) = \tilde{Y}(l)/(Z + Z_F)$ , (here  $Z$  is the input resistance of the antenna with  $Z_R$  taken into account), then the expression for output current may be written in terms of the antenna effective length:

$$J_0 = \frac{E(\mathbf{r}_F)h_d}{Z_a + Z_F}, \quad (6)$$

by defining the expression for  $h_d$  as:

$$h_d = \frac{1}{E(\mathbf{r}_F)} \sum A_n \left( D_n^e \tilde{P}_n^e e^{iv_n^e \theta_s} + D_n^m \tilde{P}_n^m e^{iv_n^m \theta_s} \right), \quad (7)$$

where  $\tilde{P}_n^e$  and  $\tilde{P}_n^m$  are determined by formulas (5) with the replacement of  $Y(l)$  by  $\tilde{Y}(l)$ .

### CONCLUSIONS

The electrodynamic model that has been constructed here for the receiving antenna in terms of the method of normal waves is represented by the coefficients  $P_n^e$  and  $P_n^m$ . They represent the influence of the characteristics of the receiving antenna and, primarily, its directed properties, when the energy of the incident TE and TM waves of the field transforms to the energy of current oscillations.

### ACKNOWLEDGEMENTS

This work was done with support from the Russian foundation for Basic Research grant for leading scientific schools of the Russian Federation No.00-15-98509.

### REFERENCES

- [1] Bremmer H. Terrestrial Radio Waves. Theory of Propagation. Amsterdam, 1949. 343 p.
- [2] Kurkin V.I., Orlov I.I., and Popov V.N. Normal-Mode Approach in the Problem of HF Radio Communication. Moscow: Nauka, 1981. 122 p. (in Russian).
- [3] Khakhinov V.V. Analyzing the HF Field in the Wave Zone of the Antenna Using the Normal-Mode Approach // Conf. Proc. MMET\*2000. Kharkov (Ukraine). 2000. P.298-300.
- [4] Lavrov G.A. and Knyazev A.S. Near-Surface and Underground Antennas. Moscow: Nauka, 1965. 472 p.

## EVALUATION OF THE ATMOSPHERIC AEROSOL PARTICLE SIZE IN THE REFLECTIVE LAYER PRODUCED BY STRONG SOLAR FLARES

Y.V. Goncharenko, F.V. Kivva

Institute of Radio Physics and Electronics  
of National Academy of Sciences of Ukraine, Kharkov, Ukraine  
E-mail: YGonch@ire.kharkov.ua

### ABSTRACT

It is well known, that nowadays one of the actual problem in the troposphere investigation is to connect solar activity with meteorological processes in the troposphere. But to present day there is no model, which explains all problem of solar terrestrial links. Investigation of influence of variation solar and cosmic rays on condition in the low and middle atmosphere take a significant part in determination parameters of this model. Experimental measurements of the low and middle atmosphere temperature profile [1] show, that it was changed after strong solar flares (Fig. 1). Theoretical model proposed in [1] explains this phenomena using atmospheric absorbent or reflective layer, with heights from 5 till 20 km. Good agreement between experimental data and numerical simulation was achieved for layers with 14-16 and 8-9 km height respectively, and coefficient of transparency about 90%.

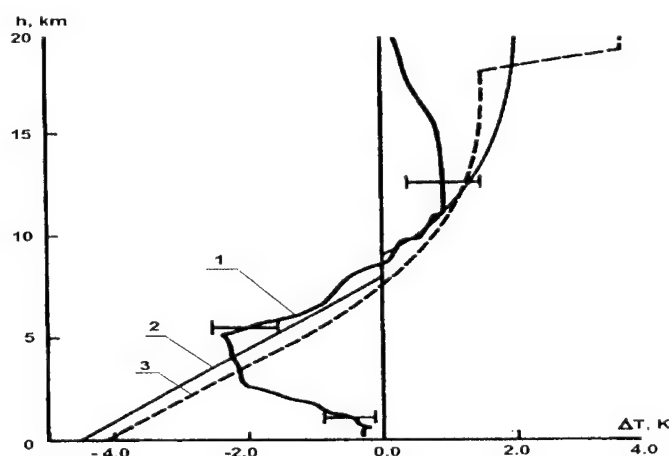


Fig. 1 Variation of temperature profile: 1- experiment, 2 – model with reflective layer on height 8-9 km., 3 – model with absorption layer on height 14-16 km.

### INTRODUCTION

Lets consider a model with reflective layer as more preferable. This layer may consist of macromolecular complexes witch include both atmospheric gases ions and water. Lets assume, that aerosols concentration proportional to ion's concentration on this height.

During strong solar flare this concentration may increase from  $100 \text{ cm}^{-3}$  to  $1000 \text{ cm}^{-3}$  [2], so aerosol concentration increase too. It is well known, that about 97% of solar energy located in the wave-length of  $0.2\text{-}3 \cdot 10^{-6} \text{ m}$ . (Fig. 2) [3] and this energy is stable in time, so, we have considered the aerosol influence of on transmission of electromagnetic energy only in this wave-length range.

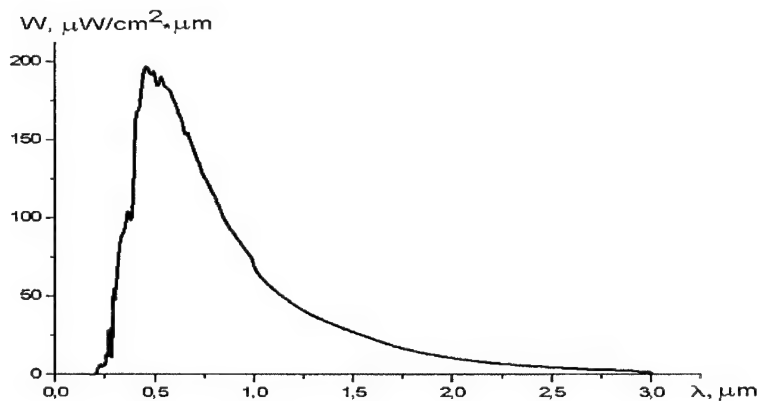


Fig. 2  $W(\lambda)$  – Solar radiation density.

As a result of small water permittivity imaginary part value of [4] we have examined only mechanism of backscattering from the little drops and didn't evaluate absorption of electromagnetic energy in water drops.

#### EVALUATION OF THE ATMOSPHERIC AEROSOL PARTICLE SIZE IN THE REFLECTIVE LAYER

It is well known, that the atmospheric aerosol particle size lies in wide range so, we have to calculate electromagnetic scattering on aerosols using Mie equation:

$$K_{bs}(m, x) = \frac{2}{\pi^2} \sum_{n=1}^{\infty} (2n+1) (|a_n|^2 + |b_n|^2), \quad (1)$$

where:

$$x = \frac{2\pi r}{\lambda}, \quad (2)$$

$$a_n = \frac{A_n(mx)\psi_n(x) - m\psi_n'(x)}{A_n(mx)\xi_n(x) - m\xi_n'(x)}; b_n = \frac{mA_n(mx)\psi_n(x) - \psi_n'(x)}{mA_n(mx)\xi_n(x) - \xi_n'(x)}, \quad (3)$$

$$\psi_n(x) = \sqrt{\frac{\pi x}{2}} J_{n+1/2}(x), \quad (4)$$

$$\xi_n(x) = \sqrt{\frac{\pi x}{2}} [J_{n+1/2}(x) + (-1)^n i J_{-n-1/2}(x)], \quad (5)$$

$$A_n(mx) = \frac{\psi_n'(mx)}{\psi(mx)}, \quad (6)$$

Where  $J_{n+1/2}$  and  $J_{n-1/2}$  are Bessel function;  $m=v-i\chi=1.322-i0.00001$  is complex water permittivity in wave-length range  $0.2-3 \cdot 10^{-6}$  m. [4].

To calculate Mie coefficients  $a_n$  and  $b_n$  (3,6) we have used Deirmenjian algorithm [4,5].

Weakening factor (dB/km) was defined by Buger low:

$$K_{scat}(x, m) = 1.346439 \cdot 10^{-2} \int_{R_1}^{R_2} r^2 N f(r) K_{hs}(x, m) dr, \quad (7)$$

where,  $N$  is concentration of aerosols,  $\text{cm}^{-3}$ ;  $r$  is radius of drops,  $\mu\text{m}$ ;  $f(r)$  is distribution density of drops size.

For simplicity sake lets assume, that radius of drops is a constant, due to similarity of the physical conditions for their appearance. Integral coefficient of transparency in wave-length range  $0.2-3 \cdot 10^{-6}$ :

$$W(r) = \frac{1}{W_0} \int_{\lambda_1}^{\lambda_2} K_{scat} \left( \frac{2\pi r}{\lambda} \right) W(\lambda) d\lambda, \quad (8)$$

where  $W_0$  is the solar constant ( $W_0=1373 \pm 20 \text{ W/m}^2$  [3]).

Calculation results for reflective layer with thickness 1 km are present in Fig. 3. As shown, supposed aerosol particle radius ( $0.2 \mu\text{m}$ , approximately) don't conflict with physical nature water aerosols.

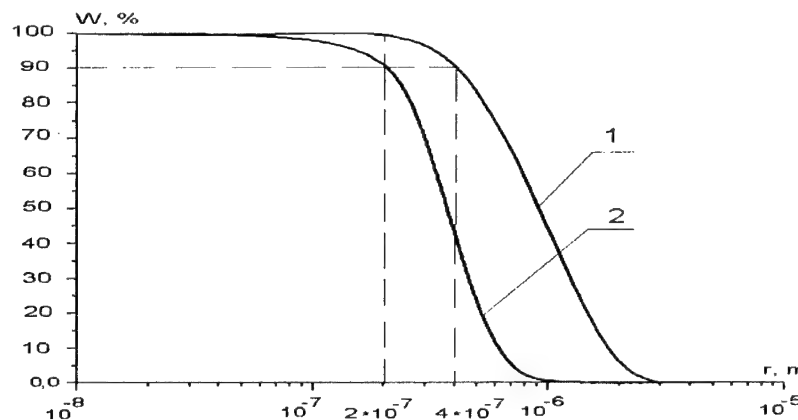


Fig.3 Coefficient of transparency; 1-for layer with  $N=100$ ; 2 - for layer with  $N=1000$ ;

## REFERENCES

- [1] M. I. Pudovkin, A. L. Dementeeva. Variation of high temperature profile in the low atmosphere during solar proton events. *Geomagnetism and Aeronomy*. Vol 37, №3, 1997.
- [2] Handbook of Atmospheric Electrodynamics, vol. 1. Edited by Hans Volland, CRC press, 1995.
- [3] Oran R. White. The solar output and its variation. Moscow, MIR: 1980.
- [4] D. Deirmenjian. Electromagnetic scattering on spherical polydispersions. Moscow, MIR: 1971.
- [5] G.M. Ajvazan. Propagation of millimeter and sub millimeter waves in clouds. Leningrad: Gidrometeoizdat, 1991.

## ON POSSIBILITY OF SCHUMANN RESONANCE OBSERVATIONS WITHIN INDUSTRIAL AREA

A.V. Shvets, V.K. Ivanov, A.V. Varavin

A. Usikov Institute for Radio Physics and Electronics NASU  
ul. Proskury 12, Kharkov 61085, Ukraine. E-mail: Shvets@ire.kharkov.ua

### ABSTRACT

Use of ADC with high resolution allowed us to embrace dynamic range both signal and powerful narrow-band interference and on this base to implement a compensative real-time algorithm for suppression of narrowband interference. The developed algorithm provides suppression of "wings" occurred due to incommensurability of a time interval of a signal that undergo to the spectral analysis and a period of a narrowband interference. Preliminary results of observations of extremely low frequency (ELF) natural electromagnetic background (Schumann resonance) performed within urban areas are presented in the paper. We demonstrate both possibilities of registration of average spectra of the Schumann resonance background signal and ELF-transients.

### INTRODUCTION

A phenomenon called Schumann Resonance (SR) is observed in spectra of the natural terrestrial radiation in the ELF range as a number of peaks at frequencies 8, 14, 20, 26 Hz. SR is excited by the worldwide lightning and represents natural oscillations of the Earth-ionosphere cavity. SR carries information both on electromagnetic properties of the lower ionosphere and ELF sources. SR measurements are used for inferring thunderstorm activity total level and its spatial distribution with the purpose of monitoring for global environmental changes [1,2]. In particular realization of idea of worldwide lightning tomography [2] will require creation of global network of the SR observatories. In this paper we consider possibility of SR observations within urban environment that would provide more regular and careful control on the receiving equipment and extending of the number of probable observation points.

As a rule the most powerful interferences are the power-line harmonics 50(60) Hz hitting into the studied frequency range. They essentially cut down the dynamic range of recorded signals. The use of traditional notch filters becomes sometimes not effective due to the suppression fails because of fluctuations of the power line frequency. Using synchronous notch filters with phase self-tuning of the rejection frequency [3] can solve the problem but relative complexity and complication in their tuning limits its using in portable systems. A data acquisition system with high resolution embracing dynamic range both signal and interference that permitted both to realize the signal filtration in a digital form and to reduce to the minimum using analogous components in the receiving system was used in the present work for the SR observations.

### METHOD FOR COMPENSATION THE NARROW-BAND INTERFERENCE

The monochromatic signal  $s(t) = a \cos(\omega_0 t + \varphi)$  multiplied by the rectangular time window  $[0..T]$  is used as a model of narrow-band interference. The spectrum of this signal includes two peaks with frequencies  $\pm\omega_0$  with a width that is determined by the number of hitting, into the interval  $[0..T]$ , of periods of the high-frequency infill. The

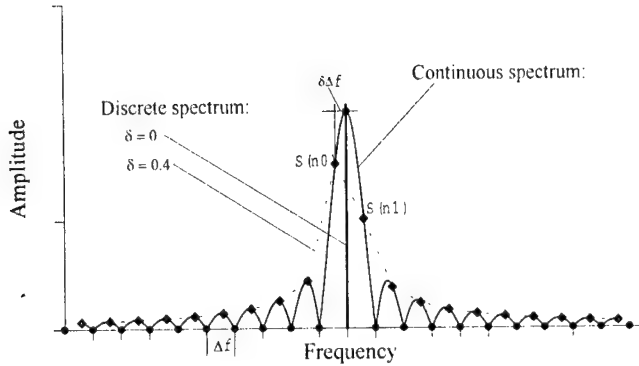


Fig.1. Formation of discrete spectrum of the bounded in time signal for fractional and integer ratios between duration of the analyzed signal and

width of these peaks will be up to the realization duration and the high-frequency infill period ratio when the transition to the discrete spectrum takes place. If the integer quantity of periods misses to  $T$ , then the infinitely narrow lines will result on the high-frequency infill frequencies in the spectrum (see Fig.1). The value of a fractional part  $\delta$  is the result of the division the interval  $T$

by the high-frequency infill period  $t_0 = 2\pi/\omega_0$  and defines both the amplitude of peaks and appearance of “wings”. These “wings” can essentially distort a spectrum at far enough frequency range.

Taking into account only positive frequencies after elementary transformations we got the next representation for the spectral density in discrete form:

$$S(n) \cong \frac{aT}{2} e^{i(\pi\delta + \varphi)} \frac{\sin \pi\delta}{\pi(n - n_0 - \delta)}, \quad (1)$$

where  $n$  is the current point in the spectrum,  $n_0$  is the result of integer dividing  $\omega_0$  by the value of  $2\pi\Delta f$ , where  $\Delta f = 1/T$  is the frequency resolution of the discrete spectrum. To compensate the interference signal we need to determine exactly its frequency  $\omega_0$ , phase  $\varphi$ , and amplitude  $a$ , that is performed by finding of parameters of two points in the discrete spectrum around the narrowband signal frequency on the basis of eq.1:

$$\delta = \frac{S(n_1)}{S(n_0) + S(n_1)}; \quad (2)$$

$$a = \frac{2}{T} [S(n_0) + S(n_1)] \cdot \frac{\pi\delta(1-\delta)}{\sin \pi\delta}; \quad \omega_0 = 2\pi\Delta f(n_0 + \delta); \quad \varphi = \arg S(n_0) - \pi(\delta + n_0 + 1)$$

## SOME RESULTS OF THE SR OBSERVATIONS

The problem of SR measurements includes two parts that reflect spectral and time presentation of a signal. This is an accumulation of average spectra of background signal formed by overlapping pulses from the aggregate of lightning discharges occurred all over the Earth. Also this is a separation of ELF transients – signals generated by the distance powerful lightning discharges and exceeded the background amplitude in 3-10 times. One of the basic problems for measurements is a radiation of power lines harmonics with amplitude exceeding the level of natural signal on 40-70 dB.

“Wings” from the strong narrowband interference can essentially distort the spectrum of measured weak signals even when high resolution ADC is used. This situation is demonstrated in Fig.2 where spectra are represented both with use compensation and without this. The effect of using of compensation method for separating the impulse signal (ELF-transient) is demonstrated in Fig.3. The suppression effectiveness is high



enough under condition if interference parameters are stable on the interval of analyzed time span. Sensitivity to sudden changes in both phase and amplitude of the narrowband interference can be reduced by fragmentation primary interval to shorter ones.

An advantage of the proposed compensation method of filtration is concluded both in absence of distortion of spectra due to its multiplying by the proper transmission characteristics when analog, digital-analog or digital filters are used and its applicability for signal separating both in time and in frequency domain.

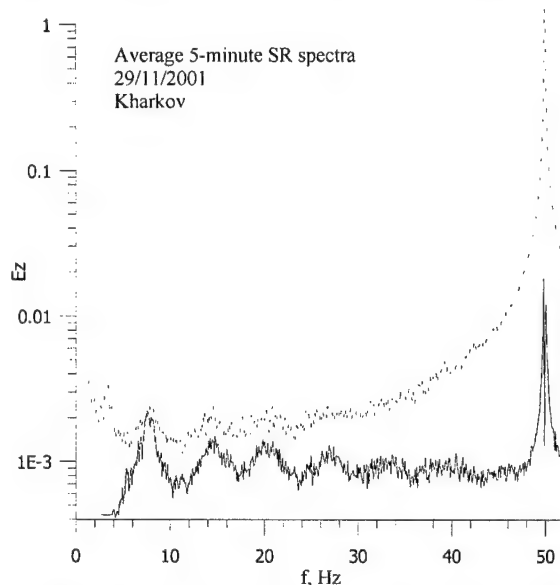


Fig.2. Average spectra of a SR background signal with compensation the power line interference and without this.

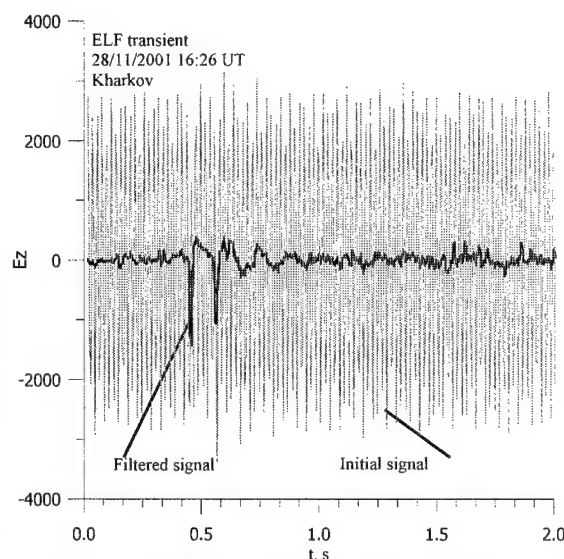


Fig.3. Revealing an ELF transient from a signal by using compensation of the 50 Hz power line interference.

## CONCLUSION

A compensation algorithm for narrowband interferences filtration is developed and realized that provides both to eliminate the influence of “wings” on the form of spectra of analyzed weak signals and to separate waveforms of impulse signals. Realization of the proposed algorithm for interference suppression is based on the using ADC with high-order resolution embracing dynamic range of signal and interference.

Results of Schumann resonance observations are demonstrated performed under condition of high level of industrial interferences within urban areas.

## REFERENCES

- [1] E. R. Williams, The Schumann resonance: a global tropical thermometer, *Science*, 1992, **256**, pp. 1184-1187.
- [2] A. V. Shvets, Worldwide lightning mapping with ELF tomography, *Proc. Wroclaw Symp. EMC*, 2000, part 2, pp. 541-545.
- [3] G. G. Belyaev, A.Y. Schekotov, A.V. Shvets and A.P. Nickolaenko, Schumann resonance observed with the Poynting vector spectra. *JASTP*, 61, 1999, 751-763.

# **BEAMS AND PLASMAS**

## BISTABILITY OF NONLINEAR SURFACE POLARITONS IN CONDUCTING ANTIFERROMAGNETS

N.N.Beletskii, S.A.Borysenko

A. Usikov IRE NASU, ul. Proskury 12, Kharkov 61085, Ukraine

Tel: +380-572-448474, E-mail: beletski@ire.kharkov.ua

### ABSTRACT

The paper deals with the theoretical investigation of the hysteresis effects and bistability states arising from the excitation of the *s*-polarized surface polaritons (SP) with the attenuated total reflection (ATR) technique at the nonlinearly conducting antiferromagnet boundary. We emphasize the analysis of influence of the electron plasma frequency on the conditions of bistability appearance. It is found that there exists a critical value of the plasma frequency at which the bistability vanishes.

### INTRODUCTION

Today the investigations of semimagnetic semiconductors attract many efforts [1-3]. This interest is stipulated by the fact that semimagnetic semiconductors possess magnetic and electron subsystems, which influence on each other. Semimagnetic semiconductors in the phase of antiferromagnetic ordering are of great interest from the viewpoint of millimeter and submillimeter wave applications. This phase is interesting because the antiferromagnetic resonance frequency of semimagnetic semiconductor lies exactly in this waveband. It can be used for both noncontact diagnostics of parameters of semimagnetic semiconductors and for the creation of radically new devices of semiconductor microelectronics.

As known, surface polaritons (SP) can exist in conducting antiferromagnets [4,5]. The propagation of large amplitude SP (nonlinear SP) results in a number of new features, which are concerned with the dependence of the dielectric permittivity of semimagnetic semiconductor on the electric field intensity [6]. For nonlinear SPs the dependence of their spectra on the electric field intensity at the media interface and the monotonic and non-monotonic character of the decaying electromagnetic field in the nonlinear medium are typical.

The present paper deals with the theoretical investigation of the hysteresis effects and bistability states arising from the excitation of nonlinear SP with the attenuated total reflection (ATR) technique at a nonlinear conducting antiferromagnet boundary. As conducting antiferromagnets, we use semimagnetic semiconductors in the phase of antiferromagnetic ordering. We place emphasis on the investigation of the influence of the electron plasma frequency on the conditions of bistability appearance.

### THE PROBLEM STATEMENT

We assume that a semimagnetic semiconductor is in the phase of antiferromagnetic ordering and can be simulated by an easy-axis two-sublattice conducting

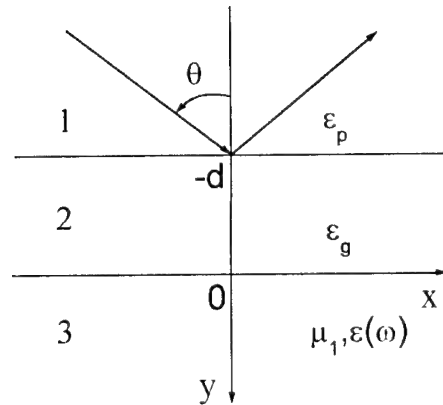


Fig.1. The geometry of the problem.

antiferromagnet with a magnetic permeability  $\mu_1$  [4,5]. Fig.1 shows the geometry of problem. Media 1 and 2 are the dielectrics with the dielectric permittivities  $\varepsilon_p$  and  $\varepsilon_g$  respectively. Medium 3 is a semimagnetic semi-conductor. We suppose that  $\varepsilon_p > \varepsilon_g$  and the external wave, which is incident at the boundary,  $y = -d$ , propagates at an

angle  $\theta$  exceeding the angle of total external reflection. The easy axis of the antiferromagnet (the z-axis) is directed along the media interface. We shall consider s-polarized nonlinear SP ( $E_x = E_y = H_z = 0$ ), the wave vector  $\vec{k}$  of which is directed along the x-axis. The antiferromagnet dielectric constant  $\varepsilon(\omega)$  is supposed to depend on the electric field intensity  $|E_z|^2$  and has the form  $\varepsilon(\omega) = \varepsilon_{(0)}(\omega) + \delta|E_z|^2$ , where  $\varepsilon_{(0)}(\omega)$  is the linear part of the dielectric constant,  $\delta$  is the nonlinearity parameter,  $\omega$  is the nonlinear SP frequency.

We have shown previously that on the antiferromagnet-dielectric boundary there exist the nonlinear SPs with both monotonic and non-monotonic decay of the electromagnetic field in the nonlinear medium [6]. The frequency  $\omega$  of the nonlinear SP is found to depend on the value of  $\Omega_p = \omega_p / \omega_r$ , where  $\omega_p$  and  $\omega_r$  are the electron plasma frequency and antiferromagnet resonance frequency, respectively.

In this paper we have found a reflection coefficient  $R$  of the external wave which is incident at the boundary  $y = -d$ . We have revealed the bistability states in the dependence of  $R$  on the intensity of the incident wave. It has turned out that the appearance of the bistability depends also on the value of  $\Omega_p$ . It has been found that there exists the critical value  $\Omega_{pc}$ , at which the bistability vanishes. The dependence of  $\Omega_{pc}$  on the value of dimensionless frequency  $\Omega = \omega / \omega_r$  has been investigated.

## NUMERICAL RESULTS

Fig.2 shows the dependence of the reflection coefficient  $R$  (left coordinate axis, solid lines) and the reflected wave intensity  $I_r$  (right coordinate axis, dashed lines) on the incident wave intensity  $I_i$  for the nonlinear SP with a monotonic decay of the electric

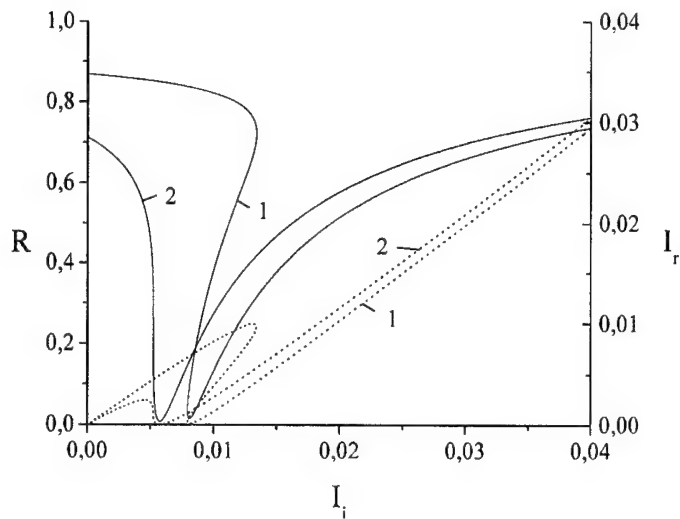


Fig.2

field at  $\Omega = 1,004\omega_r$ ,  
 $d = 0,8c / \omega_r$ ,  $\nu = 0,01\omega_r$ ,  
 $\Gamma = 0,0001\omega_r$  for two values  
of  $\Omega_p$ : 1 -  $\Omega_p = 0,5$ ; 2 -  
 $\Omega_p = \Omega_{pc} = 0,641$ . ( $c$  is the  
velocity of light,  $d$  is the  
dielectric-gap thickness,  $\nu$   
and  $\Gamma$  are the energy loss  
parameters in electronic and  
magnetic subsystems of the  
semimagnetic semiconduc-  
tors, respectively) The  
intensity of the reflected and  
incident waves are given in  
the units of  $|E_{\max}|^2$ ,

$$E_{\max} = (c\alpha_{s0} / \omega) \sqrt{2 / |\mu_1 \delta|}$$

is the amplitude of the nonlinear SP,  $\alpha_{s0}^2 = k^2 - \omega^2 \mu_1 \epsilon_{(0)} / c^2$ . It is evident from Fig.2 that at  $\Omega_p = \Omega_{pc}$  (curves 2) the bistability of the reflection coefficient of the nonlinear SP vanishes.

## CONCLUSIONS

To conclude, it should be emphasized that bistability states arising from an SP excitation on a nonlinear conducting antiferromagnet boundary can be used for the creation of the memory elements in microwaves. Besides, switching devices having parameters depending on the electron concentration in the conducting antiferromagnet can be developed.

## REFERENCES

- [1] J.K. Furdyna, Diluted magnetic semiconductors, *J. Appl. Phys.*, 1988, vol. 64, no. 4, pp. R29-R64.
- [2] O. Goede, W. Heimbrodt, Optical Properties of (Zn, Mn) and (Cd, Mn) Chalcogenide Mixed Crystals and Superlattices, *Phys. Stat. Sol. (b)*, 1988, vol. 146, no.1, pp. 11-62. See also J. Furdyna, J. Kosut, *Semimagnetic semiconductors*, Moscow: Mir, 1992 (in Russian, translated from English).
- [3] R.E. Camley, D.L. Mills, Surface polaritons on uniaxial antiferromagnets, *Phys. Rev.*, 1982, vol. B-26, no.3, pp. 1280-1287.
- [4] N.N. Beletskii, S.A. Borisenko, Determining the antiferromagnetic resonance frequency in semimagnetic semiconductors by means of surface polaritons, *Radiofizika i Elektronika*, IRE NASU Press, 2001, vol. 6, No.2, pp. 261 - 267 (in Russian).
- [5] N.N. Beletskii, S.A. Borisenko, Nonlinear surface polaritons in semimagnetic semiconductors being in a phase of antiferromagnetic ordering, *Radiofizika i Elektronika*, IRE NASU, 2001, vol. 6, No. 3, pp. 289-293 (in Russian).

## PROPAGATION OF INTRASUBBAND PLASMONS IN WEAKLY DISORDERED ARRAY OF QUANTUM WIRES

Y. V. Bludov

A. Usikov IRE NASU

ul. Proskury 12, Kharkov 61085, Ukraine. Email: bludov@ire.kharkov.ua

### ABSTRACT

The paper deals with the theoretical investigation of intrasubband plasmons in weakly disordered array of quantum wires (QWs), consisting of finite number of QWs. The array of QWs is characterized by the fact that the density of electrons of one "defect" QW is different from that of other QWs. It is shown that the amount of plasmon modes in weakly disordered array of QWs is equal to the number of QWs in array. The existence of a local plasmon mode, whose properties differ from those of usual modes, is found. We point out that the local plasmon mode spectrum is slightly sensitive to the position of "defect" QW in array. At the same time the spectrum of usual plasmon modes is shown to be very sensitive to the position of "defect" QW.

### INTRODUCTION

Quasi one-dimensional electron systems (1DES) or quantum wires (QWs) are artificial structures in which the motion of charge carriers is confined in two transverse directions but is essentially free (in the effective mass sense) in the longitudinal direction. Collective charge-density excitations, or plasmons in QWs, are the objects of great physical interest due to some unusual dispersion properties. Firstly, the plasmon spectrum depends strongly on the width of QW [1]. Secondly, 1D plasmons are free from the Landau damping [2] in the whole range of wavevectors.

From the point of view of practical application so-called weakly disordered arrays of low-dimensional systems, containing some defect, are the objects of interest. Recently the plasmons in weakly disordered superlattice, formed of finite number of equally spaced two-dimensional electron systems (2DES), were theoretically investigated [3].

This paper deals with theoretical investigation of plasmons in finite weakly disordered array of QWs consisting of a finite number  $M$  of QW located in the planes  $z=ld$  ( $l=0, \dots, M-1$  is the number of a QW,  $d$  is the distance between adjacent QWs). We suppose that all QWs possess equal 1D density of electrons  $N$  except one "defect" QW whose density of electrons is equal to  $N_d$ . So, the density of electrons in  $l$ -th QW can be expressed as  $N_l = (N_d - N)\delta_{pl} + N$ . Here  $p$  is the number of "defect" QW arranged at the plane  $z=pd$ ,  $\delta_{pl}$  is the Kronecker delta. QWs are placed into a uniform dielectric medium with dielectric constant  $\epsilon$ . We consider the movement of electrons to be free in the  $x$ -direction and is considerably confined in the directions along the  $y$  and  $z$ -axes. At the same time we suppose that the width of all QWs is equal to  $a$  in the  $y$ -direction and is equal to zero in the  $z$ -direction.

### DISPERSION RELATION AND NUMERICAL RESULTS

To obtain the collective excitation spectrum we start with a standard linear-response theory in a random phase approximation. We also take into account only the lowest

subband in each QW. The dispersion relation for intrasubband plasmons can be represented in the final form as

$$\det|\delta_{l,l'} - \Pi^{l'} U_{l,l'}| = 0, \quad (1)$$

where

$$U_{l,l'} = \frac{8e^2}{\epsilon a^2} \int_{-a/2}^{a/2} dy' \int_{-a/2}^{a/2} dy K_0 \left( q_x \sqrt{(y-y')^2 + (l-l')^2 d^2} \right) \cos^2 \left( \frac{\pi y}{a} \right) \cos^2 \left( \frac{\pi y'}{a} \right), \quad (2)$$

$K_0(x)$  is the zeroth-order modified Bessel function of the second kind,  $\Pi^{l'}$  is the noninteracting 1D polarizability ("bare bubble") function, which at zero temperature

and in the long-wavelength limit (where  $q_x \rightarrow 0$ ) can be written as  $\Pi^l = \frac{N_l}{m^*} \frac{q_x^2}{\omega^2}$ .

Fig.1 shows the intrasubband plasmon spectrum in a weakly disordered array of QW in the case where  $M=5$ ,  $d=15a^*$ ,  $a=20a^*$ ,  $p=0$  for two values of the density of electrons of "defect" QW: (a)  $N_d/N=0,5$ , (b)  $N_d/N=1,5$ . The y-axis gives the dimensionless frequency  $\omega/\omega_0$  ( $\omega_0^2 = 2Ne^2/\epsilon m^* a^2$  is the plasma frequency), and the x-axis gives the dimensionless wavevector  $q_x a^*$  ( $a^* = \epsilon \hbar^2 / m^* e^2$  is the effective Bohr radius). As seen from Fig.1, the intrasubband plasmon spectrum in finite array of QW contains  $M$  modes. So, the number of modes in the spectrum is equal to the number of QWs in the array. At the same time the propagation of plasmons in weakly disordered array of QW is characterized by the presence of local plasmon mode (LPM). In the case where  $N_d < N$ , the LPM lies in the lower-frequency region in comparison with the usual plasmon modes (fig.1a). If  $N_d > N$ , the LPM lies in the higher-frequency region (fig.1b).

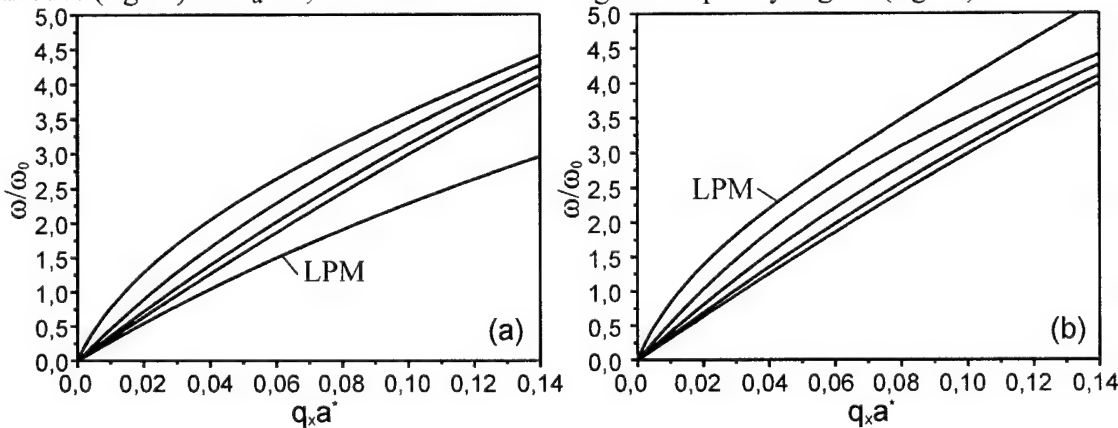


Fig.1

Now we consider the dependence of plasmon spectrum upon the value of 1D electron density in "defect" QW. Fig.2 presents the dependence of plasmon dimensionless frequency  $\omega/\omega_0$  upon the ratio  $N_d/N$  in the case where  $q_x a^* = 0,04$  and for three cases of the "defect" QW position in the array: (a)  $p=0$ , (b)  $p=1$ , (c)  $p=2$ . As seen from Fig.2, the frequency of LPM increases when the value of ratio  $N_d/N$  is increased. Also from the

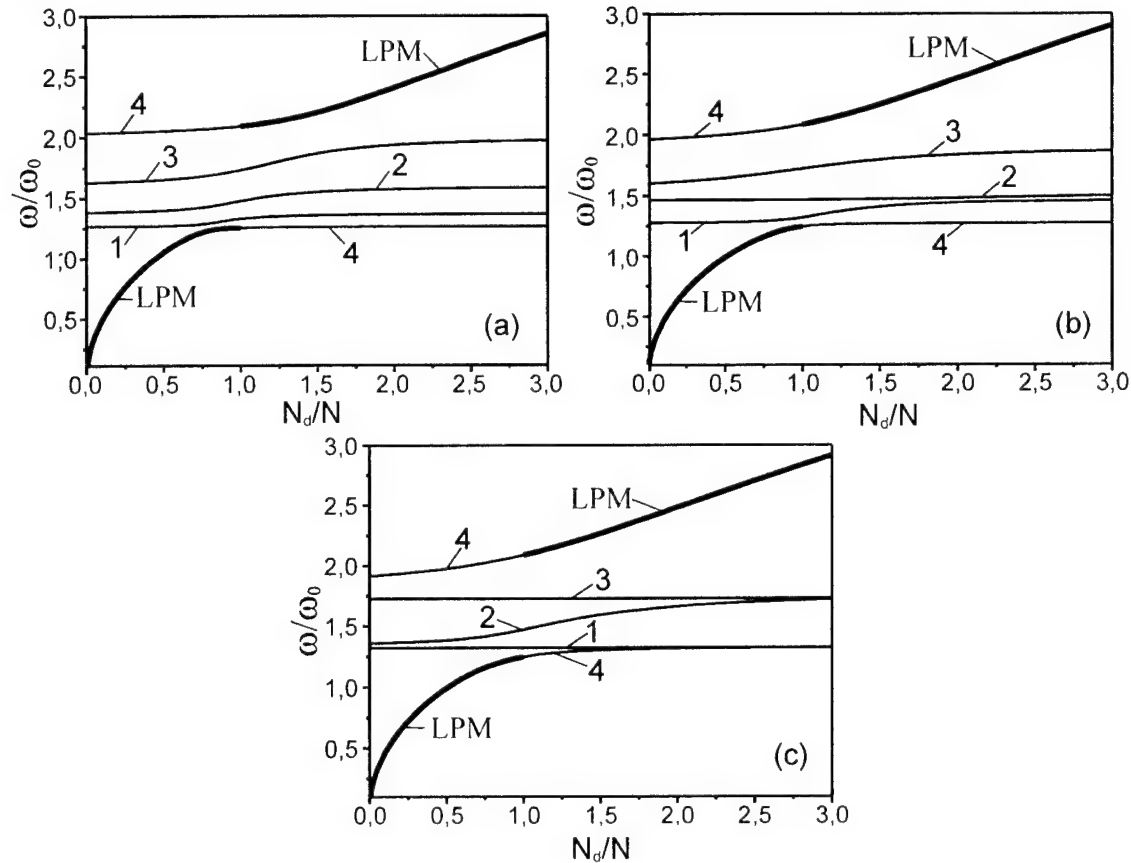


Fig.2

comparison of Fig.2a,b,c it follows that the LPM spectrum depends weakly upon the position of 'the 'defect" QW in array. However, the spectrum of usual plasmon modes is more sensitive to the position of "defect" QW in the array. At the same time, the usual plasmon mode spectrum is characterized by such a feature. As  $p=0$  (Fig.2a) when the value of ratio  $N_d/N$  is increased, the frequency of all usual plasmon modes also increases. However if  $p=1$  (Fig.2b) the frequency of one of the usual plasmon modes (curve 2) does not practically depend upon the value of the ratio  $N_d/N$ . In the case where  $p=2$  (Fig.2c), there are already two plasmon modes (curves 1 and 3) which possess such a particularity.

## CONCLUSION

In conclusion, we calculated the plasmon spectrum of finite weakly disordered array of QWs, which contains one "defect" QW. It should be emphasized that the above-mentioned features of plasmon spectra can be used for diagnostics of defects in QW structures.

## REFERENCES

- [1] S. Das Sarma and Wu-yan Lai, Phys. Rev., **B32**, 1401 (1985)
- [2] S. Das Sarma and E. H. Hwang, Phys. Rev., **B54**, 1936 (1996)
- [3] N. N. Beletskii and Y.V. Bludov, Radiofizika i Elektronika, IRE NASU Press, **4**, 93 (1999) (in Russian)



# CALCULATION OF IMPEDANCE OF A SHARP PLASMA BOUNDARY WITH A MIXED-TYPE ELECTRON SCATTERING IN ANOMALOUS SKIN-EFFECT CONDITIONS

V.I.Miroshnichenko<sup>1</sup>, V.M.Ostroushko<sup>2</sup>

<sup>1</sup>Institute of Applied Physics NASU, ul. Petropavlivska 58, Sumy 40030, Ukraine

<sup>2</sup>National Scientific Center "Kharkov Institute of Physics and Technology"

ul. Academichna 1, Kharkov 61108, Ukraine. E-mail: ostroushko-v@kipt.kharkov.ua

Some aspects of calculation of impedance change caused by oblique incidence of electromagnetic wave on a sharp plasma boundary with mixed-type electron scattering in anomalous skin effect (ASE) conditions are considered. Though the corresponding Riemann-Hilbert boundary problem can be reduced [1] to the integral equations of the Fredholm type, formal limit transition to extreme ASE causes kernels singularity. The transformation of the equations to ones with bounded kernels is made by means of partial inversion of the integral operator.

An oblique electromagnetic wave reflection from a sharp plasma boundary with a mixed-type electron scattering can be described with the functions  $\Psi_\lambda(k_z)$  and  $\Psi_\tau(k_z)$ , the linear combinations of the Fourier transforms of electric field components in plasma domain ( $z>0$ ). They should be analytical in the half-plane  $\text{Im}(k_z)\leq 0$ , together with the functions  $\Phi_\lambda(-k_z)$  and  $\Phi_\tau(-k_z)$ , and should meet two functional equations [2],

$$\begin{aligned} [1-\Omega^2 q_\lambda(\beta k_{xz})][\Psi_\lambda(k_z)+p\Psi_\lambda(-k_z)] &= \Phi_\lambda(k_z), \\ [1-k_{xz}^2-\Omega^2 q_\tau(\beta k_{xz})][\Psi_\tau(k_z)-p\Psi_\tau(-k_z)] &= \Phi_\tau(k_z), \end{aligned} \quad (1)$$

and the equalities  $\Psi_\lambda(\pm ik_x)=\pm i\Psi_\tau(\pm ik_x)$ . Here  $\beta=v_F\omega[c(\omega+i\nu)]^{-1}$ ,  $\Omega=\omega_e[\omega(\omega+i\nu)]^{-1/2}$ ,  $k_{xz}=(k_x^2+k_z^2)^{1/2}$ ,  $c$  is the speed of light,  $\omega$  is the frequency,  $\omega_e$  is the plasma frequency,  $\nu$  is the collision frequency,  $v_F$  is the velocity of electrons at the Fermi surface (spherical),  $k_x$  is dimensionless (in units  $\omega/c$ ) transverse wave number (sine of wave incidence angle),  $p\in(0,1)$  is the fraction of electrons with specular boundary scattering,  $q_\lambda(\chi)=3\chi^{-2}\{(2\chi)^{-1}\ln[(1+\chi)/(1-\chi)]-1\}$ ,  $q_\tau(\chi)=3(2\chi)^{-1}\{1-(2\chi)^{-1}(1-\chi^2)\ln[(1+\chi)/(1-\chi)]\}$ . The problem is considered under the approximation  $\beta\ll 1$ ,  $A\gg 1$ , where  $A=(\beta\Omega)^{2/3}$ , so, the distance traveled by an electron during the oscillation period is large compared with the effective field penetration depth.

Introducing new variables and functions, one can write (1) in the form

$$X_\lambda(u)+pQ_\lambda^\times(u)X_\lambda(-u)=Y_\lambda(-u), \quad X_\tau(u)-pQ_\tau^\times(u)X_\tau(-u)=Y_\tau(-u), \quad (2)$$

where  $X_\lambda(u)=\Psi_\lambda(0)^{-1}\Psi_\lambda((i\beta u)^{-1})Q_\lambda^+(u)$ ,  $X_\tau(u)=\Psi_\tau(-c_\tau u)Q_\tau^+(u)$ ,  $c_\tau=-ic_3A\beta^{-1}$ ,  $c_3=\exp(i\pi/3)$ . Here and further, a function with the upper index  $+$  should be analytic in the half-plane  $\text{Im}(u)>0$ , and it should be built for the corresponding function without upper index in accordance with the identity  $Q^+(u)Q^+(-u)=Q(u)$ . A corresponding function with the upper index  $\times$  is determined by the identity  $Q^\times(u)=Q^+(u)[Q^+(-u)]^{-1}$ . The functions  $Q_\lambda(u)$  and  $Q_\tau(u)$  correspond to the first factors in the (1) left hand sides multiplied with the constants. The identity for  $Q^+(u)$  remains its sign indefinite, and therefore the signs are chosen to provide  $Q_\lambda^+(i\infty)=1$  and  $\lim_{u\rightarrow i\infty}[Q_\tau^+(u)/u]=c_\tau$ .

By using (here and further) the tilde symbol for the Fourier transforms over all real  $u$  axes, from the first of (2) one can obtain the following equation:

$$\tilde{X}_\lambda(\zeta) + p \int_0^\infty d\xi \tilde{Q}_\lambda^*(\zeta + \xi) \tilde{X}_\lambda(\xi) + p \tilde{Q}_\lambda^*(\zeta) = 0 \quad (\zeta > 0), \quad (3)$$

(3) can be solved by iterations [3], and some values, in particular, the quantity  $F_\lambda = \lim_{u \rightarrow i\infty} \{iu[Q_\lambda^+(u) - X_\lambda(u)]\}$ , can be efficiently calculated. The function  $X_\lambda(u)$  can be written as linear combination of the functions  $X(\pm p; u)$  determined by the equations

$$X(p'; u) - p' Q_\tau^*(u) X(p'; -u) = Y(p'; -u) \quad (4)$$

(for  $p' = p$  and for  $p' = -p$ ), and with the requirements that the functions  $X(p'; u)$  and  $Y(p'; u)$  are analytic and bounded in the half-plane  $\text{Im}(u) \geq 0$ , and the condition  $X(p'; i\infty) = 1$  is satisfied. From (4), an equation similar to (3) can be obtained and the quantity  $\Psi_{\tau 1} = i \lim_{u \rightarrow i\infty} [uX(-p; u) - c_\tau^{-1} Q_\tau^+(u)]$  can be calculated, however to calculate some other quantities one has to transform the equation. Taking  $a > 0$ , for the Fourier transforms of the functions  $x(a, p'; u) = X(p'; u)(ia + u)^{-1}$ ,  $g(a; u) = Q_\tau^*(u)(ia - u)(ia + u)^{-1}$ ,  $h(a, p'; u) = Y(p'; u)(ia + u)^{-1}$ , one can obtain an integral equation:

$$\tilde{x}(a, p'; \zeta) = p' \int_0^\infty d\xi \tilde{g}(a; \zeta + \xi) \tilde{x}(a, p'; \xi) + \tilde{h}(a, p'; \zeta) \quad (\zeta > 0). \quad (5)$$

The function  $|\tilde{g}(a; \zeta)|$  for  $1 \ll \zeta \ll A$  is close to  $(\pi\zeta)^{-1}$ , so, in the limit of  $A \rightarrow \infty$ , (5) is not a Fredholm-type equation. For  $p' = p$  and bounded  $A$ , one can take  $a = 1$  and write the equation  $\tilde{x}(1, p; \zeta) = p \int_1^A d\xi [\pi(\zeta + \xi)]^{-1} \tilde{x}(1, p; \xi) + \tilde{H}(\zeta)$ , where the term  $\tilde{H}(\zeta)$  involves

the integrals with the unknown function  $\tilde{x}(1, p; \zeta)$  and kernels bounded with some functions  $[(\zeta + \xi)^{-2} \ln(\zeta + \xi) + A^{-2}(\zeta + \xi)]$  for  $\{\zeta \in (1, A), \xi \in (1, A)\}$ ,  $A(\zeta + \xi)^{-2}$  for  $\max(\zeta, \xi) > A$ , and  $\max(1, \zeta, \xi)^{-1}$  for other domains. In brackets, here and further the factors independent on  $\zeta, \xi$ , and  $A$  are omitted. Considering the function  $\tilde{H}(\zeta)$  as known, one can build the solution of the last equation applying the second of two methods used in [4]. The kernel of the corresponding regularization operator is bounded with the product  $\min(\zeta, \xi)^{-\kappa_p} \max(\zeta, \xi)^{\kappa_p - 1}$  (where  $\kappa_p = \pi^{-1} \arcsin(p)$ ), and the kernel of the obtained equation, for  $\zeta \in (1, A)$ , is bounded with the functions  $\zeta^{\kappa_p - 1}$ ,  $\zeta^{\kappa_p - 1} \xi^{-1} + A^{\kappa_p - 1} \zeta^{-\kappa_p}$ , and  $A^{1 + \kappa_p} \zeta^{-\kappa_p} \xi^{-2}$  in intervals  $\xi \in (0, 1)$ ,  $\xi \in (1, A)$ , and  $\xi > A$ , respectively. The introduction of the variable  $\bar{\zeta}$  and the function  $\bar{x}(\bar{\zeta})$ , so that the products of derivative  $d\bar{\zeta}/d\zeta$  with some factors (1 for  $\zeta \in (0, 1)$ ,  $\zeta^{2 - \kappa_p}$  for  $\zeta \in (1, A^{\kappa_p})$ ,  $A(\zeta/A)^{1 - \kappa_p}$  for  $\zeta \in (A^{\kappa_p}, A)$ ,  $\zeta^2/A$  for  $\zeta > A$ ) leads to the bounded limits for fixed  $\zeta$  if  $A \rightarrow \infty$ . The value  $\bar{x}(\bar{\zeta})/\tilde{x}(1, p; \zeta)$  is equal to 1,  $\zeta^{1 - \kappa_p}$ , and  $\zeta A^{-\kappa_p}$  in the intervals  $\zeta \in (0, 1)$ ,  $\zeta \in (1, A)$ , and  $\zeta > A$ , respectively. All this yields an equation with the kernel bounded even for  $A \rightarrow \infty$ .

In the case  $p' = -p$ , to keep the sign in the estimation of the product  $p' \tilde{g}(a; \zeta)$  for  $1 \ll \zeta \ll A$ , it is reasonable to take positive  $\delta_1 \sim A^{-1}$  and consider (5) for  $a = \delta_1$ . Denoting

$c_\sigma = c_3^2 A^{-1}$ ,  $\delta_0 = -i c_\sigma^{1/2}$ ,  $C_1 = -i X(p; i\delta_0) \delta_0^{\kappa_p}$ ,  $C_0 = -i X(-p; i\delta_0) \delta_0^{-\kappa_p}$ , and using the Euler gamma-function, for  $1 \ll \zeta \ll A$ , one can obtain  $\tilde{x}(1, p; \zeta) \Gamma(\kappa_p) \approx C_1 \zeta^{\kappa_p - 1}$ ,  $\tilde{x}(\delta_1, -p; \zeta) \Gamma(1 - \kappa_p) \approx C_0 \zeta^{-\kappa_p}$ . In the limit of  $A \rightarrow \infty$ , the quantities  $C_1$  and  $C_0$  tend to finite real values, which can be effectively calculated from the solutions of the equations with bounded kernels obtained from (5).

Suppose that the functions  $X_\sigma(p'; u)$  and  $Y_\sigma(p'; u)$  are analytic and bounded in the half-plane  $\text{Im}(u) > 0$  and obey the functional equation

$$X_\sigma(p'; u) - p' Q_\tau^*(c_\sigma/u) X_\sigma(p'; -u) = Y_\sigma(p'; -u) \quad (6)$$

and the condition  $X_\sigma(p'; i\infty) = 1$ . Then the identity  $X(p'; u) = X(p'; 0) X_\sigma(p'; c_\sigma/u)$  takes place. Applying the limit transition to the explicit solution of the equation, in which the function  $Q_\tau^*(u)$  is approximated with the relation of the polynomials, one can obtain the equality  $X(p; 0) X(-p; 0) = 1$ . From (6), an equation similar to (3) can be obtained and the quantity  $F_\sigma = i \lim_{u \rightarrow i\infty} \{u^2 (\partial/\partial u) \ln [X_\sigma(-p; u)/Q_\tau^*(c_\sigma/u)]\}$  can be calculated. Besides, (6) can be treated similarly to (4), and an equation similar to (5), but with another function instead of  $\tilde{g}(a; \zeta + \xi)$ , may be obtained. For the quantities  $C_{\sigma 1} = -i X_\sigma(-p; i\delta_0) \delta_0^{\kappa_p}$ ,  $C_{\sigma 0} = -i X_\sigma(p; i\delta_0) \delta_0^{-\kappa_p}$  (which one can effectively calculate considering now the cases  $p' = -p$ ,  $a = 1$  and  $p' = p$ ,  $a = \delta_1$  and evaluating the solutions of the corresponding integral equations for large  $\zeta$ ), and for the quantity  $F_\tau = X(-p, 0)(c_3 A)^{\kappa_p}$ , the identities  $C_0 C_{\sigma 1}^{-1} = F_\tau = C_{\sigma 0} C_1^{-1}$  take place.

Under the assumption  $\{A \gg 1, \beta \ll 1\}$ , for dimensionless impedance  $Z$  one can obtain approximate identity  $\beta(AZ)^{-1} \approx \Psi_{\tau 1} \exp(i\pi/3) + k_x^2 \beta^2 A^{-1-2\kappa_p} \exp(-2i\pi\kappa_p/3) F_Z$ , in which the quantities  $\Psi_{\tau 1}$  and  $F_Z = (F_\lambda - F_\sigma) F_\tau^2$  in the limit  $\{\beta \rightarrow 0, A \rightarrow \infty\}$  turn positive. The complex factors in the expression for the impedance are obtained explicitly due to introduction of convenient variables, for which the corresponding functions in the functional equations in the extreme ASE limit become positive for real values of arguments.

The quantities  $C_1$ ,  $C_0$ , and  $\Psi_{\tau 1}$  can also be calculated with the method of [5].

## REFERENCES

- [1] N.I. Muskhelishvili, *Singular Integral Equations*, Moscow: Nauka, 1968 (in Russian).
- [2] V.I. Miroshnichenko, *Sov. Phys. Tech. Phys.*, 1966, vol. 36, No. 6, pp. 1008–1016 (in Russian).
- [3] V.I. Miroshnichenko, V.M. Ostroushko, *Ukrainian Phys. J.*, 2002, vol. 47, No 2, pp. 147–153 (in Ukrainian).
- [4] V.G. Sologub, *USSR J. Comput. Math. Mathem. Physics*, 1971, vol. 11, No 4, pp. 837–854 (in Russian).
- [5] L.E. Hartmann, J.M. Luttinger, *Phys. Rev.*, 1966, vol. 151, No 2, pp. 430–433.

## RADIOPHYSICAL CHARACTERISTICS OF A RADIATOR BASED ON A GAS DISCHARGE PLASMA

V.V. Ovsyanikov, A.N. Gordiyenko

Dniepropetrovsk National University  
ul. Naykova 9, bld. 12, Dniepropetrovsk 49050, Ukraine  
Tel. + 380 (56) 776-9092, E-mail: root@ap1.net-rff.dsu.dp.ua

### ABSTRACT

The results of the study of characteristics of a microwave radiator based on cold plasma of a gas discharge are presented. A method of determining the plasma conductivity in the given frequency band is proposed and discussed.

As plasma always contains free charges (electrons and ions, see [1]), its excitation by a source of alternating voltage results in appearance of alternating current. For a certain electrical size of plasma segments this leads to the radiation of time-varying electromagnetic field [2].

Experimental research of a loop radiator based on cold plasma of a gas discharge [3] has shown that the bandwidth properties of its radiation characteristics and input impedance considerably exceed those of antenna based on conductors of similar configuration.

For a physical substantiation of this phenomenon we should take into account that the concentration of free carriers in gas-discharge plasma is approximately 7 orders smaller than their concentration in metals [1]. Therefore, in a plasma radiator (PR) the resistance to current excited by an external microwave field is much greater than in a conductor, especially in a perfect one. This results in the attenuation of a wave of current reflected from the end of PR antenna, establishment of a mode close to a traveling wave, and hence to stabilization of the input impedance and radiation characteristics of PR in a wider frequency band.

PR can be considered as an imperfect conductor with continuously distributed impedance along its length.

We are interested in estimation of conductivity of a PR shaped as a pole of plasma by using experimental values of input impedances PR obtained in [3] according to the following technique:

- 1) Excite, in the frequency band 150-350 MHz, the studied volume (configuration) of plasma and measure the set of values of the input impedance  $Z_{pl}(f)$  of the radiator in this range,
- 2) Solve, in accurate formulation, the problem about the distribution of current and find the input impedance  $Z_{cl}(f, \sigma)$  of PR with finite and varying values of conductivity  $\sigma$ ,
- 3) Solve the problem of optimization of  $\sigma$  variation by using the criterium of a minimum of objective function  $Z(\sigma)$  in the given frequency band:

$$\min Z(\sigma) \quad (1)$$

$$f \in [150; 350] \text{ MHz}; \quad \sigma \in (\sigma_1, \sigma_2)$$

In accordance to the above mentioned techniques, we solved the problem of optimization, where the following functions were chosen as the objective ones:

$$Z_1(\sigma) = \sqrt{\frac{\sum_{j=1}^N [K_{pl}(f_j) - K_{cl}(f_j, \sigma)]^2}{\sum_{j=1}^N K_{pl}^2(f_j)}} \quad , \quad (2)$$

$$Z_2(\sigma) = \frac{1}{N} \sqrt{\sum_{j=1}^N \left[ \frac{K_{pl}(f_j) - K_{cl}(f_j, \sigma)}{K_{pl}(f_j)} \right]^2} \quad , \quad (3)$$

$$Z_3(\sigma) = \frac{1}{N} \sum_{j=1}^N \left[ \frac{K_{pl}(f_j) - K_{cl}(f_j, \sigma)}{K_{pl}(f_j)} \right]^2 \quad , \quad (4)$$

$$Z_4(\sigma) = \frac{1}{N} \sum_{j=1}^N \left| \frac{K_{pl}(f_j) - K_{cl}(f_j, \sigma)}{K_{pl}(f_j)} \right| \quad , \quad (5)$$

where  $N$  is the total number of discrete frequencies in the given band,  $i$  is the number of the frequency value in the given band,  $K_{pl}(f_i)$  and  $K_{cl}(f_i, \sigma)$  are experimental and calculated values of the voltage standing wave ratio (VSWR) in the given frequencies, respectively.

The values of VSWR were measured and calculated in the range of 150 to 350 MHz with the interval of 10 MHz. The calculations of objective functions (2), (3), (4) and (5) in the given frequency band were performed with MATLAB. Here, 29 computed values,  $K_{cl}$ , for the conductivities in the range of  $0 < \sigma \leq 20 \text{ Sm}$  were examined.

The results of calculations are presented as plots in Fig. 1, where the curves are numbered in accordance to the numbers of objective functions (5). From these plots, we can see that all the studied objective functions display global minima at values of conductivity approximately equal to 0,5 – 0,6 Sm.

The studied PR attracts an interest of microwave researchers since it allows to combine radiation of electromagnetic power in considerably different frequency bands:

optical and microwave. Agreement between the values of optimal conductivity of PR found during optimization with different objective functions proves a reliability of the obtained results.

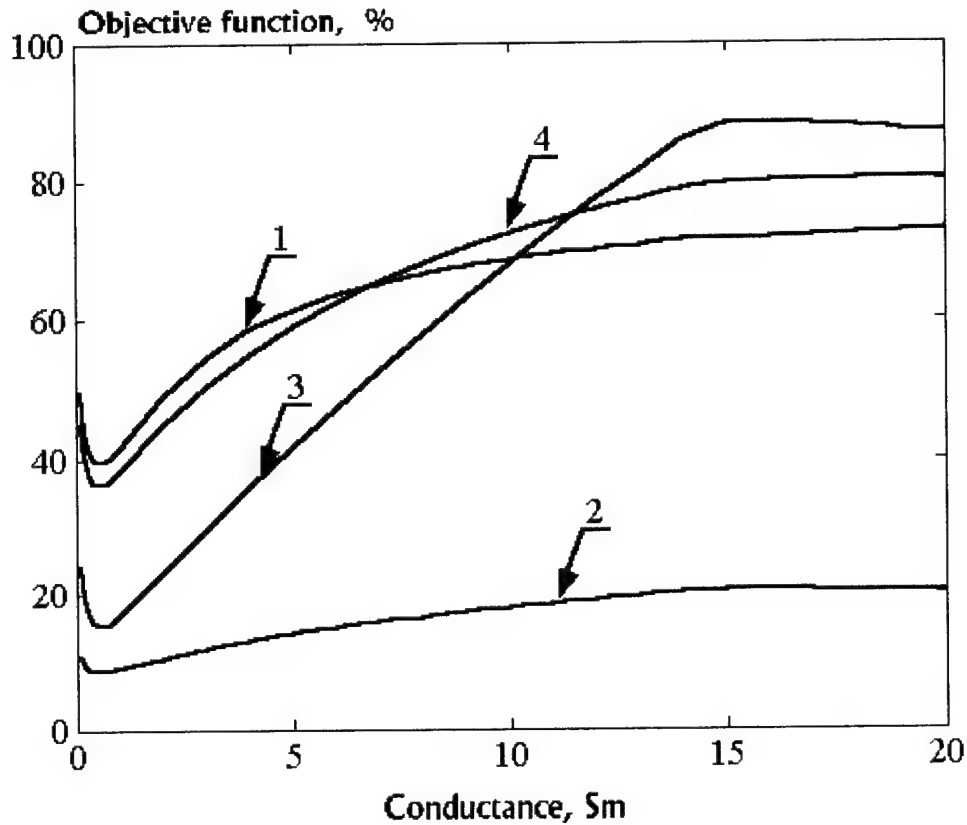


Fig.1. Objective function versus conductivity of plasma of PR

## REFERENCES

- [1] A.F. Aleksandrov, L.S. Bogdankevitch, A.A. Rukhadze, *Oscillations and Waves in Plasma Media*, Moscow: Moscow University Press, 1990 (in Russian).
- [2] S.M. Levitsky, U.P. Burikin, Radiation of electromagnetic waves by plasma waveguides, *Radiotekhnika i Elektronika*, 1973, vol. 18, no.12, pp. 2642 - 2644 (in Russian).
- [3] V.V.Ovsyanikov, Broadband microwave emitter on the basis of gas discharge plasma. *Radiophysika i Radioastronomiya*, 2001, vol. 6, no. 3, pp. 261-267 (in Russian).

# RADIATION BY SELF-OSCILLATING RELATIVISTIC CHARGED PARTICLE MOVING ALONG PERIODIC STRUCTURE

Anatoly N. Opanasenko

NSC KIPT, Akademicheskaya St. 1, Kharkov, 61108, Ukraine  
E-mail: Opanasenko@kipt.kharkov.ua

## ABSTRACT

The new elementary radiation mechanism due to the oscillatory character of a radiation friction force appearing when a relativistic charged particle moves along a periodic structure without external fields is studied by analytical methods. The equation of motion for the charged particle driven by the radiation friction force is solved by the perturbation method. It is shown that the non-synchronous spatial harmonics of the Cherenkov-type radiation (CR) can cause an oscillatory motion of the particle, which therefore generates an undulator-type radiation (UR). In the frequency range where the diffraction of the generated waves is essential, the radiation manifests itself in the interference of CR and UR. The undulator radiation takes place only in that spectral region where the wave diffraction can be neglected.

As known, a charged particle moving with a constant velocity along a periodic structure emits Cherenkov-type radiation [1]. The fields of this radiation called wake-fields can be expressed as spatial-harmonic series according to the Floquet theorem. The action of the synchronous with the particle spatial harmonics of the self-wakefield on the particle results in energy losses associated with CR. The non-synchronous spatial harmonics can cause the oscillatory particle motion resulting in generating the undulator-type radiation. This radiation is subject for discussing in this article.

As a periodic structure, we will consider a hollow corrugated waveguide with metallic surface. Suppose that a particle of charge  $e$  and of mass  $m$  moves with an ultrarelativistic velocity  $\mathbf{v}$  along the structure with the period  $D$ . The radiation friction force and the radiation power are sought for.

By using the Hamilton's method developed in [2] we can obtain the radiation friction force as

$$\mathbf{F}(\mathbf{v}(t), \mathbf{r}(t), t) = -\frac{e^2}{4c^2 V_{tot}} \sum_{\lambda}^{\omega_{\lambda} < c/r_0} \left\{ \left[ \mathbf{A}_{\lambda}(\mathbf{r}(t)) - \frac{\mathbf{v}(t) \times \text{rot} \mathbf{A}_{\lambda}(\mathbf{r}(t))}{i\omega_{\lambda}} \right] e^{i\omega_{\lambda} t} \int_0^t \mathbf{v}(t') \mathbf{A}_{\lambda}^*(\mathbf{r}(t')) e^{-i\omega_{\lambda} t'} dt' + \right. \\ \left. + \left[ \mathbf{A}_{\lambda}(\mathbf{r}(t)) + \frac{\mathbf{v}(t) \times \text{rot} \mathbf{A}_{\lambda}(\mathbf{r}(t))}{i\omega_{\lambda}} \right] e^{-i\omega_{\lambda} t} \int_0^t \mathbf{v}(t') \mathbf{A}_{\lambda}^*(\mathbf{r}(t')) e^{i\omega_{\lambda} t'} dt' \right\} + \text{K.C.} \quad (1)$$

where  $\omega_{\lambda}$  is an eigenfrequency. Seeing the force of radiation friction does not depend on the particle size  $r_0$ , so  $\omega_{\lambda} < c/r_0$  [2] ( $c$  is the velocity of light).  $V_{tot} = M V_{cell}$ , where we assume that the structure contains  $M \rightarrow \infty$  cells of volume  $V_{cell}$  and is enclosed in a "periodicity box".  $\mathbf{A}_{\lambda}(\mathbf{r})$  is the set of the eigenfunctions of the vector potential which can be represented in the Floquet form [1]

$$\mathbf{A}_\lambda(\mathbf{r}) = \sum_{n=-\infty}^{\infty} \mathbf{g}_\lambda^{(n)}(\mathbf{r}_\perp) e^{ih_n z}, \quad (2)$$

where  $\mathbf{g}_\lambda^{(n)}(\mathbf{r}_\perp)$  is the amplitude of the  $n$ -th spatial harmonic;  $h$  is the parameter of the interval:  $(-\pi/D \div \pi/D)$ ;  $h_n = h + 2\pi n/D$  is the propagation constant. The set of (2) is limited above on frequency by the electron plasma frequency  $\omega_{pe}$  in metal. As known, if  $\omega_\lambda \sim \omega_{pe}$  the diffraction conditions in the periodic structure are violated. So, for the range  $\omega_\lambda > \omega_{pe}$  the vector potential can be expanded in terms of the plane waves of free space

$$\mathbf{A}_{\lambda,l}(\mathbf{r}) = c \sqrt{4\pi} \mathbf{a}_{\lambda,l} e^{i\mathbf{k}_\lambda \mathbf{r}} \quad (3)$$

where  $\mathbf{k}_\lambda$  is the wave propagation vector;  $\mathbf{a}_{\lambda,l}$  is the real unit vector of polarization ( $l=1,2$ ) perpendicular to  $\mathbf{k}_\lambda$ .

The equation of the motion driven by the force (1) can be solved approximately in ultrarelativistic limit. As a zeroth-order approximation, we will consider the motion with a constant velocity parallel to the structure axis

$$\mathbf{v} = \mathbf{v}_0 = v_0 \mathbf{e}_z, \quad \mathbf{r}(t) = \mathbf{r}_{0,\perp} + \mathbf{v}_0 t \quad (4)$$

In this case, inserting (4) and (2) into (1), we obtain the self-wake force of zeroth order in the frequency band  $\omega_\lambda \ll \omega_{pe}$

$$\mathbf{F}(t) = -e^2 \sum_{p=-\infty}^{\infty} \mathbf{w}^{(p)} e^{ip\Omega t} + K.C., \quad (5)$$

where we have introduced  $\Omega \equiv 2\pi v_0/D$  and defined the amplitude of the  $p$ th spatial harmonic of the wake function as

$$\mathbf{w}^{(p)} \equiv \frac{Dv_0}{4c^2 V_{cell}} \sum_{n=0}^{\infty} \sum_{\lambda_j} \frac{\mathbf{g}_{z,\lambda_j}^{(n)*}}{v_0 - \frac{d\omega_\lambda}{dh}} \bigg|_{\lambda=\lambda_j} \left[ \mathbf{g}_{z,\lambda_j}^{(n+p)} - i \frac{v_0}{\omega_\lambda} \nabla_\perp \mathbf{g}_{z,\lambda_j}^{(n+p)} - \frac{\Omega p}{\omega_\lambda} \mathbf{g}_{\perp,\lambda_j}^{(n+p)} \right] \quad (6)$$

Here  $\mathbf{g}_\lambda^{(n)} \equiv \mathbf{g}_\lambda^{(n)}(\mathbf{r}_{0,\perp})$ , and  $\omega_{\lambda_j}$  satisfies the resonance conditions  $\omega_\lambda - hv_0 = n\Omega$ .

The force (5) is a periodic function of time with the period  $D/v_0$ . The synchronous harmonic of this force,  $-e^2 2w_z^{(0)}$ , determines the energy losses associated with CR in the frequency band  $\omega_\lambda \ll \omega_{pe}$ .

In the region  $\omega_\lambda > \omega_{pe}$  where the structure can be considered as free space, the radiation is absent in zeroth order approximation, i.e. at  $v_0 = \text{const}$ .

If the particle is off-axis, it experiences a periodic action of the transverse component of the non-synchronous harmonics of the self-wake force ( $\mathbf{w}_\perp^{(p)} \neq 0$ ). The radiation due to the periodic motion we will call undulator radiation. Solving the equation of the motion driven by the force (5) we find the corrected law of motion

$$\mathbf{v}(t) = \mathbf{v}_0 + \mathbf{v}_\perp(t) = \mathbf{v}_0 + ic \sum_{p \neq 0} \frac{^{(p)}}{p} e^{ip\Omega t}, \quad \mathbf{r}(t) = \mathbf{r}_{0,\perp} + \mathbf{v}_0 t + \delta \mathbf{r}_\perp(t) = \mathbf{r}_{0,\perp} + \mathbf{v}_0 t + \frac{c}{\Omega} \sum_{p \neq 0} \frac{^{(p)}}{p^2} e^{ip\Omega t} \quad (7)$$

where  $^{(p)}$  is the dimensionless vector  $^{(p)} \equiv \frac{2e^2}{mc\gamma\Omega} \left( \mathbf{w}_\perp^{(p)} + \mathbf{w}_\perp^{(-p)*} \right)$  and  $|\alpha^{(p)}| \ll 1$ .

Inserting Eq.(7) and Eq.(2) into Eq.(1) we can obtain the power radiation as



$$P \equiv -\lim_{t \rightarrow \infty} \frac{1}{t} \int_0^t \mathbf{v}(t') \mathbf{F}(\mathbf{v}(t'), \mathbf{r}(t'), t') dt' =$$

$$= \frac{e^2 D}{2V_{cell}} \sum_{n=0}^{+\infty} \sum_{\lambda_j} \frac{1}{v_0 - \frac{d\omega_\lambda}{dh} \Big|_{\lambda=\lambda_j}} \left[ \beta_0 g_{z,\lambda_j}^{(n)} + \frac{1}{2} \sum_{p \neq 0} \frac{(p)}{p} \left( \frac{D}{2\pi p} \nabla_\perp g_{z,\lambda_j}^{(n+p)} - i g_{\lambda_j}^{(n+p)} \right) \right]^2 + O(|\alpha^{(p)}|^2) \quad (8)$$

Here  $\omega_{\lambda_j}$  is a frequency found from the equation  $\omega_\lambda - \hbar v_0 = n\Omega$ ,  $\gamma$  is Lorentz factor. (8) shows that in the region  $\omega_\lambda \ll \omega_{pe}$ , the radiation manifests itself in the interference between CR and UR.

For the region  $\omega_\lambda > \omega_{pe}$  it is interesting to consider the radiation of a high energy charged particle satisfying the condition  $\omega_{pe} \ll 2\Omega\gamma^2$ . Inserting (7) and (3) into (1) and for simplicity applying the dipole limit  $k_\lambda \delta \mathbf{r}_\perp(t) \ll 2\pi$  we obtain the UR power by analogy with (10)

$$P_U \equiv -\lim_{t \rightarrow \infty} \frac{1}{t} \int_0^t \mathbf{v}(t') \mathbf{F}(\mathbf{v}(t'), \mathbf{r}(t'), t') dt' = \frac{4e^6}{3m^2 c^3} \gamma^2 \sum_{p=1}^{p \ll p_{lim}} \left| \mathbf{w}_\perp^{(p)} + \mathbf{w}_\perp^{(-p)*} \right|^2 \quad (9)$$

where the number of harmonics in the sum is limited by the condition of the small value of the oscillation amplitude resulting in  $p \ll p_{lim} = 2\pi\gamma / \max\{\alpha^{(p)}\}$ .

As follows from (9), the power grows up as square of the particle energy, so in the region  $\omega \gg \omega_{pe}$  the UR power can exceed the CR power emitted in the band  $\omega \ll \omega_{pe}$ . It should also be stated that, if a bunch of  $N$  electrons moves in the periodic structure and the bunch dimensions  $\sigma_z$  and  $\sigma_\perp$  satisfy the conditions  $\sigma_z \ll D/(2q\gamma^2)$  and  $\sigma_\perp \ll D/(2q\gamma)$ , then the radiation with the frequency  $\omega < 2q\Omega\gamma^2$  is coherent. Moreover, for the range  $\omega_{pe} \ll \omega < 2q\Omega\gamma^2$  the UR power would be proportional to  $N^4$

$$P_U = \frac{4e^6 N^4}{3m^2 c^3} \gamma^2 \sum_{p=1}^q \left| \mathbf{w}_\perp^{(p)} + \mathbf{w}_\perp^{(-p)*} \right|^2 \quad (10)$$

Finally, it should be noted that in the future super-high-power electron rf linacs there will be beam energy loss associated with the undulator radiation emitted by the electrons in the fields of the spatial harmonics of both the accelerating mode [3] and the wakefield, due to the deviation of beams from the linac axis. On the other hand, the considered above radiation mechanism can be used in the undulators based on periodic RF waveguides without external fields, where the non-synchronous wake-harmonics of an electron bunch implies a wave pump. The development of such wake-field undulators with submillimeter periods may open new frontiers in generating X and gamma rays without employing external periodic magnetic fields and RF sources.

I am grateful to Ya.B. Fainberg for the proposed method of solution and fruitful discussions.

## REFERENCES

- [1] A.I. Akhiezer, Ya.B. Fainberg, G.Ya. Liubarski, Zh. Tekh. Fiz. **25**, (1955), pp.2526-2534. Proc. CERN Symp., Geneva, 1956, Vol.1, pp. 220-230.
- [2] V.L. Ginzburg, V.Ya. Eidman, Zh. Eks. Teor. Fiz. **36**, (1959), P.1823-1833.
- [3] A.N. Opanasenko, Fizika Plazmy, **26**, (2000), no.4, P.383-386.

# INTERACTION OF A NONRELATIVISTIC ELECTRON BEAM WITH A SEMICONDUCTOR CYLINDER IN AN EXTERNAL MAGNETIC FIELD

A. F. Rusanov and V. M. Yakovenko

IRE NASU

Ul. Proskury 12, Kharkov 61085, Ukraine

E-mail: andreyrusanov@ukr.net

## ABSTRACT

The paper presents a theoretical study of electrostatic oscillations in a cylindrical system, which represents an electron beam surrounded by a semiconductor of finite thickness, adjacent to a dielectric or a perfectly conducting metal. The system is placed in a finite axial magnetic field. The results of the analysis show that space charge waves (the drift waves) and cyclotron waves could be unstable. It is also shown that, as the external magnetic field or the collision frequency of electrons increases the growth rates of the instabilities decrease.

## INTRODUCTION

Investigating interactions of charged particles beams with natural oscillations in plasmas is among the important topics of microwave plasma electronics. By now there is a great number of papers devoted to the electron beam-plasma interaction. Interactions of this kind are of considerable interest since they can be used for amplification and generation of electromagnetic oscillations of various wavelengths [1]. Also they can bring ample information on physical properties of the medium. In current literature, great attention is focused on the interaction of electron beams with the eigenmodes in plasmas of cylindrical and tubular geometry. The reason is that plasma amplifiers and generators are chiefly built around plasma formations of cylindrical geometry [2].

The interaction of electron beams with tubular solid-state plasmas of finite thickness without external magnetic field was already studied [3]. However, at conditions of experiment, the beam-plasma systems are always situated in an external magnetic field, which prevents lateral motions of electrons in the beam. This paper is aimed at investigating oscillatory processes in a cylindrical structure representing a quasi-neutral charged particle beam surrounded by a semiconductor of finite thickness adjacent to a dielectric or a perfectly conducting metal. Collisions of electrons in the semiconductor are taken into account.

## PROBLEM FORMULATION. DISPERSION RELATIONS

Let the spatial domain  $a \leq \rho \leq b$  in a cylindrical coordinate system  $(\rho, \varphi, z)$  be occupied by a semiconducting material. The spatial domain  $0 \leq \rho < a$  is filled with a dielectric of permittivity  $\varepsilon_{d1}$ , while the domain  $\rho > b$  is filled with another dielectric of

permittivity  $\epsilon_{d2}$  or with a perfectly conducting metal. The structure under analysis is infinite along the  $z$ -axis and is situated in a finite strength axial magnetic field  $\vec{H}_0$ . We will analyse the interaction of a straight, quasi-neutral nonrelativistic electron beam propagating through the domain  $0 \leq \rho < a$ , with electrostatic magnetoplasma oscillations existing in the cylindrical semiconductor structure.

Making use of Maxwell's equations, equations of motion, continuity equations for each region of the structure, boundary conditions at  $\rho = a$  and at  $\rho = b$ , and taking into account that the field magnitude should be finite at the axis of the cylindrical structure and (infinitely) far from it, we can find the dispersion relation to describe the interaction of magnetoplasma waves in the structure with the beam under analysis. The dispersion relation has the form

$$F(a, b, q, l, \omega, \nu, \omega_p, \omega_{Hs}, \omega_b, \omega_{Hb}, V_0) = 0, \quad (1)$$

where  $q$  and  $l$  are, respectively, the axial and the azimuthal wavenumbers;  $\omega$  is the signal frequency;  $\nu$  is the effective collision frequency of electrons in the semiconductor;  $\omega_p$ ,  $\omega_{Hs}$  and  $\omega_b$ ,  $\omega_{Hb}$  are, respectively, the plasma frequencies and the cyclotron frequencies in the semiconducting material and in the beam;  $V_0$  is the equilibrium velocity of electrons in the beam.

If the semiconductor borders on a metal at  $\rho = b$  or if  $b \gg a$ , then the dispersion relation takes the more simple form.

## NUMERICAL RESULTS AND DISCUSSION

(1) was solved numerically using values of parameters appropriate for n-type InSb, i.e., the permittivity of the crystal lattice  $\epsilon_0 = 16$ ; the effective mass of electrons  $m^* = 0.015m$ ; the equilibrium concentration  $N_0 = 5 \times 10^{13} \text{ cm}^{-3}$ . Throughout the discussion  $a = 10^{-1} \text{ cm}$ ,  $d = (b - a) = 10^{-3} \text{ cm}$ ,  $\omega_b = 10^9 \text{ s}^{-1}$ ,  $V_0 = 3 \times 10^9 \text{ cm/s}$ .

A numerical solution of (1) shows (see Fig. 1), that the interaction of charged

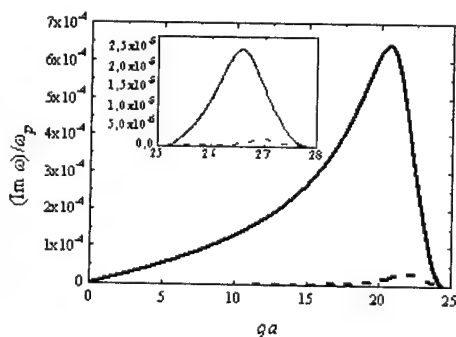


Fig. 1. The growth rates of unstable space-charge waves (solid line) and cyclotron waves (dashed line) for the structure under consideration:  $l = 0$ ;  $\Delta = \omega_{Hs}/\omega_p \approx 0.9$ ;  $\Gamma = \nu/\omega_p = 0.1$

particle beam with magnetized collisional solid-state plasmas gives rise to a broad-band instabilities of the space-charge waves ( $\omega = qV_0$ ) and the cyclotron waves ( $\omega = qV_0 - \omega_{Hb}$ ). The growth rate of any considered instability attains its maximum value under resonance conditions, when the frequency of the unstable wave coincides with that of natural oscillations of the semiconductor cylinder.

Account of two boundaries to the solid-state plasma (tubular geometry of the plasma) shows the domain of instability to be in fact divided into bands of stable and unstable states.

The growth rates of the instabilities are strongly influenced by the external magnetic field and the effective collision frequency. As the magnetic field or collision frequency increases, the growth rate of the instability decreases (see Fig. 2 and Fig. 3).

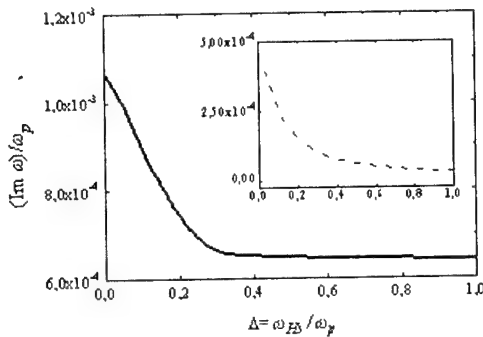


Fig. 2. The growth rates of unstable space-charge waves (solid line) and cyclotron waves (dashed line) as functions of parameter  $\Delta = \omega_{Hs} / \omega_p$ :  $l = 0$ ;  $\Gamma = \nu / \omega_p = 0.1$

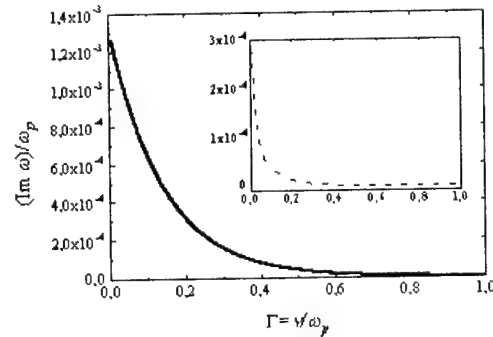


Fig. 3. The growth rates of unstable space-charge waves (solid line) and cyclotron waves (dashed line) as functions of parameter  $\Gamma = \nu / \omega_p$ :  $l = 0$ ;  $\Delta = \omega_{Hs} / \omega_p \approx 0.9$ ;

Fig. 4 shows that the maximum value reached by the growth rate at the negative values of the azimuthal wave number is higher than at the positive values of the azimuthal wave number.

If the cyclotron frequency in the semiconductor is greater than the plasma frequency, then the surface waves in considered semiconductor structure don't exist. In this case, electrons of the beam interact only with spatial oscillations of the semiconductor plasma. The growth rates of the instabilities for this kind of interaction are much less, than in the case of interaction with surface oscillations.

In order to observe the amplification effect for the space-charge wave, it is necessary to preliminary modulate the charge-particle beam.

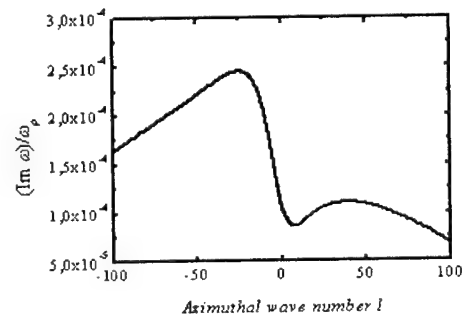


Fig. 4. The growth rate of unstable space-charge waves as a function of the azimuthal wave number  $l$ :  $\Delta = \omega_{Hs} / \omega_p \approx 0.9$ ;  $\Gamma = \nu / \omega_p = 0.1$

## REFERENCES

- [1] M. V. Kuzelev, O. T. Loza, A. A. Rukhadze, P. S. Strelkov, and A. G. Shkvarunets, Plasma Phys. Rep. **27**, 669 (2001).
- [2] A. V. Ponomarev, P. S. Strelkov, and A. G. Shkvarunets, Plasma Phys. Rep. **26**, 592 (2000).
- [3] A. F. Rusanov and V. M. Yakovenko, Telecommunications and Radio Engineering **55**, 147 (2001), and references therein.

## AN ANALYTICAL METHOD FOR CONSTRUCTION OF SINGLE PARTICLE ELECTRON TRAJECTORIES IN FREE ELECTRON LASERS

Kostyantyn V. Ilyenko, Boris P. Yefimov, Vitaly A. Goryashko\*  
and Tetyana Yu. Yatsenko\*

IRE NASU, Kharkov 61085, Ukraine  
E-mail: kost@ire.kharkov.ua

\*V.N. Karazin Kharkov National University  
pl. Svobody 4, 61077, Kharkov, Ukraine

### ABSTRACT

We apply a method of Linshedt, also called improved expansion, to solve the equations of motion and obtain single-particle trajectories of electrons moving in crossed static magnetic fields of a hybrid non-relativistic free electron laser. Making use of a natural small parameter, the ratio of the amplitude of spatially periodic magnetic field and the guide magnetic field, one can re-write the motion equations for an electron in a form, which allows their solution by an asymptotic series. In such a way the non-linear frequency shifts and renormalized mean electron velocity are calculated analytically. The analytical results are in a good compared with numerical simulations of the electron trajectories.

### INTRODUCTION

Initial analysis of properties of an electron-optical system (EOS) is performed in the approximation of geometrical optics. Namely, for unneutralised electron beam in external magnetic fields it customary to study in succession single-particle approximation, approximation of magneto-hydrodynamics and, finally, kinetic equation formalism. It turns out that even rough single-particle approximation can provide valuable insights into basic dynamics of an electron beam propagating along the studied EOS.

Attempts to find analytical expressions for description of single particle trajectories go back to the 1970s [1–3]. However, no one approach, going further the zero-approximation expression for the helical magnetic field setup [4] and the well-known formulas for the equations of mathematical pendulum in the case of absence of the guide magnetic field, has been presented [5]. This situation is rather unfortunate, since in the case of a free electron laser (FEL) with a guiding magnetic field [6,7] at non-relativistic and intermediate energies ( $< 600$  keV) such an expression could be very helpful. It can provide a qualitative analysis because of relative accessibility of the necessary values of the guiding magnetic fields for the utilization of resonances on the characteristic pump field and cyclotron frequencies.

In the present contribution we present an analytical solution by an asymptotic series of the problem of an electron motion in the harmonic transversal undulator magnetic field and strong, but finite, longitudinal magnetic field.

## IMPROVED EXPANSION

Consider the electron motion in the following static magnetic field:

$$\vec{H} = [0, -H_{\perp} \sin(2\pi z/l), -H_{\parallel}]$$

Here  $l$  is the space period of the transverse to the injection direction static magnetic field. Non-relativistic equations of motion of an electron take the form

$$m_0 \frac{d\vec{v}}{dt} = -\frac{e}{c} [\vec{v}, \vec{H}],$$

where  $m_0$  is the electron's rest mass,  $e$  is the absolute value of its charge and  $\vec{v}$  is the electron's velocity vector. Let us also introduce the following notations:

$$\tau = \omega_0 t, \quad \gamma_0 = \omega_{\parallel} / \omega_0, \quad \varepsilon = \omega_{\perp} / \omega_0, \quad \omega_0 = 2\pi v_{\parallel} / l, \quad \omega_{\parallel} = eH_{\parallel} / m_0 c, \quad \omega_{\perp} = eH_{\perp} / m_0 c, \\ \xi = x/l, \quad \eta = y/l, \quad \zeta = z/l,$$

where  $v_{\parallel}$  is the z-component of the initial velocity of the electrons,  $d\zeta/d\tau[\tau=0] = 1/2\pi$  and the rest of the initial values of the velocities and coordinates are equal to zero. Thus we can write the non-linear equations of motion in the dimensionless form

$$\frac{d^2\xi}{d\tau^2} + \gamma_0^2 \xi = -\varepsilon \frac{d\zeta}{d\tau} \sin(2\pi\zeta), \quad \frac{d\zeta}{d\tau} - \delta_0 = \varepsilon \int_0^{\tau} \frac{d\xi}{d\tau} \sin(2\pi\zeta) d\tau, \quad \frac{d\eta}{d\tau} + \gamma_0 \xi = 0. \quad (1)$$

Here  $\gamma_0$  is the dimensionless oscillation frequency and  $\delta_0 = d\zeta/d\tau[\tau=0]$ . It is easily seen that the first two equations of the system (1) define the dynamics of electrons completely.

We are interested in analytical solutions for the dimensionless frequency  $\gamma_0$  greater than 2 and the values of  $\varepsilon$  less than  $1/2$ . According to the Linshtedt method [8,9], we shall expand  $\xi(\tau)$ ,  $\eta(\tau)$ ,  $\zeta(\tau)$ , the true nonlinear-shifted frequency  $\gamma$  and mean electron velocity  $\delta$  into series in  $\varepsilon$ :

$$\xi(\tau) = \xi_0(\gamma\tau) + \varepsilon \xi_1(\gamma\tau) + \varepsilon^2 \xi_2(\gamma\tau) + \varepsilon^3 \xi_3(\gamma\tau) + \varepsilon^4 \xi_4(\gamma\tau) + \dots$$

$$\zeta(\tau) = \zeta_0(\gamma\tau) + \varepsilon \zeta_1(\gamma\tau) + \varepsilon^2 \zeta_2(\gamma\tau) + \varepsilon^3 \zeta_3(\gamma\tau) + \varepsilon^4 \zeta_4(\gamma\tau) + \dots$$

$$\gamma = \gamma_0(1 + \varepsilon f_1 + \varepsilon^2 f_2 + \varepsilon^3 f_3 + \varepsilon^4 f_4 + \dots)$$

$$\delta = \delta_0(1 + \varepsilon g_1 + \varepsilon^2 g_2 + \varepsilon^3 g_3 + \varepsilon^4 g_4 + \dots)$$

Equating coefficients at each order of  $\varepsilon$  for the system of equations (1), we find linearized sets for the functions and coefficients of (2). These sets are iterative linear non-homogeneous systems of equations, which are integrated one after another.

To  $o(\varepsilon^3)$  order the solutions have the form

$$\xi(\tau) = \frac{2\pi\delta^2\varepsilon}{\gamma[\gamma^2 - (2\pi\delta)^2]} \{ \sin[\gamma\tau] - (\gamma/2\pi\delta) \sin[2\pi\delta\tau] \}, \\ \eta(\tau) = -\frac{2\pi\delta^2\varepsilon}{\gamma[\gamma^2 - (2\pi\delta)^2]} \{ 1 - \cos[\gamma\tau] - (\gamma/2\pi\delta)^2 (1 - \cos[2\pi\delta\tau]) \}, \\ \zeta(\tau) = \delta\tau + \frac{\pi\delta^2\varepsilon^2}{\gamma^2 - (2\pi\delta)^2} \left\{ \frac{\sin[4\pi\delta\tau]}{16\pi^2\delta^2} - \frac{\sin[(\gamma+2\pi\delta)\tau]}{\gamma+2\pi\delta} + \frac{\sin[(\gamma-2\pi\delta)\tau]}{\gamma-2\pi\delta} \right\}. \quad (2)$$

The frequency  $\gamma$  and the average electron velocity  $\delta$ , up to the same order, are

$$\gamma = \gamma_0 \left[ 1 + \varepsilon^2 \frac{\gamma_0^2 + 1}{4(\gamma_0^2 - 1)^2} \right], \quad \delta = \delta_0 \left[ 1 - \varepsilon^2 \frac{\gamma_0^2 + 3}{4(\gamma_0^2 - 1)^2} \right]. \quad (3)$$

We have accomplished the calculations to the next meaningful order,  $o(\varepsilon^5)$ . They show that there exist a number of resonances at odd ratios

$$\omega_{\parallel} / \omega_0 \approx \gamma / 2\pi\delta = 2k + 1, \quad k \in \mathbb{Z}. \quad (4)$$

In the limit  $\gamma_0 \rightarrow 0$  formulas (2) and (3) provide the trajectories in the FEL without the guide magnetic field (e.g. [5, p. 37]). They as well confirm the assertions on the form of one-body trajectories of electrons in such ideal FEL magnetic field, which are usually made in the literature (cf. [1-3]).

Since in the trajectory approximation the vector potential and components of electromagnetic field in the wave zone are dependent on the time derivatives of the electron coordinates, one can expect that resonances existing in those expressions will also be present for the power of the spontaneous emission. These higher resonances one would expect to observe for experimentally accessible values of the guide magnetic field.

Numerical simulations accomplished by us for the initial system of integro-differential equations (1) verified these analytic solutions to the accuracy of 1%.

## CONCLUSIONS

As a result of this work, we are able to provide analytical solutions for electron trajectories in an ideal hybrid free electron laser-oscillator and calculate dependence of the trajectories on the parameters of the pumping magnetic fields. We have also prepared the machinery for treating the real undulator magnetic field. Thus one will be able to calculate the polar pattern of the emitted radiation in the single particle approximation in the both cases.

## REFERENCES

- [1] D.F. Alferov, et al., *Sov. J. Tech. Phys.*, vol. 43, No. 10 (in Russian).
- [2] W.B. Colson, *Phys. Lett. A*, vol. 64, No. 2, pp. 190–192 (1977).
- [3] P. Diament, *Phys. Rev. A*, vol. 23, No. 2, pp. 2537–2552 (1981).
- [4] R.A. Demirkhanov et al., *Sov. J. Tech. Phys.*, vol. 33, No. 9 (in Russian).
- [5] T.C. Marshall, *Free-Electron Lasers*, Macmillan Publ., London, 1985.
- [6] I.B. Bernstein, L. Friedland, *Phys. Rev. A*, vol. 23, No. 2, pp. 316–323 (1981).
- [7] H.P. Freund, P. Sprangle, *Phys. Rev. A*, vol. 24, No. 4, pp. 1965–1979 (1981).
- [8] A. Linshtedt, *Memoirs Acad. Sci. St.-Petersburg*, vol. 31, pp. 1 – 20 (1883) (in Latin).
- [9] A.M. Cosevich, A. S. Covalev, *Introduction into Nonlinear Dynamics*, Naukova Dumka, Kiev, 1989 (in Russian).

# COLLISIONLESS DAMPING OF SURFACE PLASMA OSCILLATIONS AND POSSIBILITIES OF ITS REVERSE AT THE INTERACTION WITH CHARGED PARTICLE FLOWS

V.M. Yakovenko. I.V. Yakovenko\*

A. Usikov IRE NASU

Ul. Proskury 12, Kharkov 61085, Ukraine

\*R & D Institute "Molnia", Ministry of Education and Science of Ukraine

ul. Schevchenko 47, Kharkov 61013, Ukraine

This paper is devoted to investigation of the interaction between the charged particle flows passing through the boundary of plasmalike media and surface oscillations.

Suppose that an external flow of charged particles crosses the boundary between the media of different electromagnetic properties, for example, dielectric (vacuum)-semiconductor. Let a semiconductor occupy the space region  $y > 0$  and vacuum (dielectric with  $\epsilon_1$ ) is at  $y < 0$ . It follows from Maxwell's equations that there are the surface electromagnetic oscillations with spectrum

$$q^2 = \frac{\omega^2}{c^2} \frac{\epsilon_1 \epsilon_2(\omega)}{\epsilon_1 + \epsilon_2(\omega)}; \quad \epsilon_2(\omega) = \epsilon_0 - \frac{\omega_0^2}{\omega^2}; \quad \epsilon_2(\omega) < 0, \quad \epsilon_1 > 0, \quad (1)$$

where  $\omega$  is the frequency of plasmon,  $\mathbf{q}$  is the wave vector along the surface,  $\omega_0^2 = 4\pi e^2 n_0 / m$  is the plasma frequency;  $n_0$  is the electron concentration,  $m$  is the effective mass of electron. If  $c \rightarrow \infty$ , the dispersion law is  $\omega = \omega_0 / \sqrt{\epsilon_0 + \epsilon_1}$ .

Hamiltonian of the system has the following form:

$$\hat{\mathbf{H}} = \hat{\mathbf{H}}^{(f)} + \hat{\mathbf{H}}^{(e)} + \hat{\mathbf{H}}^{(int)}, \quad (2)$$

where  $\hat{\mathbf{H}}^{(f)} = \frac{1}{2} \sum_q \hbar \omega_q [\hat{a}_q^+(t) \hat{a}_q(t) + \hat{a}_q(t) \hat{a}_q^+(t)]$  is the Hamiltonian of electromagnetic field (surface plasmons),  $\hat{\mathbf{H}}^{(e)} = \sum_k \epsilon_k \hat{b}_k^+(t) \hat{b}_k(t)$  is the Hamiltonian of an electron system;  $\epsilon_k = \hbar^2 k^2 / 2m$  is the dispersion law of electrons;  $\mathbf{k}$  is the wave vector of the electron;  $\hat{a}_q^+(t) = \hat{a}_q^+ \exp(i\omega_q t)$ ,  $\hat{a}_q(t) = \hat{a}_q \exp(-i\omega_q t)$ ,  $\hat{b}_k^+(t) = \hat{b}_k^+ \exp(i\epsilon_k t / \hbar)$ ,  $\hat{b}_k(t) = \hat{b}_k \exp(-i\epsilon_k t / \hbar)$ ,  $\hat{a}_q^+, \hat{a}_q, \hat{b}_k^+, \hat{b}_k$  are the birth and annihilation operators for the plasmons and the electrons in the states  $\mathbf{q}$  and  $\mathbf{k}$ ;

$$\hat{\mathbf{H}}^{(int)} = \sum_{kqk'} W_{kqk'} \hat{b}_k^+(t) [\hat{a}_q(t) + \hat{a}_{-q}^+(t)] \hat{b}_{k'}(t) \quad (3)$$

is the Hamiltonian of the electron-plasmon interaction.

To find the expression for the matrix element  $W_{kqk'}$ , it is necessary to use the expression

$$\hat{\mathbf{H}}^{(int)} = -\frac{1}{c} \sum_{\alpha=1}^2 \int \hat{\mathbf{j}}(\mathbf{r}, t) \hat{\mathbf{A}}_{\alpha}(\mathbf{r}, t) d\mathbf{r}, \quad (4)$$

where



$$\hat{\mathbf{j}}(\mathbf{r}, t) = \frac{e\hbar}{2m_0 V} \sum_{\mathbf{k}, \mathbf{k}'} (\mathbf{k} + \mathbf{k}') \hat{b}_{\mathbf{k}}^+(t) \hat{b}_{\mathbf{k}'}(t) \exp i(\mathbf{k}' - \mathbf{k})\mathbf{r}$$

is the operator of an electron current density,

$$\hat{\mathbf{A}}_{\alpha}(\mathbf{r}, t) = \sum_q \left( \frac{4\pi\hbar c^2}{V\omega_q} \right)^{1/2} \mathbf{e}_{\alpha} [\hat{a}_q(t) + \hat{a}_{-q}^+(t)] e^{i\mathbf{q}\cdot\mathbf{r}}$$

is the operator of the vector-potential of the surface wave electromagnetic field;  $\mathbf{e}_{\alpha}$  is the unit polarization vector:  $e_x = e_{1x} = e_{2x} = (q_x/|q|)\sqrt{L|q|/(\varepsilon_1 + \varepsilon_0)}$ ,  $e_{1y} = -e_{2y} = ie_x$ ,  $e_z = (q_z/q_x)\mathbf{e}_x$ ,  $\mathbf{q}_{1,2} = (q_x, \mp q, q_z)$ ,  $V = LS$  is the volume of the interaction space,  $S$  is the cross-section of the sample.

Carrying out the standard procedure [1,2] we obtain the following kinetic equation which describes the change of the surface plasmon number  $N_q$  as the result of their radiation and absorption with the electrons  $n_k$

$$\frac{\partial N_q}{\partial t} = \frac{2\pi}{\hbar} \sum_{k_1 k_2} |W_{k_1 q k_2}|^2 [(N_q + 1)n_{k_1}(1 - n_{k_2}) - N_q n_{k_2}(1 - n_{k_1})] \delta(\varepsilon_{k_1} - \varepsilon_{k_2} - \hbar\omega_q), \quad (5)$$

where [2]

$$W_{k_1 q k_2} = \frac{q_x(k_1^2 - k_2^2)}{m_0 L |q_x| [q^2 + (k_{1y} - k_{2y})^2]} \left( 2 \frac{\pi e^2 q \hbar^3}{S \omega_q (\varepsilon_0 + \varepsilon_1)} \right)^{1/2}. \quad (6)$$

From here for  $N_q \gg 1$  we obtain the expression for the decrement or increment of the surface plasmons,  $\gamma = (1/2)N_q^{-1}(\partial N_q / \partial t)$ .

Suppose that injected electron energy is distributed near some value  $\varepsilon_{k_0} = p_0^2 / 2m_0 = \hbar^2 k_0^2 / 2m_0$ . Then one can present the electron number  $n_k \ll 1$  as

$$n_k = \frac{n_{0b}(2\pi\hbar)^3}{(2\pi m_0 T)^{3/2}} e^{-\frac{\hbar^2(k_y - k_0)^2}{2m_0 T}} e^{-\frac{\hbar^2(k_x^2 + k_z^2)^2}{2m_0 T}}, \quad (7)$$

where  $n_{0b} = \sum n_k / V = \int n_k d\mathbf{k} / (2\pi)^3$  is the density,  $T$  is the temperature of the electron beam.

Taking into account the conservation laws and the conditions  $P_0^2 / 2m_0 \gg \hbar\omega_q$ ,  $P_0^2 / 2m_0 \gg T$ ,  $\omega_q / v_0 \gg q$ , we obtain

$$|W_{k_1 q k_2}|^2 = \frac{8\pi e^2 q \hbar v_{y1}^4}{V L \omega^3 (\varepsilon_0 + \varepsilon_1)}. \quad (8)$$

If the condition  $T \gg \hbar\omega_q$  is fulfilled one can consider that  $n_{k_1} - n_{k_2} \cong -\frac{\omega_q}{v_{y1}} \frac{\partial n_{k_1}}{\partial k_{y1}}$ . After

integration of equation (5) over the wave vectors  $\mathbf{k}_1$  and  $k_{y2}$  one can obtain the following expression for the decrement of the surface plasmons:

$$\gamma = -\frac{\omega_b^2 q v_0}{\omega_q^2}, \quad \omega_b^2 = \frac{4\pi e^2 n_{0b}}{m_0(\epsilon_0 + \epsilon_1)}. \quad (9)$$

However, the induced radiation processes dominate over the absorption ones under the condition  $P_0^2/2m_0 \gg \hbar\omega_q \gg T$ . In this case we obtain

$$\gamma = \frac{2n_{0b} |W_{k_0 q k_{\pm}}|^2}{\hbar^3} L V m_0 \left( \frac{1}{k_+} - \frac{1}{k_-} \right), \quad (10)$$

where  $k_{\pm} = k_0 \pm \omega_q/v_0$ ,  $v_{x1} = v_0$ .

This is due to the fact that the probability for the electron to pass to the state with a smaller energy exceeds the probability to pass to the state with a higher energy. In the former case the probability is proportional to  $k_{\pm}^{-1}$ . This mechanism of the instability of the oscillations takes place at the different inhomogeneous solid state structures: semiconductor superlattice [3], two-dimensional gas [4], and other [5]. In finding the increment (10) we put

$$n_k = (2\pi)^3 n_{0b} \delta(k_x) \delta(k_y - k_0) \delta(k_z).$$

Thus, when a directive electron beam crosses the boundary of a plasmalike media, the surface plasmons fade away if the conditions  $P_0^2/2m_0 \gg T \gg \hbar\omega_q$  are met (classical case). However, at low temperatures,  $P_0^2/2m_0 \gg \hbar\omega_q \gg T$  (quantum case), the radiation processes begin to dominate over the absorption ones and the surface oscillations grow up with increment

$$\gamma = \frac{2\omega_b^2 q v_0}{\omega_q^2}. \quad (11)$$

These processes are very important for the diagnostics of the surface of solids.

## REFERENCES

- [1] J.M. Ziman. *Elements of Advanced Quantum Theory*, 1971, Mir, Moscow.
- [2] N.N. Beletsky, V.M. Svetlichny, D.D. Khalamejda, V.M. Yakovenko. *Electromagnetic Microwave Phenomena in Inhomogeneous Semiconductors*, 1991, Naukova Dumka, Kiev.
- [3] M.V. Burtyka, O.V. Glukhov, V.M. Yakovenko. Interaction of hot electrons with two-dimensional gas in semiconductor superlattice. *Solid-State Electronics*, 1991, **34**, N 6, pp. 559-564.
- [4] M.V. Burtyka, V.M. Yakovenko, I.V. Yakovenko. Interaction of charged particle beams with plasmons in a two-dimensional electron gas. *Low Temp. Phys.*, 1995, **26**, N 6, pp. 489-492.
- [5] I.V. Yakovenko. Interaction of charged particles with surface waves at a periodically rough PEC boundary. *Radiofizika i Elektronika*, IRE NASU Press, 1998, **3**, N 1, pp. 7-10.

## PECULIARITIES OF NONLINEAR STABILIZATION OF PLASMA-BEAM INSTABILITY IN SEMICONDUCTOR GaAs

Yuri O. Averkov and Vladimir M. Yakovenko

IRE NASU, Kharkov 61085, Ukraine  
E-mail: averkov@online.kharkiv.com

### ABSTRACT

The excitation of nonlinear plasma oscillations by a monoenergetic electron beam of low density moving through a semiconductor is considered by the particle-in-cell method. An electron beam is assumed to be a sequence of electron bundles with constant density. It has been assumed that the electron collision frequency in a semiconductor is greater than the hydrodynamic increment of instability in collisionless plasma but less than plasma electron frequency is investigated. The influence both of nonparabolicity of electron dispersion law and intervalley electron transitions on the plasma-beam instability is taken into account. The nonparabolicity is shown to lead to the decrease of the maximum of the electric field amplitude while the intervalley electron transitions lead to the appearance a plateau on the temporal dependence of the slow amplitude of the electric field.

### PHYSICAL MODEL

We consider a homogeneous semiconductor GaAs placed in the strong magnetic field. Let the  $x$ -axis be directed along the direction of the magnetic field, which is parallel to the direction of a nonrelativistic monoenergetic beam moving with the velocity  $v_0 \ll c$  (where  $c$  is the speed of light in empty space). Hereinafter we consider a one-dimensional problem. We assume that the collision frequency in the semiconductor  $\nu$  satisfies the following condition:

$$\gamma_0 < \nu < \Omega_p, \quad (1)$$

where  $\Omega_p = \sqrt{4\pi e^2 N_0 / \varepsilon_0 m}$  is the electron Langmuir frequency in the semiconductor plasma,  $e$  is the charge of an electron,  $N_0$  is the equilibrium electron density in the semiconductor plasma,  $\varepsilon_0 = 12.53$  is the dielectric constant of the crystal lattice of the semiconductor,  $m = 0.067 m_0$  is the effective mass of an electron in the semiconductor,  $\gamma_0 = \sqrt{3} / 2^{4/3} \Omega_p (n_0 / N_0)^{1/3}$  is the maximum growth rate of hydrodynamic instability,  $n_0$  is the equilibrium electron density in an electron beam. In the case under consideration the most unstable oscillations are characterized by the frequency  $\omega \approx \Omega_p \approx k_0 v_0$  and the growth rate of hydrodynamic instability  $\gamma = \sqrt{\omega_b^2 \Omega_p / 2\nu} < \gamma_0$  [1]. Here  $\omega_b = \sqrt{4\pi e^2 n_0 / m_0}$  is the electron Langmuir frequency of electron beam and  $k_0$  is the wave vector of the most unstable mode.

The case described above can be realized in the highly compensated semiconductor GaAs at the liquid helium temperature. Let us consider a sample of GaAs with an n-type impurity concentration of about  $N_d = 5 \cdot 10^{17} \text{ cm}^{-3}$  and the electron concentration of  $N_0 = 4 \cdot 10^{15} \text{ cm}^{-3}$  ( $\Omega_p \approx 4.0 \cdot 10^{12} \text{ s}^{-1}$ ). In GaAs in a thermodynamic equilibrium state the majority of electrons occur in the valley with a minimum energy at the center of the Brillouin zone (the  $\langle 000 \rangle$  valley). The next several higher valleys with minimum energies in the  $\langle 100 \rangle$  directions are separated from the  $\langle 000 \rangle$  valley by the energy gap  $\Delta \approx 0.36 \text{ eV}$ . The effective electron mass in higher valleys is  $m_{\langle 100 \rangle} \approx 75 m_{\langle 000 \rangle}$ . Since the density of states is proportional to  $m^{3/2}$ , the density of states for the valley in  $\langle 100 \rangle$  directions is higher than for the  $\langle 000 \rangle$  valley. Therefore it far more probable for electron whose temperatures exceeds  $\Delta$  to occur in the  $\langle 100 \rangle$  valleys than in the  $\langle 000 \rangle$  valley. The emission or absorption of optical phonons accompanies the electron transitions between the valleys. The relaxation frequency of an electron momentum changes abruptly from  $\nu \approx 5 \cdot 10^{11} \text{ s}^{-1}$  to  $\nu \approx 10^{12} \text{ s}^{-1}$ .

### NONLINEAR STABILIZATION

With the aid of the particle-in-cell method [1] we have obtained that the valley-to-valley transitions cause the considerable changes in the temporal dependence of the slow amplitude of the wave electric field  $E_s(t)$  (i.e.,  $|dE/dt| \ll \Omega_p E$ ). The dependence  $E_s(\tau)$  (where  $\tau = \gamma t$ ) is shown in Fig.1.

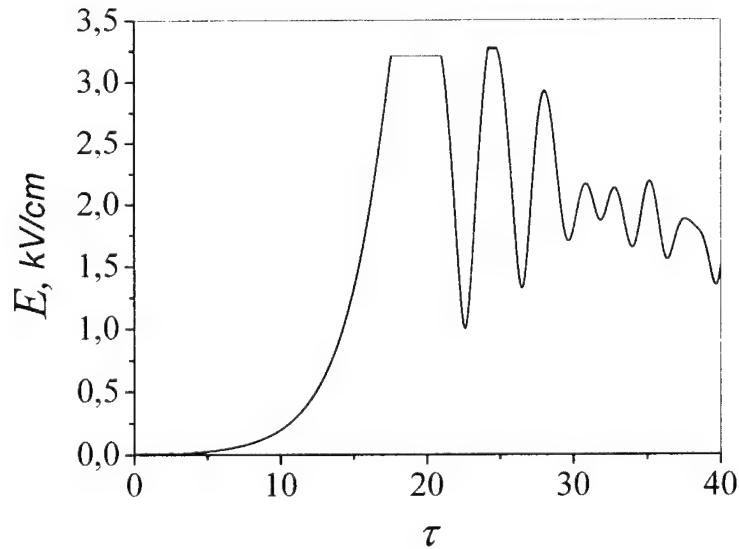


Fig. 1

The plateaus in Fig.1 appear due to the frequency  $\nu$  increases abruptly. This increase causes the abrupt decrease the growth rate of hydrodynamic instability  $\gamma$ . This situation continues until the most of beam electrons are trapped.

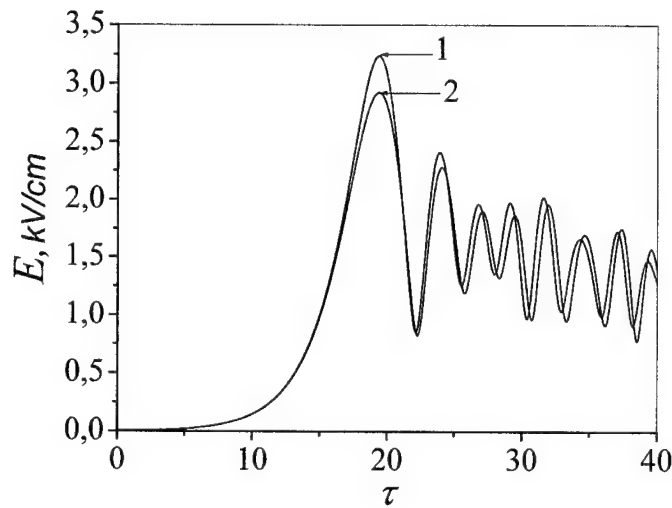


Fig. 2

The influence of nonparabolicity of electrons dispersion law in GaAs is shown in fig.2.

In this figure the curve "1" corresponds to the dependence  $E_s(\tau)$  without taken into account the nonparabolicity and the curve "2" corresponds to the opposite case. The influence mentioned above is taken into account with the help of the dependence of the electron effective mass on their temperature  $m(T_e)$ :

$$m^*(T_e) = m \sqrt{1 + \frac{4T_e(E_s)}{\theta_g}}, \quad (2)$$

where  $\theta_g$  is the energy gap between the valence and conduction bands. Fig.2 shows that the nonparabolicity causes the decrease of the maximum of  $E_s$  in which the most of the beam electrons are trapped by the wave.

## REFERENCES

- [1] A. A. Ivanov, V. V. Parail, and T. K. Soboleva, *Zh. Eksp. Teor. Fiz.* Vol.63, 1678 (1972).

# **EIGENVALUE PROBLEMS**

# EIGENOSCILLATIONS NEAR CASCADE OF THIN DISKS BETWEEN THE PAIR OF PARALLEL PLANES

Ivan S. Chikichev

Novosibirsk State University, Novosibirsk, Russia

E-mail: ChikichevIS@yukos.nsu.ru

## ABSTRACT

Eigenoscillations near cascade of thin disks between the pair of parallel planes are studied. The sufficient conditions of existence for eigenoscillations are found. The dependence of eigenfrequencies on the geometric parameters of structure is investigated. It is shown that the frequencies of eigenoscillations of given structure are discrete and they formed a bundle of resonance frequencies which is under specific conditions act as a continuous band of resonance frequencies. The number of resonance bundles is calculated.

## PROBLEM FORMULATION

The present work generalized the results obtained in [1] for periodic chain of thin disks to the structure which is shown on Fig.1. Mathematical statement of the problem based on the Helmholtz equation in cylindrical coordinate system, the assumption of rigidity of all boundaries together with the condition of local energy finiteness and could be write down in the following form:

$$\frac{1}{r} \frac{\partial}{\partial r} \left( r \frac{\partial u}{\partial r} \right) + \frac{\partial^2 u}{\partial z^2} + \lambda^2 u = 0, \quad \frac{\partial u}{\partial n} \Big|_{\Gamma} = 0 \quad E(u) = \int_{\Omega} [ |u|^2 + |\nabla u|^2 ] d\Omega < \infty \quad (1)$$

Here we assume that the process is steady-state, so the time dependence is taken to be  $\exp(-i\omega t)$  and the solution is independent on polar angle,  $\Gamma$  is the boundary of domain of oscillations including walls and cascade of thin disks. The meaning of all other designations is evident from Fig.1.

## GENERAL APPROACH

Owing to the fact that we have set the cascade of disks as a symmetrical array with respect to channel walls we can expand given problem (1) and solve it in all 3D space but with additional conditions (2) on imagine boundaries set up by the collection of parallel planes at  $\Pi_k = \{ (x, y, z) : z = H/2T + k \}, k \in Z$

$$\frac{\partial u}{\partial n} = 0, \text{ at } \Pi_k, k \in Z \quad (2)$$

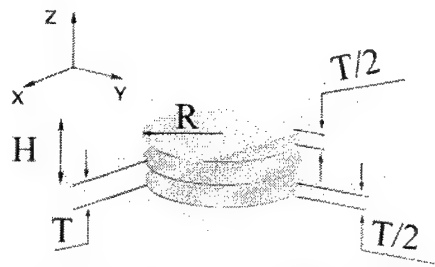


Fig.1. Region of oscillations and basic designations.

The general form of a solution for this new problem in a free space ( $x^2 + y^2 > R^2$ ) could be written in the form (3) with help of Floquet theorem:

$$u(x, y, z) = v(x, y, z) \cos(\xi z), \quad v(x, y, z+1) = v(x, y, z), \quad \xi = n\pi/N, \quad n = 0 \dots (N-1) \quad (3)$$

This follows that the solution of the problem could be understood as a stationary wave in case  $\xi \neq 0$  with phase shift in each interdisk space and as a stationary wave which is synphase in each interdisk space when  $\xi = 0$ .

In [2] it was shown that if  $R \geq \theta_0/\pi$ , here  $\theta_0$  is the first zero of Bessel function of zero order than the periodic chain of disks possesses the waveguiding properties for any  $\xi \neq 0$ . In case  $\xi = 0$  the existence of resonance frequencies is proved for  $R > 0.342$ . Coupled with existence proof the formulas (4) for dependencies of waveguiding and resonance frequencies on the geometric parameters of the chain were obtained.

$$\sin[\chi(\lambda, \xi)] = 0, \text{ here}$$

$$\chi(\lambda, \xi) = -\frac{\pi}{2} - \arctg \frac{J_1(\lambda R)}{J_0(\lambda R)} + \frac{\lambda}{\pi} \ln(2) - \arcsin \frac{\lambda}{|\xi|} - \sum_{n=1}^N \left\{ \arcsin \left( \frac{\lambda}{\xi + 2n\pi} \right) + \arcsin \left( \frac{\lambda}{\xi - 2n\pi} \right) \right\} + \sum_{n=1}^{2N} \arcsin \left( \frac{\lambda}{n\pi} \right)$$

$$\cos \sigma(\lambda, R) = 0, \text{ here} \quad (4)$$

$$\sigma(\lambda, R) = -\arctg \frac{J_1(\sqrt{\lambda^2 - \pi^2} R)}{J_0(\sqrt{\lambda^2 - \pi^2} R)} - \sum_{n=1}^N \arcsin \left( \frac{\sqrt{\lambda^2 - \pi^2}}{\sqrt{(2n\pi)^2 - \pi^2}} \right) + \sum_{n=2}^N \arcsin \left( \frac{\sqrt{\lambda^2 - \pi^2}}{\sqrt{((2n-1)\pi)^2 - \pi^2}} \right)$$

here  $N$  is a parameter, natural number, which control the approximation accuracy

The fact is that the waveguiding and resonance frequencies of the problem with additional condition (2) correspond to the eigenfrequencies of the problem (1) if one chose the appropriate values for  $\xi$  parameter (3), so the eigenfrequencies of problem (1) are discrete.

## RESULTS

From analytical and numerical investigations of expressions (4) follows that the eigenfrequencies are group into certain number of bundles in case  $\xi \neq 0$  and forms a finite set of isolated frequencies in case  $\xi = 0$ . The distant between the boundary of these bundles depends on geometrical parameters of disks cascade. Using the Neumann-Dirichlet bracket we were able to prove the following statements.

**Statement 1.** The number of resonance frequency bundles  $K$  is determined by the expression  $\mu_0 \leq K \leq \mu_1$  where  $\mu_i$  is the number of the roots for Bessel function  $J_i$  which are contained in the segment  $[0, \pi R]$ .

**Statement 2.** The number of isolated resonance frequency  $A$  can be estimate from the expression  $\mu_0 \leq A \leq \mu_1$  where  $\mu_i$  is the number of the roots for Bessel function  $J_i$  which are contained in the segment  $[0, R\pi\sqrt{3}]$ .

The boundary of resonance frequency bundles and isolated resonance frequencies are show on Fig.2. The dependence of eigenfrequencies on phase shift parameter ( $\xi$ ) is illustrated on Fig.3.



In terms of this investigation one could conclude that since the position of the boundary of resonance bundles continuously depends on the geometrical parameters of the disks cascade the methods of reduction of objectionable resonance phenomena which are based on breaking symmetry of the structure given had no fundamental basis. The second conclusion could be the following. Since the increasing of the number of disks in cascade lead to gaining of the number of resonance frequencies per bundle and due to non-linear phenomenon called "Capturing of resonance frequencies" we could finally get the continuous band of resonance frequencies instead of set discrete bundles of resonance frequencies.

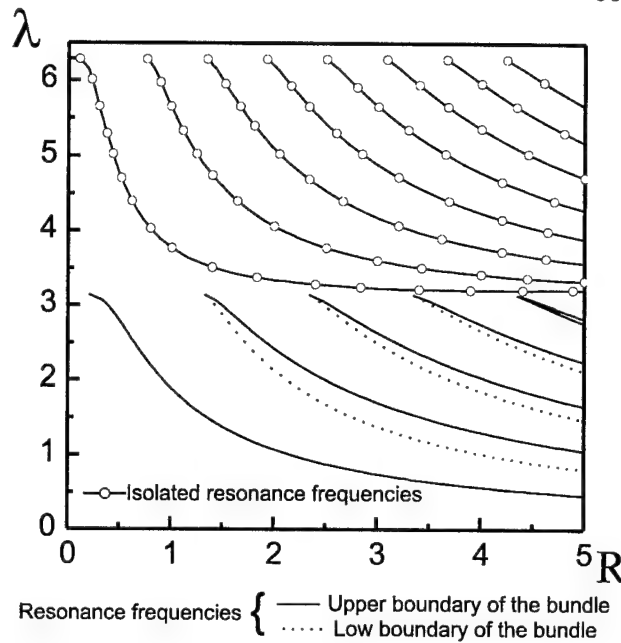


Fig.2. The dependence of boundaries of the bundles of resonance frequencies and isolated resonance frequencies on the disk radius

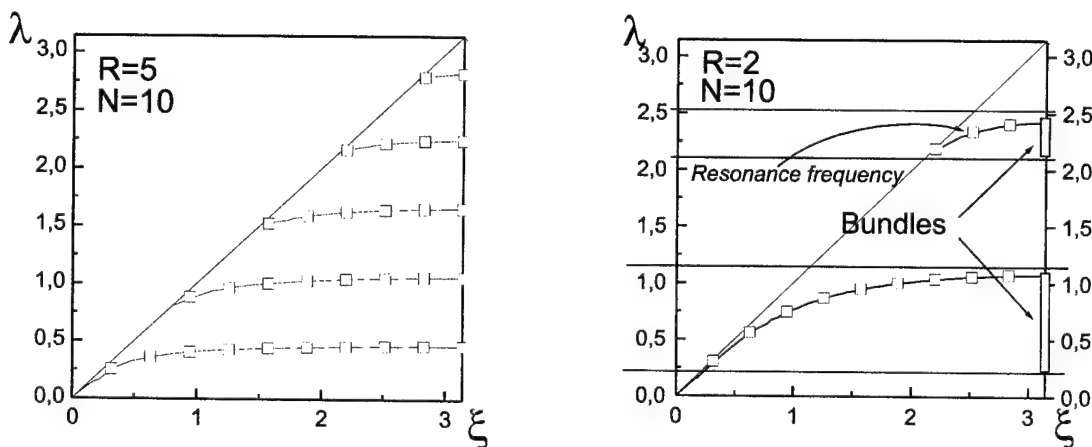


Fig.3. The dependence of eigenfrequencies on phase shift parameter ( $\xi$ ). Here  $R$  is the disk radius,  $N$  is the number of disks in cascade.

#### ACKNOWLEDGMENT

I am indebted to doctor S.V. Sukhinin who guide my research.

#### REFERENCES

- [1] I.S. Chikichev "Waveguide and anomalous properties of circular disk periodic chain" Proc. of 17th International Congress on Acoustic, Rome, Italy, 2001, pp.202-210
- [2] I.S. Chikichev "Waveguide properties of periodic chain of obstacles in 3D space" *Dinamika Sploshnih Sred*, 2000, vol 117, pp.83-88 (in Russian)

KIEV, UKRAINE, IX-TH INTERNATIONAL CONFERENCE ON MATHEMATICAL METHODS IN ELECTROMAGNETIC THEORY

## INFLUENCE OF AN ELLIPTICAL NON-UNIFORMITY OF DIELECTRIC SPHERE ON SPECTRAL CHARACTERISTICS OF RESONANCE OSCILLATIONS

Yu.F. Filipov, Yu.V. Prokopenko

Usikov Institute of Radiophysics and Electronics, National Academy of Sciences

12, Akad. Proskura St., Kharkov, 61085, Ukraine

Tel.: (0572) 448593, E-mail: prokopen@ire.kharkov.ua

The spectral task is solved for open prolate spheroid that made from homogeneous isotropic crystal and has small distance between its focuses. The approximate dispersion equation is obtained at satisfaction of the tangential component continuity conditions of electromagnetic field strengths for resonance oscillations on the spheroid surface. It allows to study spectral characteristics of resonance oscillations.

### INTRODUCTION

The open dielectric resonators are widely applied to determine the parameters of materials and to create of stable microwave standards and to use in the precision metering equipment. Thus, the measurement and research of spectral characteristics of resonance oscillations have important value. The rigorous solution of a set of Maxwell equations satisfying the radiations on infinity and the boundary conditions of electromagnetic field components was only determined for some limited dielectric structures. The numerical analysis of spectral characteristics made for the lowest types of resonance oscillations in an isotropic dielectric sphere [1]. The capability of excitation independent TE ( $E_r = 0$ ) and TM ( $H_r = 0$ ) wave modes was shown. In each of them there is a frequent degeneration at which the same frequency has  $2n+1$  modes with various dependence from the azimuth coordinate  $\varphi$ . Here  $n$  parameter is polar index determining number of field variations on the polar coordinate  $\theta$ . The influence of weak azimuthal non-uniformity leads to removing the degeneration and to arising independent EH and HE oscillations for which all six field components are not zero.

The resonance oscillations independent from azimuthal coordinate ( $\partial/\partial\varphi \equiv 0$ ) were studied in open spheroidal structures [2-4]. The mention above effects does not arise in these approximations.

### THEORETICAL CONSIDERATION

We consider an open spheroid made from homogeneous isotropic dielectric with permittivity  $\epsilon_d$  and permeability  $\mu_d$ . The prolate spheroidal coordinate system ( $\xi, \eta, \varphi$ ) obtained by rotation of plane elliptical coordinate system around of a large axis (Figure 1) is used for the solution of the spectral task. In this system  $\xi \in [0, 2\pi)$ ;  $\eta \in [-1, 1]$  and  $\varphi \in [0, 2\pi]$ , and the metrical Lamé's coefficients are equal

$$h_\xi = \tau \sqrt{\frac{\xi^2 - \eta^2}{\xi^2 - 1}}; \quad h_\eta = \tau \sqrt{\frac{\xi^2 - \eta^2}{1 - \eta^2}}; \quad h_\varphi = \tau \sqrt{(\xi^2 - 1)(1 - \eta^2)}, \text{ where } \tau \text{ is the distance}$$

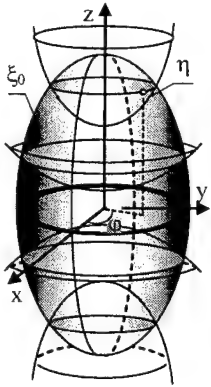


Figure 1.

between focal points. The surfaces  $\xi = \text{const}$  are prolate spheroids in spheroidal coordinate system. The value  $\eta = 0$  corresponds to crossing of the spheroid with a plane  $z = 0$ , and  $\eta = \pm 1$  correspond to spheroid poles placed on the  $z$  axis [5]. At the coordinate  $\xi = \xi_0$  it is limited by the medium with permittivity  $\epsilon_b$  and permeability  $\mu_b$ .

For fields proportionate to  $\exp i(m\varphi - \omega_p t)$ , where  $\omega_p$  is the frequency of  $p$ -th mode oscillation and  $m$  is azimuthal index, the study of the set of Maxwell equations is reduced to the solution of two coupling differential equations about  $E_\xi$  and  $H_\xi$  components

$$i\epsilon_j k \tau \Lambda_j h_\xi E_{j\xi} = -\frac{\partial}{\partial \varphi} L_j h_\xi H_{j\xi}; \quad i\mu_j k \tau \Lambda_j h_\xi H_{j\xi} = \frac{\partial}{\partial \varphi} L_j h_\xi E_{j\xi}. \quad (1)$$

Here  $k = \omega_p / c$ ,  $c$  is the light velocity and subscript  $j$  takes the value  $d$  inside or  $b$  outside of spheroid. The  $\Lambda_j$  and  $L_j$  operators are equal

$$\Lambda_j = \frac{\partial}{\partial \eta} g_{j\varphi}^{-1} \frac{\partial}{\partial \eta} + g_{j\eta}^{-1} \frac{\partial^2}{\partial \varphi^2} + \xi^2 - 1; \quad L_j = \frac{\partial}{\partial \eta} g_{j\varphi}^{-1} \frac{1}{1-\eta^2} \frac{\partial}{\partial \xi} - g_{j\eta}^{-1} (1-\eta^2) \frac{\partial}{\partial \xi} \frac{\xi^2 - 1}{\xi^2 - \eta^2} \frac{\partial}{\partial \eta},$$

where  $g_{j\eta}^{-1}$  and  $g_{j\varphi}^{-1}$  operators are reverse for operators of

$$g_{j\eta} = (1-\eta^2) \left[ a_j + \frac{\partial}{\partial \xi} \frac{\xi^2 - 1}{\xi^2 - \eta^2} \frac{\partial}{\partial \xi} \right]; \quad g_{j\varphi} = \frac{1}{(1-\eta^2)} \left[ a_j \frac{\xi^2 - \eta^2}{\xi^2 - 1} + \frac{\partial^2}{\partial \xi^2} \right].$$

Let us consider an isotropic dielectric sphere with a small ellipticity along the  $z$  axis. The transformation to spherical coordinates  $(r, \theta, \varphi)$  in (1) is carried out in the assumption  $\varphi = \varphi$ ,  $\eta = \cos \theta$  and tendency  $\tau \rightarrow 0$ ,  $\xi \rightarrow \infty$  so that the multiplication  $\tau \xi \rightarrow r$  remained final [5]. We introduce potential functions  $U_j^S$  by the expression of  $g_{j0} U_j^S = h_\xi S_{j\xi}$ , where  $g_{j0} = a_j + \partial^2 / \partial \xi^2$ ,  $a_j = \epsilon_j \mu_j k^2 \tau^2$  and  $S$  takes the value  $E$  or  $H$ . For large  $\xi$  values and  $\eta = \cos \theta$  we obtain

$$g_{j\eta} \approx \sin^2 \theta \left[ g_{j0} - \frac{\sin^2 \theta}{\xi^2} \frac{\partial^2}{\partial \xi^2} \right] + O(\xi^{-3}), \quad g_{j\varphi} \approx \frac{g_{j0}}{\sin^2 \theta} + \frac{a_j}{\xi^2} + O(\xi^{-3}).$$

The system (1) becomes

$$\begin{aligned} (\Lambda_{j0} - \Lambda_{j1}) U_j^E &\approx -g_{j0}^{-1} \frac{2i\mu_j k \tau}{\xi^2} \cos \theta \frac{\partial^2 U_j^H}{\partial \varphi \partial \xi}; \\ (\Lambda_{j0} - \Lambda_{j1}) U_j^H &\approx g_{j0}^{-1} \frac{2i\epsilon_j k \tau}{\xi^2} \cos \theta \frac{\partial^2 U_j^E}{\partial \varphi \partial \xi}, \end{aligned} \quad (2)$$

where  $\Lambda_{j0} = \Delta_\perp + \xi^2 g_{j0}$ ,  $\Lambda_{j1} = g_{0j} + g_{j0}^{-1} \frac{1}{\xi^2} \left( \frac{a_j}{\sin \theta} \frac{\partial}{\partial \theta} \sin^3 \theta \frac{\partial}{\partial \theta} - \frac{\partial^4}{\partial \varphi^2 \partial \xi^2} \right)$ ,

$\Delta_\perp = \frac{1}{\sin \theta} \frac{\partial}{\partial \theta} \sin \theta \frac{\partial}{\partial \theta} + \frac{1}{\sin^2 \theta} \frac{\partial^2}{\partial \varphi^2}$  and  $g_{j0}^{-1}$  operator is reverse for operator of  $g_{j0}$ .

At neglect by values of the order  $\xi^{-2}$  the system (2) breaks up to two independent subsystems describing TE and TM types of resonance oscillations in the spheroid. The resonance frequencies of them are accordingly determined by solving the equations

$$\sqrt{\varepsilon_d / \mu_d} \frac{j'_{v(n)}(x_d)}{j_{v(n)}(x_d)} = \sqrt{\varepsilon_b / \mu_b} \frac{h'_{v(n)}(x_b)}{h_{v(n)}(x_b)} \text{ и } \sqrt{\mu_d / \varepsilon_d} \frac{j'_{v(n)}(x_d)}{j_{v(n)}(x_d)} = \sqrt{\mu_b / \varepsilon_b} \frac{h'_{v(n)}(x_b)}{h_{v(n)}(x_b)}, \quad (3)$$

where  $x_j = \sqrt{\varepsilon_j \mu_j} k \tau \xi_0$ ;  $j_{v(n)}(x) = \sqrt{\pi x / 2} J_{n+1/2}(x)$ ;  $h_{v(n)}^{(1)}(x) = \sqrt{\pi x / 2} H_{n+1/2}^{(1)}(x)$ ,  $v(n) = n + 1/2$ ,  $J_{v(n)}(x)$  and  $H_{v(n)}^{(1)}(x)$  are the Bessel and first-kind Hankel cylindrical functions of the  $n$ -th order.

In the equations (3) the azimuthal index  $m$  is absent. Hence each resonance oscillation mode is  $2n+1$ -fold degenerate.

The taking into consideration of the addends proportionate to  $\xi^{-2}$  in (2) allows to study the influence of ellipsoidal non-uniformity upon the parameters of resonance oscillations. The TM oscillations are transformed in the HE and TE are transformed in the EH oscillations for which all six field components are already not zero. In this case the solutions of system (2) are proportionate to functions of  $j_{v(n,d)}(\sqrt{a_d} \xi)$  inside and  $h_{v(n,b)}^{(1)}(\sqrt{a_b} \xi)$  outside of the spheroid, where  $v(n, j) = [(n+1/2)^2 + (m^2 + \gamma_n) a_j / n(n+1)]^{1/2}$ ,  $\gamma_n = f_{n-1} f_{n+1} [2n^2(n+1)^2 - m^2(2n^2 + 2n + 3)]$  and  $f_n = 1/(2n+1)$ .

The resonance frequencies of oscillations are determined by solving the equations

$$\sqrt{\varepsilon_d / \mu_d} \frac{j'_{v(n,d)}(x_d)}{j_{v(n,d)}(x_d)} = \sqrt{\varepsilon_b / \mu_b} \frac{h'_{v(n,b)}(x_b)}{h_{v(n,b)}(x_b)}$$

for EH and

$$\sqrt{\mu_d / \varepsilon_d} \frac{j'_{v(n,d)}(x_d)}{j_{v(n,d)}(x_d)} = \sqrt{\mu_b / \varepsilon_b} \frac{h'_{v(n,b)}(x_b)}{h_{v(n,b)}(x_b)}$$

for HE types.

The dependence of  $v(n, j)$  parameter from the azimuthal index  $m$  arising under influence of the ellipsoidal non-uniformity of dielectric sphere removes the frequency degeneration for resonance oscillations.

## REFERENCES

- [1] Gastine N., Courtois L., Dormann J.L. // IEEE Trans. MTT, 1967, Vol. 15, No. 12, pp. 694-700.
- [2] Wait J.R. // Radio Science 1966, Vol. 1, No. 4, pp. 475-513.
- [3] Markov G.I., Tereshchenko D.Ye. // Problemi difraktsii i rasprostraneniya radiovoln (Problems of diffraction and radio-propagation). L.: -Izd. LGU, 1972, No. 11, pp. 77-94. (in Russian)
- [4] Starkov M.A. // Radiotekhnika i elektronika (Radio engineering and electronics), 1983, Vol. 28, No. 5, pp. 864-870. (in Russian)
- [5] Komarov I.V., Ponamarev L.I., Slavyanov S.Yu. Spheroidal and Coulomb spheroidal functions. / M.: Nauka, 1976, 318 p. (in Russian)

## ON PERTURBATION OF THE SPECTRUM OF PLANAR DIELECTRIC WAVEGUIDE BY REFRACTION INDEX PROFILE

Linnik V.V., Pleshchinskii N.B.  
Kazan State University  
P.O.Box 234 Kazan, 420111, Russia  
e-mai: pnb@ksu.ru, pnb@kzn.ru

### ABSTRACTS

The problem of calculating the eigenwaves of planar dielectric waveguide with arbitrary refraction index profile is considered. The iterative process based on the exact solutions of this problem in the case of piecewise constant profile is investigated. The abstract perturbation theory for operator equation with spectral parameter is extended.

### INTRODUCTION

Let the layers of planar dielectric waveguide be separated by the planes  $z = 0$  and  $z = h$ . The potential function  $F(x, z) = \exp(ik_0 \tilde{n}x) f(x)$  of the TE-waves is a solution of the Helmholtz equation and satisfies the conjugation conditions for  $z = 0$  and  $z = h$ . The function  $f(x)$  is a solution of the boundary value problem

$$f''(z) + k_0^2 [n_f^2(z) - \tilde{n}^2] f(z) = 0, \quad 0 < z < h, \quad (1)$$

$$f'(0) - \beta_s f(0) = 0, \quad f'(h) + \beta_a f(h) = 0, \quad (2)$$

here  $\tilde{n}$  is the unknown spectral parameter (longitudinal propagation constant),

$$\beta_a = k_0 \sqrt{\tilde{n}^2 - n_a^2}, \quad \beta_s = k_0 \sqrt{\tilde{n}^2 - n_s^2},$$

$n_s, n_a, n_f(z)$  are the refraction indexes of the substrate, of the external medium and of the waveguided layer respectively. The conditions (2) are to be replaced by other conditions in the case of TM-waves.

If  $n_f(z) = \text{const}$  then the exact solutions of the problem (1), (2) can be written down in the analytical form. We discuss the possibility of using these solutions for approximate calculating of the solutions of problem (1), (2) in the general case.

### ITERATIVE PROCESS

In [1] an iterative method is proposed to solve the following spectral problem

$$f''(z) + C(z, \lambda, p) f(z) = 0, \quad f'(\alpha) + A(\lambda) f(\alpha) = 0, \quad f'(\beta) + B(\lambda) f(\beta) = 0. \quad (3)$$

Let the solutions of the problem (3) be well-known for  $p = 0$ , and be unknown for  $p = 1$ . We introduce the increasing set of values  $p^{(0)} = 0, p^{(1)}, \dots, p^{(n)=1} = 1$ . Let the increments  $\delta\lambda, \delta f(z)$  correspond to the increment  $\delta p$ . The linearized equations for the calculating of increments have the form

$$\delta f''(z) + C(z, \lambda, p) \delta f(z) = - \left[ \frac{\partial C}{\partial \lambda} \delta \lambda + \frac{\partial C}{\partial p} \delta p \right] [f(z) + \delta f(z)], \quad (4)$$

$$\begin{aligned} \delta f'(\alpha) + A(\lambda) \delta f(\alpha) &= - \frac{\partial A}{\partial \lambda} \delta \lambda [f(\alpha) + \delta f(\alpha)], \\ \delta f'(\beta) + B(\lambda) \delta f(\beta) &= - \frac{\partial B}{\partial \lambda} \delta \lambda [f(\beta) + \delta f(\beta)], \end{aligned} \quad (5)$$

$$\begin{aligned} \delta \lambda \left\{ \int_{\alpha}^{\beta} f(z) \frac{\partial C}{\partial \lambda} [f(z) + \delta f(z)] dz - f(\beta) \frac{\partial B}{\partial \lambda} [f(\beta) + \delta f(\beta)] + f(\alpha) \frac{\partial A}{\partial \lambda} [f(\alpha) + \delta f(\alpha)] \right\} = \\ = - \delta p \int_{\alpha}^{\beta} f(z) \frac{\partial C}{\partial p} [f(z) + \delta f(z)] dz. \end{aligned} \quad (6)$$

### ABSTRACT APPROXIMATE SCHEME

To substantiate the numerical method we consider more general abstract spectral problem.

Let  $A$  be a linear operator acting from the space  $X$  into  $X$ ,  $\bar{A}$  be a linear operator acting from the space  $\bar{X}$  into  $\bar{X}$ , the space  $\bar{X}$  approximate the space  $X$  and  $\lambda$  be a complex parameter. The correspondence between the spaces  $X$  and  $\bar{X}$  is established by the interpolation operator  $T : X \rightarrow \bar{X}$  and the approximation operator  $S : \bar{X} \rightarrow X$ , here  $ST = I$  [2]. Let the exact spectral problem

$$Ax - \lambda x = 0, \quad x \in X \quad (7)$$

be replaced by approximate spectral problem

$$\bar{A}\bar{x} - \lambda\bar{x} = 0, \quad \bar{x} \in \bar{X}. \quad (8)$$

We introduce new spectral problem

$$\tilde{A}x - \lambda x = 0, \quad x \in X, \quad \tilde{A} = S\bar{A}T. \quad (9)$$

If  $\lambda_0, \bar{x}_0$  are the eigenvalue and the eigenelement for the problem (8), then  $\lambda_0, \tilde{x}_0 = Sx_0$  are the eigenpair for the problem (9). Therefore the eigenpair for the problem (8) can be obtained in the form

$$x = \tilde{x}_0 + \Delta x, \quad \lambda = \lambda_0 + \Delta \lambda$$

with auxiliary normalization condition.

The equation

$$(\tilde{A} - \lambda_0 I) \Delta x = \Delta \lambda (\tilde{x}_0 + \Delta x) - \Delta A (\tilde{x}_0 + \Delta x), \quad \Delta x \in X \mid (x, \tilde{x}_0) = 0 \quad (10)$$

is an abstract analogous of the problem (4), (5),

$$\Delta\lambda = (\Delta A(\tilde{x}_0 + \Delta x), \tilde{x}_0) . \quad (11)$$

The operator  $\Delta A = A - \tilde{A}$  defines the closeness between the exact and approximate operators [2].

### CONVERGENCE CONDITION

It follows from (10), (11) that

$$\Delta x = TP(\Delta x), \quad (12)$$

here  $T$  is a linear operator (inverse operator for  $\tilde{A} - \lambda_0 I$ ) and  $P$  is a nonlinear operator. It is shown that the equation (12) can be solved by iterative process if the condition

$$\|TP'(\Delta x)\| \leq q < 1 \quad \text{or} \quad 3\|T\|\|\Delta A\| \leq q < 1$$

is fulfilled.

Let  $A(\lambda)$  be a linear operator from the space  $X$  into  $X$  and  $\lambda$  be a complex parameter. Let the exact spectral problem

$$A(\lambda)x - \lambda x = 0, \quad x \in X \quad (13)$$

be approximated by problem

$$\tilde{A}(\lambda)\bar{x} - \lambda\bar{x} = 0, \quad \bar{x} \in \bar{X}, \quad (14)$$

here  $\tilde{A}(\lambda)$  is a linear operator from  $\tilde{X}$  into  $\tilde{X}$ . In this case the equation (12) is replaced by set of equations

$$\Delta\lambda = \left( [A(\lambda + \Delta\lambda) - \tilde{A}(\lambda)](\tilde{x} + \Delta x), \tilde{x} \right), \quad (15)$$

$$\Delta x = [\tilde{A}(\lambda) - \lambda I]^{-1} [\Delta\lambda I - A(\lambda + \Delta\lambda) + \tilde{A}(\lambda)](\tilde{x} + \Delta x) .$$

The sufficient condition for the convergence of the iterative process for the system (15) is obtained.

### REFERENCES

- [1] Kosolapova A.V., Pleshchinskii N.B. On perturbation of eigen waves of planar dielectric waveguide by refraction index profile // Dep. VINITI 05.12.1995. – 10 pp. (in Russian)
- [2] Pleshchinskii N.B. On the abstract theory of approximate methods for solving linear operator equations // Izv. Vuzov. Matematika. – 2000. – No. 3. – P.39-47. (in Russian)

# NUMERICAL INVESTIGATION OF EIGENOSCILLATIONS NEAR HONEYCOMB IN THE CIRCULAR CHANNEL

A.I. Makarov

Lavrentyev Institute of Hydrodynamics,  
Prospect Lavrentyeva, 15, Russia, 630090  
E-mail: Makarov@hydro.nsc.ru

## ABSTRACT

Eigenvalue problem of  $(-\Delta)$  operator with the finite-energy and Neumann conditions are investigated. The classification of possible eigenoscillations is carry out by the theory of group presentation. These modes of eigenoscillations are proved to exist and their quantity is found. Eigenvalues are studied numerically.

## STATEMENT OF PROBLEM

A system of two equal strips forming a cross in the infinite channel of circular cross-section is considered. The line of strips' intersection divides it to half-and-half. All notations are shown in figure 1. Eigenoscillations with harmonic time dependence is assumed.

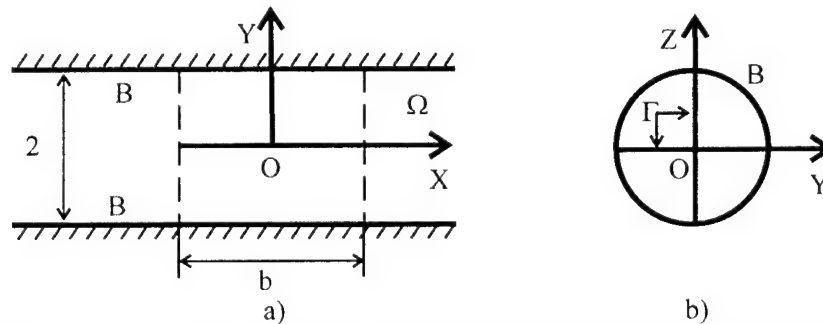


Fig. 1. Geometrical parameters of system of two strips forming a cross: a) top view; b) cross-section.

Mathematical statement of problem for potential function  $u(x,y,z)$  is:

$$\left\{ \begin{array}{ll} \Delta u + \lambda^2 u = 0 & \text{in } \Omega / B / \Gamma \quad - \text{ wave equation} \\ \frac{\partial u}{\partial \vec{n}} = 0 & \text{on } B \cup \Gamma \quad - \text{ Neumann condition} \\ \int_{\Omega_0} (u^2 + (\nabla u)^2) d\Omega_0 < \infty \quad \Omega_0 \subset \Omega & - \text{ finite-energy condition} \end{array} \right. \quad (1)$$

## CLASSIFICATION AND EXISTENCE OF EIGENOSCILLATIONS

The self-adjoint extension of  $(-\Delta)$  has positive continuous spectrum. The main difficulties is that discrete spectrum of problem (1) is imbedded in continuous spectrum of operator  $(-\Delta)$ .



Symmetry group of the cross in the channel contains subgroups  $D_4$ ,  $C_4$  (rotation on  $\pi/2$  in the plane parallel to OYZ) and  $D_1^{OYZ}$  (mirror symmetry with respect to plane OYZ) [1]. Subgroup  $D_1^{OYZ}$  means that the admissible solution space can be decomposed into solutions, which are odd and even at variable  $x$ .

Generating elements of subgroup  $D_4$  are  $r$  and  $s$ , where  $r$  is rotation at  $\pi/4$  with respect to axis  $OX$  and  $s$  is mirror symmetry with respect to plane  $OXZ$ . Irreducible representations of subgroup  $D_4$  are shown in the table 1.

	$\psi_1$	$\psi_2$	$\psi_3$	$\psi_4$
$r^k$	1	1	$(-1)^k$	$(-1)^k$
$s r^k$	1	-1	$(-1)^k$	$(-1)^{k+1}$

Table 1. Irreducible representation of  $D_4$ , where  $\psi_i$ ,  $i = 1, \dots, 4$  are their characters.

Irreducible representations  $\tau_k$  of group  $C_4$  are  $\tau_k(C_4^m) = \exp(i\pi km/2)$ , where  $k, m = 0, 1, 2, 3$ , so the admissible solution space can be decomposed into solutions, which have next property:  $C_4 < u(x, y, z) > = \exp(i\pi j/2) \cdot u(x, y, z)$ , where  $j = 0, \dots, 3$ . Oscillations with  $j=3$  and  $j=1$  are identical, they are equal to a wave moving clockwise and anticlockwise respectively.

Note that even eigenoscillations with respect to variables  $y, z$  can't exist [1]. So there are only 3 independent mode of oscillations (without consideration of evenness/oddness at  $x$ ): 1) mode corresponds to  $\psi_2$  (it will be called  $\alpha$ -mode); 2) traveling wave at  $j=1$  ( $\beta$ -mode); 3) mode corresponds to  $\psi_4$  ( $\gamma$ -mode).

Let  $\mu_{n,k}$  denote  $k$ -th root of equation  $(J_n(x))' = 0$ ,  $J_n(\mu_{n,k}) \neq 0$ ,  $k \in \mathbb{N}$ . Let  $\sigma_0^2$  be the point of the continuous spectrum of  $(-\Delta)$ . Value  $\sigma_0^2$  for  $\alpha$ ,  $\beta$ ,  $\gamma$ -modes is equal to  $\mu_{4,1}^2, \mu_{1,1}^2, \mu_{2,1}^2$  respectively. Now it is possible to investigate discrete spectrum of problem (1) located below  $\sigma_0^2$ .

**Theorem 1.**  $\alpha$ ,  $\beta$ ,  $\gamma$ -modes of the eigenoscillations always exist independent of geometrical parameters of the cross and the channel.

**Lemma 1.** The  $\alpha$ -mode eigenfrequencies belong to interval  $(\mu_{2,1}, \mu_{4,1})$ .

**Lemma 2.** Quantity  $K$  of eigenvalues located below the cut-off of problem (1) satisfies to next inequalities for  $\alpha$ -mode:  $\max(1, b\sqrt{\mu_{4,1}^2 - \mu_{2,1}^2}/\pi - 1) \leq K < b\sqrt{\mu_{4,1}^2 - \mu_{2,1}^2}/\pi + 1$ ; for  $\beta$ -mode:  $\max(1, b\mu_{1,1}/\pi - 1) \leq K < b\mu_{1,1}/\pi + 1$ ; for  $\gamma$ -mode:  $\max(1, b\mu_{2,1}/\pi - 1) \leq K < b\mu_{2,1}/\pi + 1$ .

**Theorem 2.** Finite-energy condition in any vicinity of plate edge is equivalent to next conditions (in cylindrical coordinate system chosen along a plate edge):

- 1) at the middle of the plate edge  $u(b/2 + x, \rho, \varphi) \approx f(x) + \rho \cos(\varphi) g(x)$ ;
  - 2) at other points of plate edge  $u(b/2 + x, \rho, \varphi) \approx f(x) + \sqrt{\rho} \cos(\varphi/2) g(x)$ ,
- at  $\rho \rightarrow 0$ ,  $f(x), g(x) \in W_2^1(\mathbb{R})$ .

**Lemma 3.**  $\alpha$ - and  $\gamma$ -modes have finite energy in any vicinity of plates edges. Finite-energy condition in any vicinity of plates edges for  $\beta$ -mode is equivalent to next conditions ( $\forall m_1 \in \mathbb{N}$ ):

$$\sum_{n,m=1}^{+\infty} b_{n,m} (-1)^n e^{-b\gamma_{1,m}/2} \int_0^1 r J_{2n-1,m}(\mu_{2n-1,m} r) J_{1,m_1}(\mu_{1,m_1} r) dr = 0.$$

## NUMERICAL INVESTIGATION

The linear infinite system (2) for coefficient of solution's expansion in domain  $\Omega \cap \{x \geq 0, 5b\}$  is obtained by sewing method

$$\sum_{n,m=1}^{+\infty} b_{n,m} \cdot \left( (\gamma + \gamma_1) e^{b\gamma_{1,m}/2} + (-1)^l (\gamma - \gamma_1) e^{-b\gamma_{1,m}/2} \right) \frac{f(n)}{f^2(n) - g^2(n_1)} \times$$

$$\times \int_0^1 r J_{f(n)}(\mu_{f(n),m} r) J_{g(n_1)}(\mu_{g(n_1),m_1} r) dr = 0 \quad \forall m_1, n_1 \in \mathbb{N}. \quad (2)$$

where  $\gamma(n, m) = \sqrt{\pi^2(n^2 + m^2) - \lambda^2}$ ,  $\gamma = \gamma(f(n), m)$ ,  $\gamma_1 = \gamma(g(n_1), m_1)$ ; for  $\alpha$ -mode:  $f(n) = 4n, g(n_1) = 4n_1 - 2$ ; for  $\beta$ -mode:  $f(n) = 2n - 1, g(n_1) = 2n_1 - 2$ ; for  $\gamma$ -mode:  $f(n) = 4n - 2, g(n_1) = 4n_1 - 4$ ; and  $l$  is even (odd) for even (odd) oscillations by  $x$ .

The system (2) was reduced to square and triangular partial sums, which were studied numerically. There are good coincidence between them. Figure 2 shows the variation of the eigenvalue  $\lambda$  with the cross-length  $b$  received by the first method.

I am grateful to Dr. S.V. Sukhinin, I.S. Chikichev for a number of useful notes.

This work was supported by the Russian Foundation of Basic Research, Grant 02-01-06264.

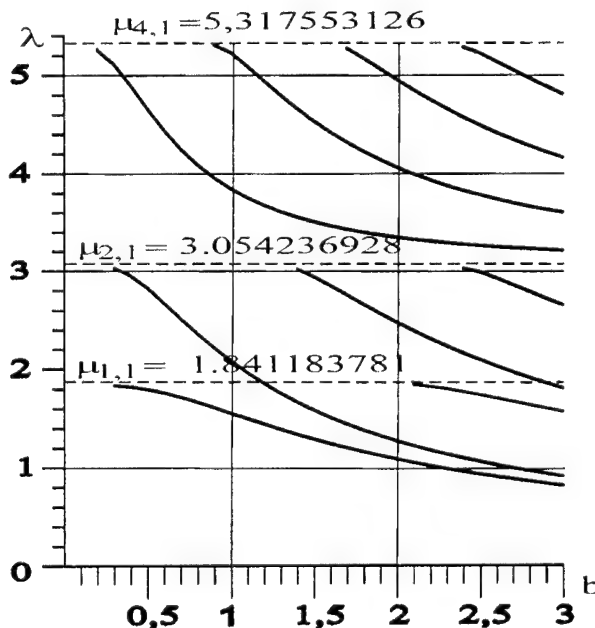


Fig. 2. Variation of the eigenvalue  $\lambda$  with the cross-length  $b$ .

## RESULTS

1. It is proved that eigenoscillations always exist.

2. It is founded the quantity of mode of oscillations.

3. The diagrams eigenvalues against length of cross are obtained.

## REFERENCES

- [1] A.I. Makarov. Eolian tones of the unit part of the honeycomb. //Journal of Applied Mechanics and Technical Physics, Vol. 43, No. 5, 2002 (in Russian).

## EXISTENCE THEOREMS FOR EIGENOSCILLATIONS IN 3D RECTANGULAR WAVEGUIDES

I.B. Yumov

East-Siberian State Technological University, Dep. of Math.

40-a Klyuchevskaya st., Ulan-Ude, 670013 Russia

E-mail: igyumov@mail.ru

### ABSTRACT

The paper deals with the problem of eigenoscillations near the obstacle with the arbitrary sufficiently smooth shape of boundary immersed in three-dimensional waveguide of rectangular cross-section. Assumed that the guide and the obstacle are rigid. For a wide range of the obstacle geometry the existence of eigenwaves has been proved and their frequencies are embedded in the continuous spectrum.

### INTRODUCTION

The investigation of eigenoscillations in unbounded waveguide regions is very important in many physics fields. First of all, the interest to the given problem is stipulated by the aeroacoustic resonance phenomenon the investigation of which is actual, e. g. when turbomachines designing (gas, vapour and hydraulic turbines, pumps, compressors), pipelines etc. (some experimental works review is in the paper[2]). A lot of papers (we'll mention only some of them [1,4-6,8]) are devoted to the investigation of eigenwaves in guide regions in two-dimensional case. The eigenwaves existence in three-dimensional guide regions has been investigated less completely. Let's note the paper [3] where the existence of the eigenoscillations being localized near sphere of the sufficiently small radius being situated in the center of the waveguide with the constant circular cross-section has been proved and also let's note the papers [7,9], where the cases of the thin-shelled obstacles in waveguides have been considered.

In the given paper by using the variational principle the sufficient conditions of the eigenwaves existence in three-dimensional waveguide with rectangular cross-section, where the obstacle with sufficiently arbitrary geometry possessing some symmetry conditions, have been obtained.

### STATEMENT OF THE PROBLEM AND THE MAIN RESULTS

The domain  $\Omega_0$  is being considered:

$$\Omega_0 = \{(x, y, z) \in \mathbb{R}^3: x \in (-d_1, d_1), y \in (-d_2, d_2), z \in \mathbb{R}\}, d_i > 0 (i=1, 2).$$

The bounded obstacle  $B$  is placed in it. This obstacle may be disconnected. According to the obstacle type the following cases will be considered:

- A.  $B$  is a compact set being bounded by the piecewise smooth surfaces and it is such one that  $\mu_3(B) > 0$ . (Here and further  $\mu_k$  means  $k$ -dimensional measure). It is supposed that  $B$  is symmetrical with respect to the plane  $y=0$ .
- B.  $B$  is an infinitely thin plate with sufficiently smooth boundary, such one that  $0 < \mu_2(B) < \infty$ . It is supposed that  $B$  is situated in the plane  $y=0$ .
- C.  $B$  is a compact set being bounded by the piecewise smooth surfaces and it is such one that  $\mu_3(B) > 0$ . It is supposed, that  $B$  is symmetrical with respect to the planes  $x=0$  and  $y=0$ .

**D.**  $B$  is an infinitely thin plate with sufficiently smooth boundary which is situated in the plane  $y=0$  and  $0 < \mu_2(B) < \infty$ . It is supposed, that  $OZ$  axis is a line of symmetry for the obstacle  $B$ .

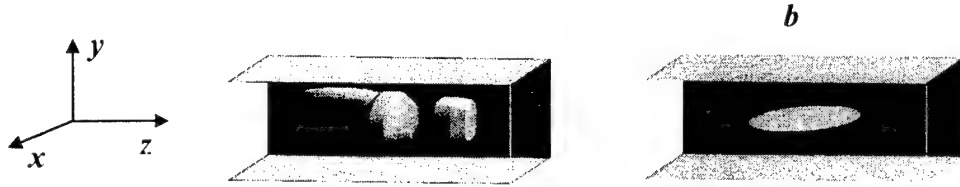


**Fig. 1.**

Waveguide regions geometry is represented in figure 1.

We seek the non-trivial solution  $u(x,y,z)$  of the boundary value problem for the equation:

$$\Delta u + \lambda u = 0 \quad (\lambda \geq 0) \quad \text{in } \Omega = \Omega_0 \setminus B, \quad (1)$$

satisfying to the Neumann boundary condition on  $\partial\Omega$ :

$$\frac{\partial u}{\partial \vec{n}} = 0 \quad (2)$$

and to the condition of finite energy:

$$E(u) \equiv \iiint_{\Omega} (|u|^2 + |\nabla u|^2) d\Omega < \infty. \quad (3)$$

Here,  $\vec{n}$  is a vector of the external normal to  $\partial\Omega$ .

Further, we'll call the problem (1)–(3) as the problem  $N$ . Besides, we are going to consider the problem  $N^{up}$  – the solution finding  $u^{up}(x,y,z)$  of the boundary value problem (1)–(3) which is odd in  $y$  for **A** and **B** cases, and the problem  $N^a$  – the solution finding  $u^a(x,y,z)$  of the boundary value problem (1)–(3) which is odd in  $x$  and  $y$  for **C** and **D** cases.

The parameter value  $\lambda$  for which the non-trivial solution of the problem  $N$  (of the problems  $N^{up}$  and  $N^a$  correspondingly) exists is called the eigenvalue of the problem  $N$  (of the problems  $N^{up}$  and  $N^a$  correspondingly). In addition, the self non-trivial solution is called the eigenfunction of the corresponding problem.

It is known, that the Neumann Laplacian possesses a continuous spectrum  $[0, +\infty)$  for the domain  $\Omega$  and the eigenvalues of the problem  $N$  (if they exist) turn out to be embedded in the continuous spectrum. It is obvious that the eigenvalues of the problems  $N^{up}$  and  $N^a$  are the eigenvalues of the problem  $N$ .

Let us introduce the notations:

$$\begin{aligned} \Omega_0^a &= \{ (x,y,z) \in \Omega_0 : x > 0, y > 0 \}, \quad B^a = B \cap \overline{\Omega_0^a}, \\ \Omega_0^{up} &= \{ (x,y,z) \in \Omega_0 : y > 0 \}, \quad B^{up} = B \cap \overline{\Omega_0^{up}}, \\ \Omega^a &= \Omega \cap \Omega_0^a, \quad \Omega^{up} = \Omega \cap \Omega_0^{up}. \end{aligned}$$

The following lemmas are valid.

**Lemma 1.** The continuous spectrum of the problem  $N^{up}$  ( $N^a$ ) is the semi-axis  $[\Lambda_{up}^2, +\infty)$  ( $[\Lambda_a^2, +\infty)$  correspondingly), where  $\Lambda_{up}^2 = \pi^2/4d_2^2$ ,  $\Lambda_a^2 = \pi^2/4d_1^2 + \pi^2/4d_2^2$ .

**Lemma 2.** Let

$$\lambda_0^{up,a} = \inf_{\substack{\psi \in H_0^1(\Omega^{up,a}) \\ \psi \neq 0}} \frac{\iiint_{\Omega^{up,a}} |\nabla \psi|^2 d\Omega}{\iiint_{\Omega^{up,a}} |\psi|^2 d\Omega}.$$

Then  $\lambda_0^{up} \leq \Lambda_{up}^2$  ( $\lambda_0^a \leq \Lambda_a^2$  correspondingly). More over, if  $\lambda_0^{up} < \Lambda_{up}^2$  ( $\lambda_0^a < \Lambda_a^2$  correspondingly), then  $\lambda_0^{up}$  ( $\lambda_0^a$ ) is the lowest eigenvalue of the problem  $N^{up}$  ( $N^a$ ), and if  $\lambda_0^{up} = \Lambda_{up}^2$  ( $\lambda_0^a = \Lambda_a^2$ ), then the eigenvalues of the problem  $N^{up}$  ( $N^a$ ) do not exist in the interval  $(-\infty, \Lambda_{up}^2)$  ( $(-\infty, \Lambda_a^2)$  correspondingly).

Using these lemmas, the existence of eigen waves has been proved.

**Theorem.** Eigenfunctions of the problem  $N^{up}$  exist:

in case **A**, if the following inequality holds:

$$\iiint_{B^{up}} \cos\left(\frac{\pi y}{d_2}\right) d\Omega > 0; \quad (4)$$

in case **B** – exist always.

And the lowest eigenvalue  $\lambda_0^{up}$  belongs to the interval  $(0, \Lambda_{up}^2)$ .

Eigenfunctions of the problem  $N^a$  exist:

in case **C**, if the following inequality holds:

$$\iiint_{B^a} \left[ \frac{1}{d_1^2} \cos\left(\frac{\pi x}{d_1}\right) + \frac{1}{d_2^2} \cos\left(\frac{\pi y}{d_2}\right) - \left(\frac{1}{d_1^2} + \frac{1}{d_2^2}\right) \cos\left(\frac{\pi x}{d_1}\right) \cos\left(\frac{\pi y}{d_2}\right) \right] d\Omega > 0; \quad (5)$$

in case **D** – exist always.

And the lowest eigenvalue  $\lambda_0^a$  belongs to the interval  $(0, \Lambda_a^2)$ .

**Corollary.** Eigenfunctions of the problem  $N^{up}$  exist in case **A**, if the obstacle  $B$  is included in the set  $\{(x, y, z) \in \Omega_0: |y| < d_2/2\}$ . And the lowest eigenvalue  $\lambda_0^{up}$  belongs to the interval  $(0, \Lambda_{up}^2)$ .

Eigenfunctions of the problem  $N^a$  exist in case **C**, if the obstacle  $B$  is included in the set  $\{(x, y, z) \in \Omega_0: |y| < d_2/2, |x| < d_1/2\}$ . And the lowest eigenvalue  $\lambda_0^a$  belongs to the interval  $(0, \Lambda_a^2)$ .

## REFERENCES

- [1] Popov A.N. // *Zhurnak Tehnich. Fiziki*, 1986, v. 56, № 10, pp.1916-1922 (in Russian).
- [2] Parker R., Stoneman S.A. // *Proc. Inst. Mech. Engr.* 1989, v.203, pp.9-19.
- [3] Ursell F. // *Proc. R. Soc. Lond.* 1991. A 435, 575-589.
- [4] Callan M., Linton C.M., Evans D.V. // *J. Fluid Mech.* 1991. v.229, pp.51-64.
- [5] Evans D.V., Linton C.M. // *Quart. J. Mech. Appl. Math.* 1993, v.46, pp.255-274.
- [6] Evans D.V., Levitin M., Vassiliev D. // *J. Fluid Mech.* 1994, v.261, pp.21-31.
- [7] S. V. Sukhinin, Dynamics of Continuous Medium: *Sb. Nauchnih Trudov/RAN Sib. Otdelen. Inst. Gidridinamiki*, 1995, v.110., pp.139-152.
- [8] S. V. Sukhinin // *Appl. Mach. and Techn. Physics*, 1998, № 2, pp.78-90.
- [9] S. V. Sukhinin // *Appl. Mach. and Techn. Physics*, 1999, № 4, pp.133-142.

# SOME ASPECTS OF THE SLOW WAVES IN THE CIRCULAR WAVEGUIDE WITH AZIMUTHALLY MAGNETIZED FERRITE ROD

Georgi Nikolov Georgiev<sup>(1)</sup> and Mariana Nikolova Georgieva-Grosse<sup>(2)</sup>

<sup>(1)</sup>Faculty of Mathematics and Informatics  
University of Veliko Tirmovo "St. St. Cyril and Methodius"  
BG-5000 Veliko Tirmovo, Bulgaria  
E-mail: gngeorgiev@yahoo.com

<sup>(2)</sup>Meterstrasse 4/2, D-70839 Gerlingen, Germany  
E-mail: Mariana.G@t-online.de

## ABSTRACT

The real Kummer function, the ordinary and modified difference Bessel functions are applied to derive the characteristic equation of slow  $\hat{TE}_{0\hat{n}}$  modes in the circular waveguide, containing azimuthally magnetized ferrite cylinder and dielectric toroid. A lemma on a remarkable property of the real zeros of the equation is formulated, based on its numerical solution. Essential features of the slow  $\hat{TE}_{01}$  mode are found out, investigating its graphically shown phase curves.

## INTRODUCTION

A few of the attributes of the slow waves in the azimuthally magnetized circular ferrite waveguides are known only [1]. The task for their propagation is rather interesting since such modes cannot be sustained, if the filling is isotropic. Very attractive in view of the variety of expected results are the stratified configurations, not treated until now, the simplest of which is examined here.

## BOUNDARY-VALUE ANALYSIS

The knowledge of the roots of the equation:

$$\frac{1-\hat{\alpha}^2}{2} \frac{\Phi(\hat{a}, \hat{c}; \hat{\rho}\hat{x}_0)}{\Phi(\hat{a}-1, \hat{c}-2; \hat{\rho}\hat{x}_0)} = \begin{cases} -\frac{1}{\hat{v}_0} \frac{\partial}{\partial \hat{v}_0} \ln \left| \frac{\partial}{\partial \hat{y}_0} bsn_{\hat{m}}(\hat{y}_0 - \hat{v}_0) \right|, & \hat{q} > 0 \\ -\frac{1-\hat{\rho}^2}{2\hat{\rho}^2}, & \hat{q} \equiv \hat{p} \equiv 0 \\ \frac{1}{\hat{w}_0} \frac{\partial}{\partial \hat{w}_0} \ln \left| \frac{\partial}{\partial \hat{u}_0} bsh_{\hat{m}}(\hat{u}_0 - \hat{w}_0) \right|, & \hat{p} = j\hat{q} > 0, \end{cases} \quad (1)$$

is a necessary condition for the study of eigenvalue spectrum and phase characteristics of the circular waveguide (radius  $\hat{r}_0$ ) with azimuthally magnetized ferrite rod (radius  $\hat{r}_1$ ) and dielectric toroid under slow  $\hat{TE}_{0\hat{n}}$  modes excitation, if the axial switching wire is dimensionless. (All quantities, related to waves mentioned are real and are marked by a hat “^” which may be omitted provided no ambiguity might arise.) The ferrite has a permeability tensor with off-diagonal element  $\hat{\alpha} = \gamma \hat{M}_r / \omega$  ( $\gamma$  - gyromagnetic ratio,

$\hat{M}_r$  - remanent magnetization,  $\omega$  - angular frequency of the wave). The relative permittivities of inner and outer media are  $\varepsilon_r$  and  $\varepsilon_d$ , resp. The left-hand side of eqn. (1) involves real Kummer functions [2]. The first and third forms of its right-hand one are written by ordinary and modified difference Bessel functions [3]. The symbols  $bsn_{\hat{m}}(\hat{y}_0 - \hat{v}_0)$  and  $bsh_{\hat{m}}(\hat{u}_0 - \hat{w}_0)$  stand for the  $\hat{m}$ th order ordinary and modified difference Bessel sine ( $\hat{m}$  - an integer) [3]. It holds  $\hat{a} = 1.5 + \hat{k}$ ,  $\hat{c} = 3$ ,  $\hat{k} = \hat{\alpha}\hat{\beta} / (2\hat{\beta}_2)$ ,  $\hat{\beta}_2 = [\hat{\beta}^2 - (1 - \hat{\alpha}^2)]^{1/2}$ ,  $\hat{x}_0 = 2\hat{\beta}_2\hat{r}_0$ ,  $\hat{\rho} = \hat{r}_1 / \hat{r}_0$ ,  $\hat{y}_0 = \hat{q}\hat{x}_0$ ,  $\hat{v}_0 = \hat{\rho}\hat{y}_0$ ,  $\hat{q} = 0.5\{(\varepsilon_d / \varepsilon_r)[1 - (2\hat{k} / \hat{\alpha}^2)] / (1 - \hat{\alpha}^2) + (2\hat{k} / \hat{\alpha}^2)\}^{1/2}$ ,  $\hat{u}_0 = \hat{p}\hat{x}_0$ ,  $\hat{w}_0 = \hat{\rho}\hat{u}_0$ ,  $\hat{p} = j\hat{q}$ ,  $\hat{m} = 0$ . The phase constant, radial wavenumber, guide and rod radii are normalized as follows  $\hat{\beta} = \hat{\beta} / (\beta_0 \sqrt{\varepsilon_r})$ ,  $\hat{\beta}_2 = \hat{\beta}_2 / (\beta_0 \sqrt{\varepsilon_r})$ ,  $\hat{r}_0 = \beta_0 \hat{r}_0 \sqrt{\varepsilon_r}$ ,  $\hat{r}_1 = \beta_0 \hat{r}_1 \sqrt{\varepsilon_r}$ ;  $\beta_0 = \omega \sqrt{\varepsilon_0 \mu_0}$ . The condition  $\hat{q}$  ( $\hat{p}$ ) - real positive or  $\hat{q} \equiv \hat{p} \equiv 0$  needs application of the first (third) or second form of eqn. (1). A numerical proof is given to the statement:

*Lemma 1:* If  $\hat{\xi}_{\hat{k}, \hat{n}}^{(\hat{c})}(\varepsilon_r, \varepsilon_d, \hat{\rho}, \hat{\alpha})$  be the  $\hat{n}$ th real positive root of characteristic equation in  $\hat{x}_0$  provided  $\hat{a}$ ,  $\hat{c}$ ,  $\hat{x}_0$  - real,  $\hat{x}_0 > 0$ ,  $\hat{c} = 3$ ,  $\hat{k} < 0$  ( $\hat{k} = \hat{a} - \hat{c}/2$ ),  $\varepsilon_r > 0$ ,  $\varepsilon_d > 0$ ,  $0 < \hat{\rho} \leq 1$ , the infinite sequences of numbers  $\{\hat{\xi}_{\hat{k}, \hat{n}}^{(\hat{c})}\}$  and  $\{|\hat{k}| \hat{\xi}_{\hat{k}, \hat{n}}^{(\hat{c})}\}$  are convergent for  $\hat{k} \rightarrow -\infty$  and their limits are 0 and  $\hat{L}$ , resp. where  $\hat{L} = \hat{L}(\hat{c}, \varepsilon_r, \varepsilon_d, \hat{\rho}, \hat{\alpha}, \hat{n})$ .

### SOME PROPERTIES OF THE SLOW $\hat{TE}_{01}$ MODE

Using the roots  $\hat{\xi}_{\hat{k}, 1}^{(\hat{c})}$  of eqn. (1) and the relations between barred quantities, the structure's phase characteristics are drawn in Figs. 1, 2 for  $\varepsilon_r = \varepsilon_d = 1$  and  $\hat{\rho} = 0.9$ . The analysis shows that propagation is possible for negative magnetization in two areas, subject to the terms:  $\hat{\alpha}_{left}^{(1),(2)} < \hat{\alpha}^{(1),(2)} < \hat{\alpha}_{right}^{(1),(2)}$ ,  $\hat{r}_{0left}^{(1),(2)} < \hat{r}_0^{(1),(2)} < \hat{r}_{0right}^{(1),(2)}$ ,  $\hat{k}_{left}^{(1),(2)} < \hat{k}^{(1),(2)} < \hat{k}_{right}^{(1),(2)}$ ,  $\hat{\beta}_{left}^{(1)} < \hat{\beta}^{(1)} < \hat{\beta}_{right}^{(1)}$ ,  $\hat{\beta}_{left}^{(2)} > \hat{\beta}^{(2)} > \hat{\beta}_{right}^{(2)}$  where  $\hat{\alpha}_{left}^{(1)} = -1$ ,  $\hat{\alpha}_{right}^{(1)} = 0$ ,  $\hat{\alpha}_{left}^{(2)} = -\infty$ ,  $\hat{\alpha}_{right}^{(2)} = -3$ ,  $\hat{r}_{0left}^{(1)} = \hat{L}^{(1)} / \left[ |\hat{\alpha}^{(1)}| (1 - [\hat{\alpha}^{(1)}]^2)^{1/2} \right]$ ,  $\hat{r}_{0left}^{(2)} = 0$ ,  $\hat{r}_{0right}^{(1),(2)} = +\infty$ ,  $\hat{k}_{left}^{(1)} = -\infty$ ,  $-1.5 < \hat{k}_{right}^{(1)} < -0.5$ ,  $\hat{k}_{left}^{(2)} = \hat{\alpha}^{(2)} / 2$ ,  $\hat{k}_{right}^{(2)} = -1.5$ ,  $\hat{\beta}_{left}^{(1)} = (1 - [\hat{\alpha}^{(1)}]^2)^{1/2}$ ,  $\hat{\beta}_{left}^{(2)} = +\infty$ ,  $\hat{\beta}_{right}^{(1),(2)} = \left\{ (1 - [\hat{\alpha}^{(1),(2)}]^2) / \left[ 1 - (\hat{\alpha}^{(1),(2)} / (2\hat{k}_{right}^{(1),(2)}))^2 \right] \right\}^{1/2}$ . The superscripts (1), (2) signify the zone to which given quantity is related; the subscripts "left", "right" - its limits. The symbols  $\hat{TE}_{01}^{(1)}$  and  $\hat{TE}_{01}^{(2)}$  are used in the first and second region, resp. In contrast to the ferrite case [1] the slowing down of waves grows, the transmission area of  $\hat{TE}_{01}^{(1)}$  mode expands towards smaller  $\hat{r}_0^{(1)}$  (compare the enve-

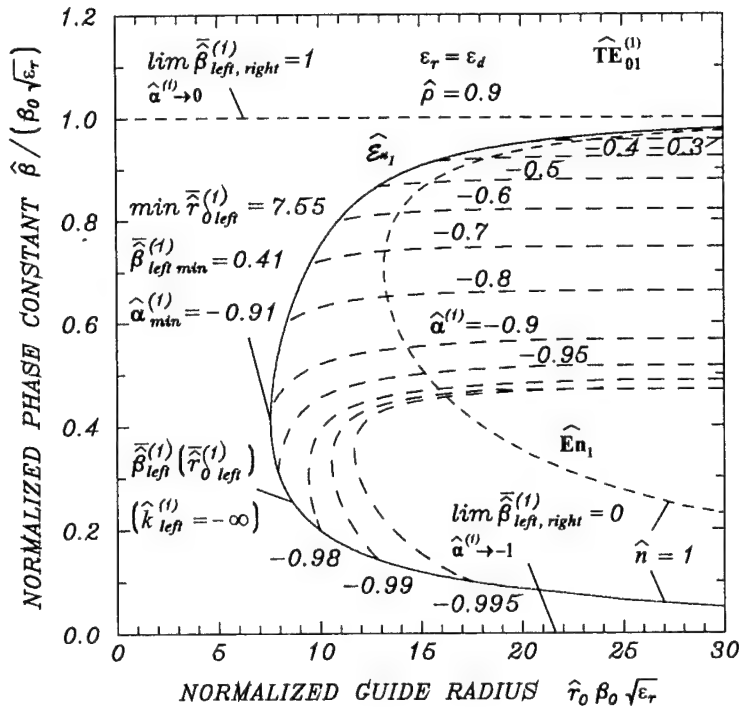


Fig.1.  $\hat{\beta}^{(1)}(\hat{r}_0^{(1)})$  curves of  $TE_{01}^{(1)}$  mode for  $-1 < \hat{\alpha}^{(1)} < 0$ .

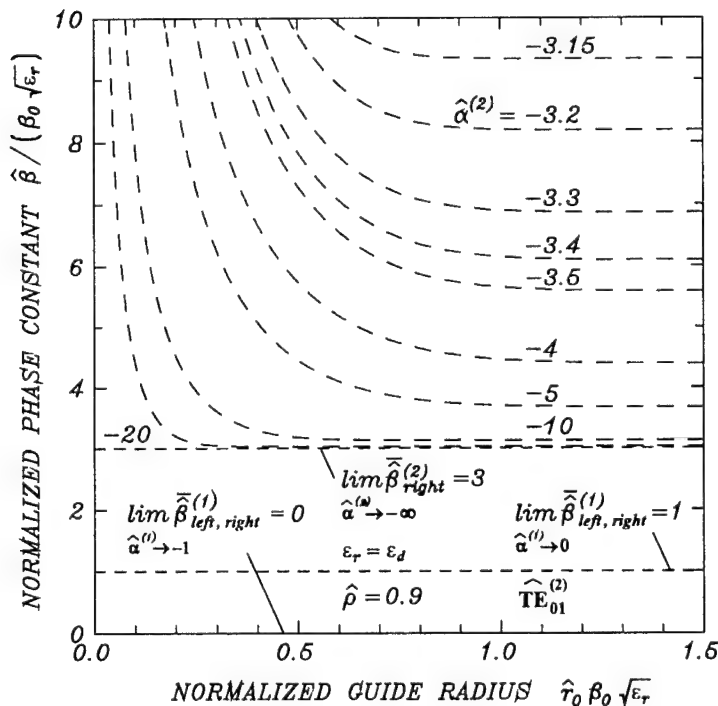


Fig.2.  $\hat{\beta}^{(2)}(\hat{r}_0^{(2)})$  curves of  $TE_{01}^{(2)}$  mode for  $-\infty < \hat{\alpha}^{(2)} < -3$ .

lopes, bounding it from the left  $\hat{\epsilon}_{n_1}$  and  $\hat{E}_{n_1}$ , for the layered and ferrite geometry, resp.) and a domain of double-valuedness appears (cf. Fig. 1).

## CONCLUSION

The propagation conditions are fixed and certain characteristics of the slow  $TE_{0n}$  modes in the azimuthally magnetized ferrite-dielectric circular structure are explored. Inseparable part of the study is a lemma on its eigenvalue spectrum. The principles for solving a new class of boundary-value problems are outlined.

## REFERENCES

- [1] G.N. Georgiev, Y.T. Siderov, M.N. Georgieva, "Slow-Wave Propagation in a Circular Ferrite Waveguide", *Chinese J. Radio Sci.*, 1995 Suppl. Issue, Proc. 1995 Intl Conf. on Radio Sci. (ICRS'95), CIE, Beijing, China, Aug.10-12, 1995, pp.678-681.
- [2] F.G. Tricomi, *Fonctions Hypergéométriques Confluentes*, Gauthier-Villars, Paris, France, 1960.
- [3] N.M. Sovetov, M.E. Averbuch, *Difference Bessel Functions and Their Application in Technics*, Saratov Univ. Publ. House, Saratov, USSR, 1968.



## DISPERSIVE CHARACTERISTICS OF A WAVEGUIDE WITH PERIODIC IMPEDANCE OF WALLS

V. Bondarev<sup>1</sup>, L. Logacheva<sup>2</sup>

<sup>1</sup>National Mining University

49026 Dnepropetrovsk, No.2 Obovanskaya Str., apt.6, nbond@fregat.com

<sup>2</sup>Zaporozhye National Technical University

### ABSTRACT

The present article is devoted to some problems of implementation of concept of a periodic impedance of walls in the process of studying wave propagation in waveguides. It enables to approach the calculation of different waveguide devices from the unified position. The implementation of such approach is shown on an example of absorbing filter of harmonics representing a sequently located round holes in a narrow or wide wall. It is shown that such tasks can be solved as Helmholtz equation with impedance boundary conditions for tangent components of electric and magnetic fields on the wall's surface.

### SURFACE IMPEDANCE OF A NARROW WAVEGUIDE WALL WITH THE SYSTEM OF HOLES

Let's study a rectangular waveguide having a periodic series of round holes on a narrow wall along the line parallel to axis  $z$ .

Let's introduce a rectangular system of coordinates which beginning coincides with one of the tops of the waveguide and cylinder system of coordinates which beginning coincides with the center of the first hole circle. Then the chosen systems of coordinates can be connected in the following way:

$$z = l + \rho \cdot \cos \varphi, \quad y = d + \rho \cdot \sin \varphi. \quad (1)$$

where  $l$  – distance from waveguide aperture to the first hole centre,  $d$  – distance from the wide waveguide wall to the holes system centre.

From the task geometry it is clear that the surface impedance is equal to zero everywhere on the narrow wall except for the holes surfaces. Let's assume that on the holes the surface impedance coincides with the characteristic resistance of the secondary round waveguides connected to the holes.

Let's disintegrate the surface impedance in the plane YOZ into the double Fourier series on the orthogonal system of functions in the rectangular ( $0 \leq y \leq b$ ,  $0 \leq z \leq h$ ,  $h$  – distance between the holes centers).

$$Z_s(y, z) = \sum_{m=0}^{\infty} \sum_{n=0}^{\infty} V_{mn} \cdot (A_{mn} \cos \frac{m\pi}{b} y \cdot \cos \frac{n\pi}{h} z + B_{mn} \sin \frac{m\pi}{b} y \cdot \cos \frac{n\pi}{h} z + \\ + C_{mn} \cos \frac{m\pi}{b} y \cdot \sin \frac{n\pi}{h} z + D_{mn} \sin \frac{m\pi}{b} y \cdot \sin \frac{n\pi}{h} z) \quad (2)$$

where  $A_{mn}$ ,  $B_{mn}$ ,  $C_{mn}$ ,  $D_{mn}$  – disintegration coefficient of Fourier series. Value  $V_{mn}$  is equal to 1,  $\frac{1}{2}$ ,  $\frac{1}{4}$ , depending on the values of  $m$  and  $n$ .

Coefficients  $B_{mn}$ ,  $D_{mn}$  are equal to zero and coefficients  $A_{mn}$ ,  $C_{mn}$  are found from the following relations:

$$A_{mn} = \frac{16\pi Z_0}{bh} \cos \frac{m\pi}{b} d \cdot \cos \frac{n\pi}{h} l \cdot \sum_{q=0} S_q^{(m,n)}, \quad (3)$$

$m \neq n.$

$$C_{mn} = \frac{16\pi Z_0}{bh} \cos \frac{m\pi}{b} d \cdot \sin \frac{n\pi}{h} l \cdot \sum_{q=0} S_q^{(m,n)},$$

$m \neq n.$

where

$$S_p^{(m,n)} = \frac{1}{2} \cdot \frac{\frac{n\pi}{h} R \cdot J_0\left(\frac{m\pi}{b} R\right) J_{-1}\left(\frac{n\pi}{h} R\right) - \frac{m\pi}{b} R \cdot J_{-1}\left(\frac{m\pi}{b} R\right) J_0\left(\frac{n\pi}{h} R\right)}{\left(\frac{m\pi}{b}\right)^2 - \left(\frac{n\pi}{h}\right)^2}, \quad (4)$$

### CALCULATION OF PROPAGATION CONSTANT OF A RECTANGULAR WAVEGUIDE WITH AN IMPEDANCE NARROW WALL

Let's study the magnetic waves propagation in a rectangular waveguide with a narrow impedance wall. As follows from the above said the impedance of a narrow wall is stipulated by the presence of round holes on it. A field in such a waveguide is determined through a longitudinal component  $H_z$  which satisfies the Helmholtz equation

$$\frac{\partial^2 H_z}{\partial x^2} + \frac{\partial^2 H_z}{\partial y^2} + \gamma_{\perp}^2 H_z = 0, \quad (5)$$

as well as boundary conditions on a narrow wall with  $E_y = -Z_s(y, z)H_z$ .

On other walls having ideal conductivity the component  $E_y = 0$ .

Due to the fact that the surface impedance is a periodic function from coordinate  $z$  the field components will be represented in the form of Floquet series

$$H_z = \sum_{n=0}^{\infty} \sum_{s=-\infty}^{\infty} A_n^{(s)} \cos \gamma_{xn}^{(s)} x \cdot \cos \frac{n\delta}{b} y \cdot e^{-j\beta_s z}, \quad (6)$$

$$E_y = -j\omega\mu_a \sum_{n=0}^{\infty} \sum_{s=-\infty}^{\infty} \frac{\gamma_{xn}^{(s)}}{\gamma_{\perp n}^{(s)2}} A_n^{(s)} \sin \gamma_{xn}^{(s)} x \cdot \cos \frac{n\delta}{b} y \cdot e^{-j\beta_s z}.$$

where

$$\beta_s = \beta + p \frac{2\pi}{h}, \quad \gamma_{xn}^{(s)2} = k^2 - \beta_s^2 - \left( \frac{n\pi}{b} \right)^2,$$

Using the boundary condition and expressions for the field components (6) as well as the orthogonality of the transverse eigenfunctions of the waveguide from (5) it is possible to receive the following system of homogeneous linear algebraic equations in regard to the field amplitudes

$$\sum_{k=0}^{\infty} \left\{ \left( Z_{po}^+ + Z_{po}^- \right) U_k^{(s)} - (1 + \delta_{nk}) \delta_{nk} \cdot V_k^{(s)} \right\} A_k^{(s)} + \frac{1}{2} \sum_{r=1}^{\infty} \left( Z_{pr}^+ U_k^{(s-r)} A_k^{(s-r)} + Z_{pr}^- U_k^{(s+r)} A_k^{(s+r)} \right) \Bigg\} = 0, \quad (8)$$

where

$$Z_{pr}^- = A_{pr} - jC_{pr}, \quad Z_{pr}^+ = A_{pr} + jC_{pr}.$$

$$U_k^{(s)} = \cos \gamma_{xk}^{(s)} a;$$

$$V_k^{(s)} = j \cdot \frac{\gamma_{xn}^{(s)}}{\gamma_{\perp k}^{(s)2}} \sin \gamma_{xk}^{(s)} a.$$

$\delta_{nk}$  – the Kronecker symbol.

Non-zero solution of the system (8) enables to receive the dispersive equation in a matrix form from which we determine the propagation constants in the structure under study. Properties of body and surface waves in an impedance waveguide are examined by numerical method in a wide range of parameters changes.

# THE PROBLEM OF ORTHOGONALITY OF EIGENWAVES IN A WAVEGUIDE PARTIALLY FILLED WITH A LOSSY DIELECTRIC

L.P.Yatsuk, A.A.Komyachko, Yu.V.Zhironkin

V.N.Karazin Kharkov National University, 4, Svobody Sq., Kharkov, 61077, Ukraine

Tel. (0572)45-75-48, Email: Ludmila.P.Yatsuk@univer.kharkov.ua

The eigenwaves orthogonality is investigated for the rectangular waveguide having a lossy dielectric slab inside it. It is shown analytically that eigenwaves of such waveguides are energetically non-orthogonal. The interaction of pair of non-orthogonal eigenwaves is discussed. The numerical estimation of their non-orthogonality has been carried out for the various slab dimensions, its permittivity and losses. Calculation results are presented.

## INTRODUCTION

The property of eigenwaves orthogonality is very important one while solving scattering problems. According to [1] there are two definitions of the orthogonality:

Mathematical orthogonality

$$\frac{1}{2} \int_{S_1} [\vec{E}_\mu, \vec{H}_\nu] \vec{e}^0 dS = \delta_{\mu\nu} N_\mu \quad (1)$$

and energetic one

$$\frac{1}{2} \int_{S_1} [\vec{E}_\mu, \vec{H}_\nu^*] \vec{e}^0 dS = \ddot{a}_{\mu\nu} P_\mu. \quad (2)$$

Here  $\delta$  is a Kronecker symbol,  $N_\mu$  is a norm,  $P_\mu$  is a longitudinal  $\mu$ -mode complex flux of power. The equality (1) is fulfilled always. As to the equality (2), it has been shown in [1], that the pairs of complex waves with propagation constants  $\pm \gamma_\mu$  and  $\pm \gamma_\mu^*$  are energetically non-orthogonal. Their joint existence results in arising active and reactive power fluxes over a waveguide cross section. We have shown that not only these waves but the modes with  $\gamma_\mu \neq \gamma_\nu$  in a waveguide filled with a layered dissipative dielectric are energetically non-orthogonal.

## SOME POINTS OF THEORY

The rectangular waveguide of  $a \times b$  cross section with a lossy dielectric slab of  $a_2 \times b$  cross section (Fig.1) is considered.. The  $\vec{E}$  and  $\vec{H}$  fields of  $LE$ - and  $LM$ -modes can be found using the magnetic Hertz vector  $\vec{\Pi}^m = \vec{x}^0 \Pi_x^m$  and electric one  $\vec{\Pi}^e = \vec{x}^0 \Pi_x^e$  correspondingly. Components  $\Pi_x^m$  and  $\Pi_x^e$  can be represented as

$$\Pi_x^{m(e)}(x, y, z) = \varphi^{m(e)}(x) f^{m(e)}(y) e^{\mp \gamma_{ym}^{m(e)} z}, \quad (3)$$

where  $\varphi^m(x)$ ,  $\varphi^e(x)$  – scalar functions which satisfy the following equation

$$\frac{d^2 \varphi_{\mu}^{m(e)}(x)}{dx^2} + (\alpha_{\mu}^{m(e)})^2 \varphi_{\mu}^{m(e)}(x) = 0 \quad (4)$$

and corresponding boundary conditions on the metal walls and dielectric interfaces. It is easy to show from (4) that for two solutions with  $\mu$  and  $\nu$  numbers of the dispersion equation root it is easy to obtain the following result.

$$\Phi_{\mu\nu} = \int_0^a \varphi_{\mu}^{m(e)}(x) \cdot (\varphi_{\nu}^{m(e)}(x))^* dx = \frac{-i2k^2 \varepsilon''}{(\gamma_{\mu}^{m(e)})^2 - (\gamma_{\nu}^{m(e)})^2} \int_{x_1}^{x_2} \varphi_{\mu}^{m(e)}(x) \cdot (\varphi_{\nu}^{m(e)}(x))^* dx. \quad (5)$$

If  $\varepsilon'' \neq 0$  and  $x_2 - x_1 \neq a$  the right side of (7) differs from zero. It proves, that scalar functions  $\varphi_{\mu}^{m(e)}(x)$  and  $\varphi_{\nu}^{m(e)}(x)$  are energetically non-orthogonal. The real part of the integral (2) for *LE*-modes with indices  $\mu$  and  $\nu$  takes the following form:

$$\begin{aligned} \operatorname{Re} P_{\mu\nu} &= \frac{1}{2} \operatorname{Re} \int_{S_{\perp}} [E_{\mu}^{LE}, (H_{\nu}^{LE})^*] \vec{z}^0 dS = \\ &= -\frac{\omega \mu_0 b}{2(2 - \delta_{0n})} \operatorname{Re} \left\{ \gamma_{\mu}^m (\kappa_n^2 + (\gamma_{\nu}^m)^2)^* e^{-i(\gamma_{\mu}^m - (\gamma_{\nu}^m)^*)z} \int_{S_{\perp}} \varphi_{\mu}^m(x) (\varphi_{\nu}^m(x))^* dS \right\} \end{aligned} \quad (6)$$

If the electromagnetic field in a waveguide consists of two eigen waves fields  $\vec{E} = \vec{E}_{\mu} + \vec{E}_{\nu}$ ,  $\vec{H} = \vec{H}_{\mu} + \vec{H}_{\nu}$  (each wave of unit amplitude for simplicity), the total flux of energy of this field  $P = \frac{1}{2} \operatorname{Re} \int_{S_{\perp}} [\vec{E}, \vec{H}^*] \vec{z}^0 dS$  consists of four fluxes:

$$P = P_{\mu\mu} + P_{\nu\nu} + P_{\mu\nu} + P_{\nu\mu}. \quad (7)$$

Two of them ( $P_{\mu\mu}$  and  $P_{\nu\nu}$ ) may be named eigen power fluxes of the waves with indexes  $\mu$  and  $\nu$ . The two others ( $P_{\mu\nu}$  and  $P_{\nu\mu}$ ) – mutual fluxes caused by field combinations of various modes:  $[\vec{E}_{\mu}, \vec{H}_{\nu}^*]$  and  $[\vec{E}_{\nu}, \vec{H}_{\mu}^*]$ .

The eigenwaves  $\vec{E}_{\mu}, \vec{H}_{\mu}$  and  $\vec{E}_{\nu}, \vec{H}_{\nu}$  propagates with different velocities. Therefore a phase shift between  $\vec{E}_{\mu}$  and  $\vec{H}_{\nu}$  ( $\vec{E}_{\nu}$  and  $\vec{H}_{\mu}$  as well) changes along  $z$ -axis. As an effect so does the phase of the complex vectors  $[\vec{E}_{\mu}, \vec{H}_{\nu}^*]$  and  $[\vec{E}_{\nu}, \vec{H}_{\mu}^*]$ . It causes variation not only magnitudes of the real part of these vectors but their sign as well. So, due to the interference effect, the mutual fluxes  $P_{\mu\nu}$  and  $P_{\nu\mu}$  depending on  $z$  may increase or decrease the total flux in comparison with  $P_{\mu\mu} + P_{\nu\nu}$ . This process is analogues to the vector addition on the phase plane. The square length of the sum vector according to the cosine theorem may be equal, less or greater than sum of squared lengths of vectors, which are summarized. As an effect of this the total flux of energy in the waveguide cross section oscillates depending on  $z$  around the exponential curve, representing the sum  $P_{\mu\mu} + P_{\nu\nu}$  (Fig.4)

## CALCULATION RESULTS

Calculations were carried out for the waveguide  $23 \times 10 \text{ mm}^2$ , various values of  $\varepsilon$ ,  $\text{tg}\delta$  and dimensions of dielectric slab. It was determined, that the orthogonality of eigenwaves can be confirmed only if the eigenvalues are determined with high accuracy ( $10^{-12}$ - $10^{-15}$ ). The value of the integral  $\Phi_{\mu\nu}$  (5) is represented on the Fig.2. Along the  $\mu, \nu$ -axis root numbers change, along  $x$ -one –width of the slab,  $\varepsilon = 10$ ,  $\text{tg}\delta = 0,1$ . The Fig.3 represents  $P_{\mu\nu}$  and  $P_{\nu\mu}$ , when  $\mu = 1$ ,  $\nu = 3$ ,  $\varepsilon = 15$ ,  $\text{tg}\delta = 0,1$ . The same parameters were used for the Fig.4.

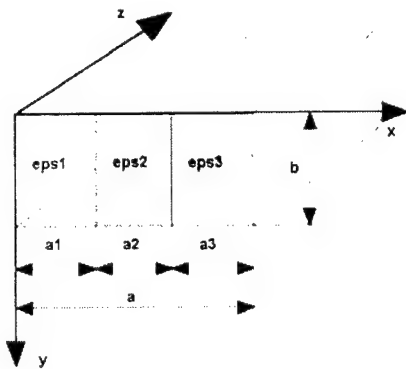


Fig. 1

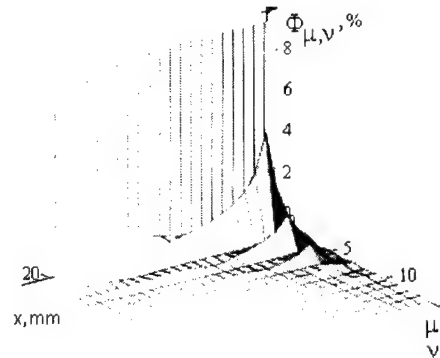


Fig. 2

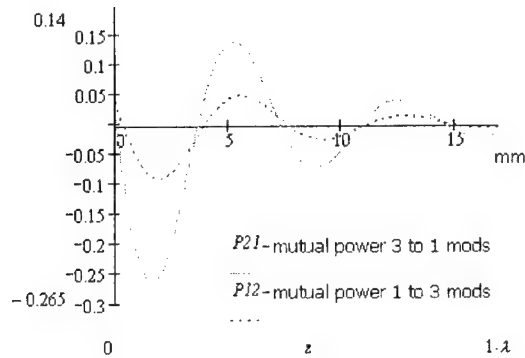


Fig. 3

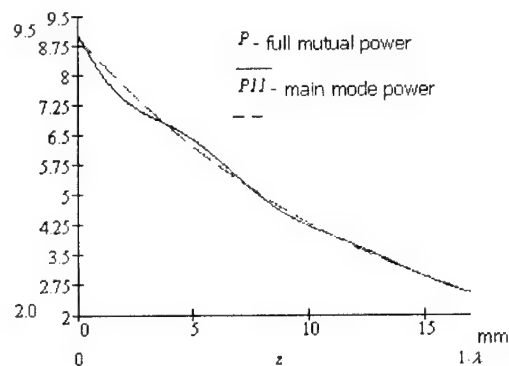


Fig. 4

## CONCLUSION

It has been shown that the energetic non-orthogonality of the eigenwaves is the more noticeable, the higher the  $\varepsilon$  and  $\text{tg}\delta$  of dielectric is. By  $\varepsilon < 5$ ,  $\text{tg}\delta < 0,01$  it can be neglected. The non-orthogonality effect diminishes with rising slab width and vanishes at all when the lossy dielectric fully fills the waveguide.

## REFERENCES

- [1] Veselov G.I., Rayevski S.B. The Layered Metal-Dielectric waveguides.-M.: "Radio and Communication".-1988, 247 p. (in Russian).

# ROTOR STATOR ACOUSTIC INTERACTION, DEATH AND BIRTH OF RESONANCE FREQUENCY

Eugene R. Bartuli

630090, Novosibirsk, RUSSIA, E-mail: bartuli@comunder.com

Guiding and resonance phenomenon near a periodic double cascade of plates has been investigated. Much attention has been paid to the difference from the oscillations near single periodic cascade of plates. It has been demonstrated that the mutual influence of the two periodic cascades decrease rapidly with the increasing distance between them, but at short distances the distortions in the oscillations localised near one periodic cascade of plates caused by the interference of the other become substantial.

## PROBLEM FORMULATION

In the present paper an elementary double cascade of plates resulting from shifts multiple to 1 of the fundamental area of the group of translations along Y axis is studied. (Fig 1)

Steady state oscillations near the structure are described with the function  $u(x, y)$  which is the potential of acoustic speed perturbation or the pressure field. In the oscillation area this function satisfies the Laplace equation:

$$(\Delta + \lambda^2)u = 0, \quad (1)$$

Here  $\lambda$  is a dimensionless oscillation frequency and it is assumed that  $(\lambda \geq 0)$ .

On the cascade elements the Neuman conditions should be fulfilled:

$$\frac{\partial u}{\partial n} \Big|_{(G_1 \cup G_2)} = 0 \quad (2)$$

In any boundary area  $\Omega_a$  which is a subarea of  $\Omega$  the local energy finiteness condition should be fulfilled:

$$\int_{\Omega_a} (|\nabla u|^2 + |u|^2) < \infty \quad (3)$$

As the structure according to the problem formulation has a translational symmetry, the function  $u(x, y)$  should satisfy the condition:

$$u(x, y+1) = e^{i\xi} u(x, y) \quad (4)$$

Where function  $v(x, y)$  satisfies the condition  $v(x, y) = v(x, y+1)$ . Here we suppose that  $0 < \xi \leq \pi$ . The problem (1) – (4) will be further referred to as problem  $B(\xi)$ .

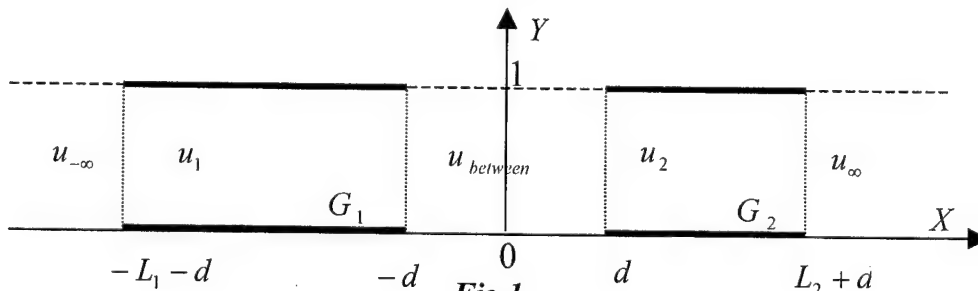


Fig 1.

**Definition.** *Waveguiding function* of the problem  $B(\xi)$  is a generalized eigenfunction localized in the neighborhood of the cascade of plates, i.e.  $u(x, y) \rightarrow 0$  as  $|x| \rightarrow \infty$ .

## THEOREM OF EXISTENCE

**Definition.** The solutions of problem  $B(\xi)$   $u(x, y)$ , which satisfy the condition  $u(-x, y) = u(x, y)$  or  $u(-x, y) = -u(x, y)$ , are called **symmetrical** ( $\alpha$ ) or **anti-symmetrical** ( $\beta$ ) modes.

**Theorem 1.** If  $L_1 = L_2$  then there are **symmetrical** modes for any geometrical parameters of the system and for all  $\xi$ .

**Theorem 2.** If  $L_1 = L_2 > 1$  then there are **anti-symmetrical** modes. If  $L_1 = L_2 < 1$  then there always exists such  $d$  that **anti-symmetrical** modes exist.

## DISPERSION RELATION

The dimensionless wave frequencies  $\lambda$  can be considered as functions of wave number  $\xi$ . These functions are so called dispersion relations.

$$\left(1 - e^{2i(\theta_1 + \lambda L_1)}\right) \left(1 - e^{2i(\theta_1 + \lambda L_2)}\right) - e^{2i\theta_2} \left(1 - e^{2i(\theta_1 + \lambda L_1 - 2i\alpha \tan(\frac{\lambda}{\theta_0}))}\right) \left(1 - e^{2i(\theta_1 + \lambda L_2 - 2i\alpha \tan(\frac{\lambda}{\theta_0}))}\right) = 0 \quad (5)$$

$$\theta_1 = -\frac{2\lambda \ln(2)}{\pi} + 2 \arctan\left(\frac{\lambda}{\delta_0}\right) + \sum_{n=1}^N \arcsin\left(\frac{\lambda}{2\pi k - \xi}\right) + \arcsin\left(\frac{\lambda}{2\pi k + \xi}\right) - \arcsin\left(\frac{\lambda}{\pi k}\right)$$

$$\theta_2 = -\frac{2\delta_0 \ln(2)}{\pi} - 2\delta_0 d + 2i \arctan\left(\frac{\delta_0}{\lambda}\right) + \sum_{n=1}^N \arctan\left(\frac{\delta_0}{\delta_n}\right) + \arctan\left(\frac{\delta_0}{\delta_{-n}}\right) - \arctan\left(\frac{\delta_0}{\pi k}\right)$$

These relations were numerically investigated.

## NUMERICAL INVESTIGATIONS

Fig. 2-5 show the results of numerical investigation of the dispersion relation (5). Fig. 2 shows the dependence of eigenwave frequencies  $\lambda$  on the wave number  $\xi$  provided that  $L_1 = L_2 = 2$  and the distance between the cascades  $d = 1$ . It coincides entirely with corresponding dependence for a singular cascade with the same geometrical parameters [2].



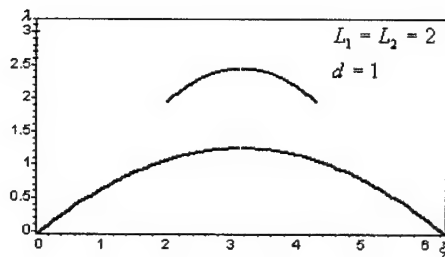


Fig 2.

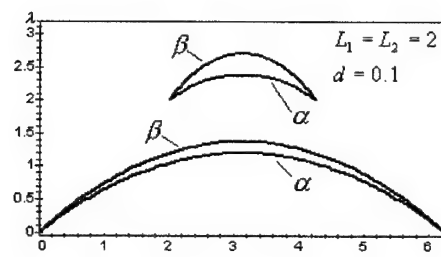


Fig 3.

Fig 3 shows the dependence of eigenwave frequencies  $\lambda$  on the wave number  $\xi$  for  $L_1 = L_2 = 2$  and the distance between the cascades  $d=0.1$ . The frequencies can be seen to part into symmetrical ( $\alpha$ ) and anti-symmetrical ( $\beta$ ) ones for each oscillation mode in the contrast to a singular cascade. This process can be called as “birth” of resonance phenomena.

The frequency parting process is shown on Fig. 4. One can see the rapid decrease of the mutual influence.. Fig 5 shows the effect of the symmetry break ( $L_1 = 0.6, L_2 = 0.5$ ) on the waveguiding eigenvalues for  $\xi = \pi$

#### ACNOLEGMENT

The author is indebted to S. V. Sukhinin, for this friendly help and useful discussion.

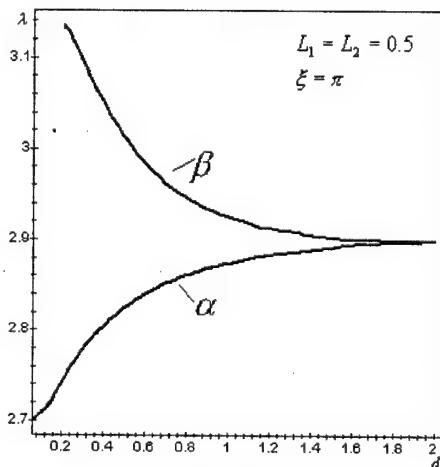


Fig 4.

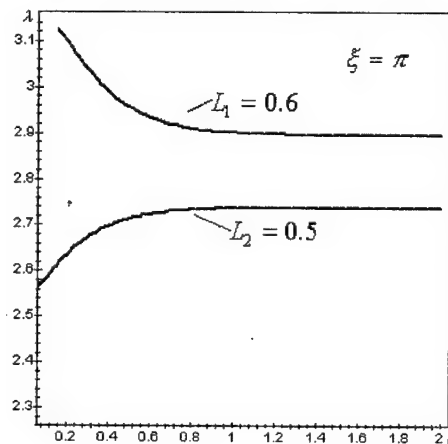


Fig 5.

#### REFERENCES

- [1] Sukhinin S.V. «Waveguiding and anomalous properties of periodical knife-type grating», J. Appl. Mech. Tech. Phys., (1998), V. 39, №2.
- [2] Bartuli E. R. Eigen oscillation Near the System of Strips in a Channel, International Conference on Mathematical Methods in Electromagnetic Theory, Ukraine, Kharkov, June 2-5, 1998), Vol. - 2, Page 841-843. 8.

## CHARACTERISTICS OF SPATIALLY-DEVELOPED SQUARE MULTIMODE RESONATORS

Viktor I. Naidenko, Hryhorii A. Borsch\*

National Technical University of Ukraine "Kiev Polytechnic Institute",

37 Prospect Peremogy, Kiev, 03056, Ukraine

E-mail: v\_naidenko@yahoo.com; \*E-mail: gborsch@hotmail.com

### ABSTRACT

By mode matching technique a problem of calculation (as well as control) of resonance frequencies and inherent Q-factors of a square resonator with final conductivity of walls loaded by square dielectric samples of complex scalar permittivity and a height, equal to the height of the resonator, has been solved.

### INTRODUCTION

When designing electron devices a problem of suppression of unwanted modes arises [1-3]. To solve this problem it is possible to use dielectric absorbing samples of finite dimensions. In the present work the dependence of resonance frequencies and inherent Q-factors of a square resonator against locations of dielectric samples, their dielectric properties and conductivity of the walls is analysed.

### FORMULATION OF THE PROBLEM

It is considered a square resonator measured  $a$ ,  $l_y$ ,  $b$  on axes  $X$ ,  $Y$ ,  $Z$  accordingly. On the height of the resonator  $l_y$  a restriction is imposed, so that in a considered frequency range there is no field variation on this direction. Modes are classified in the  $XZ$ -plane. Suppose that  $m$  half-waves are kept within  $X$ -dimension of the resonator, no one within  $Y$ -dimension and  $n$  half-waves – within  $Z$ -dimension. Under such conditions  $E$ -modes (relative to  $X$ - or  $Z$ -axis) do not arise in the resonator. Identical square dielectric samples

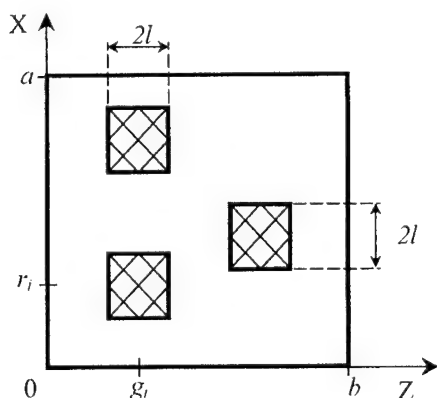


Fig. 1

are located arbitrarily (the only restriction ensued from the mode matching technique is shown below) within the resonator in parallel to axis  $Y$  (fig. 1). The centre of the  $i$ -th sample in plane  $XZ$  has coordinates  $r_i$  and  $g_i$ , accordingly. The length and the width of a sample are  $2l$  and the height is  $l_y$ . The permittivity of the  $i$ -th sample is  $\varepsilon_i = \varepsilon'_i - j\varepsilon''_i$ , the permeability is  $\mu_0$ . The resonator area outside samples has electrical characteristics of free space. The metal walls permeability is  $\mu_0$ , conductivity is  $\sigma$ . The dependence on time  $\exp(-j\omega t)$  is omitted.

## CALCULATION OF RESONANCE FREQUENCIES

The problem is solved by the mode matching technique. Planes, perpendicular to axis  $Z$  and tangent to sides of the samples, separate the resonator into partial regions. Thus dielectric samples should be placed so as not to be intersected by partial region boundaries. Also samples should abut on a partial region boundary solely either from the left or from the right.

Fields are expressed in the usual way. To determine transverse mode functions inhomogeneous partial regions have been broken into partial sub-regions by planes, perpendicular to the axis  $X$  and tangent to the sides of the samples.

System of functional equations received as a result of satisfying boundary conditions on dielectric samples was transformed by Galerkin method into the system of homogeneous linear algebraic equations (SLAE). A non-trivial solution of this SLAE can be received when its determinant equals to zero. So, we have an equation of inherent resonance frequencies of the resonator. The order  $M$  of the determinant is defined by the following formula:  $M = N \cdot (K - 1)$ , where  $N$  is the number of summand in field expressions taking into account,  $K$  is the number of partial regions. So, for a resonator with 8-0-8 working mode,  $N = 32$  and  $K = 13$  the number  $M$  will come to about 400.

To find roots of the equation and to solve the SLAE a computer program has been developed and calculations have been carried out. In a particular case, when the sample of small relative dimensions is in the maximum of electrical field, calculated results agree well with the results, received by the perturbation formula [4].

## CALCULATION OF Q-FACTORS

Q-factors have been calculated using electrical conductivity of the walls and imaginary part of the complex permittivity of samples  $\varepsilon''$ . (The influence of  $\varepsilon''$  on resonance frequencies was neglected).

## NUMERICAL RESULTS

Calculations have been carried out for resonators with the following dimensions:  $a = 300,3$  mm,  $b = 300$  mm,  $l_y = 10$  mm;  $a = 600,6$  mm,  $b = 600$  mm,  $l_y = 10$  mm;  $a = 1201,2$  mm,  $b = 1200$  mm,  $l_y = 10$  mm. The width  $a$  of a resonator is 0,1% larger than its length  $b$  in order to segregate such modes as 1-0-2 and 2-0-1 etc. The working mode of the first resonator is 2-0-2, of the second – 4-0-4, of the third – 8-0-8. These resonators are loaded by 3, 8 and 15 identical dielectric samples, accordingly. The size of a sample is  $2l = 15$  mm, the permittivity  $\varepsilon = 3 - j0,03$ . The centre of a sample is situated at the zero field value of the working mode. The metal walls conductivity is  $\sigma = 1 \cdot 10^7$  ( $\Omega \cdot m$ ).

Table 1 shows calculated resonance frequencies  $f$  and inherent Q-factors  $Q$  of the corresponding  $m$ -0- $n$  modes. Fig. 2-4 shows Q-factor of different modes as a function of  $S = \lg(\operatorname{tg} \delta)$  ( $\varepsilon' = 3$ ) for the resonators with the working modes 2-0-2, 4-0-4, 8-0-8, accordingly. It is evident that proper placing of dielectric absorbing samples (in zero value of the working mode and non-zero value of parasitic modes) allows to make the working mode competitive comparing to parasitic ones.

Table 1

$m$	$n$	$f$ , GHz	$Q$
working mode 2-0-2			
1	1	0.6921585	147.941
2	1	1.1047685	292.625
2	2	1.4123048	2171.401
4	4	2.8249589	3339.534
working mode 4-0-4			
1	1	0.3507614	344.459
2	1	0.5542424	341.500
1	2	0.5556760	456.495
2	2	0.7025874	444.960
3	3	1.0461435	381.377
4	2	1.1133991	909.652
4	4	1.4124070	2359.210

$m$	$n$	$f$ , GHz	$Q$
working mode 8-0-8			
1	1	0.1762527	570.377
1	2	0.2788432	725.184
3	1	0.3935335	593.533
3	2	0.4486148	556.588
2	1	0.2785330	618.258
2	2	0.3525262	720.958
3	3	0.5273501	492.919
2	4	0.5571264	768.097
4	2	0.5578370	1026.604
4	4	0.7053032	1238.020
6	6	1.0564086	1042.188
8	8	1.4124681	2361.398

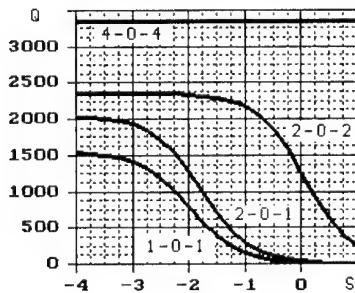


Fig. 2

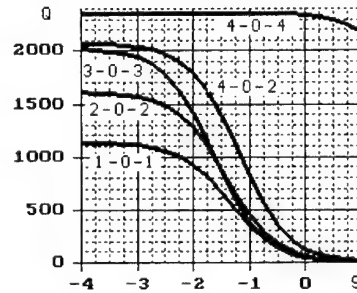


Fig. 3

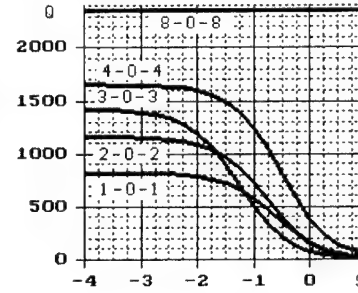


Fig. 4

## CONCLUSION

By mode matching technique a problem of calculation of resonance frequencies and inherent Q-factors of the square resonator with final conductivity of walls loaded by square dielectric samples of arbitrary complex scalar permittivity and a height, equal to the height of the resonator, has been solved. Calculated data agree well with already known. A fundamental opportunity to control the resonance frequencies and Q-factors of the resonator by certain placing within it dielectric absorbing samples is presented.

## REFERENCES

- [1]. B. Smith. Vacuum Electronics in Tomorrow's Strategic Army. "Microwave J.", 1991, v.34, No.11, pp.60-69.
- [2]. Naidenko V., Borsch H. Analysis of Resonance Frequencies and Inherent Q-factors of Partially Filled Rectangular Resonator/Proc. of Int. Conf. on Modern Problems of Telecommunications, Computer Science and Engineers Training. February 14-19, 2000. Lviv-Slavsko, Ukraine. – p. 63-64.
- [3]. Naidenko V.I. Characteristic of electromagnetic systems of spatially developed electron devices. *Radioelektronika (Izvestija vuzov)*, 1995, No.9, p.49-59. (in Russian).
- [4]. Naidenko V.I. Theory of dielectric bar parallel to the axis of periodic structure. *Radioelektronika (Izvestija vuzov)*, 1987, No.5, p.3-8. (in Russian).

# AUTHORS LIST

## A

Alkumru A.	293
Altintas A.	586
Anastassiu H. T.	505
Andreev M. V.	299
Andrenko A.	21
Andriychuk M	79
Antyufeyeva M. S.	186
Arand B.A.	316
Araz.I.	222, 455, 473
Ari N.	463, 466
Arriaga J.	124
Arslanagic S.	257
Averkov Yu.O.	653
Averyanov A.A.	275
Averyanova Y.A.	275
Ayzatsky M.I.	242

## B

Baghai-Wadji A.	27
Barkhudaryan N.V.	493
Bartuli E.R.	683
Bartolic J.	560
Batrakov D.O.	376

Baudrand H.	100
Beletskii N. N.	629
Benson T.	198, 233
Bijamov A.	407, 485
Bludov Y. V.	632
Bolshakov Y. P.	210
Bondarev V.	677
Borsch H. A.	686
Borysenko S. A.	629
Borulko V. F.	367, 551
Breinbjerg O.	257, 476, 499
Brovenko A. V.	573
Bugrova T.	432
Buharov S. V.	443
Butrym A. Y.	213
Bychkov A.	608
Bychkov A.	608

## C

Carlemalm-Logothetis C.	602
Cerezci O.	222, 463, 466 473
Chandezon J.	416
Cheremisin A.A.	570

Chikichev I.S.	659
Chumachenko V.P.	529
Churyumov G.I.	201
Colak B.	473

**D**

Damienne B.	100
Daniel J.-P.	594
Daniele V.	87, 130
Demidchik V. I.	420, 577
Demir Z.	222, 473
Derbov V. L.	67
De Vito P.	48
Dikmen F.	293, 576
Doroshenko V. A.	192, 589
Drize M. A.	210
Drobakhin O. O.	299, 599
Dubrovka F.	195
Dumin A. N.	189

**E**

Edenhofer P.	195
Engheta N.	175
Elschner G.	398

**F**

Fedorenko A.I.	508
Felbacq D.	118
Fikioris G.	73
Filipov Yu. F.	662
Freni A.	48

**G**

Gaal S. B.	239
------------	-----

Gaikovich K. P.	183
Gandel Y. V.	429
Gavrilov S.	290
Georgiev G. N.	674
Georgieva-Grosse M.	674
Gevorkyan E.A.	373
Ghvedashvili G.	485
Goblyk V.	569
Golovin D.V.	376
Gomilko A. M.	227
Goncharenko Y.	620
Gordienko A. N.	638
Gorelyshev S. A.	514
Gorobets N. N.	361, 313, 458
Goryashko V. A.	647
Goryushko D. N.	566
Gourjii A. A.	227
Gousenkova A. A.	496
Gribovsky A. V.	331
Guarab M.	325
Guseva E.	270

**H**

Hakkak M.	316
Halevi P.	124
Hanson G.	230
Hasanov E.	112
Hekim M.	455
Himdi M.	594
Hinata T.	404
Hoorfar A.	54
Hosono T.	404
Hrabar S.	560

**I**

Illyashenko L. N.	592
Ilyenko K. V.	647
Ivanchenko E. V.	452
Ivanov A. I.	517
Ivanov S. A.	469
Ivanov V. B.	611
Ivanov V. K.	623
Ivleeva S. N.	33

**J**

Jablonski T.	141
Jacob A.	163
Jorgensen E.	257, 476

**K**

Kalinchenko G. A.	387
Kamichev T. V.	469
Karamehmedovic M.	499
Karpukov L. M.	260, 310
Kartchevski E.	230
Kasyanov A. O.	266, 390
Katok V.	227, 245
Katrich V. A.	189, 328
Kazanskiy V. B.	523
Khakhinov V. V.	617
Khardikov V. V.	523
Khoroshun V. V.	429
Khraisat Y. S.	287
Kim O.S.	361, 476
Kirilenko A.	99, 482, 532, 535, 540
Kisel V. N.	508
Kivva F.	620
Kiyko V. I.	328

Klimov K. N.	210, 469
Kobayashi K.	152, 370
Komyachko A. A.	680
Kondratenko D. A.	157
Kondratyev Y. V.	599
Kornev R.V.	577
Koshikawa S.	152, 370
Kotenko M.	245
Kramarenko K. Y.	242
Krokhin A.	124
Krizhanovski V. G.	263, 267
Kulik D. Y.	535
Kulishenko S. F.	540
Kulynych Y. P.	364
Kurkin V. I.	614
Kurt M. B.	463
Kuryliak D. B.	370
Kyriacou G.	105

**L**

Lebedev A. M.	511
Le Maguer S.	136
Lerer A. M.	251, 387
Levandovskyy V. G.	227
Lewykin V. M.	379
Linnik V. V.	665
Logacheva L.	677
Lysak V. V.	236

**M**

Magath T.	42
Makarov A. I.	668
Maksymov I. S.	201
Malyuskin A. V.	566

Manuilov M. B.	322
Magro V.I.	325
Martynyuk S.	195
Matsuda T.	410
Matsushima A.	410
Meincke P.	257, 476
Melezhik P. N.	573
Minakova L.	543
Miroshnichenko V. I.	635
Mladyonov P. L.	395
Molinet F.	38
Mori A.	48
Morozov V. M.	325
Mospan L.	532
Muzychenko A. V.	296

**N**

Naidenko V. I.	270, 686
Nazarchuk Z. T.	364, 370
Nechitaylo S. V.	437
Nerukh A. G.	198, 204, 207
Nerukh D. A.	204
Nesterenko M. N.	328
Ney M.	136
Nosenko O. N.	458
Nosich A.	150, 413, 586, 594
Novacek Z.	254

**O**

Obukhovets V. A.	266, 390
Oguzer T.	586
Oinats A. V.	614
Okuno Y.	410
Oleynik M. P.	452

Ometsinska O.	245
Onufriyenko V. M.	310, 379, 382
Opanasenko A. N.	641
Ostroushko V. M.	635
Ovsyanikov V. V.	446, 638
Ozkan E.	576

**P**

Palto A. A.	302
Panin S. B.	579
Petrusenko I. V.	529
Pivnenko S. N.	361
Plastun S. V.	67
Pleshchinskii I. N.	546
Pleshchinskii N. B.	546, 665
Podlevskii B. M.	79
Ponomarchuk S. N.	614
Poyedinchuk A. Y.	416, 482, 573 579
Prokopenko I.	278
Prokopenko K.	278
Prokopenko Yu. V.	662
Prosvirnin S. L.	401, 426
Protsenko M. B.	307
Pulov R. D.	260
Puzanov O.	219

**R**

Raida Z.	254
Rassokhina J. V.	263, 267
Rathsfield A.	398
Romanenko M. V.	449
Romanenko S. N.	260, 310
Romanova E. A.	239
Rondineau S.	594



Ruchenkov V. A.	210
Rud L.	543
Rudiakova A. N.	263, 267
Rusanov A. F.	644
Ruzhytska N. N.	204
Rydberg A.	602

**S**

Sakhnenko N.	207
Saltykov D.Y.	299
Samokhin A.	169
San E.	455
Saparishvili G.	485
Savelyev V. V.	452
Savenko P. O.	79
Sazonov A. Z.	296, 437, 493
Schejbal V.	254
Schmidt G.	398
Schneider G.	163
Schuenemann K.	42
Seker S. S.	466
Semenova E. K.	589
Senkevich S. I.	540
Serov V. V.	67
Sestroretsky B. V.	210, 469
Sewell P.	233
Shchepkina Y. D.	227
Shigesawa H.	93
Shilov S. V.	67
Shishkova A. V.	361
Shlepnev Y. O.	488
Shmat'ko A. A.	566
Shulga S. N.	566
Shulika A.	236

Shvets A. V.	623
Sidina W.	100
Sidorchuk N. V.	401
Sinyavsky G. P.	251
Sitsko M. U.	420
Smirnov Y.G.	33, 502
Sorkin A. R.	526
Sorokin S. N.	452
Sukharevsky O.I.	296, 437, 493
Sukhinin S. V.	157
Sukhoivanov I.A.	236
Sulima A.V.	582

**T**

Tabatadze V.	407
Tarapov S.I.	576
Tavzarashvili K.	407, 485
Tesneli A.	466
Tkach M. D.	79
Tkachenko V.	532
Tkachuk K. I.	514
Tolstikov M. V.	611
Tretyakov O. A.	186, 213
Trifonov T.	479
Tsuji M.	93
Tsupak A. A.	502
Tuchkin Y.	576
Turetken B.	455, 473
Tveretina O.	605
Tyrnov D.O.	426

**U**

Urazghildiiev I.	602
------------------	-----

**V**

Van Thielen B.	61
Vandenbosch G.	61
Varavin A. V.	623
Vashtalov S. G.	319
Vasilets V. A.	514
Vassilyev Yu.V.	570
Vertiy A.	290
Vorgul I.	233
Vrancken M.	61
Vukovic A.	233
Vyazmitinova A. I.	216
Vytovtov K. A.	554, 563

**W**

Wallin K.	602
Watanabe K.	423

**Y**

Yachin V.V.	401
Yachmenov A. A.	387
Yakovenko I.V.	650
Yakovenko V.M.	644, 650, 653
Yakovenko Y.	569
Yamasaki T.	404
Yanovsky F. J.	275, 281
Yatsenko T. Yu.	647
Yatsuk L. P.	328, 680
Yashina N.	416, 482
Yazici M.	455, 473
Yefimov B. P.	647
Yelisseyeva N. P.	313
Yermakov G. V.	440
Yildirim O.	293

Yoshimoto K.	410
Yumov I. B.	671
Yurekli A. I.	455

**Z**

Zagorovsky V. I.	266
Zantema H.	605
Zaridze R.	407, 485
Zelenchuk D. E.	251
Zhironkin Y. V.	680
Zhou D.-Q.	410
Zich R.	130
Zinenko T. L.	413
Zolla F.	118
Zvyagintsev A. A.	517

# HISTORY OF THE INTERNATIONAL CONFERENCE ON MATHEMATICAL METHODS IN ELECTROMAGNETIC THEORY



MMET series of conferences was started in 1988 and since 1990 it has been the only regular symposium in the Former Soviet Union on electromagnetics that has English as medium of presentation and discussion. Information on the previous MMET meetings can be found in the *Antennas and Propagation Magazine*:

1. **Edward V. Jull** . Report on the Fourth International Seminar on Mathematical Methods in Electromagnetic Theory (MMET\*91), *IEEE Antennas and Propagation Magazine*, Vol. 34, No 2, April 1992, pp.79-80.
2. **Donald R. Wilton** and **Prabhakar H. Pathak** , Highlights of MMET\*94, the Mathematical Methods in Electromagnetic Theory Conference, *IEEE Antennas and Propagation Magazine*, Vol. 37, No 5, October 1995, pp.108-112.
3. **Fred Gardiol**, Report on the 6-th International Seminar on Mathematical Methods in Electromagnetic Theory (MMET\*96), Lviv, Ukraine, *IEEE Antennas and Propagation Magazine*, Vol. 38, No 6, December 1996, pp.79-80.
4. **Radovan Zentner**, Report on MMET\*98, *IEEE Antennas and Propagation Magazine*, Vol. 40, No 3, June 1998, pp. 67-69.
4. **Richard L. Dowden** and **Craig J. Rodger**, Report on MMET\*98, *IEEE Antennas and Propagation Magazine*, Vol. 40, No 5, August 1998, pp. 61-64.
5. **Nader Engheta**, Report on MMET\*2000: International Conference on Mathematical Methods in Electromagnetic Theory, Kharkov, Ukraine, September 12-15, 2000, *IEEE Antennas and Propagation Magazine*, Vol. 43, No 3, June 2001, pp. 102-106.

or on our web-page:

[www.kharkov.ukrtel.net/mmet02](http://www.kharkov.ukrtel.net/mmet02)

Signed for print 06.08.2002  
Format 60x84/8. Edition 100 copies. Volume 2.  
Order no. M-2-030802

Prepared and printed by the KONTRAST Publishing Center  
Prospekt Lenina 40, room 231, Kharkov, 61166, Ukraine  
t./f. +380-572-194913, t. +380-572-177651

Certificate of Publishing Center KONTRAST: ДК No. 178 15.09.2000